JANUARY
1982

MICROWAVES

laser technology

A Hayden Publication

Solid-state instrumentation amp challenges TWTA linearity and temperature range



Test & Measurement

Automated RF transistor testing

Tangential signal sensitivity

Safe high-power measurements

Thin-film dielectric constant

Win a cruise!
Enter **MicroWaves'** Top Ten Contest
(details inside).

MICROWAVES laser technology
A Hayden Publication

January 1982
Vol. 21, No. 1

Win a cruise! See page 48.

news

15 **Advances and the basics share spotlight at ARFTG meeting**
21 **Home satellite terminal market expansion is expected**
21 **RCA prepares for programming switch**
22 **Ariane rocket to launch Spacenet satellites**
26 **Air Force receives first improved AWACS aircraft**
26 **New lab performs FCC EMI tests**
28 **Laser range finder passes rigorous testing**
28 **Fourth satellite is acquired by SBS network**
28 **$50,000 offered to find missing ICs**
31 **Washington**
37 **International**
38 **R&D Roundup**
42 **Meetings**
46 **Industry**
54 **For Your Personal Interest. . .**

editorial

56 **Alas lexicon: Engineers versus the English language**

technical

59 **Automated Testing Needs Simplicity And Control.** Robert Rheinlander, of Motorola, tells how to avoid introducing new problems in automated tests designed to eliminate manual testing and technician mistakes.

69 **Practical Approach makes TSS Measurement Simple.** Richard Smith Hughes, of the Naval Weapons Center, shows how tangential signal sensitivity measurements can be made easier.

74 **Radiated Power Method Protects Personnel.** George J. Monser, of Raytheon, explains how technician safety is the key consideration of the peak-sampling method for measuring effective radiated power.

76 **Measurement Method Dispels Dielectric Doubt.** Protap Pramanick and Chinmoy Das Gupta, of the Indian Institute of Technology at Kanpur, present a new microwave measurement technique for finding the two components of the complex dielectric constant of thin-film materials.

86 **Locking Counter Aids Many Spectrum Analyzers.** Shmuel Shalem, of EIP Microwave, Inc., suggests a way to improve long-term stability, higher resolution, and GPIB scanning.

89 **Soft Substrates Conquer Hard Designs.** James D. Woermbke, of Westinghouse, shows how to use high-dielectric-constant soft substrates for improved reliability and increased design efficiency.

101 **MW-Oriented Program Analyzes Opamp Circuits.** Robert H. Edmonds, an independent consulting engineer, introduces a microwave-oriented program emphasizing Gunn oscillator frequency-control circuits.

*104 **Military Fiber-Optic Links: Can They Take The Heat?** Antonio N. Paolantonio, an independent consultant, shows that fiber optics likely to encounter nuclear radiation may be no better than wired systems.

departments

11 **Feedback**
*106 **Application Notes**
*106 **Bookshelf**
109 **Cover Feature**
A linear solid-state alternative to traveling wave tube amplifiers
113 **Product Features**
Spectrum analyzer system speeds phase-noise measurements. Conversion service offered for manual spectrum analyzers.
116 **New Products**
119 **New Literature**
123 **Advertisers' Index**
124 **Product Index**

Domestic only

About the cover: Litton's new solid-state class A linear power amplifier covers 2 to 6 GHz with a 1-W output. Cover photo courtesy of Litton Electron Tube Div. (San Carlos, CA.)

coming next month: Semiconductor Applications

In February *MicroWaves*, our contributors describe the fastest three-terminal device, evaluate the influence of materials on noise performance, continue a series on transistor testing, and introduce you to a promising new compound, GaAlAs.

Publisher/Editor
Stacy V. Bearse
Managing Editor
Walter J. Bojsza
Associate Editor
Jack Browne
Western Editor
Rich Rosen, PE
6043 W. Maplewood Dr.
Littleton, CO 80123
(303) 797-2575
Contributing Editor
Steven March
Washington Editor
Paul Harris
Snyder Associates
1050 Potomac St., N.W.
Washington, DC 20007
(202) 965-3700
European Correspondent
Bill Mitchell
62 Craigwell Ave.
Aylesbury
Buckinghamshire, England
HP21 7AG
(0296) 81529
Editorial Assistant
Tania Tishin
Promotion Manager
Jamie Matusow
Art Director
Janice Moscatelli
Copy/Production Editor
Michael Kachmar
Production Manager
Nick J. Tartaglia
Circulation
B. Freundlich, Dir.
G. Stone, Sub. Mgr.
P. Greenleaf, Reader Serv.
M. Sassano, Reprints
Market Research
Irene Chervin, Mgr.
Editorial Office
50 Essex St.,
Rochelle Park, NJ 07662
Phone (201) 843-0550
TWX 710-990-5071
A Hayden Publication
James S. Mulholland, Jr., President
January Press Run
43,161 copies

MICROWAVES is sent free to individuals actively engaged in microwave work. Prices for nonqualified subscribers:

	1 Yr.	2 Yr.	3 Yr.	Single Copy
US, Canada, Mexico, Central America	$30	$48	$72	$3.00
All other countries	$48	$84	$120	$5.00

Additional Product Data Directory reference issues, $20.00 each, (US, Canada, Mexico, Central America), $32.00 each (all other countries). POSTMASTER, please send Form 3579 to Fulfillment Manager, MicroWaves, P.O. Box 13801, Philadelphia, PA 19101.

Back Issues of MicroWaves are available on microfilm, microfiche, 16mm or 35mm roll film. They can be ordered from Xerox University Microfilms, 300 North Zeeb Road, Ann Arbor, MI 48106. For immediate information, call (313) 761-4700.

Hayden Publishing Co., Inc., James S. Mulholland, President, printed at Brown Printing Co., Inc., Waseca, MN. Copyright® 1982 Hayden Publishing Co., Inc., all rights reserved.

Part I

Automated Testing Needs Simplicity And Control

Even conscientious technicians can make mistakes, and manual testing can compromise quality. But automated tests must avoid new problems.

AUTOMATED testing supports the control, maintenance, and improvement of outgoing quality in today's RF market. In the past, tunable circuitry allowed much more latitude among production runs of device parameters. However, today's customers favor custom-built parts for use in broadband, fixed-tuned circuits, and set exacting specifications to fit specific applications.

This article (and a second installment in next month's *MicroWaves*) explores one approach to automating the radio frequency tests for a wide variety of transistors and functional modules. While we implemented our own high-frequency test systems, we had to keep in mind that we were not in the test systems business, much less the test instrument business. We had to concentrate our resources on semiconductor technology — which *is* our business.

Manufacturers meet twofold goal

Semiconductor manufacturers must meet two basic requirements: they must supply their customers with products of consistant quality, and they must control their internal processing to ensure high yields.

The RF power-transistor market requires the fabrication of a wide variety of devices in relatively small lots. Any automated test set used in this industry must be able to quickly adapt to different measurement requirements. If each new test requires additional equipment or set-up time, production will fall. This required flexibility should include built-in calibration facilities as well as system self-test and diagnostic capabilities.

Robert Rheinlander, Principal Staff Engineer, High Frequency and Optical Products Div., Discrete Semiconductor Group, Motorola Inc., 5005 E. McDowell, Phoenix, AZ 85008.

The costs of suitable systems can vary widely, particularly in initial capital investment. In a test system of this type final cost depends on the control of software, firmware, and hardware costs.

Above all, control of cost depends on the control of the cost of software. Specifiers almost invariably underestimate programming costs, both for the initial acquisition and for the inevitable debugging period. Software cost estimates must also look to the future, since programs which are either purchased separately or as part of a turn-key system may prove inadequate as needs change. Many "smart" programmers add to this problem by making their software difficult to modify.

The firmware provided in system ROMs trades reduced flexibility for simplified software. This tradeoff makes the most sense in commercial instrument packages (to keep them "bus" adaptable).

Any evaluation of hardware costs must primarily consider maintenance capabilities, both in trained personnel and available service equipment. The selection of vendors should depend, at least in part, on the maintenance they can provide, ranging from physical support to the provision of diagnostic software. At our facility, for example, a cost analysis prompted us to use vendor maintenance exclusively for some instruments.

"True" cost must be recognized

In all of these considerations, the cost of an automatic test set must be compared to the true cost of *not* having one. Deficient control of critical and complex testing may mean business surrendered to a competitor. And, in our case, a drastic reduction in operator-training level provided readily identifiable cost advantages.

We acquired our first automated RF system, a network analyzer, in 1969. This instrument taught us two very important lessons: First, that machine language saves memory space and decreases execution time, but is very difficult to modify. Second, that the interconnection system or bus should follow a recognized standard and be free from specialized "black box" adapters. (Keep in mind that this first system was designed and built when instrument buses were in their infancy, and memory was far more expensive than it is today.)

Development started with study

At Motorola, we began studying the available approaches to automated RF testing in 1975, with a goal of meeting 1979 demands. As we monitored the efforts and the results of others, our observations were discouraging. We had many examples of what to avoid, but few hints on the correct path to follow. We also began to realize that costs, particularly those of software development, were much higher than we anticipated.

One fault that we saw in many systems—a lack of concise definitions for the required tasks—seemed to make them overly complex and inefficiently integrated. Our studies began to indicate some necessary system philosophies:

- The system must allow hardware changes to adapt to a variety of products. Consequently, the instruments in the system must be fully interchangeable.
- All instruments serving the same function should be of the same type, model, and manufacture.
- Each system should have its own individual microcomputer facility and use an interpretive language. Each calculator/controller, however, should be readily tied to a central computer.
- All instruments must operate from a common bus system.

(continued on next page)

In addition to accepting these general philosophies, we also decided not to build anything that we could buy. Although it may seem economical to build simple adaptive devices, the savings rarely materialize when the costs of the documentation needed for servicing or duplicating the equipment is considered.

As our studies continued, new equipment became available — specifically equipment which was compatible with the IEEE-488 bus. To avoid restrictions on the interchange flexibility, we also studied various adapter systems that perform basic functions such as relay switching, bias provision, and event sensing. The model 53A smart hardware system from Computer Data Systems (Englewood, CO) and multiprogrammer systems from Hewlett-Packard (Palo Alto, CA) helped at this stage and greatly reduced the need to either build unique control apparatus or buy a variety of bus-compatible subfunctions.

Single insertion system results

Our evaluation and planning resulted in the single insertion final test (SIFT) systems. We laid down the design for SIFT I in early 1980, and had it successfully operating by October of that year (see "CATV test set came first," this page).

All combinations of functional tests, regardless of their complexity, involve gain, return loss, and power consumption. Conventionally, these tests involve the equipment shown in Fig. 1.

Although directional couplers reduce the power to levels that can be used by a thermocouple, thermistor, or diode power detector, they do so in a manner that minimizes power dissipation. The attenuation offered by a typical coupler (stripline) may vary with frequency from ± 0.3 dB to as much as ± 2 dB from its nominal coupling. Those couplers offering the best directivity seem to have the most variation in attenuation with frequency. When such couplers are used in a manually operated system, look-up tables must be read and interpreted to determine the attenuation. To avoid using the tables, a common compromise involves the selection of maximally flat couplers (with directivities of -25 dB) for the input and output power couplers, and a directionally optimal coupler to handle reflected power. (This discussion precludes lower power systems using

CATV test set came first

While SIFT I was under development, the demands of the CATV industry for amplifier modules began to tax our test capability in that area. The CATV sector, which always had its own unique test requirements, upped the ante by doubling the number of channels that had to be carried by line amplifiers (and, therefore, the required number of test sources). The variety of product "sorts," which depend on combinations of distortion, gain, and bandwidth specifications, also multiplied.

Because of their pressing nature, the CATV-amplifier measurements provided our first completed automated RF test project. The test source consisted of 60 sources which transmitted simultaneously.

Our tests were concerned with distortion within the amplifiers. The distortion product varies with the device output power in a nonlinear manner. In the former manual system, a skilled technician set the amplitude of each channel with a previously tested "standard" unit. If the channels are preset, even with great accuracy, the output power of each unit will vary with its gain because some gain variations within the test lot are inevitable.

The variable distortion products determined by the existing system represented a measurement inaccuracy, and performance could be guaranteed to the customer only by over-specifying. Of course, this tactic resulted in lost yield.

Computer loop control, on the other hand, could allow each channel to be adjusted for each unit tested. As our thoughts continued, we realized that if we could control the test sources for one type of multi-tone distortion test, we could also set up other distortion tests, and perform these tests in sequence with a single insertion into the test set.

The next step, the addition of frequency measurements and input power (and therefore gain) proved simple. This step brought input and return loss measurements in sight. And we decided that, with all that capability, we could also add a noise source and measure noise figure. The result was our DTS-1 test set which was built for us by Matrix Test Equipment (Haupauge, NY).

The DTS-1 allowed us to perform multiple distortion tests at optimal levels in a single-insertion operation. It performed five tests of four types that previously required *five* separate insertions in three different test sets. Gain and return loss testing on the DTS-1 eliminated another insertion and another test set. Noise figure tests eliminated the sixth operation previously required and the fifth test set.

The new turn-key automated system cost less than the individual equipment required to perform the same tests at the same rate. In addition to operator-training requirements, handling and sorting labor was also reduced. Yields to individual specifications improved.

Although the DTS-1 performed admirably, it was not a complete success. Some of its shortcomings were:

- Software was not formally structured into easily located, isolated subroutines. Modifications required lengthy searches.
- The original test set did not include programmable test circuit power supplies and power monitoring.
- Although the typical "handshake" controls were provided through the bus, status readings of the various source controls were not. Status reporting proved necessary for both system diagnostics and program checking.

The first and second deficiencies were corrected in the first DTS-1 system, and were assigned as criteria for the second. The third deficiency could not be corrected on the first system, but status readings were included in the second.

Even after buying a "turn-key" system that included software, several hundred hours were required to discipline and modify the programming. In comparison, hardware modifications were insignificant. The vendor can't be blamed for these shortcomings—they resulted from some mutual naivete in this cooperative design effort.●●

return-loss bridges at the input.)

An automated system has the capability of composing and storing the required look-up tables in the calculator. A corrected power reading can be generated for each frequency selected. These readings may not only be used for data, but for correcting the source level according to either the corrected device input or output.

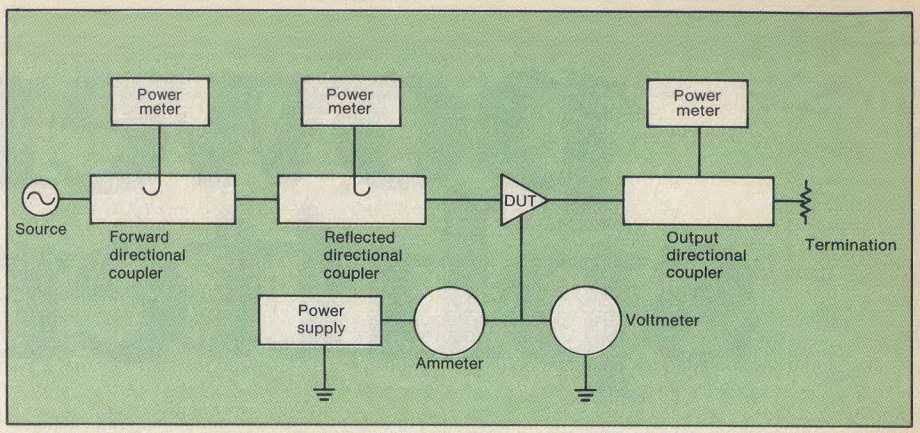
Calibration is accomplished with an attenuator/power-meter set which has been externally calibrated as a working standard. With its own errors stored in the calibration software, the attenuator/power meter is first substituted for the output-coupler/termination/power-meter subsystem (Fig. 2). Input power is applied, and the frequency swept in steps across the desired band.

Measured input power is compared to the corrected output of the standard. The resulting errors are stored in the calculator and on tape.

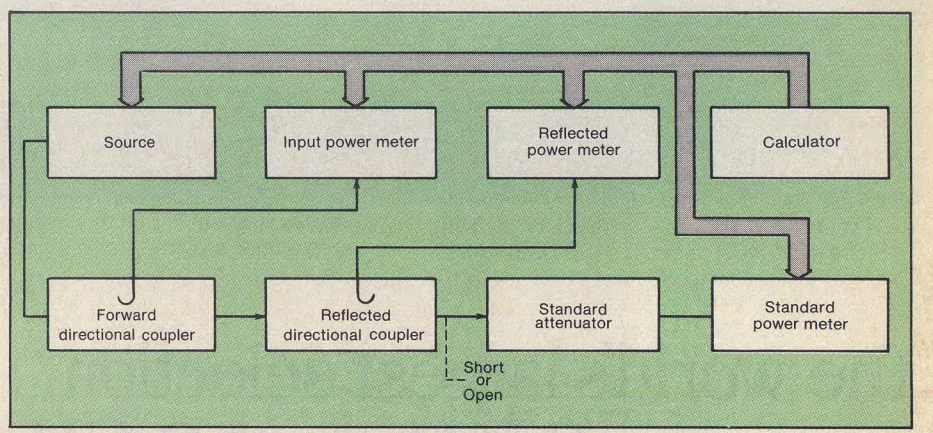
Following this work with the standard, the system is run for a reflected-power reading with first an open and then a short circuit at the output of the reflected coupler (also indicated in Fig. 2). The errors are gathered and averaged in pairs for each frequency step. These averaged errors are stored in a return-loss error array for later use. (In order for this scaler technique to be valid, the phase of the open and of the short circuit must be separated by 180 degrees at each frequency of interest.)

The calibration continues with the normal output subsystem reconnected to the test set. The input source again sweeps the frequency range, and an error table is again generated (and stored in the output array) by comparing the corrected input power reading to the uncorrected output indication. The complete RF calibration for 100 MHz to 1 GHz in 10-MHz increments requires about 20 minutes. Most of this time is used to connect and disconnect equipment. The accuracy, consistency, and speed of the calibration exceed that of manual means.

Importantly, error magnitude limits are applied within the system. These limits prevent an unrealistically large error from being entered into the tables. For example, the maximum error might be 2.0 dB if all subsystem components are within their specified limits. A detected 2.2-dB error (which could indicate the failure of some component) will not be entered and the system will interrupt with a warning to the operator.



1. The combination of functional tests that were the goal of the automated test systems *involved gain, return loss, and power consumption. These tests require the basic hardware shown.*



2. Calibration of an automated test set *begins by inserting a "working standard" power meter in place of the output subsystem. Computer control speeds the process beyond manual methods.*

Only power control homegrown

The SIFT I system is equipped with two power supplies. The main power supply for the test circuit has a 25-A capability, and can be programmed in increments of 200 Ω/V. The secondary bias supply, a 5-A constant-voltage/constant-current (CV/CI) unit, can be programmed at 200 Ω/V or 200 Ω/A. CV/CI changeover is selected with a manually changed jumper plug, and status feedback to the calculator won't allow programming in the wrong mode.

Figure 3 shows the block diagram of the final basic single-insertion test system. The only locally designed and manufactured element in the entire system, a simple power control, contains various range selection and routing switches. It also holds current shunts for both supplies.

All power supply connections are routed through the power control, which in turn is connected to the "smart hardware" system that includes the system voltmeter and scanner cards, the resistive programming card for the power supplies, an event-sense card, and relay-control cards. Each of these functions can be addressed separately through a single bus connection.

When either of the power supplies is addressed, the voltage or current is checked with the voltmeter. The voltmeter is calibrated against a working-standard voltmeter which, like the standard power meter, is connected not only across the system voltmeter, but also to the bus during calibration. The system displays and prints the program input, the system voltmeter reading, and the standard voltmeter reading.

Even though a great effort was made to identify the basic requirements of the system, to minimize

(continued on p. 65)

unique features, and to consider hardware/firmware/software trade-offs, problems emerged. The original prototype, operating within six months of funding approval, used one power meter which was switched through coaxial transfer relays. Not only was this arrangement slow, but repeatability was worse than if three separate power meters were used.

As a solution, we decided to install three recently offered, inexpensive power meters. The resulting compromise in performance could not be tolerated. After a four-months delay, we incorporated three of the *h*igh *p*riced variety, and experienced no further difficulty.

Several systems followed the prototype over a nine-month period. Some of these systems were intended for testing discrete RF power transistors with 30-W available input power over a 100-MHz-to-1-GHz range. Disregarding the power-meter problem in the prototype system, results have been excellent.

Other systems were constructed for testing RF power modules. The systems were identical to those used for discrete power testing, except that the signal source was modified to use less powerful, broadband linear amplifiers.

An outside vendor fabricated and cabled the latter systems, but new problems highlighted the inadequacies of our own documentation, and our lack of a vendor inspection system. Debugging time grew from hours to days.

Design oversight causes downtime

An oversight in our design concerned the secondary bias supply which now had to be exercised over several excursions for each module. The resistance programmer was being cycled over two more orders of magnitude than in the first systems. The MTBF of the relay that operated this subsystem quickly became a significant concern. Several outages and significant downtime were experienced.

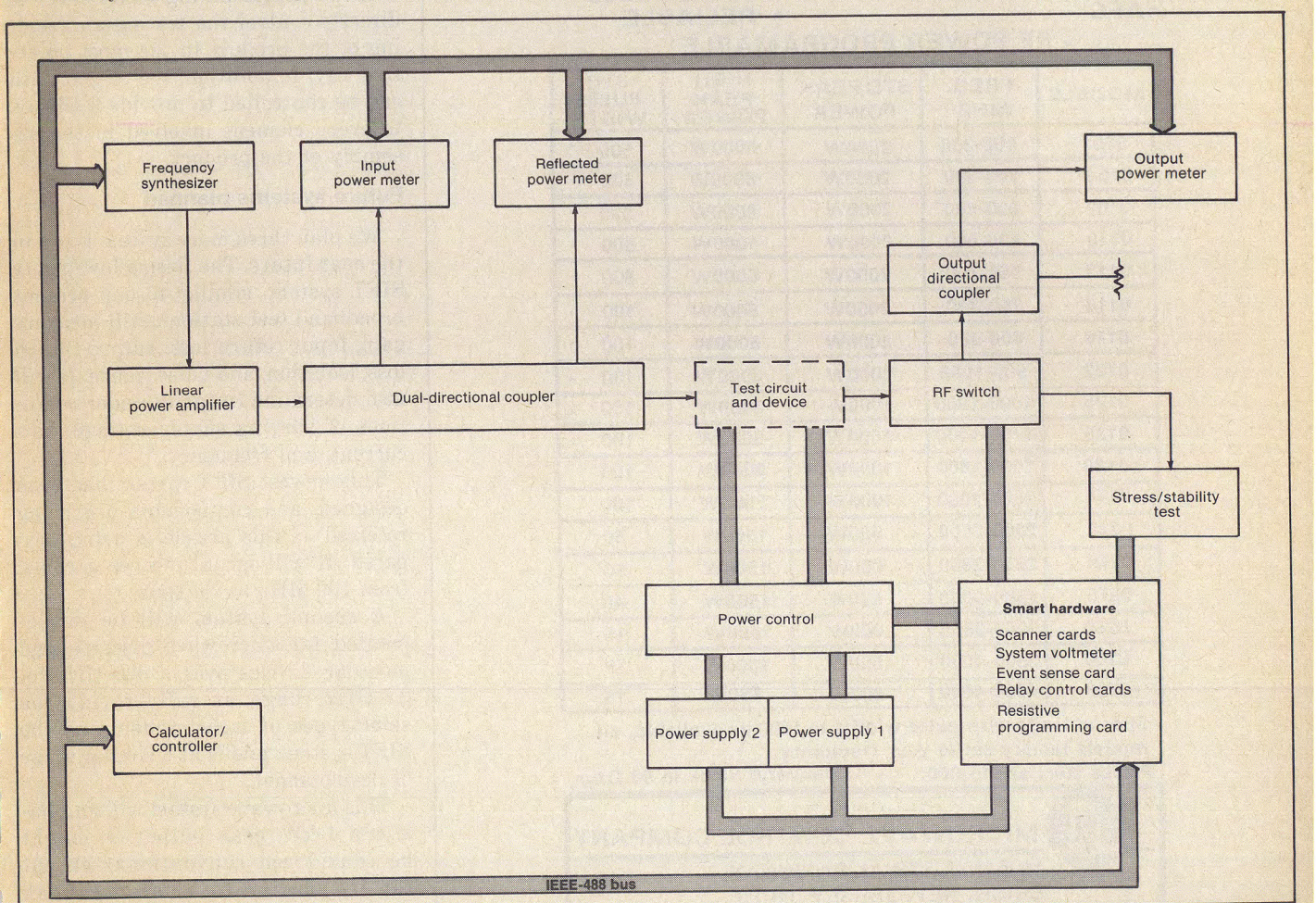
We are now retrofitting the RF power module sets with optically isolated digital-to-analog converters for programming the agile bias supply.

A solution also had to be found for RF input power transients which were producing product yield losses. The system has an input power capability of 10 W, while some products can tolerate a maximum input of only 0.5 W. We found that we had to take a "belt and suspenders" approach and add a programmable binary attenuator to the output of the signal source. This attenuator limits the maximum output of the source to a level 3 dB above the maximum test power required for that product.

Programming started with basics

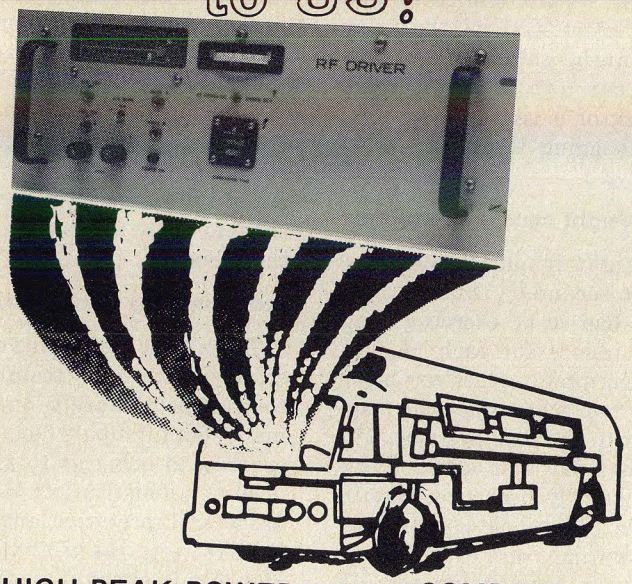
Essentially we started our software efforts from zero training level. It took approximately one year, and many helpful inputs from experienced sources, to bring us to an acceptable level of sophistication. We invariably use an interpretative language such as BASIC (in its many forms) or Hewlett-Packard Language (HPL).

(concluded on next page)



3.The basic single insertion final test (SIFT) *system includes only one locally designed and manufactured component: the power controller. All other elements were obtained from vendors.*

You Build the Bus Leave the "RF DRIVER" to US!



- HIGH PEAK POWER
- PHASE STABLE
- AFC
- COMPACT
- LONG PULSE
- RELIABLE
- RF POWER PROGRAMABLE

MODELS	FREQ. MHZ	STD PEAK POWER	HIGH PEAK POWER	STD PULSE WIDTH
0101	100-200	2000W	8000W	500 *
0104	200-300	2000W	8000W	500 *
0107	300-400	2000W	8000W	500 *
0110	400-500	2000W	5000W	500 *
0113	500-700	2000W	5000W	300 *
0116	700-800	2000W	5000W	100 *
0119	800-900	2000W	5000W	100 *
0122	900-1000	1000W	3000W	100 *
0125	1000-1200	1000W	3000W	100 *
0128	1200-1400	1000W	3000W	100 *
0130	1400-1600	1000W	3000W	100
0135	1600-2000	1000W	3000W	100
0240	2000-2500	600W	1500W	50
0268	2850-2860	600W	1500W	50
0275	2500-3000	600W	1500W	40
0280	3000-3500	600W	1500W	15
0290	3500-4000	500W	1000W	15
0300	4000-4500	400W	750W	15

* Special Units with pulse widths to 1500 µs available, all models factory set to your frequency.
Prices start at $15,000. Delivery: Stock to 90 Days

MICROWAVE CONTROL COMPANY
1105 INDUSTRIAL PARKWAY
BRICK, NEW JERSEY 08723
WE INVITE YOUR CALL, 201-458-3000
TELEX 642-651

READER SERVICE NUMBER 54

Although we sacrifice both speed and memory space with an interpretative language, its friendly nature lends itself to use by those with little computer training. Without the interpretive language, the task would be too formidable and beyond our resources.

We have developed highly structured "EXECutive" routines for each basic device to be tested. Each measurement process is divided into subroutines which apply to the function of each instrument, including its calibration correction. These sets of instructions can be maneuvered as flexible entities, and obviate the need for line-by-line corrections.

A part of the EXEC for a product group is a question-and-answer routine which allows an inexperienced operator to establish a "data file." The data file consists of the device specifications and allows several specifications to be sorted, by category, from a given product lot. This provision allows a person highly experienced with a product and its application, but without programming experience, to directly control the testing and sorting of the product in the most objective way. In addition, the output data can be controlled to provide feedback to every element involved in the assembly of the product.

Future systems planned

We plan three more system types in the near future. The first, a low-power SIFT system, similar to our present broadband test stations, will measure gain, input return loss, output return loss, isolation, and noise figure. It will also determine linearity under conditions of varying supply voltage, bias current, and frequency.

This newest SIFT system has been designed, and components are being received as this article is being prepared. It will initially cover a range from 100 MHz to 2.0 GHz.

A second system will be implemented for microwave discrete and modular devices over a 960-MHz-to-2.6-GHz range. It will provide the same types of measurements as the SIFT system, and is at a similar stage of development.

This microwave system will emphasize a 1-kW peak output. It might be considered conventional except for its ability to reference peak power to real-time comparisons of measured duty cycle or CW equivalent conditions. ●●

Practical Approach Makes TSS Measurement Simple

Tangential signal sensitivity (TSS) measurements help to evaluate low-level signal performance. A simple, repeatable technique can make these measurements more practical.

TANGENTIAL signal sensitivity (TSS), noise figure, noise temperature, and noise-temperature ratio (along with other quantities) can all specify amplifier sensitivity. Although noise figure and noise temperature are the most familiar of these measurements, they can be difficult to determine and to interpret.

TSS offers a useful alternative. In a sensitivity comparison, for example, a receiver can be specified as simply having a TSS of −55 dBm. (Noise bandwidth and signal impedance must also be stated when TSS is used.)

Tangential signal sensitivity refers to the condition in which a signal plus noise waveform (on an oscilloscope) protrudes above a noise baseline such that the bottom edge of the combined terms *just touches* the top edge of the baseline noise. Experimentally, this power ratio has been found to be 6.31 (8 dB). The input power level corresponding to this TSS condition is also referred to as tangential signal sensitivity, and is used as a tool in comparing equipment performance specs.

Richard Smith Hughes, Electronics Engineer, Naval Weapons Center, China Lake, CA 93555.

Classical TSS measurement

TSS provides several distinct advantages in specifying and comparing the signal sensitivity of noise linear systems. (Such a system exhibits no interaction or mixing of signal and noise components.) Many receivers (with square-law or linear detectors), in which the RF or IF bandwidth exceeds the video bandwidth, are noise linear systems.[1,2,3] Figure 1 shows the basic noise linear system.

TSS measurements have been complicated by the subjectivity of the words *just touches* in its basic definition. Oscilloscope sweep time and intensity settings compound the problem, and accurate TSS measurements have represented a frustrating task. But now a simple and repeatable method of measuring TSS is available.

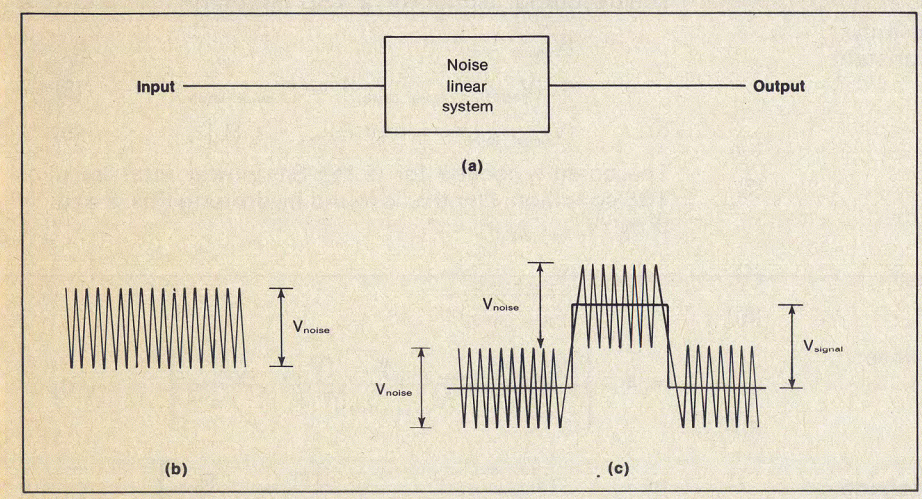
With only noise applied to the video amplifier (Fig. 2 and the "TSS equations," p. 70), the thermocouple meter indicates a value of the noise power, R_n, which is proportional to the mean-square noise voltage (Eq. 1). The 50-kHz square wave is then applied until the top of the standing noise just touches the bottom of the raised noise. The meter reading for this TSS condition is R_{s+n}, and is due to both signal and noise (Eq. 2).

At the end of the mathematical development, two equations (Eqs. 10 and 11) remain. The left-hand sides of both equations give the signal-to-noise (S/N) power ratio for a TSS condition. In the first case (Eq. 10) a true-reading RMS voltmeter is used, while the latter (Eq. 11) requires a thermocouple type. The purpose of the equations is to enable an engineer to compare similar TSS conditions mathemetically by measuring values on instruments other than oscilloscopes (or in conjunction with oscilloscopes).

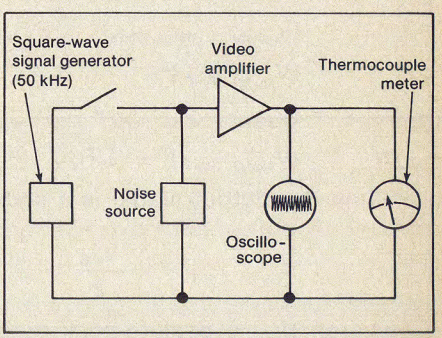
Simple scope method

A simple and repeatable (from person-to-person) technique for measuring TSS that is less subjective than the classical method and less sensitive to oscilloscope settings has been developed. The output of the noise linear amplifier is connected to a dual-trace oscilloscope (see Fig. 3). Both traces

(continued on next page)



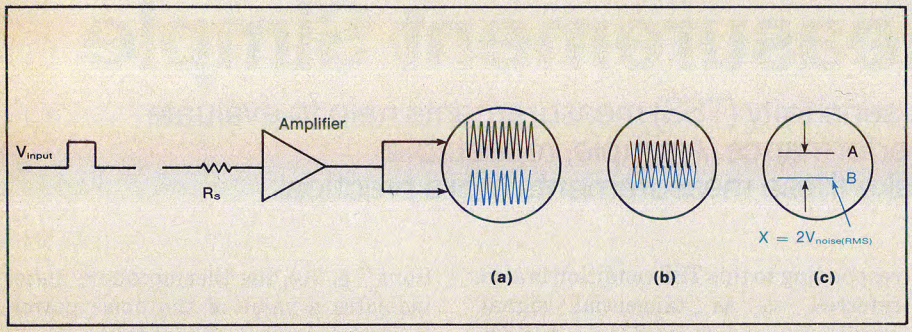
1. In the classical TSS measurement for a noise linear system, *noise alone has fairly well defined top and bottom edges, while signal plus noise shows the bottom edge of raised noise just touching the top edge of standing noise.*



2. The TSS measurement circuit *uses a scope display that can be related to a thermocouple meter indication.*

must have the same scale factor setting, and must be AC coupled to the circuit. The measurement begins by slowly bringing the two traces together (Fig. 3a and 3b) until there is no *dark band* between them. When the noise term is removed, the resultant trace separation (Fig. 3c) represents twice the RMS noise voltage.[4,5,6]

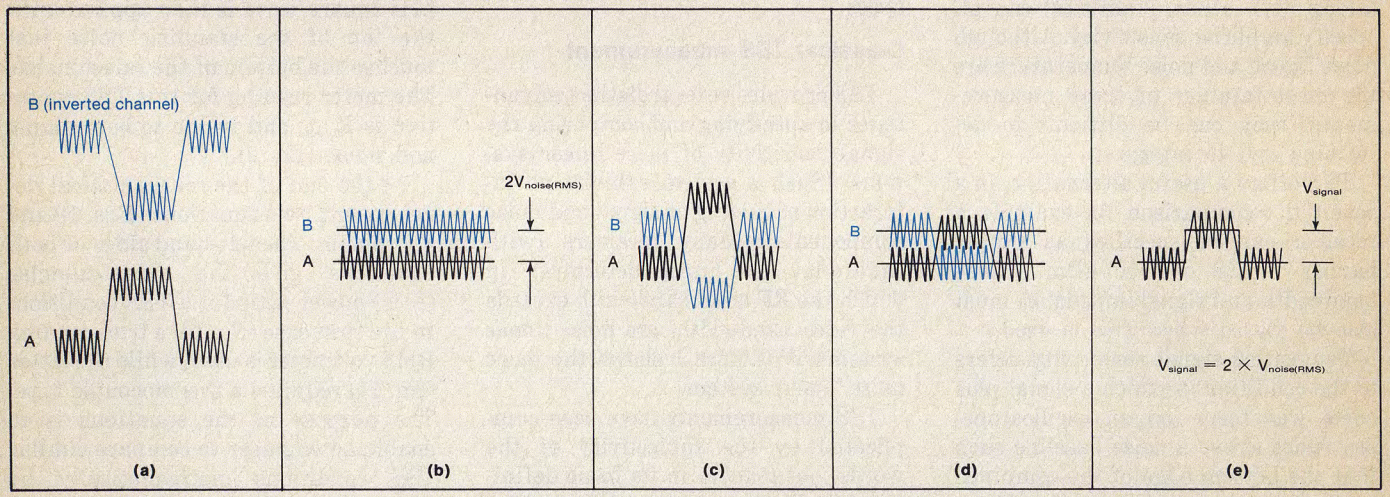
$$V_{noise\ (RMS)} = X/2 \qquad (12)$$



***3. The simple scope method of determining TSS** starts by calibrating the scope trace separation in terms of twice the RMS noise voltage.*

In Eq. 12, X = the separation of the two traces times the volts per division on the oscilloscope. This simple method of measuring the RMS output noise voltage of the noise linear system, can be used to calculate TSS.

Connect the noise linear system to be measured as before (Fig. 3), but invert the bottom trace (B) and position it above the other trace (A) (Fig. 4a). Decrease the input signal to zero, and adjust for a noise RMS condition as described earlier (Fig. 4b). Increase the input signal well above the noise (Fig. 4c), and slowly decrease the signal until the dark band disappears (Fig. 4d). The resultant output signal on channel A (Fig. 4e) is equal to twice the RMS noise



***4. The RMS signal sensitivity (RMSSS) scope display** provides the first step in the procedure to find TSS. Two signals, one inverted with respect to the other, are merged until the dark band disappears. RMSSS is on channel A.*

TSS equations

This mathetical development relates a TSS signal-to-noise-power ratio to a thermocouple reading for the special case of a square-wave input signal.

$$(V_{noise\ (RMS)})^2 = \delta\ R_n \qquad (1)$$

where: R_n = meter reading for noise only
δ = meter proportionality constant

$$(V_{signal\ +\ noise\ (RMS)})^2 = (V_{signal\ (RMS)})^2 + (V_{noise\ (RMS)})^2 \qquad (2)$$

$$(V_{(signal\ +\ noise)\ RMS})^2 = \delta\ R_{s\ +\ n} \qquad (3)$$

$$(V_{signal\ (RMS)})^2 = (V_{signal\ +\ noise\ (RMS)})^2 - (V_{noise\ (RMS)})^2 \qquad (4)$$

or $$(V_{signal\ (RMS)})^2 = \delta\ R_{s\ +\ n} - \delta\ R_n \qquad (5)$$

Since the output signal is a square-wave:

$$V_{signal\ (RMS)} = \frac{V_{p\text{-}p}}{2} \qquad (6)$$

where: $V_{p\text{-}p}$ = peak-to-peak output voltage.

The output signal mean-square voltage is:

$$(V_{signal\ (RMS)})^2 = \left(\frac{V_{signal\ (p\text{-}p)}}{2}\right)^2 \qquad (7)$$

Equations 4 and 5 may now be solved for the mean-square output signal for a TSS condition:

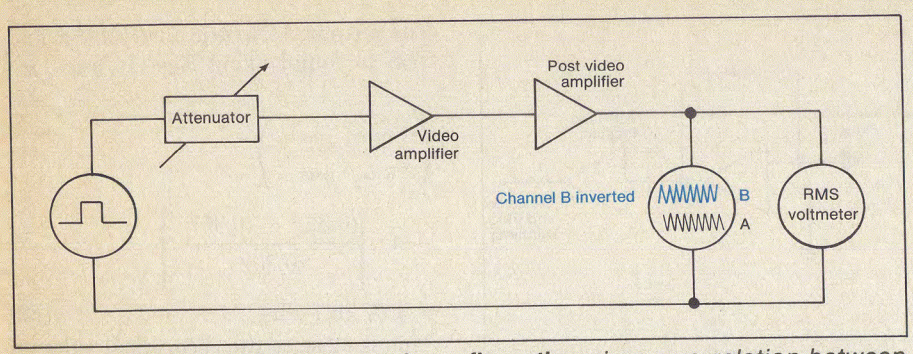
$$(V_{signal\ (p\text{-}p)})^2 = 4\ [(V_{signal\ +\ noise\ (RMS)})^2 - (V_{noise\ (RMS)})^2] \qquad (8)$$

or: $$(V_{signal\ (p\text{-}p)})^2 = 4\ [\delta\ R_{s+n} - \delta\ R_n] \qquad (9)$$

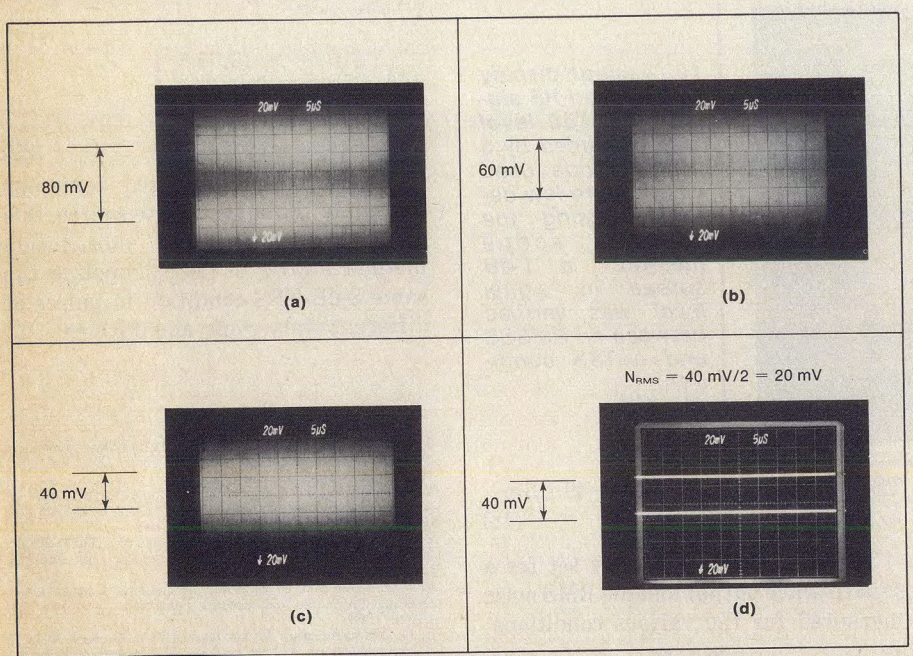
The quantity looked for is the S/N power ratio for a TSS condition, and this is found by dividing Eqs. 8 and 9 by $(V_{noise\ (RMS)})^2$:

$$\frac{(V_{signal\ (p\text{-}p)})^2}{(V_{noise\ (RMS)})^2} = 4\left[\frac{(V_{signal\ +\ noise\ (RMS)})^2 - (V_{noise\ (RMS)})^2}{(V_{noise\ (RMS)})^2}\right] \qquad (10)$$

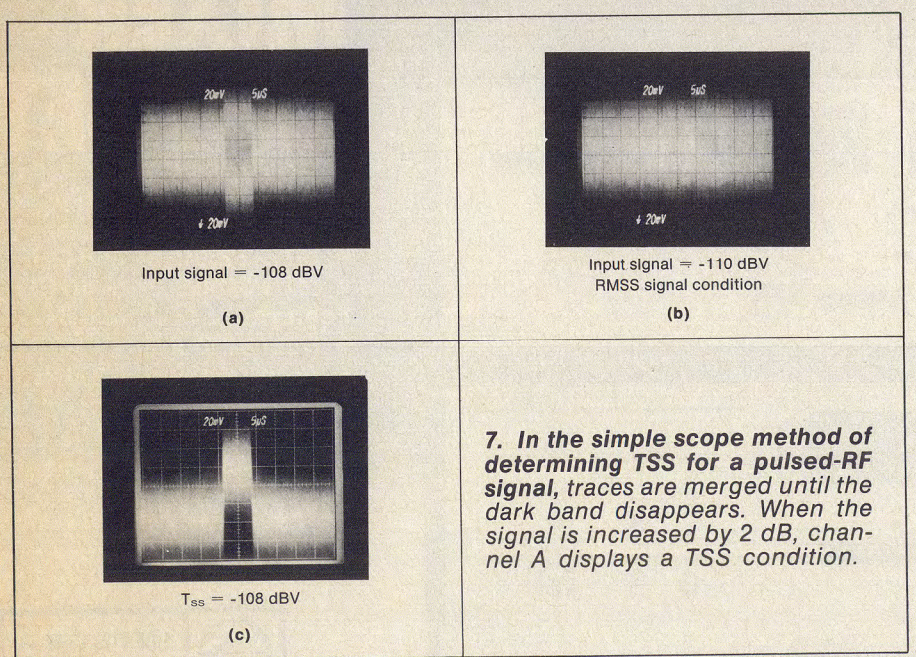
or $$\frac{(V_{signal\ (p\text{-}p)})^2}{(V_{noise\ (RMS)})^2} = 4\left[\frac{R_{s+n} - R_n}{R_n}\right] \qquad (11)$$



5. The RMSSS and TSS test circuit configuration *gives a correlation between the classical definition of an 8-dB tangential signal sensitivity and an actual measured value of 8.1 dB using the "simple scope method."*



6. The RMS noise measurement *requires the convergence of the two noise scope traces (channel A and inverted channel B) until the dark band between them disappears. When the noise is removed, two lines remain, separated by twice the RMS noise voltage.*



7. In the simple scope method of determining TSS for a pulsed-RF signal, *traces are merged until the dark band disappears. When the signal is increased by 2 dB, channel A displays a TSS condition.*

voltage. The input signal producing this condition is called the root-mean-square signal sensitivity (RMSSS).

$$V_{signal\ (p\text{-}p)} = 2V_{noise\ (RMS)} \quad (13)$$

It has been shown that TSS is that input signal which produces the output signal:[2]

$$V_{signal\ (p\text{-}p)} = 2.51\ V_{noise\ (RMS)} \quad (14)$$

Thus, the relationship between RMSSS (measured) and TSS (desired) is:

Linear: TSS=1.26 RMSSS or
TSS(dB)=RMSSS(dB) + 2 dB (15)

Square law: TSS=1.26 RMSSS or
TSS(dB)=RMSSS(dB) + 1 dB (16)

By using this somewhat less subjective "simple scope method" to arrive at a value called RMSSS, and adding the appropriate 1 or 2 dB (for a square-law or a linear detector, respectively), TSS can be determined.

Examples show applications

A low-noise video amplifier was connected to a pulse generator (Fig. 5). With the input signal removed, the RMS noise voltage was measured by slowly bringing the two traces together (Figs. 6a and 6b) until the dark band vanished (Fig. 6c). The resultant RMS noise voltage is (from Fig. 3 & Eq. 12):

$$V_{noise\ (RMS)} = \frac{40\ mV}{2} = 20\ mV \quad (17)$$

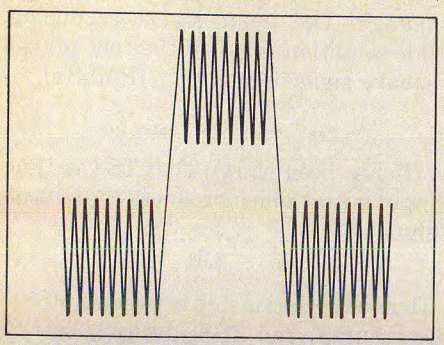
This result agrees with the measured value of 21 mV.

The input signal was increased above the noise (Fig. 7a), and decreased until the dark band vanished (Fig. 7b). This is the RMSSS condition, and represents an output S/N ratio of 6 dB. Increasing the input by 2 dB produces the desired TSS (Fig. 7c). With the input signal level at TSS, the signal generator was switched to square wave to verify Eqs. 10 and 11. The measured value was 8.1 dB (close to the accepted value for TSS of 8 dB).

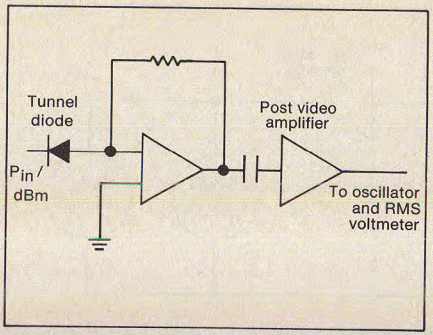
As mentioned earlier, this theory applies to any noise linear system, whether it employs mixers, RF or IF amplification, or linear or square-law detection. However, the RF or IF bandwidth must be much greater than the video bandwidth. It is fairly simple to check for noise linearity. If the raised noise is larger than the standing noise (Fig. 8), the system is noise nonlinear, and this procedure is not useful.

A tunnel diode detector[7] was used to verify the results for square-law detec-

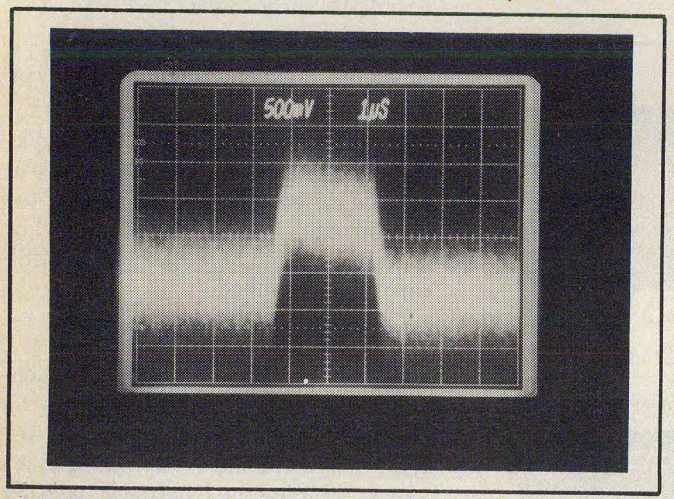
(concluded on next page)



8. Simple check for a system noise nonlinearity: *The raised noise is larger than the standing noise.*



9. A tunnel-diode detector circuit *verified the 1-dB change in TSS for square-law detection.*



10. A scope display of a pulsed-RF signal at a TSS level *was produced by a tunnel diode used as a square-law detector. Using the "simple scope method," a 1-dB spread in signal level was verified between an RMSSS and a TSS condition.*

tion (Fig. 9). The oscilloscope was set up as described earlier, and the output RMS noise voltage was measured at 360 mV. The corresponding RMSSS input was −50 dBm. Since the detector was operated well within the square-law region, increasing the input power 1 dB increased the output signal voltage 2 dB. This gave:

$$\text{TSS} = -50\ \text{dBm} + 1 = -49\ \text{dBm} \quad (18)$$

The signal generator was set for a square-wave output and the RMS noise measured for the various conditions:

$$V_{\text{noise (RMS)}} = 360\ \text{mV} \quad (19)$$

$$V_{\text{signal + noise (for RMSSS)}} = 530\ \text{mV} \quad (20)$$

$$V_{\text{signal + noise (for TSS)}} = 600\ \text{mV} \quad (21)$$

The output S/N ratio for RMSSS and TSS is found using Eqs. 10 and 11:

$$\left(\frac{V_{\text{signal (p-p)}}}{V_{\text{noise (RMS)}}}\right)^2 = 4\left[\frac{(0.52)^2 - (0.36)^2}{(0.36)^2}\right] = 4.67\ (6.7\ \text{dB}) \quad (22)$$

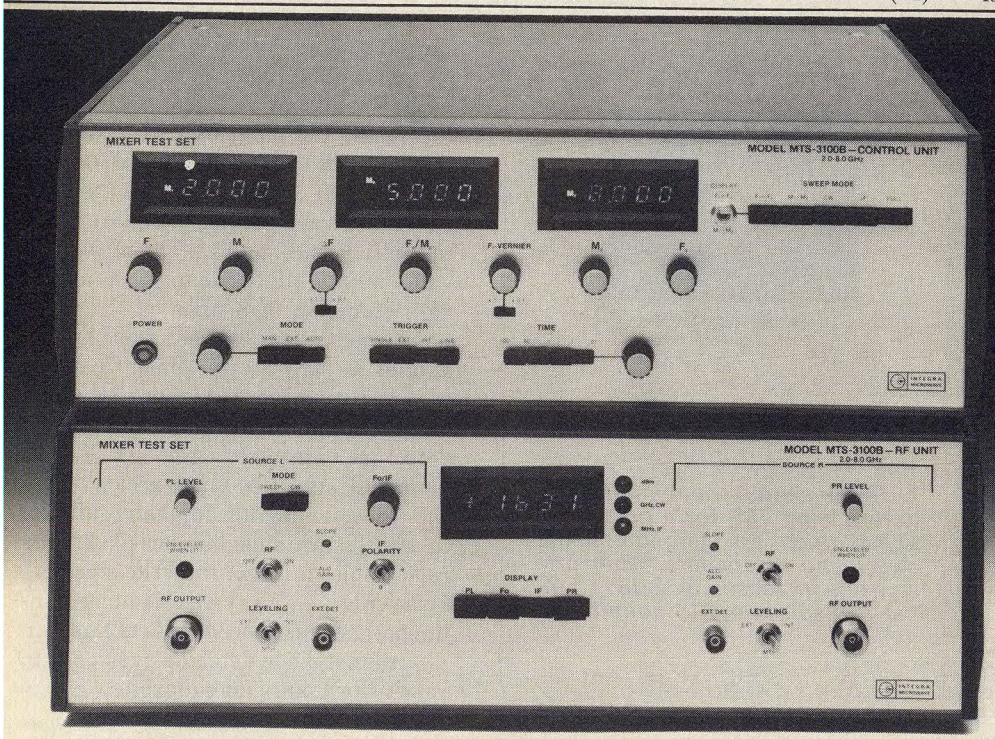
This is close to the theoretical value of 6 dB. The S/N ratio for TSS is:

$$\left(\frac{V_{\text{signal (p-p)}}}{V_{\text{noise (RMS)}}}\right)^2 = 4\left[\frac{(0.6)^2 - (0.36)^2}{(0.36)^2}\right] = 7.11\ (8.52\ \text{dB}) \quad (23)$$

Although the developed equations pertain to the square-wave source, this scope procedure and substitution method allows us to extrapolate the same 8-dB TSS condition to pulses of different duty-cycle and PRF.••

References

1. W.J. Lucas, "Tangential Sensitivity of a Detector Video System With RF Preamplification," *Proc. IEE*, Vol. 113, No. 8, pp. 1321-1330 (August 1966).
2. W.J. Lucas and E.R. Beck, "A Noise Performance of a Three-Stage Microwave Receiver," *Electronic Technology*, pp. 76-78 (February 1961).
3. J.H. Frohmaier, "Noise Performance of a Three-Stage Microwave Receiver," *Electronic Technology*, pp. 245-246 (June 1960).
4. V. Garots and C. Samuel; "Measuring Conventional Oscilloscope Noise," *Tekscope*, (Tektronix, Inc.) pp. 8-11 (April 1969).
5. G. Franklin and T. Hatley; "Don't Eyeball Noise," *Electronic Design*, Vol. 24, pp. 184-187 (November 22, 1973).
6. M. Gruchalla. "Measure Wide-Band White Noise Using a Standard Oscilloscope," *EDN*, pp. 157-160 (June 5, 1980).
7. R.S. Hughes, "Tunnel Diodes Excel as DC-Coupled Detectors," *Microwaves*, Vol. 20, No. 6, pp. 59-62 (June 1981).



MIXER TEST SET

Three models available:
- MTS-3100B, 2–8 GHz
- MTS-3100C, 8–18.5 GHz
- MTS-3100E, 26.5–40 GHz

Features:
- Dual RF Outputs
- Auto-tracking ± 3 MHz
- IF Offset to 2 GHz
- +10 dBm, leveled
- IEEE-488 Programming

INTEGRA MICROWAVE

READER SERVICE NUMBER 57

2368 Walsh Ave., Santa Clara, CA 95051 (408) 727-9601/TWX: 910-338-0585

Radiated Power Method Protects Personnel

Technician safety is the key consideration of this peak-sampling method for measuring effective radiated power. The procedure produces a typical error of ±1 dB.

SAFETY must be considered along with reliability, accuracy, and repeatability during radiated power measurements, especially with the increasing transmitter power of military systems.

The problem of establishing safe procedures is complicated by the disagreement over safe exposure levels to microwave signals. The US continues to hold to its standard of 10 mW/cm^2, while many other countries have set the maximum allowable power density at 1 mW/cm^2, or less. The USSR, for example, has set its standard at 10 $\mu W/cm^2$.

Since the US standard has been called too lax and the USSR standard too stringent, a safe approach might be to use the 1 mW/cm^2 figure as the acceptable power density. Safe approach distances can be determined for various transmitter powers based on this standard, and are shown in the table. This table applies to radiated power in a free-space environment such as an anechoic chamber. For outdoor test sites where ground reflections (which can produce a 100-percent increase in field intensity) are likely, the tabulated approach distances should be doubled.

Method uses reduced duty cycles

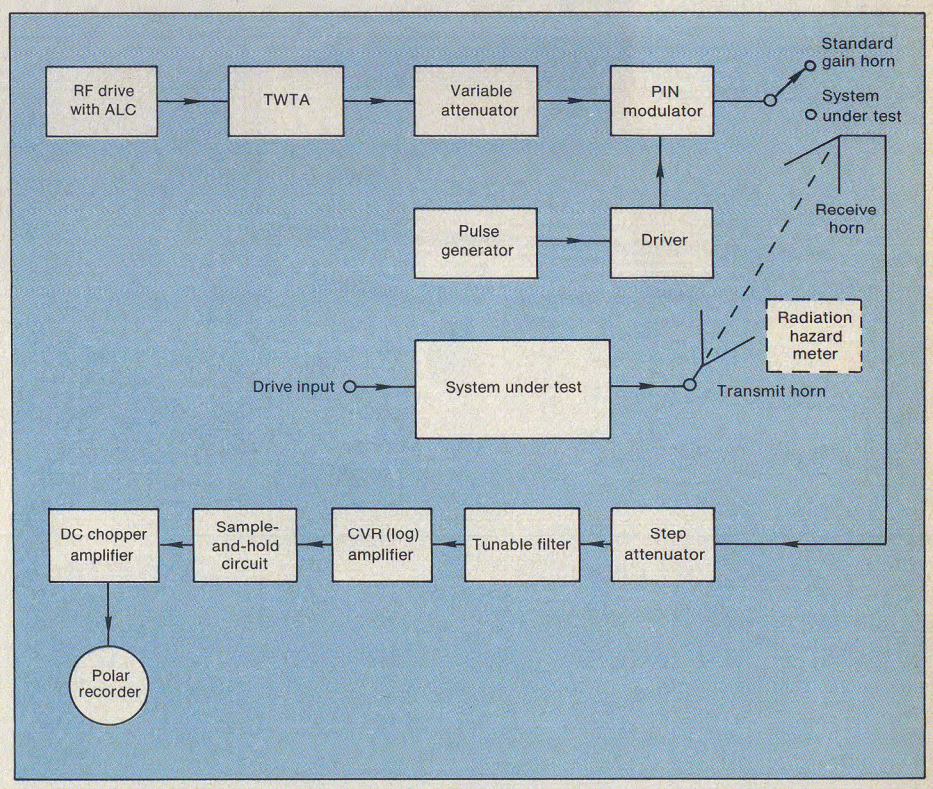
CW transmitters with high effective radiated power can be safely tested with a technique that uses pulse modulation. The pulse modulation reduces the duty cycle of the transmitter so that the *average* power presents no hazard to personnel. (Of course, exposure to high peak power from pulsed radar systems must also be avoided, but the method presented in this article pertains to modulated CW systems only.)

In principle, the measurements are made by gating the transmitter on for short time intervals. For example, if the on/off times follow a 50/50 ratio, the average power would drop to 50 percent of the CW level. Following the same logic, an on/off ratio of 1/100 would reduce the average power to 1 percent of the CW level. As the table shows, the safe approach distance decreases as the duty cycle (and therefore, the average power) diminishes.

Figure 1 shows a block diagram of the test setup used in this procedure. The measurement begins with the establishment of a calibrated signal level using a standard gain horn. The power to be delivered to the horn is measured by a power meter with the system in its CW mode and the PIN

Safe distance from a CW transmitter

Average power (kW)	Safe distance (ft.)
1.0	9.2
10.0	29.0
100.0	91.7
1000.0	289.9



1. Effective radiated power can be safely measured with this test setup. The standard gain horn sets the calibration level.

George J. Monser, Principal Engineer, Antenna and Microwave Dept., Electromagnetic Systems Div., Raytheon Co., Goleta, CA 93017.

modulator off, but still in line. The PIN modulator is then energized at a noncritical duty cycle of approximately three percent.

At the receiving end of the system, the pick-up horn delivers power to the crystal-video-receiver (CVR) detector through a tuned-filter path; pulse detection occurs in the CVR. The sampling gate of the CVR is positioned within the detected pulse window, and a sample of the pulse amplitude is stored. This sampled voltage level enters the chopper-stabilized recorder amplifier (for subsequent recording), and becomes the reference level.

The same measurement procedure is followed with the PIN modulator output connected to the input of the system under test (SUT). The recorded values for both cases are entered on the CVR transfer curve (Fig. 2), and the corresponding power levels are read in dB. For initial differences greater than 20 dB, the calibrated step attenuator ahead of the CVR detector should be reset to keep the detected signals within the 30-dB dynamic range of the CVR curve.

Array shows applications

An eight-element antenna array, of which each element is driven by its own TWT power amplifier, can illustrate the procedure. An input power level of 1 W (+30 dBm) was used to drive a 22.8-dB standard gain horn. The established calibration level corresponds to +52.8 dBm.

Following this calibration, the SUT (a TWT in this case) was energized. Since the radiated output level of the TWT was previously estimated at 20 kW (+73 dBm), an additional 10-dB attenuation was inserted to keep the signals within the dynamic range of the CVR curve.

Figure 3 indicates the test transmitter azimuthal beam pattern. The difference in the power level of beam 4 and the standard gain horn is 10.5 dB. When this figure is added to the 10-dB additional attenuation and the 52.8-dB calibrated level, a total power output of 73.3 dBm results.

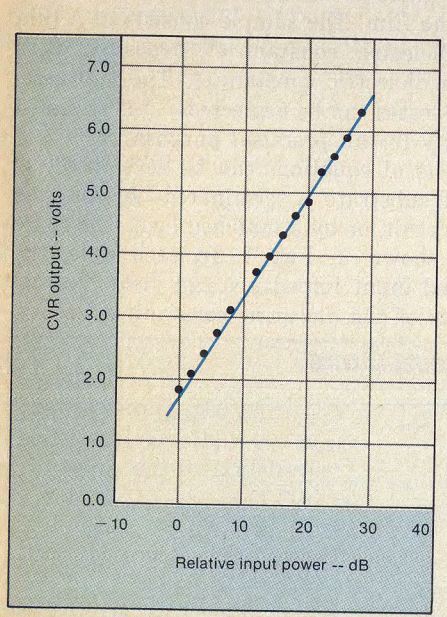
Method yields ±1 dB accuracy

A root-sum-squared (RSS) combination of the known errors produced an estimated measurement accuracy of ±1 dB. The errors which contribute to this figure are:

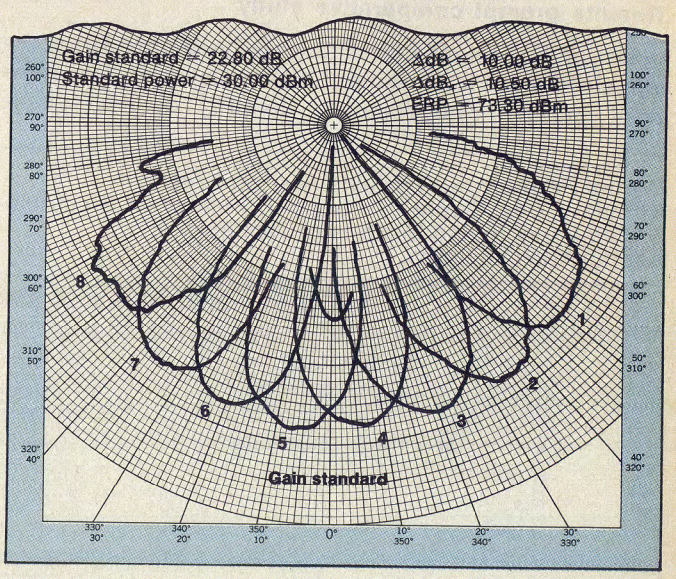
- CVR nonlinearity: ±0.25 dB
- Step attenuator accuracy: ±0.25 dB
- Drive-level adjustment: ±0.5 dB
- Standard gain horn: ±0.5 dB
- Antenna alignment: ±0.5 dB

Actual measured values taken during repeated testing of the same transmitter agreed to within 1 dB.●●

Win a cruise!
See p. 48



2. *The transfer curve of the crystal video receiver (CVR)* gives the calibration and test signal levels.



3. *A transmitter azimuthal beam pattern* verifies the test results. The eight beams of the test array are compared with the standard gain horn lobe (at 0 degrees). A 10.5-dB level difference exists between them.

Thin-Film Measurement Dispels Dielectric Doubt

A new microwave measurement technique provides a solution for finding the two components of the complex dielectric constant of thin-film materials.

THE dielectric constant of high-permittivity thin films is a complex number having real and imaginary parts. Until recently, its measurement was plagued by experimental problems at microwave frequencies. In general, most microwave measurement techniques for determining the complex dielectric constant of a bulk sample of a thin-film material are ineffective in measuring ϵ^*, the complex dielectric constant.

A new method based on measuring the input impedance of a thin film at microwave frequencies has led to the development of practical equations for calculating ϵ' and ϵ'', the real and imaginary parts, respectively, of the complex dielectric constant. The actual computations of both values can be performed simply on a programmable calculator.

Early attempts to measure the complex dielectric constant of thin film used the cavity perturbation technique.[1] The method is effective, even in the measurement of biological thin films.[2] Another of the early methods using a slab-loaded waveguide was also found to be effective.[3] However, in each of these cases, the thin-film samples were still relatively thick. As the thickness decreases, impedance methods of measuring dielectric constant falter because the imaginary impedance of a thin film becomes increasingly difficult to determine. If the film is very thin, high VSWR distorts the measurements.

Results prompt comparative study

One of the first effective microwave measurements of the complex dielectric constant of high-permittivity thin films used barium-titanium oxide ($BaTiO_3$) as the sample material.[4] But the results of the experimental work showed the ϵ' value (the real part of the complex quantity) of the sample to be much lower than that of the bulk material. Subsequent investigations determined that the low ϵ' value of the sample was caused by the formation of a surface layer on the film.

In another study, lower values of ϵ' in the sample, than in the bulk material, were observed in measurements of ferroelectric planar capacitors at microwave frequencies.[5] The same results were reported in complex dielectric constant measurements using RF techniques.[6] Because of the uncertainties regarding differing experimental methods, types of sample materials, and changes in sample composition, a comparative study was initiated, using three different measurement techniques.[7]

One is an extension of an early waveguide resonator technique.[8,9] In that method, a waveguide resonator is loaded by a double-layered sample (substrate and thin film). The resonating length of the structure gives information about the unknown dielectric constant. The input-impedance technique presented here uses the same loading method as the waveguide resonator, except that the input impedance of a double-layered sample is measured, not the resonating length.

To determine the equations for the dielectric constant of a thin film, the waveguide in Fig. 1 is loaded with a double-layered sample of the film. The sample consists of a thin film of unknown dielectric constant ϵ^*, deposited on a substrate of known dielectric constant, ϵ_s^*. The substrate is chosen so that its losses can be neglected—ϵ_s^* is assumed to be a real quantity for all practical purposes.

Three different sets of equations can be developed, depending on how the substrate is terminated—by an open circuit, by a short circuit, or by a matched load. The three configurations are shown in Fig. 1. In each case, the measured normalized input impedance can yield the real and imaginary parts of the dielectric constant, ϵ' and ϵ''.

Protap Pramanick, Graduate Assistant and
Chinmoy Das Gupta, Assistant Professor of Electrical Engineering, Indian Institute of Technology, Kanpur, 208016, India.

Table 1: Parameters of the dielectric constant equations

- ϵ^* = complex dielectric constant of the film material
- ϵ_s^* = complex dielectric constant of the substrate material
- ϵ' = $R_e\epsilon^*$
- ϵ'' = $-I_m\epsilon^*$
- ϵ_s' = $R_e\epsilon_s^*$
- t = thickness of the film, in mm
- t_s = thickness of the substrate, in mm
- f = frequency of measurement, in GHz
- C = speed of EM wave in air
- λ_o = C/f
- k_o = $2\pi/\lambda_o$ (rad/mm)
- k_c = $\frac{\pi}{a}$, cutoff wave number (rad/mm)
- β = $\sqrt{k_o^2 - k_c^2}$, guide wave number (rad/mm)
- Z_{in} = input impedance normalized by the characteristic impedance of the guide
- P_s = $\frac{\epsilon_s^* k_o^2 - k_c^2}{\beta^2}$
- K_1 = $\frac{\cot(\sqrt{P_s}\beta t_s)}{\sqrt{P_s}}$
- K_2 = $\frac{\tan(\sqrt{P_s}\beta t_s)}{\sqrt{P_s}}$

Table 1 defines all of the parameters used in the following equations:

$$\epsilon' = \frac{P'\beta^2 + k_c^2}{k_0^2} \quad (1)$$

$$\epsilon'' = \frac{P''\beta^2}{k_0^2} \quad (2)$$

In the first case, the substrate is terminated by an open circuit (Fig. 1a). The input impedance at section A-A′ is given by:

$$Z_{in} = (1/\sqrt{P^*}) \times [-j(1/\sqrt{P_s}) \cot(\sqrt{P_s}\beta t_s) + j(1/\sqrt{P^*}) \tan(\sqrt{P^*}\beta t)] \times \left[1/\sqrt{P^*} + j(-j \frac{\cot(\sqrt{P_s}\beta t_s)}{\sqrt{P_s}}) \tan(\sqrt{P^*}\beta t) \right]^{-1} \quad (3)$$

Approximating $\tan(\sqrt{P^*}\beta t)$ by $\sqrt{P^*}\beta t$, for thin films, Z_{in} becomes:

$$Z_{in} = j \left(\frac{-K_1 + \beta t}{1 + K_1 P^* \beta t} \right) \quad (4)$$

By defining the measured value of Z_{in} as $M_o e^{j\phi_o}$, Eq. 4 can be rearranged as:

$$1 + K_1 P^* \beta t = \frac{-jK_1 + j\beta t}{M_o e^{j\phi_o}} \quad (5)$$

Equating the real and imaginary parts of Eq. 5 gives:

$$P' = \frac{(\beta t - K_1) \sin\phi_o}{K_1 \beta t M_o} - \frac{1}{K_1 \beta t} \quad (6)$$

$$P'' = \frac{(K_1 - \beta t) \cos\phi_o}{K_1 \beta t M_o} \quad (7)$$

In the second case, the substrate is terminated by a short circuit (Fig. 1b). The input impedance at the section AA′ is given by:

$$Z_{in} = 1/\sqrt{P^*} \times \left[j \frac{\tan(\sqrt{P_s}\beta t_s)}{\sqrt{P_s}} + j \frac{\tan(\sqrt{P^*}\beta t)}{\sqrt{P^*}} \right] \times \left[1/\sqrt{P^*} + j \left(j \frac{\tan(\sqrt{P_s}\beta t)}{\sqrt{P_s}} \right) \tan(\sqrt{P^*}\beta t) \right]^{-1} \quad (8)$$

By approximating $\tan(\sqrt{P^*}\beta t)$ by $\sqrt{P^*}\beta t$ Z_{in} becomes:

$$Z_{in} = j \frac{K_2 + \beta t}{1 - K_2 P^* \beta t} \quad (9)$$

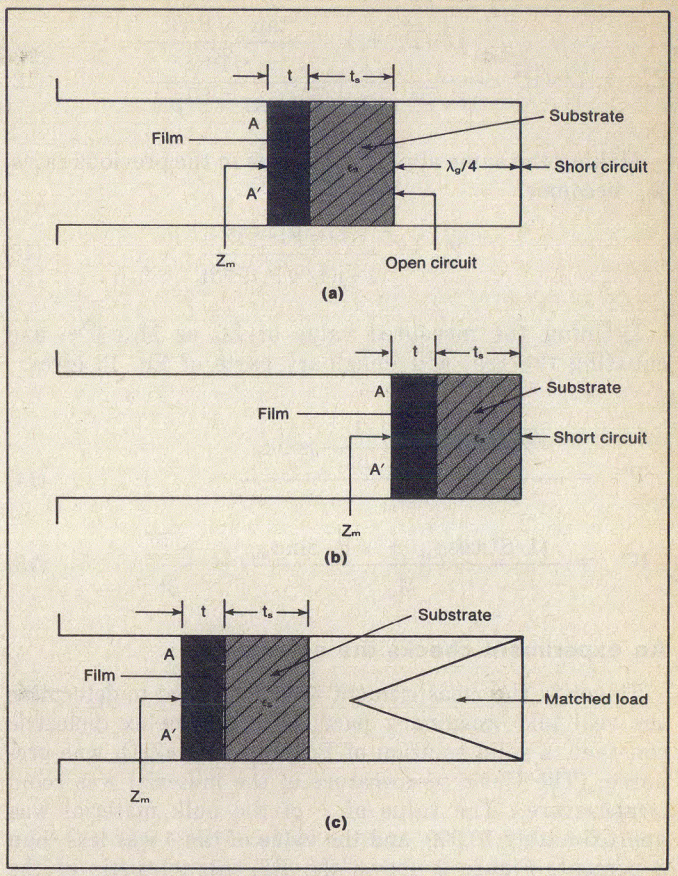
Defining the measured value of Z_{in} as $M_s e^{j\phi_s}$, and equating the real and imaginary parts of Eq. 9 gives:

$$P' = \frac{1}{K_2 \beta t} - \frac{(K_2 + \beta t) \sin\phi_s}{K_2 \beta t \, M_s} \quad (10)$$

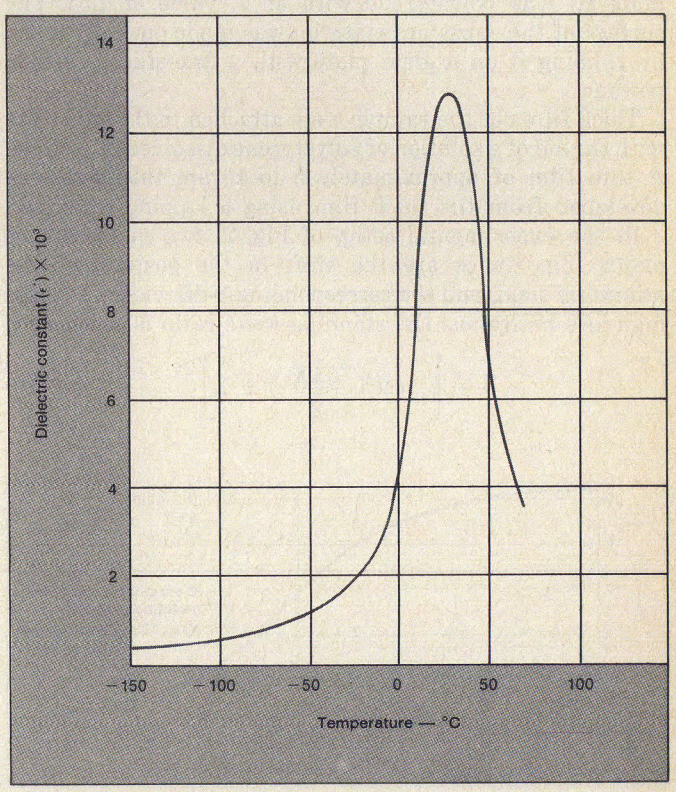
$$P'' = \frac{(K_2 + \beta t) \cos\phi_s}{K_2 \beta t M_s} \quad (11)$$

In the third case, the substrate is terminated by a matched load (Fig. 1c). The input impedance at the section A-A′ is given by:

(continued on next page)



***1. A waveguide loaded by a double-layered thin-film** sample can be terminated in one of three ways; open circuit (a), short circuit (b), and matched load (c).*



***2. The dielectric-constant versus temperature curve** of thin-film materials $BaTiO_3$ and $BaZrO_3$ shows wide variations in dielectric constant with temperature.*

$$Z_{in} = 1/\sqrt{P^*}\ \frac{1/\sqrt{P_s} + j\ \dfrac{\tan\sqrt{P^*}\beta t}{\sqrt{P^*}}}{1/\sqrt{P^*}+j(1/\sqrt{P_s})\tan\sqrt{P^*}\beta t)} \quad (12)$$

Making the same approximation as in the previous cases, Z_{in} becomes:

$$Z_{in} = \frac{1/\sqrt{P_s}+j\beta t}{1+j(1/\sqrt{P_s})P^*\beta t} \quad (13)$$

Defining the measured value of Z_{in} as $M_m e^{j\phi_m}$, and equating the real and imaginary parts of Eq. 13 gives:

$$P' = \frac{\sqrt{P_s}\cos\phi_m - (\frac{1}{\beta t})\sin\phi_m}{M_m} \quad (14)$$

$$P'' = \frac{(1/\beta t)\cos\phi_m + \sqrt{P_s}\sin\phi_m}{M_m} - \frac{\sqrt{P_s}}{\beta t}. \quad (15)$$

An experiment checks the equations

To verify the measurement technique used to determine the real and imaginary parts of the complex dielectric constant, a solid solution of $BaTiO_3$ and $BaZrO_3$ was prepared. (The Curie temperature of the material was room temperature.) The value of ϵ' of the bulk material was approximately 10,000, and the value of tan δ was less than 2 percent. Figure 2 shows the RF characteristic of the sample.

Samples were cut from 36 × 16 × 0.18 mm chips to fit exactly over the cross section of an X-band rectangular waveguide measuring 22.86 mm × 10.10 mm. The substrate material was polystyrene with an ϵ' value of 2.54. The surface of the substrate material was made optically plane by rubbing it on a glass plate with a fine silicon-carbide powder.

Thick films of the sample were attached to the substrate with the aid of a solution of polystyrene dissolved in acetone. A thin film of approximately 5 to 10 μm thickness was developed from the thick film using a lapping techique.

In the experimental setup of Fig. 2, two quantities of major importance are the shift in the position of the minimum field, and the corresponding 3-dB width, ΔX. For high-loss materials, the standing-wave ratio is given by:[10]

$$S = \left[\csc^2\left(\frac{\beta\Delta X}{2}\right) + 1\right]^{1/2} \quad (16)$$

For low-loss materials, the standing-wave ratio can be computed by $S=2/\beta\Delta X$. The input impedance (measured value) is given by:

$$Me^{j\phi} = \frac{1/S - j\tan\beta d_s}{1 - j\ 1/s\ \tan\beta d_s} \quad (17)$$

The β term can be calculated from the measurement of two adjacent node positions in the slotted section of the waveguide.

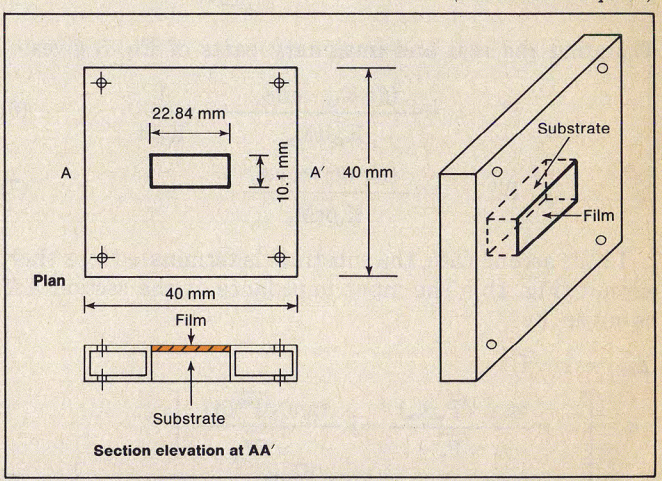
To obtain better experimental accuracy, and to simplify the working equations, the film thickness was selected to make the quantity $\sqrt{P'}\beta t$ small enough to approximate tan $\sqrt{P'}\beta t$. However, if the sample is too thin, the loss will be negligible, leading to an inaccurate measurement of the loss tangent. The sample used to test the effectiveness of the method had a dielectric constant of about 1,000. Its thickness was approximately 5 μm.

Table 2 lists the results of the experiment. Because the standing-wave ratio is so high, it cannot be measured accurately. This makes it impossible to obtain an accurate loss measurement. Thus, the experiment showed that, while it is possible to determine the value of the real part (ϵ') of the complex dielectric constant, it is not possible to determine the imaginary part (ϵ'') because of the high values of VSWR.

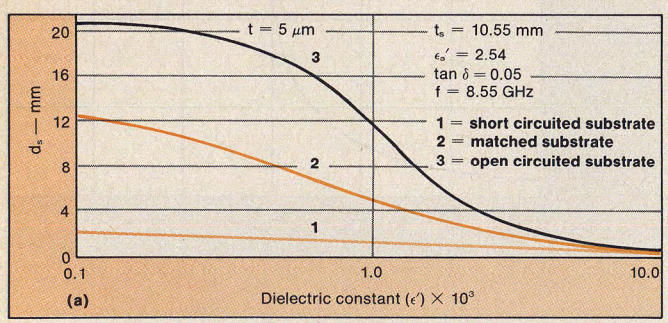
A thick film aids loss measurement

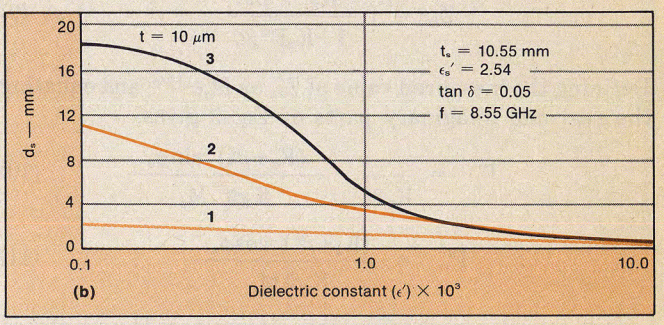
The thickness of the sample film is too small to contribute to the loss factor (the tan δ measurement), so a thicker film

(continued on p. 81)



***3. In the experimental setup for determining the dielectric constant** of a thin film, distances within the slotted waveguide can be measured to an accuracy of 0.01 mm.*





***4. When measuring thin-film dielectric constant** in the test setup of Fig. 4, the best accuracy for the real part (ϵ') is obtained with an open-circuit termination (curve 3 in both of the graphs). Graph (a) is for a sample of 5-μm thickness while graph (b) is plotted for a 10-μm sample. Both graphs are for a frequency of 8.55 GHz.*

 (continued from p. 78)

must be measured at a suitable frequency. The film must be fabricated so that the following relationships hold:

$$\tan(\sqrt{P'}\beta t) = \tan(\pi+\sqrt{P'}\beta t_e), \text{ or} \quad (18)$$

$$\sqrt{P'}\beta t = \pi + \sqrt{P'}\beta t_e, \text{ and} \quad (19)$$

$$\tan\sqrt{P'}\beta t_e = \sqrt{P'}\beta t_e \quad (20)$$

For low-loss materials, it can be shown that:

$$\sqrt{P^*} = \sqrt{P'} - j(1/2)\sqrt{P'}\tan\theta \quad (21)$$

in which:

$$\theta = \tan^{-1}\frac{P''}{P'} \quad (22)$$

$$\sqrt{P^*}\tan(\sqrt{P^*}\beta t) = (\sqrt{P'}-j(1/2)\sqrt{P'}\tan\theta) \times [\mathbf{Re}\tan(\sqrt{P^*}\beta t)+\mathbf{Im}\tan(\sqrt{P^*}\beta_t)] \quad (23)$$

$$\mathbf{Re}\tan(\sqrt{P^*}\beta t) = \frac{\sin(2\sqrt{P'}\beta t)}{\cos(2\sqrt{P'}\beta t)+\cosh(\beta t\sqrt{P'}\tan\theta)} \quad (24)$$

For low-loss materials and $\beta t\sqrt{P'}\tan\theta < 0.1$, $\cosh(\beta t\sqrt{P'}\tan\theta) \approx 1$, or:

$$\begin{aligned}\mathbf{Re}\tan(\sqrt{P^*}\beta t) &= \frac{\sin(2\sqrt{P'}\beta t)}{\cos(2\sqrt{P'}\beta t)+1}\\ &= (\sqrt{P'}\beta t)\\ &= \tan(\pi+\sqrt{P'}\beta t_e)\\ &= \tan\sqrt{P'}\beta t_e\\ &= \sqrt{P'}\beta t_e\end{aligned} \quad (25)$$

In addition:

$$\mathbf{Im}\tan(\sqrt{P^*}\beta t) = \frac{-\sinh(\sqrt{P'}\beta t\tan\theta)}{\cos(2\sqrt{P'}\beta t)+\cosh(\sqrt{P'}\beta t\tan\theta)} \quad (26)$$

Following the same type of argument, as in the derivation of Eq. 25, if follows that:

$$\mathbf{Im}\tan(\sqrt{P^*}\beta t) = -(1/2)\beta t\sqrt{P'}\tan\theta \quad (27)$$

Combining Eqs. 23, 25, and 27 gives:

$$\sqrt{P^*}\tan(\sqrt{P^*}\beta t) = P'\beta t_e - j(1/2)\beta(t+t_e)P''$$

$$= P'\beta(t-\frac{\pi}{\beta\sqrt{P'}}) - j(1/2)\beta(t+t_e)P'' \quad (28)$$

Case 1: Open-circuited substrate. Substitution of Eq. 28 into Eq. 4 yields a quadratic equation for P'. By equating the real parts:

Table 3: Experimental results, thick-film test

Sample	Type of substrate terminations	Measured ϵ' at 8.55 GHz and 25°C	Measured tanδ
A solid solution of $BaTiO_3$ and $BaZrO_3$	Short circuit (Mean of five measurements)	9889	0.026
Molecular percentage of $BaZrO_3$ is 20	Open circuit (Mean of five measurements)	9775	0.028
	Matched load (Mean of five measurements)	9870	

$$tP' - \frac{\pi}{B} - \sqrt{P'} + \frac{1}{K_1\beta}\left(1+\frac{K_1\cos\theta_o}{M_o}\right) = 0 \quad (29)$$

Once P' is known, equating the corresponding imaginary parts gives:

$$P'' = \frac{2\sin\theta_o}{M_o\beta(2t-\pi/\beta\sqrt{P'})} \quad (30)$$

Case 2: Substrate terminated by a short circuit. The equation for P' is given as:

$$tP' - \frac{\pi}{\beta}\sqrt{P'} - \frac{1}{K_2\beta}(1-\frac{K_2\cos\phi_s}{M_s}) = 0 \quad (31)$$

$$P'' = \frac{2\sin\phi_s}{M_s\beta(2t-\frac{\pi}{\beta\sqrt{P'}})} \quad (32)$$

Case 3: Substrate terminated by a matched load. The equation for P' is given as:

$$tP' - \frac{\pi}{\beta}\sqrt{P'} + \frac{\sin\phi_m}{\beta M_m} = 0, \text{ and} \quad (33)$$

$$P'' = 2\sqrt{P_s}(\frac{\cos\phi_m}{M_m\sqrt{P_s}} - 1)\left[\beta(2t-\frac{\pi}{\beta\sqrt{P'}})\right]^{-1} \quad (34)$$

(concluded on p. 84)

Table 2: Experimental results, thin-film test

Type of termination	ϵ'
Short-circuited substrate	9808
Open-circuited substrate	9754
Substrate terminated by matched load	9751 ±3

Measurement carried out at 8.55 GHz. Film is equal to 5 μm. Mean of five sets of measurements is given.

Win a cruise.

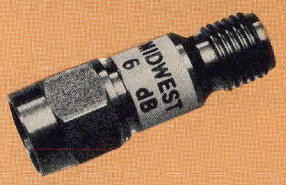
See p. 48

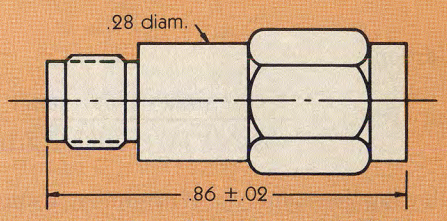
THE MINIPAD® ATTENUATOR

OUR SMALLEST, LIGHTEST, HIGH PERFORMANCE FIXED ATTENUATOR.

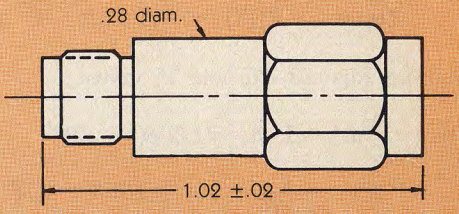
This miniature, high performance fixed attenuator has been designed to meet the needs of today's sophisticated microwave systems. The Minipad will operate within the stated specifications in most any hostile environment be it airborne, shipboard or land application. VSWR is typically less than 1.15 at 12.4 GHz and less than 1.25 at 18.0 GHz while the frequency sensitivity is normally less than 0.05 dB per GHz. The Minipad uses the Unique tube attenuator developed at Midwest Microwave. The tube attenuator is inherently a very reliable element because of its basic construction simplicity. The connectors for the Minipad attenuator are fabricated from stainless steel. The close tolerance machining plus the precise captivation techniques ensures an excellent match over the complete frequency range. All Minipads are production tested using the latest state-of-the-art swept frequency techniques. This complete testing assures that every attenuator will be within the published specifications.

- DC to 18.0 GHz
- 1 thru 30dB
- -65°C to+125°C
- 2 watts at +25°C
- MIL-E-5400 environment
- MIL-A-3933 requirements
- MIL-E-16400 environment
- 0.86 in. long × 0.28 in. diam.





1 through 12dB Weight: 5 grams (0.175 oz.)

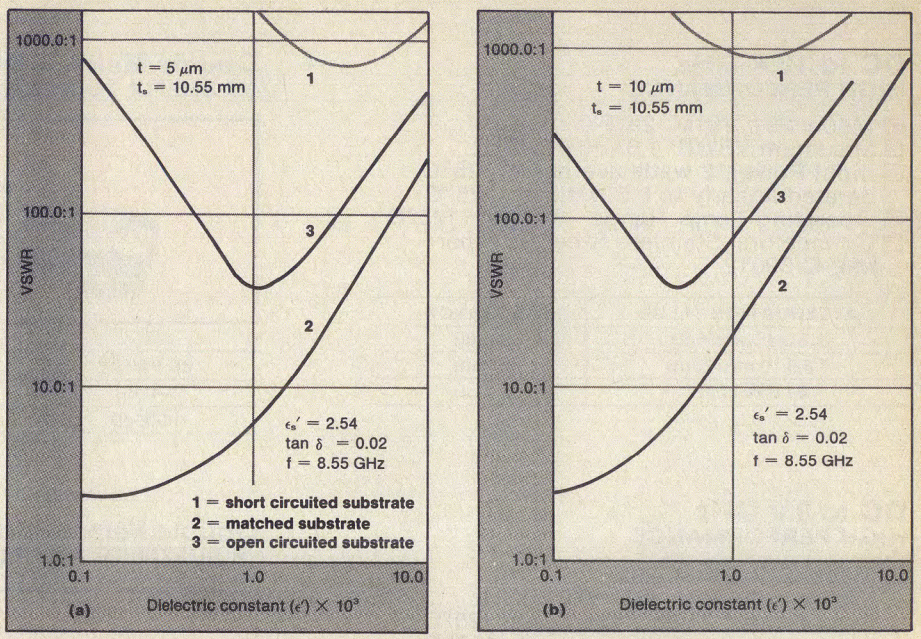


13 through 30dB Weight: 6 grams (0.212 oz.)

DC to 18.0 GHz
HIGH PERFORMANCE

- Model 290, 290M, 290F
- Maximum VSWR: 1.07 +0.015fGHz
- Input Power: 2 watts average at +25°C derated linearly to 0.5 watts at +125°C
- Operating Temp. Range: -65°C to +125°C
- Connectors: Stainless Steel SMA per MIL-C-39012

ATTENUATION VALUE	ACCURACY
1,2,3,4,5, and 6dB	±0.3dB
7,8,9,10 thru 20dB	±0.5dB
21 thru 30 dB	±1.0dB



5. The best measurement accuracy for the imaginary part *(ε″) of the dielectric constant comes in a matched-load configuration (curve 2 in both graphs). A matched load has the lowest VSWR of any of the terminations. Curve (a) shows a 5-μm sample, curve (b), a 10-μm sample.*

$$\text{for, } \beta\left(t - \frac{\pi}{\beta\sqrt{P'}}\right) \ll 1/\sqrt{P_s}$$

The experimental results of the thick-film test are shown in Table 3. Frequency measurements were made to an accuracy of 0.1 MHz using an 18-GHz Hewlett-Packard 5342A microwave frequency counter. The system excitation was an 8-to-12.4-GHz Hewlett-Packard 8690B sweep oscillator with square-wave modulation. Distances within the slotted section are measured to an accuracy of 0.01 mm.

In each measurement, the shift in the minimum distance, d_s, and the 3-dB width of the standing-wave node were fractions of a millimeter. Therefore, the influence of the slot in a slotted waveguide section (used for VSWR measurements) must be taken into account. Reflections from the slot influence the propagation constant, and distances measured with a slotted-section are larger than the actual distances. For the TE_{10} mode, the relationship between the measured wavelength, λ_{gm} and the true waveguide wavelength is given by:

$$\lambda_{gm} = \lambda_g \left(1 + \frac{W^2\lambda_g^2}{8\pi b a^3}\right) \qquad (35)$$

where: a = 22.84 mm, b = 10.10 mm, and W = 3.00 mm.

Graphing the results

Figure 3 illustrates the results of measuring a thin-film sample using three different terminations—open circuit, short circuit, and matched load. Figure 3(a) shows the results of a 5-μm thin film while Fig. 3(b) is for a 10-μm thin film. In both graphs, the curves measure the real part of the complex dielectric constant.

The graphs show that the test method is least sensitive in a short-circuit configuration (curve 1 in both graphs), and most sensitive with an open-circuit termination (curve 3 in both graphs). Sensitivity refers to the greatest slope of the d_s versus ϵ' curve. Since curve 3 is the most sensitive (greatest slope), an open circuit provides the greatest accuracy in the measurement of the complex dielectric constant.

According to Fig. 4, the best accuracy for the measurement of the imaginary part of the complex dielectric constant results with a matched load (curve 2 in Figs. 4a and 4b). This is because a matched load has the least VSWR of the three terminations. The least accuracy results with a short-circuit termination, which has the greatest VSWR. In addition, in Fig. 4(a), the slope of the log VSWR versus log ϵ'' curve for a matched termination is essentially constant from a value of $\epsilon'' = 800$ up to its greatest value on the graph. Similarly, the curve of Fig. 4(b) has a constant slope of log VSWR versus log ϵ'', except for values of ϵ'' starting at 800 and extending to the largest value.••

Acknowledgements

The authors express their gratitude to Prof. E.C. Subbarao of the Department of Materials Science of the Indian Institute of Technology for his valuable suggestions regarding preparation of the thin film. Thanks also to Dr. V. C. S. Prasad, Manager, Materials Development Laboratory, Bharat Electronics Ltd. (Bangalore, India) for supplying the film material, and to Mr. R. S. Tomar for his many helpful comments.

References

1. M.A. Rzepecka, and M.A.K. Hamid, Automatic Digital Method for Measuring the Permittivity of Thin Dielectric Films, *IEEE Transactions on Microwave Theory and Techniques*, Vol. MTT-20, pp. 30-37 (Jan. 1972).
2. H.P.S. Ahluwalia, W.M. Boerner, and M.A.K. Hamid, "Microwave Test Chamber for Measuring Relative Permittivity of Thin Films," presented at International Conference on Microelectronic Circuits and System Theory, Sydney, Australia (August 18-21, 1970).
3. Dubey and Natarajan, "Measurement of Dielectric Constant of Films by Slab-Loaded Waveguide Method, *Journal of Applied Physics* (November, 1973).
4. C. Das Gupta, "A New Microwave Method of Measuring Complex Dielectric Constant of High Permittivity Thin Films," *IEEE Trnasactions on Instrumentation and Measurement*, Vol. IM-24, No. 1 (March 1975).
5. O.G. Vendick, G.D. Loos, and L.T. Ter Matrozyan, "Planar Segnetoelectric Capacitors for Microwave Devices," *Moscow Radio Technical Electronica*, Vol. 17, pp. 2241-2243 (1972).
6. E.V. Bursian, et al., *Fiz Tverd Tela.*, Vol. 6, p. 1818, Academy of Sciences USSR (1964), translation in *Soviet J. Solid State Physics*, Plenum, New York (1964).
7. P. Pramanick and C. Das Gupta, "Comparative Microwave Measurement of Complex Dielectric Constant of High Permittivity Thin Films," *Digest of the MTT Int. Microwave Symp.* pp. 95-98, Orlando, FL 1979.
8. D.A. Roshanski *Journal of Technical Physics*, Academy of Science, USSR, No. 6, pp. 935-938 (1977).
9. E.A. Elstin, *Vestnik Moscow State University No. 1*, USSR, pp. 169-179 (1957).
10. I. Lebedev, *Microwave Engineering*, MIR Publishers (Moscow).

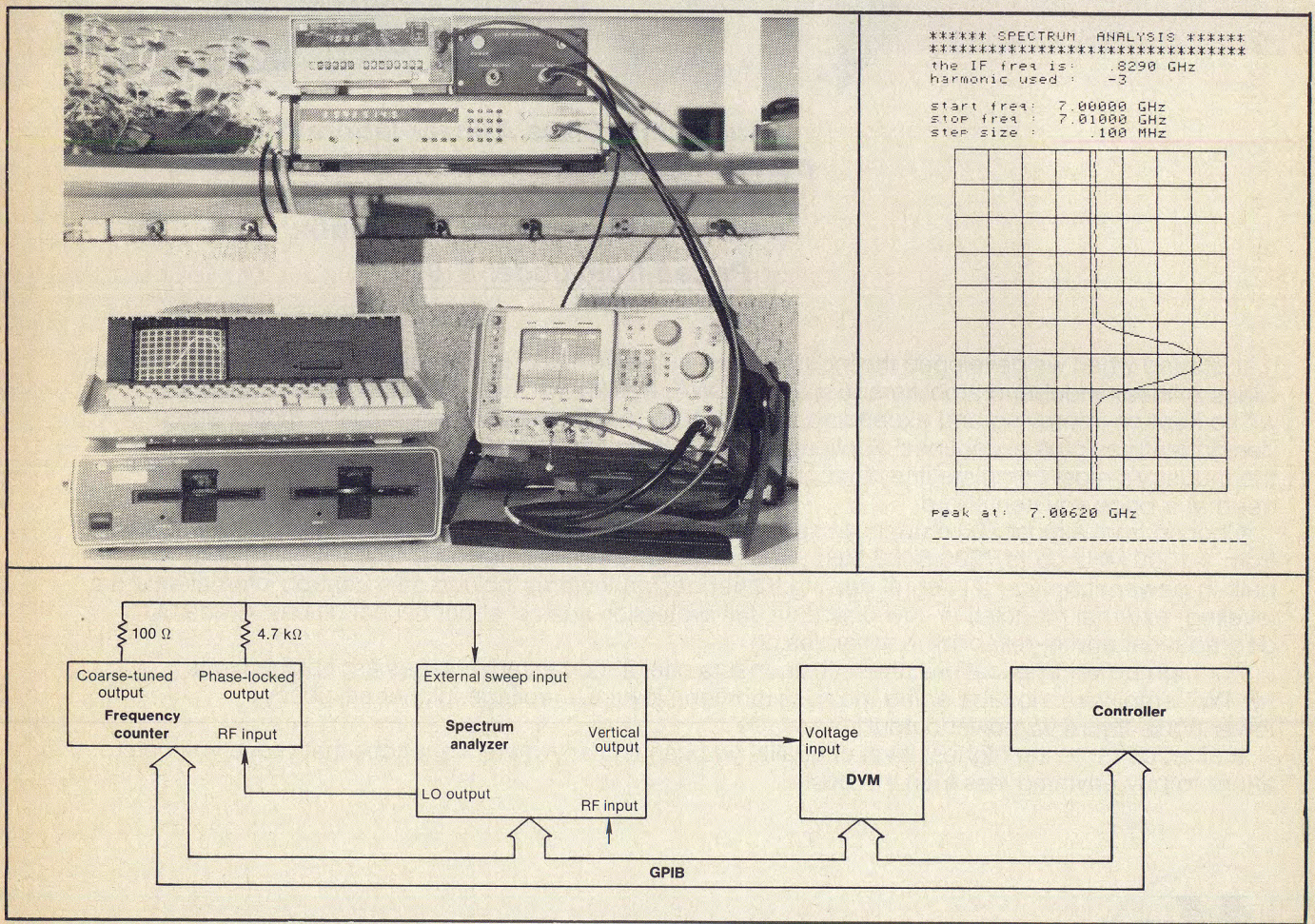
Locking Counter Aids Many Spectrum Analyzers

Stuck with a conventional, nonsynthesized spectrum analyzer? Lock it to a high-performance frequency counter for dramatically improved long-term stability, higher resolution, and GPIB scanning.

THE long-term stability of a conventional spectrum analyzer (not equipped with a synthesized local oscillator) can be dramatically improved by using a digital multimeter and a frequency counter with phase-locking capabilities. Measurements of frequency-amplitude pairs made with this test setup have an accuracy greater than the resolution of an analyzer's CRT readout.

A spectrum analyzer must meet two requirements for this application: it must have an output that allows its internal LO frequency to be sampled, and an external-sweep input port that permits the internal LO to be controlled. Most spectrum analyzers meet these criteria (particularly older models), and can be used in the configuration shown in Fig. 1. Note that if the counter and digital voltmeter (DVM) can be controlled through the general-purpose interface bus (GPIB), then the analyzer can be tuned by a computer control, even if the instrument is not equipped with a GPIB interface.

Shmuel Shalem, Test Engineer, EIP Microwave, Inc., 2731 North First St., San Jose, CA 95134.



1. The performance of a conventional analog spectrum analyzer can be improved *by locking its local oscillator to the stable reference source inside a frequency counter. Here, the EIP model 575 source-locking frequency counter teams up with a Tektronix model 492 spectrum analyzer, and Hewlett-Packard model 3438 digital voltmeter; signals are called by the HP 85F, acting as a GPIB controller.*

A desktop computer commands the GPIB network, performing needed frequency computations, instructing the counter to lock the analyzer, formatting the counter display for operator convenience, verifying a locked condition, and accumulating and processing the output of the analyzer. Data can be stored for future use, and manipulated by introducing, averaging, smoothing, normalizing, peak-hold, and peak-search functions.

The software algorithm is based on the relationship between input, local-oscillator, and IF frequencies when the analyzer is set in the external-sweep mode:

$$F_{IN} = N(F_{LO} \pm F_{IF}) \qquad (1)$$

In Eq. 1, F_{IN} is the frequency of the input signal that is being measured, and is associated with an amplitude value; F_{LO} is the frequency of the input signal that is being measured by the counter); F_{IF} is the fixed IF frequency of the counter; and N is a multiplier that depends on the frequency band of the analyzer (as does the ± sign). Inputs to the algorithm are F_{IF}, N, the ± sense, and the scanning range required (start, step, and stop frequencies).

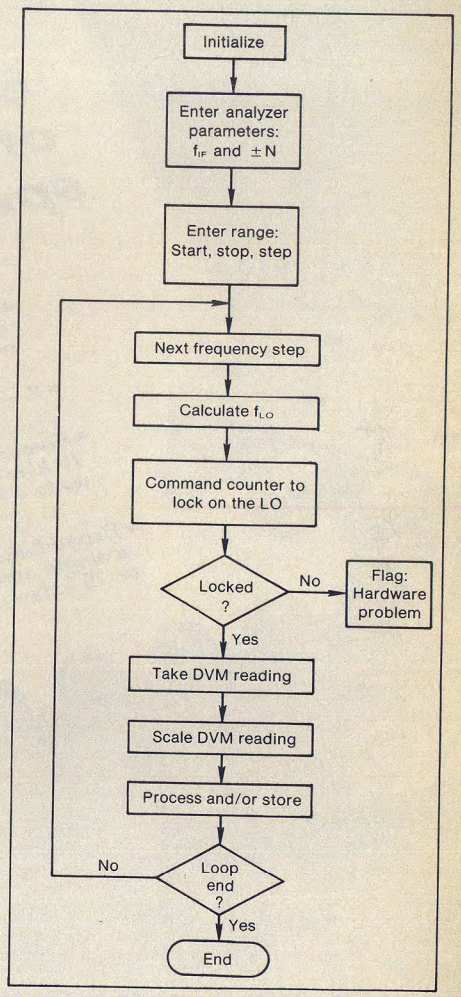
The software is written as a loop (Fig. 2), to exercise the frequency steps, and to compute F_{LO} and lock the analyzer at each step. With many analyzers, the operator's only guide to frequency is an analog indicator, which is subject to parallax and other errors. With this locking scheme, the analyzer is married to the frequency accuracy and resolution of the counter, which can be as good as $\pm 10^{-6}$ and 1 Hz, respectively.

As an enhancement, the software can instruct the counter to display the conversion to F_{IN}, using the instrument's offset and multiplier features. When the computer verifies that the counter and analyzer are locked at a specific frequency, amplitude data is extracted from the spectrum analyzer using a simple, 3 1/2-digit DVM equipped with a GPIB interface; voltage is read at the vertical-output port provided by most analyzers, scaled to dBm, and stored or processed, depending on the application.

Several important considerations must be observed when writing the software and assembling the test network:

- A time-out condition should be programmed in the "wait-for-lock" phase, in case of hardware failure or operator error.
- The execution speed of the loop must be limited intentionally, according to the specific filter being used in the analyzer.
- The tuning range of the spectrum analyzer can be checked by setting the tuning voltage of the counter to its two extremes.
- Most DVMs introduce some degree of noise averaging, often a desirable feature. However, a fast meter, such as the sample-and-hold type, should be used when averaging is not required, or when speed is of essence.
- The analyzer's attenuators and filters should be manually adjusted before measurements are made.
- The sweep of the analyzer should be set to its maximum value to allow the widest possible tuning range, unless the application dictates very close-in analysis. In the latter case, an amplifier with offset should be connected at the tuning voltage output of the counter.
- Using the EIP model 575 as the locking counter, timing cannot be faster than 200 ms/step, while step size must be at least 10 kHz.

A complete software listing for the instruments shown in Fig. 1 is available; simply send a self-addressed envelope with $0.20 postage, to: ANALYZER LOCK, Tania Tishin, *MicroWaves*, 50 Essex St., Rochelle Park, NJ 07662. ●●



***2. A simplified flowchart** points out a step-lock-read sequence. Software listing for the HP 85F is available (see text).*

Acknowledgement

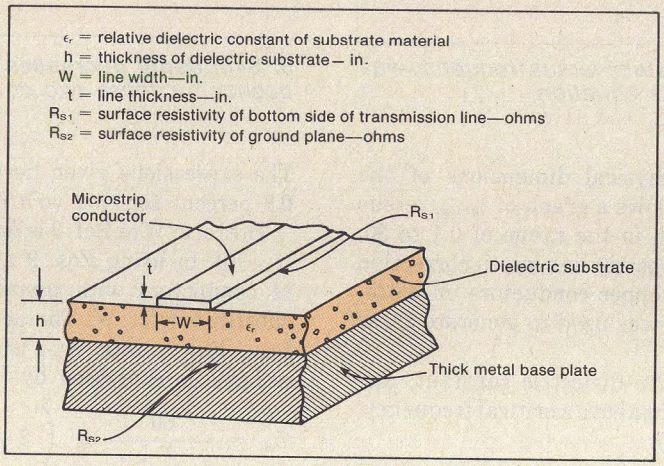
Special thanks to Andre Mathot for his conceptual inputs.

Soft Substrates Conquer Hard Designs

High-dielectric-constant, soft substrates offer improved reliability and increased design efficiency over ceramics. Learn to use them with these basic design equations.

LOW-loss, high-dielectric-constant, soft substrate materials[1] give the RF designer a way to circumvent many of the problems associated with solid ceramic or other hard substrates. This new fabrication technology offers greatly improved reliability, increased design efficiency, and reduced production costs. A designer must know, however, how the properties of these materials can affect a distributed circuit's design. The effects of conductor thickness, surface resistivities, surface finishes, dielectric constant variations, thermal stability, moisture absorption, and other characteristics become important when evaluating this new class of materials for microwave applications.

For example, thick- or thin-film gold (2.5×10^{-4} in.) usually serves as the conductor material for a ceramic substrate. For soft substrates, the conductor material is much thicker, and may not be gold. These substrates are processed like conventional printed circuit boards, and are easily machined by milling, drilling, and punching. Typically they have three layers: a copper top conductor, a middle layer of ceramic powder-filled PTFE (Teflon) resin, and a thick metallic ground plate.



1. Soft substrate materials have three layers; *the ground plane and the top conductor usually have different resistivities.*

Commercially available soft substrates are Epsilam 10 (3M Co., Minneapolis, MN), 6010 RT/Duroid (Rogers Corp., Chandler, AZ), and 810 (Keene Corp., Norwalk, CT). Most of these soft substrates use 0.25-to-2-oz. electrodeposited (ED) or rolled copper for the top conductor. A typical dielectric middle layer, with a relative dielectric constant, ϵ_r, of 10.2, is about 0.025 or 0.050 in. thick. An aluminum or copper ground plate is usually between 0.062 and 0.50 in. thick.

Although the terms microstrip and stripline are used interchangeably, the circuit topologies are not the same. Microstrip has an asymmetric geometry with an electric field that lies partially in the air above the dielectric and partially within the dielectric. As a result, the effective dielectric constant, ϵ_{eff}, is greater than the value for air $\epsilon_{eff} = 1$ and less than the value of the dielectric medium. Stripline, on the other hand, has a symmetrical or balanced configuration where the electric field lies *entirely* within the dielectric material. Thus, the effective dielectric constant is the same as the dielectric constant of the medium.

To develop a valid design approach for microstrip, the first step is a generalized conception of a microstrip conductor. In Fig. 1, the schematic shows a design where the conductor resistivity may differ from the ground-plane resistivity—a likely situation for soft substrates. Using the notation from Fig. 1, the phase velocity, v_g, of a transmission line is:

$$v_g = c(\epsilon_{eff(0)})^{-1/2} \quad (1)$$

where $\epsilon_{eff(0)}$ is the low-frequency effective relative dielectric constant, and c is the velocity of light.

Since:

$$v_g = f\lambda_g \quad (2)$$

then:

$$\lambda_g = \frac{c}{f(\epsilon_{eff(0)})^{1/2}} = \frac{2\pi}{\beta} \quad (3)$$

where:

λ_g = the wavelength in the dielectric medium,

β = the phase factor, and f = frequency, in GHz.

The low-frequency effective dielectric constant for microstrip transmission lines is given by: [2-4]

$$\epsilon_{eff(0)} = \frac{\epsilon_r+1}{2} + \frac{\epsilon_r-1}{2}\left[\left(1 + 12\frac{h}{W_{eff}}\right)^{-1/2} + 0.04\left(1 - \frac{W_{eff}}{h}\right)^2\right] \quad (w/h \leq 1) \quad (4)$$

and:

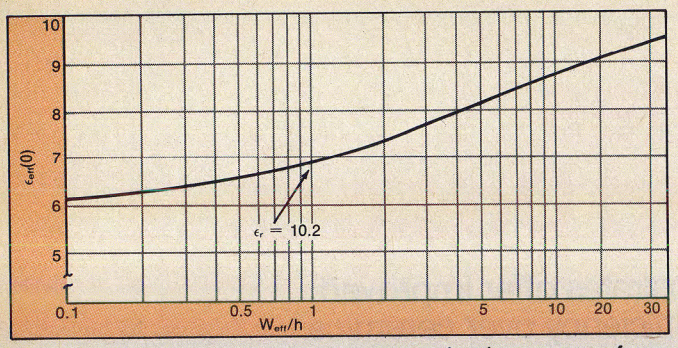
$$\epsilon_{eff(0)} = \frac{\epsilon_r+1}{2} + \frac{\epsilon_r-1}{2}\left(1 + 12\frac{h}{W_{eff}}\right)^{-1/2} \quad (w/h \geq 1) \quad (5)$$

where W_{eff} is the effective electrical conductor width, given by:

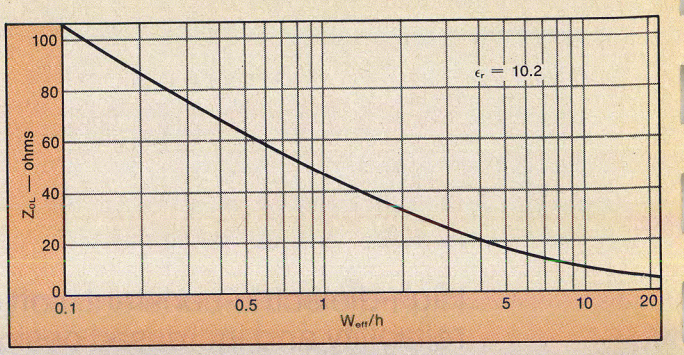
$$W_{eff} = W + \frac{t}{\pi}[1 + \ln(2h/t)] \quad (w/h \geq 1/2\pi) \quad (6)$$

(continued on next page)

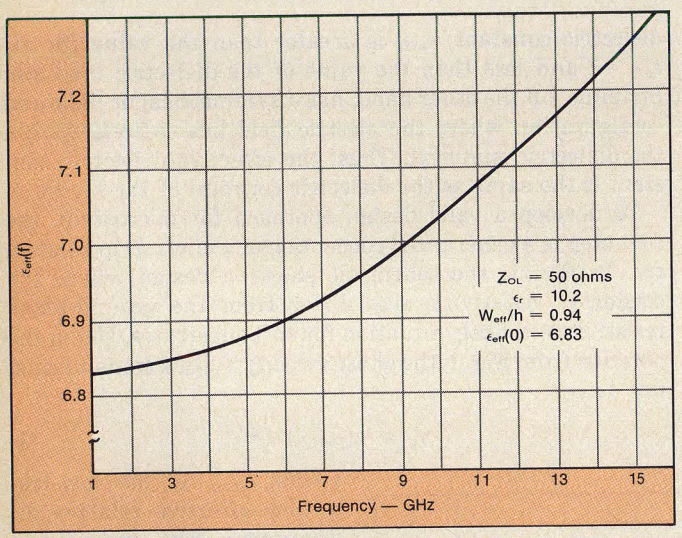
James D. Woermbke, Defense and Space Center, Systems Development Div., Westinghouse Electric Corp., Baltimore, MD 21203.



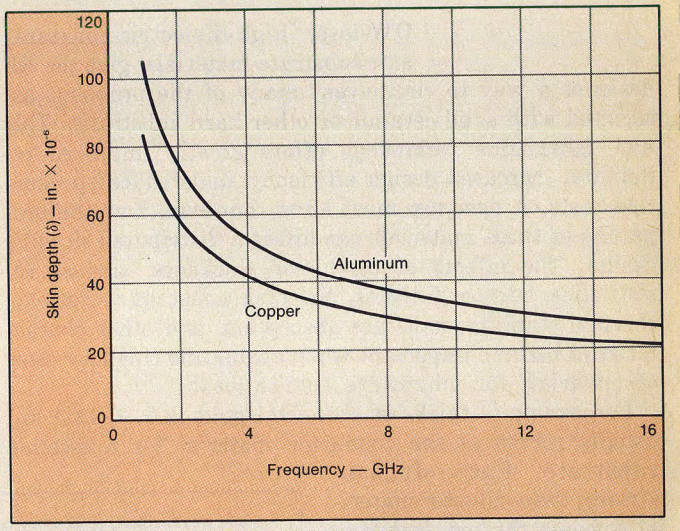
2. The effective dielectric constant *is shown as a function of the ratio of the effective conductor width/height.*



4. Low-frequency characteristic impedance, Z_{0L}, *shown as a function of* W_{eff}/h *ratio.*



3. The effective dielectric constant *versus frequency was plotted here using Getsinger's equation.*



5. Skin depth decreases *with increasing operating frequency for these two common conductor materials.*

where w, t, and h are the physical dimensions of the microstrip in Fig. 1. Figure 2 shows a graph of $\epsilon_{eff(0)}$ versus W_{eff}/h for ϵ_r = 10.2 and W_{eff}/h in the range of 0.1 to 30. Table 1 lists the calculated microstrip line width correction factors, ΔW, for 0.25-to-2-oz. copper conductors on 0.025-in. dielectric substrates. (Eq. 6 was used to generate these values).

When calculating the effective dielectric constant, dispersive effects become significant above a critical frequency, f_c, which is given by (in GHz):

$$f_c = 0.3\,[Z_{0L}/h\,(\epsilon_r - 1)^{1/2}]\ (h \text{ in cm}) \qquad (7)$$

For a 50-ohm line on 0.025-in.-thick substrate with ϵ_r = 10.2, the critical frequency is 4.83 GHz. Dispersive effects can be derived as a function of frequency[5] to show the high-frequency effective dielectric constant (Fig. 3) as:

$$\epsilon_{eff(f)} = \epsilon_r - \left[\frac{\epsilon_r - \epsilon_{eff(0)}}{1 + G\,(f/f_p)^2}\right] \qquad (8)$$

where Z_{0L} is the low-frequency characteristic impedance for $f > f_p$. In Eq. 8, $f_p = Z_{0L}/2\mu h$, and $G = 0.6 + 0.009Z_{0L}$; Z_{0L} is only valid for $f < f_p$. Also in Eq. 8, $\mu = \mu_0\,\mu_r$, $\mu_0 = 4\pi \times 10^{-9}$ H/cm, and μ_r is the relative permeability. When f is much less than f_p, the effective dielectric constant for any frequency approaches the value of the constant for zero frequency.

Closed-form expressions for Z_{0L} have been reported[3,4] in terms of w/h for the range of 0.05 to 20 and for $\epsilon_r \leq 16$. The expressions given here for Z_{0L} are accurate to within 0.8 percent for this w/h range.

The term W in Ref. 3 is for a conductor with zero thickness (t = 0). In using Eqs. 9 and 10 to account for the effects of conductors with nonzero thicknesses, W_{eff} has been substituted for W. The actual line width W can be found from Eq. 6, once W_{eff} is known. The low-frequency impedance is expressed by:

$$Z_{0L} = \frac{60}{(\epsilon_{eff(0)})^{1/2}} \ln\left(8\frac{h}{W_{eff}} + 0.25\,\frac{W_{eff}}{h}\right) \qquad (9)$$
$$(W_{eff}/h \leq 1)$$

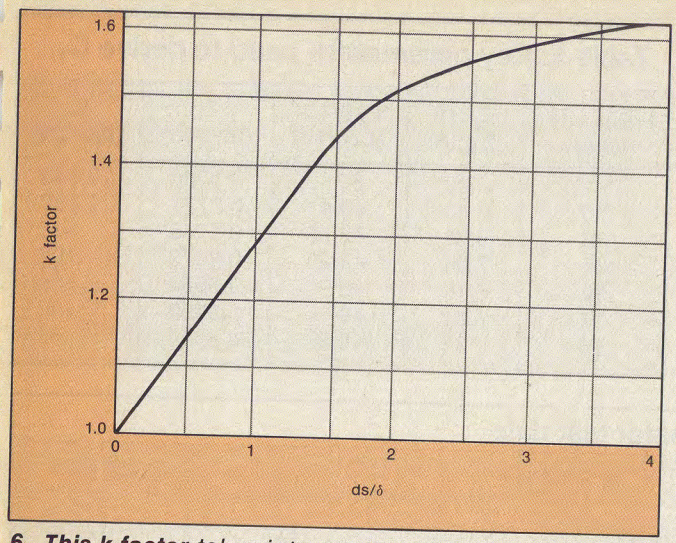
$$Z_{0L} = \frac{120\pi/(\epsilon_{eff(0)})^{1/2}}{\frac{W_{eff}}{h} + 1.393 + 0.667 \ln(W_{eff}/h + 1.444)} \qquad (10)$$
$$(W_{eff}/h \geq 1)$$

where $\epsilon_{eff(0)}$ in Eq. 9 is given by Eq. 4, and $\epsilon_{eff(0)}$ in Eq. 10 is given by Eq. 5.

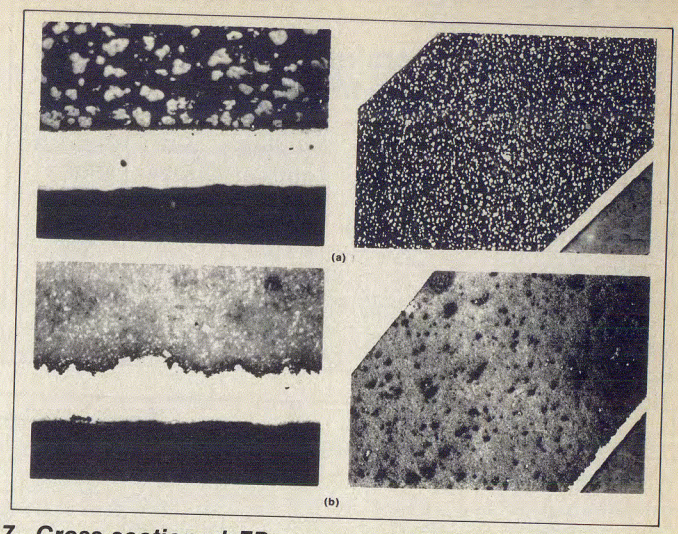
It's useful to know W_{eff}/h in terms of Z_{0L} and ϵ_r. The equations are:

$$W_{eff}/h = 8e^A/(e^{2A} - 2) \quad (W_{eff}/h \leq 2) \qquad (11)$$

$$W_{eff}/h = \frac{2}{\pi}\left\{B - 1 - \ln(2B-1) + \frac{\epsilon_r - 1}{2\epsilon_r}\right.$$



6. This k factor takes into account the effects of surface finish on surface resistivity.



7. Cross-sectioned ED copper and rolled copper conductors are compared in these photomicrographs. The photos at left are magnified 140 times, while the photos at right, used to determine surface roughness, are shown magnified 704 times.

Table 1: Calculated line-width corrections

h=0.025 in.		ΔW=W_{eff} −W
Copper weight	+ (in.)	ΔW (in.)
2 oz.	2.8×10^{-3}	3.4×10^{-3}
1 oz.	1.4×10^{-3}	2.0×10^{-3}
0.5 oz.	0.7×10^{-3}	1.2×10^{-3}
0.25 oz.	3.5×10^{-4}	0.7×10^{-3}

Table 2: Bulk resistivity (ρ), surface resistivity (R_s), and skin depth (δ) for common materials

Material	ρ(×10^{-6} Ωcm)	R_s(×10^{-2}Ω)	δ(×10^{-6} in.) (at 3GHz)
Copper	1.78	1.45	48.3
Aluminum	2.8	1.82	60.5
Gold	2.3	1.65	54.9
Silver	1.6	1.38	45.8

$$\times \left[\ln (B-1) + 0.39 - \frac{0.61}{\epsilon_r} \right] \Bigg\} \quad (W_{eff}/h \geq 2) \qquad (12)$$

where:

$$A = \frac{Z_{0L}}{60} \left(\frac{\epsilon_r+1}{2} \right)^{1/2} + \frac{\epsilon_r-1}{\epsilon_r+1}(0.23 + 0.11/\epsilon_r)$$

$$B = \frac{377\pi}{2Z_{0L}\sqrt{\epsilon_r}}$$

A graph of Z_{0L} versus W_{eff}/h for W_{eff}/h in the range 0.1 to 20 is shown in Fig. 4.

Once $\epsilon_{eff(f)}$ is known, the frequency dependence of the characteristic impedance Z_0 (f) and phase factor β(f) at a given frequency can be determined by:

$$Z_0(f) = Z_{0L}\left(\frac{\epsilon_{eff(0)}}{\epsilon_{eff(f)}} \right)^{1/2} \qquad (13)$$

$$\beta(f) = \frac{2\pi}{\lambda_g(f)} = \frac{2\pi f \sqrt{\epsilon_{eff(f)}}}{c} \qquad (14)$$

Cornering conductor losses

The unloaded quality factor, Q_u, of a microstrip line[2,6,7] is related to the total line loss α_T by:

$$Q_u = \frac{B}{2\alpha_T} = \frac{\pi}{\lambda_g \alpha_T} \quad \text{(nepers/unit length)} \qquad (15)$$

where $\beta = 2\pi/\lambda_g$.

It's possible to divide α_T into conductor loss (α_c), dielectric loss (α_d), and radiation loss (α_r). These individual losses can be related to individual Q values by Eq. 15, which can be rewritten as:

$$1/Q_u = 1/Q_c + 1/Q_d + 1/Q_r \qquad (16)$$

By substituting $\lambda_g = \lambda_0/(\epsilon_{eff(f)})^{1/2}$ into Eq. 15, this becomes:

$$\frac{1}{Q_u} = \left(\frac{\ln 10}{20} \right) \frac{\alpha_T \lambda_0}{\pi\sqrt{\epsilon_{eff(f)}}} = \frac{(\alpha_c + \alpha_d + \alpha_r)\lambda_0}{8.686\pi\sqrt{\epsilon_{eff(f)}}} \qquad (17)$$

where $\lambda_0 = c/f$ = free-space wavelength, and the individual losses are expressed in dB per unit length. By examining the three loss factors separately, it is possible to relate them to the physical characteristics of the microstrip line.

Before calculating α_c, we must know the effective resistivity of the conductor and the ground-plane material, as functions of the material and the surface finish. If the surface finish is neglected, the surface resistivity, R_s, and skin depth, δ, of the conductor are given by:[2,8]

$$R_s = \sqrt{\pi\mu f\rho})^{1/2} \text{ (ohms)} \qquad (18)$$

and

$$\delta = \left(\frac{\rho}{\pi f \mu} \right)^{1/2} = 1.981 \times 10^3 \left(\frac{\rho}{f \mu_r} \right)^{1/2} \text{(in.)} \qquad (19)$$

Depth δ is the level at which the RF currents in the

(continued on next page)

Table 3: Parameters used to plot conductor loss versus frequency in Fig. 8

Parameters	Units	Rolled copper	ED copper	Ground plane
Resistivity (ρ_1)	$\mu\Omega$-cm	1.78	1.78	—
Resistivity (ρ_2)	$\mu\Omega$-cm	—	—	2.8
Finish (ds)	in. ($\times 10^{-6}$)	7	95	10
Skin depth (δ)	in.($\times 10^{-6}$)	—	Fig. 3	—
k	—	—	Fig. 4	—

Table 5: Key parameters used to derive Q_r

Frequency (GHz)	ϵ_{eff} (f) (Eq.(8)	$Z_0(f)(\Omega)$ (Eq.(13)	P (Eq.(26)	Q_r (Eq.(25)
1	6.83	50	0.3786	19,545
3	6.85	49.9	0.3777	2,177
6	6.91	49.72	0.3746	546
10	7.04	49.26	0.3679	198
12	7.12	48.97	0.3637	138
14	7.21	48.65	0.3592	102
16	7.32	48.30	0.3544	79

Table 4: Resonator test data

Material	@ 3.3 GHz				@ 6.7 GHz
	Calculated Q_u (Eq.(17)	Measured Q_u (Eq.(40)	$\epsilon_{eff(f)}$ (Eq. (33)	ϵ_r (Eq. (34)	ϵ_r (Eq. (8)
3M standard E10-ED copper	—	165	6.6	9.8	9.9
3M low moisture E10-ED copper	155	156	6.7	10.0	10.1
Rogers 6010 rolled copper	191	181	6.8	10.2	10.3

conductor decrease to a value of 1/e relative to their surface values. As operating frequency increases, skin depth decreases. Figure 5 shows skin depth versus frequency for aluminum and copper, and Table 2 lists values for ρ, R_s, and δ for frequently used conductors.

Depending upon surface finish, there is a point where surface roughness, d_s, approaches the magnitude of skin depth. When this condition is reached, R_s increases rapidly relative to the value for a polished or smooth finish (d_s is much less than δ). The peak-to-peak value of surface roughness for ED copper is approximately 0.3t,[9] where t is the conductor thickness. Due to a smoother conductor finish, the conductor loss for 0.5-oz. copper would be less than that of 1-oz. copper.

This, of course, is an approximation of surface roughness. It neglects the true fine-grain finish characteristics (caused by the oxides and chromates on the surface of the ED copper) which are necessary in developing a good mechanical bond to the dielectric. For true accuracy, the k factor plotted in Fig. 6 versus ds/δ takes into account the effects of surface finish on surface resistivity, such that $R_s(eff) = kR_s$.

Equation 20(a) (below) gives the conductor loss, α_c, for conductor materials with equal surface resistivities; that is, $R_s = R_{s1} = R_{s2}$, where d_s is much less than δ. Surface finish effects are taken into account by substituting $R_s(eff)$ for R_s. By restricting W/h such that $\frac{1}{2}\pi < W/h \leq 2$, the expression for α_c is:

$$\alpha_c = \frac{8.68\ R_s(eff)}{2\ \pi\ Z_0\ h}\ PN\left(\frac{dB}{unit\ length}\right) \quad (20a)$$

The values of P and N are given by:

$$P = 1 - (W/4h)^2 \quad (20b)$$

$$N = 1 + \frac{h}{W} + \frac{h}{\pi W}\left(\ln\frac{2h}{t} - \frac{t}{h}\right) \quad (20c)$$

Equation 21 provides a more general expression for α_c, where the surface resistivities of the conductors are not equal (i.e., $R_{s1} \neq R_{s2}$). It accounts for the effects of a thick top conductor with a surface resistivity that differs from that of the ground plane, as well as the differing surface roughnesses of the conductor materials.

$$\alpha_c = \frac{8.686}{2\pi Z_0 h}\left\{1 - (W/4h)^2\right\}$$
$$\left\{\left[\frac{R_{s1}(eff) + R_{s2}(eff)}{2}\right]\left(1 - \frac{t}{\pi W}\right)\right.$$
$$\left. + \frac{R_{s1}(eff)h}{W}\left[1 + \frac{1}{\pi}\ln\frac{2h}{t}\right]\right\}\ (dB/unit\ length) \quad (21)$$

If the conductor quality factor, Q_c, is needed, it can be derived from:

$$Q_c = \frac{27.3\ \sqrt{\epsilon_{eff(f)}}}{\alpha_c\ \lambda_0} \quad (22)$$

Locating other losses

Once the conductor loss is known, the losses due to the dielectric and radiation remain to be found. The unloaded dielectric quality factor, Q_d, is given by:[4,6,11]

$$Q_d = 8.686\frac{\pi}{\alpha_d\lambda_g} = 27.3\frac{\sqrt{\epsilon_{eff(f)}}}{\alpha_d\lambda_0} \quad (23)$$

The dielectric loss factor, α_d, from this expression can be shown as:

$$\alpha_d = 27.3\frac{\epsilon_r}{\sqrt{\epsilon_{eff(f)}}}\frac{\epsilon_{eff(f)}-1}{\epsilon_r-1}\frac{\tan\delta}{\lambda_0}\left(\frac{dB}{unit\ length}\right) \quad (24)$$

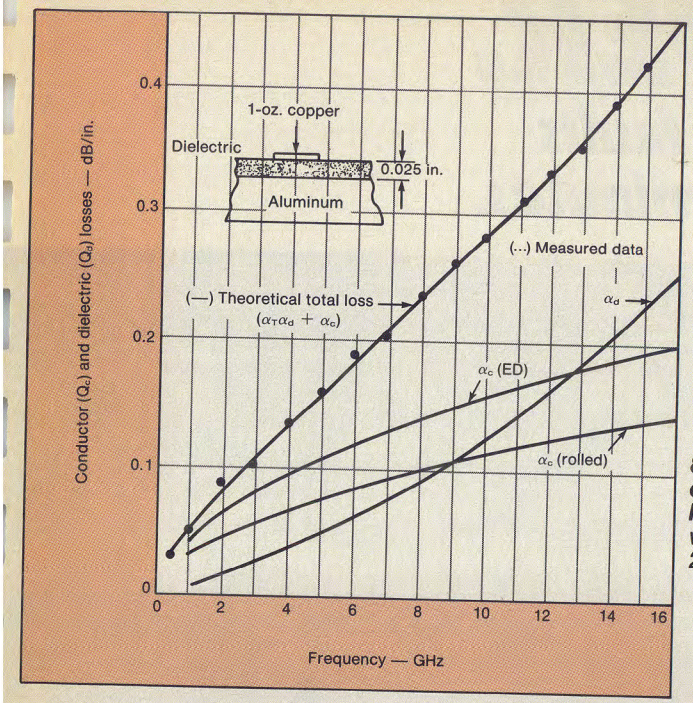
where tan δ is the loss tangent of the dielectric material.

Finally, the radiation quality factor, Q_r, can be expressed as:[7,11]

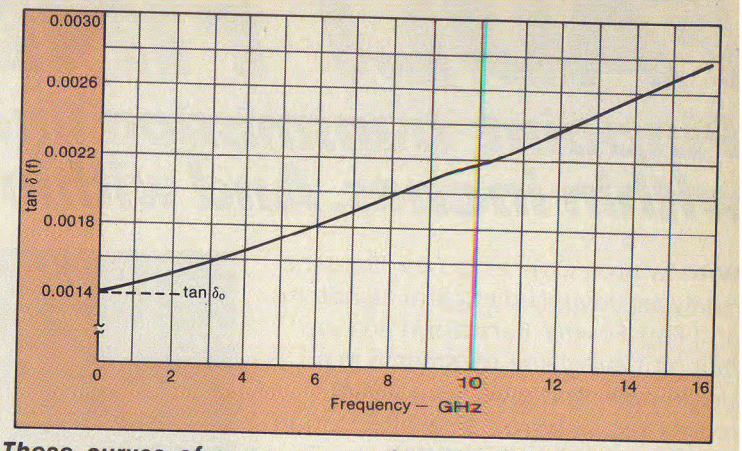
$$Q_r = \frac{Z_0(f)}{480\pi(h/\lambda_0)^2 P} \quad (25)$$

(continued on p. 94)

 (continued from p. 92)



8. These curves of conductor and dielectric losses *versus frequency were generated using Eq. 29 and Table 3.*



9. Since the loss tangent increases with rising frequency, *this curve must be used for a true evaluation of dielectric loss.*

where the value of P is:

$$P = \frac{\epsilon_{eff(f)}+1}{\epsilon_{eff(f)}} - \left\{ \frac{(\epsilon_{eff(f)}-1)^2}{2(\epsilon_{eff(f)})^{3/2}} \ln\left[\frac{\sqrt{\epsilon_{eff(f)}}+1}{\sqrt{\epsilon_{eff(f)}}-1} \right] \right\} \quad (26)$$

This loss factor is important when working with quarter- or half-wavelength resonators.

In order to calculate conductor loss, it was necessary to measure the surface roughness of the test lines. Samples of vendor materials were cross-sectioned, encapsulated, polished, and photographed, as shown in Fig. 7. The sample in Fig. 7(a) is 0.025-in.-thick dielectric clad on top with 1-oz. ED copper. The opposite surface is bonded to a 3/16-in.-thick aluminum ground plate. The 704× photo of this sample was used to determine the root-mean-square (RMS) value of surface roughness. The horizontal copper/dielectric interface line was divided into n equal segments with vertical height Y_n. The values of Y_n were then summed and averaged, so that:

$$\text{RMS (roughness)} = \left(\frac{\Sigma Y_n^2}{n} \right)^{1/2} \quad (27)$$

This equation gave a roughness value of 1.25×10^{-4} in. for ED copper and 1.0×10^{-4} in. for the aluminum base plate. Values for the 1-oz. rolled copper and the aluminum base plate in Fig. 7(b) were 7×10^{-6} and 10^{-5} in., respectively.

A simple relationship can be found for the conductor loss by substituting Eq. 18 into Eq. 20, and using the following circuit values:

Z_{0L}	= 50 ohms	ϵ_r	= 10.2
h	= 0.025 in.	W_{eff}/h	= 0.94
t	= 0.0014 in.	W	= 0.021 in.

The resulting equation gives α_c in simplified form:

$$\alpha_c \text{ (dB/in)} = 23.39k\sqrt{f\rho} \quad (28)$$

with ρ in ohm/cm and f in GHz. This relationship assumes that the top conductor and ground plane have similar finishes on similar materials. The minimum conductor loss, when k = 1, would only occur with highly polished surfaces where $d_s = 0$ (no roughness).

For the case where the conductor and ground plane are dissimilar, the relationship becomes:

$$\alpha_c = \sqrt{f}\,[\,3.25\,(k_1\sqrt{\rho_1} + k_2\sqrt{\rho_2}) + 16.9k_1\sqrt{\rho_1}\,] \quad (29)$$

where:
k_1 is the top conductor k factor,
ρ_1 is the top conductor resistivity,
k_2 is the ground-plane k factor,
ρ_2 is the ground-plane resistivity, and
f is the frequency, in GHz.

The effectiveness of Eq. 29 is shown in Fig. 8, where parameters from Table 3 were used. By using general values of bulk resistivity for the conductor materials to calculate α_c, the results are reasonably accurate for frequencies below 15 GHz. At higher frequencies, the oxides and chromates used to treat the metal surfaces modify the surface conductivity, and decrease accuracy.

It's important to understand that material selection based only on RF loss can be misleading. In Fig. 8, the total conductor loss of rolled copper/aluminum is nearly 30 percent lower than for ED copper/aluminum. This is due entirely to the differences in surface finish along the top conductor. Also, the surface finish of the ground plane introduces second-order effects on the overall conductor losses. It should be noted, however, that the physical bond of ED copper on the high ϵ_r dielectric substrate is much stronger than that for rolled copper, and this is a design feature that must also be considered.

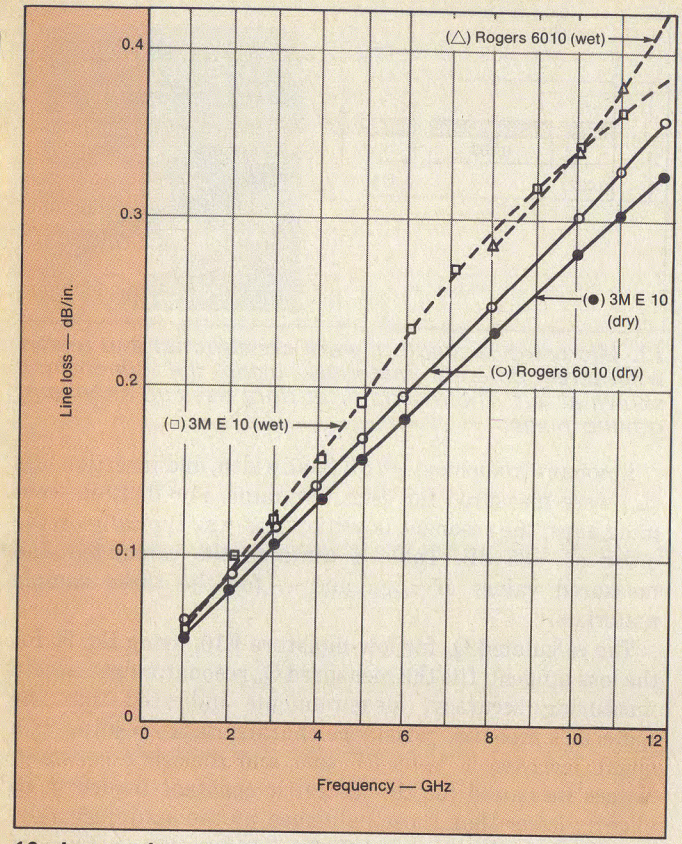
Just as a simple expression was developed for conductor loss, the same can be done for dielectric loss, by substituting $\epsilon_r = 10.2$, $\epsilon_{eff} = 6.83$, and $\lambda_0 = c/f$ into Eq. 24. What results is the following expression for 50-ohm microstrip line:

$$\alpha_d = 2.56\,f\left(\frac{\epsilon_{eff(f)}-1}{\sqrt{\epsilon_{eff(f)}}} \right) \tan\delta_0 \quad (30)$$

Unfortunately, this expression assumes that the loss tangent, tan δ_0, is constant with frequency—usually not the case with microwave dielectric materials. Because of this, a modified expression for α_d must be developed. The procedure used matched 50-ohm microstrip lines and Eq. 29 to calculate conductor loss values as functions of frequency. Since the lines were matched radiation loss could be neglected. By subtracting the conductor losses from the average total losses for these lines, what remained was a curve of dielectric loss as a function of frequency. This gives, at best, a first-order approximation that neglects second-order effects.

(continued on p. 97)

 (continued from p. 94)



***10. Losses for wet microstrip lines tend to be higher** than for dry lines, especially above 4 GHz.*

Since the calculated values of conductor loss are more accurate at low frequencies than at high frequencies, the measured value of α_d at 500 MHz was substituted into Eq. 30 to determine tan δ_0. This was calculated to be 1.1×10^{-4}. A second curve of α_d versus frequency was then generated by plugging this value into Eq. 30.

The two curves matched at 500 MHz, but diverged with increasing frequency. This divergence was attributed to the frequency effects of the loss tangent. Based on this premise, Eq. 31 was derived using curve-fitting approximations.

$$\tan \delta\,(f) = (1.2)^{f/3.4} \tan \delta_0 \qquad (31)$$

The results of this equation are shown in Fig. 9. The calculated value of tan δ (f) at 10 GHz is 1.9×10^{-4}, which is close to values measured by material manufacturers.

By substituting Eq. 31 into Eq. 30, a modified expression for α_d (dB/in) is derived:

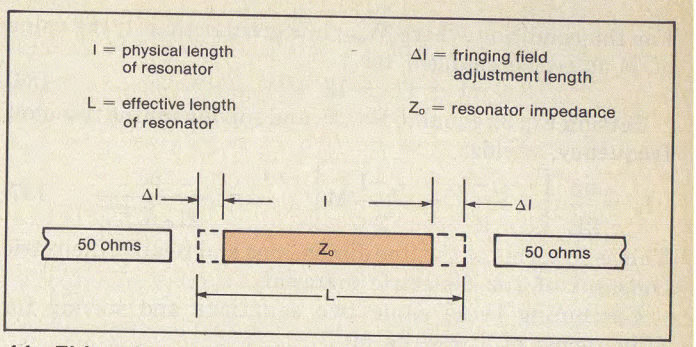
$$\alpha_d = 2.56\, f \left(\frac{\epsilon_{eff(f)} - 1}{\sqrt{\epsilon_{eff(f)}}} \right) (1.2^{f/3.4}) \tan \delta_0 \qquad (32)$$

Figure 8 includes results calculated with this equation.

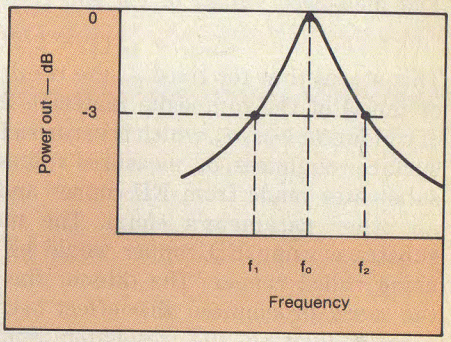
Total RF loss measurements on the 50-ohm lines were made using a long-line technique. Seven-inch-long lines were fabricated from a 0.025-in.-thick, aluminum-clad, low-moisture Epsilam 10 material. The top conductor was 1-oz. ED copper with a 3/16-in. aluminum ground plate (Fig. 7a).

After etching, the lines were vacuum-baked at 100°C for over 50 hours, prior to testing on a computerized network analyzer. Loss data was averaged at each frequency to obtain the nominal values in Fig. 8 (solid dots). In each case, the reflective and connector losses were subtracted.

The total line loss increased almost linearly from 0.03 dB/in. at 200 MHz to 0.46 dB/in. at 16 GHz. Figure 8 shows



***11. This microstrip resonator was used to collect data** on the properties of the various materials tested. The half-wavelength device has a resonant frequency which depends on its effective length, L.*



***12. The relationship of power output to frequency** provides needed information for the determination of the resonator's loaded quality factor, Q_L.*

this measured total, α_T, compared to calculated values for α_T (from Eq. 29) and α_d (from Eq. 32).

To show the effects of moisture, studies were made in a MIL SPEC 810B humidity environment. Test conditions were: ten 24-hour cycles, at a relative humidity of 95 percent, with temperature cycles from 25 to 71°C. Following removal from the thermal chamber, excess water on the surface of the test lines was carefully removed, and the lines were tested on the network analyzer. Figure 10 compares loss data in wet and dry states with previous data taken for Rogers 6010 and 3M Epsilam 10 materials.

Resonators help measurements

Microstrip resonators, such as the open-ended, half-wavelength device in Fig. 11, allow insight into the properties of a material.[12] A given length of strip will resonate at any frequency f_0 at which its effective length, $L = l + 2\Delta l$, is equal to an integral number, n, of half-wavelengths. So, at resonance, $\lambda_g = 2L/n$. By equating this with Eq. 3, it becomes:

$$\epsilon_{eff(f)} = \left(\frac{nc}{2Lf_0} \right)^2 \qquad (33)$$

Since $\epsilon_{eff(f)}$ varies with frequency, the measured value at each frequency will be unique. For the correct value of ϵ_r, the dispersive effects of $\epsilon_{eff(f)}$ must be considered.

The relative dielectric constant, ϵ_r, may be determined by solving Eq. 4 for ϵ_r in terms of $\epsilon_{eff(0)}$, as given by:

$$\epsilon_r = \frac{2\epsilon_{eff(0)} + M - 1}{M + 1} \qquad (34)$$

or:

$$\epsilon_{eff(0)} = \frac{\epsilon_r + 1}{2} + \frac{\epsilon_r - 1}{2} M \qquad (35)$$

where, for $W_{eff}/h \leq 1$:

$$M = \left[\left(1 + 12 \frac{h}{W_{eff}} \right)^{-1/2} + 0.04 \left(1 - \frac{W_{eff}}{h} \right)^2 \right]$$

(concluded on next page)

SOFT SUBSTRATES *(continued from p. 97)*

For the condition where W_{eff}/h is greater than 1, the value of M must be changed to:

$$M = (1 + 12\ h/W_{eff})^{-1/2} \quad (36)$$

Setting Eq. 33 equal to Eq. 35, and solving for the resonant frequency, yields:

$$f_o = \frac{nc}{2L}\left[\frac{\epsilon_r+1}{2} + \frac{\epsilon_r-1}{2}M\right]^{-1/2} = \frac{nc}{2L\sqrt{\epsilon_{eff(f)}}} \quad (37)$$

This is in terms of the line dimensions and relative dielectric constant of the dielectric material.

Combining these same two equations and solving for ϵ_r in terms of f_o results in:

$$\epsilon_r = \frac{(0.5\ ns/Lf_o)^2 + M - 1}{M+1} \quad (38)$$

The measured values of ϵ_{eff} and ϵ_r are related to Q by:[13]

$$\epsilon_{eff(f)} = \epsilon_r\ (1 + 1/2Q)^2 \quad (39)$$

This states that for fixed ϵ_r, the resulting ϵ_{eff} is a function of the Q of the composite material. Since Q is a function of conductor loss, α_c, which is in turn a function of conductor surface roughness, d_s, measured values of ϵ_{eff} will differ for substrates made from ED copper and rolled copper, with all other parameters equal. The measured $\epsilon_{eff(f)}$ for a substrate using ED copper would be higher than for one using rolled copper. The thinner the dielectric materials, the more pronounced this effect becomes.

In evaluating the resonator line, parasitic fringing capacitance at the open line ends can't be ignored. This capacitance is caused by the extension of electric field lines beyond the ends of the transmission lines. It makes the electrical length, L, appear longer than the physical length, l. The length correction is:

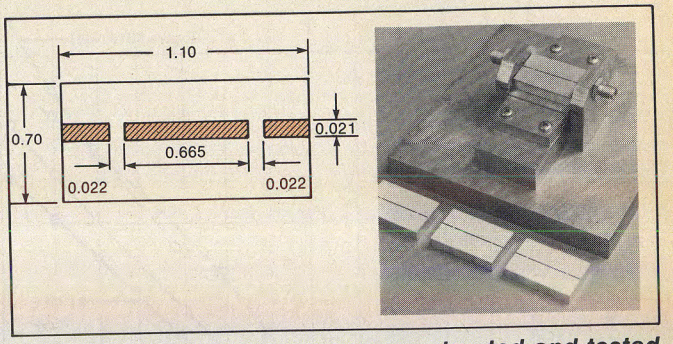
$$\Delta l = \frac{\lambda_g}{2\pi}\ \text{arccot}\left[\frac{4D + 2\ W_{eff}}{D + 2\ W_{eff}}\cot\left(\frac{2\pi D}{\lambda_g}\right)\right] \quad (40)$$

where $D = (2h/\pi)\ln 2 = 0.4413h$. The calculated Δl factor for 50-ohm microstrip lines on $\epsilon_r = 10.2$ material is approximately 0.28h. Measured data, however, indicates that this value is closer to 0.33h.[12]

The loaded quality factor, Q_L, of the resonator in a 50-ohm system can be determined by measuring the RF transmission characteristics (see Fig. 12). It's written simply as $Q_L = f_o/(f_2 - f_1)$, where the denominator is the −3 dB frequency bandwidth. The unloaded quality factor is developed from this equation and written as $Q_u = Q_L/1 - \sqrt{T})$, where T is the power insertion loss ratio of the resonator. Looking at an example, for a measured insertion loss of 30 dB, $T = 0.001$ and $Q_u = 1.030Q_L$.

Tests were run on lightly coupled 50-ohm microstrip resonators fabricated from standard 3M E10, 3M E10, and Rogers 6010 0.025-in.-thick dielectric materials. The dimensions are shown in Fig. 13 (left). In each case, the material was clad on top with 1-oz. copper and on bottom with a 3/16-in. aluminum ground plate (see Fig. 13 (right)).

It has been noted[13] that the measured values of $\epsilon_{eff(f)}$ are influenced by the width, D, of the resonator block. Therefore, it is important to clearly define test parameters. Approximately 30 test resonators were fabricated and evaluated. The final data represents an average of each grouping of information taken. Prior to testing, the resonators were vacuum-baked for a minimum of 50 hours at +100°C. Testing began immediately after removal from the thermal chamber. The spring-loaded fixture shown in Fig. 13 (right) was designed to expedite testing.



***13. Microstrip resonators were constructed and tested** with three different materials, using the dimensions shown at left. The resonator at right uses an aluminum ground plane.*

Resonant frequency, −3 dB bandwidth, and insertion loss (L_l) were measured for each resonator. For 0.022-in. coupling gaps, the resonant insertion loss was typically on the order of −35 dB. Table 4 contains the calculated and measured values of $\epsilon_{eff(f)}$ and ϵ_r for the three sample materials.

The calculated Q_u for low-moisture E10, using Eq. 30 for the loss tangent, fits the measured Q_u resonator data within measuring accuracy. Measurements indicated that the material's moisture resistance characteristics resulted in a slight increase in both RF loss and dielectric constant. Values measured for the dielectric constant tended to be slightly lower than those published by the manufacturers.

An increase in measured Q_u from 156 to 181 was brought about by switching from ED copper to rolled copper for the top conductor, a clear indication of the effect of conductor finish.

The final parameter studied for the resonators was radiation losses. Using Eq. 24, these losses were calculated, and are shown in Table 5.

Although modifications were necessary for the various microstrip transmission line-loss equations, they represent expressions which are accurate, insofar as they account for frequency effects. With them, a designer should find the road to using soft substrate materials a bit less treacherous.••

References

1. J.D. Woermbke, "Better Your MIC Designs With High-K Substrates," *MicroWaves*, Vol. 18, No. 3, pp. 66-68 (March 1979).
2. M.V. Schneider, "Microstrip Lines for Microwave Integrated Circuits," *Bell System Technical Journal*, pp. 1421-1444 (May-June 1969).
3. E.O. Hammerstad, "Equations for Microstrip Circuit Design," *Proc. European Microwave Conference*, Hamburg, Germany, pp. 268-272 (September 1975).
4. M.V. Schneider, "Dielectric Loss in Integrated Microwave Circuits," *Bell System Technical Journal*, pp. 2325-2332 (September 1969).
5. William J. Getsinger, "Microstrip Dispersion Model," *IEEE Transactions on Microwave Theory and Techniques*, Vol. MTT-21, No. 1, pp. 34-39 (January 1973).
6. Robert A. Pucel, Daniel J. Masse, and Curtis P. Hartwig, "Losses in Microstrip," *IEEE Transactions on Microwave Theory and Techniques*, pp. 342-350 (June 1968).
7. E. Belohoubek and E. Denlinger, "Loss Considerations for Microstrip Resonators," *IEEE Transactions on Microwave Theory and Techniques*, Vol. MTT-23, No. 6, pp. 522-526 (June 1975).
8. R.B. Watson, Jr., "Wide-Band Microwave Amplifier Realizations in Microstrip Employing a GaAs Schottky-Barrier Field-Effect Transistor," Cornell University, RADC-TR-76-246, Interim Report, August 1976.
9. Private discussions with I. Hutkin, Califoil, San Diego, CA.
10. R. Lending, "Surface Roughness Versus Surface Resistance at 3000 MHz," *The Microwave Engineer's Handbook*, p. 66.
11. Dr. I.J. Bahl and D.K. Trivedi, "A Designer's Guide to Microstrip Line," *MicroWaves*, Vol. 16, No. 5, pp. 174-182 (May 1977).
12. Private discussions with T. Nowicki and M. Olyphant, 3M Company, Electronic Products Division, St. Paul, MN.
13. M. Olyphant, Jr. and T. Nowicki, "Microwave Substrates Support MIC Technology," *MicroWaves*, Vol. 19, No. 12, pp. 74-80 (November 1980) and Vol. 19, No. 13, pp. 47-52 (December 1980).
14. Kurt P. Schwan, "Take the Guesswork Out of Thick Microstrip K," *MicroWaves*, Vol. 17, No. 13, pp. 184-285 (December 1977).
15. H.A. Wheeler, "Transmission Line Properties of Parallel Wide Strips by a Conformal Mapping Approximation," *IEEE Transactions on Microwave Theory and Techniques*, Vol. MTT-12, No. 5, pp. 280-288 (May 1964).
16. R.H. Jansen, "High Speed Computation of Single and Coupled MicroStrip Parameters Including Dispersion, High-Order Modes, Loss and Finite Strip Thickness," *IEEE Transactions on Microwave Theory and Techniques*, Vol. MTT-26, No. 2., pp. 75-82 (February 1978).
17. W.J. Chudobiak, O.P. Jain, and V. Makios, "Dispersion in Microstrip," *IEEE Transactions on Microwave Theory and Techniques*, pp. 783-784 (September 1971).

CALCULATOR CORNER

TI-59

MW-Oriented Program Analyzes Opamp Circuits

Opamps, formerly denizens of the lower reaches of the spectrum, have migrated to microwave applications. This program emphasizes Gunn oscillator frequency-control circuits.

OPAMPS—operational amplifiers—may be the last devices many microwave engineers expect to find in their designs. But many Gunn-diode VCO circuits (such as phase-locked-loop (PLL) acquisition sweep circuits) depend on the opamp, as do bias current supplies for step-recovery diodes, and high-gain loop amplifiers (AFC or PLL).

Figure 1 shows the most common opamp configuration used in these various control functions. The input signal is routed to the noninverting (+) input of the opamp to take advantage of the very high input impedance at this terminal.[1] The weighting resistor R_1 introduces a DC voltage to the inverting (−) input, while R_2, which returns the inverting terminal to ground, combines with R_1 to determine the noninverting (+) gain.

The program presented here analyzes this common opamp configuration, which will be shown later to take the form of a generic "summing" amplifier. Since the program can simultaneously handle 15 inputs (14 inverting and one noninverting), it can be used to study many other opamp applications as well.

Program speeds circuit analysis

Designers should welcome the ability of the program to evaluate hypothetical "what if" circuits and "worst case" situations. It allows the calculator to quickly determine the effects of variations in open-loop gain, differential input resistance, and common-mode input resistance, along with changes in R_f and R_i. And extra R_i inputs will superimpose printed-circuit board leakage resistances to different supply potentials onto the design values. The software also provides an output accumulator which allows simulated offset voltages and currents to modify the original inputs. Printer prompts assist data entry.

The equations* on p. 102 provide the basis of the program, and result in the circuit model shown in Fig. 2 (see "Definitions of terms," below).

If R_1 and R_2 in Fig. 2 are connected to a DC voltage and zero potential, respectively, the inverting (−) portion of the original configuration is a generic "summing" opamp circuit. (The summing inputs subtract from the noninverting input.) Provisions in the model account for finite open-loop gain

(continued on next page)

*Equations (1.6) and (1.7), on pages 1-16 of Reference 2, were slightly modified to accommodate more than the single R_1 input, and result in the above Eqs. (1) and (2), respectively.

Robert H. Edmonds, Consulting Engineer, 4023 Bell St., Niagara Falls, NY 14305.

Definitions of terms

The following terms and symbols are used in Eqs. 1 and 2, and for the program inputs and outputs:

Program inputs and equations

- A_{vco} — closed-loop voltage gain at DC and low frequencies. (Not an input; see program outputs below.)
- R_f — feedback resistance, in ohms.
- A_{vo} — open-loop voltage gain (often specified as "large signal voltage gain"), in V/mV × 1000. (DC and low frequencies, to opamp first pole.)
- R_{id} — opamp differential input resistance, in ohms. (Often specified as "input resistance.")
- R_{ic} — opamp common-mode input resistance, in ohms. (Not always specified. Typically, at least an order of magnitude higher than R_{id}). R_{ic} has a minimal effect and need not be entered. If entered, a new high value (e.g., 1×10^{99}) will again nullify its effect.
- R_i — R_1 to R_n, the input resistance(s) to the inverting input (−), in ohms. It is limited to 14 values R_1 through R_{14}, and must be paired with V_1 to V_n, below. (Also termed "summing resistors.")
- $V_i(-)$ — V_1 to V_n, input voltages to the inverting input resistances, in volts. Limited to 14 values which must follow associated R_i inputs. After first set of inverting output calculations, V_1 to V_n may be changed and successively entered.
- $V_i(+)$ — The input voltage to the noninverting (+) input, in volts. (Can be changed an unlimited number of times.)

Program outputs

- $A_{vco}(+)$ — The closed-loop voltage gain (noninverting, DC, and LF).
- $V_o(+)$ — The output (noninverting) in volts, paired with the above $A_{vco}(+)$ output.
- $A_{vco}(-)$ — The closed-loop voltage gain (inverting, DC, and LF).
- $V_o(-)$ — The output (inverting) in volts, paired with the above A_{vco} (−), as a result of the associated $V_i(-)$.
- ΣV_o — The summation of all V_o values (both inverting and noninverting). (Validated by superposition theorem in linear system, resulting from large amounts of negative feedback.) ΣV_o may be displayed at any time in printer mode. In manual mode, it must be displayed after the final V_o in any output calculation, to avoid interference with the completion of calculations. (Same criteria as for printer mode, which resists interruption.)••

and both differential and common-mode input resistance. The model also assumes that the opamp output impedance and common-mode voltage gain are zero.

Using the program

The program uses the normal 479.59 "turn-on" memory partition. If a printer is to be used, two magnetic cards are needed to store the program. The manual mode without the printer requires only one card.

If you anticipate using the printer, begin program storage by entering the print codes, and writing bank 3 onto card 2. After this operation, put the calculator into the **LRN** mode, and enter the program listing (available by mail, see end of article). When all of the steps have been entered, exit the LRN mode, and write banks 1 and 2 onto card 1. The program can now be entered by using the cards in any order. (For the manual mode, only card 1, which contains banks 1 and 2, is required.)

To perform a calculation, initialize the program by pressing the **E′ key.** The calculator will now accept data inputs. (For a complete guide to the operation of the software, see the procedure listed in the table.)

For convenience, scientific notation can be used to enter any input. However, to meet the printing limitations of the display, the program converts these quantities to normal notation before they are shown or printed (e.g., the number 12,100 can be entered in scientific notation as "12.1 EE 3," but appears as "12100").

The entry of "1 EE 90" will simulate an infinite input for A_{vo}, R_{id}, and R_{ic} if required. The program will also assign infinite values to these three parameters if they are not otherwise entered.

If the calculator is used in the printer mode, inputs and outputs will appear on the tape along with appropriate prompts (the prompts, inputs, and outputs are also shown in the table).

Prompts note inputs and outputs

With or without a printer, a number which corresponds to an R_i and V_i input pair will flash on the display (the flash is created by a pause mode in the program). For example, when the R_1 and V_1 values have been entered, the number "1" will flash once on the display to index each entry.

A similar indexing appears as the

(concluded on p. 123)

Equations

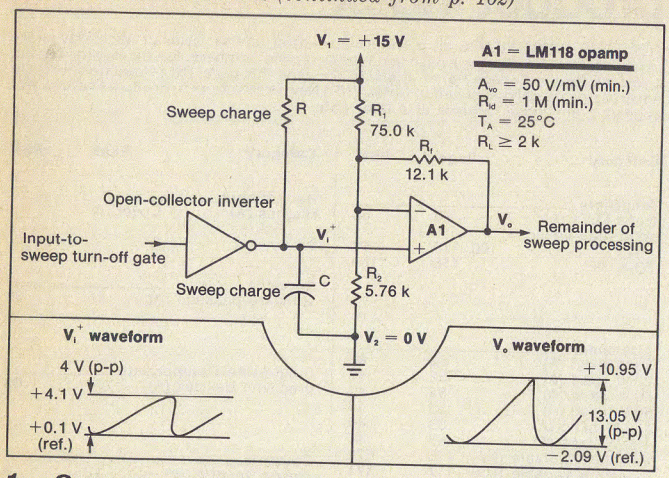
$$A_{vco}(-) = \frac{-R_f/R_i}{1 + (1/A_{vo})\,(1 + R_f/R_{ieq} + R_f/R_{id} + R_f/R_{ic})} \quad (1)$$

$$A_{vco}(+) = \frac{1 + R_f/R_{ieq}}{1 + (1/A_{vo})\,(1 + R_f/R_{ieq} + R_f/R_{id} + R_f/R_{ic})} \quad (2)$$

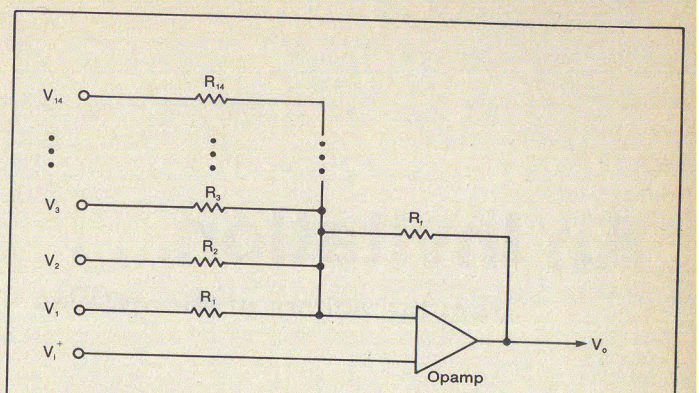
Table: Operating procedure

Printer and manual modes (enter value)	Printer prompt symbol	Press key	Printer I/O confirm symbol	Comments
		E′		Initialization. (Displayed "0".)
R_f (ohms)	⋆R F	R/S	R F	Inputs are maintained after "reinitialization."† It is then permissible to skip from any R/S input to LBL A input.
A_{vo} times R_{id} (ohms)	⋆A VO ⋆R ID	R/S R/S	A VO R ID	Scientific notation removed for all inputs.
R_{ic} (ohms)	⋆R IC	R/S	R IC	If not specified, enter high typical value for finite quantity (e.g., 1EE7), and skip thereafter. Skip input for "infinite" value.†
R_1-R_{14} (ohms, R_1-R_{14} numbers are pause displayed as man. mnemonic.)	R1-R14	A	R I	Alternate inputs with V_1-V_{14}, for first run.‡ After first run, R_1-R_{14} inputs are rejected until program has been reinitialized.† After "reinitialization," entries can skip directly to R_1, input, if desired. If an R_1-R_{14} isn't $>> R_{source}$, lump R_s into R_i value, and adjust V_1-V_{14} (V_i) value, accordingly. (R_{14} limit.)‡
V_1-V_{14} (volts; V_1-V_{14} numbers are pause displayed as man. mnemonic.)	V1-V14	B	V I−	Alternate inputs with R_1-R_{14}, even if 0.‡ After first completion of LBL D outputs, V_1-V_{14} inputs may be reentered (without V_1-R_{14}).‡ Maintain original R_1-R_{14} sequence. Use LBL E, R/S to rezero ΣV_0 (the sum of all inverting and noninverting outputs), as needed. (V_{14} limit.)‡
After the above entrees: Printer mode: Manual mode:				LBLs C, D, and E may be used in any order. LBL E must follow final V_0 of LBLs C and D, which may be used in any order. (Same criteria as printer mode. No LBL C, D interruptions.)
$V_i(+)$ (volts)	V I+	C	V I+	May be reentered as often as desired.
			AVCO	Outputs $A_{vco}(+)$.
Manual mode only		R/S	V 0	Outputs V_0 (+).
		D	n RVI−	Output (−) pair number.
			AVCO	Outputs A_{vco} (−).
Manual mode only; key R/S until all number "1" outputs have been displayed.		R/S	V 0	Outputs V_0 (−). Program must have at least one input (−) pair to yield an output. For repeat output reenter V_1-V_{14} with no "reinitialization." With "reinitialization" reenter both R_1-R_{14} and V_1-V_{14} in pairs.
		E	ΣV 0	Printer mode: Output ΣV_0 at any time. Manual mode: Only after final V_0 outputs.
		R/S		Resets ΣV_0 to zero, after any LBL E press.

†If never entered for a given calculator turn-on, will yield an "infinite" input value. After previous entries, a high value (e.g., 1EE90) will again yield an "infinite" input.
‡Rejects incorrect input or output sequence, and flashes error. Simply press **CE**, or **CLR** key, and continue in correct sequence. (**CE** key will save input.)



1. Opamps are sneaking into a growing number of microwave applications. *This common opamp configuration appears in many control functions.*



2. A circuit model, *based on equations for the inverting and noninverting closed-loop voltage gains, supports the calculator program.*

outputs for each input pair are requested. (The output is arranged in "last-in first-out" order.) The output pairs will be identified by a number that flashes twice on the display (double pause mode). Therefore, a single flash or a double flash identifies the display as either an input or an output.

The program formats the outputs in the manual mode to be identical to those in the printer mode. Every printed output will also be held on the display in the manual mode until the R/S key is depressed to start the next calculation. An instantaneous repeat of a displayed value signals the end of an output group.

You can obtain a complete program listing for this TI-59 program by sending a stamped ($0.20 US postage), self-addressed envelope to: Opamps, c/o Tania Tishin, *MicroWaves*, 50 Essex St., Rochelle Park, NJ 07662.••

References

1. G.E. Tobey, J.G. Graeme, and L.P. Huelsman, *Operational Amplifiers—Design and Applications*, McGraw-Hill Book Co., pp. 441-442 (1971).
2. D.F. Stout and M. Kaufman, *Handbook Of Operational Amplifier Circuit Design*, McGraw-Hill Book Co., pp. 1-16 (1976).
3. National Semiconductor Corp., *Linear Applications Handbook*, Application Note 29, p. 16 (1980).
4. D.F. Stout and M. Kaufman, *Handbook of Microcircuit Design and Application*, McGraw-Hill Book Co., pp. 19-14 and 19-15 (1980).

advertisers' index

Alpha Industries..... 49
Anaren Microwave Inc..... 67
ARRA..... Cover III
Astrolab, Inc..... 23
Avantek..... 35, 51
Boonton Electronics Corp..... 68
California Eastern Labs..... 36
Compact, Div. of Comsat..... 47
Daico Industries..... 38
Dynatech/UZ, Inc..... 118-119
Eaton Corp., Electronic Instrumentation Div..... 73
EIP..... 44-45
EMC Technology Inc..... 26
Engelmann Microwave Co..... 88
*Ferranti..... 106
Fluke..... 27
Ford Aerospace..... 46
Frequency Sources Semiconductor Div.. 18
Frequency Sources..... 54
Hewlett Packard Co..... 24-25, 99
Hexcel..... 64
Hughes Aircraft Co., Electron Dynamics Div..... 20, Cover IV
Hughes..... 122
Integra..... 72
Litton Industries, Electron Tube Div.. 12
Lorch..... 22
K & L Microwave Inc..... 19
M/A-Com Components..... 29
Magnum Microwaves..... 11, 13
Marconi Microwaves..... 17
Maury Microwaves..... 10
Microlab FXR..... 55
Microwave Power Devices..... 85
Microwave Distributors Co..... 116-117
Midwest Microwave, Inc..... 82-83
Microwave Control..... 66
Mini-Circuits, A Div. of Scientific Components Corp..... 1, 2, 3, 32, 33, 56, 62, 63
Motorola Inc..... 110
Narda Microwave Corp..... 7, 108
Norsal..... 58
Omni Spectra..... 43
Pacific Measurements, Inc..... 39
*Philips..... 104-105
Polarad Electronics..... 30
Precision Tube Co..... 28
Premier Microwaves..... 28
Q-Bit Corp..... 42
Raytheon Co..... Cover II
RCA..... 16
Reaction Instruments..... 21
RHG Electronics Labs, Inc..... 41
RLC Electronics..... 14
Scientific Atlantia..... 115
Systron Donner..... 93
3M Co..... 50
Tektronix..... 4-5
TRAK Microwave Corp..... 113
Transco Products, Inc..... 96
Triangle Microwave, Inc..... 79
TRW..... 103
Varian..... 95, 100
W.L. Gore..... 107
Watkins Johnson..... 16A-16FF, 80
Wavetek Indiana..... 57
Wavetek San Diego..... 111
Weinschel Engineering..... 52-53
Wiltron..... 8-9
*International Editions Only

Marketing and Advertising Staff

EAST COAST
Harry C. Dolan, District Manager
50 Essex Street
Rochelle Park, N.J. 07662
(201) 843-0550

NEW ENGLAND REP
Mitch Hall
Mitch Hall Associates
83 Nahatan St.
Norwood, MA 02062
(617) 769-4450

MID-WEST
Harry C. Dolan
200 East Ontario
Chicago, ILL 60611
(312) 337-0588

Publisher
Stacy Bearse

SALES COORDINATOR
Karen Intilli Brick
50 Essex Street
Rochelle Park, N.J. 07662
(201) 843-0550
TWX 710-990-5071

WEST COAST
Gene Roberts
MicroWaves
1307 South Mary Ave.
Suite 212
Sunnyvale, CA 94087
(408) 736-6667

TOKYO, JAPAN
Haruki Hirayama EMS, Inc.
Room 801, Shinjuku Komuro-Heim
1-22, Shinjuku 4-chome,
Shinjuku-Ku Tokyo 160, Japan
Phone: (03) 350-5666
Cable: (EMSINCPERIOD)

ABP
BPA

An Invitation. . .

from the editors of MicroWaves

Do you have a design idea that you would like to share with over 100,000 fellow engineers? We invite prospective authors to submit detailed outlines of articles related to **all** topics of interest to the microwave community.

In 1982, issues will emphasize:

January — **Test & Measurement**

February — **Semiconductor Applications**

March — **Communications**

April — **Radar Technology**

May — **Sources**

June — **Low-Noise Design**

July — **Amplifiers**

August — **Communications**

September — **Electronic Warfare**

October — **Materials**

November — **Signal Processing**

December — **Passive Components**

While we can't guarantee fortune and fame, we do pay our authors $50 per published page, and offer an international audience of microwave specialists. Send your outline to:

Stacy V. Bearse, Publisher/Editor
MicroWaves
50 Essex Street
Rochelle Park, NJ 07662

product index

FOR YOUR CONVENIENCE all products appearing in this issue of MicroWaves are categorized below with their page and reader service numbers. For more information, circle the Reader Service No. on the card opposite this page. (NL) New Literature; (A) Advertisements; (AN) Application Notes; (NP) New Products; (PF) Product Feature. Not appearing are those received at a later date.

Category	Page	RSN
Amplifiers		
GaAs FETs (A)	93	65
solid-state linear (CF)	109, 110	151
TO-8 (NP)	116	169
Attenuators		
10-W fixed (A)	52	41
25-W fixed (A)	52	42
50-W fixed (A)	52	43
50-W fixed (A)	53	44
150-W fixed (A)	53	45
150-W fixed (A)	53	46
miniature variable (NP)	116	170
miniature variable (NP)	117	171
Cables & Connectors		
coaxial connectors (NP)	117	174
right-angle OSM (A)	43	34
SMA connectors (A)	26	21
Diodes		
abrupt tuning (A)	18	14
Filters		
waveguide (NP)	118	178
YIG-tuned (A)	35	28
Materials		
Teflon substrates (A)	51	86
Mixers		
double-balanced (A)	3	88
double-balanced (NP)	116	167
miniature hermetically sealed (A)	1	2
Oscillators		
crystal (NP)	116	168
YIG-tuned (A)	82	62
Passive Components		
capacitors (NP)	116	165
90-degree power splitters (A)	33	85
parallel-plate caps (A)	36	29
phase shifter (NP)	116	166
power dividers (A)	67	55
power dividers (A)	88	64
power splitters/combiners (A)	62, 63	52
RF transformers (A)	32	84
Recruitment		
Hughes (A)	Cover. IV	
Services		
software package (A)	47	38
Solid-State Components		
precision devices (A)	100	69
Sources		
coaxial magnetron (A)	12	9
Switches		
coaxial catalog (A)	96	67
IF/RF (A)	41	33
solid state (NP)	118	179
waveguide (NP)	118	180
Systems & Subsystems		
AC regulators (NP)	117	175
D-to-A converter (NP)	118	177
driver assemblies (A)	38	30
FM demodulator (NP)	117	176
frequency converters (A)	21	17
frequency meters & attenuators (A)	50	40
mm-wave testing (A)	20	16
product catalog (A)	54	47
satellite amplifiers (A)	20	16
signal-process components (A)	2	3
spectrum analyzers (PF)	113	152
Test Equipment		
analyzer conversion (PF)	113	153
frequency counters (A)	44, 45	36, 37
frequency sweeper (A)	57	85, 86
prog. sweep generator (A)	8-9	6
signal generator (A)	17	13
signal generator (A)	68	56
spectrum analyzer (A)	73	58
spectrum analyzers (A)	4-5	4
synth. signal generator (A)	99	68
tracking sweeper controller (PF)	113	164
transmission-line analyzer (A)	40	32
Transistors		
GaAs FET (NP)	117	173
linear 5-GHz (NP)	117	172
Tubes		
TWTs (A)	Cov. II	1

Don't miss your chance to win a cruise.

The deadline for entries in *MicroWaves'* annual Top Ten contest is midnight, March 12, 1982.
(See p. 48 for details.)

laser technology
MICROWAVES
A Hayden Publication

February 1982
Vol. 21, No. 2

news

13 Researchers disclose new MIC designs for satcom applications
14 SAW oscillators: An alternative to quartz-crystal sources
14 Four-element vectored-array antenna has 1-degree beam width
17 Improvements in materials and processes advance GaAs FETS and diodes
19 Is Canada ready for her own DBS television service?
19 AEA to emphasize education and exports
20 Hawaiian fiber-optic system reaches new lengths
23 Giant antenna tracks microwaves from space
24 R&D Roundup
29 International
31 Washington
37 Industry
41 Meetings
45 For Your Personal Interest

editorial

46 In an age of technical progress the Impatt can't be forgotten

technical

SEMICONDUCTOR APPLICATIONS

49 **Automated Testing Needs Simplicity And Control.** In this month's cover feature, Part II of a two-part article, Robert Rheinlander of Motorola urges the use of available instruments to simplify the design of automated test sets needed for accuracy and economy.

55 **The Search For The Fastest Three-Terminal Device.** Edward B. Stoneham, of Hewlett-Packard, predicts that the permeable base transistor (PBT) will exhibit the most desirable high-speed performance of all the devices in the continuum between FETs and Bipolars.

67 **Improved FET Design Reaches Millimeter Waves.** John J. Berenz of TRW and G.C. Dalman and C.A. Lee of Cornell University introduce the opposed gate-source transistor, a new structure that breaks the frequency limits of conventional FETs.

77 **InP: A Promising Material For EHF Semiconductors.** James J. Gallagher, of the Georgia Institute of Technology, explains why indium phosphide may prove to be the most important semiconductor material for the range above 90 GHz.

*85 **Heterojunction Devices: Doing It With GaAlAs/GaAs.** George D. O'Clock, Jr., of Mankato State University (MN), James K. Carney of Honeywell, and L. Peter Erickson of Perkin-Elmer, warn that the blending of microwave, millimeter wave, and optic technology means system designers can no longer ignore structures such as the heterojunction.

73 **Special Feature: How to Write for MicroWaves.** The editors offer guidelines and practical tips to help you publish what you have learned in your work with microwave devices and systems.

departments

9 Feedback
28 Catalog Update
91 Product Feature
Signal generators stress simplicity of operation
92 Product Feature
Coaxial attenuators feature small price tag
93 New Products
101 New Literature
102 Application Notes
103 Advertisers' Index
104 Product Index

Domestic only

About the cover: Automated testing provides a competitive edge—when you do it right. Author Bob Rheinlander continues his two-part article on p. 49. (Cover artwork courtesy of Motorola's Semiconductor Group, Phoenix, AZ.)

coming next month: Communications

Learn how to design all-solid-state harmonic generators for 100 GHz and beyond. Witness the development of a microstrip antenna for a wideband airborne satcom terminal. Decide the winner when optics is put head-to-head with millimeter-wave technology in satellite and ground applications. And, in a special staff-written report, see how LNA technology has allowed prices to drop while quality climbs.

Publisher/Editor
Stacy V. Bearse
Managing Editor
Walter J. Bojsza
Associate Editor
Jack Browne
Western Editor
Rich Rosen, PE
6043 W. Maplewood Dr.
Littleton, CO 80123
(303) 797-2575
Contributing Editor
Steven March
Washington Editor
Paul Harris
Snyder Associates
1050 Potomac St., N.W.
Washington, DC 20007
(202) 965-3700
European Correspondent
Bill Mitchell
62 Craigwell Ave.
Aylesbury
Buckinghamshire, England
HP21 7AG
(0296) 81529
Editorial Assistant
Tania Tishin
Promotion Manager
Jamie Matusow
Art Director
Janice Moscatelli
Copy/Production Editor
Michael Kachmar
Production Manager
Nick J. Tartaglia
Circulation
B. Freundlich, Dir.
C. Stump, Sub. Mgr.
P. Greenleaf, Reader Serv.
M. Sassano, Reprints
Market Research
Irene Chervin, Mgr.
Editorial Office
50 Essex St.
Rochelle Park, NJ 07662
Phone (201) 843-0550
TWX 710-990-5071
A Hayden Publication
James S. Mulholland, Jr., President
February Press Run
43,041 copies

MICROWAVES is sent free to individuals actively engaged in microwave work. Prices for nonqualified subscribers:

	1 Yr.	2 Yr.	3 Yr.	Single Copy
US, Canada Mexico, Central America	$30	$48	$72	$3.00
All other countries	$48	$84	$120	$5.00

Additional Product Data Directory reference issues, $20.00 each, (US, Canada, Mexico, Central America). $32.00 each (all other countries). POSTMASTER, please send Form 3579 to Fulfillment Manager, MicroWaves, P.O. Box 13801, Philadelphia, PA 19101.

Back Issues of MicroWaves are available on microfilm, microfiche, 16mm or 35mm roll film. They can be ordered from Xerox University Microfilms, 300 North Zeeb Road, Ann Arbor, MI 48106. For immediate information, call (313) 761-4700.

Hayden Publishing Co., Inc., James S. Mulholland, President, printed at Brown Printing Co., Inc., Waseca, MN, Copyright® 1982 Hayden Publishing Co., Inc., all rights reserved.



Part II

Automated Testing Needs Simplicity and Control

The use of automated test sets provides greater accuracy and economy. A keep-it-simple approach using available instruments will ease the design task.

EVEN when accomplished by skilled and conscientious technicians, manual testing of RF components is affected by human error that compromises product quality. Moreover, the labor and skill costs associated with such testing are increasing at the same time specifications are tightening. While a manufacturer may discount the costs of labor and training, the penalty for any reduction in quality to the customer can be devastating.

The answer to this problem lies in automated testing. Part I of this article (*MicroWaves*, January 1982, p. 59) described the development of two single insertion final test (SIFT) systems. The lessons learned in the development of those systems—and the two systems described in this article—will be valuable to anyone designing an automated test set.

Stick to the basics

An objective, "no-frills" approach to the design of automated test sets minimizes the capital cost and reduces the burden on local resources. In addition, although it compromises speed and memory efficiency, the use of a "standard" interpretive language instead of machine language eases the development of the required software and increases its flexibility.

But perhaps the most important design philosophy should be the maximum use of off-the-shelf components. Although we found no turn-key systems that sufficiently filled our needs, we decided that the cost of a unique design would be prohibitive. A survey of the instruments and interfaces available indicated that, with cautious selection, a "bolt-together" approach would provide a nearly optimum system. In addition, we would retain control of the software and avoid the considerable documentation expenses associated with hardware design.

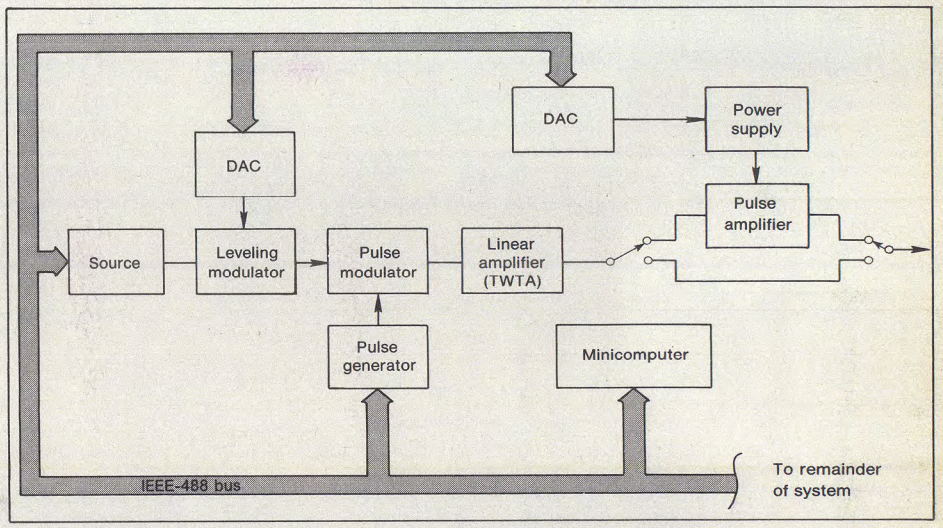
Diagnostic operations, the expensive part of maintenance, are built into the software as the operating programs are written. Thus, local control of software (made easier by the use of an interpretive language) is essential to maintain maximum flexibility.

All four systems described in these two articles incorporate desk-top minicomputers and off-the-shelf instruments compatible with the IEEE-488 bus.

The two SIFT systems discussed previously—SIFT Type I and SIFT Type II—involved CW testing with no more than simple, symmetrical modulation schemes. Pulsed RF-power measurements, especially at duty cycles of less than 10 percent, involve very different device technology and measurement technology.

The gain and output power capabilities of a pulse device usually are stated in terms of peak power under specific timing conditions. This peak power is commonly derived from the output of a high-speed detector as a video pulse, and the amplitude of that pulse must be calibrated in terms of its relationship to the RF power applied to the diode. Our experience has shown that this calibration is more difficult to define and maintain than the calibration for thermal sensing. Thus, although thermal constraints for a given power level are greatly reduced, the timing aspect of peak-power measurement introduces a whole new

(continued on p. 52)



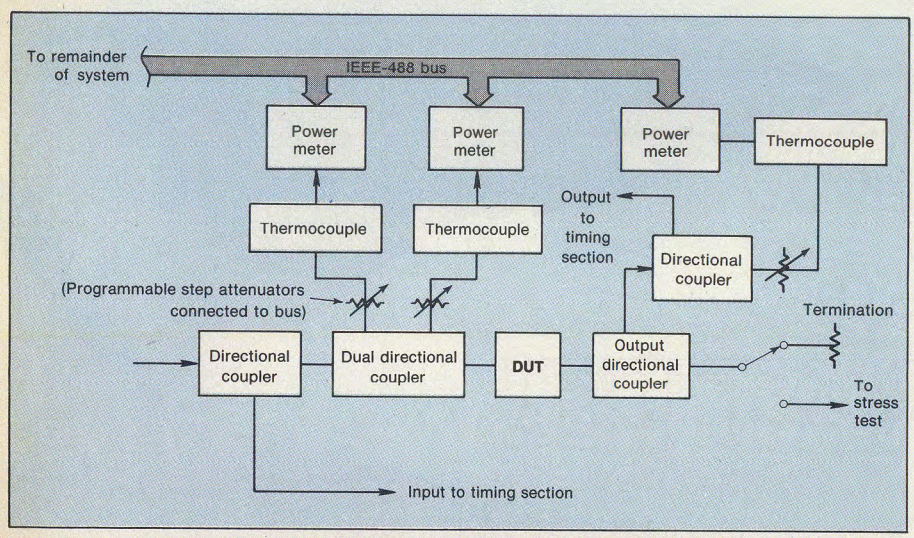
***1. The signal source for the pulse-power test set** uses a microwave generator with tuning and coarse-level setting performed through a minicomputer. The pulse-amplifier power supply is set to keep the amp near saturation.*

Robert Rheinlander, Principal Staff Engineer, High Frequency and Optical Products Div., Discrete Semiconductor Group, Motorola, Inc., 5005 E. McDowell Rd., Phoenix, AZ 85008.

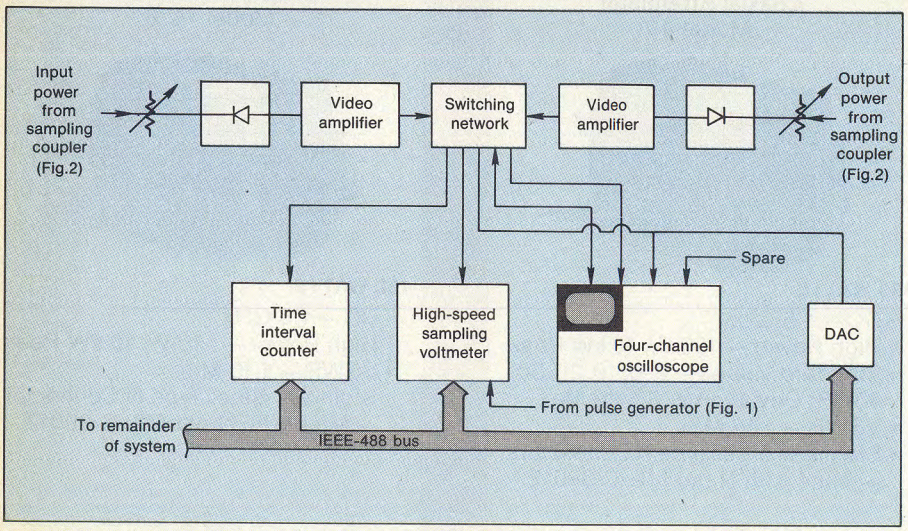
set of variables in addition to those experienced during CW testing.

Modern thermistors and thermocouplers provide reliable, long-term outputs without variations imposed by wave shape (particularly where complex modulation schemes are involved). Therefore, the use of a thermal-sensing element reduces the number of variables. Of course, the thermal-sensing method measures average power—but it is true average power, from which peak power may be calculated. We need only tie the system together through a minicomputer to combine several measurement methods, and accommodate the calculations and corrections required.

The signal source for our pulse-power test set, SIFT Type III, is shown in simplified form in Fig. 1. A microwave frequency synthesizer generates the signal, with the desired frequency and a coarse-level setting fed to the synthesizer through the bus from the minicomputer. The coarse-level setting also requires an adjustment to the output of the pulse-amplifier power supply to keep the pulse amplifier near saturation. Fine-level setting and level maintenance is accomplished by means of the leveling modulator. The modulator's digital/analog converter actually is not a separate unit as shown, but is one of several DACs included in the "smart hardware system" lined to the bus through a single connection. This DAC is fed by computer-corrected data from the input power meter. Leveling may be performed in either CW or pulse mode (CW operation locks out the pulse amplifer).



***2. The pulse-power test set measures input, reflected, and output power** as average power. The data is sent over the bus, along with duty-cycle information, to the minicomputer, where mean peak power is calculated.*



***3. The timing and video section** of the pulse-power test set currently includes a sampling voltmeter used to derive pulse amplitude and slope. This data may be used to compute peak power.*

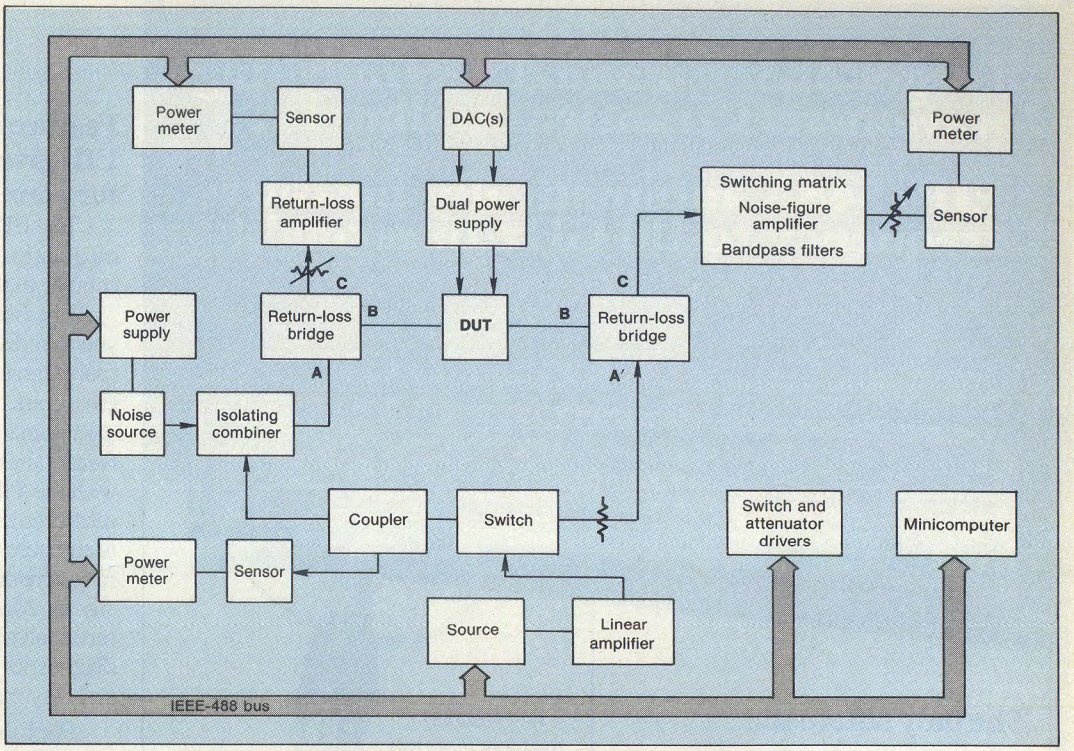
Figure 2 shows the basic RF-power measurement scheme for SIFT Type III. The only difference between it and the scheme for the CW SIFT systems is the addition of sampling couplers for the inputs to the timing and video section. These couplers are maximally flat (−10-dB) units. The dynamic range required for high-duty-cycle or CW measurement is provided by using programmable attenuators, which are diagrammed in the figures as simple variable attenuators. Input, reflected, and output power are all measured as average power, and the data is selectively sent over the bus to be corrected by the minicomputer for attenuator and coupler variations.

SIFT III's timing and video section (Fig. 3) includes a high-resolution (500-MHz clock) time-interval counter. All duty-cycle information is derived from this unit, fed over the bus, and used to compute mean peak power. The detectors are heavily buffered with high-speed operational amplifiers that drive a 50-ohm video system, which is fully terminated to minimize ringing or other pulse distortion. The sampling voltmeter currently being used in SIFT III is capable of measuring in 2-μs windows, and is primarily used to derive pulse slope. This data also may be used to compute absolute peak power and compare it to the mean.

The detected power pulses from both the input and output are fed to a four-channel oscilloscope, where they can be compared to a reference trace generated in the video-reference DAC. The DAC's output, which is sent through the bus and read through the sampling voltmeter, can be matched to a desired pulse-voltage output, or to the output of either detector operated in the CW mode. The oscilloscope is intended only for set-up and engineering use, since the entire SIFT-system concept focuses on process control and, therefore, the elimination of judgmental readings.

Linear and low-power tests

A comparison of the SIFT Type III (a test set of pulse-power devices) and the two previously described systems (test sets for CW testing) shows minimal basic differences. In fact, much of the equipment is interchangeable, as are the methods of programming and operation. We are now using the same basic approach, instruments, and skills, to develop SIFT Type IV, an automated test set



4. An extension of the pulse-power test set is SIFT IV, *which can test both discrete and modular products designed for low-power operation. It uses the basic software subroutines and hardware already developed.*

for both discrete and modular RF products designed for low-power operation. Although SIFT Type IV was not fully developed at this writing, it is merely a combination of techniques and subsystems already used successfully in automated test systems.

This latest SIFT system is diagrammed in Fig. 4. As you can see, the system uses not only the same basic hardware, but also most of the software subroutines already developed. To the basic gain, return-loss, and efficiency measurements, we have added output-return-loss and noise-figure measurements.

The principal difference between the basic measurement components is the addition of two return-loss bridges. Port C of the input bridge is terminated in the characteristic impedance, and power applied at port A is reduced by 6 to 7 dB at port B. Reflected power from port B arrives at port C attenuated by another 6 to 7 dB. At the output bridge, power applied at port B′, the TEST port, is terminated at port A′ in the nominal characteristic impedance, and arrives attenuated by 6 to 7 dB at port C′ (in a fashion similar to a directional coupler). Thus, good return-loss bridges may be used as dual-directional couplers with 6- to 7-dB tap losses. (This scheme was used in the DTS-I test set and in a preceding manually swept system, both of which were described in the previous article.) Suitable taps at A and A′ could convert this scalar measurement system into a vector analysis system. (Indeed, this was done with one of the SIFT Type I systems. We used an old vector voltmeter, which was manually programmed but read through an A-to-D converter on the bus.)

To test 75-ohm components, the B or TEST ports need only be converted to 75 ohms, and the A and C ports to 50 ohms. Wideband Engineering (Phoenix, AZ) has built return-loss bridges for us in the 1-to-500-MHz range having 50 ohms impedance at A and C and 75 ohms at B. Wiltron (Mountain View, CA) furnishes 50-75-ohm converters for use at ports A and C on the company's 75-ohm bridges.

In order to determine the noise figure of the device under test, the noise output of the device must be measured under identical "hot" and "cold" conditions for both the source and the output. The difference between the cold and hot conditions must be known to very close tolerances. This measurement is the excess noise ratio (ENR) of the noise source. Once it has been established, the relative output readings in a predetermined frequency realm can be made. These readings are analyzed by the minicomputer to establish the noise figure for the device. Since we tend to stretch the dynamic range capabilities of the power meter by using this method, the gain and level conditions must be carefully controlled. Still, this system has proven successful on DTS-I and DTS-II.

The SIFT Type IV system described above will be made effective at frequencies up to 18 GHz by the selection of suitable components. The source may be any frequency synthesizer compatible with the IEEE-488 bus. The source amplifier should provide a 2-to-3-W linear output; wideband solid-state units can be used as well as TWTAs. Return-loss bridges are available in ranges of 1 MHz to 2 GHz, and 2 GHz to 18 GHz. The biggest problem with the noise source is the establishment of the ENR.

As noted, the SIFT Type IV system was still under development at this writing, but since it employs proven techniques and subsystems, no significant problems are anticipated. Therefore, four types of SIFT systems have already evolved from off-the-shelf components used in a basic building-block concept. We have succeeded in interchanging both hardware and software without compromising flexibility.••

The Search For The Fastest Three-Terminal Device

A continuum of device configurations exists between FETs and Bipolars. One such device—the permeable base transistor (PBT)—is predicted to exhibit desirable high-speed performance.

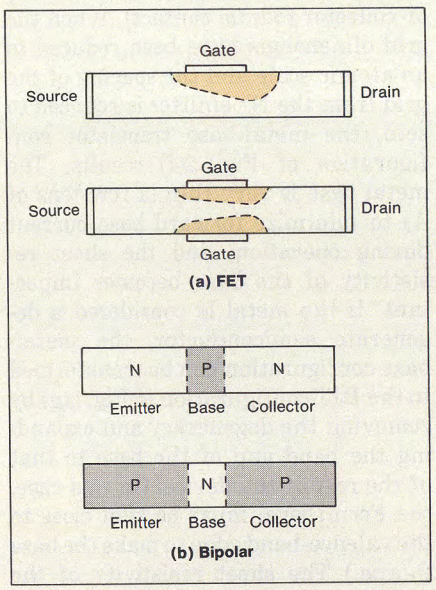
MOST people involved with semiconductor device research and development are familiar with two basic three-terminal device configurations: the *field effect transistor* (FET) and the *bipolar junction transistor* (BJT) (see Fig. 1). The FET represents a class of devices (including MOSFETs, MESFETs, and JFETs) which operate on a principle substantially different from that of the class of devices represented by the BJT (and including the metal base transistor). Some newer and less familiar devices, such as the *static induction transistor*[1,2] (SIT) and the *permeable base transistor*[3] (PBT) are often treated conceptually as special types of FETs or BJTs but appear to lie somewhere between the two classifications. We must consider, therefore, that FETs and BJTs are not totally unrelated devices, but are more appropriately viewed as *extremes* in a continuum of device configurations.

The purpose of this work is to explore the continuum of three-terminal device configurations between the FET and the BJT to find the best possible configuration for high-speed operation while uncovering a common basis for comparing the high-speed performance capabilities for all these devices.

FET to BJT via PBT

A reasonable approach to finding the most promising high-speed configuration can begin with the fastest three-terminal devices now available. This configuration can be changed one step at a time in a direction that should theoretically result in improved speed. When this process produces a configuration which cannot be further improved, it is helpful to continue gradual alterations until a BJT structure is attained. In this way, the relationships between the BJT, the FET, and the fastest device can be observed.

Edward B. Stoneham, Project Manager, Santa Rosa Technology Center, Hewlett-Packard Co., 1400 Fountain Grove Pky., Santa Rosa, CA 95404.



1. The field effect transistor, FET (a), and the bipolar junction transistor, BJT (b), *can be viewed as extremes in a continuum of device configurations.*

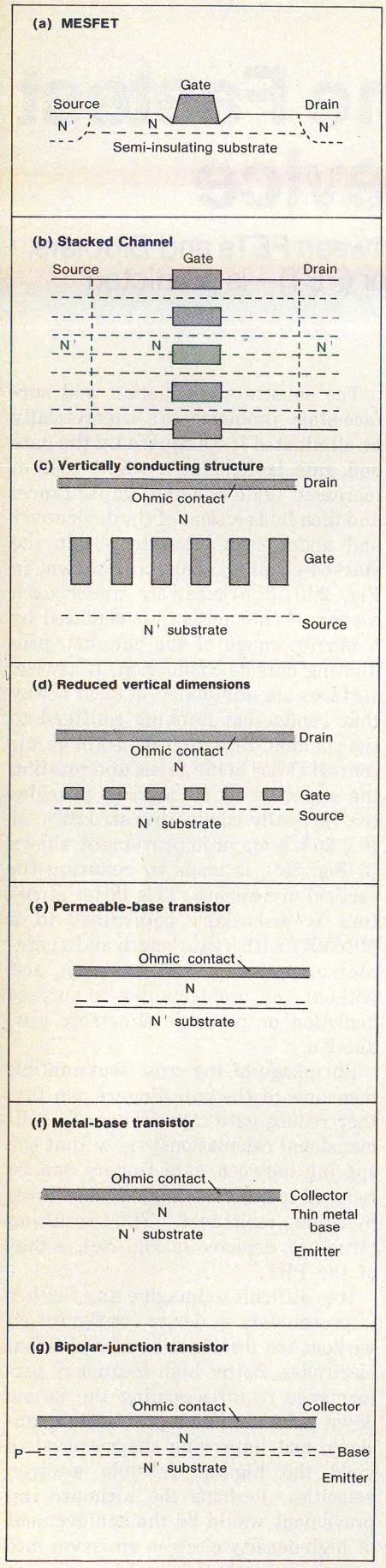
A cross-sectional, scaled drawing of a typical GaAs MESFET with a 1-μm gate length is shown in Fig. 2(a). Several changes can be made to improve the structure. Shortening the lateral dimensions, especially gate length and gate-source spacing, helps to reduce gate capacitance and source resistance. Eliminating surface states that deplete part of the channel decreases the parasitic channel resistance and improves transconductance at positive gate biases. Space-charge-limited conduction through the substrate—especially for short gate lengths—should also be prevented, since it lowers the parallel drain-source resistance.

The substrate conduction and surface-state problems can theoretically be eliminated if we square up the gate and gate trough (at a slight cost in increased gate-fringing capacitance) and then fold sections of the device over and under each other to obtain the stacked-channel structure shown in Fig. 2(b). The substrate under each section of channel is thus replaced by a mirror image of the channel, prohibiting outside conduction. Likewise, surfaces are eliminated in such a way that conduction remains confined to the channel. Bringing the drain ohmic contact closer to the gates, and rotating the structure by 90 degrees, provides the vertically conducting structure of Fig. 2(c). A major improvement, shown in Fig. 2(d), is made by reducing the vertical dimensions. This latter structure is essentially equivalent to a MESFET with a gate length and a gate-source spacing of 0.25 μm each, and without any problems due to surface depletion or parasitic substrate conduction.

Shrinkage of the cross-sectional dimensions of the gate fingers can further reduce gate capacitance. Two-dimensional calculations[3] show that the spacing between gate fingers can be reduced to maintain high drain-source dynamic resistance. The resulting structure, depicted in Fig. 2(e), is that of the PBT.

It is difficult to imagine any further improvements in device configuration without the introduction of additional electrodes. Better high-frequency performance requires scaling the device down to its minimum practical dimensions, and improving the material to yield the highest possible electron velocities. Perhaps the ultimate improvement would be the achievement of high-density electron emission into a vacuum so that there is nothing at all in the device to limit electron

(continued on next page)



velocities. As far as the device configuration is concerned, the PBT appears to be the best high-speed three-terminal arrangement.

Ending up with a BJT

The continued transformation toward a BJT configuration takes the following path: First, reducing the dimensions of the gate-finger grid, which causes scattering of electrons by the grid. Substantial forward current has to be drawn from the grid in order to allow current flow from the source or emitter (N^+ substrate) to the drain or collector (ohmic contact). When the grid dimensions have been reduced to an atomic scale and the spacing of the grid from the N^+ emitter is reduced to zero, the metal-base transistor configuration of Fig. 2(f) results. The metal base is very thin (a few tens of Å) to minimize forward base current during operation, and the sheet resistivity of the base becomes important. If the metal is considered a degenerate semiconductor, the metal-base configuration can be transformed to the BJT configuration in Fig. 2(g) by removing the degeneracy and expanding the band gap of the base to that of the rest of the device. (In this case, the Fermi level must be kept close to the valence-band edge to make the base P-type.) The sheet resistivity of the base layer is increased several orders of magnitude. High-speed performance drops dramatically as the base-series resistance increases. In practice, this effect is offset through the thickening of the base and the division of the active device into narrow fingers with low-resistivity base contacts running along both sides of each finger. However, the former remedy increases the transit delay due to minority carrier diffusion through the base, and the latter results in base areas much larger than the active device area (yielding a large collector-base parasitic capacitance).

The large collector-base capacitance is partially reduced through an increase in the base-collector depletion layer thickness, but a detrimental increase of collector transit delay results. After all trade-offs are made, the transformation of the PBT into a BJT results in a much slower device.

Using lumped-circuit models with the same circuit topology for all devices can simplify comparisons. For the BJT, the "T" model (which comes from the Ebers-Moll theory[4]) can be transformed to the "hybrid pi" model (Fig. 3) which is appropriate for modeling the FET and PBT. The "T" to "hybrid pi" transformation in Fig. 3 results in two elements, R_{BE} and C_{BE}, that are

***2. A comparison among the BJT, the FET, and the PBT** starts with a typical GaAs MESFET (a). By shortening the lateral dimensions and folding sections of the device, the stacked-channel configuration (b) can be obtained. If the ohmic contact is brought closer and the structure is rotated by 90 degrees, the vertically conducting structure (c) emerges. Reduced vertical dimensions (d) produce a structure which is essentially equivalent to a 0.25-μm vertical MESFET. A PBT (e), is produced by reducing the spacing between gate fingers. The metal-base transistor (f) results when the grid dimensions are compressed to the atomic scale. Finally, additional hypothetical alterations produce the bipolar junction transistor (g).*

Since its conception at MIT's Lincoln Laboratories (Cambridge, MA) on October 15, 1978, the permeable base transistor (PBT) has attracted attention in several research and development labs around the country. Although the largest R&D effort continues at Lincoln Labs, some investigations have also been carried out at Texas Instruments, Hughes Research Laboratory, and Hewlett-Packard Co.

Lincoln Labs

At Lincoln Labs the PBT's originators, C.O. Bozler, G.D. Alley, R.A. Murphy, and W.T. Lindley, have been joined by at least three others in the GaAs PBT effort. Also, a silicon device project aimed at generating vertical FETs that may later evolve into PBTs has been started by D. Silversmith and D. Rathman. The Lincoln Labs group has made considerable progress since their announcement in 1979 of the achievement of a maximum frequency of oscillation (f_{max}) of 17 GHz. Through reduction of the resistivity of the tungsten base material and improvement of epitaxial interfaces they achieved an f_{max} of 30 GHz by May, 1980. They also achieved a unity-current-gain frequency (f_T) exceeding 30 GHz, but with an associated f_{max} of only 10 GHz.

According to Bozler and Murphy, the best results have since been repeated but not yet improved upon. Nevertheless, they say, the tungsten resistivity has been further reduced to within three times the theoretical

dependent on frequency ω and transit time τ ($R_{BE} \approx R_{EJ}$ as a first-order approximation in ω and τ). For the input capacitance, careful modeling of transit-time effects in FETs and PBTs* yields a relationship similar to that for C_{BE} in Fig. 3. Letting C_{TOT} and C_P be the element values analogous to C_{BE} and C_{EJ} respectively, gives (to a first-order approximation in ω and τ):

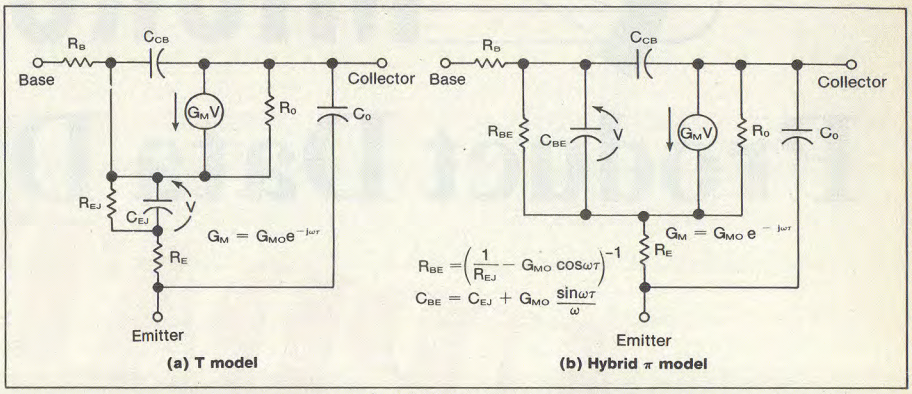
$$C_{TOT} \approx C_P + g_{mo}\,\tau \qquad (1)$$

In Eq. 1, g_{mo} is the low-frequency transconductance. The configuration in Fig. 3(b) thus becomes the common circuit model.

*A simple derivation results when a one-dimensional case is treated with electrons flowing at constant (saturation) velocity through the space-charge region from one conducting plane to another. Using Poisson's equation to calculate the displacement currents in the conducting plane through which the electrons are injected yields a capacitive effect with a dependence on ω and τ similar to that of C_{BE} in Fig. 3(b) for $\omega\tau \ll 1$.

The different device configurations can be compared by normalizing the models to the same active area, A (defined in Fig. 4 for the FET, PBT, and BJT). In normalizing circuit element values, capacitances and transconductances are altered in proportion to A, resistances are altered in inverse proportion to A, and transit-time de-

(continued on p. 61)



***3. Comparisons between configurations can be simplified** by transforming the "T" model for the BJT (a) to a "hybrid π" model (b). The latter becomes a common model that applies to FETs as well as PBTs.*

Progress on the permeable base transistor

value through changes in deposition parameters. A problem with tungsten debris in the openings of the grating has been eliminated through dry etching techniques. The mask has been redesigned to improve performance. A transmission electron microscopy study has revealed that the GaAs grown over the tungsten grating has excellent crystalline quality throughout the device's active region. The only significant problem remaining, the group believes, is the apparent presence of some deep-level traps within the openings of the tungsten grating that are not present in the absence of a tungsten grating. Bozler expresses optimism that the device will achieve an f_{max} of 100 GHz or higher during the first half of 1982. In addition, he says that recent experimentation indicates that the vapor phase epitaxial (VPE) GaAs growth process for embedding the tungsten grating can potentially be replaced with a molecular beam epitaxial (MBE) process that is more controllable.

Texas Instruments

W. Frensley at TI, operating under an Office of Naval Research contract, started a theoretical and experimental investigation of the PBT early in 1980. At the Workshop on the Physics of Sub-Micron Devices in Fort Collins, CO, in July, 1980, he presented a paper on the expected effects of ballistic transport in PBTs. The paper concluded that ballistic transport would result in measurable inductance in the output of the device but could probably not yield significant performance advantages. Using a scanning electron microscope with 10-Å resolution to study VPE GaAs overgrowth of tungsten gratings, Frensley discovered voids over the tungsten fingers which he says are a few hundred Angstrom units in size. Also, he is concerned about orientation-dependent incorporation of dopants in VPE growth over tungsten gratings, a problem called to his attention by R.A. Murphy at Lincoln Labs. Frensley says he is now concentrating on vertical FET structures until PBTs show more promise.

Hughes Research Laboratory

At Hughes (Torrance, CA), R.L. Kubena and D.E. Snyder have been investigating silicon PBTs as possible high-speed logic elements for ICs. They have used two-dimensional computer simulation to confirm Lincoln Labs' f_T predictions for GaAs PBTs, and to predict a toggle frequency of 30 GHz for logic inverters made with silicon PBTs. The Hughes group believes that focused ion beams could be used to fabricate fine gratings for silicon PBTs. Kubena says the new technique may yield gratings with lines and spaces as narrow as 1000 Å.

Hewlett-Packard

An investigation started at HP (Santa Rose, CA) in July, 1980, has yielded some microwave performance predictions and some experimental results comparing different epitaxial growth techniques for embedding tungsten gratings in GaAs. E.B. Stoneham has calculated values of f_{max} exceeding 150 GHz, and values of f_s (the frequency at which gain in an unmatched 50-ohm system drops to unity) as high as 65 GHz for structures that should be practical with existing technology. Experiments by co-workers involving overgrowth of tungsten gratings by liquid phase epitaxy (LPE), VPE, organometallic VPE (OMVPE), and MBE have demonstrated that all four techniques have potential for single-crystal embedding of fine tungsten gratings. However, LPE had severe nonuniformity problems, and VPE has been difficult to control. Also, voids were observed over tungsten fingers in the VPE growths. Current investigations are exploring the use of epitaxial germanium for the grating material, with MBE used as the embedding technique.

Cornell University

Professor Lester Eastman's group at Cornell (Ithaca, NY) is interested in the PBT as a means of studying ballistic transport effects. Presently, however, they are working with a vertical FET structure which they believe will be easier to fabricate. According to Collin Wood, they are hoping that ballistic transport can be used to extend the ultimate performance capabilities of these devices.

All things considered, there will be much attention focused on further progress of the PBT.•• *EBS*

laser technology

MICROWAVES

Product Data Directory

UPDATE

General Microwave Corporation

See pages 324 & 394 of the 1981/82 Product Data Directory for more information

GENERAL MICROWAVE

155 Marine Street
Farmingdale, L.I., NY 11735
Telephone: (516) 694-3600

AL Saber Assoc, Inc, PO Box 2311 Mobile 36601 ..... (305)973-3804
CA RF Assoc, Inc, 800 San Antonio Rd Palo Alto 94303..... (415)494-3331
CA RF Assoc, Inc, 1621 Pontius Ave Los Angeles 90025 ..... (213)478-1586
FL Saber Assoc, Inc, 2501 NW 17th Ln Pompano Beach 33064 ..... (305)973-3804
FL Saber Assoc, Inc, PO Box 1763 Bradenton 33506..... (305)973-3804
FL Saber Assoc, Inc, PO Box 3732 Indiatlantic 32903 ..... (305)973-3804
GA Saber Assoc, Inc, PO Box 2148 Acworth 30101..... (305)973-3804
IL Cain-Forlaw Co, Inc, 1203 Ironwood Dr Mt Prospect 60056 ..... (312)253-3578
MA Microwave Mktg Spec, Inc, 279 Cambridge St Ste 107 Burlington 01803..... (617)272-7530
NJ E-F Tech Sls, Inc, 21 Belgrade Ter, N Orange 07052 ..... (201)731-7203
NY E-F Tech Sls, Inc, 825 E Jericho Tpke Huntington Sta 11746 ..... (516)549-1818
OH Cain-Forlaw Co, 5280 Hopewell Church Rd Box 903 Lancaster 43130..... (614)654-4800
PA Eastern Instrumentation Inc, Street Rd & Bristol Pike Neshaminy Plaza 2, Ste 114 Bensalem 19020 ..... (215)245-6660
SC Saber Assoc, Inc, PO Box 2772 Columbia 29202..... (305)973-3804
TX Cain & Co, 13500 Midway Rd Dallas 75234..... (214)233-6809
VA Creative Mktg Assoc, 6716 Old McLean Vil Dr, McLean 22101..... (703)442-9100
FR CANADA Soquelec Ltd, 5757 Cavendish Ste 101 Montreal Que H4W 2W8..... (514)482-6727
FR CANADA Soquelec Ltd, 19 Grenfell Ste 100 Nepean Ont K2G DG3 ..... (613)226-1885
FR FRANCE Salies SA 65-67 Ave Jean Jaures, 91122 Palaiseau ..... (336)920-40-10
FR GREECE American Tech Entprs PO Box 156 Athens K 821-9470
FR HOLLAND B.V. Technische Handelsonderneming Coimex, PO Box 19, 8050 AA Hattem..... (0)5206-41214
FR INDIA Forbes Forbes Campbell & Co, Forbes Bldg PO Box 79 Bombay 400 001..... 268081
FR ISRAEL Racom Elecs Co Ltd, 60 Pinkas St, POB 21120, Tel Aviv 61210..... 3-453151
FR ITALY DSP Micronde SNC, 128 VIA Firenze, 57100 Livorno..... 0586/405036
FR ITALY Via S Bernadette, 76, 00167 Rome..... 06/6231744
FR JAPAN Seki & Co Ltd, PO Box 32, Nihonbashi, Tokyo 103-91 ..... 03(669)4121
FR JAPAN Seki & Co Ltd, Tokai Bldg, 1-50-1 Kitahorie Kamidori, Nishi-Ku, Osaka 550
FR JAPAN Seki & Co Ltd, 203, Nitto Bldg, 2-4-2 Shinohara Kita Kohoku-Ku, Yokohama 222
FR SOUTH AFRICA K. Baker Assoc Ltd, PO Box 41062, Craighall Johannesburg 2024 ..... 788-1700/05
FR SWEDEN Walmore Elecs AB, Box 6063, Sorerargatan 2, S-162 06 Vaellingby 08-38-01-30
FR SWITZERLAND Alpha-Beta Elecs AG, PO Box 88, 8060 Zurich 01/43-70-70
FR UNITED KINGDOM Walmore Elecs Ltd, 11-15 Betterton St, Drury Ln, London WC2H 985 836-1228
FR W GERMANY Kontron Elekt GMBH, Oskar-Von-Miller-Strabel, 8057 Eching, Munich

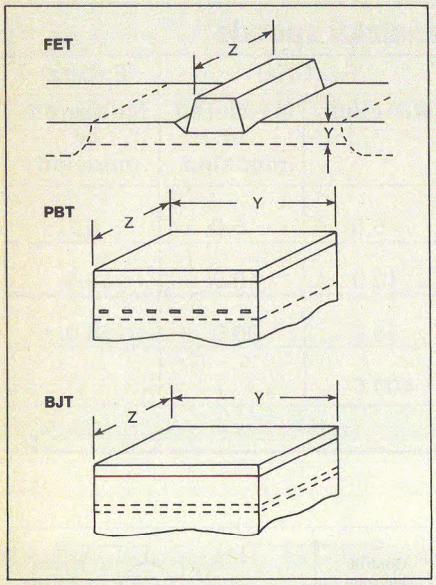
Systron Donner/Advanced Components Division

See pages 376 & 377 of the 1981/82 Product Data Directory for more information

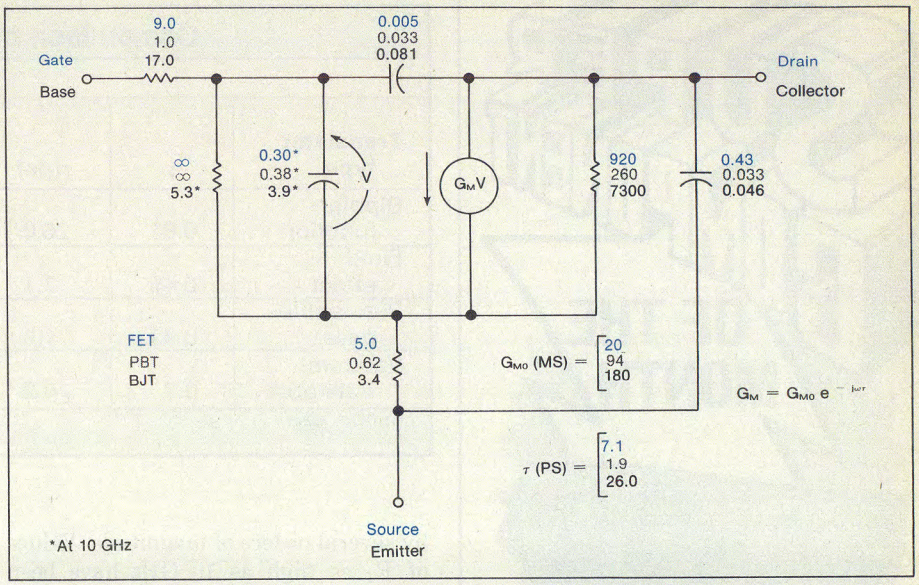
SYSTRON DONNER ADVANCED COMPONENTS DIVISION
Member THORN EMI Group

735 Palomar Avenue
Sunnyvale, CA 94086
Telephone: (408) 735-9660

AZ Territorial Mktg, PO Box 2447 Scottsdale 85252..... (602)994-8665
CA HyTech Assoc, 717B Lakefield Rd Westlake Vil 91361..... (213)991-7491
CA Jay Stone & Assoc, 399 S San Antonio Rd Los Altos 94022
IL Carter Elecs Inc, PO Box 472 Palos Park 60464 ..... (312)361-5540
MA BBC, Seventeen Wilson St Chelmsford 01824..... (617)256-6593
MD Neal Deoul & Assoc, 3104 Caves Rds Owings Mills 21117 ..... (301)363-4311
MN Scientific Devices, 7032 Willow Creek Rd Eden Prairie 55344..... (612)944-3515
MO Scientific Devices/Ramsey Assoc, 1901 Congressional Dr St. Louis 63141..... (314)569-1406
NY Phase Four, Inc, 277 N Blvd Ste 302 Great Neck 11021..... (516)482-1790
OH Scientific Devices/Ashby Assoc, 4130 Linden Ave Ste 155 Dayton 45432..... (513)298-9904
PA Scientific Devices, PO Box 201 Plymouth Meeting 19462..... (215)825-9515
TX Scientific Devices, 312 N Central Exp Ste 212 Richardson 75080 ..... (214)231-8106
WA Scientific Devices, Fraser Bldg 10843 NE 8th St Bellevue 98004..... (206)454-0990
FR CANADA Assoc, Test Equip, 3400 Pharmacy Ave Scarsborough Ont MIW 3J8 ..... (416)497-2208
FR ENGLAND Systron Donner Ltd, 2 Jacks Rd South Oakleigh, Vic 3167 (PO Box 63) 579-3622
FR FRANCE Systron Donner SA, 24, Rue de Paris, 78560 Le Port Marly (958)4863
FR GERMANY Systron Donner GMBH, Bodensee Str 113, D-800 Munich 60 ..... (089)838021



***4. The normalized active areas of the devices** also facilitate comparisons. Here the active areas of a FET, a PBT, and a BJT are defined.*



***5. The input capacitance and the transconductance shown in this model** were indicated to be the most important determinants of the speed of the device. Reducing the device models to their bare essentials simplifies the comparison among the FET, PBT, and BJT devices.*

lays are held constant.

Circuit element values, normalized to an active area of 100 μm^2 for three devices optimized for practical microwave use, are displayed in Fig. 5. The FET is a GaAs device with a 500-μm gate width, a 1-μm gate length, and an active area (A) equal to 200 μm^2. The BJT is a silicon transistor with 1-μm emitters, and an active area of 260 μm^2. Unlike the FET and BJT, which are actual production devices, the PBT is a projected device.

Two-dimensional modeling[3] was used to derive the transconductance and output conductance of each device. Other quantities were derived from geometrical considerations with particular attention paid to the effects of time-dependent space charge in the velocity-saturated region between the base and the collector.† The PBT design was chosen to optimize microwave performance by assuming 2-μm design rules for all lateral dimensions, except the base grid for which 2400-Å lines and spaces were assumed. The active area is 52 μm^2. For all devices, the parasitic capacitances and resistances caused by interconnects, bonding pads, substrates, etc., were included in the element values of the models. The parasitics are small but significant. With the exception of the output resistance (260 ohms for the PBT) all of the element values for the PBT either lie between those for the FET and the BJT or are more favorable for high-speed performance. Comparisons of model element values indicate the advantages of the PBT configuration over those of the FET and the BJT. The PBT displays superior transit time, parasitic resistances, capacitances, and conductances. The transconductance for a given active area increases progressively from FET to PBT to BJT. The high transconductance of the BJT is not sufficient, however, to overcome the other deficiencies of the BJT with respect to the FET and the PBT.

A simpler model can be used

To simplify the comparison, it helps to reduce the device models to their bare essentials. A study of the sensitivity of device broadband speed to element-value variation in the model (Fig. 5) reveals that the input capacitance and the transconductance are the most important determinants. In the simplified model of Fig. 6, the input capacitance has been divided into the two parts of Eq. 1. The capacitance $C_I \approx g_{mo}\,\tau$ is called the *intrinsic* component, since it unavoidably results from the transit-time delay in the device. The capacitance C_P, on the other hand, is termed the *parasitic* component, because it depends on the device configuration and does not seem to be an inevitable consequence of transistor action. The fraction of the total capacitance which is contributed by its intrinsic component is defined as:

$$\gamma = \frac{C_I}{C_{TOT}} \approx \frac{g_{mo}\,\tau}{C_{TOT}} \qquad (2)$$

The current gain cutoff frequency can then be found by:

$$F_T = \frac{g_{mo}}{2\pi\ C_{TOT}} \approx \frac{\gamma}{2\pi\tau} \qquad (3)$$

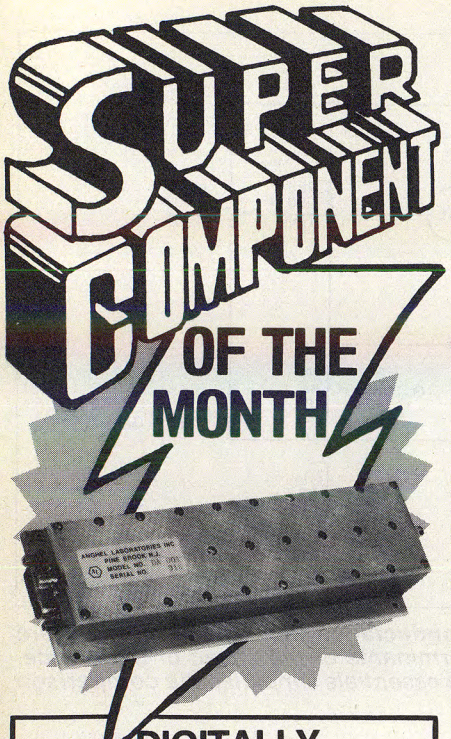
The table (p. 62) lists the values of γ, τ, and $\gamma/2\pi\tau$ for the three devices. Also included are the values for a device with the configuration of a PBT, but with vacuum rather than semiconductor between the emitter and collector. Such a device, which can be termed a *vacuum transport transistor* (VTT), shows what can be expected if electron velocities can reach nonscattering-limited velocities. Included in the table are actual measured values of F_T and F_S for the FET and BJT, and calculated values of F_T and F_S for a comprehensive model of the PBT. (F_S is the frequency at which gain with a 50-ohm source and a 50-ohm load in a common source or common-emitter configuration drops to 0 dB).††

From the table it can be seen that Eq. 3 contains all the necessary elements to estimate F_T and that F_S tends to track F_T in practical devices by an approximately constant factor. It also indicates that γ for devices optimized for practical microwave use falls within a 2-to-1 range, whereas τ varies

(continued on next page)

†The same modeling technique has been applied by the author to GaAs FETs to achieve a close match between modeled and measured S parameters at frequencies up to 14 GHz.

††F_S is one of the best indicators of the practical bandwidth capability or speed of an amplifying device.



DIGITALLY CONTROLLED ATTENUATOR

DA-001 SERIES
Featuring PIN Diode Switched T-Pads In Low Loss Microstrip Geometry

Frequency Range	915-1250 MHz
Attenuation Range (7 bits)	127 dB in 1 dB steps
Switching Speed	200 nsec max.
Operating Power	100 mW max.
Accuracy (incl. temp. effects)	± 0.25 dB for any attenuation setting
Resetability	0.1 dB
VSWR	1.20 : 1 max.
Phase Variation	± 2° max.
Control	TTL compatible
Insertion Loss	3.5 dB max.
Flatness Over Freq. Range	0.25 dB max. for any setting
Operating Temp. Range	− 55 °C to + 85 °C
DC Power Reqmnts.	+ 5 VDC 400 mA, − 5 VDC 200 mA max.
Size	8″ × 1.5″ × 1.5″
Conn.	SMA female and DC - multipin (DM type)

This device exemplifies our broad capability in Microwave Control Devices. All have super low loss, fast switching speed and, if required, high power handling capability up to 18 GHz. Contact factory for custom requirements and literature for:

- **Multi-throw Switches**
- **Voltage Variable and Digital Attenuators**
- **Voltage Variable and Digital Phase Shifters**

ANGHEL LABORATORIES INC.
333 Route 46
Fairfield, N.J. 07006
Tel: 201 575-1116

READER SERVICE NUMBER 4

Comparison of transistor speeds

Transistor type	γ	τ(ps)	F_T (GHz) Estimated[1]	F_T (GHz) Measured or modeled	F_3(GHz) Measured or modeled
Bipolar-junction	0.81	26.0	5.0	5.0	6.7
Field-effect	0.46	7.1	10.0	10.0	13.0
Permeable-base	0.43	1.9	36.0	36.0	58.0
Vacuum-transport	0.5	0.2	400.0		

(1) $F_T = \gamma/2\pi\tau$

by several orders of magnitude. Values of F_T as high as 10 GHz have been achieved for BJTs optimized for logic applications[5] and an F_T of 18 GHz has been achieved for GaAs FETs with half-micron gate lengths.[6] The table shows that the PBT is faster than the FET by at least as large a factor as the FET is faster than the BJT.

The tabulated data indicates that practical considerations (such as breakdown potential requirements and power-handling capability), and the effects of parasitics other than those included in the simple model in Fig. 6, place an upper limit on F_T. The F_T ceiling stems from the lower limit placed on the transit delay time that will be allowed by a given device configuration. To a certain extent the delay time τ in any of the device configurations discussed in this article can be varied independently of g_{mo} and C_P through appropriate changes in applied potentials and in the dimensions parallel to the current path. Equations 1 and 3 give:

$$F_T = \frac{g_{mo}}{2\pi\,(C_P + g_{mo}\,\tau)} \qquad (4)$$

Equation 5 approaches a maximum value of:

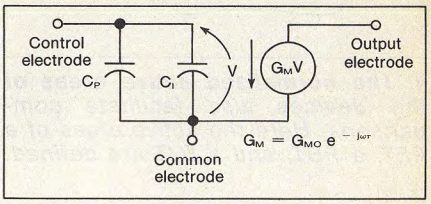
$$F_{T_{max}} = \frac{g_{mo}}{2\pi\,C_P} \qquad (5)$$

as τ, and hence γ, approach zero. From Eqs. 1, 4, and 5, we have:

$$\frac{F_T}{F_{T_{max}}} = \frac{C_P}{C_P + g_{mo}\,\tau} =$$

$$\frac{C_{TOT} - C_I}{C_{TOT}} = 1 - \gamma \qquad (6)$$

The fact that $\gamma > 0.4$ for all devices in the table indicates that $F_T/F_{T_{max}}$ does not exceed 0.6 according to Eq. 6. Hence, while C_P limits F_T (Eq. 5), other parasitics and practical considerations further restrict F_T to typically less than 60 percent of $F_{T_{max}}$. The predicted high speed of the PBT results first from the fact that the device's g_{mo}/C_P, according to two-dimensional modeling, will exceed that of a BJT or that of a FET. Second, practical considerations and parasitics other than C_P allow designs with short transit times and therefore small values of C_I.



6. Input capacitance can be divided into two components. *The intrinsic component (C_I) is an unavoidable result of the transit time. The parasitic component (C_P), on the other hand, depends on the device configuration.*

How much further device speed can be pushed is indicated by the F_T for the VTT in the table. In the author's opinion, the speed of a VTT will be reached after about four more technological advances as great as the advance from the silicon BJT to the GaAs FET. The permeable base transistor configuration, which lies between that of a field-effect transistor and that of a bipolar junction transistor, yields distinct advantages with regard to parasitic capacitances, resistances and conductances. As a result, the PBT can take advantage of shorter transit times to gain speed advantages. Comprehensive

(concluded on p. 65)

THREE-TERMINAL DEVICE

(continued from p. 62)

modeling predicts an F_s of 60 GHz and an F_{max} of 130 GHz for a practical GaAs PBT design. Such a device would make as great a speed improvement over the GaAs FET as the latter has made over the silicon BJT.

Although the PBT has the best three-terminal device configuration envisioned in this paper for achieving high speed, a GaAs version of it will not come close to achieving the maximum conceivable frequency limits. Improvements in materials, use of ballistic transport, and possible developments in electron emission into vacuum could boost speeds an order of magnitude further.••

References

1. A.I. Cogan and P.O. Haugsjaa, "Two-Dimensional Field and Potential Analysis in Static Induction Transistors," Device Research Conference, Ithaca, New York (June 23-25, 1980).
2. J. Nishizawa, et al., "Field-Effect Transistor Versus Analog Transistor (Static Induction Transistor)," IEEE Transactions on Electron Devices, Vol. ED-22, pp. 185-197 (1975).
3. C.O. Bozler and G.D. Alley, "Fabrication and Numerical Simulation of the Permeable Base Transistor," IEEE Transactions on Electron Devices, Vol. ED-27, pp. 1128-1141 (1975).
4. J.J. Ebers and J.L. Moll, Proceedings of the I.R.E., Vol. 42, p. 1761 (1954).
5. A. Wang, Hewlett-Packard Co., private communication.
6. C. Li, Hewlett-Packard Co., private communication.



SR. MICROWAVE CIRCUIT DESIGN ENGINEER

Alpha Industries, a respected and rapidly expanding manufacturer of microwave semiconductor components with a 40% annual growth rate, offers a talented professional exceptional challenge and professional rewards.

An excellent opportunity exists at Central Microwave Corporation for an individual with a strong background in GaAs devices, Gunn oscillators, or FET's. Position is located in St. Louis at this wholly owned subsidiary of Alpha Industries. Qualified candidate must have at least a BSEE or MSEE with 5 years proven experience.

Please forward resume with salary history and requirements, in confidence, to Margaret S. Doyle, Alpha Industries, Inc., 20 Sylvan Road, Woburn, MA 01801, USA. Resumes which do not include the requested salary information will not be considered.

Alpha

The Alpha Advantage

An Equal Opportunity Employer

READER SERVICE NUMBER 2

Moving?

1. For FASTEST service you must attach old mailing label in space below.

If mailing label is not available print your old Company name and address in this box

Please allow 6 weeks for change to take effect

2. Print your NEW business address here

NAME_____TITLE_____

COMPANY_____

ADDRESS_____

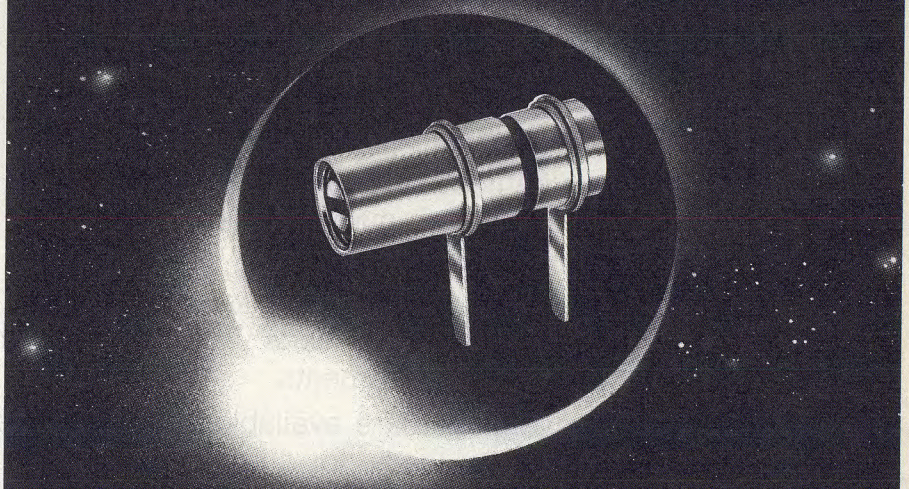
CITY_____STATE_____ZIP_____

M-282

3. Mail to:

MicroWaves
P.O. Box 13801
Philadelphia, Pa. 19101 USA

JOHANSON ENGINEERING ECLIPSES THE INDUSTRY



For over 35 years Johanson engineering has set the standard of quality for the variable capacitor industry. The Giga-Trim* (gigahertz trimmers) are tiny variable capacitors that are a cost effective means of fine tuning RF hybrid and microwave circuits. Now, a new improved series provides an increased Q factor of >3000 to >5000 and a zero temperature coefficient. *Electronic Accuracy through Mechanical Precision.*

U.S. Patent No. 3,469,160

Johanson

Manufacturing Corporation
400 Rockaway Valley Road
Boonton, New Jersey 07005
201-334-2676 TWX 710-987-8367

READER SERVICE NUMBER 35

Improved FET Design Reaches Millimeter Waves

A new transistor structure, the opposed gate-source transistor, promises to break the frequency limits of conventional FETs. It features increased transconductance and submicron gates.

ALTHOUGH conventional FETs have undergone many refinements in the pursuit of millimeter-wave performance,[1,2,3] current designs have failed to satisfy the need for operation at higher and higher frequencies of oscillation. The advent of a completely different FET structure, the opposed gate-source transistor (OGST), promises to break the frequency limitations of current designs.

The new transistor structure places the gate and source on opposite sides of a thin conductive channel. The drains are situated at opposite ends of the channel, but electrically connected at the output end of the transistor. This design has certain advantages over conventional FETs:

- it practically eliminates parasitic source resistance;
- it effectively doubles transconductance;
- it greatly relaxes the dimensional requirements on the physical gate length (effectively achieving submicron gates); and
- it provides integrated gate and drain transmission lines as input and output.

These improvements extend the upper limit of the maximum frequency of oscillation to 300 GHz—quite an advance from the present ceiling of 120 GHz for a conventional FET.[4]

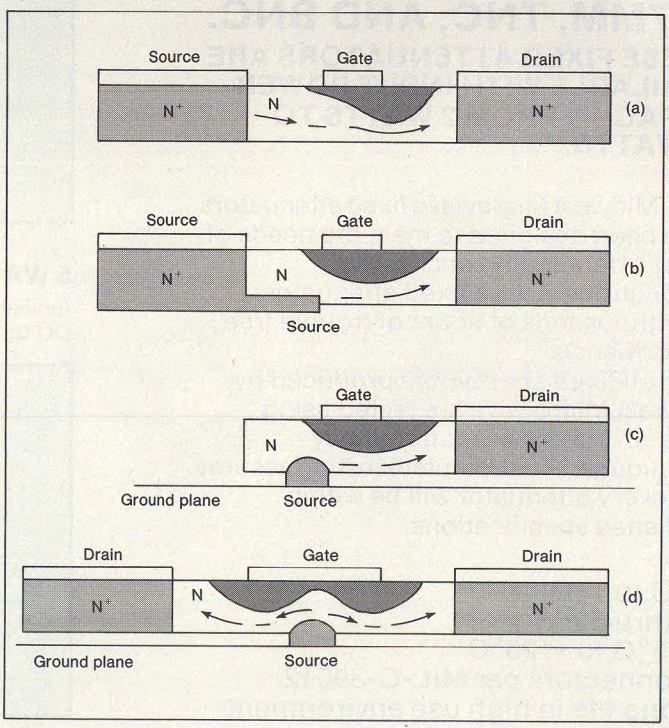
The evolution of the OGST from the conventional FET structure is traced in Fig. 1. The device in Fig. 1(a) is a typical FET. The electrons from the source flow beneath the gate and are collected by the drain. The depletion region, formed by reverse-biasing the gate electrode, controls channel current by constricting the electron flow. Excessive source resistance and inductance, and circuit parasitics associated with input and output connections, limit the high-frequency performance of this structure.

A modification of this structure, shown in Fig. 1(b), adds a buried source beneath the gate. The current is controlled in a fashion similar to that of the first device, but, by placing the source closer to the gate, the source-gate resistance is reduced. The effective gate length is also reduced, by an amount proportional to the extension of the source beneath the gate. By adding a ground plane, as in Fig. 1(c), the source inductance can be reduced, and the input and output connections

(continued on p. 70)

Table 1: OGST parameters at different frequencies

Parameter	Units	44 GHz	60 GHz	94 GHz
Physical gate length	μm	0.50	0.30	0.25
Source-drain spacing	μm	1.14	0.83	0.53
Channel doping	cm^{-3}	2×10^{17}	3×10^{17}	4.2×10^{17}
Channel thickness	μm	0.2	0.15	0.1
Physical gate width	μm	43	33	21
Pinchoff voltage	V	5.7	4.9	3.0



***1. The evolution of the OGST** can be traced from the conventional FET (a). By adding a buried source (b), a ground plane (c), and finally, by paralleling transistor structures (d), the OGST results.*

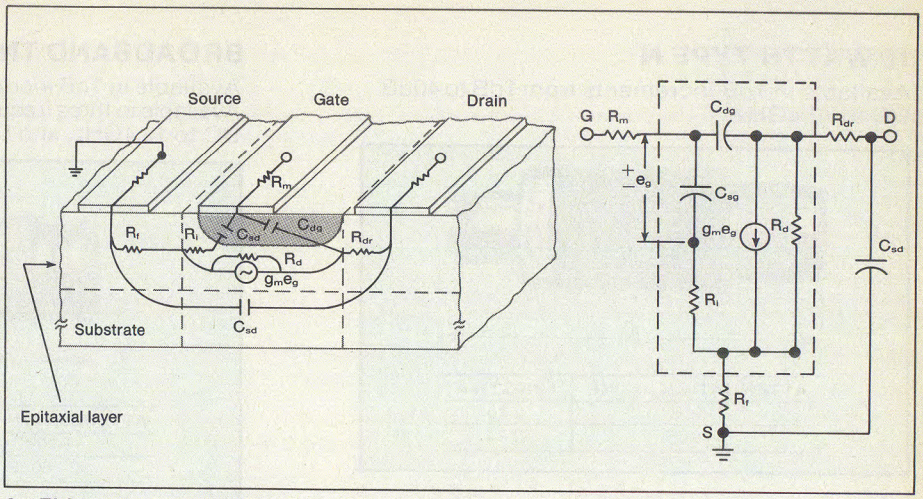
John J. Berenz, Senior Scientist, TRW Defense and Space Systems Group, Redondo Beach, CA 90278, and **G. C. Dalman** and **C. A. Lee,** Professors, School of Electrical Engineering, Cornell University, Ithaca, NY 14853

can be simplified using microstrip lines.

Figure 1(d) shows the final opposed gate-source transistor topology. Two parallel mirror-image transistors of the type shown in Fig. 1(c) are connected at the gate-source electrodes. This gives the resulting transistor twice the transconductance of the original single-transistor configuration, and doubles the physical length of the gate. Since the drains are physically separated, heat is dissipated much more readily.

Of course, for millimeter-wave operation, physical gate length must be made small (about 0.3 μm). The effective gate length will actually be smaller because of the dual-channel structure.

Figure 2 presents a perspective sketch of a conventional FET, illustrating the equivalent circuit elements associated with the different regions of the transistor.[4] Compare this to the OGST representation and circuit in Fig. 3. The equivalent circuits are basically the same, except that the values of specific elements for the OGST will differ considerably from those of the conventional FET. For example, the OGST transconductance will be twice as large. For an effective 0.15-μm gate length, the OGST transconductance will be about 400 mS/mm.



***2. This conventional FET** sketch and schematic illustrate the planar placement of the source, gate, and drain.*

Another benefit of the new design is that source-gate resistance shrinks. For the 0.15-μm gate length, this resistance will be about 0.1 ohm-mm for the OGST, compared to 0.45 ohm-mm for a conventional FET. The OGST's source inductance can also be made smaller. By directly connecting the source to the underlying ground plane via a line V-groove, the resulting inductance will be less than that of a conventional FET.

As long as the source length is a small fraction of the gate length, the source-gate capacitance of the OGST will not be significantly greater than that of the conventional FET. The source-drain capacitance of the new design will also be small, providing the source contact is isolated from the drains by a sufficiently thick semi-insulating layer.

Since these differences in the equivalent circuit element values can significantly affect the maximum frequency of oscillation and the general high-frequency performance, they have been collected and compared in Tables 1 and 2.

Because the opposed gate-source transistor is still an experimental design, the best way to compare its performance is to select a particular frequency, for example, 60 GHz. For operation at this frequency, an effective gate length of 0.15 μm is required. Assuming that a moderate electron velocity of 1×10^7 cm/s is possible, the cutoff frequency (f_T) will be:

$$f_T = \frac{V_{sat}}{2\pi L_g} = 106 \text{ GHz} \qquad (1)$$

The maximum frequency of oscillation (f_{max}) is then approximated by:

$$f_{max} \approx \frac{f_T}{2}\left(\frac{g'_m}{g_{ds}}\right)^{1/2} \qquad (2)$$

where g'_m, the reduced transconductance, is:

$$g'_m = \frac{g_m}{1 + g_m r_{sg}} \qquad (3)$$

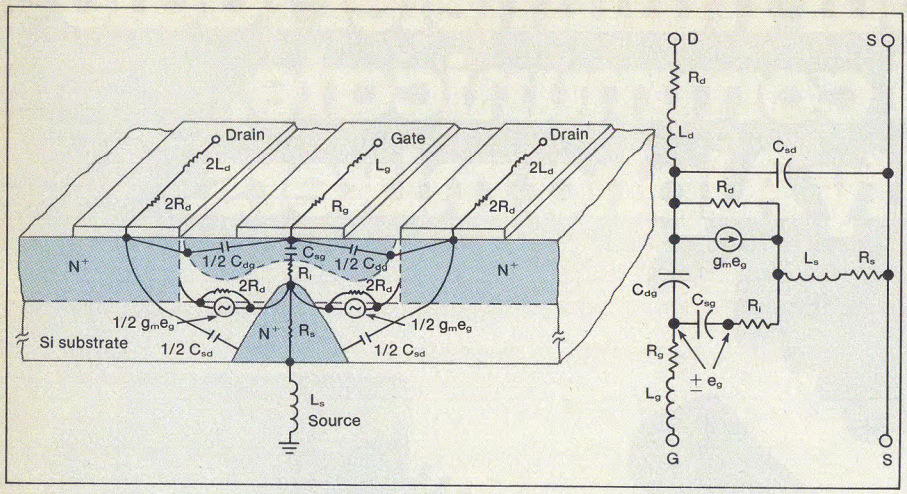
In Eq. 3, g_m is the intrinsic device transconductance, r_{sg} is the source-gate resistance, and g_{ds} is the drain-source conductance.

For a 60-GHz OGST, g'_m is

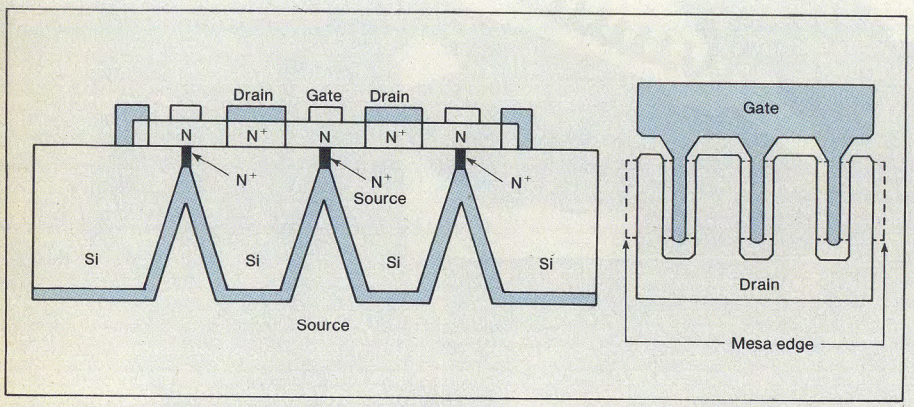
Table 2: OGST performance estimates

Parameter	Units	Estimate A	Estimate B	Estimate C
Gate length	μm	0.5	0.25	0.3
Transconductance (g_m)	S/mm	0.12	0.21	0.4
Source-gate resistivity (R_{sg})	Ω-mm	1.05	0.45	0.1
Drain-source conductance (G_{ds})	S/mm	≅0.01	—	≅0.01
Cutoff freq. (f_T)	GHz	—	—	106
Reduced Transconductance (g'_m)	S/mm	—	—	0.38
Max. osc. freq. (f_{max})	GHz	—	—	330
Power output (P_o)	mW	—	—	4.5
DC characteristics				
Drain-source current (I_{dss})	mA	—	—	5
Breakdown voltage (V_B)	V	—	—	8.5
Pinchoff voltage (V_p)	V	—	—	4.9
Threshold voltage (V_T)	V	—	—	0.5
Schottky barrier height (ϕ)	V	—	—	0.9

Estimate A: Schellenberg, et al.[1]
Estimate B: Bandy, et al.[2]
Estimate C: Proposed 60-GHz OGST



3. The improved FET, the OGST, *reduces parasitics by placing the source directly underneath the drain.*



4. Higher power devices are possible *by paralleling two or more single-gate DIFETs. The top view of the OGST at right serves as a comparison.*

calculated to be about 385 mS/mm. For a channel doping of about 3×10^{17} cm^{-3}, g_{ds} is about 10 mS/mm. Thus, the maximum frequency of oscillation for this particular OGST is estimated to be about 330 GHz.

Of course, this estimate is very conservative. Because of the short effective gate lengths, velocity "overshoot" may increase the effective electron velocity to as high as 4×10^7 cm/s, increasing f_{max} in direct proportion.

The power output of the OGST is limited by two factors: avalanche breakdown voltage and maximum allowable current density. The breakdown voltage for a 60-GHz OGST is about 8.5 V, depending on the source-drain spacing and the breakdown field. The maximum allowable current density will be:

$$J_{max} = 0.1\ Ne\ v_{sat} = 48\ kA/cm^2 \quad (4)$$

where N is the channel doping (3×10^{17} cm^{-3}), e is electronic charge, and v_{sat} is the same 1×10^7 cm/s assumed above. Thus, the limitations on the maximum input power are clearly established.

Since the maximum power output of a FET results from class B operation, the OGST was analyzed under class B conditions, giving it an output of:

$$P_o = \frac{2}{\pi^2} I_{dss} (V_B - V_p - V_T)(1 + \frac{\phi}{V_p})^2 \quad (5)$$

where I_{dss} is the drain-source current in saturation, V_B is the breakdown voltage, V_p is the pinchoff voltage, V_T is the threshold voltage for saturated current flow, and ϕ is the height of the Schottky barrier.

For a 60-GHz OGST with a channel thickness (a) of 0.15 μm, and a gate width (Z) of 35 μm, the maximum drain current will be twice that of a single transistor:

$$I_{dss} = 2\ aZ\ J_{max} = 5\ mA \quad (6)$$

Pinchoff voltage is found from:

$$V_p = \frac{eNa^2}{2\epsilon} = 4.9\ V \quad (7)$$

where ϵ is the dielectric permittivity of GaAs.

If V_T is about 0.5 V, and ϕ is about 0.9 V, then the anticipated power output at 60 GHz is about 4.5 mW, under class B conditions. This is equivalent to about 130 mW/mm of gate length.

In this configuration, the individual drain contacts are connected to form a three-terminal device. Another method is to use separate drain contacts in a "dual-drain" configuration to obtain operation analogous to that of a dual-gate FET. This mode of operation lends itself to mixing, multiplying, and injection-locking applications.

A special feature of the OGST is that gate and drain transmission lines are electronically coupled. When these lines have equal phase velocities, the OGST operates in a distributed interaction (DI) mode (i.e., as a DIFET). In this mode, signals propagating down the gate transmission line is electronically coupled in synchronism to the drain transmission line. Essentially, the transistor functions as a distributed traveling wave amplifier.

As a result, the output power of the OGST can be boosted by increasing the gate width until line losses are excessive. For the 60-GHz OGST, the gate width can be increased by a factor of five over the value in Table 1. Because output current adds coherently along a transmission line with constant characteristic impedance, the output power of the DIFET will be increased by more than a factor of seven.

By paralleling two or more single-gate DIFETs (Fig. 4), even higher output power is possible. This approach promises to deliver up to 100 mW of CW power at 60 GHz. The DI mode also should provide increased bandwidths.

In short, the OGST and DIFET are new approaches to the design of a higher frequency transistor. This transistor can be readily incorporated into either monolithic or hybrid microwave and millimeter-wave integrated circuits, and can be used in both analog and digital applications.••

Acknowledgement

This work is supported by the Defense Advanced Research Projects Agency (DARPA) under Contract N00123-81-C-1225, EHF Monolithic Arrays, and is monitored by the Naval Ocean Systems Center (San Diego, CA).

References

1. J.M. Schellenberg, G.W. Keithley, C.K. Kim, V.K. Eu, H.B. Kim, and G.O. Ladd, "RF Characteristics of Ka-band GaAs FETs," Proceedings of the Cornell Conference on Active Microwave Semiconductor Devices and Circuits, pp. 289-296 (August 1979).
2. S.G. Bandy, D.M. Collins, and C.K. Niohmoto, "Low-Noise Microwave F.E.T.S. Fabricated by Molecular-Beam Epitaxy," *Electronic Letters*, pp. 218-219 (1979).
3. J.M. Schellenberg, H. Yamasaki, and D.W. Maki, "A 69 GHz FET Oscillator," paper presented at the 1981 IEEE/MTT-5 International Microwave Symposium, June 15-17, 1981, Los Angeles, CA.
4. R.A. Pucel, H.A. Haus, and H. Statz, "Signal and Noise Properties of Gallium Arsenide Microwave Field-Effect Transistors," *Advances in Electronics and Electron Physics*, Vol. 38, Academic Press, New York, NY, pp. 195-265 (1975).

InP: A Promising Material For EHF Semiconductors

Indium phosphide can be considered the third most important semiconductor material for microwave use, behind Si and GaAs. Above 90 GHz, it may well rank first.

THE development of indium phosphide (InP) semiconductor devices is expected to contribute significantly to the extension of microwave techniques into the millimeter-wave and near-millimeter-wave (NMMW) regions. Potential applications are as low-noise local oscillators, drivers for tube amplifiers, medium-power stand-alone transmitters, and low-noise amplifiers in radiometry, target acquisition, missile guidance, communications, and fuzing systems.

InP opens NMMW region

System concepts for the NMMW range have often been deemed unrealistic because of high attenuation relative to the microwave region, poor angular resolution relative to the visible/infrared region, and the lack of suitable solid-state power sources. However, in view of recent technological advances, NMMW frequencies prove to be an attractive compromise between RF and light, and, in adverse weather conditions, clearly better than atmospherically limited light/IR systems.[1] Mature InP processing technology could supply system architects with compact, efficient power generators needed for their NMMW plans.

In many respects, indium phosphide is similar to gallium arsenide (GaAs). Both are III-V semiconductor compounds that exhibit very similar electronic properties, and both can be used to design the same types of solid-state devices. With significant performance differences, transferred-electron (Gunn) diodes, Impatt diodes,

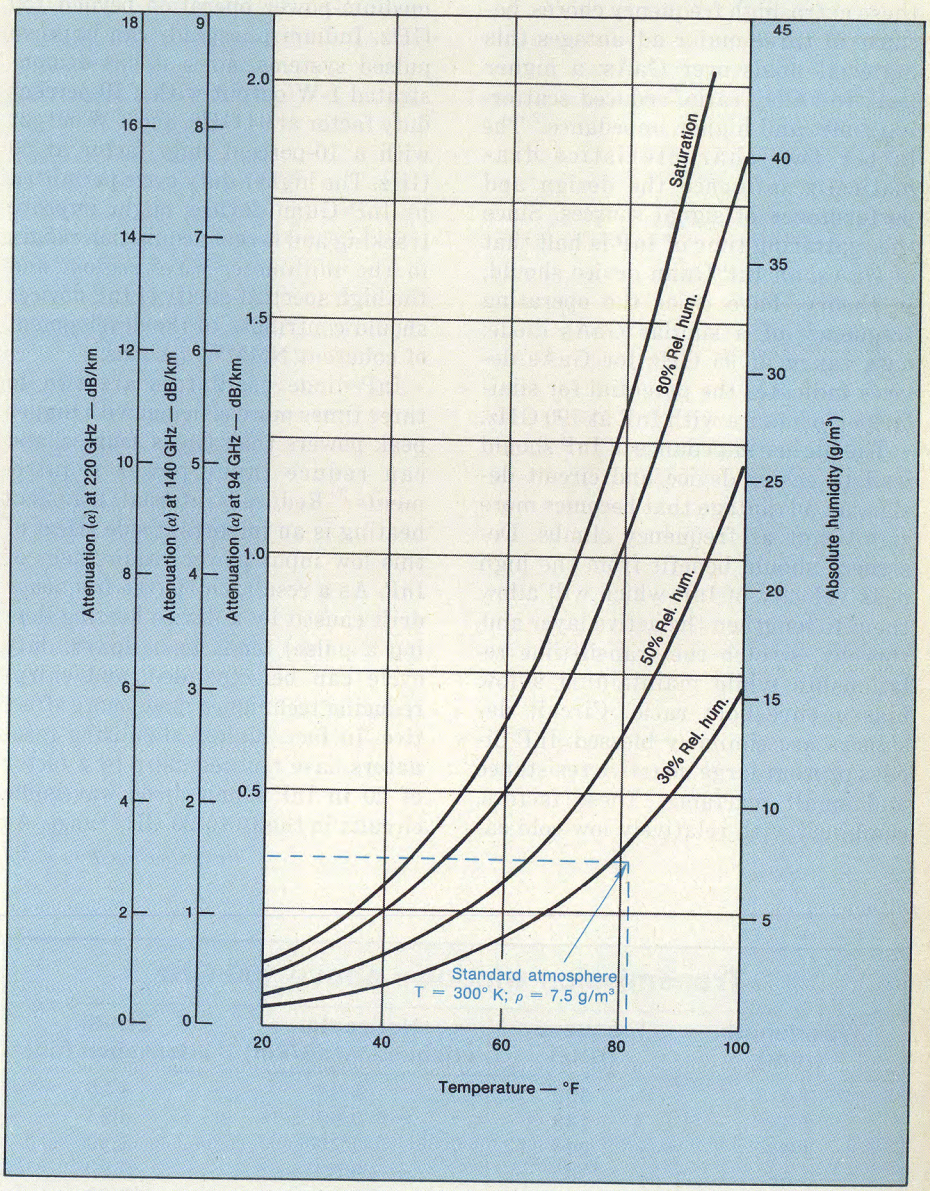
(text continues on next page)

James J. Gallagher, Principal Research Scientist, Engineering Experiment Station, Georgia Institute of Technology, Atlanta, GA 30332

Adverse weather clouds the choice of wavelength

The near-millimeter spectrum spanning 90 to 900 GHz is usually dismissed as a region of high attenuation relative to the microwave region, and as a region of poor angular resolution relative to the visible/infrared (IR) spectra. It is, however, an attractive frequency range for tactical systems that must function

(continued on next page)



***1. Attenuation depends greatly** on wavelength and relative humidity.*

InP: A PROMISING MATERIAL *(continued from p.77)*

and field-effect transistors can all be constructed with InP and GaAs.

InP devices are expected to play their most important role in transmitter and local oscillator circuits in the NMMW spectrum that extends from 90 to 900 GHz. Existing devices fabricated from silicon (Si) and GaAs can meet today's system requirements through 60 GHz, although InP might provide some performance enhancements in this region as well. The lively 94-GHz vicinity is currently covered by Si Impatts and tube sources; in many applications, InP will provide greater efficiency and stability. Vacuum-tube sources have been developed to provide power to 300 GHz, but are difficult to phase lock, and not suitable for coherent radar applications. Gunn diodes fabricated with InP are very attractive candidates for these extra-high frequency chores, because of three major advantages this material holds over GaAs: a higher peak-to-valley ratio, reduced scattering time, and higher impedance.[2] The latter two characteristics dramatically influence the design and performance of signal sources. Since the scattering time of InP is half that of GaAs, an InP Gunn device should, in theory, have twice the operating frequency of a similar GaAs diode; data taken at 95 GHz for GaAs devices indicates the potential for similar performance with InP at 190 GHz.

The higher impedance of InP should lead to easier device and circuit design, an advantage that becomes more significant as frequency climbs. Designers should benefit from the high peak velocity of InP which will allow them to lengthen the active layer and, thereby, stretch the transit-time relationship while maintaining a low bias-to-threshold ratio. Circuit designers are similarly blessed: InP diodes present large negative resistance and small reactance. These factors, combined with relatively low cold capacitance should make it possible to employ larger InP devices (with more power capability than their GaAs counterparts) to diminish power-combining challenges.

The advantages of InP over GaAs can be seen in the progress of current research and development programs directed to applications below 60 GHz. Based on lessons learned in the design of conventional diodes (such as those for intruder alarms at 10 GHz, klystron replacements for marine radar, ECM components, C- and Ku-band radar systems, and paramp pumps for the 25-to-50-GHz spectrum), several characteristics of InP Gunn sources, which are outlined in the following paragraphs, can be predicted.

InP Gunn oscillators will provide higher power than GaAs alternatives through 100 GHz—and low-noise medium-power operation beyond 150 GHz. Indium phosphide can improve pulsed systems, since it has demonstrated 1-W output with a 10-percent duty factor at 94 GHz, and 3-W output with a 10-percent duty factor at 60 GHz. The higher duty cycle permitted by InP Gunn devices might improve tracking and target acquisition radars in the millimeter-wave region, and the high spectral purity of InP devices should contribute to the development of coherent NMMW systems.

InP-diode oscillators are two to three times more efficient with higher peak powers than GaAs sources, and can reduce input power requirements.[3] Reduced internal transient heating is an important side effect of this low input power requirement of InP. As a result, chirp (the frequency drift caused by a device heating during a pulse) tends to be lower, duty cycle can be expanded, and chirp-reducing techniques made more effective. In fact, high-Q stabilizing resonators have reduced chirp by a factor of 20 in InP Gunn diode waveguide circuits in the 10-to-20-GHz range. As

(text continued on p. 80)

Transmission windows above 100 GHz

Wavelength (mm)	Frequency (GHz)	Horizontal attenuation(dB/km)	Zenith attenuation (dB)
3.0	100	0.30	1.25
2.1	143	0.50	0.91
1.3	231	1.75	2.10
0.88	341	9.00	9.90
0.72	417	17.00	22.00

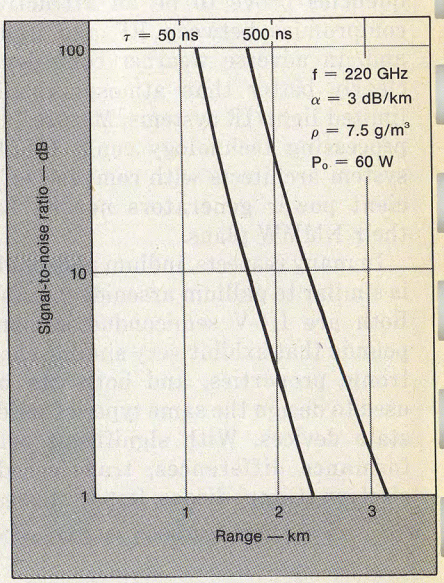
ADVERSE WEATHER...

(continued from p. 77)

under adverse atmospheric conditions.[5]

Transmission in bad weather improves considerably as wavelength grows longer. Ideally, a centimeter wavelength would be best for a radar, seeker, or link under these circumstances. Accuracy requirements, however, often eliminate this region. For example, the required accuracy for target tracking or designation usually falls within the range of 0.1 to 0.5 mrad, calling for antenna diameters of 0.5 to 1.0 m for millimeter wavelengths, and 5 to 10 m for centimeter wavelengths. The advantage of higher-frequency systems for vehicle- or aircraft-mounted weapon systems is obvious.

Several disadvantages of NMMW systems should diminish as technology progresses, but the effect of the atmosphere should remain a limiting factor for systems applications. Because of strong absorption by water vapor and oxygen, the performance of a NMMW system is governed by the moisture, smoke, or aerosols present in the atmosphere according to $e^{\alpha}R$ (where α is the atmospheric attenuation and R is the target range). The table lists the clear-weather transmission windows available for tactical ground-to-ground or ground-to-air applications. Horizontal values are based on

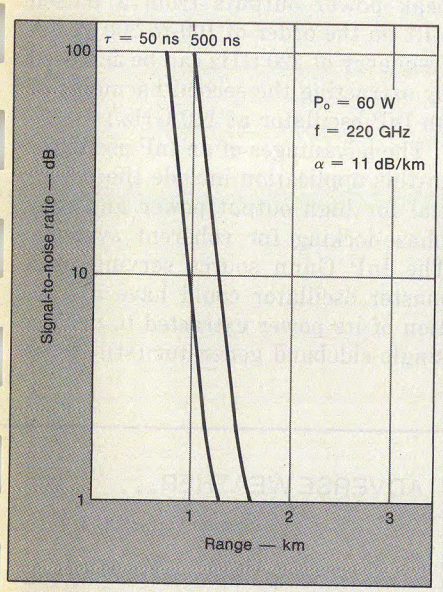


2. Long- and short-pulse systems behave differently; *atmospheric conditions are warm and dry for this link at 220 GHz.*

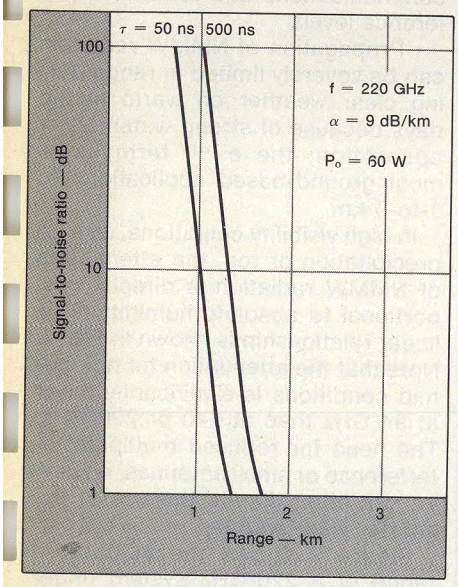
a water concentration of 5.91 g/m^3 at sea level (290°K), while zenith listings assume 7.5 g/m^3. Four general statements can be made about atmospheric effects:

- Rain attenuation of NMMW radi-

(continued on next page)



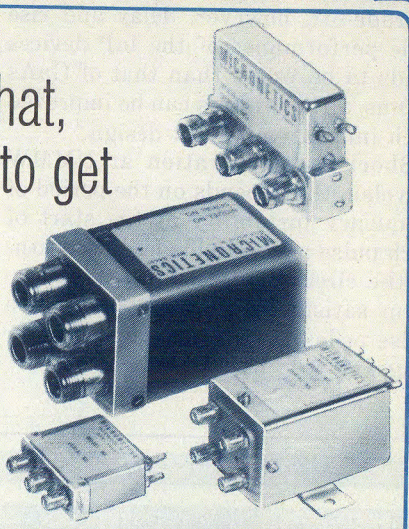
***3. Compare these curves with those of Fig. 2** to see the effect of 100 percent relative humidity, 30-mi-visibility, fog, and 32°F temperature.*



***4. Rain degrades** the performance of a 220-GHz system; in this case, rain rate is 4 mm/hr, relative humidity is 100 percent, and temperature is 68°F.*

Puzzled about what, where, and how to get

Coaxial Switches?



Make Micronetics your dependable source for quality and fast delivery!*

High Frequency SPDT Switch DC-18 GHz RSM Series

Model	Operating Voltage**	Mode
RSM-2-D	28V DC	Failsafe
RSM-2-D-TTL	28V DC	Failsafe TTL
RSM-2-A	115V AC	Failsafe
RSM-2-D-L	28V DC	Latching
RSM-2-D-L-TTL	28V DC	Latching TTL

High Power SPDT Switch DC-12.4 GHz RSN Series

Model	Operating Voltage**	Mode
RSN2-D	28V DC	Failsafe
RSN2-D-TTL	28V DC	Failsafe TTL
RSN2-A	115V AC	Failsafe
RSN2-D-L	28V DC	Latching
RSN2-D-L-TTL	28V DC	Latching TTL

High Frequency Transfer Switch DC-18 GHz RSTM Series

Model	Operating Voltage**	Mode
RSTM-D	28V DC	Failsafe
RSTM-D-TTL	28V DC	Failsafe TTL
RSTM-A	115V AC	Failsafe
RSTM-D-L	28V DC	Latching
RSTM-D-L-TTL	28V DC	Latching TTL

Life: 1,000,000 cycles Min. Indicator: Optional

**Most types are now available off the shelf.*

***Operating voltages as low as 10V DC are also available.*

Write or call for additional information.

micronetics inc.

36 Oak Street · Norwood · NJ · 07648

(201) 767-1320 twx: 710-991-9603

READER SERVICE NUMBER 40

InP: A PROMISING MATERIAL *(continued from p. 79)*

a trade-off, however, delay and rise time performance of the InP devices tends to be worse than that of GaAs Gunns, although this can be improved with innovative circuit design.[3]

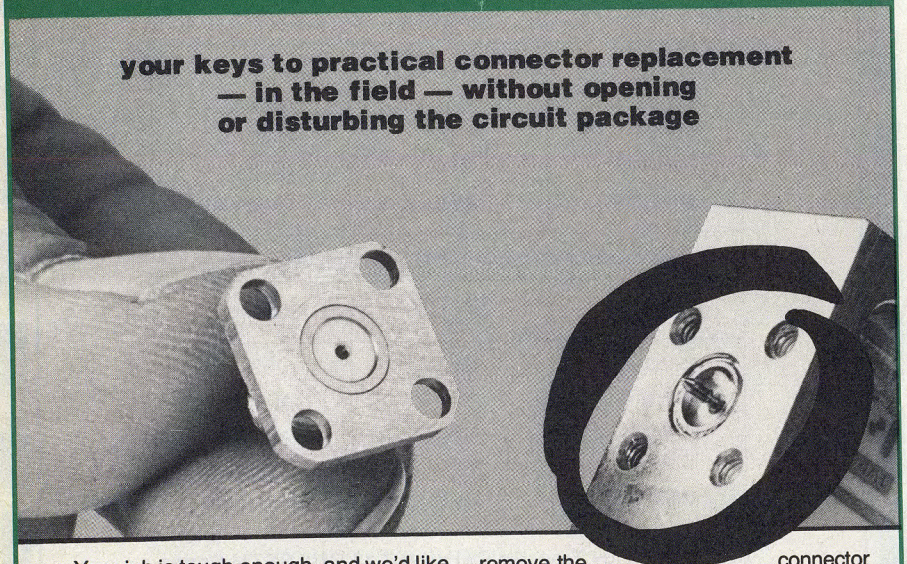
Short-pulse operation at NMMW wavelengths depends on the period of frequency instability at the start of each pulse as the fields build up within the circuit. InP-diode sources perform satisfactorily when they use a pulse pedestal approach in the driver stage.

One particularly exciting development involves InP as an image-line, self-mixing Gunn oscillator that will have many applications in three areas: fuzing;[4] very short-range, high-resolution tracking; and short-range remote sensing systems. The integration of image-line technology could provide the small, compact devices required for these uses.

Another application for InP Gunn oscillators is in 50-to-100-W transmitters operating between 100 and 300 GHz. It's interesting to note that the contribution of the solid-state source might depend on its synergy with the new breed of extended-interaction amplifiers (EIA). The EIA can provide 33-dB gain with 1-to-2 kW peak power outputs at 94 GHz. This gain should extend into the 220-GHz atmospheric windows. If a power combining technique could provide 50-mW CW power from InP Gunn oscillators at 220 GHz, one could expect peak power outputs from a pulsed EIA on the order of 100-to-200 W. (A frequency of 220 GHz can be achieved by extracting the second harmonic of an InP oscillator at 110 GHz.)

The advantages of an InP oscillator in this application include the potential for high output power and easy phase-locking for coherent systems. The InP Gunn source serving as a master oscillator could have a fraction of its power extracted to drive a single-sideband generator (still to be

Interchangeable transition pins:



Your job is tough enough, and we'd like to help. What better way than with our interchangeable transition pin connectors. The pins slip-fit into the connector and are soldered to the circuit. So you can remove the connector without disturbing the circuit contact. And that means in-the-field connector replacement is a sweetheart instead of a heartache. *Even on hermetic packages.*

And if that one advantage isn't enough to make life easier, we've got four more for you. *Our SMA flange connectors with interchangeable pins also:*

- *Increase package design options*
- *Assure mechanical integrity for improved electrical performance*
- *Simplify testing procedures*
- *Reduce inventory costs*

Of course these connectors meet all applicable specifications of MIL-C-39012. We'd like to say a lot more about these unique connectors. About their simplicity, practicality and economy. And if you'd care to listen, get in touch soon for full technical details or applications assistance.

EMC TECHNOLOGY, INC.
1971 OLD CUTHBERT ROAD
CHERRY HILL, NEW JERSEY 08034
Phone: (609) 429-7800 • TWX: 710-896-0193

Authorized distributors and technical sales representatives in all major metropolitan areas.

EMC TECHNOLOGY is a full line MIC product manufacturer. Our products include SMA connectors, terminations, attenuators, resistors and DC blocks for stripline, microstrip and SMA coax.

READER SERVICE NUMBER 22

ADVERSE WEATHER...

(continued from p. 79)

ation is comparable to rain attenuation in the IR region.

- Propagation of NMMW radiation through cloud, fog, smoke, and battlefield aerosols is superior to that in the visible/IR regions.
- Strong absorption in the windows listed in the table allows for covert communications and reduced interference levels.
- Propagation of NMMW radiation can be severely limited in range during clear weather on warm humid days because of strong water-vapor absorption; the $e^{-\alpha R}$ term limits most ground-based applications to 1-to-3 km.

In high visibility conditions, with no precipitation or fog, the attenuation of NMMW radiation is directly proportional to absolute humidity. This linear relationship is shown in Fig. 1. Note that the attenuation for hot, humid conditions is significantly lower at 94 GHz than at 140 or 220 GHz. The need for reduced multipath interference or small antennas, however, will often dictate the use of the shorter wavelengths.

Figure 2 shows the calculated range of a 220-GHz system under warm, dry conditions. The peak power of 60 W corresponds to the output of the extended interaction oscillators (EIO) at 220 GHz. The two

developed in this frequency range) to serve as the local oscillator for a subharmonic receiver. One stabilized InP Gunn oscillator combined with an EIA amplifier might provide all the NMMW power required for both the system's transmitter and receiver.

The InP Gunn oscillator and EIA offer several interesting combinations which may further aid systems development:

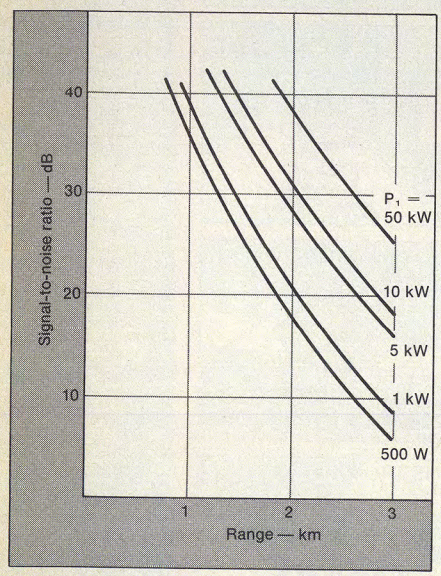
- A pulsed Gunn oscillator, capable of being injection locked, might drive (as a fundamental or doubled signal) a CW EIA to provide a high repetition rate or narrow signal pulses; a suitable EIA must be developed for this scenario.
- A CW Gunn oscillator/pulsed amplifier combination could drive the EIA so that stability can be established by phase locking the CW oscillator. The pulsed Gunn amplifier would give greater peak drive power for the EIA.
- The pulsed EIA can be driven by an injection-locked, pulsed InP Gunn oscillator.

InP Gunn diodes can also be used in low-noise amplifier circuits. At twice threshold, the hot-electron diffusion coefficient of InP is much lower than that of GaAs—indicating a lower noise measure for the former material (computations and experiments point to an advantage of 4 or 6 dB).

A brief survey of reported results illustrates the promise of the InP amplifier. In one program, Gunn-effect devices were developed for noise figures in the 7-to-9-dB range, with associated gains of 5-to-8-dB between 25 and 60 GHz. Reflection-type amplifiers built with notch diodes yielded noise figures of 7 or 8 dB at 36 GHz, with an instantaneous bandwidth of 4 GHz and dynamic range as large as 90 dB for linear amplification. In terms of bandwidth, full Ka-band coverage has been demonstrated with a single diode, and 18-dB gain with two half-

(concluded on p. 84)

curves show that, for short pulses, ranges of 2-to-3 km are possible for low signal-to-noise ratio (S/N); the calculations were performed for single pulse operation so that signal processing will increase the S/N when it is included. Figures 3 and 4 show how range is regraded for 30-m-visibility fog and a 4-mm/hr rainfall.[6]

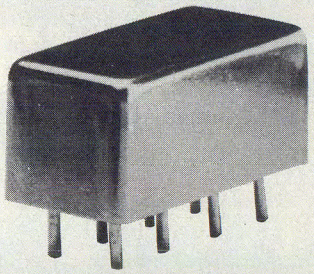


***5. Increased power does not significantly increase range** for a 220-GHz system in warm, humid conditions (T = 30°C; relative humidity = 80 percent).*

Figure 5 demonstrates the range as a function of transmitter power. Power does not significantly increase the range of the system, doubling the transmitter power for a given S/R only increases the range by about 10 percent under clear, dry conditions—and even less in more severe weather.

What does this mean for indium phosphide? It can be concluded that, at NMMW wavelengths, the operating range for ground-based systems is between 1 and 3 km, depending upon the atmospheric conditions, and that increasing transmitter power does not produce large range increases. The power requirements exceed the capabilities of solid-state devices, but recent developments in tube amplifiers (EIAs) offer the potential of using a solid-state driver. Thus, InP may contribute toward providing sufficient power with improved capability for a totally coherent system. The coherent system would provide an increase in the signal integration by a factor of n (n = the number of pulses integrated). In addition, a S/N increase is possible resulting from potential receiver improvements with an InP local oscillator. ●●

ultra hi-level mixers
(+27 dBm LO)



.05 to 500 MHz
only $74.95 (1-9)

IN STOCK . . . IMMEDIATE DELIVERY

- **low distortion, +38 dBm intercept point, (two-tone, 3rd order)**
- up to +24 dBm RF input
- low conversion loss, 6 dB
- hi isolation, 40 dB
- miniature 0.4 x 0.8 x 0.4 in.
- hermetically-sealed
- MIL-M-28837/1A performance*
- one year guarantee

*Units are not QPL listed

VAY-1 SPECIFICATIONS

FREQUENCY RANGE, (MHz)			
LO-RF		0.05-500	
IF		0.02-500	
CONVERSION LOSS, dB		TYP.	MAX.
One octave from band edge		6.0	7.5
Total range		7.5	8.5
ISOLATION, dB		TYP.	MIN.
low range	LO-RF	47	40
	LO-IF	47	40
mid range	LO-RF	46	35
	LO-IF	46	35
upper range	LO-RF	35	25
	LO-IF	35	25

SIGNAL 1 dB Compression level +24 dBm Typ.

For other Mini-Circuits Lab products see ads on p. 1, 2, 3, 32, 33, 46

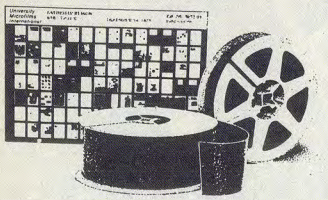
finding new ways . . .
setting higher standards

Mini-Circuits
A Division of Scientific Components Corporation
World's largest manufacturer of Double Balanced Mixers
2625 E. 14th St. B'klyn, N.Y. 11235 (212) 769-0200

C74-3 REV. B

READER SERVICE NUMBER 43

MICROWAVES is available in microform



Please send me additional information.

University Microfilms International

300 North Zeeb Road
Dept. P.R.
Ann Arbor, MI 48106
U.S.A.

18 Bedford Row
Dept. P.R.
London, WC1R 4EJ
England

Name _____

Institution _____

Street _____

City _____

State _____ Zip _____

band stages has been reported in the 30-to-40-GHz region. The limiting factor appears to be the bandwidth of the circulator required for the negative-resistance amplifier circuit.

InP can also be expected to develop as a material for high-peak-power Impatt oscillators, with good spectral purity, high efficiency, and low noise in the millimeter-wavelength region. A comparison of the efficiency of InP Impatts with that of other types indicates that the optimum projected profile for InP exceeds that of GaAs and Si to the region of 90 GHz, after which it continues to exceed GaAs but falls slightly below Si. (InP Impatts may never be competitive with Si diodes above 100 GHz.)

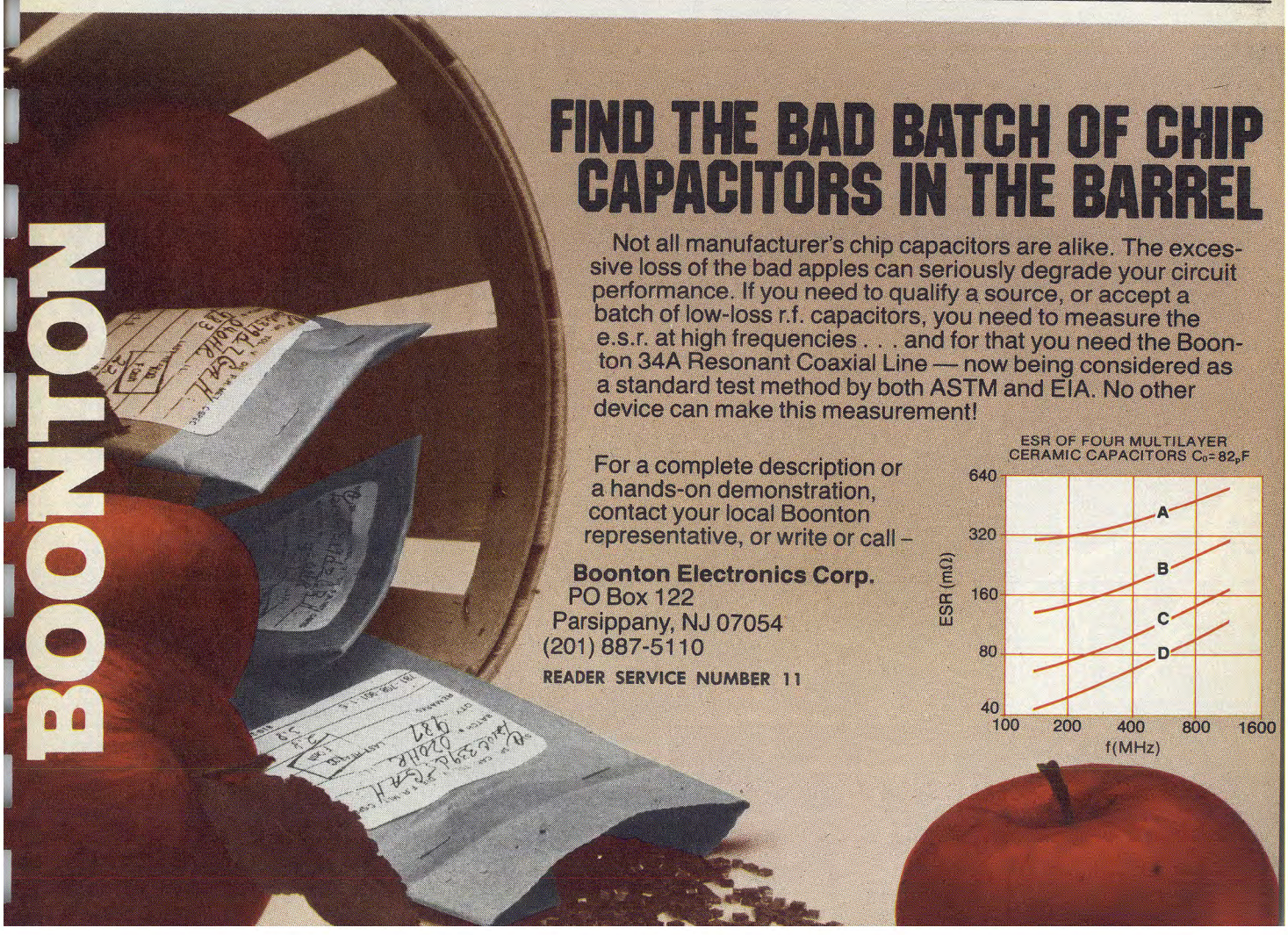
Although InP promises to expand transistor circuits to higher frequencies, GaAs offers high standards for InP to exceed. Plessey, for instance, has reported a 3.5-dB noise figure at 18 GHz for a GaAs device. Still, designers are discovering subtle advantages of the newer material. Indium phosphide FETs have larger geometries for a given frequency. Thus, while a GaAs FET needs a submicron gate length at 12 GHz, an InP FET could have a gate length greater than 1 μm. InP FETs should also offer improved gain above 10 GHz.●●

Acknowledgement

This article is based on a longer paper given at the NATO-sponsored InP Workshop which occurred under the auspices of the Rome Air Development Center (AFSC), Deputy for Electronic Technology, Hanscom AFB, MA 01731 (June 1980).

References

1. J.J. Gallagher, R.W. McMillan, and R.G. Shackelford, "Military Applications at Near-Millimeter Wavelengths," *Proceedings of the Society of Photooptical Instrumentation Engineers*, Vol. 197, pp. 170-190 (August 1979).
2. F.B. Fank, J.D. Crowley, and J.J. Berenz, "InP Material and Device Development for mm-Waves," *Microwave Journal*, pp. 86-91 (June 1979).
3. F.A. Myers, "Efficient InP Gunn Diodes Shrink Power Requirements," *MicroWaves*, Vol. 19, No.5, pp. 80-85 (May 1980).
4. S. Dixon and H. Jacobs, "Millimeter-Wave InP Image Line Self-Mixing Gunn Oscillator," presented at The Fifth International Conference on Infrared and Millimeter Waves, Wurzburg, Germany, October 6-10, 1980.
5. S.M. Kulpa and E.A. Brown,"Propagation and Target/Background Characteristics," *Near Millimeter Wave Technology Base Study, Vol. 1*, Report No. HDL-SR-79-8, Harry Diamond Laboratories (1978).
6. R.W. McMillan, R.E. Forsythe, R.A. Bohlander, R.G. Shackelford, R.N. Trebits, and W.A. Holm, "Near Millimeter Wave Radar Technology," Georgia Institute of Technology, Contract No. DAAK70-79-C-0108 (January 11, 1980).



FIND THE BAD BATCH OF CHIP CAPACITORS IN THE BARREL

Not all manufacturer's chip capacitors are alike. The excessive loss of the bad apples can seriously degrade your circuit performance. If you need to qualify a source, or accept a batch of low-loss r.f. capacitors, you need to measure the e.s.r. at high frequencies . . . and for that you need the Boonton 34A Resonant Coaxial Line — now being considered as a standard test method by both ASTM and EIA. No other device can make this measurement!

For a complete description or a hands-on demonstration, contact your local Boonton representative, or write or call –

Boonton Electronics Corp.
PO Box 122
Parsippany, NJ 07054
(201) 887-5110

READER SERVICE NUMBER 11

MICROWAVES
laser technology
A Hayden Publication

March 1982
Vol. 21, No. 3

news

15 Advanced Westar: NASA and Western Union ready an orbiting giant
17 LNA sales skyrocket as prices plummet
26 Kevlin cited for excellence
28 MARISAT hits 1000 mark in shipboard terminals
28 Martin Marietta completes fiber-optic network
31 Hughes doubles silicon output; relieves reliance on foreign supply
33 Washington
38 Industry
47 International
49 R&D Roundup
53 Meetings
54 For Your Personal Interest

editorial

56 The microwave industry can no longer rest on "glad tydings"

technical

COMMUNICATIONS

59 **Optical And MM-Wave Links Face-Off For The Future.** George D. O'Clock, Jr., C. Hendrickson, and Wayne Schaefer, of Mankato State University (MN), explain why the choice between millimeter-wave and laser optical systems depends on the application.

65 **Discriminator Boosts Phase-Noise Testing.** Fred Labaar of TRW introduces a new design that combines the strengths of delay-line FM discriminators and high-Q cavity discriminators.

77 **Shielded Microstrip Aids V-Band Receiver Designs.** Michael Dydyk and B. David Moore, of Motorola, introduce new substrate materials for use in shielded microstrip transmission lines that yield higher performance, lower cost millimeter-wave integrated circuits.

84 **Harmonic Generators Have High Efficiency.** John W. Archer, of the National Radio Astronomy Observatory, and Bart B. Cregger, Robert J. Mattauch, and James D. Oliver, Jr., of the University of Virginia, show why the increasing availability of high-cutoff frequency Schottky-barrier diodes makes it possible to develop millimeter-wave harmonic generators.

*88G **Military Fiber-Optic Links: Can They Take The Heat?** Antonio N. Paolantonio, an independent consultant, shows that fiber optics likely to encounter nuclear radiation may be no better than wired systems.

91 **GaAs Compounds Promise Lower Noise MESFETs.** Rimantas L. Vaitkus and Tom H. Miers, of Motorola, present two GaAs compounds that promise to improve semiconductor noise performance.

product technology

99 **Use A Waveform Recorder To Simplify VCO Testing.** Douglas Nichols, of Hewlett-Packard, suggests substituting a waveform recorder for an oscilloscope to reduce test time and increase accuracy.

departments

11 Feedback
101 Product Feature
Waveform recorder captures transients
102 Product Feature
Synchronizer system phase locks sources
106 New Products
114 Application Notes
115 New Literature
118 InfoCenter

120 **Looking Back**
A retrospective view of past issues of *MicroWaves*

Foreign only

About the cover: Advanced Westar, one of the four satellites in the joint NASA-Western Union TDRSS program, will surpass the capacity and size of any communications satellite in commercial service. The giant's particulars are given on p. 15. (Cover artwork courtesy of Western Union, Upper Saddle River, NJ.)

coming next month: Radar Technology

In April, *MicroWaves* will scan the radar fields. Design articles will detail the optimum parameters for phased arrays, review pulse compression with low-power, solid-state sources, explain the role of software in reducing system downtime, and extoll the merits of CW radar.

Publisher/Editor
Stacy V. Bearse
Managing Editor
Walter J. Bojsza
Associate Editors
Jack Browne
product technology
Barry Manz
news
Western Editor
Rich Rosen, PE
6043 W. Maplewood Dr.
Littleton, CO 80123
(303) 797-2575
Contributing Editor
Steven March
Washington Editor
Paul Harris
Snyder Associates
1050 Potomac St., N.W.
Washington, DC 20007
(202) 965-3700
European Correspondent
Bill Mitchell
62 Craigwell Ave.
Aylesbury
Buckinghamshire, England
HP21 7AG
(0296) 81529
Editorial Assistant
Tania Tishin
Promotion Manager
Jamie Matusow
Art Director
Janice Moscatelli
Copy/Production Editor
Michael Kachmar
Production Manager
Nick. J. Tartaglia
Circulation
B. Freundlich, Dir.
C. Stump, Sub. Mgr.
P. Greenleaf, Reader Serv.
M. Sassano, Reprints
Market Research
Irene Chervin, Mgr.
Editorial Office
50 Essex St.
Rochelle Park, NJ 07662
Phone (201) 843-0550
TWX 710-990-5071
A Hayden Publication
James S. Mulholland, Jr., President
February Press Run
43,496 copies

MICROWAVES is sent free to individuals actively engaged in microwave work. Prices for nonqualified subscribers:

	1 Yr.	2 Yr.	3 Yr.	Single Copy
US, Canada Mexico, Central America	$30	$48	$72	$3.00
All other countries	$48	$84	$120	$5.00

Additional Product Data Directory reference issues, $20.00 each (US, Canada, Mexico, Central America), $32.00 each (all other countries).

Back Issues of MicroWaves are available on microfilm, microfiche, 16mm or 35mm roll film. They can be ordered from Xerox University Microfilms, 300 North Zeeb Road, Ann Arbor, MI 48106. For immediate information, call (313) 761-4700.

Hayden Publishing Co., Inc., James S. Mulholland, President, printed at Brown Printing Co., Inc., Waseca, MN. Copyright® 1982 Hayden Publishing Co., Inc., all rights reserved.

Optical And MM-Wave Links Face-Off For The Future

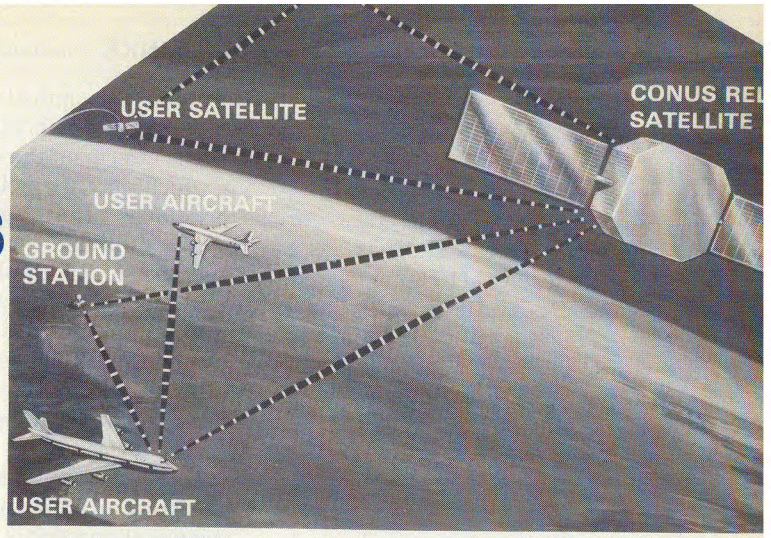


Photo courtesy of McDonnell Douglas Corporation

Millimeter-wave and laser optical systems exhibit specific strengths and weaknesses in satellite and terrestrial communication systems. The ultimate choice depends on the application.

TRADE-OFFS between millimeter-wave and optical communication systems have been evaluated for more than two decades. In both satellite and terrestrial applications, each brings its own set of advantages and disadvantages.[1-4]

The optical system offers the potential for very wide bandwidths, immunity from a wide range of electromagnetic interference (EMI), smaller transmitters and antennas, reduced weight, and a lower probability for interception. However, limiting its performance are modulation restrictions, pointing accuracy, laser lifetimes, and narrow beam widths (which causes signal acquisition and tracking problems).

In contrast, the millimeter-wave system has the advantages of easier acquisition, longer transmitter lifetime, more modulation technique flexibility, and, in some cases, a more advanced development cycle. However, the millimeter-wave system is more susceptible to EMI, and has a higher probability of interception. Production costs also continue to plague millimeter-wave technology, although some cost-reduction progress has been made over the past.

(For a more detailed discussion of the contrast between optical and millimeter-wave communication systems, see "RF and optical system parameters," p. 60.)

George D. O'Clock, Jr., Professor, **C. Hendrickson,** Associate Professor, and **Wayne Schaefer,** Graduate Assistant, Dept. of Physics and Electronic Engineering Technology, Mankato State University, Mankato, MN 56001.

Transmitter options

Transmitter candidates for millimeter-wave links include the traveling-wave tube (TWT) and the Impatt diode. If an application calls for transmitter output power significantly in excess of 1 W, the TWT is often the best choice. However, satellite applications which demand low-voltage operation and high transmitter lifetimes favor the

(continued on next page)

Table 1: Partial listing of semiconductor laser candidates

Material	Wavelength (μm)	CW output at 300°K (mW)	Lifetime (hrs)
GaAs	≈0.9	≤50	10^3-10^4
GaAs/GaAlAs	0.78-0.94	≤20	10^4-10^5
InP/InGaAsP	1.0-1.6	≈5	5×10^3-10^4
InGaAs	1.0-4.0	—	$\approx10^3$
PbSnTe	6.5-13.5	—	$\leq10^3$

Table 2: Millimeter-wave and optical systems comparative link analyses

	60-GHz link	10-μm CO_2 laser	1-μm GaAs/GaAlAs DH laser
Transmitter power	0 dBW	0 dBW	−17 dBW
Transmitter losses	1.4 dB	1.5 dB	1.5 dB
Transmitter antenna/ aperture gain	49.0 dBi	96.0 dBi[d]	115.6 dBi[d]
Pointing loss	0.5 dB	1.5 dB	3.0 dB
Propagation loss (44,000 nmi)	225.5 dB	280.0 dB	300.0 dB
Conical scan loss	—	1.0 dB	2.0 dB
Receiver antenna/ aperture gain	49.0 dBi[b]	96.0 dBi[d]	115.6 dBi[d]
Receiver tracking and polarization losses	1.0 dB	—	—
Receiver losses	3.0 dB	1.0 dB	1.0 dB
Total received power	−133.4 dBW	−93.0 dBW	−93.3 dBW
Noise power (P_n)	−149.4 dBW[c]	−133.3 dBW[e]	−109.3 dBW[e]
Signal-to-noise ratio[a]	16.0 dB	40.0 dB	16.0 dB

[a] Atmospheric losses, thermal defocusing, and modulation/demodulation losses not considered.
[b] Two-foot diameter reflector, 55-percent efficiency.
[c] $P_n = kT_{eff}B$ [k = Boltzmann's constant; T_{eff} = effective receiver front-end temperature (assuming 8-dB noise figure for mixer/preamp, 160°K for antenna and receiver noise, 130°K for LO leakage, AM/PM conversion, and transmitter noise); and B = bandwidth (40 kHz to account for data and Doppler shift)].
[d] Aperture diameter = 24.6 cm, 80-percent efficiency.
[e] $P_n = (\eta/2hf)B$[h = Planck's constant; η = quantum efficiency; f = frequency; and B = bandwidth (500 kHz for data and Doppler shift)].

solid-state Impatt. (See "Impatt diode: structure is the key to future improvements," p. 61.)

Optical transmitters may come from the ranks of gas, solid-state, or semiconductor lasers. The gas laser family includes CO_2(10.6-μm wavelength) and He-Ne (0.63 μm). Solid-state lasers include ruby (0.69 μm) and Nd:YAG (1.06 μm). Semiconductor lasers offer a wide variety of wavelengths, output power, and lifetime options (Table 1).[5,6,7]

Although some semiconductor laser structures can achieve higher output powers than those shown in Table 1, they do so at the expense of higher beam divergence and astigmatism. (See "Semiconductor laser research aims for better system performance," p. 62.)

Aside from the obvious contrast between the optical and millimeter-wave device, each alternative has intrinsic effects on the design of systems in which they are included. Modulation techniques offer one example.

In a millimeter-wave system, various types of RF amplitude modulation can be achieved by using the nonlinear properties of diodes and transistors. Frequency and phase modulation require frequency dispersive or phase-delay elements along with the nonlinear devices.

Optical modulators can use the birefringent properties of certain electrooptical materials such as $LiNbO_3$, $LiTaO_3$, KDP and $Ba_2NaNb_5O_{15}$. In these cases, an RF field applied across the electrooptic crystal causes the polarization of the incident light beam to rotate. Optical modulation can also be obtained by applying an electric field to certain electrooptic materials. Often, electrooptic modulators require high voltages ($\geq$ 1 kV) to achieve a significant modulation depth or a high percentage modulation.

Many of these electrooptic materials are also piezoelectric and allow certain types of modulation to be obtained through the acoustooptic effect.

Various forms of pulse modulation (amplitude, position, and code) can be applied to an optical communication system, as well as standard amplitude modulation, frequency modulation, and frequency-shift keying (FSK). Practical problems exist for optical phase-shift key modulation (PSK), although work has been initiated with differential phase-shift keying (DPSK).[8,9]

Table 2 provides link analyses for a millimeter-wave and an optical com-

RF and optical system parameters

An understanding of the following system parameters will assist in comparing millimeter-wave and optical communication systems.

Frequency. Although higher frequencies (shorter wavelengths) help reduce system size and weight, the higher frequencies also increase acquisition and tracking problems. For example, a 1-μm-wavelength optical receiver will have a field of view (FOV) of less than 5-μrad. A spacecraft can be stabilized to approximately $\pm$ 1.75 mrad.[1] Under these conditions, the spacecraft instability represents approximately 700 optical beam widths.

Noise. The minimum noise power (P_n) in a heterodyne receiver is given by the fundamental expression:[1–11]

$$\frac{P_n}{B} = \frac{hf}{(e^{hf/kT} - 1)} + hf/\eta \qquad (1)$$

In Eq. 1, B = the receiver bandwidth, h = Planck's constant, f = frequency, k = Boltzmann's constant, and T = temperature. The quantum efficiency (η) indicates the number of usable charge carriers generated by incoming photon energy.

The exponential term in Eq. 1 can be expanded to the series:

$$e^{hf/kT} = 1 + hf/kT + \left(\frac{hf}{kT}\right)^2/2! + \left(\frac{hr}{kT}\right)^3/3! + \ldots \qquad (2)$$

For frequencies up to 600-GHz, the ratios hf/kT become quite small. Therefore:

$$e^{hf/kT} \approx 1 + hf/kT \qquad (3)$$

and:

$$P_n \approx KTB, \text{ (for } f \leq 600\ GH_z) \qquad (4)$$

Eq. 4 is the familiar RF noise power expression derived from conventional thermal noise concepts.

The RF heterodyne receiver sensitivity will be determined, in part, by the output power of the local oscillator and the effective temperature of the front end (including the effects of ambient temperature, receiver noise figure, mismatches, and external noise sources).

At optical frequencies, the exponential term in Eq. 1 becomes very large, and the entire first portion of the noise expression approaches zero, leaving:

$$P_n \approx \frac{hf}{n} B \qquad (5)$$

Eq. 5 is the general expression for noise power in an optical system.

The sensitivity of the optical heterodyne receiver is determined by the quantum efficiency, bandwidth, local oscillator output power, and the type of photomixer, photodiode, or photomultiplier used in the receiver front end. Photo detectors often require cooling to reduce the effects of the diode dark (reverse) current. A temperature increase of 25°C can increase the diode dark current by a factor of 10.

Antenna gain. Antenna gain (G) can be a misleading term. It is not a power gain, but a parameter that compares the directional properties of an antenna to a nondirectional isotropic or omnidirectional antenna.[1,3] Antenna gain, therefore, measures the ability of the antenna to direct the propagating electromagnetic energy along a specified path, and is given by the following expression (for both RF and optical systems):

$$G = \frac{4\pi A}{\lambda^2} \eta_A \qquad (6)$$

In Eq. 1, B = the receiver bandwidth, h = Planck's constant, f = frequency, k = Boltzmann's constant, The antenna efficiency (η_A) includes the losses from I^2R, polarization, spillover, blockage, mismatch, structural distortion, tolerance deviations, etc.

Propagation loss. The term propagation loss (P_L) can also be misleading since it represents a decrease in the power density (W/m^2) of a propagating electromagnetic wave, rather than a dissipative power loss. P_L is a function of distance or propagation time, and is given by the expression:

$$P_L = [37.8 + 20\ Log\ r + 20\ Log\ f] \qquad (7)$$

In Eq. 7, r = the distance (nmi) between the transmitter and the receiver, and f = the carrier frequency (MHz).••

munications system. The comparison between the laser and the millimeter-wave systems indicates that the received signal-to-noise ratio is adequate for communications in either case. However, the tracking capabilities of the laser optical system are marginal.

The field of view (FOV) of the 24-cm aperture at a 1-μm wavelength is approximately 5 μrad. If a satellite stability of ± 0.1 degrees (± 1.75 mrad) is considered, tracking becomes significantly difficult for a simple 1-μm optical receiver. Although beam defocusing can overcome this limitation by increasing the beam width, it does so at the expense of the signal-to-noise ratio.

A higher power gas laser with a longer wavelength could replace the lower power semiconductor laser in the above example. A wide beam-width millimeter-wave system can help to reduce the acquisition and tracking problems. Some studies have proposed hybrid systems that would combine millimeter-wave components (for acquisition and coarse tracking) with optical components (for secure, relatively interference-free communications and fine tracking).[2]

The MTBF of a semiconductor source is, of course, a vital planning statistic. However, a direct comparison between the MTBF of a semiconductor laser and that of a millimeter-wave Impatt diode can be like comparing apples and oranges. The laser and the diode operate at very different output power and prime-power levels.

Ideally, the high directivity of the optical communications system allows a much lower output for the optical transmitter (i.e., the laser). In fact, if acquisition, pointing, Doppler, and atmospheric-loss limitations are ignored, the semiconductor laser could have an output power that is fifty times lower than the millimeter-wave Impatt.

(continued on next page)

Impatt diode: structure is the key to future performance

The maximum device power density for an Impatt diode ($\rho r_{RF(MAX)}$) can be expressed as:

$$\rho_{RF(MAX)} = 2\eta_c v_s E_c^2 \quad (8)$$

In Eq. 8, η_c = the DC-to-RF conversion efficiency, v_s = the scattering-limited velocity, and E_c = the electric field.

According to Eq. 8, the maximum power density for an Impatt diode at a given DC-to-RF efficiency should ideally depend only upon material parameters and not on operating frequency.[12] In reality, size and thermal constraints impose practical limitations which cause the maximum power density to decrease as frequency increases.

Fig. 1 shows the equivalent circuit for an Impatt diode. The reactances in this model—C_{jB}, the depletion layer junction capacitance at breakdown, and L_D, the avalanche inductance (which accounts for carriers in the depletion layer)—can be derived from the relationship:

$$(2\pi f_A)^2 \approx 1/L_D C_{JB} \quad (9)$$

In Eq. 9, f_A is the avalanche frequency defined as:

$$f_A = v_s/2W \quad (10)$$

Equation 10 shows the dependence of the two equivalent circuit reactances on the depletion layer width (W).

The output power of the device (ignoring the effect of L_D) can be found from the expression:

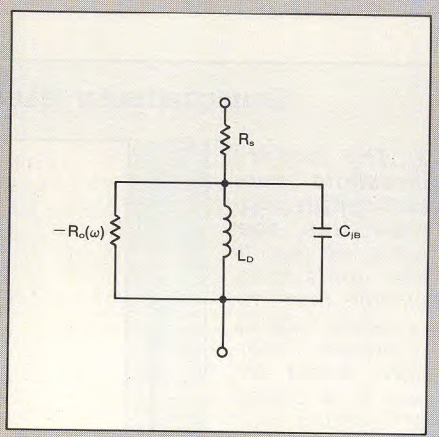
$$P_o \approx V_o^2/4\left[1/R_D(\omega) - R_s/R_D(\omega) - \omega^2 C_{JB}^2 R_s\right] \quad (11)$$

In Eq. 11, V_o = the applied voltage, R_s = the fixed equivalent series resistance of the diode, and $-R_D(\omega)$ = the frequency-dependent negative resistance.

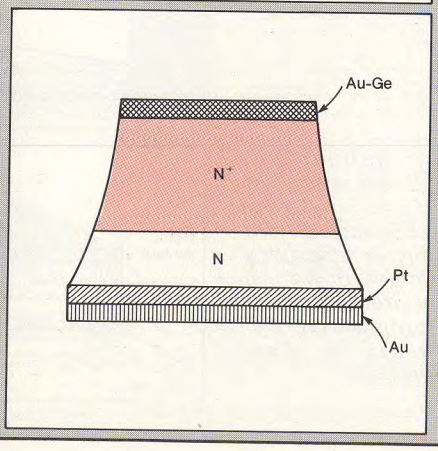
The above relationships show that improved Impatt performance will depend upon refinements to the structure of the device (Fig. 2). High quality thin-film layers and contacts can lower the value of R_s and produce higher efficiencies and output power. In addition, more precise control of device structure and the fabrication of more abrupt doping profiles will help reduce L_D, which can limit output frequency, efficiency, and yield.

Impatt development continues to emphasize the incorporation of materials and structures that allow efficient heat removal from the active portion of the device—one of the diode's most perplexing problems. Since Impatts operate under high DC-power conditions, CW output power for a single double-drift silicon Impatt at 60 GHz is limited to approximately 1.5 W at 8-to-10-percent efficiency.[13] The remaining power is converted to heat and must be removed.

Solving the heat problem involves the application of special heat-sink materials (metallized BeO, diamond/copper combinations, and silver) along with the fabrication of thin device structures which promote efficient heat transfer between the semiconductor chip and the heat sink.••



1. The equivalent circuit for an Impatt diode *shows C_{jB}, the depletion layer junction capacitance at breakdown; L_D, the avalanche inductance; R_s, the equivalent series resistance; and $-R_D(\omega)$, the frequency-dependent negative resistance.*



2. The profile of a GaAs Schottky-barrier Impatt *shows the structure that must be improved to upgrade the diode's performance. Thin-film layers and high quality contacts can lower R_s, and better control of the structure and doping profile will help increase f_A.*

COMPARING OPTICAL AND MM-WAVE LINKS *(continued from p. 61)*

In this example, a 20-mW (CW) semiconductor laser—with a prime power requirement below 0.5 W, a current density under 3.5×10^3 A/cm², and junction temperatures less than 150°C—is being compared with a 1-W millimeter-wave Impatt diode operating under 10-W prime power, an approximate 50×10^3-A/cm² current density, and a 250°C junction temperature.

Similar mechanisms can cause the failure of either semiconductor device: contact metal migration, impurity migration, and defect migration. All of these occur under the influence of high temperatures, high electric fields, and mechanical stress.

Certain defects propagating into the active region of the laser can cause reductions in the internal quantum efficiency, and can increase optical losses. As a result, threshold current variations occur that cause large changes in optical power output.

Although the 20-mW semiconductor laser is very sensitive to a wide variety of failure mechanisms, lifetimes for these devices now range from 10,000 hrs to 50,000 hrs under normal operating conditions. The 1-W millimeter-wave Impatt diode, which is subject to the same failure mechanisms, has lifetimes in the 50,000-to-100,000-hr range.

The higher power, solid-state, and gas laser lifetimes are often in the 5,000-to-15,000-hr range. The seals and impurities in the gas-discharge tube limit the lifetime of the gas laser. The solid-state laser lifetime is limited primarily by the flash lamp.

Doppler shift and performance

The Doppler shift, another frequency/wavelength-dependent constraint, must also be evaluated for its effect on the performance of the systems. The Doppler-frequency shift (Δf) is given by the expression:

$$\Delta f = \frac{f_o V_r}{c}$$

In the equation above, f_o = the frequency, c = the velocity of light, and V_r = the relative velocity between the transmitter and receiver.

If the transmitter and receiver are nearly stationary with respect to one another, the Doppler shift will be minimal. However, the relative velocities in certain applications (e.g., low-earth-orbiting satellites and satellite-to-satellite transmission) can approach 7.8 km/s.[1] At 1-μm wavelengths, the Doppler-frequency shift could exceed 7 GHz and would extend far beyond the bandwidth of most optical photomixers used in heterodyne receivers.

Under these circumstances, a 10-μm wavelength system would be more acceptable, since the Doppler-frequency shift would be less than 1 GHz. The Doppler shift associated with a millimeter-wave system would drop to below 10 MHz.

Distance favors guided optics

In comparisons between fiber-optic and millimeter-wave guided systems for terrestrial applications, the fiber-optic system displays significant advantages for transmitter-receiver distances exceeding 75 ft. Millimeter-wave guided systems have some advantages for shorter distances because of the 10-dB or greater coupling loss experienced with optical fiber.

Dispersive losses limit the bandwidth and, therefore, the information-carrying capacity of optical fiber. Although the development of 1-km fiber-optic links with bandwidths up to several gigabits continues, commercially available fibers are normally limited to 50-Mbit bandwidths.

For long distances, the low attenuation of the various optical fibers available for 1-μm wavelengths (ranging from 0.0003 dB/ft to 0.002 dB/ft) offers significant advantages over a WR-15 waveguide (approximately 0.3 to 0.4 dB/ft at 60 GHz). In addition,

Semiconductor laser research aims fo

Satellite optical systems, which have been discussed and analyzed since the early 1960s, offer system designers the possibility of extremely high data rates and increased operating distances. These advantages, together with the security offered by the highly directional laser signal, and its relative immunity to RF interference, have offered the incentives for both military and commercial investigation and investment.

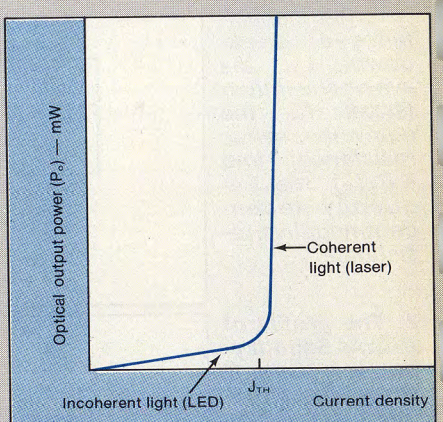
Semiconductor laser component performance constraints can be analyzed by examination of the following expressions for the structurally dependent current density (J), and the laser-threshold current density (J_{TH}) shown in Fig. 3:

$$J \approx dqn/\tau \qquad (12)$$

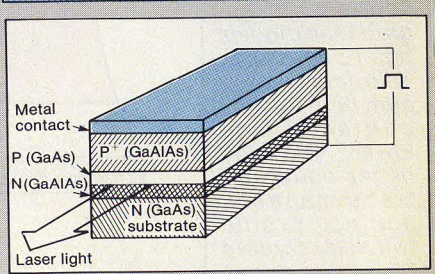
$$J_{TH} = \frac{8\pi q n^2 d \nu^2 \Delta\nu}{\eta_q c^2}\left[\alpha + \frac{1}{L}\ln\left(\frac{1}{R}\right)\right] \qquad (13)$$

In these expressions (which apply for 0°K), d = the thickness of the active layer, η = the refractive index, τ = carrier lifetime, υ = frequency, $\Delta\upsilon$ = line width at half intensity, η_q = quantum efficiency (the fraction of excitation that produces radiation), α = loss/unit length (free carrier absorption and defect center scattering), L = cavity length, R = the reflectivity at the ends of the cavity, q = the electron charge, and c = the speed of light.

3. The laser-threshold current density, J_{TH}, *identifies the point at which the emissions change from incoherent light to coherent laser light. Some research is aimed at lowering J_{TH}.*



4. Refinements to the semiconductor laser structure *will improve efficiency, lower power requirements, and promote more efficient heat transfer.*



the fiber-optic cable has cost advantages over an RF waveguide.

Application dictates choice

As the information presented here shows, the choice between optical and millimeter-wave communication systems depends upon the intended application. For example, the present state of the art favors millimeter-wave technology for satellite-to-satellite links, but earth-satellite transmissions benefit from the interference rejection and low interception probability offered by an optical system using a gas or solid-state laser transmitter. The exact performance of the laser optical system depends upon the selection of a wavelength that overcomes atmospheric and weather-related attenuation. Also the acquisition and tracking performance of the laser optical system will depend on wavelength and laser output power.

Relatively wide (1-GHz) bandwidths can be achieved for satellite coverage of three to six ground stations at millimeter-wave frequencies (40 to 50 GHz).[10]

For terrestrial applications, semiconductor lasers with low prime power requirements and improved lifetimes can be used in fiber-optic systems. A fiber-optic link can have important cost and interference-rejection advantages over a millimeter-wave system that uses either a waveguide or conventional RF transmission.••

Acknowledgments

The authors wish to acknowledge previous discussions with D.V. Haffner, Rockwell International.

References

1. J. H. McElroy, et al, "CO_2 Laser Communication Systems for Near-Earth Space Applications," *Proceedings of the IEEE*, Vol. 65, pp. 221-251 (February 1977).
2. G. J. Donelle, "Some Considerations for Millimeter Wave Space Communications," 1970 IEEE International Communications Conference, IEEE Cat. 70C21 COM (June 1970).
3. M. Ross, P. Freedman, J. Abernathy, G. Matassov, J. Wolf and J. D. Barry, "Space Optical Communications with the Nd:YAG Laser," *Proceedings of the IEEE*, Vol. 66, pp. 319-344 (March 1978).
4. T. Giallorenzi, "Optical Communications Research and Technology: Fiber Optics," *Proceedings of the IEEE*, Vol. 66, pp. 744-780 (July 1978).
5. P. D. Wright and R. J. Nelson, "High-Efficiency Stripe Geometry InGaAsP DH Lasers (λ = 1.3 μm) with Chemically Etched Mirrors," *IEEE Electron Device Letters*, Vol. EDL-1, pp. 242-243 (November 1980).
6. T. E. Stockton and R. B. Gill, "Semiconductor Light Sources for Fiber Optic Applications," *Microwave Journal*, Vol. 24, pp. 48-56 (October 1980).
7. D. Zeskind, "Semiconductor Lasers Shine Thanks to Improved Performance, Reliability," *EDN*, Vol 24, pp. 43-50 (June 24, 1981).
8. G. Borsuk and W. J. Thaler, "Frequency-Modulated Laser Communication System," *IEEE Transactions on Sonics and Ultra-Sonics*, Vol. Su-17, pp. 207-209 (October 1970).
9. T. L. Paoli and J. E. Ripper, "Direct Modulation of Semiconductor Lasers," *Proceedings of the IEEE*, Vol. 58, pp. 1457-1465 (October 1970).
10. L. D. Holland, N. B. Hilsen, J. J. Gallagher, G. Stevens, "System Analysis for Millimeter-Wave Communication Satellites," *Microwave Journal*, Vol. 24, pp. 35-43 (June 1980).
11. B. M. Oliver, "Thermal and Quantum Noise," *Proceedings of the IEEE*, Vol. 53, pp. 436-454 (May 1965).
12. W. E. Schroeder and G. I. Haddad, "Nonlinear Properties of IMPATT Diodes," *Proceedings of the IEEE*, Vol. 61, pp. 153-182 (February 1973).
13. H. J. Kuno, "Solid State Millimeter-Wave Power Sources and Combiners," *Microwave Journal*, Vol. 25, pp. 21-34 (June 1981).
14. A. A. Bergh and J. A. Copeland, "Optical Sources for Fiber Transmission Systems," *Proceedings of the IEEE*, Vol. 68, pp. 1240-1247 (October 1980).

better system performance

In a situation similar to that discussed for Impatt diodes, Eq. 12 and 13 show that improvements to the laser structure (Fig. 4) will upgrade performance. Thinner active regions, for example, will produce lower laser threshold currents and reduce input power requirements. Better crystallinity, homogeneity, and material interface compatibility will yield higher values of τ and lower values of α. As a result, J_{TH} can drop even more, while device lifetimes climb.

Reduced J_{TH} can also be obtained from the increased quantum efficiencies that can come from more precise control of the device structure. And, as J_{TH} continues to improve, power dissipation will decrease, lowering device temperatures and increasing device lifetime.

Lower, more stable temperatures lie at the root of better performance. Threshold current variations ranging from 0.4 mA/°C to 0.8 mA/°C commonly occur in semiconductor lasers. These variations depend upon the laser structure and are particularly pronounced in the longer wavelength InP-based lasers.[14]

Temperature variations also effect the wavelength of the laser: a 1°C temperature variation can create a 4-to-5-change in wavelength. Consequently, increases in output power levels will often require the laser to be cooled.••

Moving?

1. For FASTEST service you must attach old mailing label in space below.

If mailing label is not available print your old Company name and address in this box

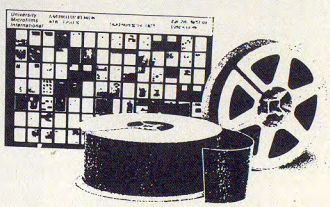
Please allow 6 weeks for change to take effect

2. Print your NEW business address here
NAME_____TITLE_____
COMPANY_____
ADDRESS_____
CITY_____STATE_____ZIP_____

M-382

3. Mail to:
MicroWaves
P.O. Box 13801
Philadelphia, Pa. 19101 USA

MICROWAVES is available in microform



Please send me additional information.

University Microfilms International

300 North Zeeb Road
Dept. P.R.
Ann Arbor, MI 48106
U.S.A.

18 Bedford Row
Dept. P.R.
London, WC1R 4EJ
England

Name _____
Institution _____
Street _____
City _____
State _____ Zip _____

New Discriminator Boosts Phase-Noise Testing

Delay-line FM discriminators and high-Q cavity discriminators have their separate strengths. This new design combines the best of both—and yields high sensitivity.

HIGH-SENSITIVITY phase noise measurements close to the RF carrier frequency are critical to the design and operation of high-grade communication systems and Doppler radars. The delay-line FM discriminator, a widely used phase detector, provides economy, easy implementation, wide frequency coverage, and a high tolerance for source frequency drift (a characteristic of all self-mixing or homodyne systems).[1,2,3] However, the sensitivity of this type of discriminator decreases with the offset frequency, and its maximum power input is dictated by the mixer.

The high-Q cavity discriminator can attain much higher sensitivities within the range of its practical Q values because its maximum power input is limited by the leakage of the carrier signal into the mixer. In the cavity type, carrier suppression alone can produce higher sensitivities than those of its delay-line counterpart. However, at millimeter-wave frequencies, fabrication of high-Q cavities becomes prohibitively complex and costly.[4]

The delay-line RF bridge shown in Fig. 1 combines the attributes of the "classic" delay-line discriminator (Fig. 2) with those of the cavity discriminator by providing carrier suppression before the signal is applied to the mixer. Improvements in sensitivity of 35 dB have been demonstrated in the S band and increases of 70 dB might be attainable. The transfer function (RF in, IF out) duplicates that of the classic design, and the physical process is simply the interference of two equally strong signals. The level-set attenuators and phase shifters used are relatively inexpensive, commercially available to 325 GHz, and cover at least one waveguide band. For lower frequency use, coaxial components provide an even wider frequency range. The RF bridge technique can, in principle, be extended into the optical region, and has been incorporated into an RF noise measurement system (Fig. 3).

Fred Labaar, Senior Staff Engineer, Operations and Support Group, Measurement Engineering Dept., TRW Electronics and Defense, Redondo Beach, CA 90278.

Approach differs with frequency

At frequencies below 20 GHz, where low-noise amplifiers are readily available, the sensitivity improvement can equal the carrier suppression obtained by using the proper amount of gain in the pre- and post-bridge RF amplifiers. For frequencies above 20 GHz, two approaches are possible:

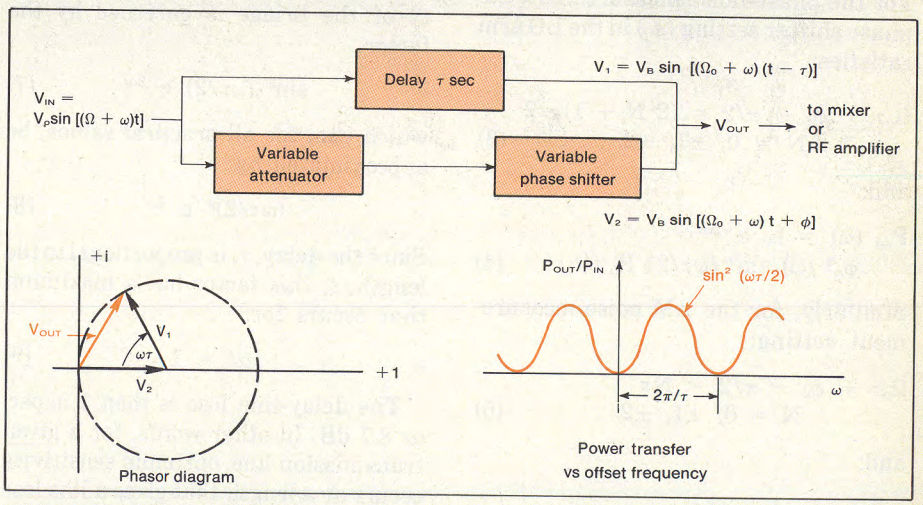
- *Using a harmonic mixer* to down-convert to a convenient lower frequency below 20 GHz, and then using the delay-line RF bridge technique. This approach takes advantage of the delay-line discriminator's relative insensitivity to frequency drift. However, a separate measurement must be performed to measure the fundamental LO signal.
- *Performing a direct measurement.* This offers sensitivity improvement only if the necessary input power is available.

It is not very difficult to obtain 40 or 50 dB of carrier suppression, even in the higher millimeter-wave frequency bands.

The sensitivity of the delay-line RF bridge method and the classic delay-line method are compared in Fig. 4 (RF=2 GHz). When studying this illustration, the following should be noted:

- Overlap of the classic discriminator traces is noticeably worse below 1 kHz because a sensing thermistor mount was not removed during one of the measurements. Despite the use of so-called noise suppressors or DC blocks, this thermistor attachment coupled noise into the system via a weak ground loop.
- Measurements are for comparison purposes only because the classic delay-line discriminator's sensitivity can be boosted by nearly 10 dB if

(continued on next page)

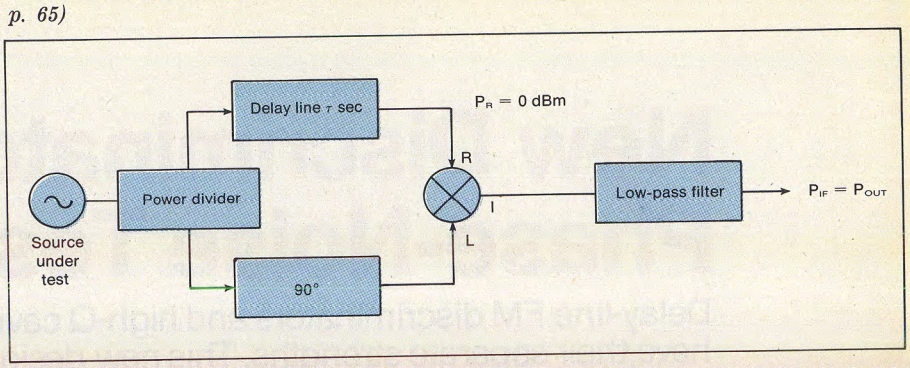


***1. The delay-line RF bridge** combines the advantages of the classic delay-line discriminator (see Fig. 2) and the cavity discriminator by suppression of the carrier before the signal is applied to the mixer for down-conversion to the baseband frequency.*

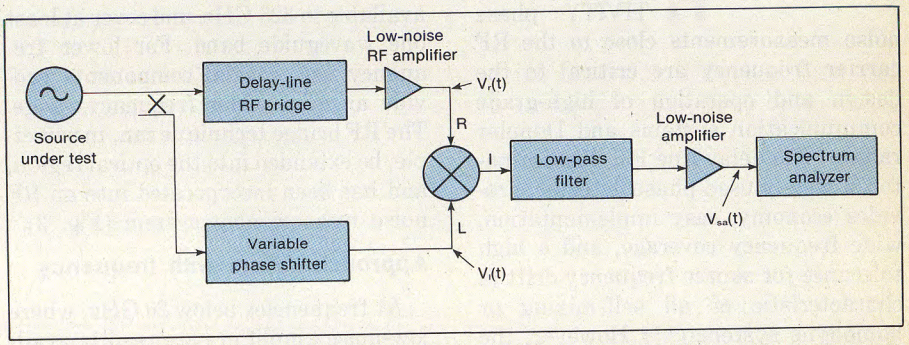
larger-diameter, lower-loss coax is used.

- Noise measurements must be presented together with the system noise floor. Without showing the noise floor, a source that easily meets specifications may be rejected. The classic delay-line trace below 1 kHz is a case in point.

The actual minimum suppression during measurement was more than 90 dB, which gives an idea of what is possible in this frequency range. An additional 20 dB of padding gives a potential improvement of 70 dB. Full use of this potential was not made because no extra RF amplifier was available.



2. The economical "classic" delay-line FM discriminator *used in the author's single-oscillator phase-noise test system measures phase noise (phase shift 90 degrees) and AM noise (phase shift = 0 degrees).*



3. The delay-line RF bridge incorporated into the RF noise measurement system *significantly improves sensitivity without impairing the advantages inherent in the delay-line technique.*

RF-power transfer function

The RF signal voltage has the following form (see "Definitions of terms," p. 68):

$$V(t) = \{V_o + \epsilon(t)\} \times \sin\{\Omega_o t + \phi(t)\} \quad (1)$$

In Eq. 1:

$$|\epsilon(t)| \ll V_o$$

$$|\phi(t)| \ll 1 \text{ rad}$$

The delay-line RF bridge transfer function is $T(\Omega)$:

$$T(\Omega) = A_{tr}(\Omega) \exp\{j\phi_{tr}(\Omega)\} \quad (2)$$

in which:

$$A_{tr}(\Omega_o + \omega) = e^{-\alpha\ell} \sin\{\omega\tau/2\}$$

$$\phi_{tr}(\Omega_o + \omega) = \pi/2 - \Omega_o\tau - \omega\tau/2$$

For the phase-noise measurement, the phase shifter setting (ϕ_ℓ) in the LO arm satisfies:

$$\Omega_o\tau + \phi_\ell - \pi/2 = (2N + 1)\pi/2 \quad N = 0, \pm1, \pm2\ldots \quad (3)$$

and:

$$P_{sa}(\omega) = L_c e^{-2\alpha\ell} \phi_o^2(\omega) \sin^2(\omega\tau/2) P_o(\Omega_o) \quad (4)$$

Similarly, for the AM noise measurement setting:

$$\Omega_o\tau + \phi_\ell - \pi/2 = N\pi \quad N = 0, \pm1, \pm2\ldots \quad (5)$$

and:

$$P_{sa}(\omega) = L_c e^{-2\alpha\ell} \epsilon_o^2(\omega) \sin^2(\omega\tau/2) P_o(\Omega_o) \quad (6)$$

The required sensitivity of the phase-noise measurement system at the lowest frequency determines the test system's parameters. The first requirement is that, at the lowest frequency (f_{min}), the output of the delay-line RF bridge lies above the post-bridge amplifier's noise floor (see Fig. 3) or, in the absence of an amplifier, lies above the mixer's noise floor. This requirement is met by having adequate input power or high bridge sensitivity. According to Eqs. 4 and 6, the sensitivity of the bridge is governed by the factor:

$$\sin^2(\omega\tau/2)\, e^{-2\alpha\ell} \quad (7)$$

which can, for all practical values, be approximated by:

$$(\omega\tau/2)^2\, e^{-2\alpha\ell} \quad (8)$$

Since the delay, τ, is proportional to the length, ℓ, this factor has a maximum that occurs for:

$$\alpha\ell = 1 \quad (9)$$

The delay-line loss is then 1 neper, or 8.7 dB. In other words, for a given transmission line, optimum sensitivity occurs at a length that gives a line loss of 8.7 dB. The choice of the transmission line is, of course, restricted by considerations of size.

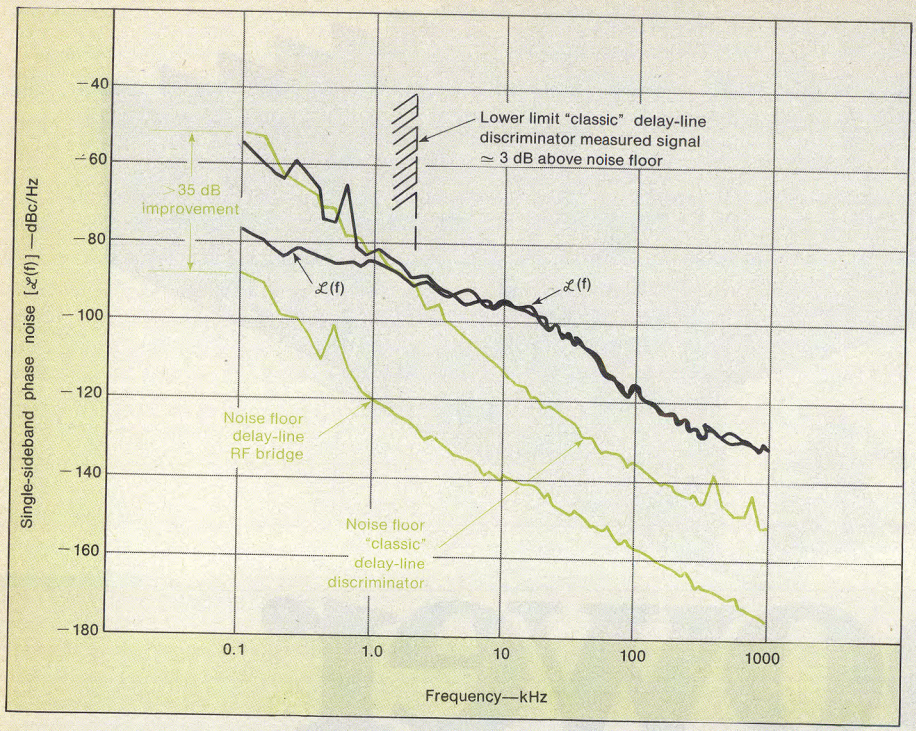
The choice of the delay time itself is a function of f_{min}, and the suppression of the carrier that can be maintained by the bridge. This occurs because the transfer function (Eq. 3) is derived under the assumption that complete suppression of the RF carrier is obtained. The suppression is given by 10 log δ^2, where $\delta \ll 1$. A similar limitation holds true for the classic delay-line discriminator, but for AM instead of carrier suppression.

It is easy to verify that the transfer function becomes invalid when the magnitude of $\sin\{\omega\tau/2\}$ is comparable to δ. The attenuation term $e^{-\alpha\ell}$ occurs also in the suppression and drops out. The following constraint must then be imposed:

$$\omega_{min}\,\tau/2 \gg \delta \quad (10)$$

The output of the post-bridge amplifier should be high enough to overcome the mixer's IF noise. For commercially available balanced mixers through X band, this noise has been verified to vary as 1/f from about 10 kHz to at least 10 Hz. The measurement system giving the results shown in Fig. 4 will serve as an example: for an f_{min}=100 Hz, the gain of the amplifier must be at least:

(continued on p. 68)



***4. A comparison of phase-noise measurements** between the classic delay-line discriminator and delay-line RF bridge shows the 35-dB improvement in sensitivity delivered by the latter design.*

Definitions of terms

The following terms and symbols are used in the equations

L_c = mixer's conversion loss
m = modulation index
$P_o\ (\Omega_o)$ = input power RF bridge
ℓ = delay-line length
$\mathscr{L}\ (f)$ = (single sideband phase-noise power density)/carrier power) (dBc/Hz) $\approx \frac{1}{2}\phi_{RMS}^2\ (\omega)$
$\mathscr{M}\ (f)$ = (single sideband amplitude noise power density)/(carrier power) (dBc/Hz) $\approx \frac{1}{2}\epsilon_{RMS}^2\ (\omega)$
α = delay-line loss/length
$\epsilon\ (t)$ = amplitude noise parameters
$\phi\ (t)$ = phase-noise parameter
Ω = RF angular frequency
Ω_o = carrier angular frequency
$\omega = \Omega - \Omega_o$ = angular offset frequency from carrier $= 2\pi f$

$$G = 10 \log \{10^4/f_{min}\} = 40 \text{ dB} \quad (11)$$

The delay line is 100 ft of Andrew FHJ-50 Heliax coax No. 35375 A02H. The coiled delay line measures 12 in. (diameter) × 3 in. The RF loss at 2 GHz is approximately 10 dB, and the delay time is 0.133 μs. This gives:

$$\omega_{min}\ \tau/2 = (2\pi)(100)(1/2)(0.133)\ 10^{-6} \approx 4 \times 10^{-5} \quad (12)$$

This means that the minimum RF carrier suppression should be:

$$10 \log (4\times10^{-5})^2 = -88 \text{ dB} \quad (13)$$

With an available input power of 23 dBm (200 mW), a delay-line loss of 10 dB and an amplifier noise figure of 3 dB, the maximum sensitivity at f_{min} is determined as follows:

$$\text{Power (dBm)} - \text{Loss (dB)} - (10 \log \times \omega_{min}\ \tau/2)^2 + 3 + \mathscr{L}_{min}\ (f_{min})\ \text{(dBc)} = \text{kTB (dBm)} + \text{Noise Figure (dB)} = 23 - 10 - 93 + \mathscr{L}_{min}\ (f_{min}) = -174 + 3 \quad (14)$$

so:

$$\mathscr{L}_{min}\ (f_{min}) = \mathscr{L}_{min}\ (100 \text{ Hz}) = -91 \text{ dBc} \quad (15)$$

This value is close to the value of the noise floor at 100 Hz. Usually the situation is reversed: $\mathscr{L}_{min}$ is given and the input power must be determined.

Establishing calibration

Calibration power level measured by the low-frequency spectrum analyzer for a phase-modulated input is:

$$P_{cal}\ (\omega_c) \approx \frac{1}{8} L_c\ e^{-\alpha\ell}\ (m\omega_c\tau)^2\ P(\Omega_o) \quad (16)$$

if:

$$2m \sin\left(\frac{\omega_c\tau}{2}\right) \ll 1 \quad (17)$$

Power measured by the spectrum analyzer is in a frequency band ($\Delta\omega$), centered on ω:

$$\Delta\omega = 2\pi \times \text{bandwidth setting of spectrum analyzer} \quad (18)$$

$$P_{meas}\ (\omega) = \overline{P_{sa}\ (\omega)} = 1/\Delta\omega \int_{\omega-\Delta\omega/2}^{\omega+\Delta\omega/2} P_{sa}\ (\omega)\ d\omega \quad (19)$$

From Eqs. 4, and 16 to 19:

$$\mathscr{L}\ (f) = 10 \log \left(\overline{P_{sa}\ (\omega)}\right) - 10 \log \left(P_{cal}\ (\omega_c)\right) + 10 \log \left(K_\phi\ (\omega)\right) + 2.5 \quad (20)$$

where:

$$K_\phi\ (\omega) = \frac{1}{8}\left[\frac{(m\ \omega_c\tau)^2}{1 - \frac{\sin\ (\Delta\omega\tau/2)}{\Delta\omega\tau/2} \cos\ (\omega\tau)}\right]$$

Similarly, for AM noise:

$$P_{cal}\ (\omega_c) = 1/4\ L_c e^{-2\alpha\ell} m^2\ P(\Omega_o) \quad (21)$$

$$\mathscr{M}\ (f) = 10 \log \left(\overline{P_{sa}\ (\omega)}\right) - 10 \log \left(P_{cal}\ (\omega_c)\right) + 10 \log \left(K_a\ (\omega)\right) + 2.5$$

where:

$$K_a\ (\omega) = \frac{1}{8}\left[\frac{m^2}{1 - \frac{\sin\ (\Delta\omega\tau/2)}{\Delta\omega\tau/2} \cos\ (\omega\tau)}\right]$$

Although Eq. 19 suggests that one can measure through a bridge null (resonance), in practice the factors $K_\phi\ (\omega)$ and $K_a\ (\omega)$ "blow up" at the

resonance frequency:

$$\omega = N\ 2\pi/\tau$$
$$N = 1,2,3\ \ldots \qquad (22)$$

Although the resonance of the bridge (in this case, 7.5 MHz) can be accurately determined at any particular moment, temperature variations that can occur throughout the measurement cycle can shift it by several analyzer bandwidths (30 kHz in the example). Therefore, the calculated output is correct to within four or five spectrum analyzer bandwidths of the correct resonant frequency.

"Tweaking" aids measurement

To obtain carrier suppression of at least 90 dB during the measurements, a slight mechanical modification of the attenuator and phase shifter is required. The slack in the major moving parts (those interacting directly with the EM field) can be removed by applying spring pressure at appropriate points without impeding their overall movement.

Continuous tuning of the phase trimmer may be necessary during the test because ambient temperature variations cause changes in delay-line length. This change in the nominally 100-ft delay line is dictated by the change in length of the center conductor and not the corrugated outer conductor. The cable is constructed so that the center conductor is thermally well insulated from the outer conductor.

The thermal isolation from the environment is enhanced in this system by the use of DC blocks at both ends of the delay line to prevent ground loops, and the packaging of the coiled delay line, which is intended to suppress acoustic pickup. The resulting thermal time constant (the time it takes the transient to fall to 33 percent of its final value) was estimated to be at least four hours, since the rate of phase trimming did not appreciably change after eight hours (indicating *at least* two time constants had passed) while the ambient temperature had already leveled off.

The rate of change in electrical length was about 0.3 degrees per °C. The need for continuous phase trimming is understandable because a 90-dB suppression requires about 0.025-milliradian, or about 0.01-degree phase balance. If this system is to be a dedicated test apparatus, enclosing the delay line in an automatically controlled oven is advisable. An oven temperature of 10° C above the maximum expected ambient temperature would make the delay line virtually immune to ambient temperature variations.

Practical considerations for design

This RF bridge has been used successfully with a cavity instead of a delay line in one bridge arm (see Fig. 1). This is a much easier configuration to implement and tune than the circuits using a circulator, described by other authors.[4,5,6]

Although the main function of the discriminator is phase detection, the same circuit can be used for amplitude detection. However, if amplitude detection is the only goal, there are better methods to use.

The suppression of AM noise while measuring phase noise normally does not constitute a problem. This is not because the inherent AM noise suppression is so high, but because the AM noise of the RF signal is usually much lower than the phase noise. On occasion, however, the AM noise can be very high (as once experienced when testing a missile transmitter under vibration), and the leakage of AM noise causes the system noise floor to go up. For the classic delay-line discriminator in Fig. 4, below 1 to 2 kHz the detected phase noise is drowned in the system noise floor. It is therefore good practice to measure the suppression of AM noise when measuring phase, and vice versa, and to measure both the phase noise and amplitude noise. This information ensemble will allow correct measurement interpretation.

Because of L-to-R-port leakage, it is difficult to obtain high AM suppression. The recommended procedure is to set the phase shifter in the LO arm for minimum AM sensitivity when measuring phase noise. The result is not always adequate because the RF signal carrier leakage through the discriminator interferes with the L-to-R-port leakage. Depending on the circuit layout and RF carrier frequency, minimum AM sensitivity may coincide with minimum phase modulation sensitivity. The author is now evaluating a promising simple compensation circuit to solve this leakage problem.

The circuit described here may be converted to a cavity type discriminator by replacing the delay line with a cavity. Given practical constraints, cavity discriminators can be more sensitive than delay-line discriminators. However, two factors favor the use of the delay line:

- Transmission lines of any size or configuration are easier to obtain, less costly, and cover wide frequency ranges.
- The delay-line discriminator can be adapted to phase noise measurements of pulsed RF signals because coaxial waveguide offers little or no frequency dispersion.••

Acknowledgments

The author wishes to thank Algie Lance and Wendell Seal of TRW, and Dr. Donald Halford of NBS for sharing their knowledge of RF noise measurement techniques and for their unlimited support; to TRW Inc.; the Ford Aerospace and Communications Corp., Aeronautic Division, where this concept was conceived; and Karen Wilmarth for her efforts in producing this article.

References

1. A. L. Lance, Wendell D. Seal, Frank G. Mendoza, and N. W. Hudson, "Automated Phase Noise Measurements," *Microwave Journal* (June 1977).
2. A. L. Lance, Wendell D. Seal, Frank G. Mendoza, and N. W. Hudson, "Automating Phase Noise Measurements in the Frequency Domain," *Proceedings of the 31st Annual Frequency Control Symposium* (June 1977).
3. D. Halford, notes on "The Delay Line Discriminator," NBS Notebook, F 10, pp. 19-38 (April 1975).
4. J. G. Ondria, "Noise Measurements of W-Band (75-110 GHz) CW GaAs GUNN and Silicon IMPATT Oscillators," *1980 IEEE-MTT-S International Microwave Symposium Digest*, pp. 24-25.
5. J. R. Ashley, T. A. Barley, G. J. Rast, "Measurement of Noise in Microwave Transmitters," *IEEE Transactions on Microwave Theory Tech.*, Vol. 25, No. 4, pp. 294-318 (April 1977).
6. J. G. Ondria, "A Microwave System for Measurements of AM and FM Noise Spectra," *IEEE Transactions on Microwave Theory Tech.*, Vol. 16, pp. 767-781 (September 1968).

Moving?

1. For FASTEST service you must attach old mailing label in space below.

Please allow 6 weeks for change to take effect

If mailing label is not available print your old Company name and address in this box

2. Print your NEW business address here
NAME_____TITLE_____
COMPANY_____
ADDRESS_____
CITY_____STATE_____ZIP_____

M-382

3. Mail to:
MicroWaves
P.O. Box 13801
Philadelphia, Pa. 19101 USA

Distributed Line Analysis For Microstrip Antennas

Providing a broadband microstrip satcom antenna for aircraft will take some fancy circuitry. The design must begin with an accurate equivalent circuit.

MICROSTRIP antennas have advantages for aircraft use because of their low physical profiles and economical installation. They would be more widely used if their present signal bandwidth (approximately 3 percent) could be increased.

The research described in this article was aimed at just such an extension of the bandwidth of a printed-circuit microstrip antenna in the 225-to-400-MHz band. However, the design work was actually done in the 2.0-to-4.0-GHz range because better measurement equipment was available for these frequencies. The design has applications in nearly all bands, and to uses other than communications.[1]

The principal desired mode, the stripline mode (see inset, Fig. 1), has a symmetrical distribution of electric field under the upper conductor, with electrical fringing out in the air. This fringing has caused major difficulties in the mathematical description of the distribution and characteristic impedance of this transmission mode. No known method of finding a closed formula exists for either.

All of the methods which have been used for this task are approximate and depend on numerical procedures. Charts have been published for Z_o, the characteristic impedance,[2] and other competing methods can be used.[3]

The transmission line mode is quasi-TEM—that is, it is slightly TE because of the fringing. For wide strips, such as those used in this type of rectangular microstrip radiator, however, this mode may be assumed to be completely TEM because very little fringing energy exists in comparison to the energy between the plates (except at the radiating edge during resonance).

In this study, the circuit properties of microstrip antennas were explored using distributed network analysis, rather than the field-theory analysis most widely reported. This analysis suggested that the coupling of signals from the basic parallel-plate radiator to a series of half-wave auxilary strips could conquer the bandwidth limitation (Fig. 1).

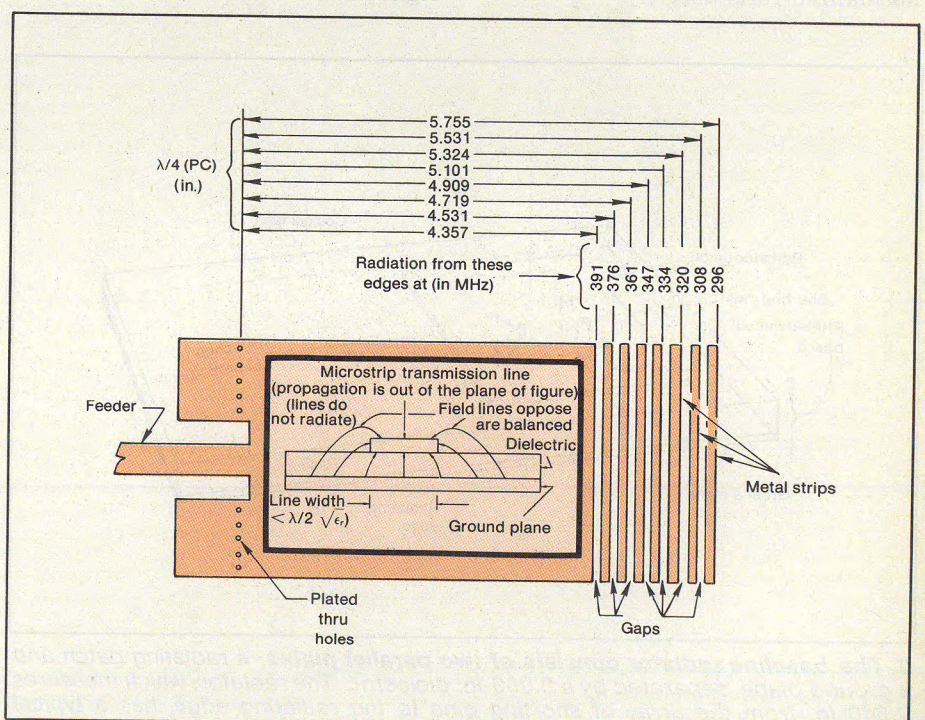
Auxilary strips extend bandwidth

The launcher is sized to resonate and, consequently, to radiate at the highest frequency in the band of interest. Auxilary strips are placed near the launcher and are separated from it and each other by a series of gaps. Circuits must be developed which will cause the strips to progressively join themselves to the launcher, effectively making it longer as the frequency goes down.

The baseline radiator will launch a wave which can excite any of a number of edges located in the axial direction. Since the launcher must be able to propagate a driving TEM wave in a *single* direction, the baseline antenna was shorted at one end by closely spaced pins. These pins connect the radiating patch to the ground plane (Fig. 2). The other end of the launcher was left open. The microstrip launcher now consisted of a quarter-wavelength TEM cavity for waves in the dielectric medium between the conductors.

The cavity was excited by a coaxial probe located in the central axial plane, and was expected to resonate in

(continued on next page)



1. Auxilary strips can expand the bandwidth of the basic radiator *if the proper coupling network can be found. (Inset shows desired microstrip mode.)*

Murray Hoffman, Department Staff in Satellite Communications Systems, The Mitre Corporation, Burlington Rd., Bedford, MA 01730

 (continued from p. 71)

the dominant TEM mode regardless of the probe's axial (Z) location. The location of the probe in the central axial plane prevented it from contributing to the excitation of odd-order TE modes. Its exact position would only determine the match of the 50-ohm coaxial system to the TEM mode.

Before the basic quarter-wave radiator could be combined with the more complex auxilary strips, an equivalent distributed transmission-line circuit for it had to be found. This equivalent circuit had to accurately describe the combined behavior of the coaxial probe and the TEM cavity. The significant line lengths would be given by distances from the probe to the short and to the radiating edge. A radiation resistance (a real impedance) would be assigned to the radiating edge that would be variable to allow adjustments for computation.

Equivalent circuit developed

The equivalent circuit developed for the launcher (Fig. 3) consists of two transmission lines which are in parallel at the coaxial connector. (The 0.424-nh inductance in the coaxial line will be discussed later.) It shows a line, ℓ_2, terminated in a short which presents a normalized impedance at the plane of the connector given by:

$$Z_2 = j\tan\beta\ell_2 \qquad (1)$$

The second line, ℓ_1, is terminated in a normalized resistance (r):

$$r = \frac{R}{Z_o} \qquad (2)$$

In Eq. 2, R = the terminating resistance, and Z_o = the characteristic impedance of the microstrip radiator in the TEM mode.

The characteristic impedance can be found from the current flowing in the TEM line and the voltage across it. The voltage is the field E_y, times the separation of the plates, h. Similarly, the current equals the product of the field, H_x, and the width of the line, w. Consequently:

$$Z_o = \frac{hE_y}{wH_x} \qquad (3)$$

A determination of Z_o, therefore, requires the ratio E_y/H_x. Using the solution for E_y in the forward direction:

$$E_y = A_1 e^{-j\beta z} \qquad (4)$$

This expression permits H_x to be found from E_y through a reduced curl equation for the TEM mode which states:

$$\frac{\delta E_y}{\delta z} = j\omega\mu H_x \qquad (5)$$

Performing the differentiation and making the proper substitutions:

$$\frac{E_y}{H_x} = -\sqrt{\frac{\mu}{\epsilon}} = -\frac{377}{\sqrt{\epsilon_r}} \qquad (6)$$

The minus sign only assures that power flows in the +Z direction for a right-hand coordinate system according to E × H. It follows that:

$$Z_0 = \left(\frac{h}{w}\right)\left(\frac{377}{\sqrt{\epsilon_r}}\right) \qquad (7)$$

For the microstrip line used in this study, ϵ_r = 2.55, h = 0.06, and w = 1.250. These values lead to a Z_o of 11.33 ohms. Thus, the normalized r is :

$$r = \frac{R}{11.33} \qquad (8)$$

Therefore, the second line extending from the connector to the radiating edge presents an impedance at the connector of:

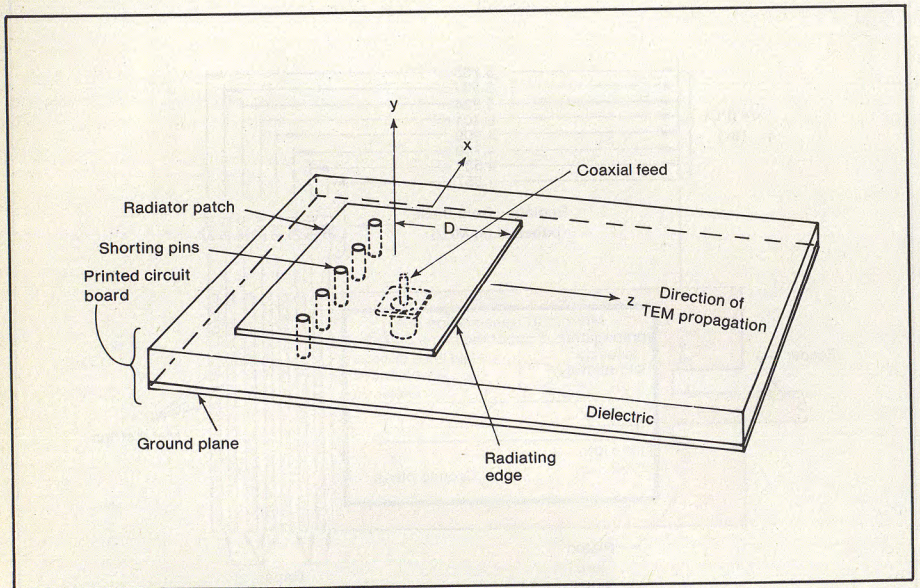
$$Z_1 = \frac{r + j\tan\beta\ell_1}{1 + jr\tan\beta\ell_1} \qquad (9)$$

The impedance (admittance) presented to the connector by the parallel combination of the two lines is given by the sum of the two admittances:

$$\frac{1}{Z_p} = \frac{1}{j\tan\beta\ell_2} + \frac{1 + jr\tan\beta\ell_1}{r + j\tan\beta\ell_1} \qquad (10)$$

Computer program written

A special computer program was written which performs the distributed line network analysis and plots the impedance as a function of frequency. This program, which is in



***2. The baseline radiator consists of two parallel plates**, a radiating patch and a ground plane, separated by a 0.060-in. dielectric. The radiator, which measures 0.640 in. from the array of shorting pins to the radiating edge, has a typical characteristic impedance of 10 ohms. When not resonating, it can be expected to have a reflection coefficient, Γ, of 0.948, which corresponds to a VSWR of 37.5:1.*

Symbols used

- Γ = reflection coefficient
- Z_o = characteristic impedance of baseline radiator in TEM mode
- ℓ_1 = equivalent line length, coaxial connector to radiating aperture
- ℓ_2 = equivalent line length, coaxial connector to shorting pins
- Z_2 = normalized impedance of ℓ_2 at connector plane
- r = normalized impedance of ℓ_1
- R = radiating resistance of aperture
- E_y = electric field in Y direction
- H_x = magnetic field in X direction
- h = dielectric thickness
- w = width of radiating patch
- A_1 = amplitude of forward wave
- β = space phase constant $= \pm\Omega\sqrt{\epsilon\mu} = \frac{2\pi f}{\nu_m} = \frac{2\pi}{\lambda_m}$
- z = distance in Z direction
- Ω = angular velocity
- ϵ = actual permittivity of dielectric
- ϵ_r = relative dielectric constant (dielectric between plates)
- μ = permeability
- f = frequency
- ν_m = wave velocity in dielectric
- λ_m = wavelength in dielectric
- Z_p = parallel impedance presented by ℓ_1 and ℓ_2 to the coaxial connector

extended BASIC for graphics plotting, runs on a Tektronix 4052 Graphics Computer System. (See "Obtaining the program," p. 74.)

The form of Eq. 10 was maintained to take advantage of convenient computer inversion routines for complex numbers and fractions. It accepts values for the variables R, ℓ_1, ℓ_2, and calculates Z_p over a band of frequencies. It then normalizes Z_p to a 50-ohm system and computes the complex reflection coefficient, Γ, that would be measured at the input to the 50-ohm coaxial connector.

This phase of the study validated the equivalent circuit by correlating the measured impedance of the baseline radiator with the computed impedance. Both the network analyzer used in the measurements and the computer produce graphical outputs. The network analyzer drives a rectangular recorder which plots the measured impedance as a function of frequency on a Smith Chart. This chart lies within the unit circle in the complex reflection coefficient plane.

The computer drives a rectangular plotter which depicts Γ in the same plane as that shown by the network analyzer. Thus, the two plots can be compared directly (Fig. 4).

The measured impedance locus shown in Fig. 4 is plotted as a function of frequency in the Γ plane. Frequency points along the impedance locus were measured using a microwave frequency counter. At each frequency point, the sweep was halted and a dot was made by depressing the recorder pen. The measured locus describes a circle.

Short inhibits radiation

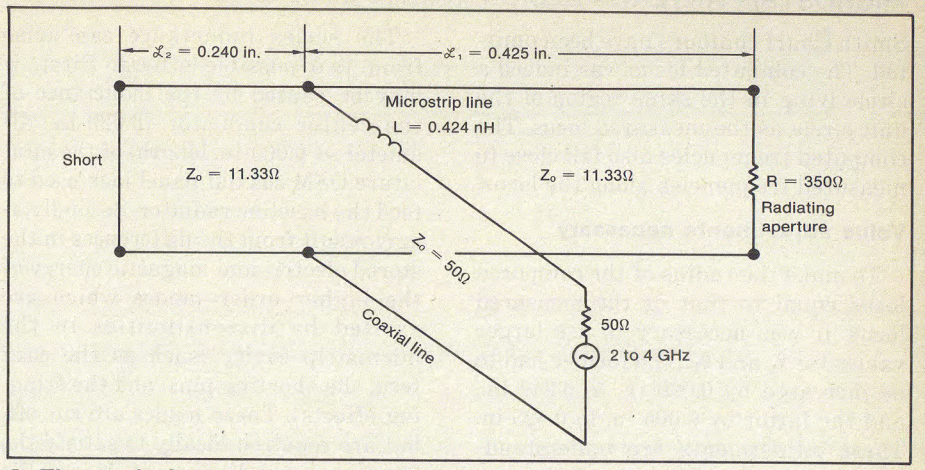
The radiator patch (see upper right corner, Fig. 4) was etched to provide enough material for soldering the short. The short itself consists of five ten-gauge copper wires which pass through the patch, the dielectric, and the ground plane. The wires were soldered to the patch and the ground plane, and closely spaced to prevent a wave from propagating past them.

The 0.150-in. spaces between the 0.100-in. wires acted as waveguides below cutoff. That is, the wave is reactively attenuated between the wires, which form a screen and reflect the wave forward. The effective location of the reflection was assumed to be the plane containing the centerline of the wires. The distance from this plane to the radiating edge is 0.640 in., and is composed of ℓ_2, the distance from the centers of the wires to the center of the coaxial feed-point, and ℓ_1, the distance from the coaxial feed-point to the radiating edge. These distances—0.220 in. and 0.420 in., respectively—were the initial values used in the computer program.

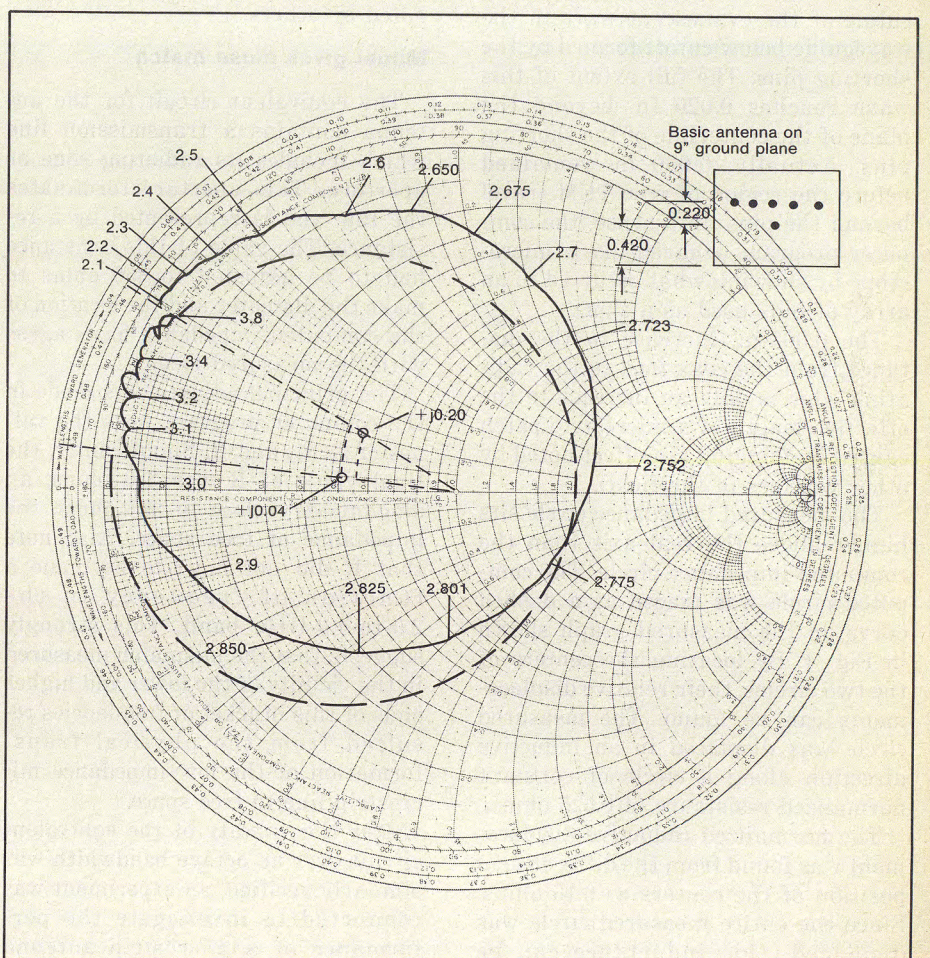
The top portion of Fig. 5 shows the initial impedance plot computed using the equivalent circuit and drawn by the 4052 graphics system. The computer draws the complex reflection coefficient plane with the unit circle the same size as it is on the measured recording.

For convenience, axes accompany circles which represent VSWRs of 1.2, 1.4, 1.6, 1.8, 2.0, 3.0, and 4.0:1, while the

(concluded on next page)



***3. The equivalent circuit for the baseline radiator** was used in a computer program. Measured and computed results verified the circuit.*



***4. The computer (dashed line) and the network analyzer (solid line) produce plots in the same plane** that can be compared directly. The comparison led to refinements in the equivalent circuit for the baseline radiator.*

Smith Chart contours have been omitted. The computed locus was indeed a circle lying in the same region of the unit circle as the measured locus. The computed frequencies also fall close to measured frequencies along the locus.

Value adjustments necessary

To make the radius of the computed locus equal to that of the measured locus, it was necessary to use larger values for ℓ_2 and ℓ_1. The former had to be increased by 0.020 in. to 0.240 in., and the latter by 0.005 in. to 0.425 in. These adjustments are understandable and do not affect the theory.

The larger increase arises from the cutoff of the evanescent wave in the waveguide below cutoff formed by the shorting pins. The full extent of this wave reaches 0.020 in. beyond the plane of the centerline of the shorting pins. Actually, 0.050 in. remained before the region of free TEM travel beyond the pins. In a sense, the computer program behaved like a microscope by showing what occurred in an array of pins used as a short.

The 0.005-in. increase in the distance from the coax feed to the radiating edge is only an increase in the effective length of a microstrip patch caused by fringing (an effect noted by other workers in the field).

The measured impedance circle sits higher above the real axis than the computed impedance circle. The computed circle was traced as a dashed curve on the measured graph shown in Fig. 4. By locating the centers of the two circles, their relative displacements can be found. The measured circle was displaced in an inductive direction along a circle of constant normalized resistance of 0.525 ohms.

The normalized inductive displacement was found from the difference in position of the centers as 0.16 ohms. Since the entire measured circle was displaced, this inductance can be confidently assigned to the input reference plane at which the network analyzer measurements were being made. Since the inductance lay along a constant resistance circle, it was in series with the microstrip circuit.

Normalized to the 50-ohm measuring system, the inductance had a reactance of 8 ohms, which corresponds to 0.424×10^{-9} h at a frequency of 3.0 GHz. When this series reactance was added, the computed locus fell exactly over the measured locus (bottom portion of Fig. 5).

The series inductance can arise from two possible effects. First, it may be caused by the inductance of the center conductor (0.020-in. diameter × 0.060-in. length) of the miniature OSM coaxial panel jack used to feed the baseline radiator. Secondly, it may result from the differences in the stored electric and magnetic energy of the higher order modes which are excited by discontinuities in the microstrip cavity (such as the coax feed, the shorting pins, and the fringing effects). These modes are cut off, but are required locally to satisfy the boundary conditions of Maxwell's equations. (These modes have been noted by others.[4])

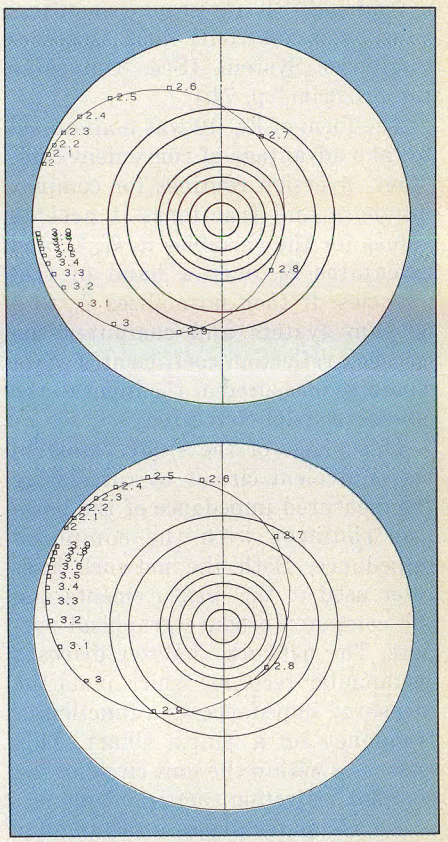
Model gives close match

The equivalent circuit for the antenna contains a transmission line which includes its radiating edge or aperture. This aperture terminates the line and is represented by a resistance. The value of this resistance had to be adjusted to 350 ohms to make the diameter and the location of the computed impedance locus agree with the measured locus.

The principal adjustments made in the computer program were the values of ℓ_1, ℓ_2, and R. Significantly, the final value of R was 350 ohms, an amount very close to 377 ohms, the impedance of free space. Also note that R did not have to be made a function of frequency in the 2.0-to-4.0-GHz band. This strongly suggests that the mismatch measured in the vicinity of the lower and higher ends of this bracket of frequencies resulted from the physical transformation of the low impedance microstrip line to free space.

After the validity of the equivalent circuit over an octave bandwidth was similarly verified, an experiment was conducted to investigate the performance of a microstrip antenna with coupling between the basic radiator and an auxilary strip. Transfer of the site of radiation from one edge on the radiator to another on the auxilary strip was demonstrated.

Radiation measurements confirmed the proper antenna-pattern shapes. The frequency band over which the VSWR was less than 5.0:1 was increased from 5.6 percent for the basic radiator, to 14.7 percent for the improved design with the auxilary strip. These measurements confirm the validity of this design approach.



***5. Computer plots show** the original (top) and adjusted (bottom) equivalent circuit performance for the radiator.*

The initial band broadening observed in these measurements encourages further development of the parasitic-strip approach. It also demonstrates that the distributed line approach can be used in the design of all quarter-wave microstrip radiators. ●●

References

1. M. Hoffman, "Broadband Low Profile Microstrip Antenna IR&D Project Report for Fiscal 1979," WP-22663, Bedford, MA: The MITRE Corporation (January 16, 1980).
2. H. Wheeler, "Transmission Properties of Parallel Strips Separated by a Dielectric Sheet," *IEE Transactions on Microwave Theory and Techniques*, Vol. 13, No. 3, p. 172 (March 1965).
3. Matthaei, Young, and Jones, *Microwave Filters, Impedance Matching Networks, and Coupling Structures*, p. 165, McGraw-Hill, New York, NY (1964).
4. Y.T. Lo, "An Analysis of the Disk Microstrip Antenna Part II," RADC TR-79-132, University of Illinois (May 1979).

Acknowledgment

The author wishes to thank Norman Cox for his support on this project and his painstaking efforts in the microstrip laboratory in developing our measurement capability and in making the baseline radiator measurements. This work was performed under the Mitre Corp. internal research and development program as project 90140.

Obtaining the program

To obtain the 199-step, extended BASIC program mentioned in this article, send a stamped ($0.20 US postage), self-addressed envelope to "Microstrip Radiator," c/o Ms. Tania Tishin, *MicroWaves*, 50 Essex St., Rochelle Pk., NJ 07662.

Shielded Microstrip Aids V-Band Receiver Designs

Higher performance, lower cost millimeter-wave integrated circuits result from new substrate materials used in shielded microstrip transmission lines.

THE recent development of thin, flexible, and relatively low dielectric-constant substrate materials (such as Cuflon) has simplified the design of shielded microstrip transmission media for millimeter-wave integrated circuits. Before such transmission materials were available, conventional millimeter-wave integrated circuits relied on fused-quartz-dielectric substrates. Fused quartz is extremely smooth, has low dielectric losses, reduces conductive losses, and can be made thin enough for operation up to 100 GHz. On the other hand, it is expensive, breaks easily, and is difficult to drill. Moreover, fused-quartz circuits are small, and require greater precision in processing than if they were fabricated on a lower dielectric-constant material.

Using Cuflon, a cost-effective V-band receiver module with shielded microstrip as the transmission media can be designed. The module consists of a Gunn-diode, dielectric-resonator-controlled local oscillator, an isolator (circulator with one port terminated), a directional filter, a single-diode mixer, and a waveguide-to-shielded-microstrip transition.

Since all millimeter-wave circuits require metallic shielding to control higher-order modes, reduce radiation losses, and eliminate external electromagnetic interference, the receiver must have a rectangular magnetic shield. Together, the metallic shield and the shielded microstrip pave the way for improved millimeter-wave integrated circuits.[1]

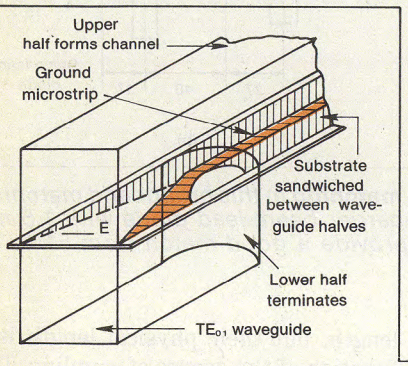
A transition to microstrip

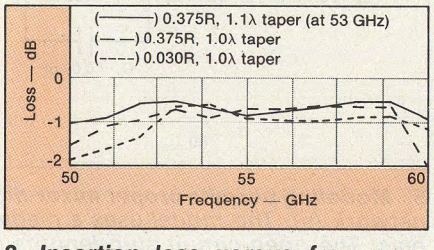
Since all V-band test equipment uses TE_{01} rectangular waveguide, a transition must be made to the shielded microstrip mode. The transition must have low losses, low VSWR, and broad bandwidth. It must be simple to fabricate, and be reusable with good performance.[2] Figure 1 shows such a transition. The substrate is suspended in the plane of the E-field lines of the WR-15 split-block waveguide.

The launching mechanism is similar

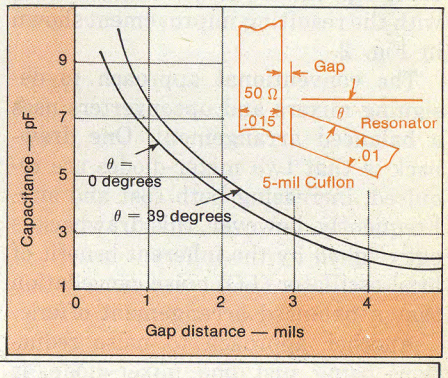
(continued on next page)

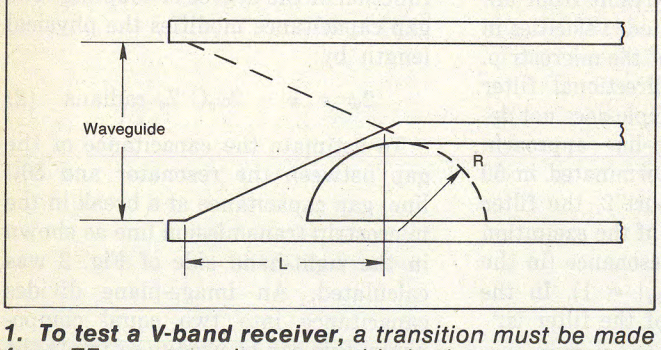
Michael Dydyk, Technical Staff, Microwave Section, and **B. David Moore,** Staff Engineer, Microwave Section, Motorola Government Electronics Division, 8201 E. McDowell Rd., Scottsdale, AZ 85252.



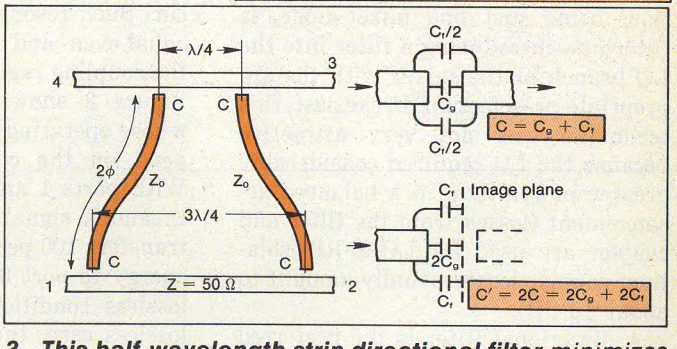


***2. Insertion loss versus frequency** reveals that the optimum value of the semicircular cutout in the transition region (radius R) is 0.0375 in.*





***1. To test a V-band receiver,** a transition must be made from TE_{01} rectangular waveguide in the test equipment to the microstrip used in the receiver. This configuration offers advantages such as simple fabrication, durability, and good performance over time.*



***3. This half-wavelength strip directional filter** minimizes local oscillator power (LO) dissipation while maintaining good LO-to-RF isolation. The dependence of physical length on gap capacitance can be calculated by the boxed equations, and is shown by the curve at top.*

to that of fin line; that is, as the wave progresses down the transition, the tapered ridges on opposite sides of the dielectric gradually increase the impedance until the 50Ω microstrip value is reached. Unlike fin line, however, the E field gradually rotates 90 degrees to match the microstrip mode. The half of the waveguide under the microstrip ground plane terminates 270-mil beyond the beginning of the transition. The half of the waveguide above the microstrip line continues, forming a shielded channel. The channel is above cutoff and will not support a waveguide mode.

The performance of the tapered transition depends on two dimensions —the radius (R) of the semicircular cutout in the transition region, and the length (L) of the tapered region. In tests, the first transition was $1\lambda_g$ long at 53 GHz, with R equal to 0.030-in. (Note that λ_g is the wavelength for microstrip.)

Plotted insertion loss for the two transitions is shown in Fig. 2 along with radius-transitions of $1\lambda_g/0.0375$ in. and $1.1\lambda_g/0.0375$ in. Tests showed that an R of 0.0375 in. was close to the optimum value. For example, increasing R to 0.045 in. rapidly decreases both VSWR and insertion loss above 56.5 GHz. A $1.1\lambda_g/0.0375$-in. radius-transition test substrate was fabricated to bring up the low-end insertion loss, with the resulting improvement shown in Fig. 2.

The conventional approach to designing mixers and upconverters uses a balanced arrangement. One drawback is that two mixer-diodes are required, increasing both cost and size. Frequently, however, this drawback is outweighed by the inherent benefit of local-oscillator (LO) noise cancellation that a balanced arrangement offers.

Another approach to noise reduction, using just one mixer-diode, is filtering—introducing a filter into the LO branch of the mixer with the appropriate preselection. In the past, this technique was not very attractive because the LO required considerably greater power than in a balanced arrangement (losses from the filter and coupler are used for LO-to-RF isolation; coupler losses usually amount to about 10 dB).

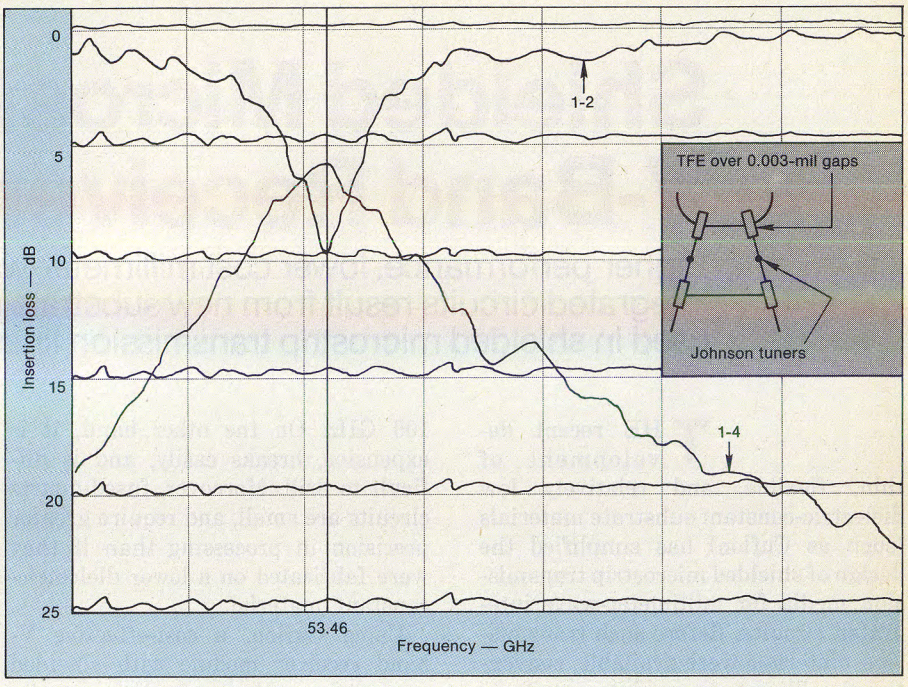
A directional filter is the preferred method for minimizing the LO power while maintaining a reasonable LO-to-RF isolation. Investigations found the resonant-ring approach to be unsuitable because dual resonances occur. Such resonances result from unequal even- and odd-mode velocities in the coupling regions of the microstrip. Figure 3 shows a directional filter whose operating principle does not depend on the coupled-line approach. With ports 1 and 4 terminated in 50 Ω, and a signal at port 2, the filter transfers 100 percent of the excitation energy to port 3 at resonance (in the lossless condition, $|S_{32}| = 1$). In the lossless case, the Q of the filter is:[3]

$$\frac{1}{Q_L} = \frac{\omega_2 - \omega_1}{\omega_0} = \frac{2\omega_0^2 C^2 Z Z_0}{\pi} \quad (1)$$

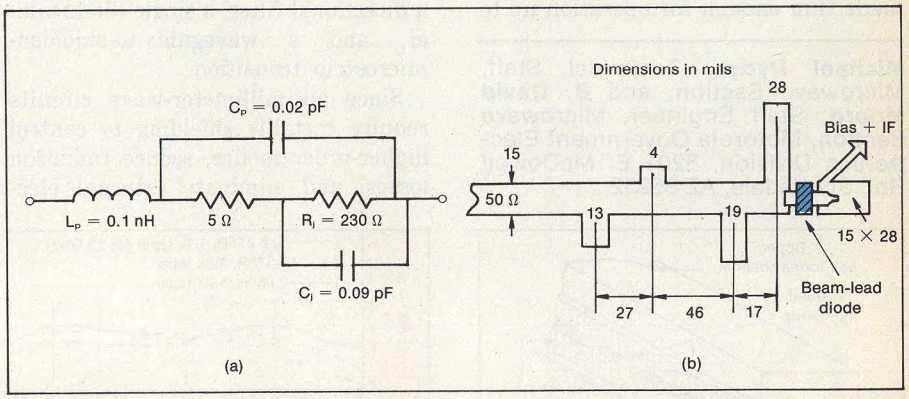
The resonators are $\lambda/2$ in electrical length, but their physical length is a function of the degree of coupling. The gap capacitance modifies the physical length by:

$$2\phi = \pi - 2\omega_0 C Z_0 \text{ radians} \quad (2)$$

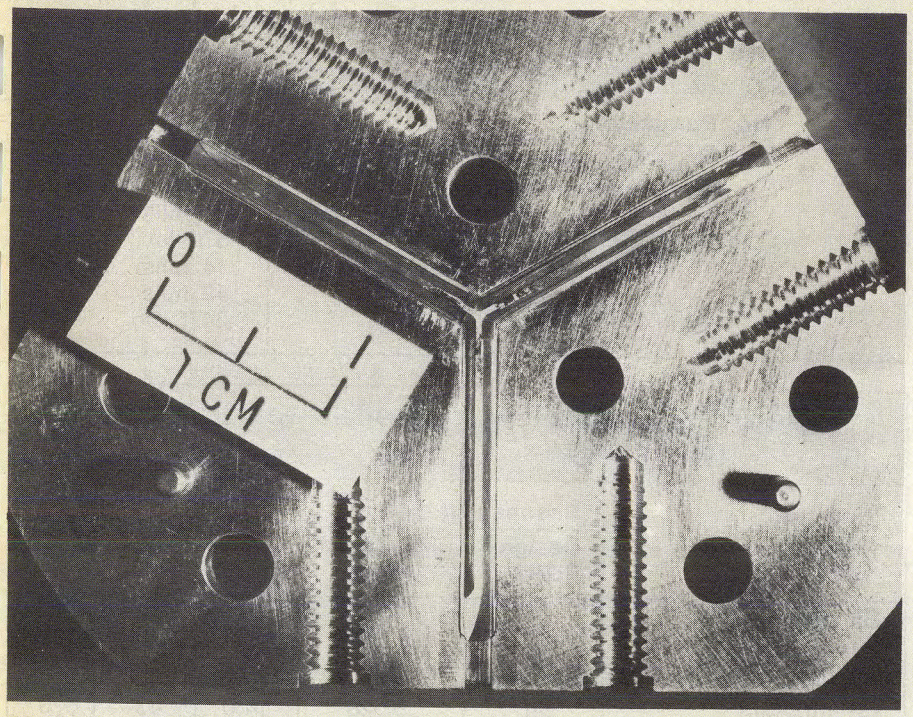
To estimate the capacitance of the gap between the resonator and 50Ω line, gap capacitance at a break in the microstrip transmission line as shown in the right-hand side of Fig. 3 was calculated. An image-plane divides capacitance into two equal components; this can be used to estimate the capacitance between an open-ended line perpendicular to an infinite line at the image plane (see Fig. 3).



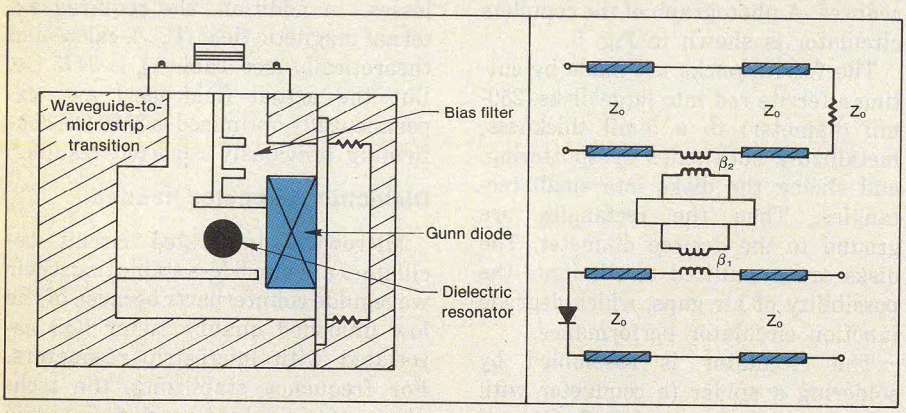
***4. The response curve of the V-band receiver's directional filter** shows an insertion loss of 5.5 dB at 53.46 GHz. Normally, the loss should be just 3 dB, but deviations in resonator spacing make it greater than anticipated.*



***5. Modeling permits proper mixer-diode matching** in this broadband matching network (a). The model uses a medium-barrier beam-lead diode with 1.5 mA bias. The open-circuit stub lengths (b) provide a good match from 51 to 57 GHz.*



6. This microstrip junction circulator *is designed by conventional techniques, but requires careful construction of the ferrite pucks to optimize operation at the desired frequency.*



7. One of the simplest techniques for frequency stabilization *employs a dielectric-resonator-controlled oscillator, shown with its equivalent circuit. Power output soars to 30 mW in the 54-to-55-MHz range, with temperature stability of 18 ppm/°C.*

Capacitance versus gap in microstrip has been calculated previously for ϵ_r equal to 1, 6, and 9.6.[4] An interpolation of the results made for Cuflon ($\epsilon_r = 2.1$) and gap capacitance is plotted versus the gap in Fig. 3 (for both a perpendicular and a slanted resonator on 0.005-in. Cuflon).

A slanted resonator provides somewhat more capacitance for a given gap because of the increased length of the gap. The gap must be as small as possible to achieve the best LO power-coupling to the mixer diode. With conventional print-and-etch techniques, it is impossible to accurately etch a 1- or 2-mil gap because of the lack of resolution of the etch resist. The first test circuits were constructed using thin-film techniques and glass-mask artwork to achieve a 1-mil gap (0.0065 pF).

The design dimensions of the filter, centered at 53 GHz, are: Z = 50Ω, Z_0 (resonator) = 67Ω, 2ϕ = 2.854 radians, and a gap of 1-mil (0.0065 pF). Several test filters were etched with gaps as wide as 2.0 mils, but higher resonant frequencies and dual resonances resulted. Small pieces of Teflon tape can increase the gap capacitances and lower the resonant frequencies of the two resonators. Dielectric tuners are placed above each resonator to fine tune them to the same frequency. A plot of the filter's response characteristics is given in Fig. 4.

Excluding transition losses, the filter insertion loss at 53.46 GHz is 5.5 dB. This is slightly greater than the 3-dB loss expected when considering microstrip line losses at this frequency. The discrepancy is probably due to small deviations from the $\lambda_g/4$ and $3\lambda_g/4$ resonator spacings. This results in imperfect phase addition of the signal at resonance. Radiation effects due to discontinuities can also be a factor.

Matching mixer-diodes

In a broadband receiver, a good match to the mixer diode is desirable, not only at the LO frequency, but over the RF bandwidth. To obtain an image response, the matching band must be even greater. For an LO center frequency of 53 GHz, and an IF bandwidth of 2 to 4 GHz, the diode match must be good from 49 to 57 GHz.

One approach to diode matching models the parasitics of a beam-lead mixer diode using COMPACT to generate a broadband matching network. The model, shown in Fig. 5(a), is for a medium-barrier diode with 1.5 mA bias current.[5]

A matching network designed on COMPACT assumes four shunt, open-circuit stubs of 70Ω (0.010 in. wide). The optimization results in the dimensions shown in Fig. 5(b). The calculated VSWR is less than 2.0:1 from 51 to 57 GHz, and peaks to 3.9:1 at the low end (49 GHz). When this network was tested the input match was better than 2.0:1 between 52 and 59 GHz, with a diode bias current of 1.5 mA. Lengthening each stub by 0.004 in. results in an improved match at 50 GHz, but the match degrades sharply above 57 GHz. The dimensions given in Fig. 5(b) offer the best performance.

With an LO frequency of 53 GHz, the following IF conversion losses are observed using a Ka-band beam-lead diode: 6.9 dB at 750 MHz, 7.5 dB at 2 GHz, and 12.5 dB at 4 GHz. The higher conversion loss at higher IF frequencies is attributed to the length of the IF ground return on the RF side of the diode. The return is made through the tapered transition. This can be corrected with a modified layout to achieve flat conversion loss over a wide IF band.

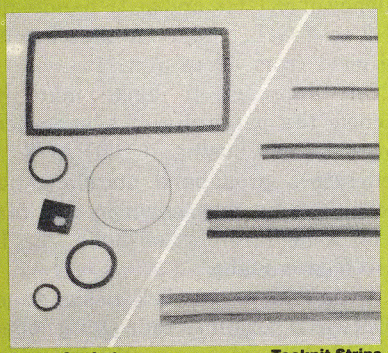
The design parameters for a microstrip junction circulator (Table 1)

(continued on next page)

#1 in EMI Shielding for MICROWAVE Applications

Die-Compressed Mesh Gaskets, high volume, low-cost gaskets manufactured to custom applications requiring rings and special rectangular shapes with holes or slots, corner radii and other essential features.

Tecknit Strips, knitted wire mesh providing low compression closure force. A cost-effective material available in a wide variety of customized and standard cross sections.



Mesh Gaskets Tecknit Strips

THINK OF US AS THE EMI EXPERTS YOU ALWAYS WANTED ON YOUR STAFF.

Write for the TECKNIT Data Guide or call to discuss an EMI shielding problem.



TECKNIT®

EMI Shielding Products
129 Dermody Street,
Cranford, NJ 07016
(201) 272-5500
320 North Nopal Street
Santa Barbara, CA 93103
(805) 963-5811
TWX (710) 996-5951
TELEX 685-3079TCKNT

LS-1-81

READER SERVICE NUMBER 60

Table 1: Design parameters for millimeter microstrip junction circulator

No.	Parameter	Values
1	Center frequency	53 GHz
2	Saturation magnetization	5000 G
3	Diameter of ferrite disk	38 mils
4	Thickness of ferrite disk	5 mils
5	Transformer inner conductor width	14 mils
6	Length of transformer	42 mils
7	External magnetic field (H_{ext})	3475 Oe

Table 2: Dielectric resonator materials—parameters and performance

Dielectric material	Resonant frequency		t (mils)	2R (mils)	Q_0
	Design (GHz)	Measured (GHz)			
Barrium tetratitanate	53	52.25	15.5	50	750
Zirconium tin tetratitanate	59	57.28	14.0	43	575

are generated using established procedures. A photograph of the complete circulator is shown in Fig. 6.

The ferrite pucks are made by cutting a ferrite rod into large disks (250-mil diameter) to a 5-mil thickness, metallizing both sides by sputtering, and slicing the disks into small rectangles. Then the rectangles are ground to the desired diameter. The disks are metallized to eliminate the possibility of air gaps, which degrade junction circulator performance.

The circulator is assembled by soldering a spider (a conductor with three arms) to the top of the ferrite and inner conductor. Then a 1-mil copper disk is soldered to the bottom of the ferrite and ground-plane of the shielded microstrip.

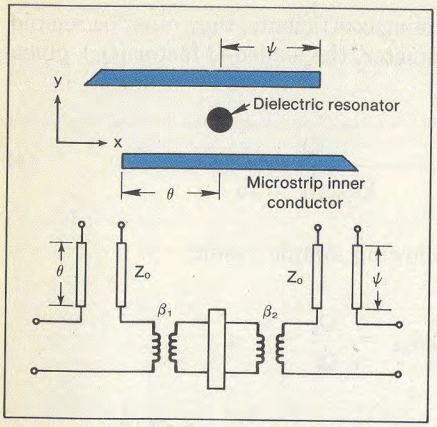
The operating center frequency of the circulator is 56.8 GHz, 3.8 GHz above design frequency. In the microwave bands, the actual operating frequency occurs below the design frequency. The discrepancy results primarily from variations in the relative dielectric constant with frequency. At this time, however, the ferrite material has not been characterized in the frequency range of interest. To get the operation down to 53 GHz, it is necessary to increase the ferrite diameter by 42 mils.

The circulator insertion loss of 0.7 dB —over a 3-GHz frequency range—is determined after subtracting the intrinsic input/output transmission line losses. In addition, the required external magnetic field (H_{ext}), calculated theoretically (see Table 1), is 3475 Oe. But the actual field used and experimentally optimized is 2550 Oe, confirming previously reported results.[6]

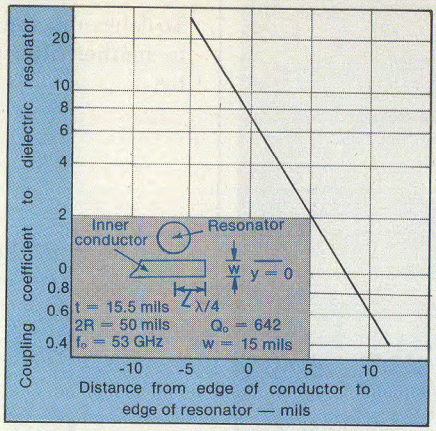
Dielectric resonator needed

Microwave integrated circuit oscillators are much less stable than their waveguide counterparts because of the low unloaded quality factor (Q_0) associated with microstrip resonators. For frequency stabilizing, the techniques used include passive dielectric resonators,[7] active orthogonal microstrip resonators,[8] and diplexers.[9] By far, the simplest approach is the use of a dielectric resonator, and this technique was pursued for its potential applications in controlling the frequency of a Gunn-diode oscillator at V-band frequencies.

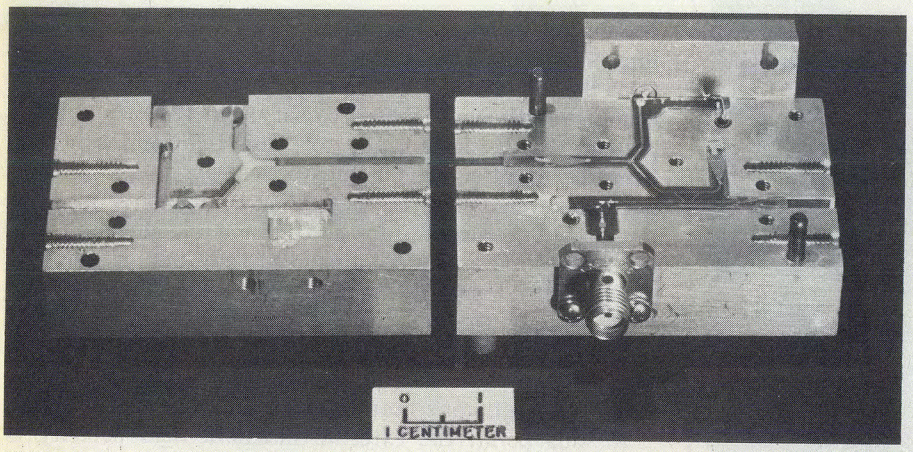
Figure 7 shows a conceptualized dielectric-resonator-controlled oscillator along with its equivalent circuit. An impedance characteristic of the active device is vital to the design of any oscillator, but it requires special diagnostic equipment that was unavailable. And without knowledge of the Gunn-diode impedance, it is impossible to directly design a dielectric-resonator-controlled oscillator. Therefore, it is necessary to establish oscillations from the Gunn diode with a



8. In a bandpass-filter *the resonator's coupling coefficients depend on the x-y positions of the resonator between the transmission lines.*



9. Coupling reactance at resonance *can be eliminated by fixing the resonator's horizontal (x) position while varying the vertical (y) position.*



10. The entire V-band receiver is integrated and tested *as a module to determine its performance. At the right is a diagnostic port for testing and aligning the Gunn-diode oscillator. Frequency is adjusted by monitoring the signal level between the RF port on the left and the diagnostic port.*

method that can be easily converted to the dielectric resonator circuit. The technique, the coupled-line transformer oscillator circuit, sets up the conditions necessary to obtain Gunn-diode oscillations at the desired frequency, disregarding output power. The coupled line can be removed and replaced with a dielectric resonator. The position of the dielectric resonator between the transmission lines and its resonant frequency are varied to optimize the output power. By varying the position of the resonator between the transmission lines, the coupling coefficients vary, thus changing the impedance to the Gunn diode.

With this approach, as much as 30 mW of output power is available in the 54-to-55-MHz range. A temperature stability of 18 ppm/°C is achieved with barium tetratitanate as the dielectric resonator. The measured Q_{ext} is 145. Note that the temperature stability figure includes the stability of the Impatt-diode oscillator used as a local oscillator.

To gain complete control of the oscillating frequency, it is necessary to reduce or eliminate the step discontinuity between the microstrip ground plane and the Gunn diode. This is accomplished by placing a washer with an inner diameter of 50 mil around the Gunn diode.

A new resonator material

Microstrip dielectric resonator parameters have been described previously (see "Applying High-Q Resonators To MM-Wave Microstrip," *Micro Waves*, December 1980, p. 62). The parameters are given in Table 2. The table includes experimental results of resonant frequency and the unloaded Q factor (Q_0). Comparing the theoretical and experimental data gives excellent results.

The table also contains experimental results regarding zirconium tin tetratitanate (ZST), a new dielectric resonator material. Introduced a year ago by the Murata Company, ZST features:

- a highly stable temperature coefficient,
- a wide selection of temperature coefficients, and
- a high quality factor (Q_0 = 6000 minimum at 7.0 GHz).

These features suggest applications such as: high-quality and temperature-insensitive filters; ultratemperature-stable oscillators (in which the dielectric resonator compensates for the temperature characteristics of circuits); and active devices.

The results in Table 2 are for type C ZST with a temperature variation approaching 0 ppm/°C. While the quality factor of ZST is 25 percent lower than that of barium tetratitanate, it has the very attractive feature of temperature stability.

The actual oscillator realization requires that the dielectric resonator operate in the bandpass-filter configuration of Fig. 8. The key to achieving specific input and output coupling coefficients in the oscillator design is knowing the location of the dielectric resonator between the input and output transmission lines.

The best way to obtain such information is by the experimental characterization of the coupling coefficients. This objective is important in the millimeter-wave frequency range because of the limitations of diagnostic instrumentation, and the need for accuracy. These constraints necessitate a novel coupling-coefficient characterization based strictly on insertion loss and frequency measurements. The technique uses a microstrip dielectric resonator operating in the bandpass-filter mode as shown in Fig. 9. The input and output coupling coefficients can be changed by varying the vertical (y) or horizontal (x) position of the microstrip dielectric resonator between the transmission lines. However, it is preferable not to have any coupling reactance at resonance. This dictates that the horizontal position be fixed and the vertical position be changed to vary coupling coefficients.

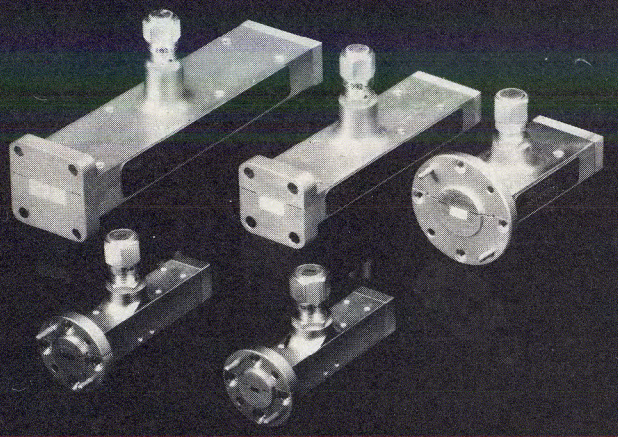
The insertion loss (IL) of the bandpass filter depends on the input (β_1) and output (β_2) coupling coefficients given by:

$$IL = 20 \log_{10} \left[\frac{1 + \beta_1 + \beta_2}{2\sqrt{\beta_1 \beta_2}} \right] \quad (3)$$

(concluded on next page)

TEK WAVEGUIDE MIXERS

Now from Tektronix: amplitude calibrated waveguide mixers to 140 GHz.



These Tektronix waveguide mixers together give you frequency coverage from 18 to 140 GHz, with −75 dBm sensitivity at 140 GHz and frequency response of ±3 dB. The two microwave mixers, WM490K and WM490A, cover ranges 18-26.5 and 26.5-40 GHz and include field replaceable diodes. The three millimeter-wave mixers, WM490U, WM490E and WM490F, cover ranges 40-60, 60-90 and 90-140 GHz. The WM490 Series is designed for use with the Tektronix 492 and 7L18 Spectrum Analyzers. Sets come complete with a container for spare diodes, 28″ cable, instruction manual and storage case.

For more information contact your nearest Tektronix Field Office (listed in major city directories). Or call 800-547-6711 for a data sheet.

Tektronix, Inc., P.O. Box 4828, Portland, OR 97208.
In Europe: European Marketing Centre, Postbox 827, 1180 AV Amstelveen, The Netherlands.

Tektronix
COMMITTED TO EXCELLENCE

Copyright © 1981 Tektronix, Inc. All rights reserved. 962

READER SERVICE NUMBER 61

SHIELDED MICROSTRIP *(continued from p. 81)*

To determine the coupling coefficients, they must be related to another filter parameter, the loaded-Q factor (Q_L), given by:

$$Q_L = \frac{Q_0}{1 + \beta_1 + \beta_2} \tag{4}$$

This leads to the following simple result:

$$2\beta_{1,2} = \frac{Q_0}{Q_L} - 1 \pm \left[\left(\frac{Q_0}{Q_L} - 1\right)^2 - \left(\frac{Q_0/Q_L}{\log_{10}^{-1} \frac{IL}{2_0}} \right)^2 \right]^{1/2} \tag{5}$$

Figure 9 shows typical results using this technique. The important point is that the reference for the vertical position (y) is the edge of the lower inner conductor. To achieve large coupling-coefficients, it is necessary that the resonator be placed over the inner conductor. This is indicated in Fig. 9 by the negative sign in the vertical position.

After development, the individual components are integrated and fabricated into the final module shown in Fig. 10. The evaluation and alignment of the Gunn oscillator is accomplished using the diagnostic port shown on the right side of Fig. 0, together with the appropriate polarity of the external magnetic field on the circulator. The position and frequency of the dielectric resonator are adjusted to maximize the oscillator's output power to 22 mW at 55 GHz.

At this point, the external magnetic-field polarity is reversed, which directs the oscillator power to the directional filter. To maximize the circulator isolation and minimize size, an internal resistive-film load must be introduced. This load has a full-wavelength taper and is constructed from 55Ω/□ resistive-film on Mylar. The test also evaluates the circulator performance.

The directional filter's frequency is adjusted by monitoring the signal level between the RF and diagnostic ports (shown in Fig. 10). The performance of this integrated V-band receiver over an 8-GHz bandwidth, in a form of conversion loss, varies from 7.5 to 11 dB. A variation in conversion loss with a frequency of 3.5 dB results primarily from the impedance variation of the RF port at IF frequencies. The module's temperature sensitivity measures 22 ppm/°C over 0 to 70°C.••

References

1. Michale Dydyk, "Shielded Microstrip: Transmission Media for MM-Wave Integrated Circuits," *1981 IEEE MTTS-S International Microwave Symposium Digest*, pp. 99-101.
2. D.L. Saul and D.T. Rubin, "Millimeter Wave Microstrip Filters and Multiplexers", *NOSC Technical Note 287* (October 1977).
3. G. Matthei, et al., *Microwave Filters, Impedance Matching Networks, and Coupling Structures*, Artech House Books, Dedham, MA, p. 864 (1964).
4. A Farrar and A.T. Adams, "Matrix Methods for Microstrip Three-Dimensional Problems," *IEEE Transactions of the MTT-S*, Vol. 20, pp. 497-504 (1972).
5. Diode and Transistor Designers Catalog, 1980, Hewlett-Packard Catalog No. 5952-9880 (7/79) F, p. 180.
6. Michael Dydyk, "Take Two Steps Toward Better Circulator Design," *MicroWaves*, Vol. 18, No. 3, pp. 53-62 (March 1979).
7. J.K. Plourde, et al., "A Dielectric Resonator Oscillator with 5 PPM Long-Term Frequency Stability at 4 GHz," *1977 IEEE Microwave Symposium Digest*, pp. 273-276.
8. B. Glance and W. Snell, Jr., "A Discriminator Stablized Microstrip Oscillator," *IEEE Transactions of the MTT-S*, Vol. 24, pp. 648-650 (1976).
9. D. Rubin and D. Saul, "MIC Millimeter-Wave (Channelized Downconverter," *NOSC's Technical Note 550* (October 1978).

Harmonic Generators Have High Efficiency

The increasing availability of high-cutoff frequency Schottky-barrier diodes has made it possible to develop millimeter-wave harmonic generators. They offer usable LO power with solid-state reliability.

SINCE solid-state millimeter-wave sources began competing with tube devices, such as reflex klystrons or backward-wave oscillators, as the power sources for low-noise heterodyne receiver LOs,[1] the race has been on to push these sources to higher frequencies and power levels. The development of IMPATT diodes and Gunn oscillators has hastened the replacement of the higher power, but less reliable, tube devices. Now, by combining high-cutoff-frequency Schottky-barrier varactor diodes with lower frequency solid-state oscillators,[2,3] it's possible to create all-solid-state sources for frequencies above 100 GHz (Fig. 1).

The key lies in the optimization of the varactor diodes and the mount. For a high-quality multiplier, the combination should offer the highest possible conversion efficiency/bandwidth product. The conversion efficiency (η) for an ideal varactor harmonic generator is defined as:[4]

$$\eta = \exp(-\alpha f_{out}/f_{co}) \qquad (1)$$

where f_{out} is the output frequency, f_{co} is the dynamic cutoff frequency (a figure of merit for a given varactor diode), and α is a parameter related to the output harmonic number and the input drive level. The greatest conversion efficiency occurs at the highest dynamic cutoff frequency. However, high conversion efficiency strongly depends on the performance of the varactor diode and its surrounding waveguide circuitry as well as an adequate impedance match between the two at the fundamental pump frequency (ω_0) and the desired output harmonic ($n\omega_0$).

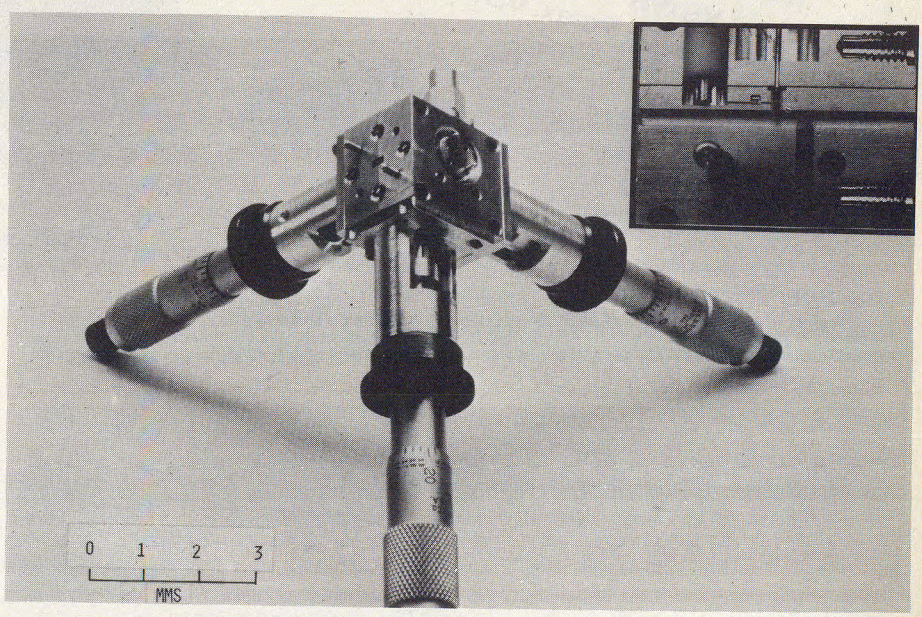
John W. Archer, Research Engineer, National Radio Astronomy Observatory, Charlottesville, VA 22901, and **Bart B. Cregger, Robert J. Mattauch,** and **James D. Oliver, Jr.,** University of Virginia, Charlottesville, VA 22901.

Mount design is important

The first step in the development of a high-efficiency frequency multiplier is the design of a suitable mount. The mount and varactor should be designed so they are well-matched over a broad band of frequencies. On the other hand, the diode impedance should be poorly matched to the mount embedding impedance at undesired pump harmonics, so power flow at these frequencies is minimized, and conversion efficiency is optimized.

One such mount, the crossed waveguide type, is shown in Fig. 2. The power incident in the full-height imput waveguide is fed via a tunable transition to a seven-section suspended-substrate low-pass filter. The filter passes the pump frequency with low loss, but cuts off higher-order harmonics. It also transforms the impedance of the pumped varactor at the input frequency to a convenient value at the plane of the input waveguide-to-stripline transition. Two adjustable waveguide stubs with sliding contacting shorts perform the impedance matching for the pump circuit. One stub operates as a backshort for the waveguide-to-stripeline transition and the second acts as an E-plane series stub located approximately $\lambda_g/2$ (at the pump wavelength) towards the source from the plane of the transition. Typically, by adjusting these tuners, the mount can be matched to the diode at any pump waveguide operating frequency. Additionally, the short positions can be optimized for good fixed-tuned pump performance over a bandwidth of greater than 30 percent of a given center frequency.[3]

The whisker-contacted varactor chip (mounted on the filter substrate) is located, along with a tuning backshort,



***1. This crossed-guide harmonic generator** outputs 110 to 170 GHz. The inset shows the input waveguide running horizontally and the output waveguide running vertically, out of the plane of the photo at top.*

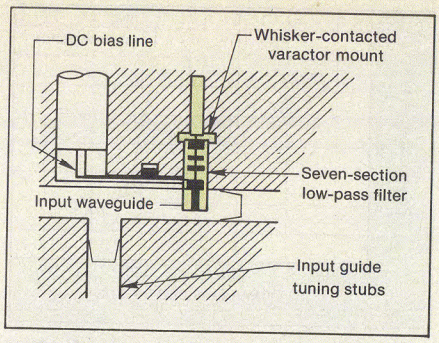
in the reduced-height output waveguide. The varactor receives DC bias through a transmission line filter. This quarter-wavelength-long 140-ohm transmission line consists of a 0.001-in.-diameter gold center conductor, bonded at one end to the low-impedance section of the low-pass filter and at the other end to a 100 fF quartz dielectric bypass capacitor. For shielding purposes, it is enclosed in a rectangular housing machined into the mount.

The reduced-height guide is coupled to the full-height output guide by means of a quarter-wave, three-section, step impedance transformer. The position of the transformer relative to the plane of the varactor diode can significantly affect the performance of the multiplier mount.

In general, the steps in waveguide height in the transformer excite nonevanescent, higher-order waveguide modes in the output guide at frequencies above the desired output harmonic. Since spurious mode coupling influences the mount embedding impedance which the diode "sees" at these higher harmonics, it has been used to enhance mount performance by empirically optimizing the design and position of the transformer.

By designing the transformer so that it is cut off at the second harmonic and spaced approximately $\lambda_g/2$ (at the second harmonic wavelength) from the plane of the diode, the transformer provides a second harmonic idler termination when implementing a frequency tripler.

Through computer-aided analysis, it's possible to determine the characteristics of the reduced-height waveguide cavity. The computer simulation, based on previous studies,[5] was used as an initial design procedure to determine the complex embedding impedance of the waveguide cavity as a function of backshort position at harmonic frequencies of the pump. Unfortunately, this analysis assumes an idealized mount geometry, and doesn't take into account mode coupling at the waveguide transformer at high pump harmonics. As a result, the accuracy is limited at these high harmonic frequencies. However, scale-modeling frequency doubler mounts at lower frequencies, where circuit impedances can be checked with a network analyzer, shows that the computer simulation can reasonably approximate a practical multiplier up to about the fourth harmonic.



***2. This waveguide mount** was used to develop the high-frequency multipliers. It must be matched to the impedance of the varactor diode at the fundamental input frequency, but mismatched at unwanted harmonics.*

Because, in general, there is no unique diode for a given mount which will provide simultaneous pump and output impedance matching, the choice of this component represents a trade-off among several competing requirements. Since the output guide is cut off at the pump frequency, the embedding impedance seen by the varactor diode at this frequency is not influenced by the tuning of the output backshort, except when the backshort is positioned very close to the diode. Ideally, the diode reactance at the pump center frequency should be near resonance with the mount impedance, in order to simplify broadband impedance matching of the input circuit. However, the diode parameters determined on this basis should not preclude adequate tuning by the backshort at the output harmonic frequency. In satisfying these requirements, it may be necessary to examine many different mount and diode parameter combinations.

Diode parameters are limited by practical considerations. The dimensions of the output waveguide are constrained by mechanical requirements, and guide impedances of much less than 200 ohms are difficult to achieve.

Two assumptions are made. The first is that the pump voltage is a sinusoidal waveform which swings between zero bias and the breakdown voltage. The second is that an inverse one-half-power capacitance law is valid in this voltage range for the reverse-biased Schottky-barrier varactor. Then for a suitable diode reactance, the required approximate diode zero-bias junction capacitance can be estimated in a straightforward manner. This approximate capacitance, along with an assumed practical value for the series resistance of the varactor-mount combination, are the foundations of a dynamic, large-signal, nonlinear analysis based on earlier techniques.[6,7]

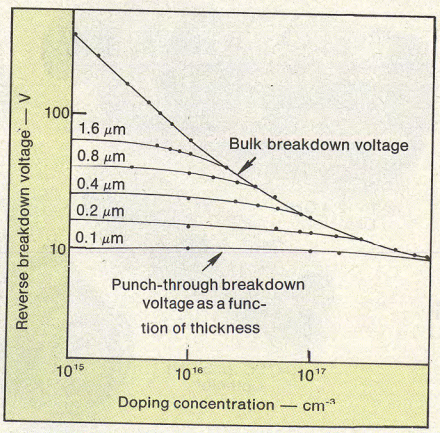
The analysis determines instantaneous voltage and current waveforms in the mounted diode for one pump cycle. For each multiplier mount, conductance capacitance, voltage, and current waveforms must be determined. From these waveforms, it's possible to verify the performance of each mount-diode combination, and to determine the maximum reverse breakdown voltage of the diode for a given pump power-handling capacity.

Designing the diode

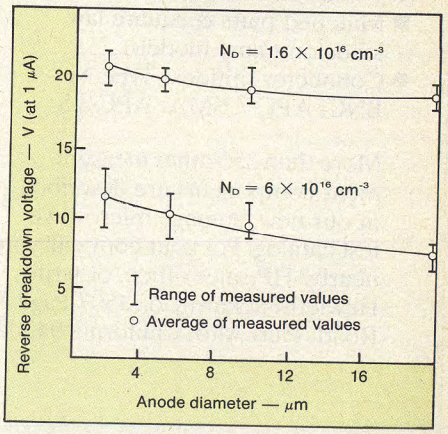
Three varactor diode electrical parameters must be chosen to achieve high-efficiency harmonic generation:

- zero-bias junction capacitance,
- device series resistance, and

(continued on next page)



***3. Bulk and punch-through breakdown voltages** are shown as functions of doping concentration for various layer thicknesses.*



***4. Reverse breakdown voltage** increases slightly for decreasing anode size. This effect was studied for two different doping concentrations.*

• reverse breakdown voltage.

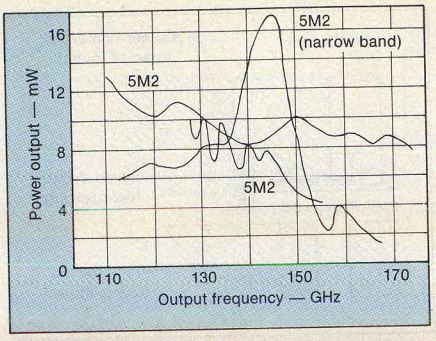
These parameters are intimately related to the varactor epitaxial-layer doping concentration and thickness, as well as the nature of the metal-semiconductor contact area. By considering them carefully, it's possible to achieve an optimum match between laboratory measurements and computer predictions.

It has been noted that the common figure of merit used to characterize harmonic generator varactors is the dynamic cutoff frequency,[8] given by:

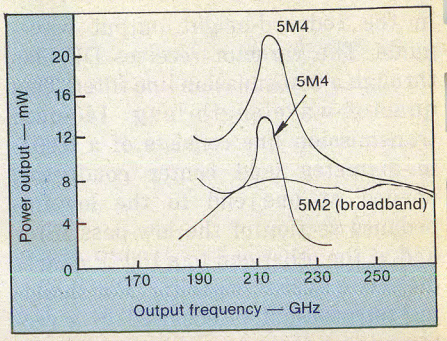
$$f_{co} = (S_{max} - S_{min})/2\pi R_s \quad (2)$$

where S_{max} and S_{min} are maximum and minimum device elastances (inverse capacitances), respectively, and R_s is the device series resistance. Highest dynamic cutoff frequencies are attained when the range of voltage-variable elastance (or capacitance) is maximum and series resistance is minimum.

In theory, highest conversion efficiencies are obtained when no appreciable conduction current flows in the varactor at any time during a complete cycle of the pump. Thus, in general, harmonic generator varactor diodes are operated in the current-voltage region between reverse breakdown and forward turn-on with only displacement current flowing in the device.



***5. These performance curves for the 110-to-170-GHz frequency multipliers** show the results for different varactor diodes.*



***6. These curves of output frequency versus power output** are for the 190-to-260-GHz multipliers, using different varactor diodes.*

Material parameters significantly affecting reverse breakdown voltage are epitaxial layer thickness and doping concentration. When reverse voltage breakdown is of a bulk nature, the doping concentration is chosen so that the varactor will support the full peak-to-peak swing of the pump voltage without being driven into forward turn-on or avalanche breakdown.

Avalanche breakdown is expressed by setting the ionization integral to unity.[9] For GaAs, where electron and hole ionization rates are considered equal, this becomes:

$$\int_0^W A \exp\left[-(b^2/E^2_{max}) \times \left(1-\frac{x}{W_s}\right)^{-2}\right] dx = 1 \quad (3)$$

where A and b are the ionization coeffi-

HP's Small Wonders

A wide selection of detectors

- 11 Coaxial models for 1000 MHz, 12.4 GHz, 18 GHz & 26.5 GHz
- 9 Waveguide models to 40 GHz
- Matched pairs & square law loads on many models
- Connector options: Type N, BNC, APC-7, SMA, APC-3.5

More than 350 other measurement components are described in our new, 96-page microwave test catalog. For your copy call your nearby HP sales office, or write Hewlett-Packard Co., 1507 Page Mill Road, Palo Alto, California 94304.



04911

HEWLETT PACKARD

READER SERVICE NUMBER 63

cients of GaAs, E_{max} is the maximum electric field present, W_s is defined as $[2(V_{app} + 0)\ \epsilon_o\ \epsilon_{rel}/qN_D]^{1/2}$ (for an abrupt junction), and W is the width of the space-charge region.

It is sometimes necessary to consider a premature, *punch-through*, breakdown voltage which can occur when breakdown voltage is reached at lower voltage levels than expected. This takes place when particular epitaxial-layer doping thicknesses can't support the breakdown voltage associated with that of bulk material.

By using computer analysis, the ionization integral for GaAs was evaluated so that bulk and punch-through breakdown voltages could be determined as functions of doping concentration and thickness. The results appear in Fig. 3. The analysis is invaluable in choosing the initial epitaxial doping concentration and thickness —on one hand, to avoid avalanche breakdown, and on the other hand, to find the lowest possible series resistance.

There is a subtle, but important, consideration when studying reverse breakdown voltage: the effect of the small anode size generally associated with these devices. Because of edge effects, the reverse breakdown voltage (measured at 1 μA) increases slightly with decreasing anode diameter for a given epitaxial layer doping. Figure 4 shows the experimental results of such an effect, for multisize platinum anodes defined on 0.016 × 0.010-in. samples of GaAs, doped to 1.6×10^{16} cm^{-3} and 6.0×10^{16} cm^{-3}. For each chip, the material was assumed to be homogeneous.

Of course, there may be more than one doping concentration and thickness combination for a desired reverse breakdown voltage. As a rule, higher-doped epitaxial layers will result in lower device series resistance, and, in turn, yield devices with higher dynamic cutoff frequencies. Thus, doping and layer thickness should be chosen with two guidelines in mind: to give the required reverse breakdown voltage for the varactor, and to minimize device series resistance.

Once an epitaxial layer is chosen, device geometry (anode diameter for circular junctions) must be determined for the predicted zero-bias junction capacitance. Including edge effects, this circular anode, zero-bias junction capacitance has been modeled as:[10,11]

$$C_{j0} = \frac{\epsilon_{rel}\ \epsilon_0\ \pi D^2}{4d}\left(1 + \frac{2yd}{D}\right) \quad (4)$$

where D is the anode diameter, d is the zero-bias depletion width (given by $d = [2\epsilon_{rel}\epsilon_o\phi/qN_d]^{1/2}$ for an abrupt junction), and y is given by the relation[11] ($y = 1.416 + 1.72/\epsilon_{rel}$). Using the predicted zero-bias junction capacitance, the epitaxial layer, an assumed relative dielectric constant, ϵ_{rel}, and ϕ, barrier height potential, the necessary diameter of the varactor device may be determined.

In order to evaluate series resistance, an applicable model was chosen.[12] It shows that for devices with micron-sized diameters, series resistance is dominated by the undepleted epitaxial layer. For this reason, particular attention should be paid to the choice of the highest possible doping concentration with the thinnest possible epitaxial layer, consistent with the desired reverse breakdown voltage.

Using the results

With these design techniques in hand, varactors were fabricated on vapor-phase epitaxial GaAs with epilayer Si doped to 4 to 5 × 10^{16} cm^{-3}. Standard pyrolytic oxide deposition and photolithographic techniques were used to define 4-to-5-μm-diameter windows in the SiO_2. The windows were subsequently pulse-plated with Pt to form Schottky barriers.

Performance curves for various harmonic generators are shown in Figs. 5 and 6. Figure 5 includes 110-to-170-GHz output frequency doubler test results, while Fig. 6 presents 190-to-260-GHz output device performance. The RF results from these figures, along with the varactor DC characteristics, are collected in the table. The results are identified by the different batches tested.

The power levels shown in Figs. 5 and 6 are sufficient for most low-noise heterodyne receiver mixing purposes. Through experimental investigation of the 110-to-170-GHz doublers, the pump frequency-matching configuration and the step-impedance transformer design were optimized. This optimization has resulted in a fixed-tuned, fixed-bias frequency doubler. It exhibits a median conversion efficiency of 12 per-

(concluded on next page)

Table: Summary of varactor frequency multipliers

Batch	DC characteristics				RF characteristics		
	V_{BR} (V)	C_{jo} (fF)	R_s (ohms)	f_{co} (THz)	Output frequency (GHz)	P_{max}/η_{max} (mW/percent)	P_{min}/η_{min} (mW/percent)
5M2	14.5	21	11	2.7	110-170	10/20 (@131 GHz)	3/6
					110-170(broadband)	13/16	8/10
					110-170(narrow band)	16/20 (@145 GHz)	—
					190-260(broadband)	8/10	6/75
5M4	14	15	6.3	6.6	190-260(narrow band)	215/27 (@215 GHz with 80 mW pump power)	
					190-260(narrow band)	14/28 (@213 GHz with 50 mW pump power)	

cent for 50 mW pump power, with a total variation of less than 2.5 dB, over the 80 to 120 GHz range.[3]

The effect of varactor characteristics on the harmonic generator output performance was investigated for devices with approximately the same zero-bias junction capacitance. Those with significantly higher dynamic cutoff frequencies resulted in improved multiplier performance (higher conversion efficiency and broader bandwidth). Furthermore, for the limited number of devices which were available for testing, those with slightly higher zero-bias junction capacitances (due likely to material and/or metal-semiconductor contact area inhomogeneities) and lower DC series resistance values consistently resulted in better multiplier performance for any given mount.

It's interesting to note that the 80-to-120-GHz doubler with the greatest reported efficiency/bandwidth product used a 5M2 varactor with a zero-bias junction capacitance of 21 fF and a series resistance of 8 ohms.[3] Even though the dynamic cutoff frequency of the 5M2 device was significantly less than that of the 15-fF 5M4 device, better performance came with the higher capacitance device. This is probably due to a better impedance match at the input and output frequencies.

Very recently, a 215-GHz frequency tripler, using a 5M2 varactor, was developed and tested. For a pump power of 80 mW, the output at the center frequency was 4.8 mW, with an instantaneous 1-dB bandwidth of 3 GHz.[2] When a 5M4 device was substituted, the performance was comparable, with slightly higher peak efficiency but more restricted tuning ability.

Present work is aimed at the development of 80-to-120-GHz varactor devices capable of supporting much higher pump power levels (about 150 to 200 mW), without a significant reduction in the dynamic cutoff frequency. Higher zero-bias junction capacitance devices are desirable for devices in this frequency range, since they permit a better device-waveguide impedance match at both input and output frequencies. Devices with significantly increased voltage/variable-capacitance levels (possibly hyperabrupt epitaxial layers) may also result in the improvement of the efficiency/bandwidth products of these multipliers.••

Acknowledgement

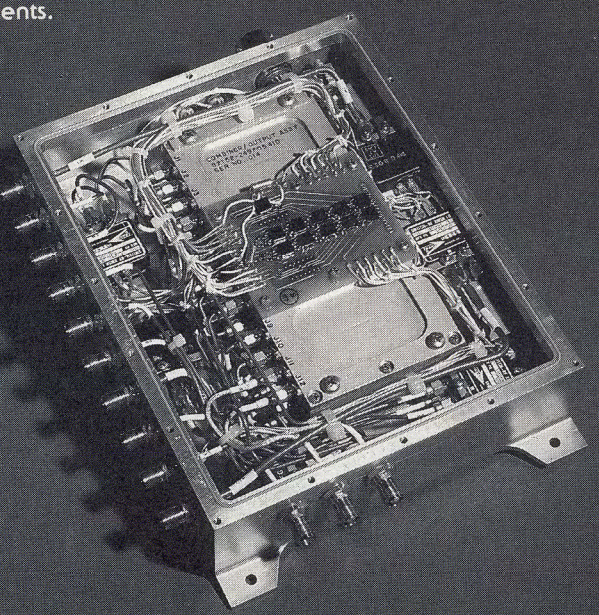
This work was supported in part by the National Radio Astronomy Observatory, which is operated by Associated Universities, Inc. under contract with the National Science Foundation, and by the National Science Foundation under Grant ECS80-22937.

References

1. J. W. Archer, "A Portable All-Solid-State Low-Noise Receiver for 230 GHz," presented at the 1981 IEEE International Conference on Infrared and Millimeter Waves (December 7-12, 1981).
2. J. W. Archer, "Millimeter Wavelength Frequency Multipliers," *IEEE Transactions on Microwave Theory and Techniques*, Vol. MTT-29, No. 6, pp. 552-557 (June 1981).
3. J. W. Archer, "A High Performance Frequency Doubler for 80 to 120 GHz," *IEEE Transactions on Microwave Theory and Techniques*, Vol. MTT-30, No. 5 (May 1981).
4. J. W. Gewartowski, *Microwave Semiconductor Devices and Their Applications*, H. A. Watson, ed., McGraw-Hill, New York, NY, Ch. 8 (1969).
5. R. L. Eisenhart and P. J. Khan, "Theoretical and Experimental Analysis of a Waveguide Mounting Structure," *IEEE Transactions on Microwave Theory and Techniques*, Vol. MTT-19, pp. 706-719 (August 1971).
6. P. H. Siegel and A. R. Kerr, "A User Oriented Computer Program for the Analysis of Microwave Mixers, and a Study of the Effects of the Series Inductance and Diode Capacitance on the Performance of Some Simple Mixers," NASA Goddard Space Flight Center, Greenbelt, MD, NASA Tech. Memo, No. 80324 (July 1979).
7. D. N. Held and A. R. Kerr, "Conversion Loss and Noise of Microwave and Millimeter-Wave Mixers: Part II—Experiment," *IEEE Transactions on Microwave Theory and Techniques*, Vol. MTT-20, No. 2, pp. 49-61 (February 1978).
8. P. Penfield and R. P. Rafuse, *Varactor Applications*, MIT Press, Cambridge, MA (1962).
9. S.M. Sze, *Physics of Semiconductor Devices*, Wiley-Interscience, New York, NY, Ch. 3 (1969).
10. J. A. Copeland, "Diode Edge Effects on Doping-Profile Measurements," *IEEE Transactions on Electron Devices*, Vol. ED-17, No. 5, pp. 404-407 (May 1970).
11. E. Wasserstrom and J. McKenna, "The Potential Due to a Charged Metallic Strip on a Semiconductor Surface," *Bell System Technical Journal*, Vol. 49, No. 5, pp. 853-877 (May 1970).
12. E. R. Carlson, M. V. Schneider, and T. F. McMaster, "Subharmonically Pumped Millimeter-Wave Mixers," IEEE *Transactions on Microwave Theory and Techniques*, Vol. MTT-26, No. 10, pp. 706-715 (October 1978).

LOOK WHAT'S IN THE BOX!

10 of our QPL* SPDT Coaxial switches with SMA connectors along with the following special TRANSCO products. 1 TTL compatible switch driving network. 34 cable assemblies with RG 188 flexible cable and UT 085/UT 141 rigid cable. 10 directional couplers, 20 to 1 bandwidth and 1 10 way power combiner. All of that assembles into TWO 20 to 1 bandwidth RF distribution networks, packaged ever so sweetly into a 10" x 8" x 2" rugged, EMI/moisture sealed enclosure to pass stringent RF leakage tests and withstand the most severe airborne environments.



If you have a packaging problem, remember we're not just in the component business. We can provide quality component integration as well. TRANSCO quality. Nothing less, since 1942.

Request a set of the TRANSCO component data sheets.

*Qualified Product List MIL-S-3928

TRANSCO PRODUCTS, INC.

4241 Glencoe Ave.
Marina Del Rey, California 90291 U.S.A.

FOR EMPLOYMENT OPPORTUNITIES IN RF ENGINEERING, CALL CHARLIE TALBOT.
AN EQUAL OPPORTUNITY EMPLOYER M/F.
Tel: (213) 822-0800 Telex 65-2448 TWX 910-343-6469
1-800-441-7513 EXT 310

TPI

Military Fiber-Optic Links: Can They Take The Heat?

Fiber optics are being evaluated for use in military vehicles likely to encounter nuclear radiation. These computations show they may be no better than the wired systems they replace.

FIBER-OPTIC communication systems have been proposed as alternatives to wired wideband and microwave links in military equipment which will be exposed to nuclear radiation. For example, the Lockheed-Georgia Company demonstrated a fiber-optic system in 1979 installed in their jet-powered Caproni research aircraft.[1] The McDonnell-Douglas Astronautics Company uses a fiber-optic link in the Ground Launch Cruise Missile,[2] and a fiber-optic system is scheduled for installation in the MX intercontinental ballistic missile (ICBM).[3] And, in a unique, simulated radiation environment, a complete satellite will be exposed to radiation in a test cell, while a fiber-optic system will connect the satellite to instrumentation outside the radiation chamber.[4]

Both silica and plastic fiber sustain optical degradation when exposed to nuclear radiation, and lengths as short as 10 m can fail to provide reliable communications in such an environment. The length of the optical fibers used in the stated examples range from 30 m in the Caproni aircraft to 90 m in the satellite test chamber.

In order to demonstrate the susceptibility of optical fibers to damage from nuclear radiation, four factors must be considered: the operational scenario, radiation penetration energy, system dynamic range, and communications link margin. These factors are used to predict the expected lifetime of the fiber-optic system when operating in a radioactive environment.

Nuclear environment

At least three types of military vehicles may be exposed to nuclear radiation: an intercontinental ballistic missile, a fractional orbiting bomb (FOB), and a satellite in either circular or synchronous orbit. All of these vehicles may encounter quasi-steady-state nuclear radiation for extended periods of more than ten minutes. The vehicle need not be attacked directly by a nearby nuclear blast; radiation clouds or fallout are known to linger for long periods of time. When a nuclear device was detonated about 400 km above Johnston Island in 1962, the ensuing radiation cloud extended for a distance of some 1000 km from the drop site, and produced a slowly decaying artificial electron belt.

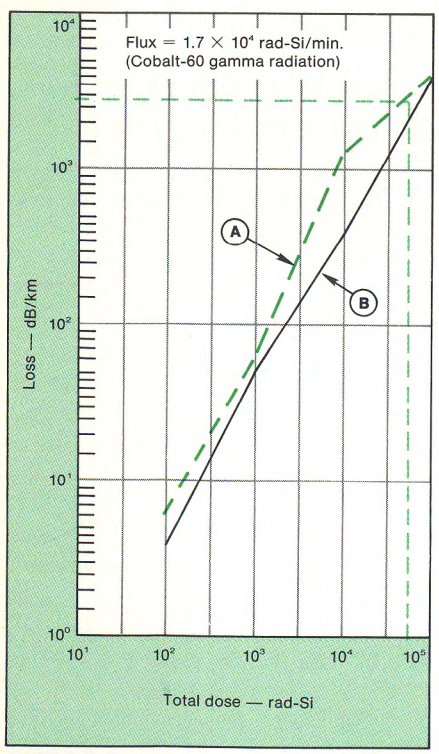
By 1968, six years later, calculations showed that about 50 percent of the electrons in this radiation belt had energies of between one- and three-million electron volts (MeV) for a circular, near-polar orbit at 1200 km.[5] Hence, an ICBM or satellite may be exposed to relatively high-energy nuclear particles for at least several minutes during one pass.

The radiation damage sustained by a device or material depends upon factors such as: the type of radiation (protons, electrons, neutrons, X rays, gammas, etc.), the particle energy in MeV, the radiation flux or dose rate, and the fluence (electrons/square centimeter), also called total dose (Rad-Si). Some data concerning the equivalence between displacement damage and ionization damage for several types of radiation particles was presented by the Jet Propulsion Laboratory.[6] However, the authors observed that the correlation between indicated damage constants may vary by a factor of three to one, depending upon particle injection energy.

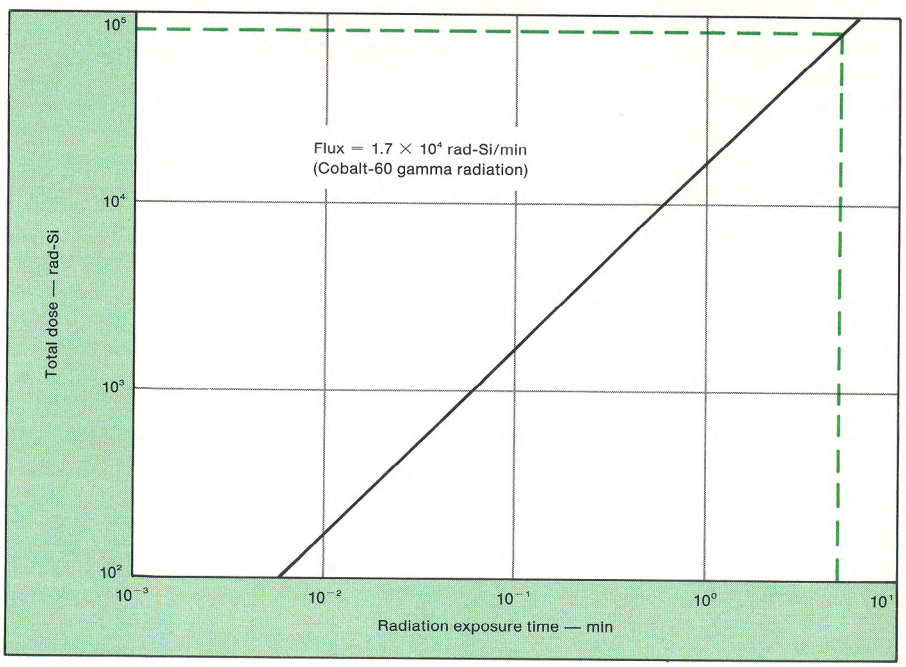
Despite this seemingly poor precision of measurement, the particle energy band of interest has been estimated to be about 0.3 to 30 MeV.[7]

(concluded on next page)

Antonio N. Paolantonio, PE, Radio and Communications Consultant, 17806 Elkwood St., Reseda, CA 91335.



***1. Signal losses for a given dose of nuclear radiation** provide the basis for determination of the usable lifetime of a fiber-optic system.*



***2. Computing total radiation doses for a selected time period** with transmission loss shown in Fig. 1, illustrates that the usable lifetime of a fiber-optic system is quite short. The length selected for study, 10 m, is 20 m shorter than the shortest length cited here.*

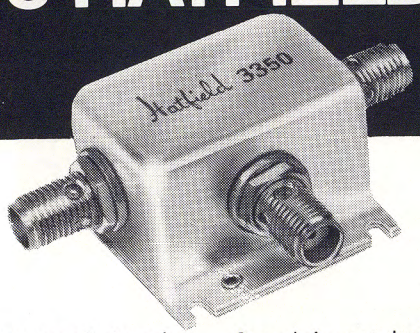
Call them what you like–



Power Dividers
Hybrid Couplers
Signal Dividers
Passive Couplers
Signal Combiners

But get the name right.

It's 'HATFIELD'!



This range of signal processing components consists of passive, constant impedance devices for passing r.f. signals from one to a number of output ports with minimum of loss and high isolation between output ports.

2 and 4-way devices are manufactured in a wide variety of enclosures covering the broad frequency range from 1 kHz to 600 MHz. Send for details of our 3100 Series or our complete signal processing components catalogue.

W&G
W & G Instruments Ltd.
Burrington Way, Plymouth,
Devon, PL5 3LZ
Telephone: 772773
Telex: 45592

MILITARY FIBER OPTICS *(cont. from p. 88G)*

An energy level of 0.5 MeV (electron pulse) impinging the fiber optics has resulted in severe transmission losses.[8]

Fiber-optic communication systems are available with dynamic range from 16 to 23 dB when new. At least one manufacturer claims that a dynamic range of 27 dB for a bit error rate (BER) of 10^{-8} is obtainable for a digital system, and a system power margin of 28 dB for step-index fiber.[9]

The dynamic range is the ratio of maximum to minimum signal power at the receiver which will provide reliable communications with a specified BER, such as 10^{-8}. The link margin is the received power in excess of that required to produce this specified BER. Although one system is specified to have a power margin of 28 dB,[9] a more common figure for link margin is about 10 to 15 dB.

The lifetime of fiber-optic communication systems exposed to nuclear radiation may be defined as the time required for the radiation-induced losses in the fiber cable to exceed the link margin, or when the system signal-to-noise ratio drops below the minimum required for a given BER. In order to compute the cable lifetime, link margin, the length of fiber in the system, and the relationship of the fiber-optic transmission loss and radiation exposure level must be considered.

Assume that the maximum link margin is 28 dB, and that the fiber-optic cable is 10-m long (which is the longest run practical in an ICBM). Radiation test data for several optical fibers is available. Curves of loss versus total dose for two doped silica (radiation-hardened) fibers are presented in Fig. 1. Curve A is for a doped silica fiber manufactured by ITT with the fiber designation of SiO_2 - GeO_2 - P_2O_5 - B_2O_3 (graded). Curve B is for a doped silica fiber manufactured by Schott with the fiber designation of SiO_2 - GeO_2 - B_2O_3- P_2O_5 - Sb_2O_3.

As our hypothetical test cable is 10-m long, a length factor of 100 is used to obtain the total expected cable loss for the 28 dB of link margin. The total loss now becomes 100×28, or 2800 dB. Enter the ordinate of Fig. 1 at 2800 dB, draw a horizontal line across to the fiber-loss curves, and drop to the abscissa to determine total dose. The figure is 8.0×10^4 Rads-Si. Now use Fig. 2 to determine the exposure time required to absorb this total dose. Enter the ordinate of Fig. 2, at 8.0×10^4 Rads-Si, draw a horizontal line to intersect the plotted curve, and drop to the abscissa to find the exposure time. This becomes five minutes.

Therefore, this fiber-optic communication system, 10-m long with a link margin of 28 dB, will be degraded to a margin of zero in about five minutes when exposed to nuclear radiation. If the link margin were only 15 dB, the lifetime of the system would be only two minutes. Thus, a relatively short fiber-optic system is highly susceptible to failure in a single pass of a vehicle through a decaying radiation belt. Attempting to improve radiation resistance of the fiber optics by adding mechanical shielding will only negate the advantages of the fiber optics—light weight compared to coaxial or shielded-wire cables.••

References

1. Rick Cotta, "Fiber Optic Flight Control—Avioptics Progress Slowed By Cable/Connector Mismatches," *Military Electronics/Countermeasures*, April 1980, pp. 59-63.
2. "Fiber Optics in Tactical Systems—Digitized Data at 100 MBaud With No EMI/EMP," *Military Electronics/Countermeasures*, June 1980, pp. 38-41.
3. James B. McNeely and Richard I. Klien, "What About the Longer Wavelengths?" *Optical Spectra*, November 1980, pp. 52-55.
4. James C. Blackburn, "Only With Fibers: Space Radiation Testing," *Optical Spectra*, May 1980, pp. 46-50.
5. Donald F. Heath and Paul A. Sacher, "Effects of a Simulated High-Energy Space Environment on the Ultraviolet Transmittance of Optical Materials Between 1050 A and 3000 A," *Applied Optics*, Vol. 5, No. 6, June 1966, pp. 937-943.
6. Alan G. Stanley, Keith E. Martin, and William E. Price, "Voyager Electronic Parts Radiation Program—Volume II: Test Requirements and Procedures," Jet Propulsion Laboratory Publication 77-41, December 15, 1978.
7. Richard H. Parker, Edward L. DiVita, and Gunter Gigas, "Jupiter's Radiation Belts and Their Effects on Spacecraft," Jet Propulsion Laboratory, internal, 1974.
8. George H. Sigel Jr., "Fiber Transmission Losses in High-Radiation Fields," *Proceedings of the IEEE*, Vol. 68, No. 10, October 1980, pp. 1236-1240.
9. "Operation of ITT Model 2-D Digital Terminals in Optical Fiber Digital Transmission Systems," ITT Electro-Optical Products Division, Optical Fiber Communications, Technical Note R-2, April 1977.

GaAs Compounds Promise Lower Noise MESFETs

Efforts to improve semiconductor noise performance are shifting from reduced device size to more promising materials. Two GaAs compounds stand out in early research.

SIGNIFICANT noise-figure improvements in metal-semiconductor field-effect transistors (MESFETs) is the promise held by two compound semiconductor materials: the ternary $Ga_{0.47}$ $In_{0.53}$ As and the quaternary $Ga_{0.27}$ $In_{0.73}$ $As_{0.6}P_{0.4}$. Potentially superior to GaAs itself in the fabrication of low-noise MESFETs, the quaternary material offers at least a 1-dB improvement over a GaAs MESFET of the same geometry when operated at frequencies above 10 GHz.

The search for new semiconductor materials marks a change in the efforts made to extend the frequency limits of transistors. For decades, research centered on the reduction of the dimensions of silicon bipolar devices. Buoyed by the success of GaAs devices in low-noise and power applications, the attention of researchers has now turned toward even better semiconductor materials.

Although the ternary and quaternary III-V materials have produced encouraging results, work with indium phosphide (InP) MESFETs has not shown significant improvement in noise performance. Fundamental problems exist in the epitaxial growth of quality layers with all three materials, and in the fabrication of large Schottky-barrier-height gate contacts, but many of these problems will be solved in the next five years.

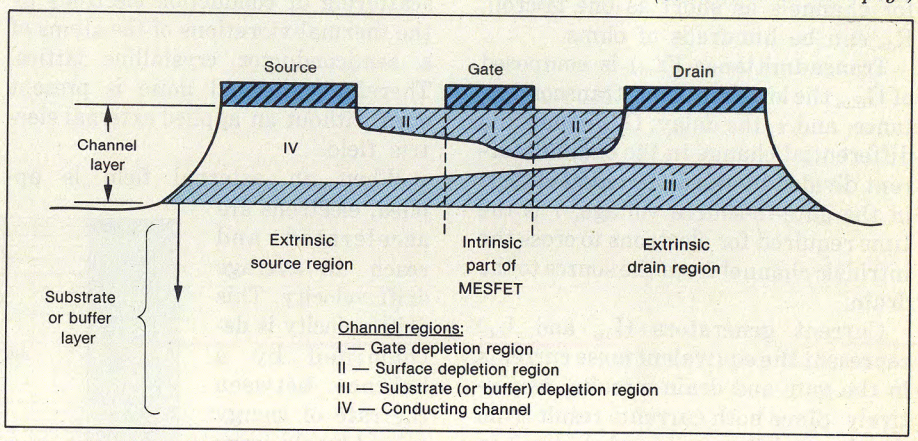
The basic MESFET consists of an n-type active-channel layer on top of either a semi-insulating substrate or a high purity buffer layer that covers the semi-insulating substrate. The active layer is selectively etched to form an electrically isolated mesa, and source, drain, and gate metal contacts are added (Fig. 1). The source and drain contacts are ohmic, and the gate is a rectifying Schottky contact.

The drain-to-source channel current is controlled by the gate-to-source voltage (V_{gs}). When V_{gs} is made more negative, the depletion region under the gate expands, increasing channel resistance and reducing channel current. For a fixed V_{gs}, channel current increases with increasing drain-to-source voltage (V_{ds}). This is only true for low values of V_{ds}, since channel current will saturate at a value that is nearly independent of the drain-to-source voltage when that voltage is high enough. This results from the saturation of the electron drift velocity. The exact value of V_{ds} at which this will occur depends on the semiconductor material, device dimensions, and gate-to-source voltage.

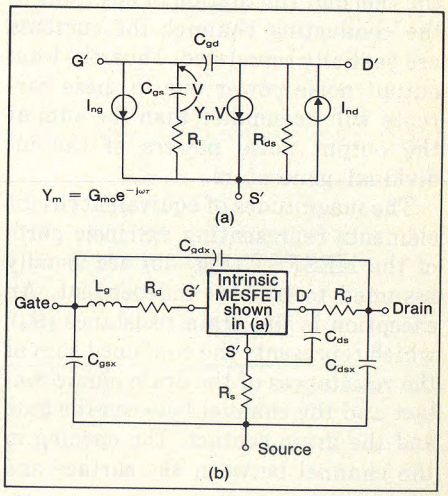
Building an equivalent circuit

The AC equivalent circuit shown in Fig. 2 represents the small-signal operation of a low-noise MESFET at microwave frequencies. Figure 2(a) represents the channel under the gate metal contact, the intrinsic part of the device. The magnitudes of the components of this equivalent circuit will

(continued on next page)



1. In this mesa-type MESFET, *the drain is assumed to be positive and the gate negative with respect to the source. The source and drain contacts are ohmic; the gate is a rectifying Schottky contact.*



2. The small-signal operation of a low-noise MESFET *is represented by these AC equivalent circuits. The first (a) shows the intrinsic part, and the second (b) the extrinsic part of the device.*

Rimantas L. Vaitkus, Research Scientist, and **Tom H. Miers,** GaAs Research Engineer, Semiconductor Research and Development Laboratories, Motorola, Inc., 5005 E. McDowell Rd., Phoenix, AZ 85008.

depend on device dimensions, the semiconductor material, and the values of V_{gs} and V_{ds}. The gate-to-source and the gate-to-drain capacitances (C_{gs} and C_{gd}) appear across the depletion region separating the gate metal from the conducting channel. These are differential capacitances that are due to changes in the dimensions of the depletion region induced by changes in the gate-to-channel potential differences. Under typical bias conditions, the gate and the substrate depletion regions on the drain end of the channel are separated by only a very thin residual conducting channel. Therefore, dimensional changes in the depletion layer in this region are very limited. However, the conducting channel on the source end represents a considerable fraction of the total channel thickness, and the depletion region is free to expand and contract. Thus, the value of C_{gd} will typically be five to 50 times smaller that that of C_{gs}.

The equivalent resistance (R_i) which the channel offers to the gate-to-source AC current represents only a small fraction of R_{ds}, the total drain-to-source intrinsic channel resistance. Under typical bias conditions, the drain end of the channel is pinched to a narrow residual channel, and even for channels as short as one micron, R_{ds} can be hundreds of ohms.

Transadmittance (Y_m) is composed of G_{mo}, the low-frequency transconductance, and τ, the delay. G_{mo} equals the differential change in the channel current divided by the differential change in the gate-to-source voltage; τ is the time required for electrons to cross the intrinsic channel from the source to the drain.

Current generators (I_{ng} and I_{nd}) represent the equivalent noise currents in the gate and drain circuits, respectively. Since both currents result from the thermal fluctuation of electrons in the conducting channel, the currents are partially correlated. Thus, the total output noise power due to these currents will be smaller than the sum of the output noise powers of the individual generators.

The magnitudes of equivalent circuit elements representing extrinsic parts of the MESFET (Fig. 2b) are usually assumed to be bias independent. An exception is the drain resistance (R_d), which represents the combined sum of the resistances of the drain ohmic contact and the channel between the gate and the drain contact. The opening in the channel between the surface and the substrate depletion regions depends on the drain voltage. However, an adequate analytical model for this dependence is not available. Similarly, source resistance (R_s) represents the sum of ohmic contact and the channel resistances at the source.

The inductance (L_g) and resistance (R_g) represent the equivalent impedance of the gate metal strip. Equivalent noise generators for R_s, R_d, and R_g are part of the equivalent circuit, but are not shown.

The fringing electric field in the substrate produces the drain-to-source capacitance (C_{ds}). The capacitances between the gate, drain, and source metal patterns (C_{gsx}, C_{gdx}, and C_{dsx}) include the effects of the wire bonding pads. If a MESFET chip is mounted in a package, additional elements will be needed in the equivalent circuit to represent wire-bond impedances and interelectrode capacitances.

Scattering creates thermal noise

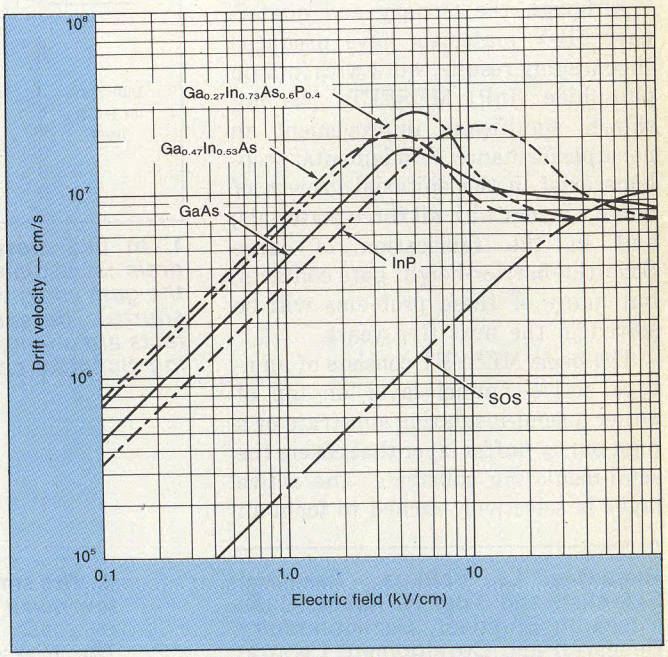
Thermal noise (produced by the electron transport process in semiconductors) predominates among the types of noise that have been identified in MESFETs operating at microwave frequencies. It originates in the random scattering of conduction electrons by the thermal vibrations of the atoms of a semiconductor crystalline lattice. Therefore, thermal noise is present even without an applied external electric field.

When an external field is applied, electrons are accelerated and reach an average drift velocity. This drift velocity is determined by a balance between the rate of energy gained by electrons from the field and the rate of energy lost to the atoms of the semiconductor through collisions. More collisions mean more electron scattering and, hence, more noise. Thus, electron scattering determines the magnitudes of the noise and of the electron drift velocity, which is characterized by a parameter called mobility at low values of electric-field strength. Higher values for mobility produce higher current and lower mean-square noise voltage. This is characteristic of noise generated in the ohmic regions of a channel (those regions represented by the parasitic resistances R_s and R_d) as well as the ohmic part of R_{ds}.

Electron diffusivity, the rate at which a localized electron concentration spreads or diffuses in a semiconductor, is also determined by electron scattering. Low scattering rates result in faster electron diffusion. At low electric fields, diffusivity is proportional to electron mobility.

Intervalley scattering occurs at high electric fields and causes electrons to change from a "light," high-mobility state to a "heavy," low-mobility state. These changes are accompanied by abrupt changes in velocity that produce noise current. Intervalley scattering also produces negative differential mobility regions in the drift velocity versus the electric field characteristics of compound semiconductors.

Channel mean-square noise current at high electric fields is proportional to the high-field diffusivity of the semiconductor. This is characteristic of the noise generated on the drain end of the intrinsic MESFET channel that is biased in the saturated current region. Thus, the magnitude of the electric field determines the level of generated noise in the channel.



***3. Drift velocity is shown versus electric field** for n-type channels with 10^{17} cm^{-3} donor concentrations at 300°K.*

Noise figure is defined as the ratio of the total output noise power to the fraction due solely to the amplified noise of the signal source. Noise figure depends on the MESFET parameters as well as the output admittance of the signal source. Only one value of signal-source admittance allows the best or minimum value of noise figure for any device at a given bias condition; that value is assumed for results presented here.

Approaching low-noise design

A strategy for the design of low-noise MESFETs requires maximum gain and minimum parasitic noise resulting from source, drain, and gate resistances. High gain minimizes the effect of the drain-noise current (I_{nd}) on the noise figure.

MESFET gain can be increased by reducing the gate length. Although a practical limit exists, E-beam lithography is pushing this limit to the 0.25-m region.[1]

Improvements to noise figure due to increased gain with shorter gate lengths can be offset by increases in gate resistance. An increase in gate metal thickness as gate length is reduced can remedy this problem up to microwave skin depth. In addition, there are reliability and process limitations on the gate metal thickness. As an alternative, smaller structures can be fabricated in parallel to achieve the required channel width. Design and fabrication become increasingly difficult, however, as the number of paralleled structures increases.

Source resistance, the sum of ohmic contact and extrinsic channel resistances, plays a significant role in determining noise figure. Contact resistance can be reduced by using epitaxial growth or ion implantation to insert a heavily doped region between the channel and the contact. Extrinsic channel resistance decreases when the space between the source and the gate is reduced, or when a gate recessing process is used. As the spacing becomes smaller, alignment of the contacts becomes more difficult. Self-aligned processes can be used, but these often result in other problems.

The gate recessing procedure starts with a thick channel and places the gate within a recess that has been etched to the proper depth. A variation of this technique forms a heavily doped layer on top of the channel; the gate is recessed through this layer.

Searching for better materials

The optimum semiconductor material for a low-noise microwave MESFET must have a high low-field mobility and a large saturated drift velocity. Since the present low-noise devices have very short channels, low bias voltages on the drain create high fields in the channel, which make the saturated drift velocity one of the dominant parameters for the intrinsic device. A high value of low-field mobility causes drift velocity to saturate at lower values of field strength and is very important in determining the value of the source resistance.

Three possible processes limit drift velocity:[2] increased lattice losses dominate in silicon, electron transfer to heavy conduction band minimums dominate in GaAs, and, avalanching occurs before the peak velocity is attained in materials such as InAs. Avalanching can be prevented if the semiconductor has a large forbidden energy gap. (This is also important for temperatures encountered in normal device operation.) Unfortunately, this solution conflicts with the need for high low-field mobility, since a large energy gap implies electrons with high effective mass and, therefore, a low low-field mobility.

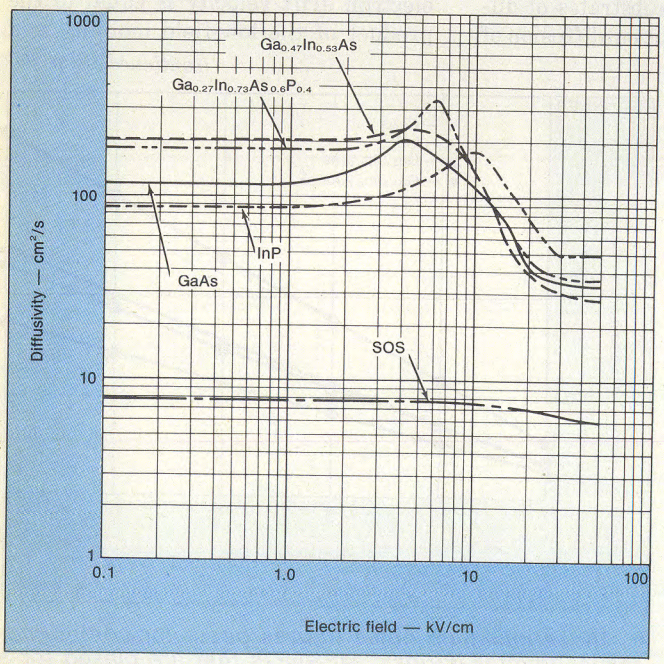
Velocity limitation through intervalley transfer makes it necessary that a MESFET's semiconductor material have a large valley separation. Direct energy gap semiconductors are best for this because of low effective mass and weak scattering of high energy electrons.

Substrate resistivity also affects the choice of a semiconductor material. The planar MESFET structure requires a semi-insulating substate with a resistivity of $10^7\Omega$-cm to provide channel isolation and to minimize the substrate capacitance. In some materials, even the intrinsic resistivity is not high enough at normal operating temperatures. High resistivity is achieved by doping with either chromium or iron to trap free electrons. Only two semiconductors, GaAs and InP, now have high low-field mobilities and saturated velocities that can be prepared as substrates with this kind of resistivity. Therefore, interest has centered on these materials and others that can be lattice-matched to them. Silicon, which can be epitaxially grown on insulating sapphire (SOS) serves as a useful reference.

Two compound semiconductors that can be lattice-matched to semi-insulating InP substrates offer promise for low-noise MESFET design. These are the ternary compound $Ga_{0.47}In_{0.53}As$ (with a theoretical saturated drift velocity slightly higher than that of GaAs and an electron low-field mobility almost twice as high), and the quarternary compound $Ga_{0.27}In_{0.73}As_{0.6}P_{0.4}$ (with a higher saturated velocity than GaAs or InP, and a low-field mobility more than twice the InP value).

The drift velocity of the five promising MESFET semiconductor materials—SOS, GaAs, InP, $Ga_{0.47}In_{0.53}As$, and $Ga_{0.27}In_{0.73}As_{0.6}P_{0.4}$—is shown in Fig. 3. The diffusivity dependence on electric field strength for these materials is shown in Fig. 4. In both figures, donor concentrations of 10^{17} cm^{-3} at 300°K are assumed. The curves represent both theoretical and experimental work. The diffusivity

(continued on next page)



***4. Diffusivity is plotted against field** for n-type channels with 10^{17} cm^{-3} donor concentrations at 300°K.*

shown in Fig. 4 is parallel to the field. The diffusivity component transverse to the field does not play a role in this noise model and is not shown.

Process and material limitations

GaAs MESFETs are currently the most popular devices. Although InP, $Ga_{0.47}In_{0.53}As$, and $Ga_{0.27}In_{0.73}As_{0.6}P_{0.4}$ appear very attractive, there are still a number of basic process and material limitations to overcome.

Just as silicon processing was not readily adaptable to GaAs, neither will GaAs MESFET processing be compatible with InP, $Ga_{0.47}In_{0.53}As$, or $Ga_{0.27}In_{0.73}As_{0.6}P_{0.4}$. The ohmic contact technology differs for each material. However, good quality ohmic contacts can be fabricated to InP, the ternary, and the quarternary alloys,[3] just as to silicon and GaAs. Unfortunately, this is not true for the Schottky-barrier gate contact, which, because of the low barrier heights on these materials, will conduct excessively for the bias levels encountered in normal MESFET operation. This leakage degrades the ability of the Schottky gate to modulate the channel. One solution requires the insertion of a thin (less than 100 Å) oxide layer between the gate and the channel,[4] while another uses a thin undoped layer of the same material between the gate and the channel to increase the barrier height.[5] These process steps are difficult and may degrade the device performance.

In addition to the processing problems, there are also some basic, practical material considerations that can degrade MESFET performance. Although extensive work has been done with GaAs to reduce substrate effects, conversion of the substrate from semi-insulating to conducting during thermal cycling still occurs in GaAs and is known to occur in InP. Substrate currents are blamed for the reported poorer performance of some InP MESFETs when compared to GaAs. However, here the ternary and quarternary compounds have an advantage due to the confinement of electrons to the channel by the difference in energy gap between the channel and the substrate.

The interface between the active channel and the underlying high resistivity substrate is extremely important in the fabrication of a low-noise device. For optimum noise figure, a MESFET must be biased so that the gate depletion edge is only a few hundred angstroms from this interface. Therefore, a high-quality interface is needed to assure that the low-field mobility and saturated velocity remain high in this region. Trapping centers, unwanted impurities, and crystal defects must be at a minimum near the interface.

Unfortunately, a high-quality interface is difficult to achieve in ternary and quarternary alloys that must be lattice-matched to the InP substrates. This is especially true for SOS because of the differing crystal structures of silicon and sapphire. Not only do crystal defects occur in the thin channel layers grown on substrates of different composition, but outdiffusion of substrate impurities takes place during epitaxial growth.

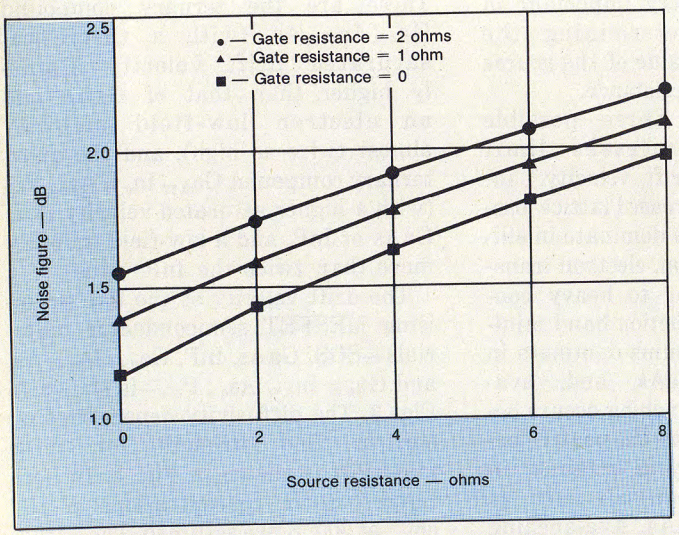
These problems can be reduced in GaAs and InP, but not entirely eliminated. In GaAs, crystal defects, trapping centers, and outdiffusion can be minimized by the growth of a high-purity buffer layer between the substrate and the channel layer. Unfortunately, this technique has not been developed for these other materials.

There are two undesirable depletion regions in the channel: the surface depletion region that results from surface states in the energy gap, and the substrate depletion region that results from the change in impurity concentrations or in crystal composition. Since these depletion regions reduce the thickness of the conducting channel, they increase the magnitude of the parasitic source and drain resistances.

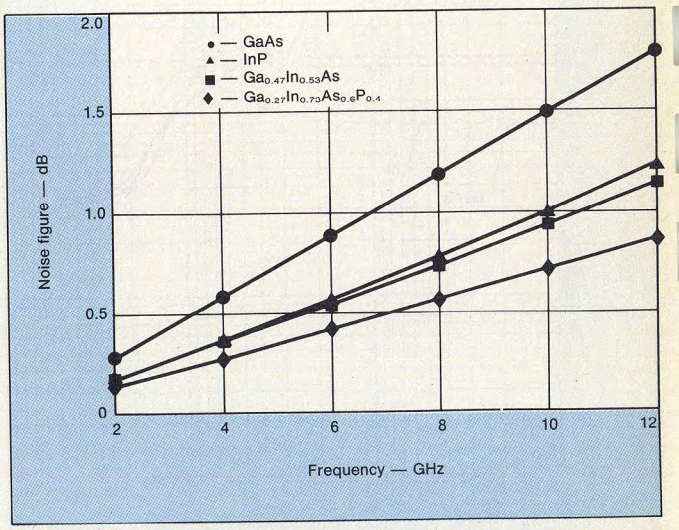
Modeling MESFET performance

Electric field and current density at every point of the MESFET channel are governed by a set of differential equations, which, when solved under an appropriate set of boundary conditions, yield a theoretical estimate of device performance. By using a set of simplifying assumptions, explicit analytical expressions for the values of the intrinsic MESFET equivalent circuit elements shown in Fig. 2(a)—with the exception of R_i—have been derived.[6] For simplicity, the conducting channel under the gate was subdivided into two regions: an ohmic region, where the electron drift velocity is equal to the product of the low-field mobility and

(continued on p. 96)



5. *The effects of gate and source resistances on the noise figure* *of a MESFET with a 300-μm width and a 1-μm gate length are shown. The device is in the common-source configuration.*



6. *These minimum noise figures* *occur for compound-semiconductor intrinsic MESFETs that are biased for a 10-mA drain current and a 3-V drain-to-source potential. SOS results aren't included.*

Material parameter values used in noise analysis

	H_o (cm^2/V-s)	v_s (10^7cm/s)	D_h (cm^2/s)	δ	E_s (kV/cm)	n	ϵ_r	E_g (eV)	ϕ_b (V)
GaAs	4500	1.3	35.0	1.2	2.9	3	12.9	1.42	0.85
InP	3300	1.6	50.0	0.4	4.85	3	12.4	1.35	0.50
$Ga_{0.47}In_{0.53}As$	7800	1.4	30.0	0.34	1.79	3	13.7	0.78	0.30
$Ga_{0.27}In_{0.73}As_{0.6}P_{0.4}$	7000	1.77	36.0	0.56	2.53	3	13.2	0.92	0.40
SOS	250	1.0	6.5	16.4	40.00	2	11.7	1.12	0.85

the electric field strength; and a saturated velocity region, where the electron drift velocity is equal to a fixed maximum value (v_s). Electron diffusivity was assumed to be equal to its low-field value in the ohmic region and to a lower, high-field value (D_h) in the saturated velocity region.

The equivalent AC resistance of that part of a channel that conducts the gate-to-source voltage (R_i) equals some fraction of the resistance of that region of the channel (called the ohmic channel) where the depletion region boundaries are free to move. Therefore, R_i was calculated using an earlier ohmic theory that did not consider the effects of velocity saturation.[7] Because of this approach, R_i has been made inversely proportional to the low-field mobility of the material even though the device operates with part of the channel in velocity saturation. This is consistent with the experimental evidence for GaAs and InP.

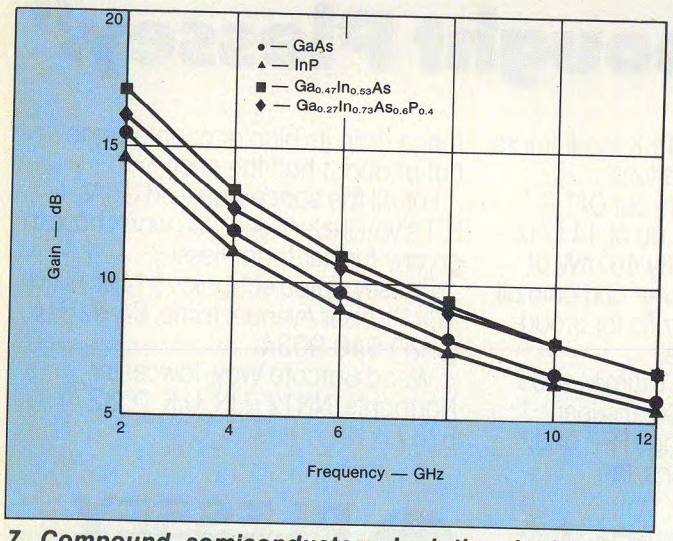
The dependance of electron noise temperature on the electric field was approximated by:

$$T_e = T_o [1 + \delta (E/E_s)^n] \quad (1)$$

In Eq. 1, T_o = the lattice temperature; E = the local applied field; and δ, E_s, and n = material constants.

The material parameters needed for the model are low-field mobility (μ_o), saturated drift velocity (v_s), high-field diffusivity (D_h), dielectric constant (ϵ_r), and the constants E_s, δ, and n used in the expression of electron temperature (Eq. 1). The values used in the analysis correspond to channel doping of 10^{17} on character space cm^{-3} and a temperature of 300°K (see table, above). The energy gap (E_g) is shown, along with typical values of the Schottky barrier height (ϕ_b).

The values of low-field mobility are close to theoretical values and are indicative of those that can actually be obtained. As shown in Figs. 3 and 4, saturated drift velocity and high-field diffusivity are not simple constants above some value of electric field (E_s). Thus, a drift velocity has been selected midway between the peak value and the value at 50 kV/cm. The diffusivity at 30 kV/cm was chosen for the model parameter (D_h). Values for v_s and D_h have been in good agreement with experimental results for GaAs MESFETs and are considered reasonable for other materials.



***7. Compound semiconductors had the depicted associated gains** when terminated for minimum noise figure. The devices were biased for a 10-mA drain current and a 3-V drain-to-source voltage.*

Noise factors

Gate and source resistances are detrimental to noise performance in two ways: the addition of thermal noise, and the degradation of device gain. Successful low-noise device designs depend on the reduction of source and gate resistances. Multiple, parallel MESFET cells result in the lowest reported values of gate resistance, equivalent to 0.3Ω for 300-Mm-wide GaAs devices. However, 1-ohm gate resistances are more common. Deep-recess gate structures have yielded source resistances of approximately 2 ohms for 280-μm-wide GaAs devices.

The effects of the gate and source resistances on the noise figure of a 300-μm-wide GaAs MESFET with a 1-μm gate length at 8 GHz (in the common-source configuration) are shown in Fig. 5. A gate resistance of 1Ω coupled with a source resistance of 2Ω can add 30 percent to the noise figure of the intrinsic MESFET. Drain resistance was set to equal source resistance, while other extrinsic elements were ignored. The device was assumed to be biased at 10 mA of drain current with 3 V from drain to source. This is the optimum bias for low-noise operation reported for many devices of this size.

The intrinsic part of a MESFET is common to all such devices. The complicating effects of the extrinsic elements, on the other hand, are highly dependent on device geometry and doping. Consequently, differences due only to material parameters are presented here in terms of the noise figure of the intrinsic part of the MESFET.

The optional noise figure predicted for the intrinsic MESFET by the model occurs at drain currents that are much lower than those normally found for GaAs MESFETs. This may be caused, in part, by the high voltage drop in the extrinsic drain region of the channel when the drain-to-source voltage exceeds the channel pinchoff voltage. This voltage drop results from the narrowing of the channel by the expansion of the surface and substrate depletion regions resulting from the positive drain potential. Comparison with measured performance becomes more meaningful when calculated results are presented at a fixed bias of 10 mA (drain current) with 3 V across the intrinsic channel from drain to source. At this bias condition, the contribution of the noise originating in the saturated velocity region of the channel to the noise figure is small.

The results for GaAs, InP, $Ga_{0.47}In_{0.53}As$, and $Ga_{0.27}In_{0.73}As_{0.6}P_{0.4}$ are shown in Figs. 6 and 7. SOS results were substantially poorer and were not included in the figures. SOS noise

figures ranged from 1.5 dB at 2 GHz to 6.8 dB at 12 GHz, and the associated gains ranged from 10.7 dB at 2 GHz to 1.1 dB at 12 GHz. Intrinsic noise figures are lowest for $Ga_{0.27}In_{0.73}As_{0.6}P_{0.4}$, and highest for GaAs. Both low-field mobility and saturated velocity are important in determining the relative magnitude of the intrinsic noise figure, are larger for $Ga_{0.27}In_{0.73}As_{0.6}P_{0.4}$ than for GaAs, and account for the better noise performance of the quarternary compound. InP has a lower low-field mobility than GaAs, but its higher saturated velocity apparently dominates the noise figure. The ternary $Ga_{0.47}In_{0.53}As$ has a higher low-field mobility and a lower saturated velocity than InP. These differences, however, balance out to give InP and $Ga_{0.47}In_{0.53}As$ approximately the same intrinsic noise figures. Since source resistance is inversely proportional (approximately) to low-field mobility, the effects of source resistance will be most pronounced in InP and smallest in $Ga_{0.47}In_{0.53}As$. It is likely, therefore, that experimental noise figures for InP devices may not be lower than those for GaAs. For the same reason, measured values of noise figure for $Ga_{0.47}In_{0.53}As$ and $Ga_{0.27}In_{0.73}As_{0.6}P_{0.4}$ should be even better in relation to GaAs.

The associated gain shown in Fig. 7 is for the intrinsic MESFET terminated at its input with an admittance that gives a minimum noise figure at 10 mA. Gain is strongly correlated with low-field mobility: the higher the low-field mobility, the higher the gain. Therefore, it is reasonable to assume that the extrinsic gain of these semiconductors will show the same relationship due to the inverse relation of source resistance to low-field mobility. Differences in the noise figures increase monotonically with frequency. Thus, the potential improvement in noise figure when using the quarternary alloy instead of GaAs, while small at 2 GHz, grows to nearly 1 dB at 12 GHz. The lower source resistance for the quarternary will enhance this improvement even more. The difference in the associated gain show an opposite trend, but not nearly as significant as the noise figure.

Predictions should be viewed in light of the limitations of the model, the available information on material parameters, and the available processing and material growth technology. The treatment of drift velocity and diffusivity versus electric field in the model is approximate. However, the agreement between predicted and measured noise figures for GaAs MESFETs is quite good.

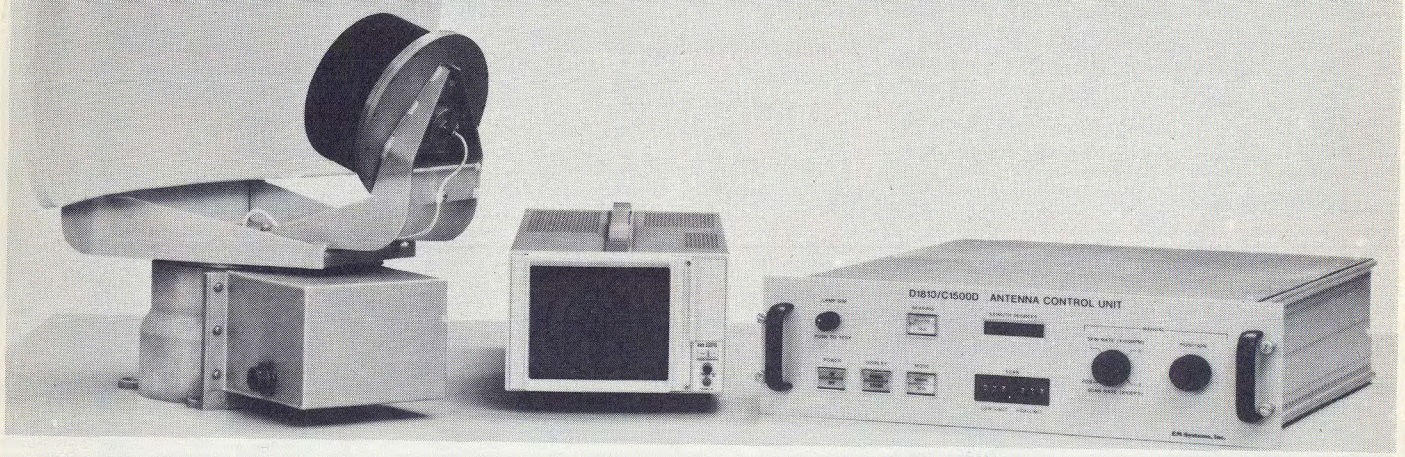
The electron transport properties of these materials—the ternary and the quarternary alloys in particular—are not well known in the high-field regime. Much of the knowledge in that area comes from Monte Carlo calculations. Also, transport properties are functions of impurity level, temperature, and crystalline quality.••

References

1. K. Kamei, et al, "Extremely Low-Noise MESFETs Fabricated by Metal-Organic Chemical Vapour Deposition," *Electronics Letters*, Vol. 17, No. 13, pp. 450-451 (1981).
2. W. Fawcett, C. Hilsam, and H. Rees, "Optimum Semiconductor for Microwave Devices," *Electronics Letters*, Vol. 5, No. 14, pp. 313-314 (1969).
3. H. Morkoc, T. Drummond, and C. Stanchak, "Schottky Barriers and Ohmic Contacts on n-Type InP Based Compound Semiconductors for Microwave FET's," *IEEE Transactions on Electron Devices*, Vol. ED-28, pp. 1-5 (1981).
4. D. Morgan and J. Frey, "Increasing the Effective Barrier Height of Schottky Contacts to n-$In_xGa_{1-x}As$," *Electronics Letters*, Vol. 14, No. 23, pp. 737-738 (1978).
5. H. Morkoc, J. Andrews, and S. Hyder, "Effects of an n-Layer Under the Gate on the Performance of InP MESFET's," *IEEE Transactions on Electron Devices*, Vol. ED-26, pp. 238-241 (1979).
6. R. A. Pucel, H. A. Haus, and H. Statz, "Signal and Noise Properties of Gallium Arsenide Microwave Field-Effect Transistors," *Advances in Electronics and Electron Physics*, Vol. 38, pp. 195-265 (1975).
7. J. R. Hauser, "Small Signal Properties of Field Effect Devices," *IEEE Transactions on Electron Devices*, Vol. ED-12, pp. 605-618 (1965).

Broadband DF SYSTEMS

0.5 to 18 GHz or 18 to 40 GHz with a single feed.
Includes sector scan, manual, and continuous rotation modes.
Other coverage available from 0.1 to 40 GHz.
Digital interface for computer control.
New technology lowers cost.



EM Systems, Inc. 290 SANTA ANA CT., SUNNYVALE, CA. 94086 (408) 733-0611 TWX: 910-339-9305

Use A Waveform Recorder To Simplify VCO Testing

It's easier to measure VCO settling time and post-tuning drift with a waveform recorder: It reduces test time and increases measurement accuracy over the traditional "scope."

Testing a voltage-controlled oscillator (VCO) often proves to be difficult and time-consuming. By using an oscilloscope, an operator runs the risk of interpolating data incorrectly or missing a transient completely. But if a waveform recorder is substituted for the oscilloscope in a VCO test setup, these risks are minimized and time and expense are saved as well.

Although each VCO type has different performance characteristics, VCOs are evaluated by the same parameters. As a result, a waveform recorder can serve a wide range of VCO tests. (A comparison of VCO types can be found in the "1980 Solid-State Microwave Voltage-Controlled Oscillators Catalog" from Frequency Sources, Inc. (Santa Clara, CA). For a free copy, circle reader service number 155.)

Two of the most important, and most difficult, VCO tests benefiting from the use of waveform recorders are settling time and post-tuning drift. Both are transient response tests that measure VCO output behavior resulting from an abrupt change in VCO tuning voltage. Settling time occurs in a very short time interval—the time it takes for the VCO output to slew to within a specified Δf of the intended final frequency. Post-tuning drift (the largest frequency drift occurring between two specified times) takes place over a longer time. Examples of both characteristics appear in Fig. 1.

A test setup designed to evaluate settling time and post-tuning drift is shown in Fig. 2, and an automated system appears in Fig. 3. It improves the quality of VCO testing over an oscilloscope in several ways. Since the waveform recorder can capture all necessary data from a single switching action, the VCO no longer has to be repeatedly switched from V_1 to V_2. (Using an oscilloscope requires repeated VCO switching in order to see any output.) And, because only a single voltage tuning step is needed for data acquisition, the VCO is tested under conditions more like actual use.

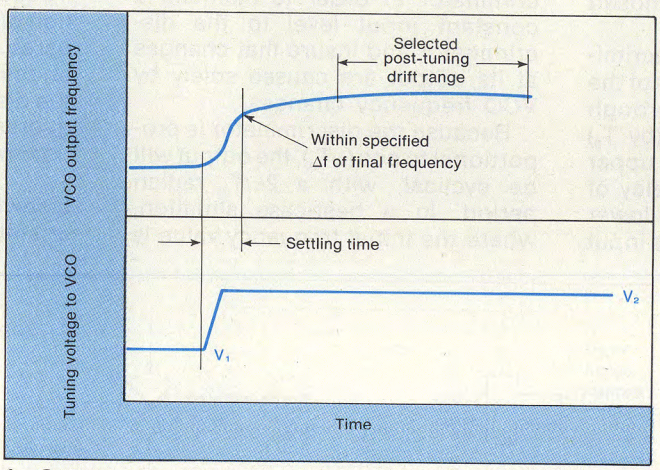
Moreover, VCO repeatability can be evaluated, since the waveform recorder provides "single-shot" data. Repeatability measurements are difficult with an oscilloscope because of the manner in which the scope functions—the oscilloscope display represents only the average VCO response to a particular tuning step. This average results from the number of repetitions needed to maintain a viewable image on the screen.

Data can be viewed after the measurement, since the VCO output is stored in the recorder's memory. This data can also be processed because it is in digital form. Data can be used as documentation of the performance of each VCO, or it can be automatically processed between any desired time limits to determine if the VCO meets a prescribed performance requirement.

The recorder can capture far more information at a glance than a scope. Modern waveform recorders allow as many as 16,000 data points to be stored in one pass. This extensive memory can be used to capture (in a single measurement) VCO data from *before* the tuning step, to beyond ten seconds after the tuning step. If a mixed time-base sampling mode is provided, the sample rate can be changed during the measurement to optimize resolution and use the available memory more efficiently.

A waveform recorder generally provides better amplitude resolution than an oscilloscope, usually to about 0.1 percent of the full-scale reading. This translates into a more accurate determination of VCO output frequency.

Another bonus gained from using a waveform recorder is that the tuning voltage can be sampled while the VCO output is being captured (an active probe may be needed). By establishing a correlation between tuning voltage and the variations in VCO output, one source of testing error can be eliminated.



1. Curves of settling time and post-tuning drift (top) and the VCO tuning voltage (bottom) *illustrate the time difference between these two VCO parameters. Settling time is the more rapid event of the two, requiring a test sample rate of a few micoseconds.*

Preparing the test setup

Once a discriminator has been selected for a particular test (see "Discriminator discourse," p. 100), the discriminator can be calibrated by using a source of known frequency and sampling the discriminator output. If a linear response approximation is unacceptable, the calibration values can be stored and referenced when performing the actual VCO tests.

Settling time and post-tuning drift measurements can be made with the configuration shown in Fig. 2. For

(continued on next page)

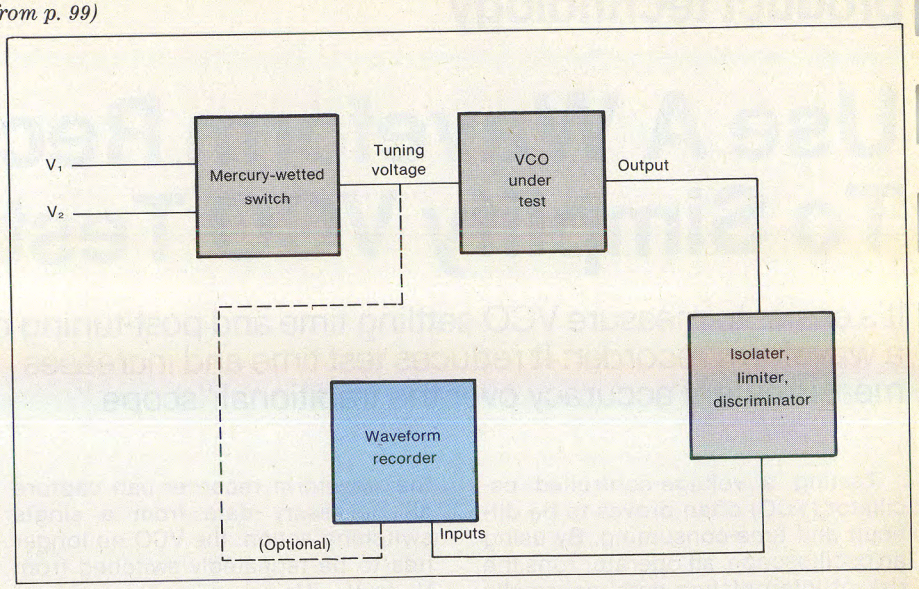
Douglas Nichols, Product Marketing Engineer, Hewlett-Packard Co., Santa Clara, CA 94050.

SIMPLIFY VCO TESTING *(continued from p. 99)*

these tests, the easiest way to use the waveform recorder is by external triggering because the tuning voltage step from V_1 to V_2 is an available reference. Newer model waveform recorders provide digital triggering, which results in greater control when setting the trigger level, and greater confidence in triggering action. Other waveform recorder parameters that can be selected prior to the measurement include input range, trigger position, and sampling rate.

Although setting the input range on a waveform recorder and an oscilloscope is similar, control of the other two parameters is unique to waveform recorders. The primary measurement benefit of selectable trigger position is that data can be captured prior to the trigger. This capability allows monitoring of the VCO output frequency prior to the tuning step.

Setting the sample rate depends on the desired time resolution. Typically, VCO settling-time testing requires a fast sample rate. This usually spans several microseconds after the tuning step is applied. Depending on the type of VCO being tested, the range of the settling time measurement may be more or less than this typical value. By dedicating the entire waveform recorder memory to the settling time measurement, a single 0.8-ms measurement is possible given the 50-ns/sample resolution typical of modern waveform recorders.



***2. This VCO test setup** replaces the traditional oscilloscope with a more accurate waveform recorder.*

Discriminator discourse

A discriminator's job in a VCO test setup is to convert frequency to voltage. This conversion process must be understood before the proper discriminator can be chosen for a VCO test.

Consider the delay-line discriminator in the figure. Regardless of the frequency, the delay time through the lower branch is longer (by T_0) than the delay time of the upper branch. The added phase delay of a signal passing through the lower branch will be $\phi(\omega) = \omega T_0$. At its input ports, the mixer sees the VCO output and this same output shifted by $\phi(\omega)$. Given a VCO output of A sin $(\omega\tau)$, the input to the mixer will be:

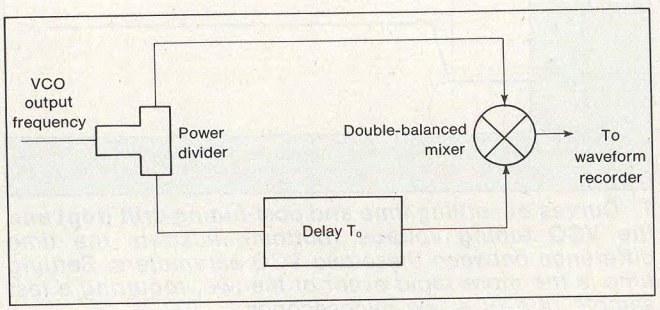
$$\begin{aligned} &A \sin(\omega\tau)\ AK \\ &\times \sin[\omega\tau + \phi(\omega)] \\ &= (A^2K/2)\cos\phi \\ &- \cos(2\omega\tau + \phi) \end{aligned}$$

where K is an attenuation factor due to insertion loss in the delay line. By using a low-pass filter, or allowing the input bandwidth of the waveform recorder to act as a low-pass filter, the equation becomes:

$$\left(\frac{A^2K}{2}\right)\cos\phi = \left(\frac{A^2K}{2}\right)\cos(\omega T_0)$$

This shows the proportional relationship between discriminator output level and the product of the amplitude and the frequency of the VCO output. Since the discriminator must detect frequency change, a limiter should precede the discriminator in order to maintain a constant input level to the discriminator and insure that changes at its output are caused solely by VCO frequency changes.

Because the discriminator is proportional to $\cos(\omega T_0)$, the output will be cyclical, with a $2\pi/T_0$ radian period. In a best-case situation, where the initial frequency value is a multiple of 2π, the range for unambiguous frequency measurement will be π/T_0 radians, or $1/2T_0$ Hz. Besides determining the unambiguous frequency range, T_0 plays a role in determining the sensitivity of the test system to frequency change. Unfortunately, although decreasing T_0 increases the useful frequency range, it also reduces frequency sensitivity.



The important relationships are:

$$\Delta f = R/2T_0 \text{ Hz}$$
$$f_{UN} = 1/2T_0 \text{ Hz}$$

where Δf is the smallest detectable frequency change, R is the resolution of the waveform recorder (compared to full scale), and f_{UN} is the unambiguous frequency range of the discriminator. In other words, to guarantee a desired Δf, the relationship is:

$$T_0 \geq R/2\Delta f$$

Likewise, to guarantee a desired unambiguous measurement range, simply compute:

$$T_0 \leq 1/2f_{UN}$$

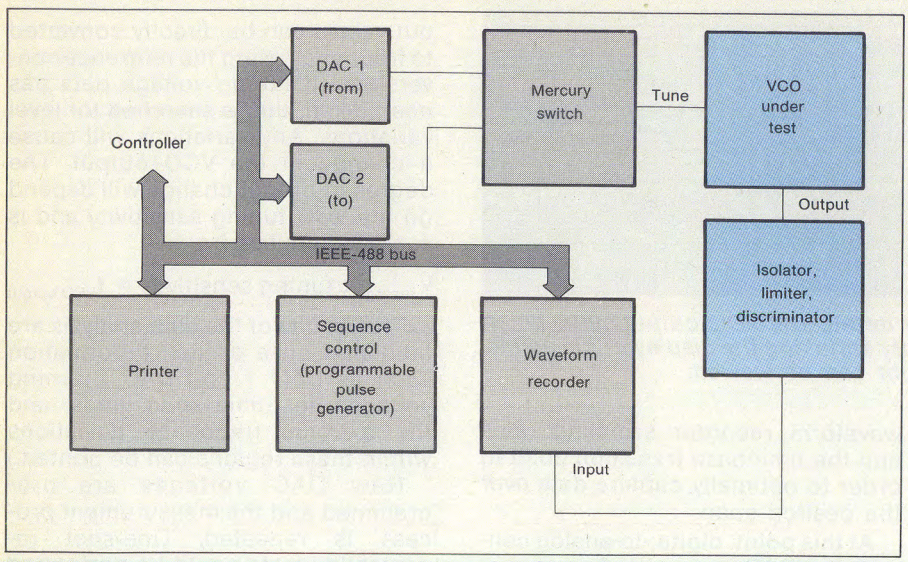
As an example, suppose that 100-kHz sensitivity is needed and the waveform recorder has a known resolution of 1 part in 1000. The minimum allowable delay time is thus:

$$\frac{R}{2\Delta f} = \frac{10^{-3}}{2\,(10^5)} = 5 \text{ ns}$$

Using the same example, the delay time for an unambiguous 50-MHz bandwidth is:

$$T_0 \leq \frac{1}{2f_{UN}} = \frac{1}{2(50)(10^6)} = 10 \text{ ns}$$

Therefore, in this case, only discriminators with a delay time in the 5-to-10-ns range should be considered.••



3. The VCO test setup can easily be automated, *with the addition of a controller and two DACs.*

For post-tuning drift measurements, where the VCO output usually changes less rapidly than during settling time, a slower sampling rate can be used. A sample rate of 500 μs/sample will span nearly ten seconds. By setting the recorder in a fast-slow sample sequence, settling time and post-tuning drift measurements can be made in a single-shot test.

The VCO test data can be utilized in many ways. Since data is stored in memory, it may be viewed at leisure. If viewing an entire data record crowds the data too much for detailed analysis, portions of the record can be enlarged, creating a window of desired data (see Fig. 4). Also, absolute voltage and time relative to the trigger can be obtained by positioning a cursor on any sample point. In this way, minimum and maximum values, which indicate peak VCO frequency excursions, can be determined over any selected time span.

For a more elaborate evaluation of the captured data, the entire sample record (or selected portions) can be dumped to a controller for automatic analysis. Any number of time ranges can be selected, over which minimum and maximum values can be located. Once extremes are located, they can be converted to frequency using the reference conversion values generated during discriminator calibration. The results of the analysis may then be sent to a printer for automatic

(concluded on next page)

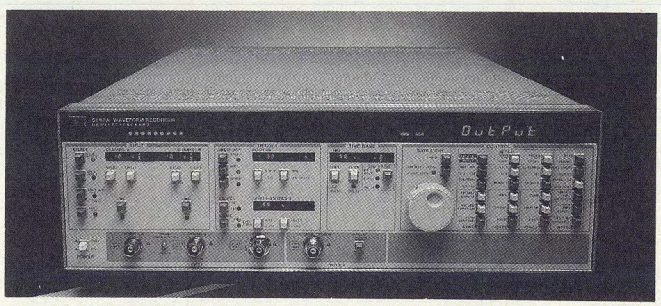
product feature

Waveform recorder captures transients

The 5180A waveform recorder is the key to improved VCO testing. Basically an analog-to-digital converter (ADC) with a memory, the measuring instrument can digitize analog waveforms at rates as high as 20 MHz and store them using up to 16K words of digital memory. It's an invaluable tool for recording any transients that fall below 10 MHz, such as turn-on or switching characteristics. In addition, it can handle either single-shot or repetitive events.

The recorder's two inputs accept voltages from ±100 mV to ±10 V. Sampling can alternate between the two channels, with a sampling rate of 5 MHz/channel. The input bandwidth is 40 MHz. By using a "TR1−TR2" function, two waveforms can be subtracted to highlight variations between them.

The unit features a flexible time base which will sample transients at intervals from 50 ns to 5 ms in a 1-2-5 sequence. (For example, a 50-ns first interval will be followed by second and third time segments of 100 and 200 ns, respectively.) Triggering may be performed internally, based on the incoming signal waveform, or manually, by using an external trigger. The time of the trigger can be recorded with 50-ns resolution. With these pretrigger capabilities, up to 100 percent



of the information recorded during a test can be collected before the trigger occurs. And post-trigger delay has been built in, to compensate for delays between the trigger and the signal of interest.

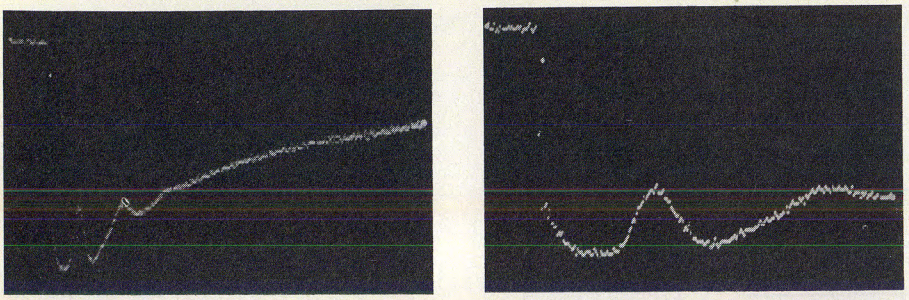
The memory is a large, 10-bit, 16,384-word storage system which may be divided into 1, 2, 4, 8, 16, or 32 equal-length records. An automatic advance function will move the memory from one record to the next as each becomes filled. Conceivably, as many as 32 different waveforms could be recorded in one pass.

Any two records can be viewed simultaneously on a CRT. Cursors displayed on the CRT provide voltage and time readouts and help avoid interpolation errors. The memory is fast enough to read data records at rates up to 10^6 words/s.

The performance of the 5180A waveform recorder owes much to the development of a specially designed 20-MHz, 10-bit ADC. The ADC circuitry features a monolithic 4-bit flash converter capable of 350-MHz rates, and a monolithic high-speed opamp with a 150-MHz bandwidth.

The 5180A will provide an output to an oscilloscope, a CRT, or a digital plotter for hard-copy results. For multichannel, simultaneous sampling, several units can be interconnected. P&A: $18,000; 8 wks. **Hewlett-Packard Co., 1820 Embarcadero Rd., Palo Alto, CA 94303 (415) 857-4101.**

CIRCLE NO. 154



4. Data can be manipulated for greater detail. *The VCO output curve at left results from displaying 1024 data points. By shrinking the display to 256 points, the close-up section of the curve at right can be viewed.*

logging. By running the output to a plotter, a hard-copy record can be made without a controller.

Automating the test setup

At times it may be necessary to have the use of an automated VCO test system. Such a system (Fig. 3) could perform an entire series of tests at the touch of a button. It would work in the following manner.

First, the desired sequence of tuning voltages is stored in the controller. The values can be entered, or, if the sequence is used often, loaded from a disk or cassette. Then, test time spans are entered. Many spans can be analyzed from a single measurement. For example, minimum and maximum information might be required from tuning to 1 μs (for settling time) and from 30 μs to 100 ms (post-tuning drift). The controller automatically determines waveform recorder sampling rates and the time-base transition point in order to optimally capture data over the desired span.

At this point, digital-to-analog converters (DACs) 1 and 2 are programmed to the first test voltages. Next, the waveform recorder setup is programmed, and the recorder is armed, awaiting a trigger.

The controller programs the pulse generator to output a single pulse. This pulse throws the mercury-wetted relay, (switching VCO tuning voltage from the DAC 1 output level to the DAC 2 output level) and triggers the waveform recorder to begin collecting data. If the tuning voltage is being captured with the discriminator output, the waveform recorder will have been programmed to record it on a second channel.

The waveform recorder sends data to the controller. Discriminator output values can be directly converted to frequency using the reference conversions. If tuning voltage data has been taken, this is searched for level variations. Any variations will cause a change in the VCO output. The degree of output change will depend on the VCO tuning sensitivity and is easily computed from:

$$V_{tuning} \times \text{tuning sensitivity} = f_{VCO\ output}$$

The results of the data analysis are tabulated on a printer. (Information such as DAC 1 and DAC 2 tuning voltages, test-time span limits, and the extreme frequency deviations within these regions can be printed.)

New DAC voltages are programmed and the measurement process is repeated. One-shot repeatability tests could be performed by leaving the DAC voltages unchanged and repeating the measurement. This could lead to worst-case and typical VCO performance specifications, since statistical information can be generated from several one-shot tests.

A waveform recorder can provide fundamental measurement capabilities invaluable to VCO testing. As part of an automated VCO test setup, the recorder permits the acquisition of meaningful data, along with considerable savings in money and time. Once its many benefits are considered, the waveform recorder should become a key performer in many future VCO test systems.••

product features

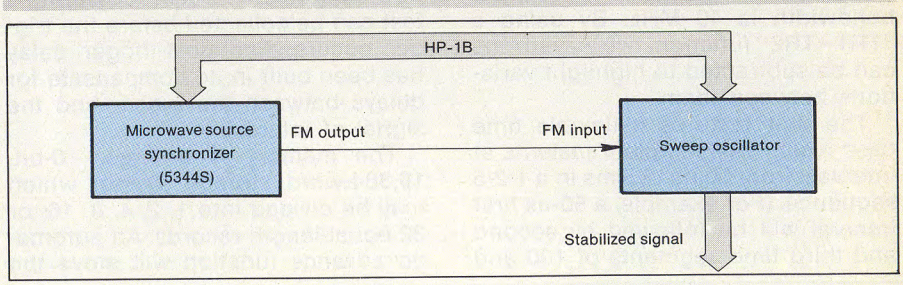
Synchronizer system phase locks sources

Many new products reveal their true value when coupled to an older instrument. In this way, the older component assumes the characteristics of the new model, thus achieving performance levels never before possible. The 5344S microwave source synchronizer is one such new product. With it, CW or swept sources from 0.5 to 18 GHz are phase-locked to a quartz oscillator in the 5344S. The results: source resolution as high as 1 Hz with signal drift no greater than 5×10^{-10} per day.

The synchronizer is actually a two-component, self-contained system (see figure, top). It includes a model 5342A microwave counter (with HP-IB interface and high-stability time base) and the 5344A source synchronizer. Both units are half-rack models, electrically and mechanically integrated at the factory.

(concluded on p. 106)





MICROWAVES
laser technology
A Hayden Publication

April 1982
Vol. 21, No. 4

news

15 **Exacting Military Demands Drive A Vast Radar Market.** In this month's cover feature, news editor Barry Manz talks with leading designers, engineers, and scientists to determine the current state of the radar market. His report also includes: *Future appears bright for commercial sector (p. 23), Millimeter-wave radar: An emerging market? (p. 25), Seeking new ways to exploit radar (p. 26), and Tale of a 60-ton gunfighter (p. 26).*
31 **Optics link Vegas phones**
31 **Pay-TV venture planned**
32 **Remote sensing detailed**
33 **Pair plead innocent to IC theft**
33 **Titan IIIC booster lifts its last load**
34 **GE boosts silicon MESFET**
34 **NJ Bell enters optics age**
78 **IEEE highlights VLSI advances**
37 **Washington**
43 **International**
49 **R&D Roundup**
52 **Meetings**
53 **Industry**
56 **For Your Personal Interest**

editorial

58 **Prudent decisions can devalue the MTT budget surplus**

technical

RADAR TECHNOLOGY

61 **Matched Filters Up Power, Reduce Noise In Radar.** Fulvio Ananasso, of Telespazio S.P.A. per le Communicazioni Spaziala, introduces advances in solid-state technology that boost the output power of transmitters.
69 **Design Method Optimizes Scanning Phased Array.** Dr. Ernest Jacobs, of The Aerospace Corp., presents an expression for the minimum number of elements required to construct an array with a specified gain and scan angle.
73 **Array Radars Solve Communication Jams.** H.D. Lewis, of the RCA Government Systems Division, tells how tactical multifunctional phased-array radars can support new command, control, and communication systems very resistant to electronic countermeasures.
80 **Higher System Availability Is Achieved With Software.** Benson Scheff, of Raytheon, explains that mature diagnostics and fault elimination are recent developments in digital computers that control radar systems and monitor performance.
89 **CW Radars Find New Uses In The '80s.** Andrzej B. Przedpelski, of A.R.F. Products, Inc., introduces Doppler parameters and statistical data reduction methods that yield an effective miss-distance indicator.

product technology

97 **The QPL: Whom does it serve?**
98 **Transfer switches allow circuit paths alternate routes.**
100 **Product Feature.** Power differential amplifier is a multifunction performer.
105 **Product Feature.** Reflectometer sheds light on fiber-optic flaws.
106 **Product Feature.** Economical signal generator uses solid-state source.

departments

11 **Feedback**
54 **Bookshelf**
106 **New Products**
117 **New Literature**
118 **InfoCenter**
120 **Looking Back**

About the cover: The Navy's new AN/SPS-48E radar system, shown on our cover during land-based tests at John Hopkins Applied Physics Laboratories, typifies the military requirements which set the pace in the radar marketplace. (See this month's cover feature, p. 15). Photo courtesy of ITT Gilfillan, Van Nuys, CA.

coming next month: Sources & Special Conference Coverage

May's issue will feature a complete guide to the International Microwave Symposium (Dallas, TX, June 15-17). Our coverage will be an invaluable guide, whether or not you attend the event. Also look for design articles on a millimeter-wave synthesizer which integrates three Impatts and a microprocessor, a mechanically tuned post-coupled 45-GHz Gunn oscillator, a new, tunable, coherent millimeter-wave source called the orotron, and the computer-assisted design and manufacture of SAW devices.

Publisher/Editor
Stacy V. Bearse
Managing Editor
Walter J. Bojsza
Associate Editors
Jack Browne
product technology
Barry Manz
news
Western Editor
Rich Rosen, PE
6043 W. Maplewood Dr.
Littleton, CO 80123
(303) 797-2575
Contributing Editor
Steven March
Washington Editor
Paul Harris
Snyder Associates
1050 Potomac St., N.W.
Washington, DC 20007
(202) 965-3700
European Correspondent
Bill Mitchell
62 Craigwell Ave.
Aylesbury
Buckinghamshire, England
HP21 7AG
(0296) 81529
Editorial Assistant
Tania Tishin
Promotion Manager
Jamie Matusow
Art Director
Janice Moscatelli
Copy/Production Editor
Michael Kachmar
Production Manager
Libby Wayman
Circulation
B. Freundlich, Dir.
C. Stump, Sub. Mgr.
P. Greenleaf, Reader Serv.
M. Sassano, Reprints
Market Research
Irene Chervin, Mgr.
Editorial Office
50 Essex St.
Rochelle Park, NJ 07662
Phone (201) 843-0550
TWX 710-990-5071
A Hayden Publication
James S. Mulholland, Jr., President
April Press Run
42,655 copies
MICROWAVES is sent free to individuals actively engaged in microwave work. Prices for nonqualified subscribers:

	1 Yr.	2 Yr.	3 Yr.	Single Copy
US, Canada Mexico, Central America	$30	$48	$72	$3.00
All other countries	$48	$84	$120	$5.00

Additional Product Data Directory reference issues, $20.00 each (US, Canada, Mexico, Central America), $32.00 each (all other countries).

Back Issues of MicroWaves are available on microfilm, microfiche, 16mm or 35mm roll film. They can be ordered from Xerox University Microfilms, 300 North Zeeb Road, Ann Arbor, MI 48106. For immediate information, call (313) 761-4700.

Hayden Publishing Co., Inc., James S. Mulholland, President, printed at Brown Printing Co., Inc., Waseca, MN. Copyright® 1982 Hayden Publishing Co., Inc., all rights reserved.

Matched Filters Up Power, Reduce Noise In Radar

Advances in solid-state technology have revived matched filter and pulse-compression techniques for boosting the output power of radar and communication transmitters.

A KEY requirement in the design of advanced radar equipment or RF telecommunication links such as satellite communication systems is the range of signal transmission. Such systems must maximize the transmission distance while allowing useful information to be extracted easily from the noise.

A unique solution for reducing receiver noise—made possible by developments in solid state technology—is the matched filter, based on the concept of transversal filters[1] or the correlation of one waveform with another.[2] Transversal filters are tapped delay lines designed to respond to one class of frequencies or waveforms (the signal) while discriminating against all others (the noise).

Since the early 1960s, much attention has been focused on matched filter development.[3] Until recently, however, many proposed analog techniques were impractical because of the large size and weight of transversal filters that used tapped coaxial or stripline transmission lines. Attempting to implement matched filters with digital techniques results in significant signal degradation when the received RF or IF wave is demodulated.[4] Moreover, at high clock speeds and bit rates, conventional digital logic is costly and consumes a great deal of power.

Because of solid-state technology advances in charge-transfer devices (CTDs) and surface acoustic waves (SAW), some classes of matched filters have become practical. Both technologies can simplify filter design, and lead to production of small, low-power, low-cost filters.

Obviously, signal-to-noise ratio (S/N) can be improved by other techniques. For example, sophisticated microwave tubes such as magnetrons, klystrons, and gyrotrons boost the radiated signal, but prevent straightforward use of the new angular modulation techniques based on phase coherence. In addition, tubes counter the trend toward all solid-state transmitters, which increase system reliability while decreasing cost.

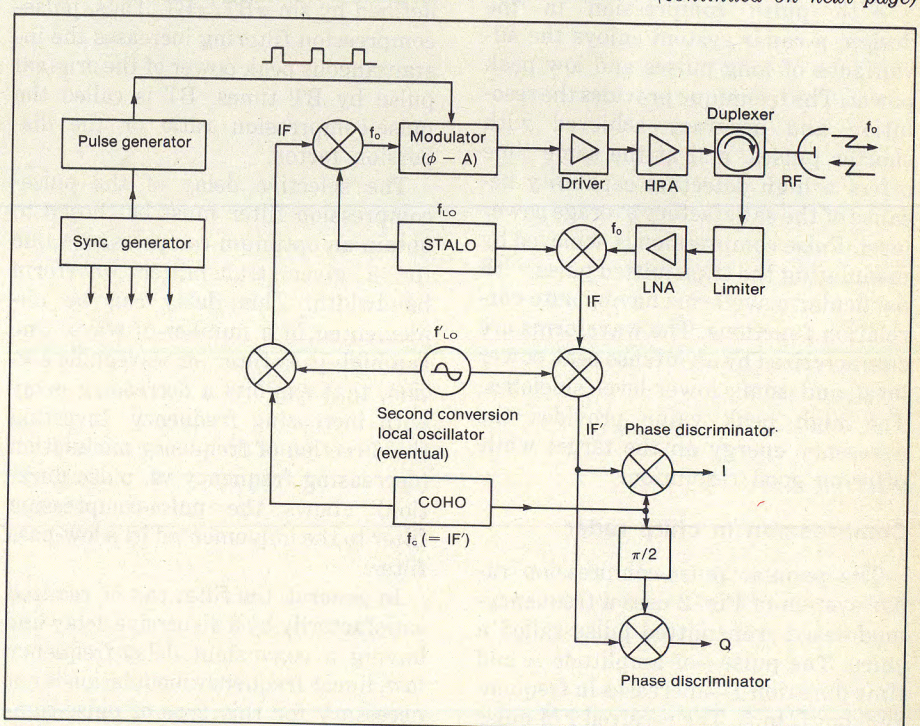
To understand the application of matched filters, a coherent radar system can serve as an example of the pulse-compression concept. When the average power level available from a solid-state transmitter is low, pulse-compression methods are required. For example, because of the high cost of transmitted power, a satellite navigation system is an excellent candidate for pulse compression and matched filters. Although a radar system illustrates the concept, the principles apply equally well to a telecommunications system.

A coherent radar system

The coherent radar system in Fig. 1 is widely used in military applications, especially those involving MTI (moving target indicator) systems. By using the Doppler effect to cancel clutter and fixed-obstacle-generated echoes, it only detects moving objects.

Phase difference is produced by a coherent oscillator (COHO), usually a high-stability 30-MHz quartz oscillator. The phase difference is impressed on the stable local oscillator (STALO), creating the proper phase relationship between the transmitted and received signals. When converted

(continued on next page)



***1. A coherent radar system** is an ideal candidate for matched-filter and pulse-compression techniques. The techniques improve accuracy and resolution, and increase the output power.*

Fulvio Ananasso, Senior Engineer, Telespazio S.P.A. per le Comunicazioni Spaziali, Corso d'Italia, 00198 Rome, Italy.

 (continued from p. 61)

to a video frequency, the received signal contains only the phase corresponding to the Doppler shift. From the mixing between the IF-converted RF signal and the COHO output, a double-phase discriminator extracts the in-phase (I) and quadrature (Q) components of the Doppler vector. Successive video elaborations give the target's velocity, while distance is determined from the attenuation of the received signal.

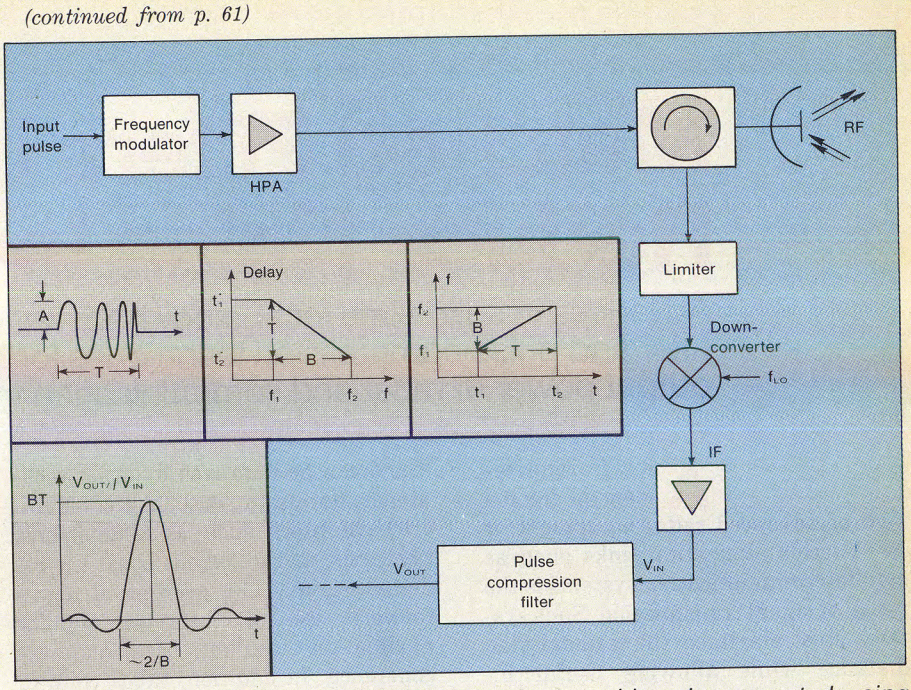
The HPA (high-power amplifier), the final power stage of the coherent radar, is an RF amplifier instead of an oscillator. This stage is normally a traveling-wave tube amplifier (TWTA) driven by a solid-state transmitter. Solid-state sources drive many of the recently developed phased-array systems that use large numbers of radiators. And the power output levels, averaging tens of kW, are as great as those of the traditional but less reliable microwave tubes.

While TWTAs and solid-state transmitters deliver satisfactory average power levels, serious problems exist in generating high peak-power levels. To maximize the energy on the target, the transmitted pulses must not be too narrow. Unfortunately, wider pulses cause the distance resolution to decrease. One way to obtain pulses of the proper dimension is through the pulse-compression technique.

With pulse compression in the design, a radar system enjoys the advantages of long pulses and low peak power. The technique provides the resolution and accuracy achieved with shorter pulses, and at the same time offers a high detection capability because of the satisfactory average power level. Pulse compression is achieved by modulating the transmitted pulse with particular waveforms having auto-correlation functions. The waveforms are characterized by an intense peak power level and some lower-level sidelobes. The high peak value provides the necessary energy on the target while offering good resolution.

Compression in chirp radar

The popular pulse-compression radar system of Fig. 2 uses a frequency-modulated transmitted pulse called a chirp. The pulse—of amplitude A and time duration T—increases in frequency from f_1 to f_2. The received FM pulse (echo) passes through the pulse-compression filter which is designed to provide a frequency dependent propagation velocity.



***2. A frequency-modulated transmitted pulse**—a chirp—is generated using pulse compression. A pulse-compression filter can greatly increase the peak power of a transmitted pulse.*

In this system, the pulse-compression filter causes the higher frequencies at the end of the pulse to move more rapidly with respect to the lower frequencies at the beginning of the pulse. This results in the filter's output energy being compressed into a shorter pulse, having a duration of 1/B, where $B = f_1 - f_2$, and having a shape defined by $\sin \pi BT/\pi BT$. Thus, pulse-compression filtering increases the instantaneous peak power of the original pulse by BT times. BT is called the pulse-compression ratio or the dispersion factor.

The selective delay of the pulse-compression filter must be chosen to obtain an optimum compression value for a given transmitter waveform bandwidth. This delay can be implemented in a number of ways. One is a high-pass filter, or waveguide section, that exhibits a decreasing delay with increasing frequency. Inverting the direction of frequency modulation (decreasing frequency vs. pulse duration) allows the pulse-compression filter to the implemented by a low-pass filter.

In general, the filter can be realized satisfactorily by a dispersive delay line having a convenient delay-frequency law; linear frequency modulation is not necessary for this type of pulse-compression system. The system can use any type of modulating law provided the filter has a suitable matched characteristic. In addition, the transmitted waveform need not be rectangular.

Matched-filtering basics

A chirp radar system shows how to maximize signal power by suitably modulating the transmitted pulse to a particular receiver matched to the transmitted signal. Matched filtering is the processing of the received signal that allows pulse compression over a short time interval. Moreover, matched filtering is based on the autocorrelation of the received signal, which makes it easier to extract signal from noise, provided that the received waveform is at least known approximately.

Correlation factor (R) is defined as a coefficient that expresses the degree of similarity between two functions. For electrical signals, R is normalized with respect to the signal energy, and is given by:

R = 0 for two noncorrelated functions,
R = +1 for two identical functions,
R = −1 for two symmetrical functions.

The correlation function, $R(\tau)$, expresses the variation in the area of overlap of two functions a(t) and b(t) as a function of the time difference between them. Thus $R(\tau)$ is:

$$R(\tau) = \int_{-\infty}^{+\infty} a(t)b(t+\tau)dt$$

$$= \frac{1}{T_p}\int_0^{Tp} a(t)b(t+\tau)dt \qquad (1)$$

In Eq. 1, a(t) and b(t) are periodic over the period T_p.

If a(t) = b(t), $R(\tau)$ becomes the autocorrelation function of the signal a(t) alone. The autocorrelation function of a rectangular pulse of duration T is a triangular pulse having a base 2T. By definition, a matched filter is one whose output signal is the autocorrelation function of its input signal. Thus, the energy in the transmitted signal is compressed into a short time interval, depending on the shape of the waveform.

Mathematically, the necessary and sufficient condition for a filter to be matched is that its transfer function, $F(\omega)$, be the complex conjugate $S_i^*(\omega)$ of the spectrum of the input signal, $s_i(t)$. The complex conjugate $S_i^*(\omega)$ is given by the product of the transmitted signal's Fourier Transform, $S'(\omega)$, and the channel transfer function, $H(\omega)$. $H(\omega)$ is generally set equal to 1. The transfer function is:

$$F(\omega) = S_i^*(\omega) = [S'(\omega)H(\omega)]^*$$
$$F(\omega) \cong S'^*(\omega) \qquad (2)$$

The filter's output signal spectrum is:

$$S_o(\omega) = S_i(\omega)F(\omega)$$
$$= |S_i(\omega)|^2$$

That is, the output signal $s_o(t)$ is indeed the autocorrelation function of the input signal, $s_i(t)$. The impulse response of the filter matched to $s_i(t)$ is theoretically $s_i(-t)$, but because of the filter's own delay (τ_f), it becomes $s_i(\tau_f - t)$.

Using Barker's codes

An alternative to the chirp radar technique that uses frequency codes is a military radar system that uses more efficient phase-codes. With these phase, or Barker, codes, the transmitted pulse is divided into N sub-pulses or "chips," all having the same frequency, f_o, and exhibiting 0- or 180-degree phase—(binary phase-shift keyed) depending on a suitable, or arbitrary, code.

The frequency modulator of a chirp radar can be replaced by a phase/amplitude (on/off) modulator such as the one shown in Fig. 3. This modulator can be inserted directly at the RF output (see Fig. 1) or in the IF path of a single side-band IF-to-RF modulator. It provides on/off amplitude modulation for creating the transmitted pulses. In addition, the modulator can produce 0/180-degree phase modulation or both amplitude and phase modulation according to the truth table of Fig. 3. Thus, the modulator provides phase control of the pulsed RF signal by on/off amplitude modulation.

In a Barker's code system having N sub-pulses of duration τ, and an RF pulse width of $T=N\tau$, the matched filter can be implemented by a digital transverse filter of (N − 1) τ-delay elements, N amplifiers—some of them inverting—and an output adder (see Fig. 4). The output signal consists of a main lobe whose amplitude is N times the amplitude attainable without modulation, a duration of about 2τ, and a number of secondary lobes. The location of the peak of the signal determines the maximum S/N ratio. This type of system is called a Barker's (or magic) code with N elements.

Figure 5(a) illustrates a magic code having N = 6 sub-pulses per pulse in the transmitted waveform. Depending on the type of code used, some sub-pulses exhibit 180-degree phase transitions at the beginning. The code can be chosen in many ways, depending on the desired shape of the autocorrelation function. Figure 5(b) shows the magic code corresponding to the waveform of Fig. 5(a). Plus (+) symbols indicate 0-degree phase, and minus (−) symbols indicate 180-degree phase. In other words, Fig. 5(b) represents the modulating sequence applied to the Fig. 5(a) waveform after it has been multiplied by the RF carrier frequency, f_o. A two-phase modulation or binary phase-shift keying is equivalent to suppressed-carrier amplitude modulation.

The components of the matched filter will consist of five (i.e., N−1) τ-delay elements, N = 6 amplifiers, each having unity gain for simplicity, and an output adder. The phase shift of each amplifier varies according to the modulating sequence. For example, the last or Nth amplifier must be inverting ($\theta_N = 180°$), if the first sub-pulse has 180-degree phase. If the first sub-pulse has 0-degree phase, the Nth amplifier is noninverting. If the second sub-pulse has 180-degree phase, the next to last or (N − 1)th amplifier must have 180-degree phase. In general, the (N−j)th amplifier's phase shift must correspond to the phase of the j-th pulse or chip.

Using the scale in Fig. 5(c), the occurrence of a compression lobe can be predicted at the output of the matched filter. In effect, this results in the modulation envelope as illustrated in Fig. 5(d). The modulation envelope has output values along the time scale shown in Table 1. The complete modulated waveform that would appear on a CRT display is shown in Fig. 5(e).

Matched filter benefits

A comparison of the characteristics of a matched filter with a traditional receiver is shown in Fig. 6. Assume that an input pulse, $s_i(t)$, of duration T is subdivided into N sub-pulses over the interval $\tau = T/N$, with the frequency ω_o, and having a peak-to-peak RF amplitude of 2 A. Also assume that the receiver is subjected to a white-noise input N_i of 2 A rms. The bandwidth of the receiver is about 1/T.

For the traditional receiver, these input conditions result in an S/N ratio of −6 dB. Signal detection under these conditions is quite difficult, not only because the noise level is greater than the signal level, but the RF front-end itself degrades the signal. On the other hand, a matched-filter receiver has a bandwidth of approximately $1/\tau$, which is about N times wider than that of a traditional receiver. The amplitude response, $|F(\omega)|$, is equal to the input signal spectrum, $|S_i(\omega)|$. Thus, the out-

(continued on next page)

Table 1: Modulation envelope output values

$t = t_1$	→	output = −A+0=−A
$t = t_2$	→	" = +A+A+0=2A
$t = t_3$	→	" = −A−A+A+0=−A
$t = t_4$	→	" = −A+A−A+A+0=0
$t = t_5$	→	" = −A+A+A−A−A+0=−A
$t = t_6$	→	" = +A+A+A+A+A+A=6A → compression peak
$t = t_7$	→	" = 0−A+A+A−A−A=−A
$t = t_8$	→	" = 0−A+A−A+A=0
$t = t_9$	→	" = 0−A−A+A=−A
$t = t_{10}$	→	" = 0+A+A=2A
$t = t_{11}$	→	" = 0−A=−A

put noise (N_o) exhibits a voltage level of $K\sqrt{T/\tau} = K\sqrt{N}$ times that of a traditional receiver, where K depends on the filter's characteristics.

The particular spectrum shape, $S_o(\omega)$, of the output signal, $s_o(t)$, produces an output waveform envelope having a peak of width of about 2τ. The amplitude is about NK times greater than that of a receiver without matched filtering. Therefore, at the output of a matched filter, the S/N ratio is N times greater than at the input.

The so-called processing gain, defined as:

$$X = 10\ (\log_{10} N) = 10\ (\log_{10} T/\tau) \qquad (3)$$

represents the improvement in dB due to pulse compression in a matched receiver. For example, a code having 6 sub-pulses per pulse gives an improvement of:

$$X = 10\ (\log_{10} 6) = 7.78\ \text{dB}$$

in the S/N ratio. Compared to the S/N ratio of −6 dB in the conventional receiver, the improvement to 7.78 dB represents a change of +1.78 dB, but only at the peak value (see t_6 in Table 1). Nevertheless, the improvement considerably simplifies detection of the signal.

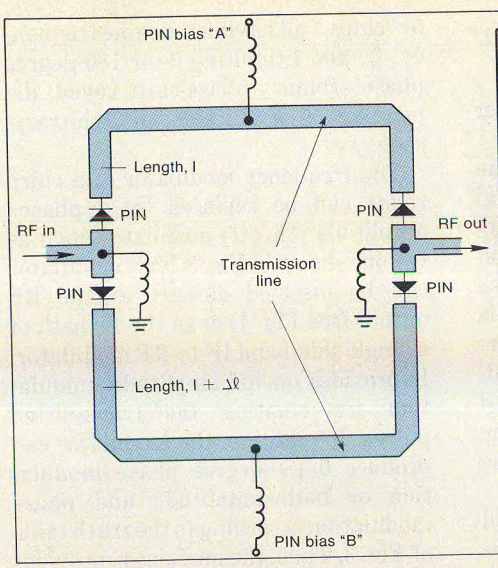
If N is increased, the compression peak becomes more intense and narrow, with a corresponding improvement in the S/N ratio at the peak of the signal. Unfortunately, increasing N also widens the receiver bandwidth. Moreover, the complexity of the threshold decision circuitry becomes greater, since it must react in shorter time intervals.

The usual values of N range from 8 to 10 in civilian telecommunication applications (telemetry or telecommands) and up to 50 through 80 in military applications that call for high efficiency in a noisy environment.

Different waveforms can be obtained by using codes with 4, 8, etc., phase states. Each time however, the maximum output S/N ratio is achieved for a matched receiver.

Communications application

Pulse-compression techniques and matched filters apply to telecommunications transmission as well as radar systems. One such application is a satellite navigation system in which the signal's arrival time—after transmission from the satellite—must be determined accurately by a navigation receiver. Navigation systems often operate in noisy environments, with interference coming from man-made and atmospheric sources.[15] In addition, there is normal degradation of the satellite's circuitry.



Truth Table		
"A" bias	"B" bias	Output
Reverse	Reverse	No RF signal (off)
Forward	Reverse	Reference phase // (on)
Reverse	Forward	Phase // + 180° (on)
Forward	Forward	——

***3. A phase/amplitude modulator can replace a conventional frequency modulator** in a chirp-radar system. The modulator imparts modulation characteristics to the RF output shown in the truth table.*

The received power (P_R) for an earth or near-earth based navigation receiver is calculated from the equation:

$$P_R = \frac{P_T G_T G_R (T/\tau)}{L_A L_{stat}} \qquad (4)$$

where P_T is satellite transmitted power, G_T is the satellite transmitter's antenna gain, G_R is the ground receiver's antenna gain, $T/\tau = N$ is the number of sub-pulses or chips per pulse (see the S/N ratio improvement due to matched filtering, Eq. 3), L_A is the free-space satellite-to-ground attenuation, and L_{stat} is the statistical attenuation due to various transmission system degradations such as atmospheric fading, signal depolarization, and spurious coupling.

Converting Eq. 4 into logarithmic form, the worst-case received power is:

$$[P_R]_{dBm} = [P_T]_{dBm} + [G_T]_{db} + [G_R]_{dB} + [X]_{dB} - [L_A]_{dB} - [L_{stat}]_{dB} \qquad (5)$$

Assuming a 1-MHz RF bandwidth (B_{RF}), an antenna noise temperature (T_A) of 100 K, and a receiver noise figure of F = 3 dB, the effective noise level at the input is:

$$[N_R]_{dBm} = 10 \log_{10} K(T_A + FT_o)B_{RF} = 10 \log_{10} (1.38 \times 10^{-23} \times 680 \times 10^6) = -110.3\ \text{dBm} \qquad (6)$$

where K is Boltzmann's constant and T_o = 290 K, ambient temperature.

Now, assume the following values for the variables in Eq. 5:

P_T = 40 W (+46 dBm)
G_T = 15 dB
G_R = 4 dB
L_A = 170 dB
L_{stat} = 8 dB

Inserting these values into Eq. 5 gives a received power of:

$$[P_R]_{dBm} = [X]_{dB} - 113 \qquad (7)$$

Ignoring the signal-to-noise degradation of the receiver, the received signal level is about 3 dBm below the level of the noise (in the absence of pulse compression, X = 0). But to obtain relatively error-free detection of the received signal requires an S/N ratio of 8 dB. Substituting from Eq. 6 and 7 gives:

$$[S/N]_{min} = [P_R]_{dBm} - [N_R]_{dBm} = X_{db} - 113 + 110.3 = 8 \qquad (8)$$

Therefore, X_{min} = 10.7 dB. Going back to Eq. 3:

$$N = T/\tau = 10^{X/10)} = 11.8, \text{ or } N \geq 12$$

Thus, a code of N ≥ 12 chips assures the required detection quality.

Matched filter technologies

Current implementations of matched filters are based either on surface-acoustic wave (SAW)[5,6] or charge-transfer device (CTD) technology.[7,8] Table 2 provides a comparison of both technologies as applied to matched

(continued on p. 66)

 (continued from p. 64)

filters.

SAW technology is used in analog signal processing and filtering over the frequency range of 3 MHz to 2 GHz. A SAW device is a passive electro-acoustic component that requires neither clocking nor complicated matching to other circuit elements. The CTD mechanism, on the other hand, is based on the transfer of charge in a metal-oxide semiconductor (MOS), with a multiphase clocking scheme acting as the energy-propagating means. CTDs currently permit signal processing and filtering in the range of 100 Hz to 30 MHz.

Because surface-acoustic waves propagate with a velocity four to five orders of magnitude lower than electromagnetic waves, SAW technology dramatically reduces the size and weight of matched filters. Smaller size, simpler design, and low power consumption all result in lower cost compared to transmission-line filters.

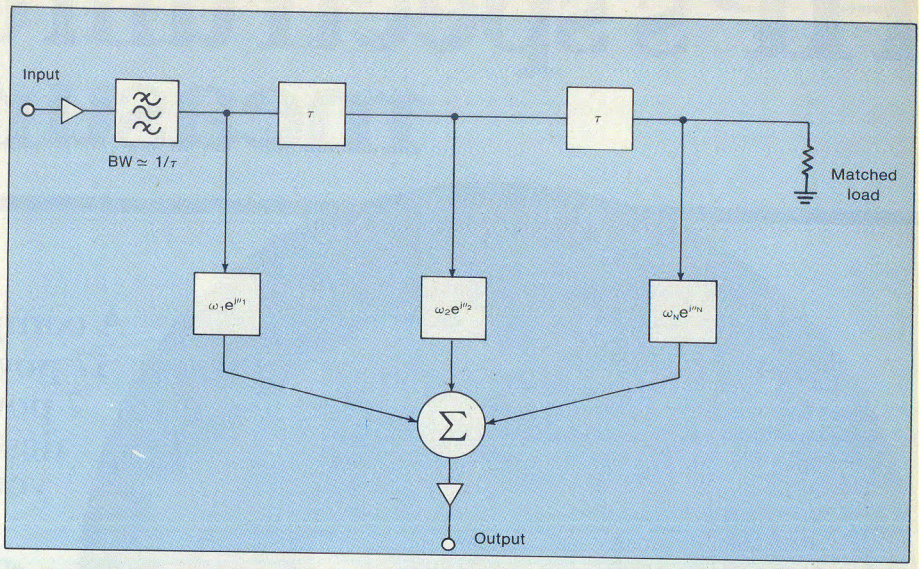
Propagation losses in SAW filters stem from the thermal phonon scattering of coherent surface waves, impurities, and surface imperfections. Propagation losses range from 0.2 dB/μs to 0.4 dB/μs at VHF (30 to 300 MHz) for piezoelectric materials such as quartz and lithium niobate. At 1 GHz, propagation losses for lithium niobate increase to approximately 1 dB/μs.

As Fig. 4 shows, transversal filters can provide both amplitude (W_i) and phase weighting (θ_i). By adjusting individual fingers of the interdigitated structures, SAW technology is capable of providing both types of weighting.

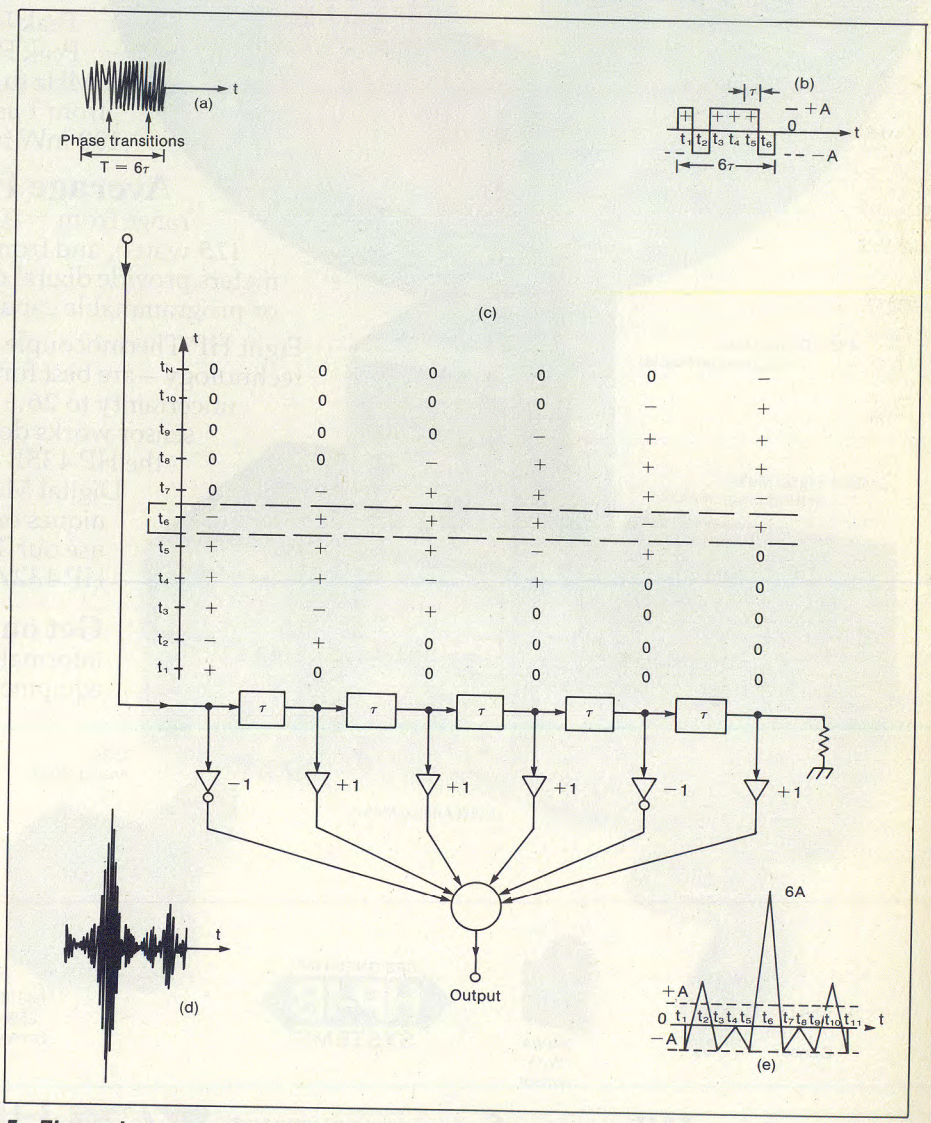
The family of CTDs includes charge-coupled devices which transfer a bidirectional flow of electric charge along the surface of a semiconductor, and the so-called bucket brigade devices, which transfer the charge through transistor action.[9,11] One of the newer family members, the peristaltic charge-coupled device overcomes some of the carrier diffusion and transport-drift problems by storing active charges in a region well below the semiconductor surface.[12]

With clock frequencies below 3 MHz, typical losses are 0.01 percent. At 10 MHz, charge transfer losses of surface CTDs rise to 0.1 percent while those of peristaltic CTDs remain at 0.01 percent. In transversal filter applications, CTDs can provide W_i, but θ_i must be accomplished with external circuitry.

Both SAW and CTD devices can perform a variety of filtering and pre-



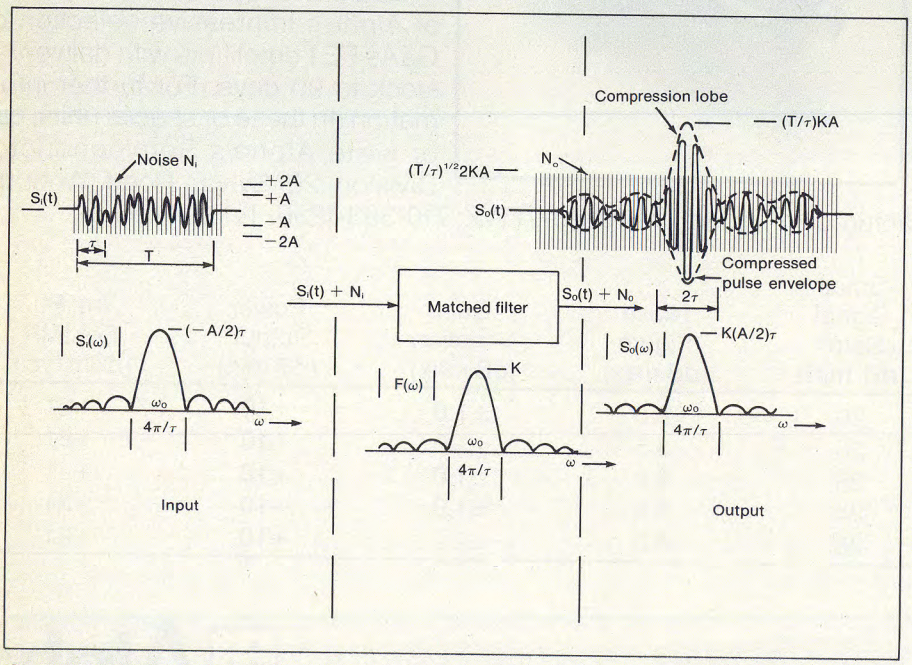
4. One implementation of a matched filter is this digital transversal filter. *The output signal consists of N sub-pulses as generated by a Barker's or magic code. (Note: ω_1, ω_2, and ω_N should read W_1, W_2 and W_N.*



5. The pulse compression produced by an RF matched filter *(c) with a binary phase-shift keyed input (a) is illustrated by a modulating sequence (b), compressed envelope (d), and AC waveform (e).*

Table 2: Comparison of SAW and CTD technologies

Parameter	SAW	CTD
1. Device origins	White & Voltmeter Interdigital Transducer (1965)	Sangster - Bucket brigade device (1969) Bell Labs - Surface charge device (1970)
2. Energy transport mechanism	Acoustic phonon propagation	Electrical charge propagation
3. Velocity of propagation	$v_s = C/\rho$ (C = coeff. elasticity ρ = substrate material density)	$v_c = 1/f_c$ = 1/(multiphase clock frequency)
4. Material medium	ST-quartz	Silicon
5. Size of 15-dB processing gain matched filter (substrate or chip)	4.5 in. × 0.3 in. (11.4 cm × 0.76 cm)	< 80 mil × 40 mil (< 2 mm × 1 mm)
6. Power requirement	< 100 mW, amplifier to compensate for insertion loss	< 60 mW, for peripheral circuitry
7. Current practical IF range	15 MHz to 120 MHz (can cover from 3 MHz to 2.5 GHz depending on material and fabrication techniques)	2 MHz to 5 MHz (can cover from 0.5 kHz to 120 MHz under limited operation)
8. Dynamic range	60 dB to 70 dB	70 dB to 85 dB
9. Clocking requirement	None	Two- or three-phase clock required (5 MHz)
10. Receiver IF requirement	Possibility of only one IF stage	Double conversion required



***6. An input signal below the input noise level** can be amplified to produce an output compression lobe greater than the output noise level.*

processing functions.[13,14] They offer programmability and adaptability, and in many respects are complementary technologies. Typically, CTDs operate above 2 MHz for materials such as lead zirconate titanate, and above 10 MHz with materials such as quartz and lithium niobate.

In synthesis applications, SAW devices offer high-frequency capability and wide bandwidth, but have limited delay time because of the small size of the piezoelectric crystal substrate. CTDs can provide milliseconds of delay, but with standard silicon MOS technology they are presently limited in frequency and bandwidth. As Table 2 shows, a SAW filter requires just one RF stage and needs no clock, making it preferable to the CTD.

SAW filter technology is apparently evolving towards specific bandpass filter and matched filter applications at high frequencies, with some programmability and adaptability. CTDs, on the other hand, are aimed at the IF or video-frequency range, in applications requiring long delay or integration times with a high degree of adaptability.••

Acknowledgment

The author extends his thanks to Dr. Maurizio Rizzo for his discussions concerning the manuscript, and to Dr. G. D. O'Clock, Jr. for providing valuable documentation.

References

1. H.E.Kallman, "Transversal Filters," Proceedings of the *IRE*, pp. 302-310 (July 1940).
2. D.O.North, "An analysis of the factors which determine S/N discrimination in pulsed-carrier systems," RCA Technical Report PTR-6c (June 25, 1943).
3. M.Bernfeld, et al., Matched Filtering; Pulse Compression and Waveform Design," *Microwave Journal*, pp. 57-64 (October 1964).
4. G.Turin, "An Introduction to Digital Matched Filters," *Proceedings of the IEEE*, pp. 1092-1112 (July 1976).
5. R.M. White, "Surface Acoustic Waves," *Proceedings of the IEEE*, pp. 1238-1276 (August 1970).
6. C.Grasse, "Tips on Specifying Acoustic-Wave Devices," *MicroWaves*, pp. 48-57 (June 1975).
7. C.H.Sequin and M.F.Tompsett, "Charge-Transfer Devices," Academic Press, New York (1975).
8. W.F.Kosonocky and D.J.Sauer, "The ABCs of CCDs," *Electronic Design*, pp. 58-63 (April 12, 1975).
9. L.Altman, "The New Concept for Memory and Imaging: Charge Coupling," *Electronics*, pp. 50-59 (June 21, 1971).
10. G.D.O'Clock Jr., "Acoustic-Wave Filters Improve Radar," *Electronic Design*, pp. 56-59 (July 5, 1973).
11. F.L.J.Sangster, "The Bucket-Brigade Delay Line, A Shift Register For Analogue Signals," *Philips Technical Review*, pp. 97-110 (1970).
12. L.J.M.Esser, "The Peristaltic Charge-Coupled Device: A New Type of Charge Transfer Device," *Electronics Letters*, p. 620 (December 1972).
13. W.S.Jones, et al., "Evaluation of Digitally Coded Acoustic Surface-Wave Matched Filters," *IEEE Transactions on Sonics and Ultrasonics*, pp. 21-27 (January 1971).
14. D.D.Buss, et al., "Transversal Filtering Using Charge Transfer Devices," *IEEE Transactions on Solid-State Circuits*, pp. 138-146 (April 1973).
15. C.L.Cuccia and R.S.Davies, "Operation of Information Satellites in an Interference Environment," *Microwave Journal*, pp. 33-42 (June 1972).

Design Method Optimizes Scanning Phased Array

An expression can be developed for the minimum number of elements required to construct an array with a specified gain and scan angle. The result offers a starting point for design.

ARRAYS have received widespread use in both radar and communication systems, primarily because an array can be steered or scanned very rapidly and does not require mechanical movement (Fig. 1).

Array system designers are always looking for the optimum configuration that will answer their particular requirements. Although the definition of "optimum" depends on the application, in this case it describes antenna parameters that minimize the number of elements required to achieve a given array gain, $G(\phi_s)$, at the *maximum scan angle*, ϕ_s.

In general, the gain of an antenna is inversely proportional to the square of the pattern's half-power beam width (given identical E- and H-patterns). Scanning loss, the reduction in the sensitivity of the system as it scans off boresight (mechanical axis), must also enter design considerations. Higher array element gains imply narrower beam patterns with a resulting increase in scan loss at fixed angles. While the element gain increases the magnitude of the array gain at the maximum scan angle, the scanning loss reduces it. However, an optimum element gain exists which can maximize the array gain at ϕ_s.

Deriving the optimum parameters

The relationship between element gain (g_e) and its half-power beam width (ϕ_o) is:[1]

$$g_e \approx \frac{k}{\phi_o^2} \qquad (1)$$

The factor k can vary slightly for different classes of antenna elements. However, it is essentially constant for a limited range of beam widths.

The main lobe element pattern is approximated by the $(\sin x/x)^2$ function with the half-power beam width of the actual pattern and the function matched. The element gain function, $g(\phi)$, is:

$$g(\phi) \approx g_e \left[\frac{\sin\ (2.78\ \phi/\phi_o)}{(2.78\ \phi/\phi_o)} \right]^2 \qquad (2)$$

From data on uniform arrays[2] the array gain, $G(\phi)$, is approximated by:

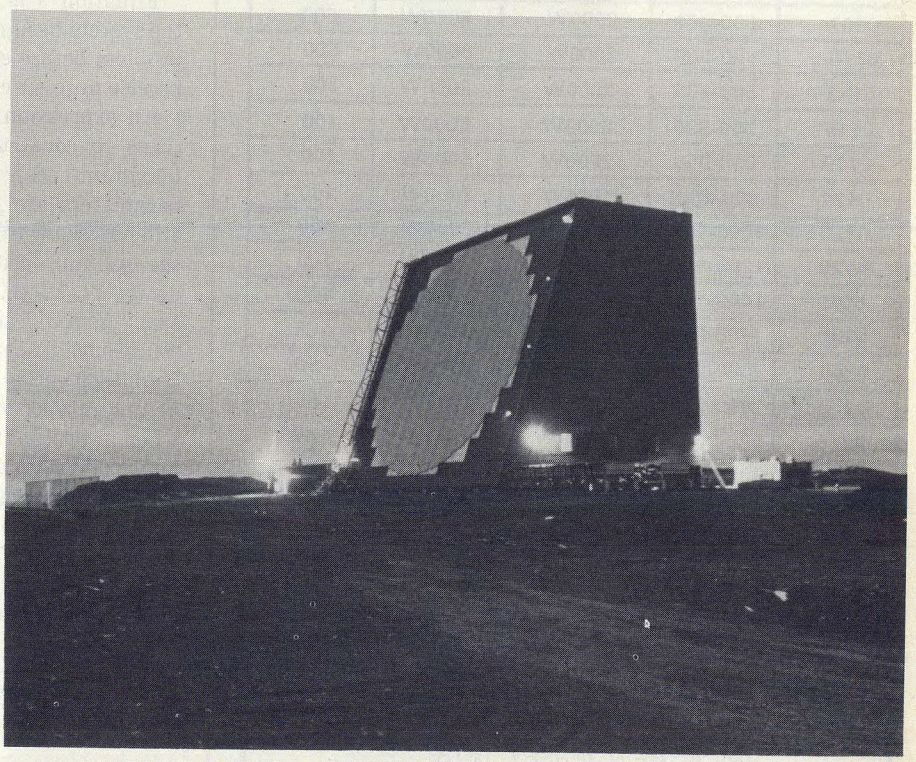
$$G(\phi) \approx N_o f(d/\lambda) g(\phi) \qquad (3)$$

where N_o = number of elements, and $f(d/\lambda)$ is a function dependent on the spacing between elements in wavelengths. For a small range of spacing, $f(d/\lambda)$ is essentially constant and for $d \geq \lambda$, $f(d/\lambda) \approx 1$. Combining Eqs. 1, 2, and 3, with ϕ taken at maximum scan angle, gives:

$$N_o \approx \frac{G(\phi_s)\ (2.78\ \phi_s)^2}{kf(d/\lambda)\ \sin^2(2.78\ \phi_s/\phi_o)} \qquad (4)$$

Equation 4 determines the required number of elements as a function of $G(\phi_s)$, ϕ_s, and ϕ_o. Since the required array gain, $G(\phi_s)$, at the maximum scan angle, ϕ_s, is given, element half-power beam width, ϕ_o, is the only variable.

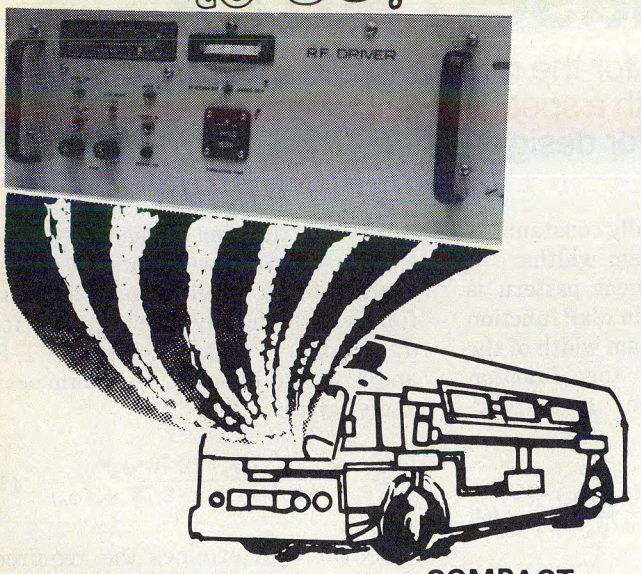
(concluded on next page)



1. Phased-array systems, *such as the giant COBRA DANE radar at Shemya AF Station near the western tip of the Aleutian Islands, are becoming more common. They have applications in communications as well as radar.*

Dr. Ernest Jacobs, Project Engineer, The Aerospace Corp., P.O. Box 92957, Los Angeles, CA 90009.

You Build the Bus Leave the "RF DRIVER" to US!



- HIGH PEAK POWER
- PHASE STABLE
- AFC
- COMPACT
- LONG PULSE
- RELIABLE
- RF POWER PROGRAMABLE

MODELS	FREQ. MHZ	STD PEAK POWER	HIGH PEAK POWER	STD PULSE WIDTH
0101	100-200	2000W	8000W	500 *
0104	200-300	2000W	8000W	500 *
0107	300-400	2000W	8000W	500 *
0110	400-500	2000W	5000W	500 *
0113	500-700	2000W	5000W	300 *
0116	700-800	2000W	5000W	100 *
0119	800-900	2000W	5000W	100 *
0122	900-1000	1000W	3000W	100 *
0125	1000-1200	1000W	3000W	100 *
0128	1200-1400	1000W	3000W	100 *
0130	1400-1600	1000W	3000W	100
0135	1600-2000	1000W	3000W	100
0240	2000-2500	600W	1500W	50
0268	2850-2860	600W	1500W	50
0275	2500-3000	600W	1500W	40
0280	3000-3500	600W	1500W	15
0290	3500-4000	500W	1000W	15
0300	4000-4500	400W	750W	15

* Special Units with pulse widths to 1500 µs available, all models factory set to your frequency

Prices start at $15,000. Delivery: Stock to 90 Days

MICROWAVE CONTROL COMPANY
1105 INDUSTRIAL PARKWAY
BRICK, NEW JERSEY 08723
WE INVITE YOUR CALL, 201-458-3000
TELEX 642-651

READER SERVICE NUMBER 49

OPTIMIZING PHASED ARRAYS *(continued from p. 69)*

To find the minimum N_o, Eq. 4 is differentiated with respect to ϕ_o and set equal to zero:

$$\frac{dN_o}{d\phi_o} = \frac{2(2.78\ \phi_s)^3\ G(\phi_s)\ \cos\ (2.78\ \phi_s/\phi_o)}{kf(d/\lambda)\ \sin^3\ (2.78\ \phi_s/\phi_o)} = 0 \qquad (5)$$

The set of solutions to Eq. 5 is $2.78\ \phi_s/\phi_o = (2n\text{-}1)\ \pi/2$ (where n = 1,2,3...). The only physically correct solution is for n = 1; all other solutions are for local minimums and result in array scanning into the side-lobe region. Letting n = 1:

$$2.78\ \phi_s/\phi_o = \pi/2, \text{ or} \qquad (6a)$$

$$\phi_o \approx 1.77\ \phi_s \qquad (6b)$$

Thus, *regardless of the desired gain at the maximum scan angle, the optimum element half-power beam width is approximately 1.77 times the maximum scan angle.* (Note that the array scans $\pm\phi_s$.)

The scanning loss (L_m) at the maximum scan angle is obtained by substituting Eq. 6(a) into Eq. 2:

$$L_m \approx \left[\frac{\sin\ \pi/2}{\pi/2}\right]^2 = -3.9\ \text{dB} \qquad (7)$$

The maximum scan angle occurs when the element pattern is down by approximately 3.9 dB from its peak.

The gain of the optimum element is obtained by substituting Eq. 6(a) into Eq. 1. A k value must first be selected. The value of k found to be most consistent with medium gain element antennas is $\approx 2.57 \times 10^4$. Using this value the gain expression becomes:

$$g_e \approx 39.1 - 20\ \log\ \phi_s\ (\text{dB}) \qquad (8)$$

where ϕ_s is in degrees.

Letting $k = 2.57 \times 10^4$ and $f(d/\lambda) = 1$ in Eq. 4 and substituting Eq. 6(a), an expression is obtained for the minimum number of elements required to achieve the gain, $G(\phi_s)$, at the maximum scan angle, ϕ_s:

$$N_{min} \approx 3.02 \times 10^{-4}\ G(\phi_s)\ \phi_s^2 \qquad (9)$$

Equation 9 is an approximate expression which allows the system designer to estimate the magnitude of the design problem before expending significant engineering effort. A precise number can only be obtained from a detailed design.

An expression for the minimum number of elements it takes to construct an array with a gain of $G(\phi_s)$ at a maximum scan angle of ϕ_s has been developed. These parameters are just the starting point of the design. It's still necessary to find a suitable antenna element that meets the optimum criteria and a configuration that meets good design practices. For example, a correct choice of element spacing would significantly minimize grating lobe energy "suck-out." The minimum number of elements gives a lower bound estimate of what it would take to do the job. The actual number of elements could possibly exceed this value when practical matters such as aperture symmetry, feeding network design and side-lobe levels are taken into account.

It is quite possible that the available suitable element antennas will be lower in gain than the specified optimum. In this case, an optimum can be obtained by configuring the elements into subarrays that conform to the optimum element pattern.

Acknowledgments

This work was supported by the US Air Force under Contract No. F04701-79-C-0080. The author wishes to thank Messers. F.L. Hennessey and H.E. King for their helpful discussions and suggestions.

References

1. J.D. Kraus, *Antennas*, McGraw-Hill, New York, NY, p. 25 (1950).
2. H.E. King and J.L. Wong, "Directivity of a Uniformly Excited N × N Array of Directive Elements," *IEEE Transactions on Antennas and Propagation*," Vol. AP-23, pp. 401-404 (May 1975).

Array Radars Solve Communication Jams

The widely used tactical multifunctional phased-array radars can support new command, control, and communication systems that are very resistant to electronic countermeasures.

PHASED-ARRAY radar systems can automatically perform both of the classic radar duties: search (initial detection) and tracking. In the recent past, phased-array systems have been installed as fixed land-based radars, mobile land-based radars, shipboard radars, and airborne radars. While each of these radars differs in use and system parameters, each is inherently capable of adding one more function—communications.

Tactical data communications between a master station—the data gathering and processing radar system—and any of several remotely located slave stations is essential to successful command and control during military operations. But, when multiple highly mobile stations must be included in the links, and high jamming levels must be overcome, this communication can be seriously degraded.

Multifunctional array radars can improve this situation by assuming the additional function of data transmission and reception. The radar can beacon-track the cooperating mobile (slave) stations, which can be equipped with suitable transponders. Such a system can provide positive identification of each slave station as well as highly accurate data on its position. The system can be applied to surface-to-air command and control, air-to-surface targeting and tracking (long range), and surface-to-surface coordination in both monostatic and multistatic operations.

The concept exploits the inherent high-power aperture product and low antenna side lobes of the phased-array radar to combat ECM. Moreover, the ability of the multifunction phased array to revisit the cooperating station as often as required permits a reliable interchange of data on an interrogation/reply basis. A waveform suitable for the combined radar and communications function can be designed as part of the system.

H. D. Lewis, Principal Member, Engineering Staff, RCA Government Systems Div., Missile and Surface Radar, Moorestown, NJ 08057.

Radar classification

Radar can be classified as search radar, tracking radar, or multifunction radar. (The multifunction radar classification encompasses both rotating and electronically steered antenna configurations. For example, a track-while-scan (TWS) radar can use off-axis measurements obtained during mechanical rotation of a search antenna to provide target track data.)

A pure search radar has little value in data transfer. At least some degree of track memory must be part of the system to allow proper timing of message transmissions. A rotating radar of this type, even with TWS capability, is limited by the complexities of rotational speed, azimuth beam width, and maximum message lengths. All of these parameters must be carefully balanced to insure that a control/reply message pair can be transmitted and received during the time a communicating slave station is illuminated by the radar. If the radar must cover a complete 360 degrees in azimuth, the message rates involved may be fairly low.

In spite of these limitations, a search radar with a rotating antenna and limited TWS capability could produce some enhancement of data communications in the presence of jamming when compared to the conventional isotropic antenna system.

Tracking radars suffer none of the constraints of search radars. However, the single-target-track limitation of a tracking radar restricts it to communication with a single slave data-exchange system. Thus, a multistation link would require several tracking radars.

The electronically steered phased-array radar can serve as an ideal master data-communications station. In such a system, targets detected by steering the highly directive, electronically agile antenna through a spatial scan pattern are revisited by the beam and tracked. Thus, the modern multifunction phased-array radar can handle a multiplicity of simultaneous targets and can easily service many slave stations. In operation, the antenna can be instructed to dwell on an individual slave station. Each dwell consists of positioning the antenna beam precisely on the slave station, transmitting a message, and receiving a reply. The radar is then free to move on to another beam position or even transmit a second message to the same slave. Dwells need not be identical, but can be adapted to message lengths and the distance to the slave station.

Note that the communication link can be achieved as part of the process of tracking the station. From the perspective of the radar hardware, no new duties have been added. A fixed master phased-array system aboard a ship, for example, can communicate with friendly aircraft as part of its normal functions within a battle area.

Phased-array system concepts

A phased-array system can position its directive antenna beam anywhere in the radar coverage volume within a few microseconds. This capability separates the search and track functions which are tied together in a rotating-antenna radar system.

Search is performed by scanning the array's beam, in a predetermined fashion, through the coverage volume.

(continued on p. 75)

Each angle cell which provides a detection can be revisited as often as necessary to obtain the range and angle data needed for tracking.

The particular radar doctrine that was incorporated in the design of the radar will determine the revisit rate. This tracking data rate may be increased as the signal-to-noise or jamming-to-noise ratio decreases, or it may be decreased when a slow-moving, long-range target holds little interest in comparison with a rapidly moving, close-in target. Regardless of the doctrine, the radar is caused to modify its tracking rates to perform at peak tactical efficiency. As a result, most phased-array systems can track an enormous number of targets. If required, the search function can be interrupted to update tracking information, and then resumed.

A target 100 miles away might require a single dwell that takes a round-trip time of 1220 μs, plus an extra few microseconds allotted for radar dead time and antenna beam positioning. Perhaps 700 to 1000 such dwells can be transmitted in a one-second interval. If half of these dwells are dedicated to the search function, approximately 300 tracking dwells remain available at a one-per-second revisit rate. And, of course, the number of tracking dwells available will increase if the radar's mission can accommodate a slower tracking rate. This simplistic example illustrates the immense quantity of high quality data that can be extracted from a phased array.

Data transfer considerations

The phased-array radar seldom exists as a separate entity making exclusive use of its own data. In the real world, the data must be disseminated to multiple users and is essential to proper radar and control system operation. The transfer of this data is not easily achieved, especially when hostile jamming must be overcome.

If the using stations must be mobile (aircraft, tanks, ships, etc.), the problem of data transfer becomes even more complex. The master disseminating station (the radar complex) must either keep track of all user station positions or broadcast data in all directions. Broadcasting data with omnidirectional antennas has been the traditional approach in tactical communication systems, since the master station need not worry about user location in this kind of master/slave data link (Fig. 1).

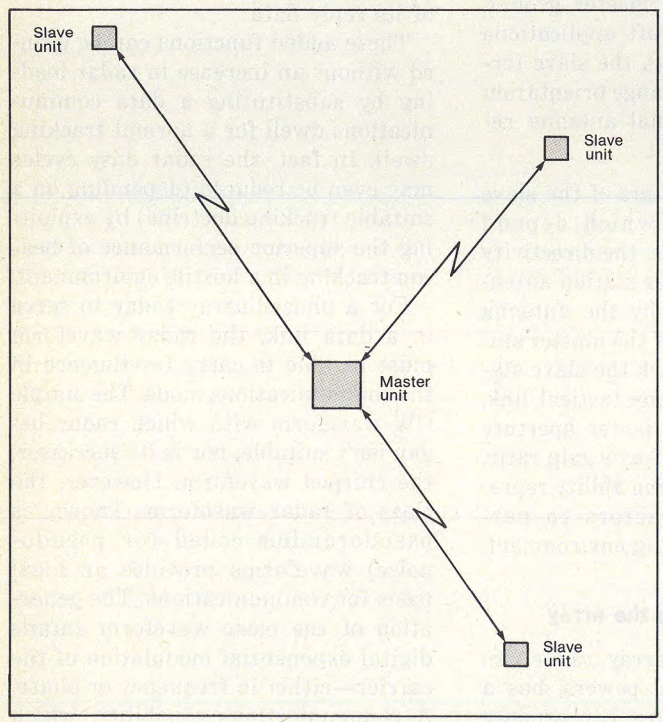
When jamming is encountered, the system must satisfy the parameters shown in Fig. 2. The jammer is located at a range, R_{jm}, from the master station, and at a range, R_{js}, from the slave. It radiates P_jG_{jm} Watts toward the master, by virtue of its transmit power in the master-station receiver bandwidth, P_j, and its antenna gain in the direction of the master station, G_{jm}.

In like manner, the jammer radiates P_jG_{js} Watts toward the slave (G_{js} = the jammer antenna gain in the direction of the slave). For the purpose of this discussion, the receiver bandwidth of the master and the slave are assumed to be identical.

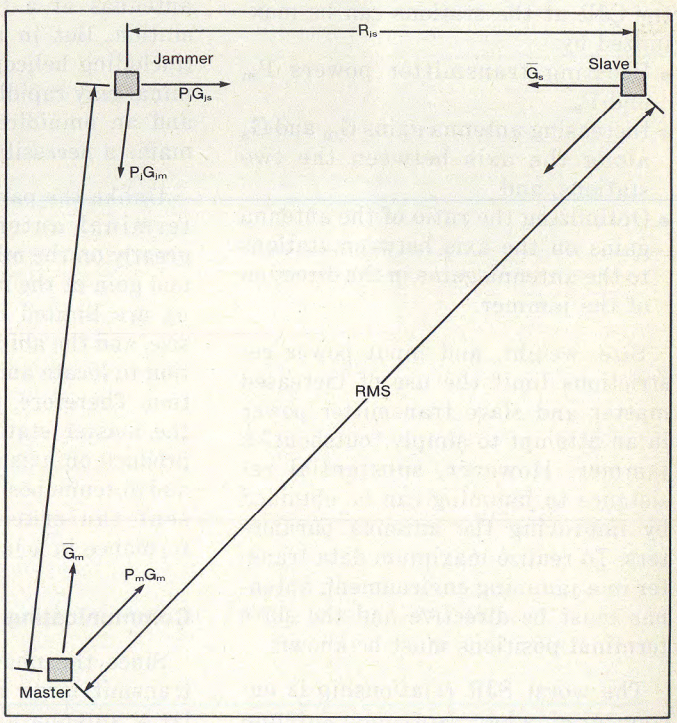
The master station transmits P_mG_m Watts in the direction of the slave, which is at a distance R_{ms} removed from the master (P_m = the power radiated by the master, and G_m = the master station's antenna gain in the direction of the slave). At the slave station, the signal is received by an antenna with a gain G_s, and the jamming energy is received by the same antenna with a gain $\overline{G_s}$ in the direction of the jammer.

The reply, from slave to master, is transmitted at a power P_sG_s (P_s being the slave's transmitter output). The master antenna receives the reply signal with a gain G_m, and the jamming signal with a gain $\overline{G_m}$.

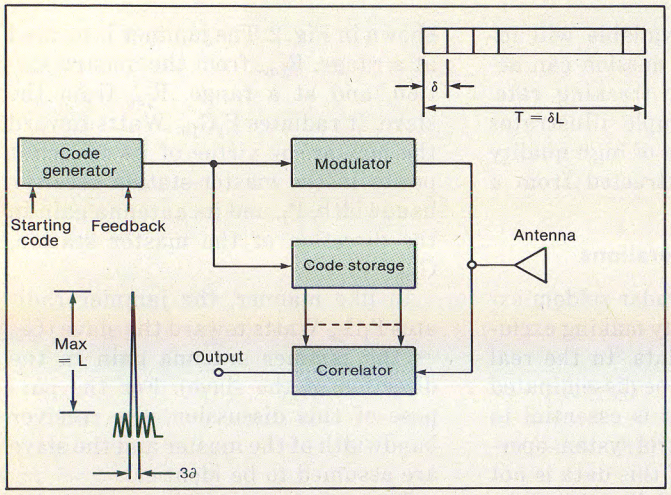
(continued on next page)



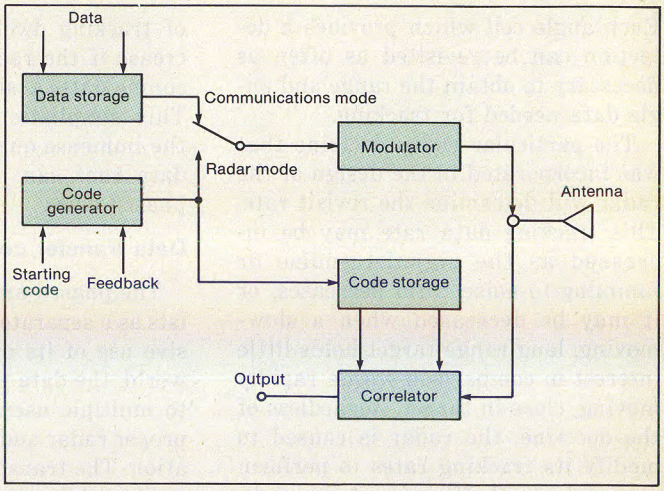
***1. The traditional approach to tactical communication systems** has been the broadcasting of data with omnidirectional antennas.*



***2. Jamming disrupts the flow of data** between the master and the slave stations. It can be overcome with increased transmitter power, and greater antenna gain and directivity.*



3. A pseudorandom code can be generated in a radar, *used to modulate the carrier for transmission, and stored for latter correlation with the received signal.*



4. Data transmission can be handled by a radar *equipped to transmit a coded waveform without degrading its primary mission.*

The signal-to-jamming ratio (SJR) at the slave will be:

$$(SJR)_s = \left(\frac{P_m G_m}{P_j G_{js}}\right)\left(\frac{G_s}{G_s}\right)\left(\frac{R_{js}}{R_{ms}}\right)^2 \quad (1)$$

While the SJR experienced at the master station can be found from:

$$(SJR)_m = \left(\frac{P_s G_s}{P_j G_{jm}}\right)\left(\frac{G_m}{G_m}\right)\left(\frac{R_{jm}}{R_{ms}}\right)^2 \quad (2)$$

For any given set of jammer radiated power and range relationships, the SJR at the stations can be maximized by:

- Boosting transmitter powers P_m and P_s,
- Increasing antenna gains G_m and G_s along the axis between the two stations, and
- Optimizing the ratio of the antenna gains on the axis between stations to the antenna gains in the direction of the jammer.

Size, weight, and input power restrictions limit the use of increased master and slave transmitter power in an attempt to simply "outshout" a jammer. However, substantial resistance to jamming can be obtained by improving the antenna parameters. To realize maximum data transfer in a jamming environment, antennas must be directive and the slave terminal positions must be known.

The worst SJR relationship is encountered when isotropic antenna systems are used for both the master and slave terminals. Such systems provide no increase in effective radiated power during transmission, and no off-axis rejection during reception.

In some cases, slave terminal antennas can exhibit a more desirable degree of directivity. A shipboard system, which can be steered at a slow rate to compensate for changes in heading, would only be required to have sufficient beam width to compensate for pitch and roll variations. Trucks or tanks can train broad beamed, but still partially directive, antennas at a fixed master ground station. But in aircraft applications (including helicopters), the slave terminal may rapidly change orientation and an omnidirectional antenna remains a necessity.

Unlike the parameters of the slave terminal antenna which depend greatly on the mission, the directivity and gain of the master station antenna are limited only by the antenna size, and the ability of the master station to locate and track the slave station. Therefore, for any tactical link, the master station's power aperture product, on-axis to off-axis gain ratio, and antenna positioning ability represent the crucial factors to performance in a jamming environment.

Communicating with the array

Since the phased-array radar can transmit large signal powers, has a large antenna aperture, can produce high ratios of on-axis to off-axis antenna gains, and can accurately and rapidly position its antenna beam, it offers a great number of benefits for communications.

The phased-array radar, with its automatic detection and tracking capabilities, usually tracks the slave terminals as part of its normal operation. The transfer of data requires the addition of a data transponder to the communicating slave station. This transponder extends the tracking range and establishes a positive means of identification by permitting beacon tracking of the slave by means of its reply data.

These added functions can be gained without an increase in radar loading by substituting a data communications dwell for a normal tracking dwell. In fact, the radar duty cycles may even be reduced (depending on a suitable tracking doctrine) by exploiting the superior performance of beacon tracking in a hostile environment.

For a phased-array radar to serve in a data link, the radar waveform must be able to carry intelligence in the communications mode. The simple CW waveform with which radar began isn't suitable, nor is its successor, the chirped waveform. However, the class of radar waveforms known as pseudorandom-coded (or pseudo-noise) waveforms provides an ideal basis for communications. The generation of the basic waveform entails digital exponential modulation of the carrier—either in frequency or phase. A communications capability, which also requires modulation and demodulation of a digital bit stream, is inherent in such a radar design.

The pseudorandom-coded waveform preserves the advantages of chirp radar (i.e., good range resolution and high average power). In addition, such waveforms can provide good approximations of the "thumb tack" range-velocity ambiguity functions, in which only one range-velocity solution exists in the region of interest.

In operation, a radar using this concept (Fig. 3) generates the pseudorandom code, uses it to modulate the carrier for transmission, and stores it for correlation with the received signal. The correlator output provides range resolution commensurate with the width (δ) of a single bit of the code, and offers signal enhancement (relative to noise, jamming, or a false code) equal to the number of bits (L) in the code. Standard techniques may involve the use of "M-sequence" or shift-register codes.

Shift-register codes can be distinguished by their starting code (the binary code loaded into the register) and their register feedback tap configuration (which determines the output code for any specific register length and starting code). The period, N, of a shift register sequence is given by:

$$N = 2^n - 1 \qquad (3)$$

In Eq. 3, n = the initial register length. Range ambiguities are spaced $N\delta$ apart. The uniform range side lobes have an amplitude (1/N) with respect to the correlated output. If a truncated sequence is used with a length, L, that is less than the cyclic length, N, the range side lobes will be greater than 1/L and will depend on the specific starting code and feedback taps. For most truncated codes of reasonable length, a number of starting codes and feedback taps can be found which will generate an output code having range side lobes below some arbitrary value suitable for radar (and communication). These codes and taps are stored as part of the radar waveform inventory.

Since the pulse compression or integration gain of the radar is equal to the length of the truncated code, the radar is adaptive. Performance in the presence of noise or interfering signals can be increased by increasing this code length.

A radar equipped to transmit a coded waveform is ideally suited to transmit digital data to a slave station (Fig. 4). Since the tracking of the slave station can use a beacon reply, all of the L bits are available for addressing, labeling, and data. Moreover, the high power-aperture product of the phased-array radar for one-way transmission can be used to counter jamming of the master station transmission, while its inherent side-lobe structure aids in rejection of reply jamming.

In addition, the reply from the slave station can use the inherent integration gain of the radar to good advantage: encoding data in such a way that the transmission of one of two codes of length L indicates a "one," and transmission of the other indicates a "zero." The generation of the coded waveform is shown in Fig. 5. The radar processing (Fig. 6) involves simultaneous correlation of the received reply against both codes.

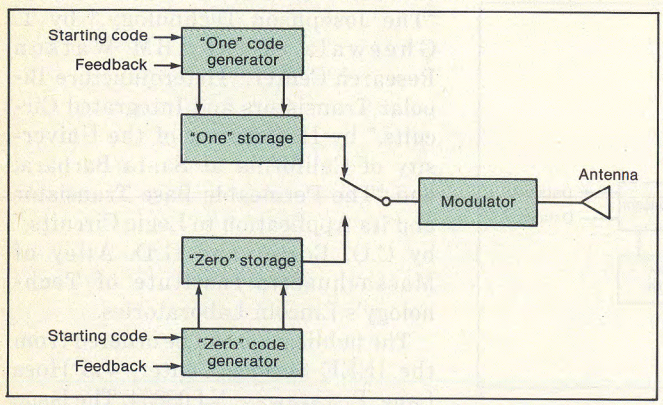
If the radar thresholds are properly set, the reply can be self-checking. If the reply is not confused by noise or jamming which exceeds the threshold, an output will exist at only one correlator for each bit in the message. Should a bit not be present at one of the two correlator outputs (indicating that a bit has not been detected), the bit is declared in error. When the bit error rate exceeds a prescribed value, the slave station is commanded to increase the length of each bit. As the bit error rate drops below a prescribed value, bit length is decreased. In this manner, the average power contained in the reply is adapted to the environment.

Slave station acquisition

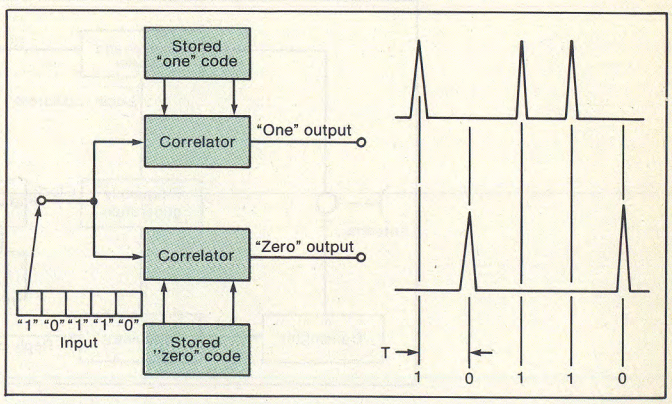
Since the master station is a radar, it can beacon-track the slave unit. It extracts range and angular position data from the reply and uses it to establish tracking files. Angle data is used to position the antenna beam for subsequent dwells, while range data is used to gate the desired range interval and avoid false alarms. Beacon links must be established by interrogation techniques, which imply that the radar has sufficiently accurate information of the slave position to direct an initial interrogation message. Several alternate methods are possible.

If the radar can skin track the cooperating slave unit, highly accurate tracking data can be used to position the initial interrogation. Acquisition simply becomes a matter of switching from skin tracking to beacon tracking. This technique is ideally suited for applications in which short-range skin tracks can be established on slave

(continued on next page)



5. Two codes can be used to take advantage of the inherent integration gain of the radar. *One code represents a logic "one," the other signifies a "zero."*



6. The reply received by the master station from a slave *must be simultaneously correlated against both communication codes. If neither code appears, the bit is in error.*

units that are traveling away from the master unit. As the range between the master and the slave unit increases, the high-quality beacon track replaces the less jamming-resistant skin track. (Note that if the radar addresses a noncooperating unit, no beacon reply is received.)

In many instances, only coarse designation data will be available. In these cases, acquisition can be performed by transmitting interrogations in a scan pattern which covers the area of uncertainty. In the rare event that no initial designation data is available, the radar can transmit beacon interrogations over large spatial areas using normal search patterns.

Dealing with frequency uncertainty

Some penalty accompanies the use of pseudo-noise-coded radar waveforms to achieve integration of reply data and, thereby, increase immunity to jamming. Correlation of pseudo-noise-coded waveforms is a coherent, matched filtering process. As code length increases (increased integration gain), the matched filter bandwidth decreases. Eventually, it becomes difficult to insure that a reply transmission can be maintained in the matched filter bandwidth, because of the tolerances between the independent clocks used at master and slave stations, which is translated to the actual transmission frequency.

The loss in signal-to-noise ratio (or signal-to-jamming ratio), which results from a difference in frequency between the two stations, is given by:

$$\text{Loss} = \sin(\Delta\omega T/2)^2 \qquad (4)$$

In Eq. 4, $\Delta\omega$ = the radian frequency difference, and T = duration of the pseudorandom-coded bit.

A low transmission frequency can eliminate the problem, and allow the clock tolerances to be more easily maintained. But, since many systems operate at frequencies which can lead to substantial losses, several other available solutions can be applied. These include frequency synchronization, "Doppler" processing, measurement and compensation of the frequency offset, and noncoherent integration of several coherently integrated short bits.

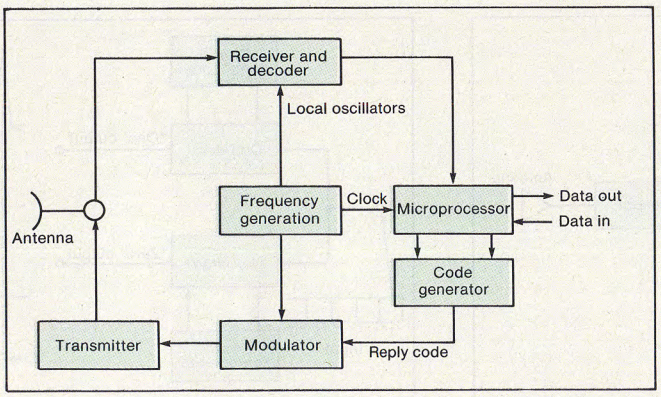
Slave terminal design

A slave terminal suitable for use with the phased-array radar consists of three basic building blocks (Fig. 7):

- A receiver, matched to the digital modulation impressed on the radar transmission, with suitable decoding,
- A modulator and transmitter capable of generating two or more pseudorandom sequences identical to the radar waveform, and
- An interface unit that can output received data, format reply data, and provide the internal control functions required by the unit.

The advantage of using the phased-array radar for tactical communication has been verified initially by the construction and test of a prototype transponder. Bench and boresight-tower-link tests have revealed substantial immunity to jamming which is in agreement with calculated performance. Additional testing of the transponder using aircraft vectoring has been initiated. The radar automatically acquires the aircraft skin track, then initiates two-way link acquisition and beacon tracking using a discrete address.

Following establishment of the link, the aircraft is vectored to waypoints or directed to intercept other aircraft with the master radar computing the intercept solution. ••



7. A slave station for use with the phased-array radar has three building blocks: *a receiver, a modulator and transmitter, and an interface unit.*

Acknowledgment

This article is an extension of material originally presented at the National Aerospace Electronics Conference, Dayton, OH, May 19-21, 1981. The original paper, "Using Phased Array Radar For Communications," can be found in the proceedings of that conference (© IEEE).

IEEE highlights VLSI advances

Proceedings of the IEEE has devoted its January 1982 issue (Vol. 70, No. 1) to the rapid development of very large scale integration (VLSI) technologies. The guest editor, Dr. Richard C. Eden, has assembled seven papers on the subject, three of which concern gallium arsenide (GaAs) techniques.

The issue includes: "Comparison of GaAs Device Approaches for Ultra-High-Speed VLSI," authored by Eden; "High-Speed GaAs Integrated Circuits," by S.I. Long, et al., of Rockwell International; "Electron-Beam-Fabricated High-Speed Digital GaAs Integrated Circuits," by P.T. Greiling, et al., of Hughes Research Laboratory; "The Josephson Technology," by T. Gheewala of the IBM Watson Research Center; "Heterojuncture Bipolar Transistors and Integrated Circuits," by H. Kroemer of the University of California at Santa Barbara; and "The Permeable Base Transistor and its Application to Logic Circuits," by C.O. Bozler and G.D. Alley of Massachusetts Institute of Technology's Lincoln Laboratories.

The publication can be ordered from the IEEE Service Center, 445 Hoes Lane, Piscataway, NJ 08854. The issue costs $6 for IEEE members and $12 for non-IEEE members. Specify item number JH57141. •• *SM*

Higher System Availability Is Achieved With Software

Digital computers have been controlling radar systems and monitoring their performance for two decades. But mature diagnostics and fault elimination are relatively recent developments.

THE change from hard-wired to programmable devices, and the use of commercial data processing hardware and software, is allowing the radar system designer to create and use better fault detection and recovery mechanisms. Because of these options, hardware and software development have become intertwined, and the availability of radar systems has improved.

Fault detection, fault recovery, and data collection have become an integral part of today's real-time radar system. The emphasis on these functions is being driven by the need to increase the time the system is available to fulfill its primary mission (i.e., increased system availability).

The problem becomes two-fold: during operation the system must respond rapidly to remedy any failure condition, and, during maintenance, operational data must supplement diagnostics to minimize repair time. Increasingly, system designers are recognizing that the operational and maintenance phases represent a processing continuum requiring the same data to be acquired and, ideally, the same analyses to be applied.

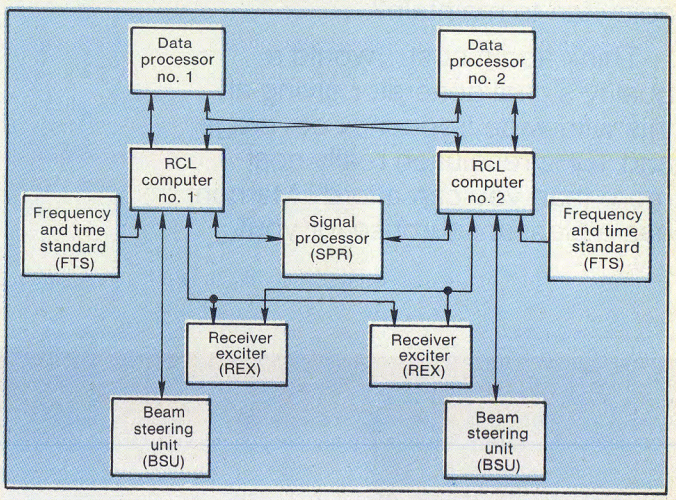
New software/hardware roles

Diverse digital system architectures and programmable digital devices allow the effect that every on-line process has on the availability of the entire system to be anticipated in the system software. This technology has established new roles for software and hardware in monitoring performance, preventing downtime, detecting failures, and reconfiguring the system to avoid them.

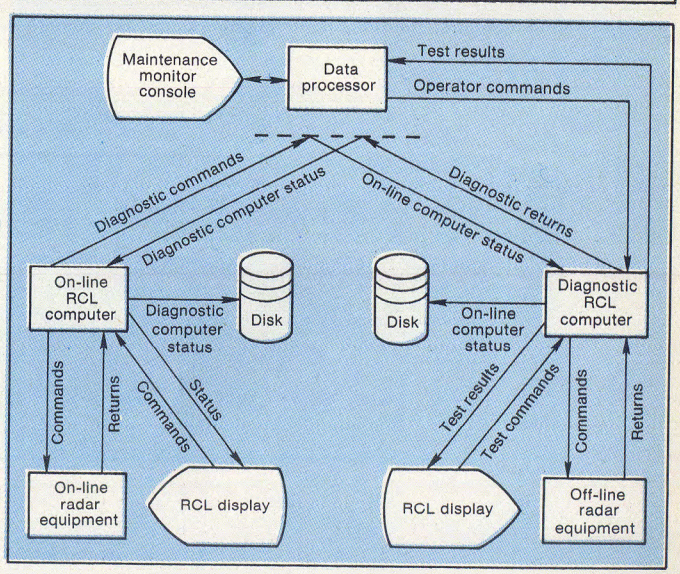
Benson H. Scheff, Principal Engineer, Equipment Div., Raytheon Co., Wayland, MA 01778.

A wide spectrum of practical digital architectures has resulted from the design community's greater understanding of the mechanisms of problem partitioning, processor interference, interprocess communication, protocols, distributed data bases, and fault tolerance schemes. Digital system architectures are no longer restricted simply to the typical central monolithic processor of the 1960s and the early 1970s. Today, networks of distinct processing elements can be coupled under software control that permits functions to be partitioned and assigned to subsidiary processing elements.

Distributed systems are produced from the separation of functions into independent and semi-independent tasks by assigning the partitioned tasks to a number of processing elements. The result has been improved system capacity, increased system memory, and faster response times—all coupled with decreased cost and size.



***1. The PAVE PAWS system** insures the radar's availability by using a redundant system. The dual-system philosophy applies both to the data processing and the radar hardware.*



***2. The on-line RCL performs tactical tasks,** checks the on-line radar units, and manages the radar equipment configuration. The off-line RCL continuously assess the off-line radar subsystem.*

The state-of-the-art programmable digital devices—from discrete components to integrated circuits to MSI/LSI—has advanced dramatically. The earliest integrated circuits contained the equivalent of a dozen transistors and could perform only elemental functions. Today, advances in lithography and fabrication techniques permit chips to contain as many as 100,000 active elements. Through custom design, all of the functions of a data processor can be performed on a single chip: a CPU, clock, I/O (input/output) capability, read-only memory (ROM), and random-access memory (RAM).

These microprocessor developments are complimented by software support systems which can include higher-order language and translation capabilities. They can also supply extensive software development maintenance tools, as well as emulation features.

Microprocessor cost savings

The value of the microprocessor is that it can be programmed. When embedded as a processing element within a radar system as a "replacement" for logic circuits, it can save cost in system design, parts, and correction and modification. (It is easier to test and correct a line of code than to layout, test, and debug the complete hardware.)

The microprocessor also provides more flexible control and greater processing ability. Diagnostics or testing can be incorporated as an adjunct to the primary application processes. The diagnostic routine can command system components to produce a specific output, and compare the real-time response to self-computed values. Data can be acquired as an intermediate output of the on-line application computations, or by "eavesdropping" on data as it is transferred between processing elements.

Phased arrays, because they use diverse computation and control processes, provide a good illustration of these hardware and software techniques. The PAVE PAWS and WAAS radar systems serve as examples.

Systems show alternate schemes

PAVE PAWS, which was developed for the US Air Force, was built on the concept of redundant, reconfigurable devices, with functions off-loaded into different standard general purpose digital computers. In this system, each of these data processors generally controls its own set of functions, while one central data processor maintains system control.

The Wide Area Active Surveillance System (WAAS) was developed for the US Navy and uses microprocessor-type devices built into radar units. These microprocessors contain relatively complete programmable processing capabilities and are integrated into the unit they control.

The PAVE PAWS system is a fixed-base phase-array warning system with a primary mission of detecting and attacking characterization of submarine-launched ballistic missiles which penetrate other radar coverage. As a secondary mission, PAVE PAWS supports the USAF SPACETRACK system with earth satellite surveillance, tracking, and data collection.

Before the detection and resolution of hardware and software failures by the PAVE PAWS system can be discussed, these terms must be more clearly defined. Once in operation, hardware errors can generally be classified as either failures in design or implementation, or as failures in equipment. Unfortunately, software problems and failures cannot be as neatly categorized.

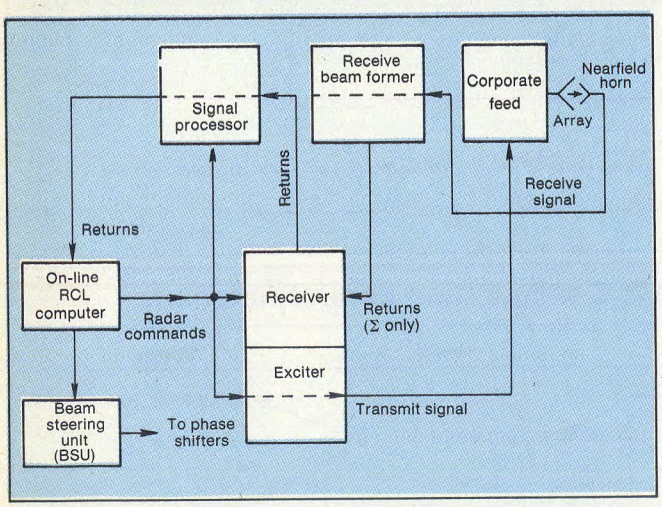
Software does not decay with time. However, design or coding errors can cause limits to be exceeded, buffers and tables to overflow, and input data to be lost. Software errors, like hardware errors, can be transient, especially if defensive design and code (which automatically commands faulty data to be retransmitted or recalculated) has been used for the specific operational process. Whether the failure is rooted in hardware or software, the effect is the same. The operational process can continue if a failure is recognized and if remedial action is accomplished.

The main objective, then, is to have the software recover the system from a failure. The classification of that failure as a hardware or software error is completely secondary. It may not even be critical for the software to identify a specific fix during maintenance—software modifications have been known to correct problems that were due solely to hardware.

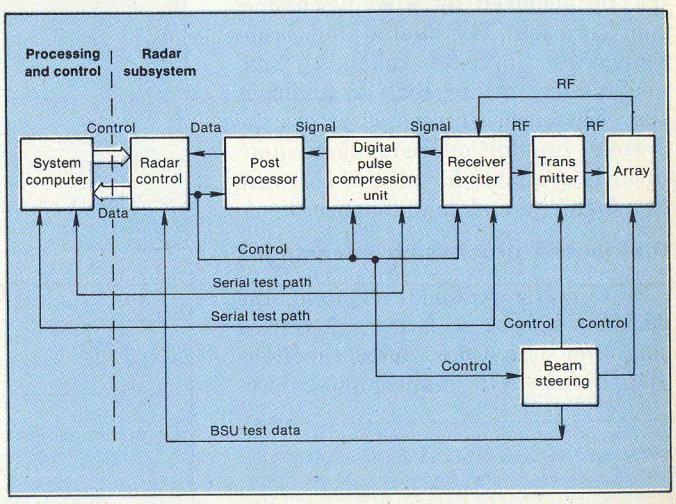
Software chooses most likely failure

The PAVE PAWS system uses reconfiguration in layers based on considering failures as single point events that can be attributed to the function

(continued on next page)



3. In the PAVE PAWS array test configuration, *failure reports and out-of-tolerance data are used to isolate hard faults and identify the components involved.*



4. The Wide Area Active Surveillance (WAAS) system *is controlled by a standard DEC KL-10 computer. The KL-10 downloads instructions to distributed microprocessors.*

most likely to have failed. Consider, for example, a process containing the generic functions A and B. "A" could denote the central data processor, and "B" the tactical applications software. They could also indicate two radar subsystem elements, each containing both hardware and embedded software (or "firmware").*

Each function is backed by a redundant partner (for example, B1 can be replaced by B2). If a process containing the function A1 and B1 fails, the software reconfigures the system by replacing the element that has been determined to be the most likely to fail.

If B1 is the most likely failure candidate, it will be replaced by B2. If the resulting process, A1 and B1, remains nonoperative, the system will take one of two possible actions, depending on the particular elements and process. Either A1 will be replaced with A2 (forming an A2 and B2 process), or A1 will be replaced with A2, *and* B2 will be replaced with B1 (forming an A2 and B1 process).

The PAVE PAWS data processor and radar control architecture was determined largely by the requirement that the system be maintained at 99-percent availability for seven days a week, 24 hours a day (including all preventative maintenance). In addition, a specified one-hour mean time for repairs was coupled with a very stringent downtime restriction (downtime was to occur no more than once every 323 hrs).

Various dual computer and multiprocessing configurations had to be considered to achieve increased availability through redundancy, since the required system performance could not be achieved by a single-channel configuration. The dual system is intended to increase reliability and availability, rather than to augment the capacity (throughput) of the system. In addition, redundant equipment is available for off-line software development and maintenance.

Distributed processing advantages

Within the redundant system, the decision to use a large, centralized computer with radar control functions distributed to a minicomputer pro-

*"Firmware" is microcode which is generally not accessible to the applications programmer/engineer. It may exist as privileged instructions in RAM, or, as in the case cited here, in ROM. ROMs cannot be modified since data is stored by the pattern of connections permanently made between elements on a chip. "Programming" is accomplished only by changing the fabrication mask.

Table 1: Radar interface functions

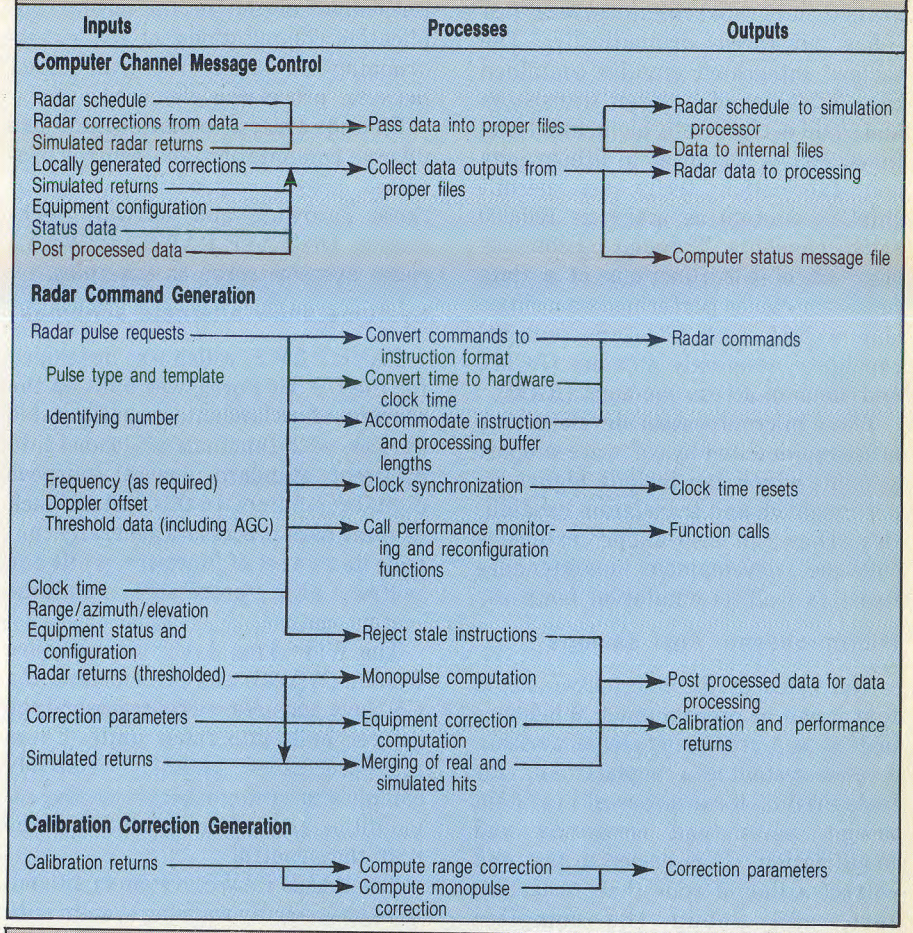


Table 2: Operability assessment functions

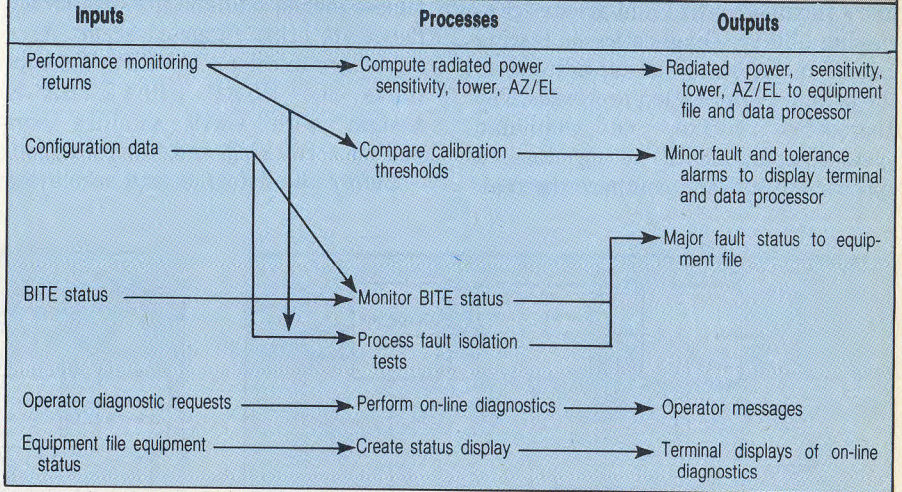
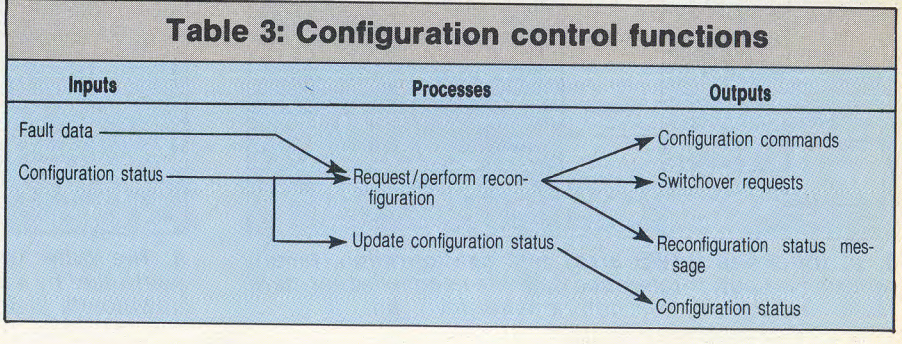


Table 3: Configuration control functions



vided the following advantages:

- Off-loading the radar processing functions reduced the central computer requirements,
- Using software in a general purpose computer provided a more flexible radar system, and
- Development, testing, and maintenance of the radar and radar control subsystem (hardware and software) could be accomplished independently of the software/data processing subsystem activity.

The PAVE PAWS system uses redundant data processors (Control Data CYBER 174 computers) and radar controllers (RCLs, MODCOMP IV/25) arranged in the dual system (Fig. 1). Redundant radar equipment continues this dual-unit philosophy throughout the system. The RCL directs the radar subsystem units: the beam-steering unit (BSU), the frequency time standard (FTS), the general purpose signal processor (GPSP), the receiver exciter (REX), and the array. In the event of a single hardware or software fault, hardware is automatically reconfigured by the software to eliminate the fault and resume the primary mission of the system.

The operational software samples hardware status bits, performs "sanity and health" checks on itself and all processing equipment, computes and verifies parity bits and check sums, and monitors input and output processes. The detection of a nontransient failure event, or the occurrence of an abnormally high number of transient failures during a specific time period, triggers a specific reconfiguration algorithm.

Reconfiguration is software controlled, and is accomplished by "closing" the device or subsystem to be "dialed out," and "opening" the redundant device to be used in its place. The device address in the appropriate input/output software is changed, and the proper protocols executed. In certain critical situations, reconfiguration is subject to operator override (e.g., when reconfiguration is requested to an element which is capable of only degraded operation).

Table 4: Principal test categories

Function	Test	
	On-line (Automatic)	Operator Call Up
Calibration	Angle Boresight Range Zero Calibration Satellite Tracks Propagation Corrections Monopulse Gain and Phase Radar Cross Section	Calibration Data
Performance	Transmit Power and Gain Receive Gain and Sensitivity Receive Noise Figure Module (Transmit and Receive)	Range Side lobes Antenna Patterns
Fault Monitoring and Correction	Fault Sensing Redundancy Switching Status Reporting	Diagnostics Detailed CI Status Module Status

Table 5: On-line diagnostic software tests

Unit	Test
Signal Processor (SPR)	Operability Assessment/ Verification
Receiver/Exciter (REX)	Operability Assessment/ Verification Stabilization Power Supplies Operability LRU Isolation
Beam Steering Unit (BSU)	Operability Assessment/ Verification
Entire System	Monitors Tactical Noise Environment Calculates Performance Indices Calibration

Table 6: Off-line diagnostic software tests

Unit	Test
Signal Processor (SPR)	Pulse Compression Side-lobe Blanking Threshold Computation Data Thresholding Beam Steering Computation Range Interpolation Amplitude Interpolation GPSP Diagnostics (Hardware)
Receiver/Exciter Unit (REX)	RCL Interface Waveform Generator Pilot Pulse Test Target Status
Beam Steering Unit (BSU)	RCL Interface Registers Time of Commands Array Interface Status
Frequency and Time Standard (FQT)	RCL Interface Status
Test Assist Mode	Antenna Pattern Measurement Azimuth and Elevation System Test (Gain, Dynamic Range, Linearity)

Three reconfiguration levels

Reconfiguration can take place:

- At the data processor level (the tactical software resident in the off-line data processor assumes responsibility for the tactical processing),
- At the RCL level (the tactical software resident in the on-line data processor directs the alternate RCL to assume responsibility for the tactical processing), and
- At the radar unit level (the software resident in the on-line RCL reconfigures the system to put different radar units on-line).

In the case of the central processor, recovery is based upon the ability of one of the two data processors to take one of two alternate actions:

- Detect a fault (hard failure) such as power failures and tactical software aborts, or
- Suspect that the data processor itself is in a condition which could provide erroneous processing (a soft failure identified by out-of-tolerance checks and an excessive number of parity errors).

In the on-line computer, hard failures cause an immediate data processor reconfiguration. Soft failures are logged and analyzed by the tactical software; reconfiguration may or may not be commanded depending on the total system status. For example, data transmission anomolies between the data processor and the RCL (i.e., failure to respond properly within a predetermined time period to communication directives issued by the tactical software in the on-line processor) are characterized as soft

(continued on next page)

failures, since one failure does not indicate that either the on-line RCL or the on-line processor are inoperative.

The data processor and RCL reconfiguration processes are intertwined. Assume, for example, that the tactical software in the data processor had requested the closing of the on-line RCL and the opening of the alternate RCL for processing. If the correct RCL-processor communications cannot be established and maintained after the RCL reconfiguration, the input/output hardware in the on-line processor is most likely to be malfunctioning. The software in that processor, by requesting mainframe reconfiguration, transfers tactical control to the alternate processor to continue the mission.

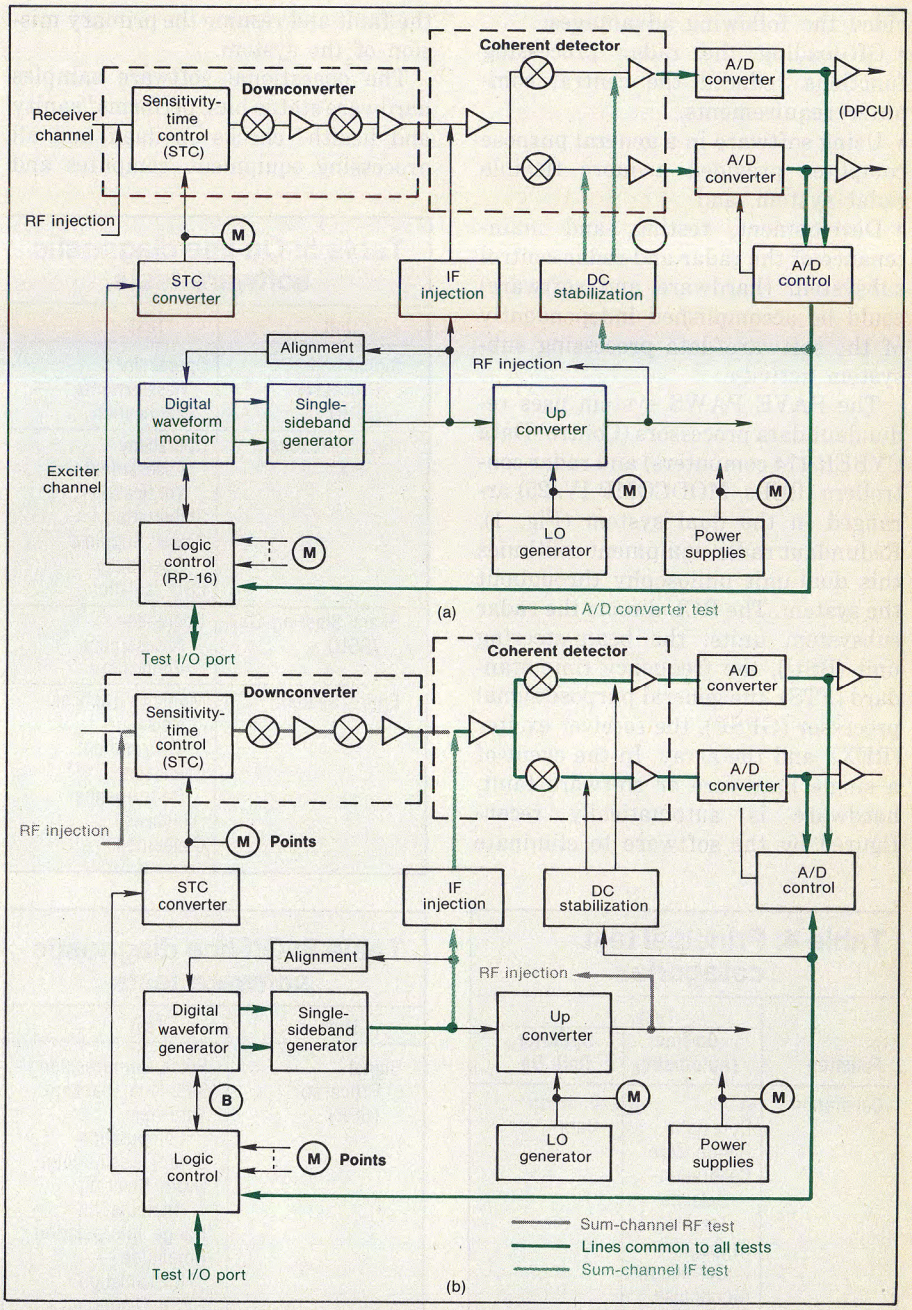
Architecture sets recovery action

Within the radar system, the specific architecture determines whether or not the faulty unit can be switched off-line and replaced. The beam-steering unit (BSU) consists of two identical units each dedicated to a single RCL. When the on-line BSU fails, its associated RCL must be reconfigured to obtain the usable BSU. Similarly, each frequency time standard (FTS) is dedicated to a single RCL. In this case, however, the software in each RCL communicates by passing a signal from its FTS to the other RCL. Thus, while one FTS cannot replace another, drift between the two units can be detected.

The signal processor (SPR) consists of four identical general purpose signal processors (GPSPs). Only three GPSPs are required for tactical operation; the fourth acts as a spare. Periodically, the on-line RCL software swaps the spare GPSP with one of the on-line units, which then becomes the spare. In contrast, the receiver contains four pairs of on-line RF channels which are dedicated to specific functions, and a fifth pair which is spare. When one of the on-line channels fails, the RCL software substitutes the spare pair. However, none of the on-line channels can substitute for another.

In the transmit mode, there are two exciters—one for each radar face. Should one exciter fail, the RCL software commands the remaining one to drive both PAVE PAWS radar faces.

In the operational environment (Fig. 2), the on-line RCL performs tactical tasks (Table 1), verifies the correct operation of the on-line radar units (Table 2), and manages the radar equipment configuration (Table 3). The



***5. A subset of the WAAS REX diagnostic sequence** illustrates the control scheme. The A/D test (a) is accomplished with a signal injected after DC stabilization at point A. The receiver IF is tested (b) when the waveform generator is activated over path B to generate nonchirped pulses. For the final test (b) RF is injected as shown by the gray lines. (The circled "M's" indicate points monitored by the RP-16 microprocessor in the REX.)*

off-line RCL continuously assesses the off-line radar subsystem by diagnosing faults and subsequently isolating them. Software-controlled tests (Table 4) are performed with built-in test equipment to maintain calibration, verify performance and operating status, and diagnose faults. The on-line tests are performed automatically according to a schedule; the off-line tests are under operator control.

A system fault for the PAVE PAWS radar is specified as one that continues for eight seconds—the time required for a short range target to fly through the search fence. Consequently, fault status is scanned once every four seconds, leaving four seconds to reconfigure and verify that the fault has been cleared.

Schedule follows resource periods

Scheduling in the PAVE PAWS radar subsystem is based on a scheme which divides time into fixed resource periods. The scheduler in the data pro-

cessor controls resource usage by sending a schedule to the on-line RCL which specifies the operations to be performed in that resource period.

Based on this schedule, the RCL software formulates detailed radar-subsystem commands for the radar. It also processes the returns, applies the monopulse amplitude and phase corrections, computes the angle errors, and sends the post-processed data to the central data processor.

During resource periods for which tactical operations are not planned, the RCL schedules calibration, operability assessment, and diagnostic functions (Table 5).

Figure 3 shows a typical test configuration in which receiver, subarray, and element tests are conducted. Interference monitoring data is also processed and sent to the central processor. Failure reports and "out-of-tolerance" data are used to isolate hard faults which affect system performance and identify them with reconfigurable radar units.

To maintain system operability, the RCL software either reconfigures the radar equipment by replacing a faulty unit with a redundant unit (as in the case of the REX and SPR), or, if the RCL software cannot switch the failed unit (FTS, BSU, RCL), requests the data processor to switch RCLs. After reconfiguration, the appropriate diagnostic software is requested by the operator.

The off-line RCL radar diagnostics perform operability assessment and fault isolation functions for the off-line radar equipment (Table 3), while the on-line RCL continues to operate the on-line radar equipment.

Operator interfaces occur at the RCL and at the central data processor. The system maintenance monitor display shown in Fig. 2 provides complete status information. This information includes the status of all hardware elements (on-line active, on-line standby, or off-line) in the radar subsystem. The operator interface at the RCL display primarily supports off-line radar subsystem maintenance.

WAAS uses embedded processing

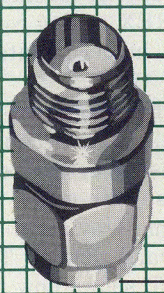
The Wide Area Active Surveillance system (WAAS) is a range instrumentation radar with missions that include range safety, control of fleet training exercises, and recording high quality track data for post-mission analysis. The radar, which is controlled by a standard DEC KL-10 computer (Fig. 5), can operate as a stand-alone sensor or as an integrated component of the range instrumentation.

Tactical considerations led to the integration of programmable microprocessing devices into the receiver exciter (REX) and the digital pulse compression unit (DPCU). The REX uses a Raytheon RP-16 bit-slice microprocessor, while the DPCU uses a sequence controller.

In the REX, the RP-16 handles the complex algorithms needed for calibration phase and gain corrections of the chirp waveform. In the DPCU, the sequence controller handles the signal processor operations. Each microprocessor controls the routing of signals through its radar unit. The diagnostic approach was aimed at coupling these built-in control functions with the computational and logic-decision capability inherent in the microprocessors.

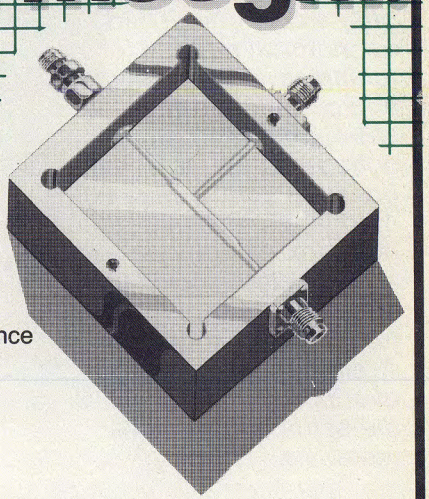
(concluded on next page)

Our thought.



Your afterthought.

EMC's 3mm SMA attenuator is a small solution to a big problem.



It's funny that one of our first thoughts is one of your last. We're speaking about attenuation for your MIC package. And since we do think of it first, you can be sure our attenuators are the very best.

Proof:

- EMC attenuators are the smallest available - just 3/4" long to accommodate your package without creating new design problems
- Our attenuators are low in cost - the lowest in the industry - with guaranteed performance to 18 GHz
- Stainless steel construction assures rugged service, gold plated beryllium-copper center conductors add reliability
- For highest flexibility, attenuators are available in 1 dB increments up to 20 dB - choose the precise model to match your needs
- All EMC attenuators are offered with full calibration (optional) and in flange mount configurations as well

Don't give a second thought to your next noise problem. Instead, quietly pick up the phone and call us or any EMC stocking distributor. We'll have an attenuator on its way to you the same day. After all, why should such a small solution stand in the way of such a large problem. Let us hear from you today.

EMC TECHNOLOGY, INC.
1971 OLD CUTHBERT ROAD
CHERRY HILL, NEW JERSEY 08034
Phone: (609) 429-7800 • TWX: 710-896-0193

Authorized distributors and technical sales representatives in all major metropolitan areas.

EMC TECHNOLOGY is a full line MIC product manufacturer. Our products include SMA connectors, terminations, attenuators, resistors and DC blocks for stripline, microstrip and SMA coax.

READER SERVICE NUMBER 54



MICROWAVE TO MILLIMETERS

Microwave tuning elements offer a convenient and economical method for tuning cavities, waveguides and other microwave structures. The unique Johanson self-locking constant torque drive mechanism eliminates the need for locking nuts and assures stable noise free adjustment in applications from L to W band. Available in a variety of applications in metallic, dielectric and resistive materials.

Electronic Accuracy Through Mechanical Precision

Johanson

Manufacturing Corporation

400 Rockaway Valley Road
Boonton, New Jersey 07005
201-334-2676
TWX 710-987-8367

READER SERVICE NUMBER 75

SOFTWARE AND RADAR SYSTEMS *(continued from p. 85)*

These microprocessors can compare programmable inputs with sampled digitized outputs and use the results to make system decisions.

Standard time-sharing used

In operation, the software-controlled tests for the REX and the DPCU use the standard KL-10 time-sharing system. From the viewpoint of this time-sharing system, each microprocessor is identified as a standard teletype output channel and, thus, does not need a special interface. The software for the DPCU microprocessor is down-loaded from the KL-10, but the REX software exists as firmware in its microprocessor's ROM. Although the REX software could have been similarly downloaded, operational considerations dictated that REX testing could not depend on the host computer's availability.

A subset of the REX diagnostic sequence (the A/D test, the sum-channel IF test, and the sum-channel RF test) can illustrate the ease with which the WAAS control scheme provides diagnostics under software control. The REX diagram (Fig. 5) shows how the RP-16 monitors the outputs of the selected units to insure that the signals are generated.

In the first test, the RP-16 establishes the signal paths shown in Fig. 5(a) to test the A/D converter. A signal is injected (under RP-16 control) after DC stabilization at point A. The digitized output from the A/D converter is sampled and compared with the injected signal.

To test the receiver IF, the RP-16 establishes the signal paths shown in Fig. 5(b). The RP-16 then activates the waveform generator over path B to generate nonchirp pulses. Again, the A/D output is sampled and evaluated by the RP-16.

For the final test (also shown in Fig. 5b), RF is injected under RP-16 control, and the A/D output is similarly evaluated.

Changing design considerations

The growth of hardware technology has resulted in an ever-increasing improvement in the speed, capacity and flexibility of the building blocks which are used in the architecture of a system. In addition, software control allows processors of dissimilar architectures to function in concert.

These new building blocks allow designers to partition attributes which apply to the entire system (availability, for example) and to assign these subfunctions to specific elements. But the designer must be careful not to limit the inherent flexibility of the system elements by arbitrarily assigning processes to the hardware or software domain. This pitfall must be avoided when the problem is defined in the initial design phase.

Therefore, system designers pay for the increased flexibility by facing increased complexity in design issues. Details like process design, timing, and synchronization no longer exist as a sequence of processes residing merely in a single computer, but as a set of processes spread across a configuration of distinct processing elements in a computer network.

The use of programmable microprocessors is motivated by their size, power consumption, cost, and the ease with which they can be embedded within the hardware they control. Standard hardware and components, which can be programmed through existing software support systems, can be used to tailor a data processing device for specific requirements and enhanced performance. And, when designers replace hardware with software control, the resulting efficiencies can be immediately noticed in predesign trade-offs, design, production, system reliability and availability, and manufacturing. Completed products can be more easily corrected and modified.

To realize the full potential of the off-the-shelf hardware created by technological advances, a designer must thoroughly consider the trade-offs posed by the computing elements and communications network, as well as software control and existing software development tools. This understanding must include the answers to questions inherent in the sharing of devices by a process, by bus protocols and mechanizations, and the data base design. Processor coupling and interaction are important parts of these considerations.

Above all, designers must learn to characterize the problem (or process) in terms of computing specifications, and to translate these specifications to computing resources. The computing resources, in turn, must be structured into a processing network which, in combination with the radar hardware, is consistent with the original characterization of the problem.••

CW Radars Find New Uses In The '80s

Doppler parameters and statistical data reduction methods yield a miss-distance indicator (MDI) using a CW-type radar that gives real-time value for intercept distance, range, and time.

ALTHOUGH the radars of the 1920s and 1930s provided range information by operating primarily in a CW mode, the trend has veered toward pulse-type equipment since then. Pulsed radars have so dominated the field that most authorities share the belief that CW radars do not give range information. However, CW systems can provide both range and relative velocity data in several applications involving the relative motion between a target and a radar set.

A basic CW radar configuration is shown in Fig. 1. The detected, reflected wave is shifted in frequency (Doppler effect) by an amount which is a function of the relative velocity between the target and the transmitter/receiver. Range data is extracted from the *change* in Doppler frequency (versus time).

A miss-distance indicator (MDI) is a typical application of a CW-type radar. It uses RF (or supersonic, subsonic, or audio frequencies) to determine the relative velocity between two objects, the time of "intercept" (i.e., the time at which the distance between the two will be at its minimum), and the actual value of that minimum distance. The main requirement for the simplest systems is that the two objects travel in straight lines (not necessarily parallel) at constant velocities during the time of intercept. More sophisticated data reduction is required to handle any curvature of the paths and the acceleration of either object.

A typical Doppler shift curve just before and after the time of intercept is shown in Fig. 2. Both "closing velocity" (relative velocity between the two objects) and "miss distance" (minimum approach distance) can be determined from the data.

Formulas for the slant range (R), the Doppler frequency (f_d), and the miss distance (d_m), can be derived from the relationships shown in Fig. 3:

$$R = \sqrt{d_m^2 + (vt)^2} \qquad (1)$$

$$f_d = \frac{2\, f_o\, v \cos\left[\tan^{-1}\dfrac{d_m}{vt}\right]}{c} \qquad (2)$$

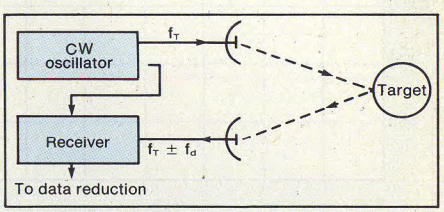
$$d_m = \frac{\left(\dfrac{df_d}{dt}\right)_{max} f_d^2 t^2 c}{2\, f_o \left[\left(\dfrac{df_d}{dt}\right)_{max} t^2 - f_d^2\right]} \qquad (3)$$

The miss distance, d_m, can be calculated with Eq. 3 if the Doppler curve's maximum slope and any point on the curve are known. The choice of the point closest to the maximum curvature yields the best accuracy. The velocity (v) can be found from Eq. 1 or 2, depending on the known quantities.

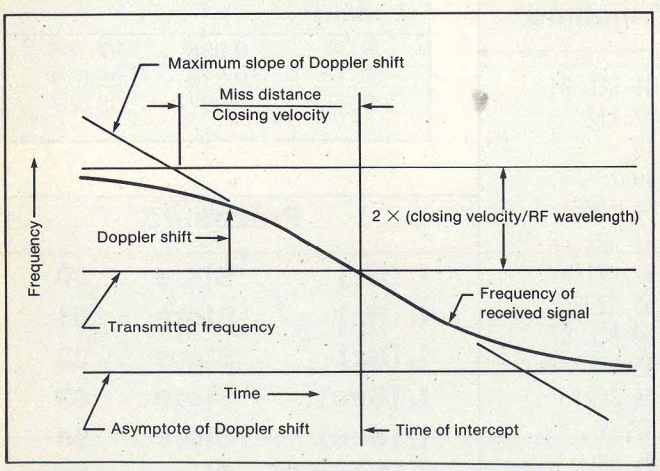
However, use of the maximum slope technique is not always desirable. Slope of the curve is difficult to ac-

(continued on next page)

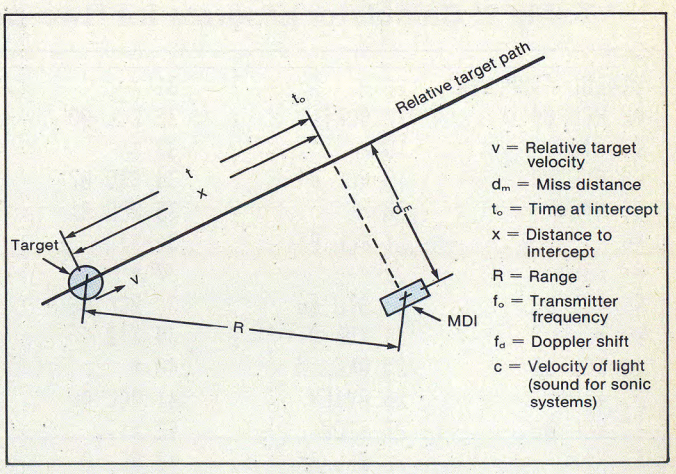
Andrzej B. Przedpelski, Vice-President, Development, A.R.F. Products, Inc., 2559 75th St., Boulder, CO 80301.



***1. This homodyne CW-type radar** displays a Doppler-shifted return.*



***2. The miss-distance indicator (MDI) Doppler curve** represents received signal frequency variations prior, during, and after "intercept."*



***3. Time, distance, and velocity relationships** are displayed for the miss-distance radar application. Equations 1, 2, and 3 are derived from this figure.*

curately measure, is further complicated by the presence of noise, and does not lend itself readily to automatic data reduction. Alternate means of finding d_m and v are available with the following formulas:

$$d_m = \frac{ct_1t_2f_1f_2(\sqrt{t_2^2-t_1^2}(\sqrt{f_2^2-f_1^2})}{2f_o[f_2^2(t_2^2-t_1^2)-t_2^2(f_2^2-f_1^2)]} \quad (4)$$

$$\left(\frac{df_d}{dt}\right)_{max} = \frac{f_1f_2\sqrt{t_2^2-t_2^1}}{t_1t_2\sqrt{f_2^2-f_1^2}} \quad (5)$$

$$v = \frac{cf_1f_2\sqrt{t_2^2-t_1^2}}{2f_o\sqrt{f_2^2(t_2^2-t_1^2)-t_2^2(f_2^2-f_1^2)}} \quad (6)$$

where t_1, f_1 and t_2, f_2 are the coordinates for any two points on the Doppler curve. For greatest accuracy, these two points should not be too close together on the curve.

This technique and its advantages are best illustrated by the following example. Three points, P_1 (4 ms, 248 Hz), P_2 (6 ms, 342 Hz), and P_3 (10 ms, 470 Hz), were arbitrarily chosen on the Doppler shift curve in Fig. 4. An f_o of 1.0 GHz was assumed. The calculated values of d_m and v for each pair of points closely correlate (as shown in Table 1).

Table 1 indicates the built-in redundancy of this two-point method. It is used to good advantage in high-noise environments in which several initial pairs provide preliminary data and, by statistical methods, other pairs improve the accuracy. Handheld calculators, such as the HP-41 (program delineated in Table 2), greatly simplify the calculation of d_m, v, and $(df_d/dt)_{max}$.

The CW mode enjoys several other advantages over pulse-type operation. With the availability of continuous real-time intercept information including Doppler shift, an *a priori* determination of "direct-hit" parameters can be predicted.

Alternate method required

A target (Fig. 3) traveling at 2 km/s toward the stationary CW radar misses it by 0.1 m. Most of the Doppler frequency shift occurs within 100 μs of the "intercept" as shown in Fig. 6. However, it is difficult to measure the actual Doppler frequencies within this period. Data reduction using the maximum slope *or* the two-point method is only suitable for relatively *slow* events, where the change in Doppler frequency is *smaller* than the Doppler frequency itself. Time has to be available to determine the instantaneous Doppler frequency at any given moment during the intercept. As velocities increase and miss distances decrease, it becomes impossible to obtain Doppler frequency values directly from the S-curve (Fig. 2). All the information is still available in the received signal, and, using a different data reduction method (one that uses the actual Doppler voltage), the velocity, range, and miss-distance values can still be obtained.

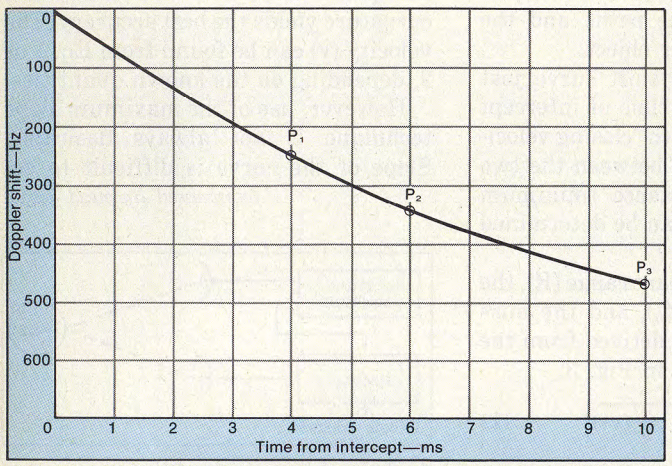
The actual Doppler voltage (i.e., the difference between the transmitted and received signals) can be described in the following expression:

$$V_d = K\left[\frac{d_m^4}{(v^2t^2+d_m^2)^2}\right] \times \left[\cos\left(\frac{4\pi f_o}{c}\sqrt{v^2t^2+d_m^2}\right)\right] \quad (7)$$

where K = product of transmitter power output, antenna gains, receiver gain, and so forth.

The first bracketed term in Eq. 7

(continued on p. 92)



***4. A segment of the Doppler shift curve** provides data for use in the two-point method of determining closing velocity and miss distance.*

Table 1: Calculated miss distance and velocity

Chosen points	d_m (m)	v (m/s)
P_1,P_2	0.938	97.188
P_1,P_3	0.978	99.074
P_2,P_3	0.997	99.687

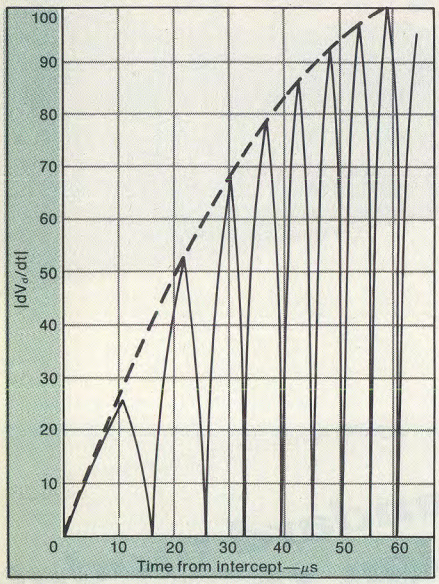
Table 2: Calculator program for "two-point" method

```
01♦LBL "DOPPLER"   16 -          31 /          46 RCL 01
02 RCL 04          17 SQRT       32 RCL 00     47 X↑2
03 X↑2             18 /          33 /          48 -
04 RCL 03          19 RCL 04     34 STO 07     49 /
05 X↑2             20 /          35 RCL 01     50 "DM= "
06 -               21 RCL 03     36 X↑2        51 ARCL X
07 SQRT            22 /          37 *          52 AVIEW
08 RCL 02          23 STO 06     38 RCL 03     53 STOP
09 *               24 "DF/DT= "  39 X↑2        54 RCL 07
10 RCL 01          25 ARCL X     40 *          55 *
11 *               26 AVIEW      41 RCL 06     56 SQRT
12 RCL 02          27 STOP       42 X↑2        57 "V= "
13 X↑2             28 RCL 05     43 RCL 03     58 ARCL X
14 RCL 01          29 *          44 X↑2        59 AVIEW
15 X↑2             30 2          45 *          60 .END.
```

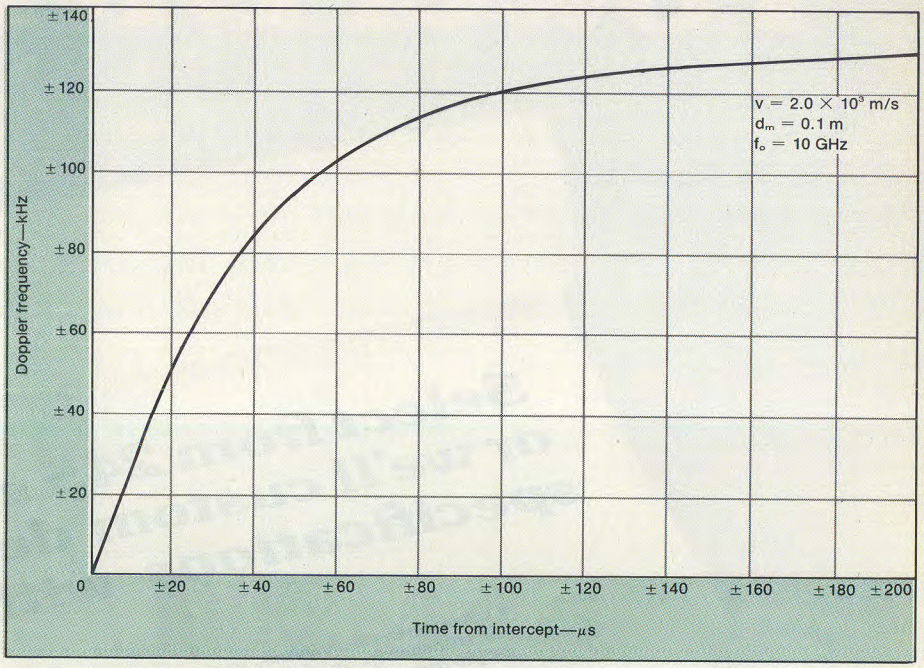
Procedure

f_o [Hz]	Store	00
f_1 [Hz]	Store	01
f_2 [Hz]	Store	02
t_1 [Sec]	Store	03
t_2 [Sec]	Store	04
c [3 × 10^8]	Store	05
	XEQ "Doppler"	

indicates a signal-strength range dependency while the second term is the actual Doppler voltage, from which, for low velocity/high miss-distance cases, the Doppler frequency is obtained. Both bracketed terms in Eq. 7 (the first, which concerns amplitude, and the second, which pertains to frequency) contain useful data. However, the constant K varies in an uncontrolled manner (since antenna gains may change due to pattern effects, receiver



5. The time rate-of-change of the leveled Doppler voltage *when smoothed provides an envelope that is a segment of the standard Doppler S-curve.*



6. The Doppler S-curve for the fast intercept case *(high velocity, narrow miss) shows that most of the Doppler shift occurs within the first 100 μs.*

Procedure

f_o [Hz]	Store	01
v [m/s]	Store	02
t_n [s]	Store	03
c [3 × 10^8]	Store	04
t_{n+1} [s]	Store	05

XEQ "DM"

Table 3: Calculator program for "fast intercept" method (Eq. 10)

```
01♦LBL "DM"     15 X↑2          29 RCL 03
02 RCL 05       16 /            30 X↑2
03 X↑2          17 -            31 *
04 RCL 03       18 X↑2          32 -
05 X↑2          19 RCL 04       33 SQRT
06 -            20 X↑2          34 2
07 RCL 02       21 4            35 *
08 X↑2          22 /            36 RCL 01
09 *            23 RCL 01       37 *
10 RCL 04       24 X↑2          38 RCL 04
11 X↑2          25 /            39 /
12 16           26 RCL 02       40 .END.
13 /            27 X↑2
14 RCL 01       28 *
```

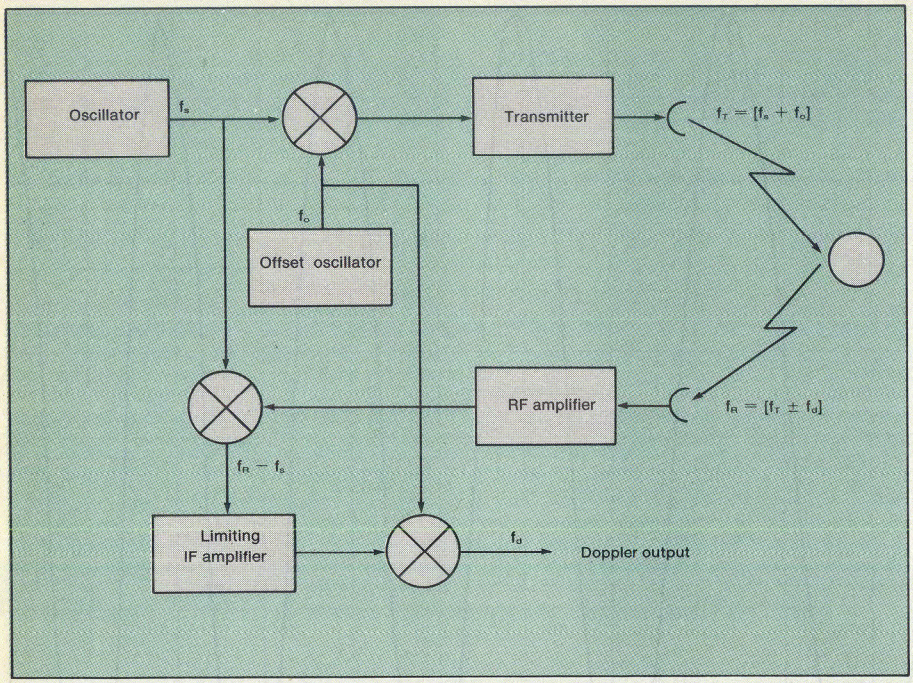
Table 4: Calculator program for "fast intercept" method (Eq. 13)

```
01♦LBL "V"      13 2            25 -
02 RCL 03       14 /            26 X↑2
03 X↑2          15 RCL 05       27 -
04 RCL 05       16 X↑2          28 /
05 X↑2          17 RCL 03       29 SQRT
06 +            18 X↑2          30 RCL 04
07 RCL 06       19 -            31 *
08 X↑2          20 X↑2          32 2
09 -            21 RCL 07       33 /
10 RCL 07       22 X↑2          34 RCL 01
11 X↑2          23 RCL 06       35 /
12 -            24 X↑2          36 .END.
```

Procedure

f_o [Hz]	Store	01
t_n [s]	Store	03
c [3 × 10^8]	Store	04
t_n + 1 [s]	Store	05
t_n + 2 [s]	Store	06
t_n + 3 [s]	Store	07

XEQ "V"



***7. The block diagram of a CW-type radar** is configured to provide a leveled-voltage Doppler output, needed for fast intercept target resolution.*

gains may vary with signal strength, etc.) and may thus make the first (amplitude) term unusable in practice. Furthermore, a very large receiver dynamic range would be required to accommodate the widely varying signal levels. In any case, the second term (frequency) still contains adequate information for data reduction, even if a limiting (FM) type receiver is used. The limiting is usually accomplished in the IF amplifier, as shown in a typical circuit in Fig. 7. The amplitude-leveled Doppler voltage ($\overline{V}_d$) is:

$$\overline{V}_d = \cos\left(\frac{4\pi f_o}{c}\sqrt{v^2t^2+d_m^2}\right) \quad (8)$$

A plot of the leveled Doppler voltage is given in Fig. 8.

One possible way to obtain the desired data is to differentiate Eq. 8:

$$\left|\frac{d\overline{V}_d}{dt}\right| =$$

$$\left|-2\pi f_d \sin\left(\frac{2\pi f_o}{c}\sqrt{v^2t^2+d_m^2}\right)\right| \quad (9)$$

The envelope of Eq. 9, as shown in Fig. 5, is the *standard* Doppler S-curve. Equations 4 and 6 can then be used to obtain d_m and v.

(concluded on next page)

Table 5: Fast intercept example results

Data	v (m/s)	Error	Program
$t_1\ t_2\ t_4\ t_5$	1.905×10^3	−5%	Table 4
$t_1\ t_2\ t_3\ t_4$	2.057×10^3	+3%	Table 4

Microwave Specialists

Communications Satellite Payload Equipment

Marconi Space and Defence Systems, Europe's acknowledged No 1 in the development of advanced satellite systems, are seeking the following specialists to play key roles in new communications satellite projects at their Stanmore location which is pleasantly located in rural surroundings some 12 miles north of London. We would like to hear from suitably qualified and experienced men or women who want the chance to work in a high technology environment that offers total involvement and lots of excitement.

MICROWAVE EQUIPMENT MANAGERS

Will be responsible for an Equipment forming part of the Communication Payload programme. This will involve original design, manufacture and test of breadboards; engineering; qualification and flight model hardware; and will entail liaison with European prime contractors on all aspects of the programme. The programmes are usually of an international nature, requiring high technology designs, coupled with demanding timescales.

MICROWAVE DEVELOPMENT ENGINEERS

Will report to the Equipment Manager and will be responsible for development work on the payload equipments. Tasks will include the design of microwave circuits with the emphasis being on lightweight, high reliability designs including extensive use of MIC technology.

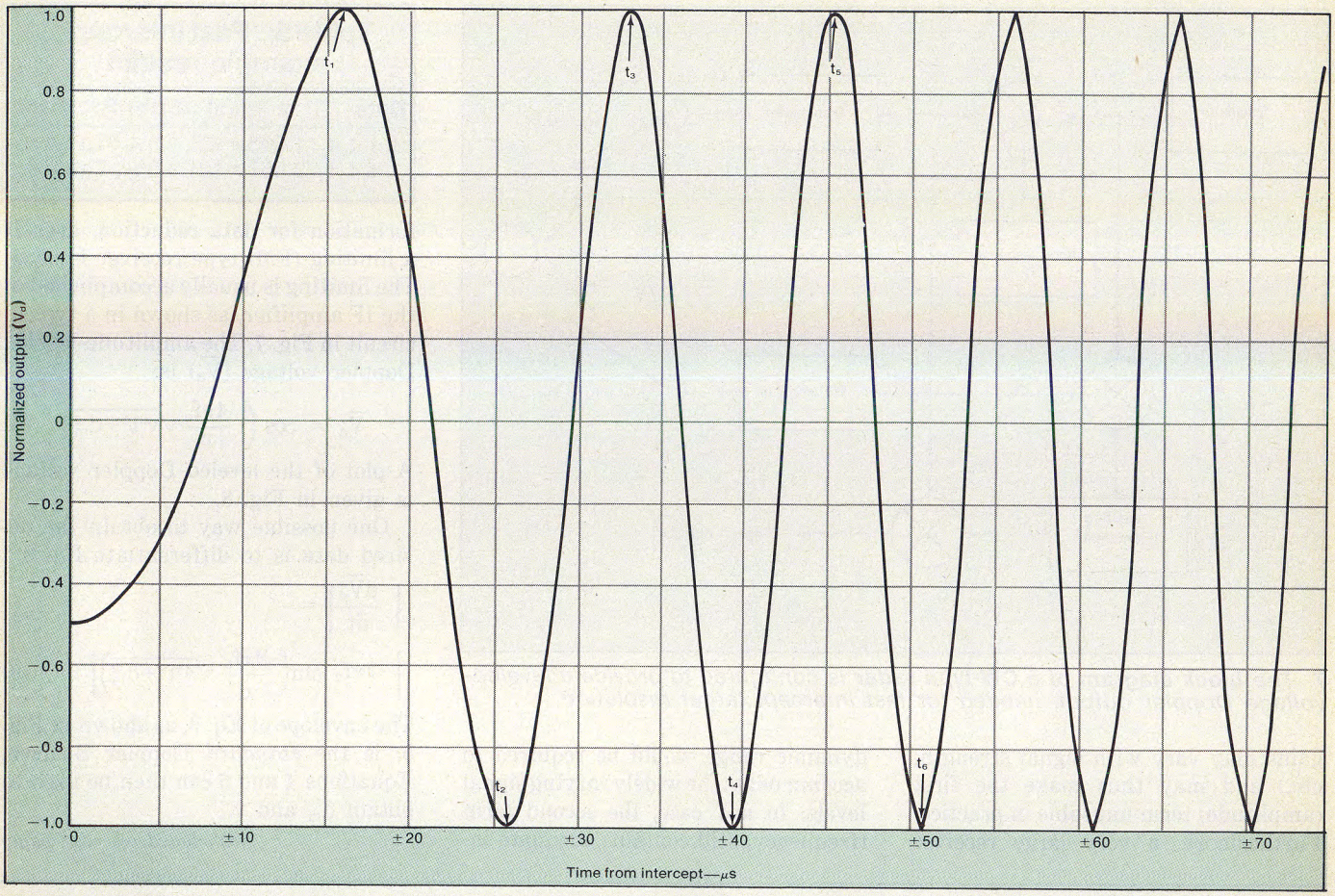
Applicants for both positions should hold a degree or equivalent qualification and have had at least 2 years' relevant experience.

Salaries will be negotiable and accompanied by an excellent range of benefits.

To find out more details, write or telephone Bill Seton, Personnel Manager with brief details of your career to date.

Marconi Space and Defence Systems, The Grove, Warren Lane, Stanmore, Middx. HA7 4LY, England. Tel: 011441-954 2311 ext. 18.

Marconi
Space & Defence Systems



***8. The leveled Doppler voltage curve provides the data points** required for miss distance calculations. The points appear at successive peaks of the curve.*

If the relative velocity, v, is known, the miss distance can be calculated using:

$$d_m = \frac{2f_o}{c}\left(\left[v^2(t_{n+1}^2-t_n^2)-\frac{c^2}{16f_o}\right]^2-\frac{c^2}{4f_o^2}\,v^2t_n^2\right)^{-2} \quad (10)$$

where t_n and t_{n+1} are times of successive peaks (for example, t_3 and t_4 in Fig. 8). A similar equation can be derived for t_n and t_{n-2}.

$$d_m = \frac{f_o}{c}\left(\left[v^2(t_{n+2}^2-t_n^2)-\frac{c^2}{4f_o}\right]^2-\frac{c^2}{f_o^2}\,v^2t_n^3\right)^{-2} \quad (11)$$

Velocity, v, needed in Eqs. 10 and 11, is obtained from:

$$v = \frac{cf_d}{2f_o}$$

where f_d is the asymptotic value of $\overline{V}_d$(frequency) for large values of t. This value can easily be obtained if adequate signal strength and time are available.

If only a small portion of the $\overline{V}_d$ curve is available and velocity is not directly obtainable from Eq. 12, it can still be calculated using:

$$v = \frac{c}{2f_o}\times\left(\frac{t_n^3+t_{n+1}^2-t_{n+2}^2-t_{n+3}^2}{2[(t_{n+1}^2-t_n^2)-(t_{n+3}^2-t_{n+2}^2)]}\right)^{-2} \quad (13)$$

$$v = \frac{c}{\sqrt{2f_o}}\times\left(\frac{1}{(t_5^3-t_1^2)-2(t_3^2-t_1^3)}\right)^{-2} \quad (14)$$

or other combinations derived from Eq. 11 and 12. Once v is known, Eq. 11 or 12 can be used to calculate d_m.

Fast intercept results

HP-41C programs solving Eq. 10 and 13 are given in Tables 3 and 4. Using these programs and the curve of Fig. 8, v and d_m can be calculated for the fast intercept example with the following data points: t_1 = 16 μs, t_2 = 26 μs, t_3 = 33 μs, t_4 = 39.5 μs, and t_5 = 45.5 μs. The results of these calculations are shown in Table 5.

Using the average (calculated) velocity of 1.981 x 103 m/s and estimated values for t_2 and t_3 in the Table 3 program, a miss distance of 0.091m (with 9 percent) is obtained.

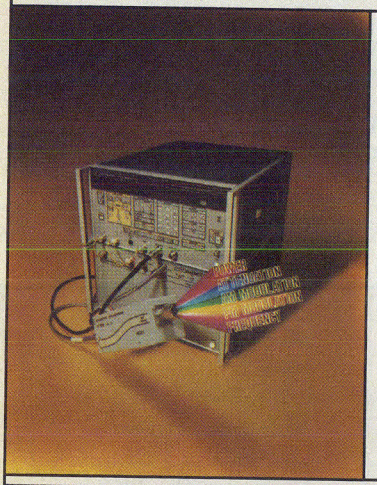
Further statistical reduction of other data-point sets will improve the accuracy of closing velocity and miss distance, especially in the presence of noise.••

May 1982

Vol. 21, No. 5

MICROWAVES laser technology

A Hayden Publication



about the cover

The VM-24 signal generator calibrator is a two-cabinet test system capable of making six different measurements. The successful integration of the instrument's many functions allows a moderately skilled operator to calibrate a signal generator with microprocessor controlled precision. (Cover artwork courtesy of Weinschel Engineering, Gaithersburg, MD. Design by Keith Dean, ANR Advertising, West Caldwell, NJ.)

p. 149

departments

8 Feedback
44 For Your Personal Interest
47 R&D Roundup
55 Editorial
110 Catalog Update
131 Bookshelf*
168 InfoCenter
170 Looking Back
170 Looking Ahead

news

57 **Special Feature: The 1982 International Microwave Symposium**
Thirty-four pages of abstracts, products, and expert commentary.

17 Millimeter-wave seeker guides a smart, sleek missile . . . **18** The MTT national lecturer: "The Year of the GaAs FET" may mark solid-state's turning point . . . **24** Papers shed light on optics progress . . . **25** NASA, Columbia contractors track transponder failure . . . **25** New firm joins DBS race . . . **28** Engineer pay hikes up 9 percent in '81 . . . **28** Productivity conference stresses proven techniques . . . **31** Hughes satcom facilities hum after $1-billion Intelsat award . . . **32** Radiation guidelines imminent from ANSI
34 International • **39** Washington • **48** Industry • **50** Meetings

design features

119 **MM-Wave Synthesizer Has 8-to-15-GHz Bandwidth.** M. P. Fortunato and K.Y. Ishikawa, of Hughes Aircraft Co., describe the use of sweeper Impatts with a microprocessor in a W-band synthesizer.

126 **The Orotron Emerges As A Millimeter-Wave Source.** Donald E. Wortman and colleagues from the Army's Harry Diamond Laboratories report on recent results with this possible alternative to existing devices.

*__135__ **Calculate GaAs MESFET Equivalent Circuits.** Allan A. Sweet, a private consultant, shows how a calculator program can simplify GaAs MESFET design.

139 **U-Band Gunn Oscillator Rivals Impatt Performance.** J. Siegenthaler, from the Swiss Post Office Research Laboratory, details the design of a post-coupled waveguide oscillator with a 10-GHz tuning range.

143 **Computer Design Package Aids SAW Development.** John W. Arthur, of Scotland's Racal MESL Microwave Ltd., explains how simulation software is making SAW fabrication more cost effective.

product technology

152 **Control high-speed circuits with PIN diode switches.** Brian Bedard, of Adams Russell's Anzac Div., writes that the use of PIN diodes as high-speed controllers is a matter of a few important trade-offs.

149 **Cover Feature**—Calibration system is six instruments in one . . . **155** **Product Features**—PIN diode switches . . . **156** Synthesized signal generator has pulse modulation to 26 GHz

157 Application Notes • **158** New Products • **167** New Literature

**Foreign Editions Only.*

MM-Wave Synthesizer Has 8-to-15-GHz Bandwidth

Millimeter-wave sweeper Impatt diodes are combined with microprocessor control and opamp circuitry in a fast and accurate W-band synthesizer.

QUALITY millimeter-wave instrumentation is often the key to developing millimeter-wave components and systems. Unfortunately, available techniques and equipment often present technical compromises.

Fixed frequency oscillators, for example, have limited use as generators. Mechanically-tunable oscillators (klystrons and Gunns) and sweepers (backward-wave oscillators and Impatts) are needed for broadband measurements. Sweepers are convenient because their tuning is automatic. However, the phase noise and frequency stability of these oscillators are not adequate for measurements where crystal oscillator quality is required. Phase-locked oscillators offer the best stability, phase noise, and accuracy of all the sources but are usually fixed in frequency.

Millimeter-wave engineers use several phase-locked sources or a phase-locking system with tunable source for stable, low-noise, broadband sources. However, these systems are limited in tuning range (typically 500 MHz or less[1]) and are difficult to use.

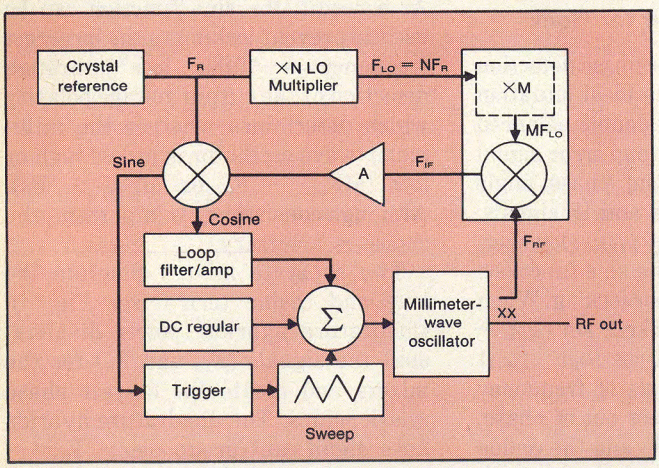
A third alternative utilizes a microwave/millimeter-wave frequency counter to lock an oscillator to the counter's crystal reference. This stabilizes the source frequency but does *not* improve the phase noise because of a limited loop bandwidth of approximately 100 Hz. One solution entails using sweeper Impatts (Impatts which can be bias-tuned over 8 to 15 GHz) and a programmable LO source under microprocessor control. This fully automatic, low phase-noise, solid-state synthesizer, detailed in Fig. 1, provides the desired capability.[2,3]

Bias-tuned Impatts are the only solid-state devices presently capable of oscillation over a wide tuning range. However, sweeper Impatts exhibit greater phase noise than other millimeter-wave oscillators. Figure 2 plots the SSB phase noise of a free-running sweeper Impatt, fixed-tuned Impatt and Gunn oscillators, and the noise floor of the phase-locked loop (PLL) circuit. Locked oscillator phase noise outside of loop bandwidth is determined by the free-running phase noise. Within the loop bandwidth, the phase noise approaches the circuit's noise floor. For optimal phase noise the loop should be closed at the frequency at which the noise floor and free-running phase noise spectra intersect. Figure 2 illustrates how a loop bandwidth of 2 to 7 MHz is sufficient for locking a fixed-tuned Impatt or Gunn oscillator, while a sweeper Impatt requires a bandwidth of about 30 MHz for equivalent performance.

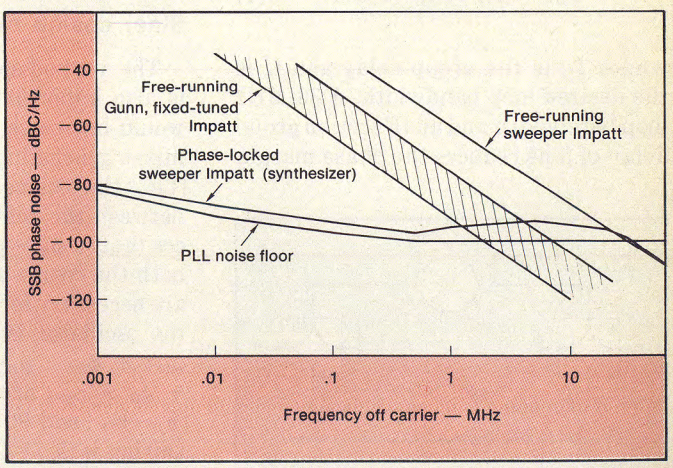
The breakthrough in millimeter-wave frequency synthesizer development is related to the ability to lock virtually any millimeter-wave Impatt. The considerable improvement in SSB phase noise of a phase-locked sweeper Impatt versus a free-running Gunn, fixed-tuned Impatt, and free-running sweeper Impatt is also illustrated in Fig. 2. Notice how close the phase-locked Impatt response is to the

(continued on next page)

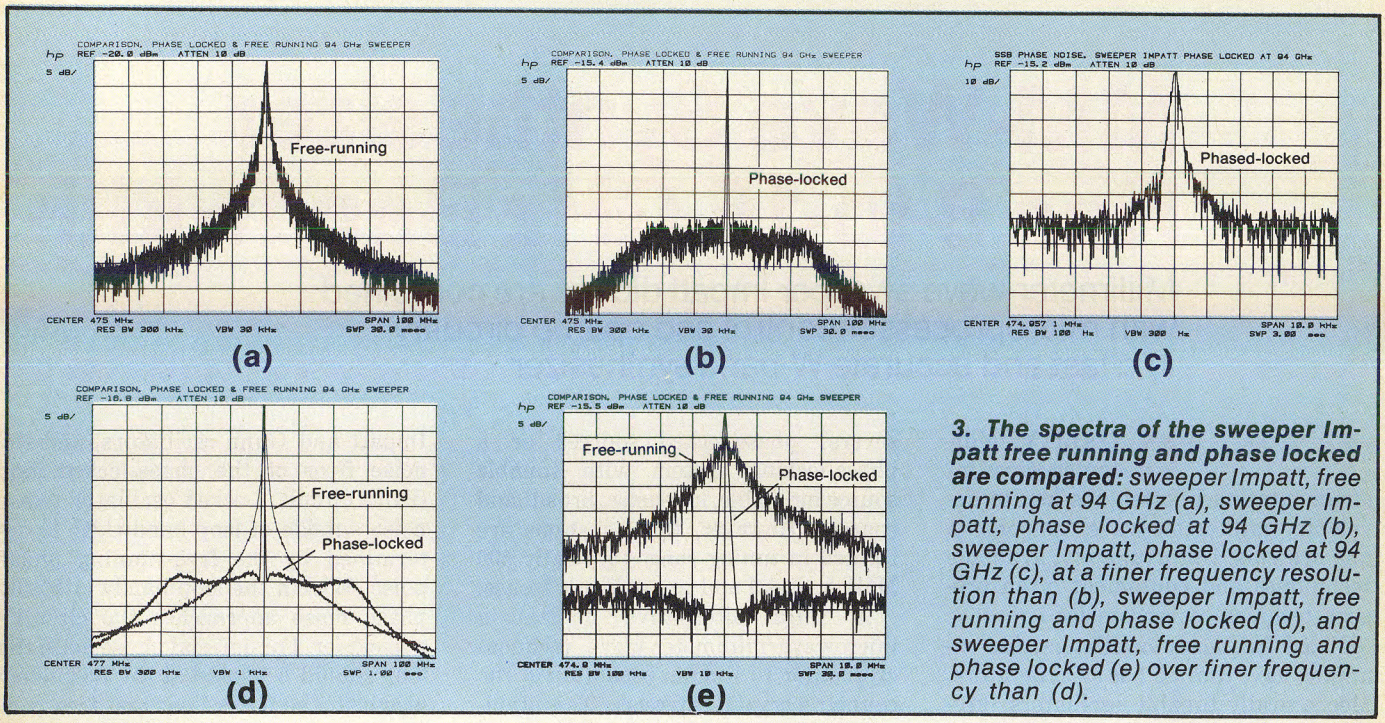
M.P. Fortunato, Staff Engineer, and **K.Y. Ishikawa,** Section Head, Hughes Aircraft Co., Torrance, CA 90509.



1. The preferred method of generating stable low-phase noise millimeter-wave signals *is shown in the blocked diagram. It incorporates sweeper Impatts and a programmable LO under microprocessor control.*



2. SSB phase-noise comparison *between free-running Gunn, fixed-tuned Impatt, sweeper Impatt and phase-lock sweeper Impatt oscillators is illustrated. The advantages of the latter are clearly indicated.*



3. The spectra of the sweeper Impatt free running and phase locked are compared: *sweeper Impatt, free running at 94 GHz (a), sweeper Impatt, phase locked at 94 GHz (b), sweeper Impatt, phase locked at 94 GHz (c), at a finer frequency resolution than (b), sweeper Impatt, free running and phase locked (d), and sweeper Impatt, free running and phase locked (e) over finer frequency than (d).*

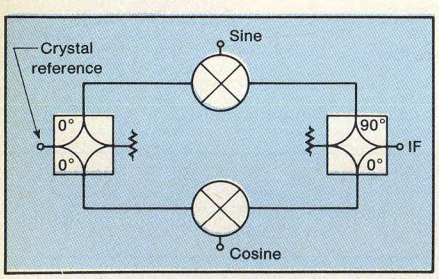
theoretical optimum (PLL noise floor). Figure 3 compares the spectra of a free-running and a phase-locked sweeper Impatt. Examining frequency terms close to the carrier reveals the advantages inherent in phase-locking.

Low group delay shown

Phase-locked bandwidths of up to 20 MHz are achieved by using wide-bandwidth hybrid operational amplifiers. Further increases in bandwidth require minimizing the group delay of the IF section. Group delay directly decreases the phase margin of the loop by an amount ϕ_D:

$$\phi_D = T_G \times f_L \times 360° \qquad (1)$$

where T_G is the group delay and f_L is the desired loop bandwidth. A 30-MHz loop bandwidth and an IF section group delay of 5 ns reduces the phase margin by 54 degrees, whereas a 2 MHz bandwidth reduces the phase margin by less than 4 degrees for the same delay.



4. Method of generating both sign and cosine "error" terms *is accomplished using two separate mixers and quadrature hybrid.*

A VCO with its K_0/s frequency domain representation (where K_0 is the VCO tuning sensitivity in rad/sec/amp or rad/sec/volt) introduces a single pole which diminishes the loop's phase margin by 90 degrees. Therefore the largest allowable phase shift through the IF, phase detector, and loop electronics, for stable operation, is 90 degrees. Consequently, a loss of 54 degrees due to the hybrids leaves only 36 degrees allowable phase shift for the phase detector and loop electronics at 30 MHz for a loop with *no* phase margin.

Sine, cosine needed for "lock"

The method used for phase detection is also important. The ideal situation would have a solitary double balanced mixer generating the loop error signal [i.e., the cosine of the phase angle between the reference and IF signals: $\cos(\omega_R t + \phi_R - \omega_{IF} t - \phi_{IF})$]. However, both the cosine and the sine functions are necessary for proper locking. When the oscillator is unlocked, $\sin(\omega_R t - \omega_{IF} t + \phi_R - \phi_{IF})$ and $\cos(\omega_R t - \omega_{IF} t + \phi_R - \phi_{IF})$ are signals of frequency $|F_R - F_{IF}|$ and 90 degrees out of phase. During lock, $|F_{IF}| = F_R$ and the cosine and sine terms equal constants. Lock is achieved by using one of these signals (cosine in this case) as the error signal. The signal is forced to zero by the loop when lock is achieved. Of course, when the $\cos(\omega_R t - \omega_{IF} t + \phi_R - \phi_{IF}) = 0$, $\sin(\omega_R t - \omega_{IF} t + \phi_R - \phi_{IF}) = \pm 1$. Since $F_{IF} = F_{RF} - MF_{LO}$ (M is the harmonic number used in the harmonic mixer), the cosine term equals zero when $F_{RF} = MF_{LO} \pm F_R$. It's possible, therefore, to lock on two different RF frequencies. In both cases $|F_{IF}| = F_R$. In one case F_R leads F_{IF} by 90 degrees and:

$$\sin(\omega_R t - \omega_{IF} t + \phi_R - \phi_{IF}) = \sin(90°) = 1$$

In the other case, F_R lags F_{IF} by 90 degrees and:

$$\sin(\omega_R t - \omega_{IF} t + \phi_R - \phi_{IF}) = \sin(270°) = -1$$

As a result, the sine function can be used to prevent locking to the incorrect frequency—a "false lock"—through detection of the output voltage polarity which determines whether the millimeter-wave oscillator is locked high or low ($MF_{LO} + F_R$ or $MF_{LO} - F_R$). Although consistency is important, the choice is arbitrary.

Two separate mixers generate the sine and cosine terms (see Fig. 4). Quadrature hybrids (power dividers) split the signals (F_{IF} and F_R) for the mixers and create the correct phase relationships. The quadrature hybrids have significant group delay, T_G: [4]

$$T_G = \frac{T_0}{4}\left(\frac{S}{S^2\cos^2\theta + \sin^2\theta}\right) \qquad (2)$$

(continued on p. 123)

In Eq. 2, $T_0 = 1/f_0$, S = the voltage coupling coefficient for the main line, $\theta = .5\pi(f/f_0)$, and f_0 = the center frequency of the hybrid.

In our case:

$$S = \frac{1}{\sqrt{2}} \qquad \theta = \frac{\pi}{2}$$

$$f \cong f_0$$

Therefore:

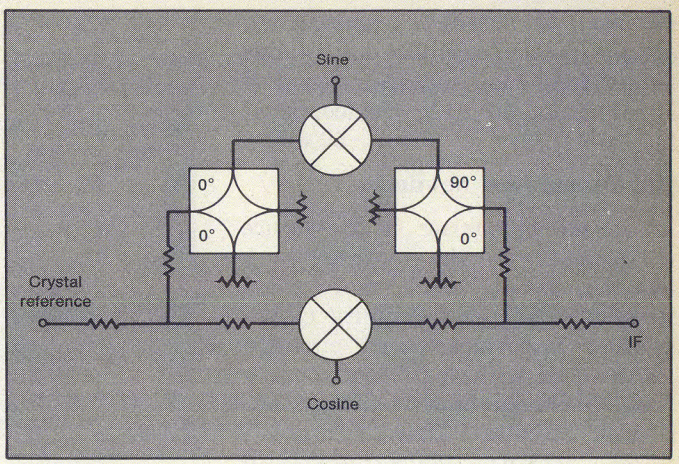
$$T_G = \frac{T_0}{4} \quad S = \frac{T_0}{4\sqrt{2}}$$

with:

$f_0 = F_R = 100$ MHz
$T_0 = 10$ ns
$T_G = 1.77$ ns

Using Eq. 1, this gives a decrease in phase margin of 19 degrees for a loop bandwidth of 30 MHz. To minimize the group delay and still allow power splitting for the sine processing, resistive dividers are used for the power splitting, and the hybrid power divider and mixer assembly are used strictly to generate the quadrature signal needed for lock alarm[3] (see Fig. 5). The loss introduced by dividers requires increasing the IF gain by several dB.

5. Addition of resistive power splitters *reduces group delay in a standard phase detector.*



Varying loop gain

Even with sufficient loop bandwidth for proper noise reduction of the sweeper Impatt, wide loop frequency range stabilization is difficult. The loop gain needs to be changed in order to phase-lock the Impatt at significantly different RF frequencies. The loop gain of a second order PLL is given by:[5]

$$\frac{\phi_o}{\phi_i} = \frac{K_0 K_d K_f (s+a)}{s^2 + 2\delta\omega_n s + \omega_n^2} \qquad (3a)$$

where:

$$\delta = \frac{1}{2}\sqrt{\frac{K_0 K_d K_f}{a}} \qquad (3b)$$

and:

$$\omega_n = \sqrt{K_0 K_d K_f a} \qquad (3c)$$

where the transfer function of the loop amplifier and filter is:

$$F(s) = K_f (s+a)/s$$

In Eq. 4, K_0 is the tuning sensitivity of the Impatt (rad/sec/amp) and K_d is the transfer function of the phase detector (volt/rad).

Any change in the Impatt's tuning sensitivity causes equivalent variations in the loop gain. If K_f or K_d is varied inversely with K_0, the loop gain will remain constant and stable at any RF frequency.

Two methods have been applied at lower frequencies. The first uses multiplying DACs in the loop filter and varies K_f inversely with K_0.[6] This method is impractical because of the limited bandwidth of MDACs. The second method uses a divide-by-N stage in the IF which effectively changes the gain of the phase detector to K_d/N. The loop gain remains fairly constant when N is adjusted in proportion to K_0. This method is useful for reference frequencies up to 5 MHz. However, due to the required loop bandwidth, this method is impractical since the reference frequency must be at least 50 MHz.

Impatt linearizing techniques

A programmable attenuator, placed between the phase-detector and the error amplifier (loop electronics) is used to vary K_f inversely with K_0 under microprocessor control. An alternative method that lowers the loop noise floor places a linearizing circuit, comprising resistors and switching elements, after the error amplifier. The linearizer, with its Impatt shunting resistors, decreases the effective "gain" of the Impatt, K_0, to the minimum value in its tuning range. An opamp detects Impatt current levels and switches the appropriate shunt resistors in or out. The current levels at which each resistor is switched are preset and don't require microprocessor control.

Noise presents problem

Even with a wide bandwidth and fully stable loop "noise," harmonically-related spurious signals must be dealt with. In the mixing process, both at the harmonic mixer and the phase detector, harmonics of the 100 MHz IF frequency are generated. These spurious signals are partially filtered out by the loop filter/amplifier but still show up at the output of the loop amplifier *and* RF spectrum. The 200-MHz second harmonic of the IF appears as a 100 MHz signal after the phase detector. Since the loop filter/amplifier has a single pole, "roll-off" crossover frequency of 30 MHz, the spurious signal is attenuated by 20 log 100/30 or 10.46 dB. With this harmonic typically 30 to 40 dB down (i.e., below the level of the fundamental) after the phase detector, its total spectrum contribution is consequently −40 to −50 dBc. The third harmonic, however, is only about 10 to 15 dB down. It is attenuated by 20 log 150/30 + 40 log 200/150 or 18.48 dB (a second pole is added at 150 MHz due to the frequency limitations of the opamp) for a final level of −28.5 to −32.5 dBc. A third spurious signal comes in at 50 MHz from the carrier. This, due to the harmonic mixer's tendency to generate subharmonics at some RF and IF frequencies, provides spectrum contributions as high as −30 dBc.

These spurious signals can be significantly reduced by doubling the reference signal, F_R, to 200 MHz before applying it to the phase detector, raising the IF frequency to 200 MHz. In this case the second harmonic (400 MHz) is at 200 MHz after phase detection and is attenuated about 20 dB which gives a −50 to −60 dBc level in the reference spectrum. The third harmonic is at 600 MHz and is slightly attenuated by the IF amplifiers (500 MHz nominal bandwidth). It is mixed down to 400 MHz after the phase detector and is essentially eliminated by the loop filter by the added poles around 300 MHz. The subharmonics are moved out to 100 MHz by this doubling. They

(concluded on next page)

 (continued from p. 123)

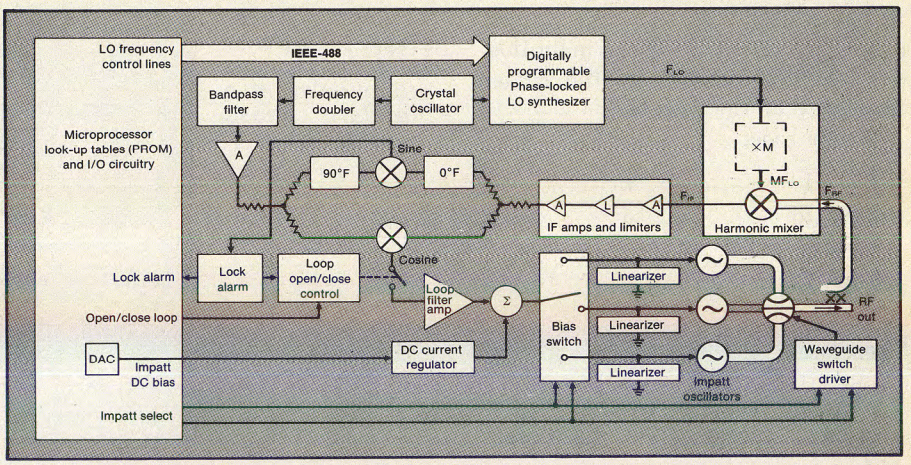
are about 10 dB less in magnitude out of the harmonic mixer due to this higher frequency and are attenuated an additional 10 dB by the loop filter for a final level of about −50 dBc.

Microprocessor needed

The microprocessor is the device which makes all the hardware work together as a flexible unit of instrumentation. The majority of the microprocessor-associated circuitry can be used with any Impatt on any band. To change Impatts all that need be replaced is the PROM memory (i.e., stored "look-up" tables) associated with the Impatts in use. One of these look-up tables is "RF vs. LO frequency." This data is used to select and program the correct LO frequency for the requested RF frequency. The second table is "Impatt bias current vs. RF frequency" which is used to set the DC bias of the Impatt closest to the desired frequency. This data is unique to each Impatt and must be directly measured before it can be burned into the PROM. If a programmable attenuator is used, a third set of data, the Impatt's tuning sensitivity, is needed. It must also be measured for each individual Impatt.

Upon receiving a command, either from the keyboard or the IEEE-488 bus, the microprocessor opens the loop (see the synthesizer block diagram of Fig. 6). It then goes to its look-up tables and finds the appropriate LO frequency and Impatt bias current. It sends the appropriate data to the LO source and, through a DAC, sets the DC current regulator to the correct level. It also sets the loop gain with the programmable attenuator. If the RF signal is within 5 MHz of the requested frequency, the lock alarm closes the loop and lock is achieved. If the RF frequency is not correct (due to factors such as thermal drift) the microprocessor goes into its acquisition mode. It steps the input data to the DAC and sweeps the bias current. When the Impatt frequency is within 5 MHz of the desired frequency, the lock alarm signals the microprocessor to hold the DAC level and closes the loop. Switching from one frequency to another takes 10 ms.

Three Impatts must be used for full waveguide band coverage. This necessitates the use of a waveguide switch and a DC bias line switch (see Fig. 6). The microprocessor switches on the correct Impatt before setting the bias current and either closing the loop or going into the acquisition mode.



***6. Block diagram of the complete millimeter-wave synthesizer** combines the modified phase-detection scheme, LO linearizer, multiple Impatt oscillators and control circuitry to provide stable low-phase noise automatic millimeter-wave synthesizer.*

Typical W-band synthesizer specifications

Frequency Range	75-110 GHz
Step Size	550 to 750 kHz
Switching Speed	10 ms max
SSB Phase Noise	−80 dBc 1 kHz from carrier
per Hz Bandwidth	−87 dBc 10 kHz from carrier
	−96 dBc 100 kHz from carrier to 10 MHz from carrier
	−120 dBc 100 MHz from carrier
Spurious Signals	−50 dBc
Power Output	1 mW min
Accuracy	5 ppm

The fully automatic synthesizer finds many uses in the lab. Its low phase noise, crystal-oscillator stability, and full waveguide bandwidth facilitate the use of highly accurate network analyzers and automated test instrumentation (the W-band synthesizer specifications are listed in the table above). A synthesizer with these capabilities makes testing easier, faster, and more accurate.••

Acknowledgments

The authors wish to acknowledge the contributions of W.F. McFaddin and R. Wetzel in the laboratory, S. Canell for his work on the microprocessor, and M. Crandell, P.A. Gianfortune, H.J. Kuno, J. A. Paul, F.J. Bernues, and J. Cadwallader for their helpful discussions and criticisms.

References

1. P.S. Henry, "Frequency Agile Millimeter-Wave Phase Lock System," *Review of Scientific Instruments*, pp. 1020-1025 (September 1976).
2. J. Baprowski, C. Smith, and F.J. Bernues, "Phase-Locked, Solid State Millimeter-Wave Sources," *Microwave Journal* (October 1976).
3. M.P. Fortunato and K.Y. Ishikawa, "A Broadband Solid State Millimeter-Wave Synthesizer," *IEEE MTT-S International Microwave Symposium Digest* (June 1982).
4. J. Curtis, "Octave and Decade Band Quadrature Networks and Their Application to Various Signal Processing Components," *Olektron Corp. Technical Note C-3* (May 1981).
5. S. Wetenkamp, "Combining Phase-Lock Loop 'Transportation Lag'," *MSN*, pp. 101-106 (March 1978).
6. A. Boulouard, "Improved Phase Locking Stabilizes EHF Sources," *MicroWaves*, pp. 77-78 (November 1981).

Advertisers...
Products...
Literature.

Find them fast in our **InfoCenter** (see p. 168)

The Orotron Emerges As A Millimeter-Wave Source

The orotron represents a possible alternative to existing devices as an intermediate-power source of CW or pulsed millimeter-wave energy. It's lightweight and can be tuned electrically or mechanically.

A new challenger has emerged in the race for frequency generation at millimeter and submillimeter wavelengths: the orotron. It can be tuned mechanically and electronically, will operate at intermediate power levels as a pulsed or CW source, and can be made lightweight and portable.

The orotron,[1–3] which is based on the Smith-Purcell effect,[4] is also known as a ledatron[5] or diffraction radiation generator.[6] Figure 1 shows how the device works. A sheet-like electron beam passes over the surface of a metallic diffraction grating and radiates into a mode of an open resonator formed by two metallic mirrors; the grating partially covers the lower mirror. The radiation from the resonator is then fed back into the beam, causing the electronics to bunch together. If the proper conditions of synchronism between the electron beam velocity and the phase velocity of an evanescent wave traveling along the grating are met, coherent radiation will result.[7–9]

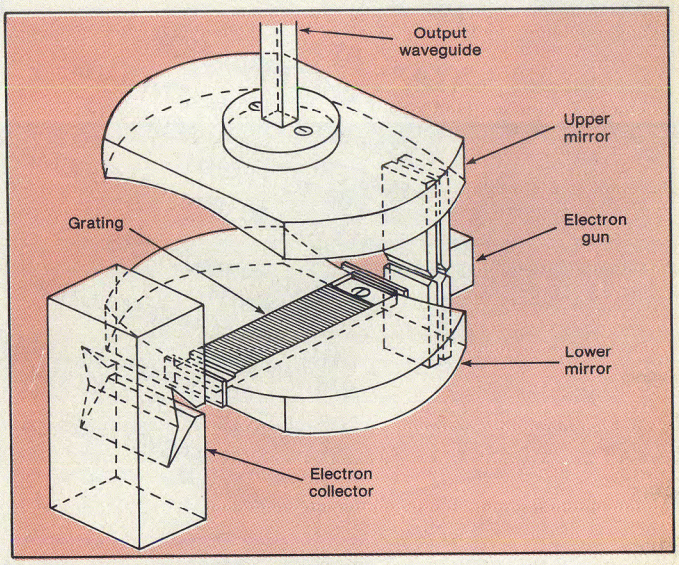
The orotron has other attractive features:

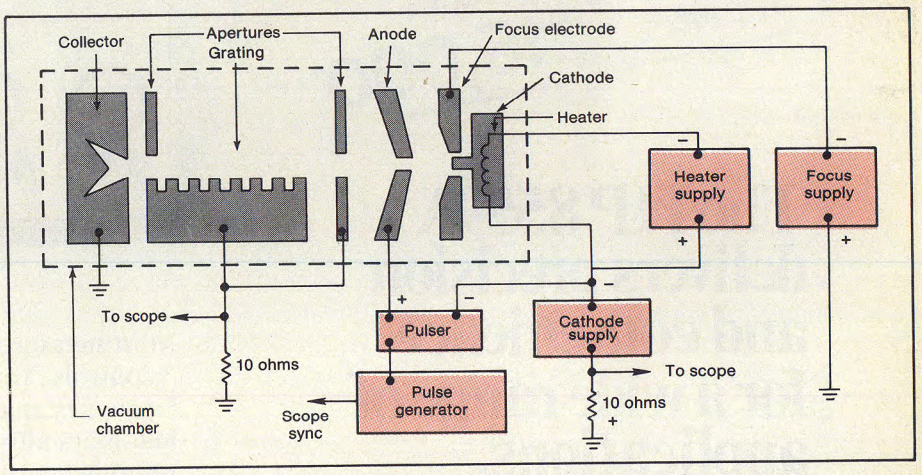
- it can be pulsed at high repetition rates with narrow pulses;
- it can be pulsed by low-voltage signals; and
- it can generate outputs with very narrow bandwidths.

Unfortunately, US experience with the orotron is still limited. Soviet workers claim[10] that the tube is the most widely used source of millimeter-wave radiation for plasma diagnostics in the world. Soviet and Japanese researchers, using the dense electron beams required for high output powers and frequencies, have already designed devices capable of operating up to 200 GHz.[6,11,12]

Donald E. Wortman, Richard P. Leavitt, and **Herbert Dropkin,** US Army Electronics Research and Development Command, Harry Diamond Laboratories, Adelphi, MD 20783.

1. The 50-to-75-GHz orotron *relies on synchronism between the velocity of the electron gun's beam and the phase velocity of an evanescent wave which travels along the metal diffraction grating. The upper and lower mirrors together form an open resonator.*





2. This wiring diagram *includes a focus electrode which can be used to control electron-beam current or to minimize beam ripple.*

One US contribution to orotron technology, developed at the Harry Diamond Laboratories (HDL, Adelphi, MD), is shown in Fig. 2. This device is the result of corroboration of the Soviet and Japanese research, and the authors' own success in developing linear and nonlinear theories of orotrons as well as the tube's observed tuning characteristics. The device is designed to operate from 50 to 75 GHz and can be pulsed with low-voltage (about 10-V) signals.[13] The electron source is a "Pierce-type" ribbon-beam electron gun that works under space-charge-limited conditions. The electron speed at the grating is determined by the potential difference, V_c, between the cathode and the grating. The elec-

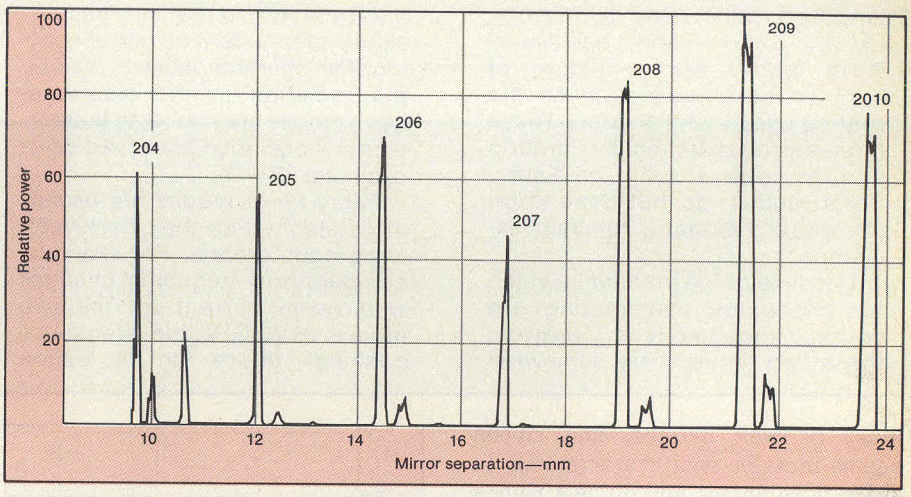
tron current is usually determined by the potential difference, V_a, between the anode and the cathode. The focus electrode voltage, V_{fe}, can be used to minimize beam ripple or to control the beam current.

The apertures mounted on the ends of the grating aid in aligning the electron beam and in electrically isolating the grating from the gun optics. The entire gun and grating structure are immersed in a uniform magnetic field (with field strength usually between 1 and 5 kG) along the direction of electron flow in order to confine the electron beam to the interaction structure.

Different modes possible

When the electron beam grazes the grating at a fixed cathode voltage, oscillation can be achieved in several modes by varying the spacing between the resonator mirrors. For example, Fig. 3 displays the results when the mirror spacing is varied and a fixed cathode voltage of 2412 V is applied. As the mirror spacing is opened from 10 to 24 mm, the mode changes from TEM_{204} to TEM_{2010}. The left-hand side of Fig. 4 reveals the threshold characteristics of the orotron for a TEM_{207} mode, showing a starting current of 55 mA. The right-hand side of the same figure shows the results of measurements made by varying the cathode voltage and keeping the distance between resonator mirrors fixed. Oscillation was achieved with cathode voltages from 2092 to 2153 V. Not shown in Fig. 4 is a sharp cutoff at 2153 V with no hysteresis.[14] By setting the cathode voltage at some level beyond this cutoff point, 2155 V for instance, a small negative voltage pulse applied to the grating will create the appropriate potential difference between the cathode and the grating for maximum power generation.

After this small voltage is applied to the grating, oscillation rapidly resumes. This feature permits the orotron to be pulsed rapidly with low-voltage signals while the current is on, and negates the leading-edge jitter caused by thermal effects when the beam current is simultaneously pulsed.



3. The relative output power varies with the separation distance between the two resonator mirrors. *This spectrum was generated while cathode voltage and beam current were kept constant.*

In the laboratory, the HDL orotron has been tuned continuously from about 50 to 75 GHz in a TEM_{208} Fabry-Perot mode, with power outputs of more than 1 W. By tuning the device to 65.65 GHz, and operating in a TEM_{209} mode, it was possible to achieve 5-W output power. The tuning transconductance was found to be 0.25 MHz/V at 70 GHz.

Although the HDL orotron principally operates in Fabry-Perot modes, it was also found to oscillate on backward-wave modes. (For a look at these two operating modes, see "A more than one mode device, p. 128.) Still, with the orotron oscillating in Fabry-Perot modes, performance is closer to ideal and the output tends to be more stable.

Improving beam quality

One of the prerequisites for further improvement of the orotron is an increase in the density of the electron beam. It was found that electron trajectories could be modified; by varying the voltage on the focus electrode of the electron-beam gun, it was possible to improve the quality of the beam. This method nearly doubled the power output for a fixed-beam current and beam voltage. As a consequence, the starting current could be reduced by a factor of two.[15]

Although the orotron represents a promising source of millimeter-wave energy, it is largely an experimental device. A cathode must still be developed* that is capable of producing thin, dense, monoenergetic electron beams. Beam stability requirements

(concluded on next page)

*Dr. C. Spindt of SRI (Stanford, CA) is currently testing cathodes that produce 50 A/cm² current density. The authors' theory (see Ref. 12) suggests that a current density of 50 A/cm² should produce 400 W of RF power.

A more than one mode device

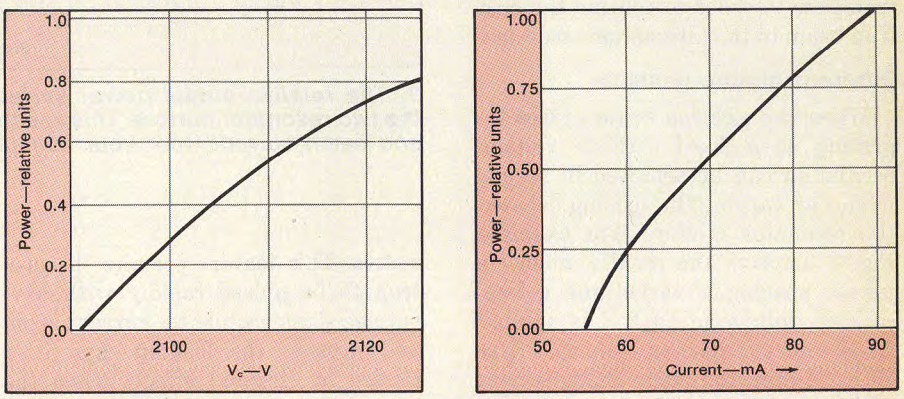
The grating-resonator system that is the heart of the orotron can support two distinct mode types: Fabry-Perot and backward wave. Fabry-Perot type modes are characteristic of any open resonant system; they are much like the modes of a laser cavity or the standing waves on a string. At any given frequency, these modes will occur at mirror spacings that allow a half-integral number of wavelengths to fit between the mirrors. On the other hand, backward-wave modes are a feature of periodic structures such as the grating used in the orotron. These modes propagate on the grating and, in contrast with the Fabry-Perot modes, do not depend on the mirror resonator for their existence.

Because of the manner in which the resonator and grating are coupled together in the orotron, these two modes vary somewhat from their pure forms. Of necessity, the grating imposes a fine structure on the Fabry-Perot modes so that one of its components can interact resonantly with the electron beam. This interaction of beam and grating-resonator produces the coherent radiation with desirable characteristics due to the high Q factor of the open resonator. In contrast, the backward-wave modes couple to the resonator so that they become slightly dependent on mirror spacing. The characteristics of the output radiation in the backward-wave modes are similar to those of a poorly designed backward-wave oscillator (BWO).

Fabry-Perot modes are usually more stable than their backward-wave counterparts. For example, compare how frequency changes with beam current for the two modes. At 70 GHz, the "frequency pushing" figure for the Fabry-Perot modes is 0.05 MHz/mA. This value jumps to 2.0 MHz/mA for the backward-wave mode at the same frequency. Another parameter useful for comparing the two modes is electronic tuning transconductance—the change in frequency with changing beam voltage. At 70 GHz, this transconductance is only 0.25 MHz/V for the Fabry-Perot modes, but increases about 15 times for the backward-wave modes. Obviously, the ultimate performance of an orotron design will be limited by competition between these two types of modes. Fortunately, there are several techniques available for reducing the influence of spurious backward-wave modes on orotron output, including one which involves tapering the grating's grooves towards the ends of the grating and filling these outer grooves with an absorbing substance.••

must be well defined, and ribbon beams must be well characterized. In order to compress and guide a ribbon beam across a metallic diffraction grating, methods must be found for determining the optimal shape of the surrounding magnetic field. Finally, open resonators must be examined so that dominant and parasitic modes can be characterized. This resonator knowledge can help lead to configurations that will produce maximum interaction between the RF fields and the electron beam.

The orotron would seem to be valuable as a driver for high-power millimeter-wave amplifiers such as gyrotrons, as a signal generator in high-resolution millimeter-wave spectroscopy, or as a source in high-density plasma diagnostics. A multitude of applications in radar, communications, and signal-processing equipment are also possible. Much of the device's future depends on the development of novel techniques for prebunching the electrons in the beam, phase-locking the output, and recovering the unspent longitudinal beam energy by the use of depressed collectors. Solution of these design problems will make the orotron a formidable millimeter-wave source.••



***4. Output power is compared to the input beam current** for the TEM_{207} orotron mode at 63 GHz (left). The power profile (right) for the same single orotron mode shows how the device oscillates over a 61-V range in the beam accelerating voltage.*

References

1. F. S. Rusin and G. D. Bogomolov, "Generation of electromagnetic oscillations in an open resonator," *JETP Letters*, Vol. 4, pp. 160-162 (September 15, 1966).
2. D. E. Wortman, H. Dropkin, and R. P. Leavitt, "Millimeter-wave orotron oscillation—Part II: Experiment," *IEEE Journal of Quantum Electronics*, Vol. QE-17, pp. 1341-1348 (August 1981).
3. D. E. Wortman, R. P. Leavitt, H. Dropkin, and C. A. Morrison, "Generation of millimeter-wave radiation by means of a Smith-Purcell free-electron laser," *Physical Review*, Vol. A24, pp. 1150-1153 (August 1981).
4. S. J. Smith and E. M. Purcell, "Visible light from localized surfaces moving across a grating," *Physical Review*, Vol. 92, p. 1069 (November 1953).
5. K. Mizuno, S. Ono, and Y. Shibata, "Two different mode interactions in an electron tube with a Fabry-Perot resonator—the ledatron," *IEEE Transactions on Electron Devices*, Vol. ED-20, pp. 749-752 (August 1973).
6. V. P. Shestopalov, *Difraktsionnaya Elektronika*, University Press, Kharkov, USSR (1976).
7. R. P. Leavitt, C. A. Morrison, and D. E. Wortman, "The orotron—a free-electron laser using the Smith-Purcell effect," *Applied Physics Letters*, Vol. 35, pp. 363-365 (September 1979).
8. F. J. Crowne, R. P. Leavitt, and T. L. Worchesky, "An exactly solvable nonlinear model for a Smith-Purcell free-electron laser," *Physical Review*, Vol. A24, pp. 1154-1157 (August 1981).
9. R. P. Leavitt, D. E. Wortman, and H. Dropkin, "Millimeter-wave orotron oscillation—Part I: Theory," *IEEE Journal of Quantum Electronics*, Vol. QE-17, pp. 1333-1340 (August 1981).
10. A. I. Skibenko, I. P. Fromin, and V. A. Skubko, "The use of two operating regimes of millimeter-wave generators in millimeter-wave interferometry," *Radiotekhnika i Elektronika*, Vol. 25, pp. 2474-2476 Moscow, USSR (1980).
11. S. Suto, Y. Nakanishi, M. Ikezawa, and K. Mizuno, "Construction of a wide band millimeter wave oscillator of the ledatron," *Japanese Journal of Applied Physics*, Vol. 20, pp. 1611-1612 (1981).
12. R. P. Leavitt and D. E. Wortman, "The effects of space charge on the performance of an orotron," manuscript in preparation.
13. D. E. Wortman, H. Dropkin, and R. P. Leavitt, "Means of modulating electron-beam-powered radiation devices," patent pending.
14. R. P. Leavitt and D. E. Wortman, "Nonlinear self-consistent theory of the orotron," *IEEE Transactions on Microwave Theory & Techniques*, submitted for publication, 1982.
15. D. E. Wortman, R. P. Leavitt, and H. Dropkin, "Improved orotron performance in the 50 to 75 GHz frequency region," *IEEE Transactions on Electron Devices, submitted for publication, 1982.*

Calculate GaAs MESFET Equivalent Circuits

Designing a GaAs MESFET based on a handful of necessary physical parameters can often lead to surprises when performance is evaluated. This program helps eliminate the guesswork.

TAILORING a GaAs MESFET design to a specific electrical requirement can be an agonizing affair, since any modification in physical parameters can result in drastic changes in device performance. However, with this HP-41C program, it's possible to accurately predict a MESFET's performance given its physical parameters.

The key to the program lies in linking a MESFET's physical parameters to its final electrical performance. Parameters affecting performance are shown in the figure, along with an equivalent circuit. Specifically, these parameters are: gate length (μm), gate width (μm), doping concentration (cm^{-3}), channel depth (μm), gate metal resistivity (ohm-cm), gate metal height (μm), frequency (Hz), drain voltage (V), pinchoff voltage (V), and gate capacitance/area (pF/cm^2). The last two parameters can be determined from the "Ideal GaAs Schottky barrier nomograph" on p. 136.[1] By plotting doping impurities and channel depth, and drawing a straight line through the two points, the graph yields values for gate capacitance/area and pinchoff voltage, respectively.

Using these design parameters as inputs, the program (p. 136) will furnish the following: drain current, I_{DSS} (mA); transconductance, G_m (mmhos); gate capacitance, C_g (pF); drain capacitance, C_d (pF); gate resistivity, R_g (ohms); drain resistivity, R_d (ohms); maximum available power gain, or MAG (dB); and power output (dBm).

Using the program is simple. Insert either three memory modules, or a memory "quad" module, into the HP-41C. If an HP-41CV is used, its built-in memory is more than adequate to handle the program. Next, connect the card reader, and make the following keystrokes:

(SHIFT) (GTO) (.) (.)

Then, insert the magnetic cards containing the program, starting with track #1 and ending with track #3. (Note that the program is not available on prepared cards, but must be manually inserted before following these procedures.) Once this is completed, the card reader can be removed and the printer plugged into port #4. With the printer in the "NORM" mode, key in:

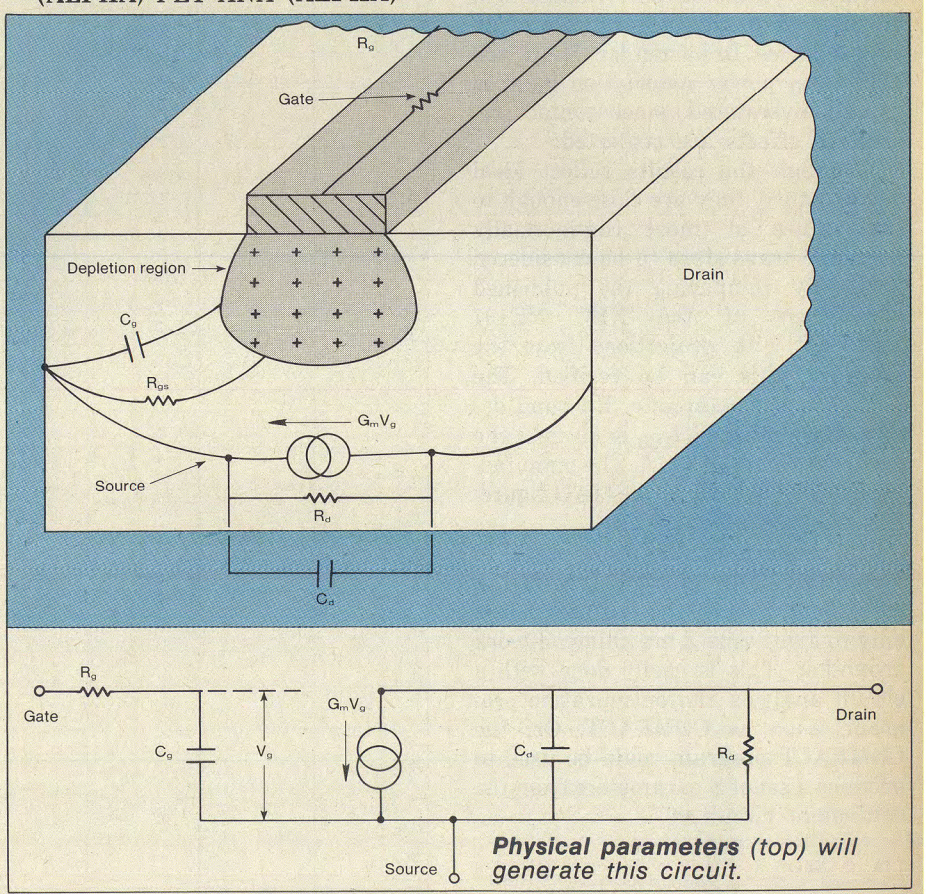
(ALPHA) SIZE (ALPHA)
0 5 0
(ALPHA) FET ANA (ALPHA)

Inputs must now be entered. Key these in after each prompt from the calculator and then press the **R/S** key.

Certain assumptions must be made with this program:

- the channel is composed of ideal, high-mobility GaAs;
- contact is made to the gate structure at its physical center;
- the gate is an ideal Schottky barrier;
- all contacts are ideal (i.e., they have zero contact resistance);
- the drain voltage is less than the breakdown voltage;
- DC drain current is 0.5 I_{DSS};
- the calculation of power is based on 30-percent efficiency; and
- the channel length is three times the

(concluded on next page)



***Physical parameters** (top) will generate this circuit.*

Allen A. Sweet, Private Consultant, 404 Grayson Ct., Menlo Park, CA 94025.

GaAs FET program listing

```
01*LBL "FET ANA"
02 "GATE LENGTH"
03 PROMPT
04 STO 01
05 "GATE WIDTH"
06 PROMPT
07 STO 02
08 "DOPING"
09 PROMPT
10 STO 03
11 "DEPTH, CHANNEL"
12 PROMPT
13 STO 04
14 "GATE METAL RESI"
15 PROMPT
16 STO 05
17 "GATE METAL HEIG"
18 PROMPT
19 STO 06
20 "FREQUENCY"
21 PROMPT
22 STO 07
23 "GATE CAP/AREA"
24 PROMPT
25 STO 08
26 "PINCH OFF VOLTS"
27 PROMPT
28 STO 09
29 "DRAIN VOLTAGE"
30 PROMPT
31 STO 10
32 1.602 E-19
33 ENTER↑
34 .7 E7
35 *
36 RCL 03
37 *
38 RCL 02
39 *
40 RCL 04
41 *
42 1 E-5
43 *
44 STO 11
45 "IdSS="
46 ARCL X
47 AVIEW
48 RCL 11
49 ENTER↑
50 2
51 *
52 .707
53 *
54 RCL 09
55 /
56 STO 13
57 "GM, .5IdSS="
58 ARCL X
59 AVIEW
60 RCL 11
61 ENTER↑
62 2
63 *
64 .447
65 *
66 RCL 09
67 /
68 "GM,.2IdSS="
69 ARCL X
70 AVIEW
71 RCL 08
72 ENTER↑
73 RCL 01
74 *
75 RCL 02
76 *
77 1 E-8
78 *
79 STO 14
80 "C, GATE="
81 ARCL X
82 AVIEW
83 RCL 05
84 ENTER↑
85 RCL 02
86 *
87 12
88 /
89 RCL 01
90 /
91 RCL 06
92 /
93 1 E4
94 *
95 STO 12
96 8 E-2
97 ENTER↑
98 RCL 01
99 *
100 RCL 02
101 /
102 2
103 /
104 RCL 04
105 /
106 1 E4
107 *
108 RCL 12
109 +
110 STO 15
111 "R, GATE="
112 ARCL X
113 AVIEW
114 13
115 ENTER↑
116 8.85
117 *
118 RCL 04
119 *
120 RCL 02
121 *
122 3
123 /
124 RCL 01
125 /
126 1 E-4
127 *
128 2
129 /
130 STO 16
131 "C, DRAIN="
132 ARCL X
133 AVIEW
134 1.8
135 ENTER↑
136 RCL 01
137 *
138 RCL 02
139 /
140 RCL 04
141 /
142 2
143 *
144 1 E4
145 *
146 STO 17
147 "R, DRAIN="
148 ARCL X
149 AVIEW
150 RCL 13
151 ENTER↑
152 2
153 /
154 PI
155 /
156 X↑2
157 STO 18
158 RCL 17
159 ENTER↑
160 RCL 15
161 /
162 SQRT
163 STO 19
164 RCL 07
165 ENTER↑
166 RCL 14
167 *
168 1/X
169 X↑2
170 RCL 18
171 *
172 RCL 19
173 *
174 1 E18
175 *
176 LOG
177 10
178 *
179 "MAG="
180 ARCL X
181 AVIEW
182 RCL 11
183 ENTER↑
184 2
185 /
186 RCL 10
187 *
188 .3
189 *
190 LOG
191 10
192 *
193 "POWER="
194 ARCL X
195 AVIEW
196 "END"
```

(continued from p. 135)

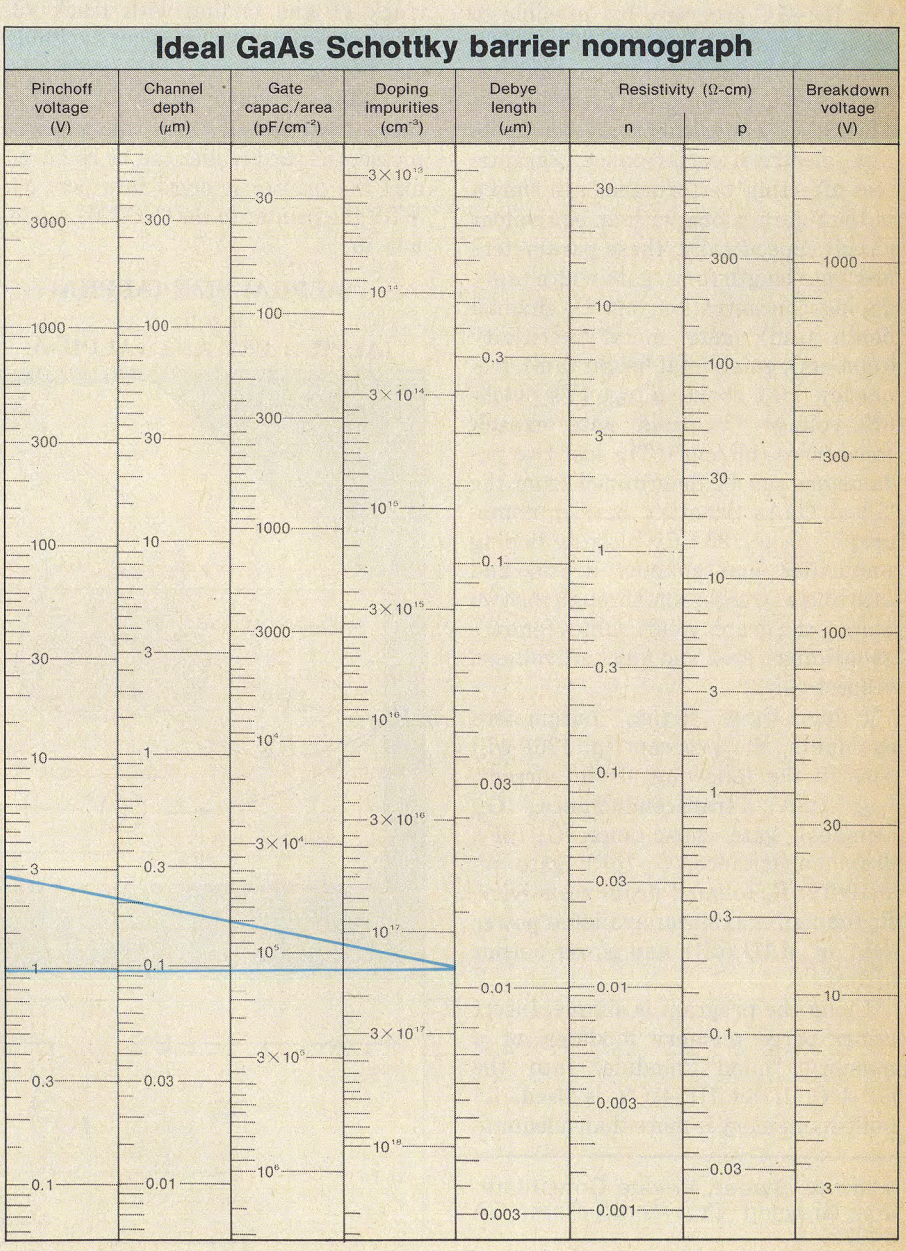
gate length.

These assumptions clearly represent an idealized FET. As a result, the calculator-predicted performance will be superior to the performance of an actual device. In particular, MAG, the maximum power association gain, is usually overstated, since contact resistance effects are neglected.

Although the results reflect ideal performance, they are close enough to the values of most commercially available transistors to be considered valid. By comparing the published parameters of the NEC NE137 MESFET with projections from the program, this can be verified. The NE137 is a 0.5-μm-gate, Ku-band device. Its published I_{DSS} is 50 mA: the program yields 58.3 mA. The manufacturer gives 19.8 dB as the MAG figure: the program gives 15 dB.

The program should prove useful to monolithic IC designers. It provides an equivalent circuit; the engineer needs only to synthesize a matching network around it. This is easily done with a circuit analysis and optimization program, such as COMPACT. Or, the COMPACT program could be used to produce a set of S parameters from the equivalent circuit.••

Ideal GaAs Schottky barrier nomograph



References

1. A. G. Milnef, *Semiconductor Devices in Integrated Electronics*, p. 35, Van Nostrand-Reinhold, NY (1980).

U-Band Gunn Oscillator Rivals Impatt Performance

Post form, diode height, and supply voltage effects are key considerations in this 45-GHz, mechanically tuned design. Measurements confirm a 10-GHz tuning range.

MILLIMETER-WAVE oscillators are less than common as commodities. In early 1981, the Swiss Post Office Research Laboratory could not find one suitable for use in a millimeter-wave radiation measurement receiver which we were assembling from available components. Our solution was to design and build a mechanically tuned, post-coupled, waveguide, Gunn oscillator in the 45-GHz band.

The receiver design required that the oscillator signal be injected directly into the mixer. The conversion loss experienced with harmonic mixers was too high to be accommodated, and frequency multipliers could not generate sufficient power to drive commercially available high quality mixers.

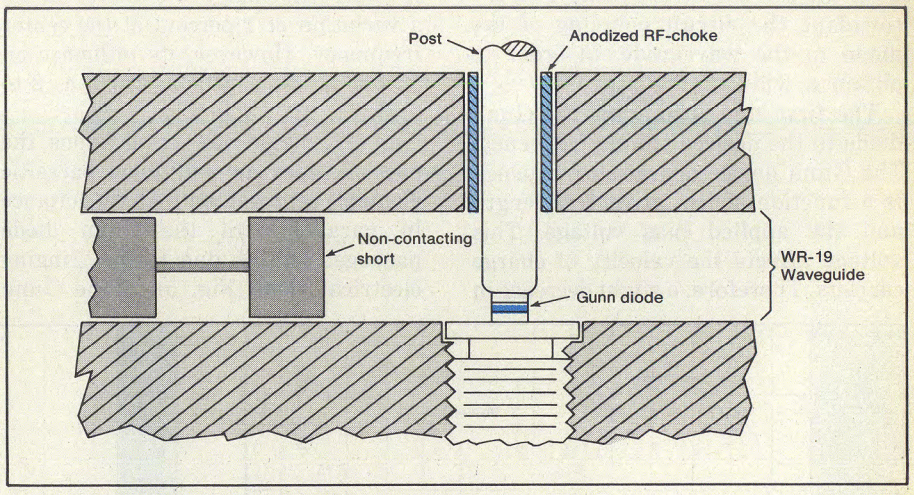
Among the candidates for a direct-injection source, the Gunn oscillator—one of the simplest to design—has outstanding advantages. Millimeter-wave backward-wave oscillators (BWOs) are very delicate and expensive. Impatt-diode oscillators, on the other hand, produce too much noise, and YIG-tuned oscillators are only available to 26 GHz. In comparison, the Gunn-effect oscillator can offer low noise and relatively high stability in applications that can bear the restriction of its narrow tuning capability.

Recent technical advances in commercial GaAs and InP Gunn diodes have extended their useful operation to 100 GHz. And even the narrow tuning range is falling to known technology and precision components.

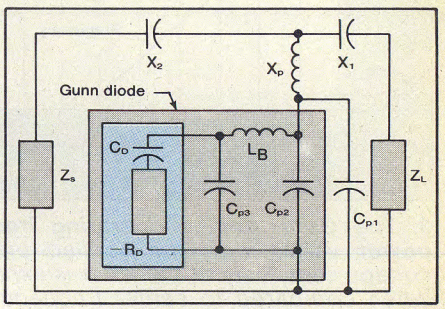
Gunn effect well understood

The theory of post-coupled Gunn-effect waveguide oscillators dates from the early 1970s.[1,2] The electrical configuration is a post-coupled Gunn diode mounted in a WR-19 waveguide and tuned by a movable noncontacting short (Fig. 1). The load is directly coupled (i.e., there is no coupling iris). Therefore, the oscillator must be isolated from the load.

The frequency of oscillation is determined by the complex impedances presented to the Gunn device. Data sheets available from manufacturers provide the values of the parallel capacitances C_{p2} and C_{p3}, and the encapsulation bonding inductance, L_B (Fig. 2). The post impedance, X_p, and the post fringing capacitance, C_{p1}, can be determined by the designer. The capacitive reactances X_1 and X_2 result from field distortion due to the finite diameter of the post, compared to the waveguide width. Z_L denotes the load impedance and Z_S the impedance of the short-circuited waveguide, both transformed to the device plane. This leads to X-band oscillators with a 33-percent tuning range and an ability to apply results extrapolated from 8.2-to-12.4-GHz and 18-to-26-GHz bands to a 40-to-50-GHz, millimeter-wave Gunn oscillator design.



***1. A post-coupled Gunn diode,** mounted in a WR-19 waveguide, is tuned by the noncontacting short shown at left.*



***2. The electrical model of a Gunn oscillator circuit** shows all of its frequency and power contributing parametric terms.*

Tuning range determined

Six 50-mW diodes in the standard MA 138/P6 package made by Plessey and Microwave Associates were used in this study. Two 100-mW types in the pill package were also obtained from Hughes Aircraft. The 50-mW units are screw-mounted, whereas the 100-mW types (6-W DC power dissipation) are soldered onto one waveguide half-section. The other half-section carries the post with the RF choke. In the 100-mW

(continued on next page)

J. Siegenthaler, Member of the Technical Staff, Swiss Post Office Research Laboratory, 3000 Bern 29, Switzerland.

oscillator, a low reflection, full-band step transformer is used to match the diode impedance to the waveguide.[3] The oscillator frequency is tuned by means of a noncontacting nonresonant short[4] moved by a calibrated micrometer screw. No other tuning elements are required to achieve the full tuning range.

Wide tuning ranges possible

Millimeter-wave Gunn oscillator designers have two options. They can specify a narrow tuning range with any diode at the center frequency, or try to adapt the circuit coupling of the diode to the waveguide, in order to obtain a wide tuning range.

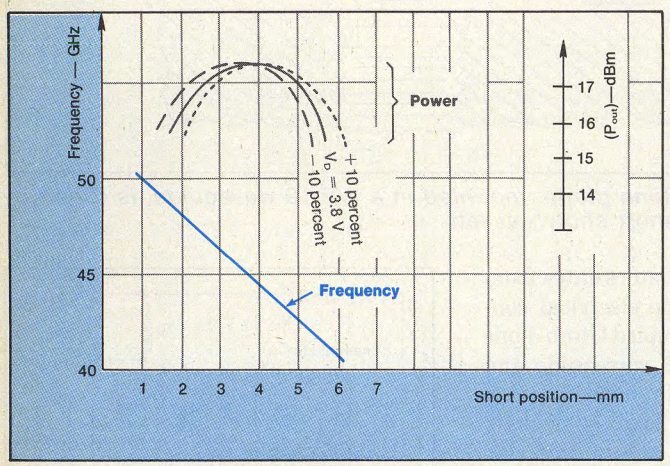
The first step is to adapt the Gunn diode to the desired tuning frequency. The Gunn device operating frequency is a function of its active area length and the applied bias voltage. This voltage affects the velocity of charge carriers. Therefore, a slight decrease in voltage causes an increase in the operating frequency (Fig. 3). While the power at the center frequency exhibits minimal supply voltage sensitivity, the same is not true at the tuning range extremes. A 10-percent change in the applied voltage can cause a 1-to-2-dB output power variation.

Post diameter is the second adjustable oscillator parameter and appears as an inductance determined by the ratio of post diameter and waveguide width.[5] In theory,[1,2] its influence on frequency is not significant. A 10-percent change in diameter causes a variation of 1 percent at the center frequency. However, its influence on output power can be as much as 2 to 3 dB, as shown in Fig. 4.

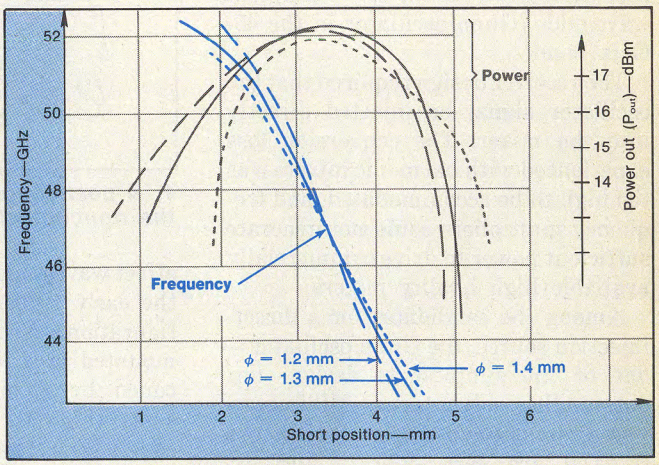
In millimeter-wave applications, the post includes an additional parasitic element, represented by a capacitance in parallel with the Gunn diode package. This is due to the fringing electrical field (Fig. 5) at the Gunn diode transition. To obtain the lowest possible post inductance, its diameter should be larger than that of the diode package. In addition, smooth mechanical transitions to the Gunn diode aid considerably in increasing the upper frequency tuning limit. In some cases, the frequency range can be extended by 1.5 GHz, depending upon the diode used in the circuit.

The third parameter that effects oscillator tuning range is the height of the Gunn diode above the waveguide wall. Earlier publications proposed frequency tuning by altering the diode height[6] or diode recess[7] in order to change the diode package inductance. Increasing the Gunn diode's height in steps of 0.07 mm can produce a change of as much as 2 GHz in the tuning range (Fig. 6).

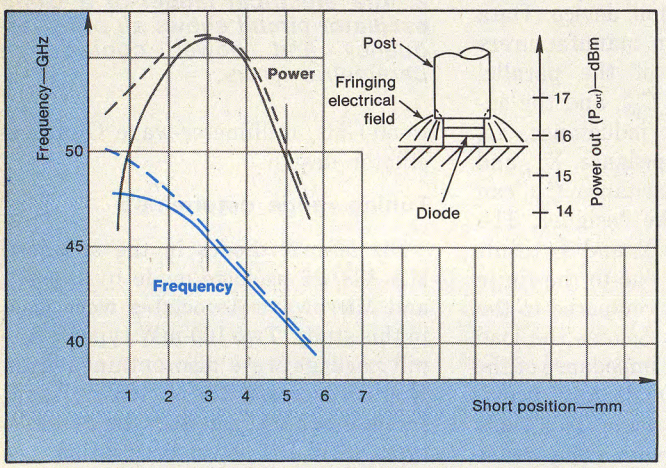
In general, a diode mounted on the bottom of the waveguide extends the low frequency tuning range. The high frequency end shows some saturation



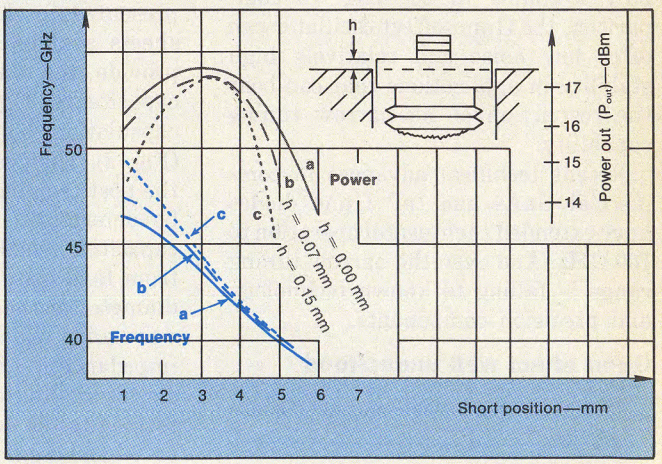
***3. The Gunn device operating frequency and output power** varies with the applied bias voltage. Greater voltage sensitivity of the latter is exhibited at band edges when compared to center frequency.*



***4. Two sets of curves show contrasting differences in post diameter sensitivity.** The frequency term varies slowly while output power exhibits larger changes versus diameter variations.*



***5. The capacitive reactance term** that represents the Gunn diode post's fringing electrical field limits its upper frequency response.*



***6. A method of oscillator tuning** is illustrated by raising the diode (height "h") above the bottom waveguide wall to change its package inductance.*

and the output power response is flattened. On the other hand, if the diode is mounted on a pedestal, a more linear high-frequency tuning behavior results while the lower frequency end and the power output flatness suffers.

Consequently, since parametric influences are mutually dependent, they must be considered simultaneously to achieve optimum oscillator performance. A carefully designed combination of values will provide sufficient margin to obtain the desired range. This necessitates monitoring frequency, power, spectrum, and frequency-tuning capability during the optimization routines. To avoid unwanted frequency pulling effects by load impedance reflections, an isolator is inserted between the test circuit (Fig. 7) and the oscillator. The power is measured through a 10-dB coupler and an absorption-wavemeter. To observe spectrum and tuning characteristics, the oscillator signal is mixed with a very stable synthesizer signal driving a 13-to-18-GHz frequency tripler.

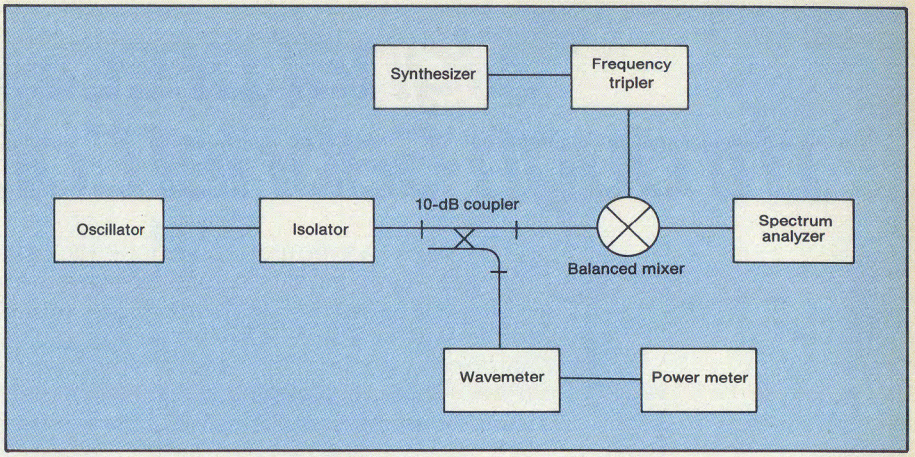
Measurements verify design

This study shows oscillators can be optimized to have a frequency tuning range of more than 20 percent with no more than a 3-dB power variation. If the power (variation) spec can be loosened to 6 dB, a tuning range of up to 28 percent can be achieved without exhibiting discontinuities such as jumping or frequency pulling effects. Typical frequency tuning and power output curves are illustrated in Fig. 8.

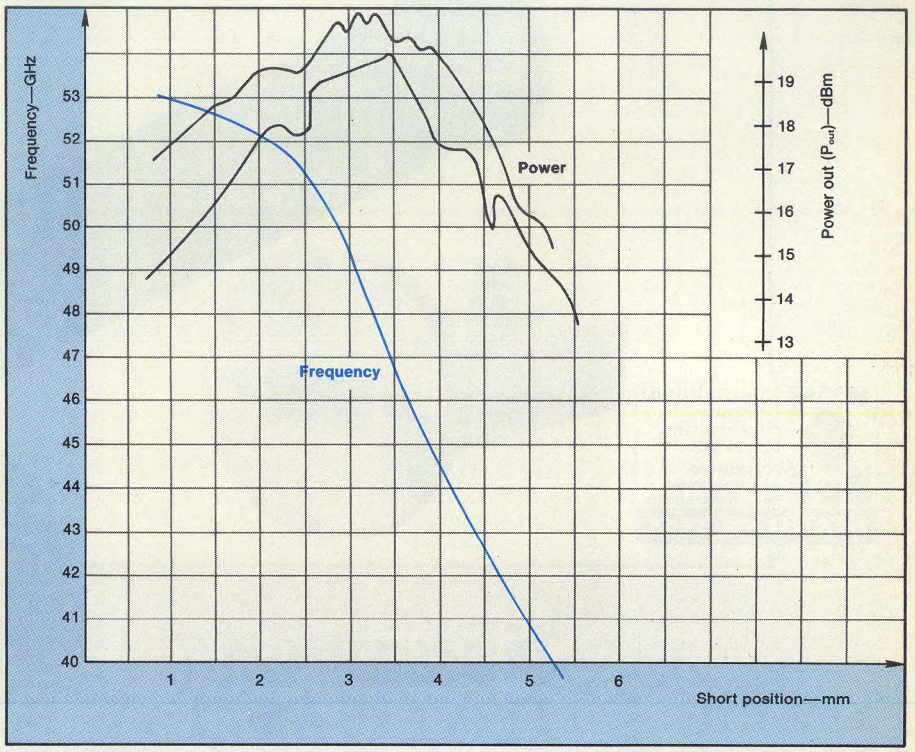
The actual oscillator output power is 1 to 2 dB higher with less variation than the values measured in the test circuit when the insertion loss and the relatively high reflection coefficient of the full band isolator are considered. The 100-mW type diode in the reduced waveguide (25-percent height) shows similar results within a 3-dB output power increase.

The signal from this Gunn-diode design, which is very stable over the full tuning range, was compared with the output of a high quality, commercially available, mechanically tuned Impatt oscillator with a range of 46 to 49 GHz. The FM stability of the Gunn oscillator is higher at the low frequency tuning end because of the higher Q of the cavity.[1]

With a measured temperature coefficient of −2 MHz/°C, no oscillation start-up problems occurred in the 3-dB frequency range between the temperatures of 0 and 50°C. Some oscillators may show mode-switching problems[1] at the lowest frequency end (−6-dB point) and temperatures below 0°C, but for laboratory applications, this is not a significant disadvantage.••



7. A test circuit is used *to simultaneously measure the oscillator's frequency, power, spectrum, and frequency-tuning capability while running through the optimization routines.*



8. Typical frequency-tuning and power-output curves *are shown for an optimized Gunn diode oscillator. Greater than 20-percent frequency range with no greater than a 6-dB power variation is illustrated.*

Acknowledgments

The author thanks K. Hilty for helpful discussions and continuous support, Dr. P. Kartaschoff for help in editing, and M. Mori for excellent machine shop work of the mechanical parts.

References

1. W.C. Tsai, F.J. Rosenbaum, and L.A. Mackenzie, "Circuit Analysis of Waveguide Cavity Gunn Effect Oscillators," *IEEE Transactions MTT*, Vol. 18, No. 11, pp. 808-817 (November 1970).
2. C.P. Jethwa and R.L. Gunshor, "Circuit Characterization of Waveguide-Mounted Gunn Effect Oscillators," *Electronic Letters*, Vol. 7, No. 16 pp. 433-436 (July 1971).
3. Matthaei, Young, Jones, *Microwave Filters, Impedance-Matching Networks, and Coupling Structures*, McGraw-Hill, New York, NY pp. 255-354 (1964).
4. G. Epprecht and P. Herrmann, "Kontaklose, Verschiebbare Kurzschlusse fur Rechteck-Hohlleiter," 67-04 (internal report), Swiss Federal Institute of Technology, Zurich, Switzerland (September 1967).
5. N. Marcuvitz, *Waveguide Handbook*, MIT Rad. Lab. Series, No. 10, p. 262 (1964).
6. J. Ondria, "Wide-band Mechanically Tunable and Dual In-Line Radial Mode W-Band (75-110 GHz) CW GaAs Gunn Diode Oscillators," presented at the Seventh Biennial Conference on Active Microwave Semiconductor Devices and Circuits, Cornell University, Ithaca, NY (August 14-16, 1979).
7. "Microwave Power Generation and Amplification Using Impatt Diodes," Application Note 935, Hewlett-Packard (1971).

Computer Design Package Aids SAW Development

Simulation software and measurement hardware have combined to meet the challenges of SAW development and manufacturing. The final system can emulate performance using measured data.

SAW (surface acoustic wave) devices challenge the designer. The interdigital transducers which launch and receive the SAW waves that travel across the substrate must be precisely sized and spaced to obtain the required response. And the small physical scale of the devices virtually precludes any adjustments or trimming after fabrication.

This new breed of technology, like many others, depends heavily on computer-aided design (CAD). Indeed, most of designers' initial efforts in the SAW field are invested in the CAD programs themselves. Afterwards, the designer's role becomes one of selecting the appropriate design parameters and transducer structures. The actual determination of the dimensions of the device and its constituent parts can be left to the software.

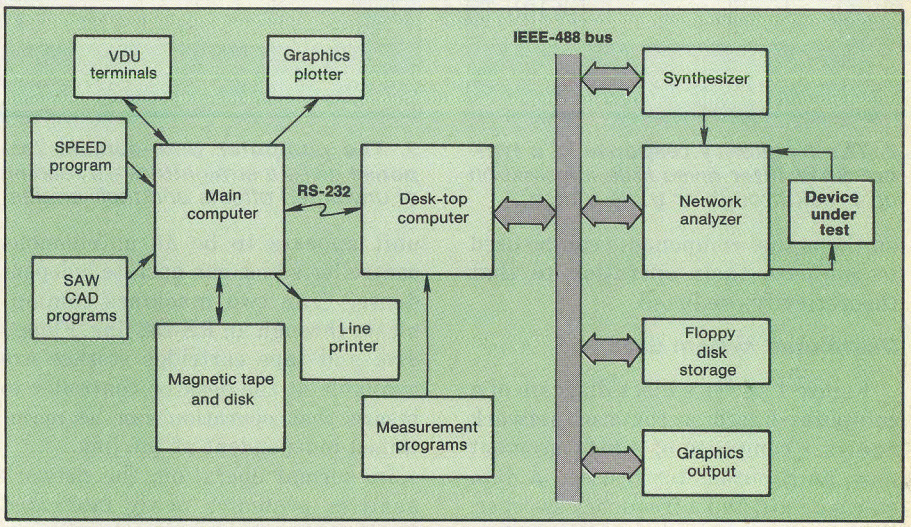
Design only part of the process

Although critical, the design of SAW devices stands as only one aspect of the total process of developing such complex structures. To achieve the highest levels of device and subsystem performance, the design loop must be closed by integrating design, measurement, and evaluation. We have devised a three-tiered system for this purpose:

- A CAD package for SAW devices,
- A measurement package for the fabricated devices, and
- A simulation package for subsystems and devices.

The first two software elements offer nothing fundamentally unique, although the measurement package does require a relatively comprehensive and expensive set of test equipment. However, the simulation package plays a key role as a developmental tool. On a broader front, it also provides a way to evaluate devices, subsystems, and systems by synthesizing their performance from the measured data.

John W. Arthur, Chief Engineer, SAW Applications, Racal MESL Microwave Ltd., Newbridge, Midlothian, Scotland.



***1. The network analyzer** comprises a measurement unit, an S-parameter test set, a storage unit, and a frequency sweeper. A synthesized source replaces the sweeper for automated measurements.*

The simulation software that we developed, the Simulation Package for Electrical Engineering (SPEED), is not restricted to SAW design. It can cover nearly all conceivable linear systems, as well as a restricted class of nonlinear operations (amplitude limiting, mixing, detection, and so forth).

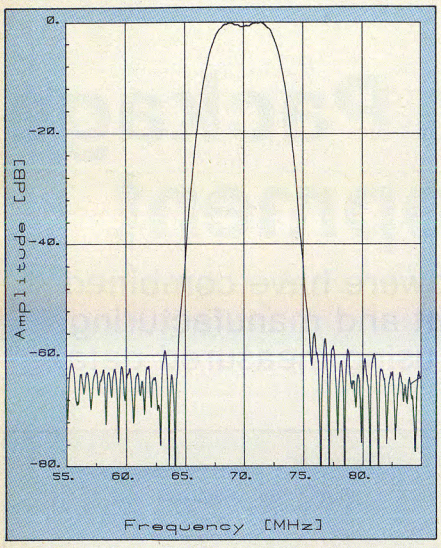
SPEED provides an ideal environment for the theorist or the designer, in large part because the program allows theoretical and measured data to be interchanged at any stage. The question "Will it work?" has been addressed by allowing noise sources and other synthetic perturbations and distortions to be introduced. Of course, the question "Does it work?" must be answered in real-life applications.

The design of a SAW device begins with a complex specification based on a customer's requirements. First, the specification writer must determine the critical parameters and assign sensible values to them. This formidable task is further complicated by the awkward trade-offs that must be made among these parameters.

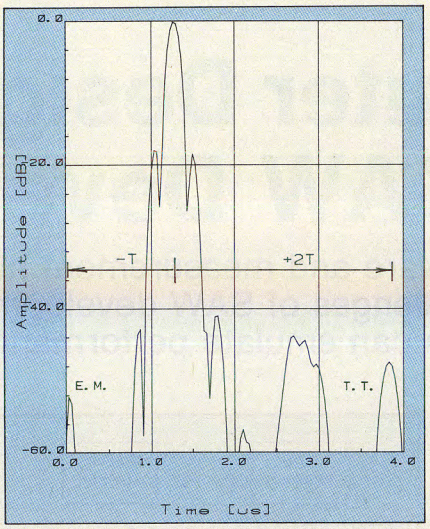
Next, the specification must be followed in detail during fabrication. Devices that deviate from the required performance must be identified early enough during manufacture to save both time and money. A short visit to the bench can easily verify the performance of a simple component. But a SAW device is a good example of a complex component which is not as easily tested.

The direct, closed-loop approach suggested here answers both these needs. The specifier can use SPEED to verify that the device or subsystem will yield the performance required by clients. Likewise, measurements made

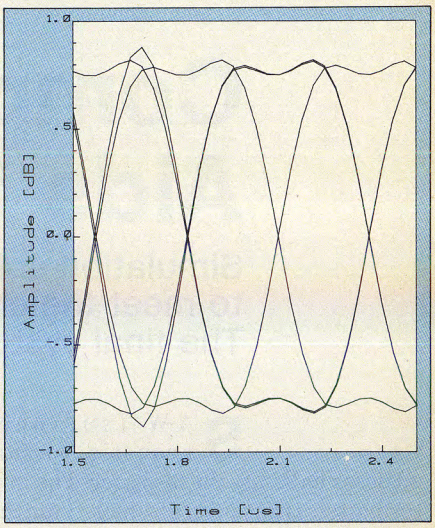
(continued on next page)



***2. The frequency response of a typical SAW filter** gives little information on breakthrough or triple transit.*



***3. The computer time-domain response** gives a straightforward reading of unwanted effects and their origins.*



***4. The "eye" diagram for a 3.75-MHz PSK signal** shows the effect of the filter shown in Fig. 2.*

on the actual components can be used to compare their operation to that theoretically predicted.

Distributed system used

Figure 1 shows a block diagram of a computer-based automatic network analyzer composed of a measurement unit, an S-parameter test set, a data storage unit, and a frequency sweeper. For automated measurement work, a highly accurate and stable synthesized source replaces the sweeper, and an IEEE-488 bus provides remote control of the entire system.

The operator controls the system through a local desktop computer which also provides graphics output for routine measurements. To the main computer, the satellite desktop unit appears to be an autonomous controller which can operate independently. The two machines communicate through an RS-232 link. Floppy disk and tape cartridge storage are available at the desktop controller to insure that operation can be maintained independent of the link.

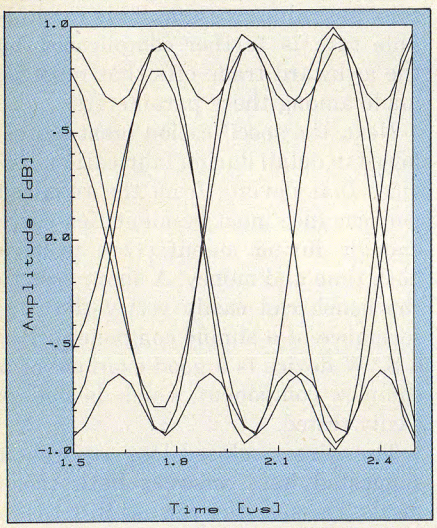
In normal operation, the network analyzer evaluates newly fabricated SAW devices in a conventional manner. If these preliminary results indicate that all is well, a program in the desktop machine steps the network analyzer across the bandwidth of the device, and a record is made of the transmission amplitude and phase characteristics as functions of the frequency. The evenly spaced measurement points are symmetrical about the center frequency. Data must be recorded at a sufficient number of points (N) to unambiguously resolve the total delay of the device. The required number of points can be determined from the following rule:

$$N \geq BT \qquad (1)$$

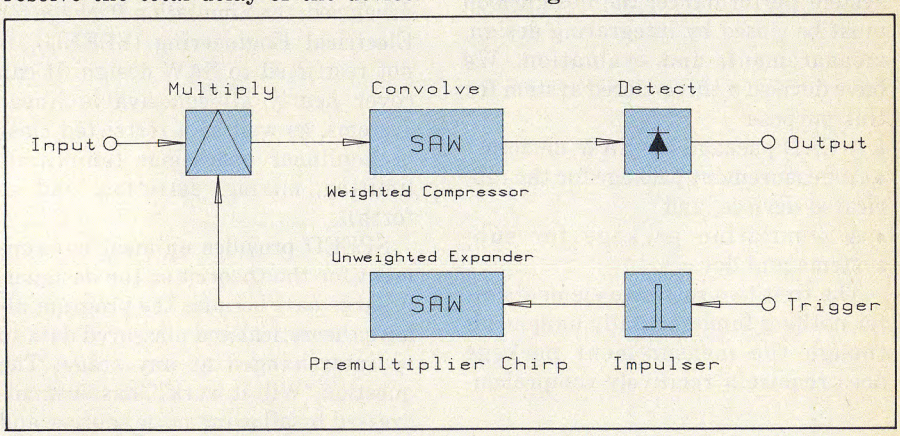
In Eq. 1, B = the total bandwidth covered and T = the maximum delay within the measurement bandwidth.

If the rule expressed in Eq. 1 is broken, 2π phase ambiguities will create wrap-around effects in the time domain. Conventionally, measurements of the π-points (i.e., those points where the phase changes by 180 degrees) offer the most accurate readings of the response of a device with a long electrical length. These measurements, however, are quite inconvenient for computation, particularly with dispersive devices, and measurements at equal frequencies have been adopted instead.

To execute this procedure, the accuracy of the phase calibration of the network analyzer must be very high. Although errors tend to be random



***5. A similar "eye" diagram** shows the effect of an interfering signal in a channel 4 MHz away.*



***6. The design of a SAW spectrum analyzer** or "compressive receiver" shows the simulation package applied to a subsystem. The pictured realization is known as the "M(long)C" or "sliding transform" type.*

(and, therefore, non-accumulative) for dispersive devices, this situation may not occur for a linear phase network, and it is useful to calibrate from a delay line. In general, any line with a delay slightly greater than 1/B will suffice, provided it remains non-dispersive within this measurement bandwidth (i.e., B).

A simple program can measure the delay, check for dispersive effects, and recalibrate any phase measurements. This procedure can improve the 1-degree typical accuracies at the ±180-degree points to ±0.1-degree nominal figures. Similar improvements (to 0.1 dB) can be gained in amplitude measurements by programming the attenuators through the measurement processor according to the level of the signal.

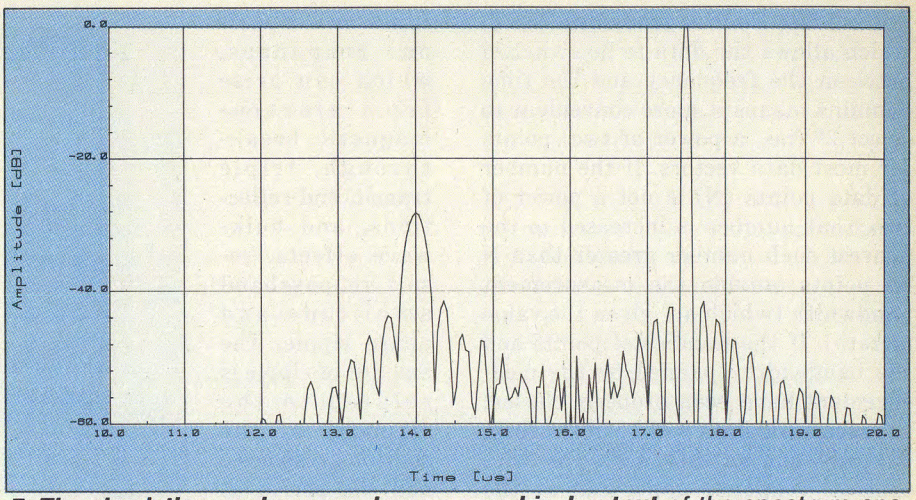
The synthesized source must have high accuracy and long-term stability to avoid major problems in measuring long lines to high accuracy. At a center frequency of 100 MHz and a delay of 25 μs, the total allowable phase excursion is 1.8×10^6 degrees and the required accuracies better than 1 in 10^7. To achieve this accuracy with confidence, source stability and repeatability should be specified at ±1 Hz.

After the device has been measured, the data can be temporarily stored or sent directly to the main computer for filing on a mass storage device (usually disk). When batches of devices are to be measured, the devices which conform to the central band of the manufacturing distribution are selected either in the measurement phase, or later, on the main computer.

SPEED emulates performance

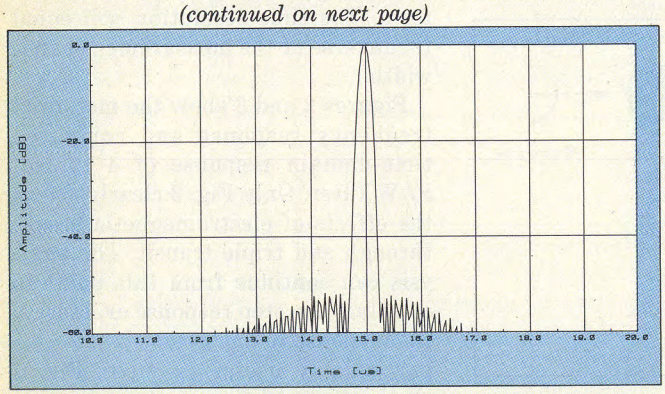
Once within the main computer system, data for each device is given a descriptive name and is converted to the standard SPEED format. The

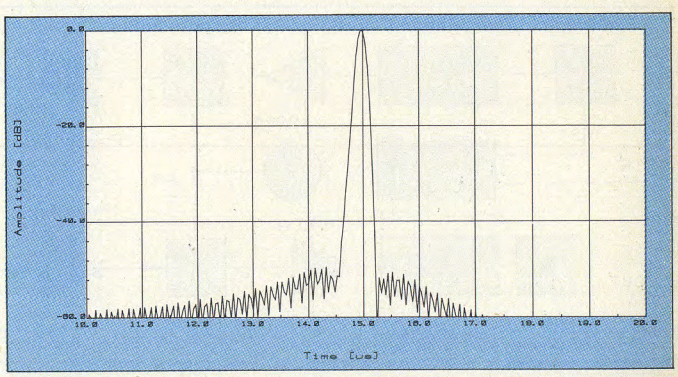
(continued on next page)



***7. The simulation package produces a graphical output** of the spectrum analyzer's performance for a specific input signal. The depicted response is based on actual device measurements. See table below.*

```
!                    M LONG C SPECTRUM ANALYSER SIMULATION
!
!
DEFINE ,PREM=1024,COMP,SIG,TEMP                    ! DATA VECTORS
DEFINE,PEAK,POS                                    ! SIMPLE VARIABLES
DEFAULT,DEV=1,LU=1,N=1024                          ! DEFAULT VALUES
SETUP,BMAX=25_MHZ,N=1024_SAMPLES
TIME                                               ! START OFF IN
                                                   ! TIME DOMAIN
!
CHIRP,PREM,B=20_MHZ,T=20_US,SLOPE=1                !PREMULTIPLIER CHIRP
GET_TEMP,FILE='#CHEBE'
MULT,PREM,TEMP,PREM                                !MATCHING NETWORK RESPONSE
MULT,PREM,TEMP,PREM
CHIRP,COMP,B=10_MHZ,T=10_US,SLOPE=-1               !COMPRESSOR CHIRP
GET_TEMP,FILE='#CHEBC'
MULT,COMP,TEMP,COMP                                !MATCHING NETWORK RESPONSE
MULT,COMP,TEMP,COMP
!
!          APPLY 50DB TAYLOR WEIGHTING TO COMPRESSOR
WINDOW,COMP,TYPE=27_(TAYLOR),CENTRE=5_US,LENGTH=10_US,SUB=50_DB
!
TONE,SIG,F=0_MHZ                                   ! INPUT SIGNAL
!
MULT,SIG,PREM,SIG                 ! MULTIPLY SIGNAL AND PREMULTIPLIER CHIRP
CONVOLVE,SIG,COMP,SIG               ! CONVOLUTION IN WEIGHTED COMPRESSOR
!
!              DEFINE GRAPHICS HEADERFORMAT
!
HEADER,STITLE='M-LONG-C',TITLE='MClong?C Analyser Output'
HEADER,XTITLE='Time [usJ',YTITLE='Amplitude [dBJ
HEADER,XMIN=10_US,XMAX=20_US,YMIN=-60,YMAX=0
                                                   ! SELECT OUTPUT DEVICE
SKIP,STRING='HARD COPY?'
DEFAULT,DEV=3
PEAKMAG,SIG,PEAK,POS                               ! GET PEAK HEIGHT
GRAPH,SIG,NORM=PEAK                                ! EXECUTE GRAPH
SWITCH                                             ! RETURN TO INTERACTIVE
                                                   ! MODE
!
```

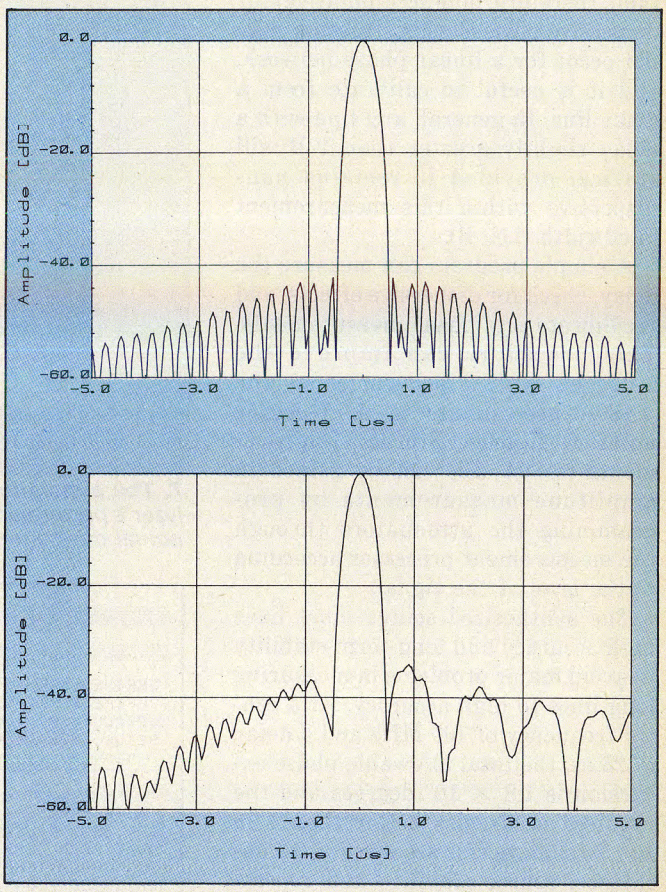




***8. A 0.5-dB ripple Chebyshev bandpass matching network** can be simulated at the input and output transducers of each SAW device. This capacity allows a designer to examine different circuit options without reverting to costly and time-consuming hardware fabrication and testing.*

radix-2 fast Fourier transform (FFT) which allows the data to be switched between the frequency and the time domains makes it more convenient to select 2^n (i.e., a power of two) points for most data vectors. If the number of data points (N) is not a power of two, that number is increased to the nearest such number greater than N by points outside the measurement bandwidth (which are given the value of zero). If the number of points and the bandwidth spanned by the measurement have been properly chosen, the measured data will be in the form entirely compatible with the theoretical response generated at the simulation or design level.

The measured data can be interchanged with the simulated data. For example, a simulated compressed-pulse resulting from the design of a pair of matched SAW filters can be compared with a synthetically measured compressed-pulse virtually as soon as the devices have been measured. Even if the simulation doesn't represent the physical response of an actual system in complete detail, the effect that the practical devices have on system performance can be readily observed. As the following examples show, an entirely new means of evaluating devices in a system context has been opened with this relatively straightforward and widely applicable procedure.



***10. A distortion is introduced** when a time-varying gain is applied to compensate for the R^{-4} range dependency of the radar's return signal. The distortion is greatest at the critical short ranges.*

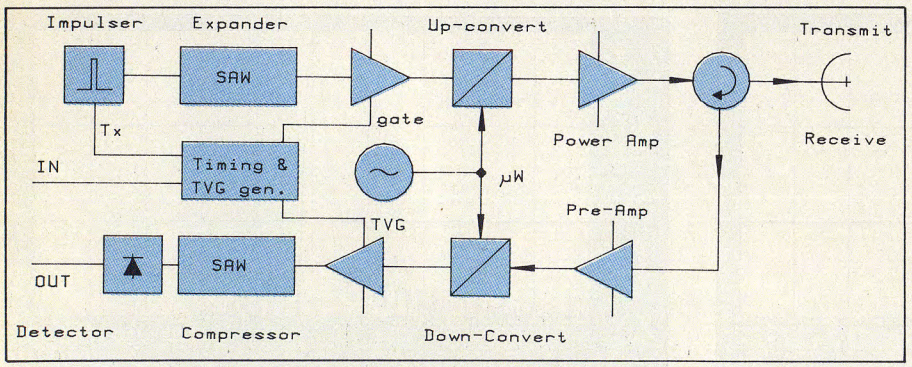
SAW bandpass filters

SAW bandpass filters, which are normally realized as transversal filters, have a characteristically linear phase response. The passband shape is composed of the responses of the input and output transducers (each of which has a frequency response closely approximated by the Fourier transform of its spatial weighting function). Spurious responses, which can arise from electromagnetic breakthrough, triple transit, end reflections, and bulk-wave effects, result in passband amplitude and phase ripple. The amount of ripple is related to the strength of the spurious responses and the period at which they occur (which, in turn, depends on their effective delay time).

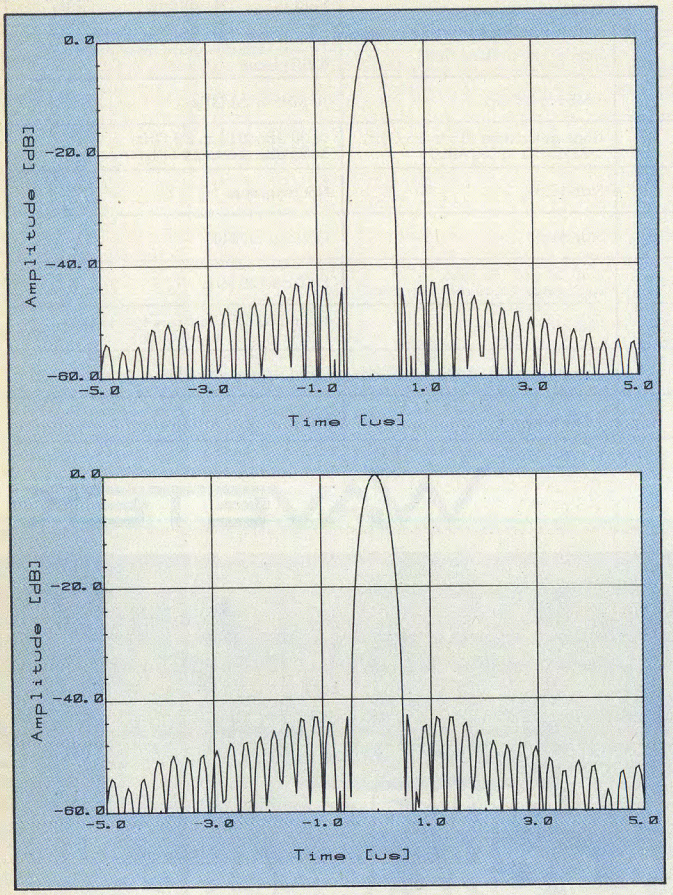
A simple observation of the frequency response will not easily establish the extent of the unwanted spurious response or its origins—except when a single dominant source is involved. In the time domain, however, electromagnetic breakthrough and triple transit have respective characteristic delays of $-T$ and $+2$ relative to the main response (T = the group delay of the filter) and are easily identified. Similarly, end reflections can be determined by calculating the delays involved in the round trip between each transducer and the substrate boundaries. (Bulk waves, with their potential for complex propagation paths, are not as easily related to observable time-domain responses, but these can often be determined from the frequency response with little difficulty.)

SAW measurements, therefore, require a simple means of measuring time-domain responses as a diagnostic method. Frequency domain measurements in both amplitude and phase over a sufficient bandwidth allow the time-domain response to be produced directly via a Fourier transform. The time resolution will equal the inverse of the measurement bandwidth.

Figures 2 and 3 show the measured frequency response and computed time-domain response of a typical SAW filter. Only Fig. 3 clearly shows the effects of electromagnetic breakthrough and triple transit. The analysis can continue from this point to calculate the step response or, indeed, the response to any given signal. As a particularly useful example, Fig. 4 shows the "eye" diagram (so called because of its characteristic shape) for a 3.75-MHz chip rate PSK signal after it



***9. A pulse-compression radar** serves as an example of the system-level potential of the SAW CAD package. The SAW pulse-compression loop shown here was designed and simulated according to the procedures illustrated earlier.*



***11. The SPEED software guided the design of new compensation** for the distorted return. The compressed pulse distortion has dropped to almost negligible levels at the close ranges.*

has passed through the filter with the response shown in Fig. 2. The filter has nearly optimal bandwidth, shape factor, and step response. The effect of an interfering signal in a channel just 4 MHz away and of equal magnitude and chip rate can be seen in Fig. 5.

The technique allows system performance to be simulated at the design phase and proven at the time of device measurement. While extremely effective as a developmental tool, it also leads to a new range of possibilities for production testing in which the test signals are synthetic and of infinite variety. The responses can be extracted with only one standard measurement facility.

Subsystems equally accommodated

The foregoing SAW bandpass-filter example illustrates the design and evaluation of a device and, to some extent, the performance of that device as part of a subsystem. However, complete subsystems, such as the SAW compressive receiver,* can also be handled by the software.

Figure 6 shows the "M(long)C" or "sliding transform" realization of this type of SAW subsystem.

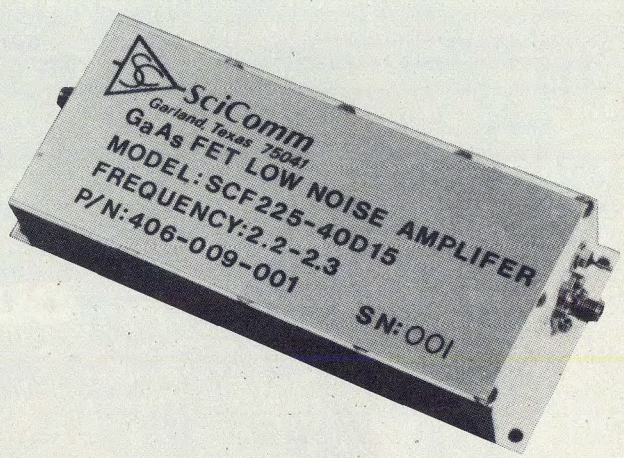
Fortran, the source language for SPEED, was selected to decrease execution time and increase code economy. Fortran also makes the software package reasonably machine

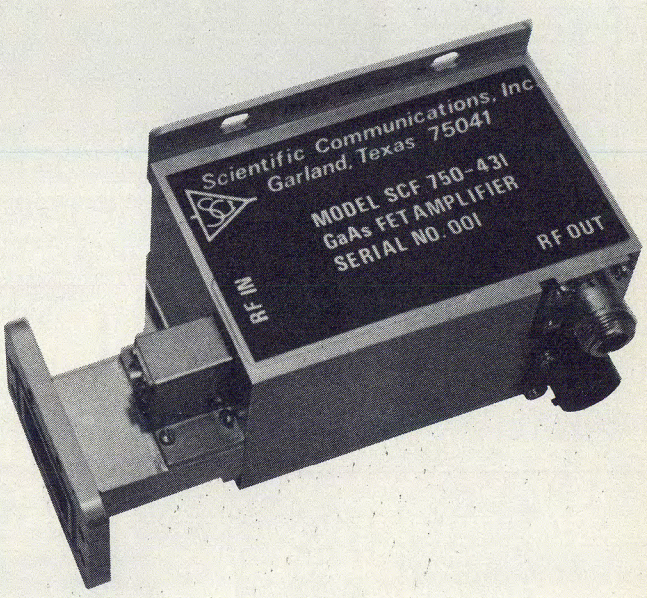
(continued on p. 162)

*The more conventional name for this subsystem is SAW spectrum analyzer. The term compressive receiver is used in the text to avoid confusion with the spectrum analyzer in the measurement system.

SciComm

Designing and supplying very low noise amplifiers for a multiplicity of military, industrial and commercial applications, SciComm has built a reputation of providing maximum amplification and minimum noise by means of Parametric, GaAs, FET and Bipolar technology.





SCIENTIFIC COMMUNICATIONS, INC.
3814 Cavalier Drive, Garland, TX, 74042
TEL (214) 487-0684 TWX 910 860 5099

READER SERVICE NUMBER 80

Control high-speed circuits with PIN diode switches

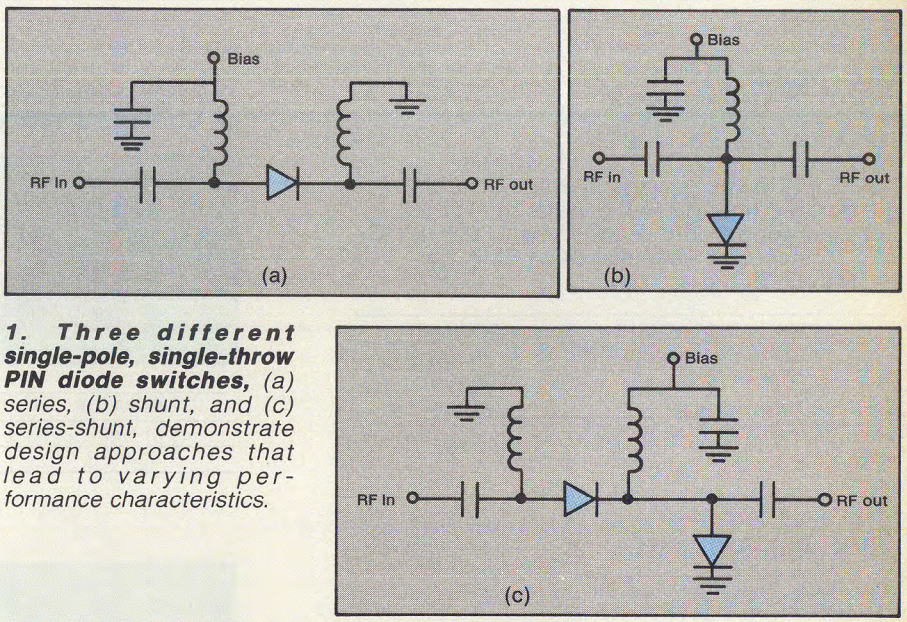
PIN diode switches act as powerful traffic controllers for high-speed circuits. Learning to use them is merely a matter of understanding a few important design trade-offs.

A PIN diode switch is one of the devices available to a designer who needs to control the path of an RF signal. It works well with small signals (less that +20 dBm) and can handle a wide range of frequencies, usually from 5 MHz to 18 GHz. Since it controls the signal path with a biased PIN diode, it is fast enough to be used for pulse modulation, signal sampling, and switching antenna arrays.

The most basic diode switch configurations[1-7] are series and shunt types. The series switch, shown in Fig. 1a, features low insertion loss—because of its simplicity—and good isolation at frequencies below 2 GHz. By connecting several switches together, multithrow switches can easily be constructed. The shunt switch, shown in Fig. 1b, has better isolation at frequencies above 2 GHz. It works effectively up to 18 GHz, after which it encounters excessive insertion loss and VSWR due to the shunt capacitance of the diode.

Shunt switch isolation can be improved by using several shunt diodes separated by quarter-wavelength transmission lines. Such a layout will more than double the isolation characteristics of a single-diode design. Although limited in bandwidth, the layout can provide isolation from 70 to 90 dB. Unfortunately, the additional components (e.g., bias chokes, shunt diodes, and transmission lines) cause an increase in insertion loss over the basic shunt design.

Shunt multithrow switches are difficult to construct; it's much easier to combine series and shunt switches into a layout such as the one in Fig. 1c. It's easy to increase the order of this switch by merely adding arms to the basic series-shunt topology (Fig. 2).



1. Three different single-pole, single-throw PIN diode switches, *(a) series, (b) shunt, and (c) series-shunt, demonstrate design approaches that lead to varying performance characteristics.*

The three main performance parameters for PIN diode switches are insertion loss, isolation, and VSWR. Insertion loss is usually determined by the complexity of a particular layout. An ideal switch would have an insertion loss of 0 dB but, unfortunately, typical values are usually between 0.5 and 2 dB. The parameter is explained by the following equation:

$$\text{Insertion loss} = 10 \log P_1/P_2$$

where P_1 and P_2 represent the power levels delivered to a load with the switch in and out of the signal path, respectively.

Isolation is sometimes referred to as the on/off ratio. It's a measure of the degree to which an unwanted signal is attenuated when the switch is in the off position. Its equation is similar to that for insertion loss:

$$\text{Isolation} = 10 \log (P_1/P_2)$$

except that P_1 and P_2 refer to the power delivered to the load with the switch in its on and off positions, respectively. Of course, the maximum possible isolation is a finite value. It's important to realize that for high isolation designs, insertion loss is sacrificed. Consequently, the judicious designer is one who never specifies more isolation than is needed.

In its isolated (off) state, a switch has reflective termination at each port. This design can be modified in order to present a matched termination to the RF signal in both the on and off states. This type of switch is called a "matched" or "terminated" switch.

The third switch parameter, voltage standing wave ratio (VSWR), refers to the degree of impedance matching present at a PIN diode switch RF port. It is usually given by the following equation:

$$\text{VSWR} = \frac{1+|\Gamma|}{1-|\Gamma|}$$

where the magnitude of Γ is equal to the square root of the ratio of the incident power at the switched RF port to the reflected power at the same port. Good VSWR usually follows from careful insertion loss design. For low VSWR, internal switch transmission line media, component parasitics,

Brian Bedard, Product Line Manager, Control Devices, Adams Russell, Anzac Div., 80 Cambridge St., Burlington, MA 01803.

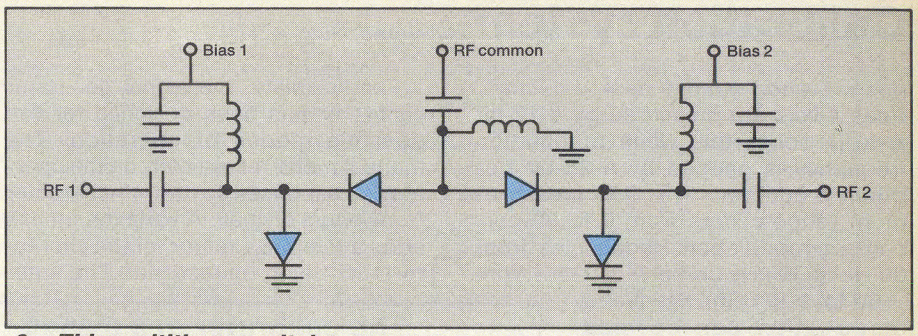
and RF port transitions must be considered. By reducing parasitics and creating an efficient switch topology, VSWR can be kept to a minimum.

Switching speeds

One of the special characteristics of PIN diode switches is fast switching time. For frequencies below 2 GHz, switching speeds as high as 1 to 2 μs are typical. Above this frequency, achievable speeds increase to 10 to 30 ns. Because of these speeds, PIN diode switches are often called upon to perform as pulse modulators or time multiplexers.

There are four main parameters used to define switching speed: rise time, fall time, on time, and off time. The first two are the most significant and are used to determine the upper limit in switching rate, as well as to indicate the minimum time needed for the switch to change states (on, off). It should be noted that a switch is considered "on" when 90 percent of the RF signal (a stable signal) is passing through it. By the same measure, a switch is "off" when only 10 percent of the RF signal is conducting through it. The rise and fall times are simply the times it takes a switch to climb or descend these high and low percentage levels.

On and off times take into account the trigger control pulse used to operate the switch. They are a measure of the total switching times for a particular design. The on time is a record of how long it takes a switch to reach the 90 percent level after 50 percent of the control pulse is applied. In contrast, off time signifies the time needed to reach the 10 percent level once 50 percent of the pulse command has been received. Although the on/off time parameter includes the pulse delay (which is internal to the switch), this delay can be designed out of a system by allowing adequate control lead time to anticipate the delay.



2. *This multithrow switch* *was constructed by adding arms to the basic configuration of Fig. 1c.*

Switching transients

Fast switching speed does not come without a price, and the cost is in switching transients. These appear at the RF ports as a result of the DC shifts that occur in the switch during the switching process. The spectral content of these transients can cause false signals to occur during switching. As switching speed increases, so does the amplitude of these transients.

There are a number of ways to specify switching transients. One approach is by calculating the maximum allowable amplitude of the transients found at each RF port. Another method measures only the spectral content of the transients that lies in the bandwidth of the switch.

Distortionless devices

Distortion is not a common problem with PIN diode switches because of the diodes they use. The PIN diode's intrinsic (I) layer provides enough spacing between the low-resistance positive (P) and negative (N) layers to create a relatively long transition time for charge carriers crossing the intrinsic boundary. The long transition time reduces the effects of nonlinear diode resistance on an RF signal. As a result, switches in the 2-to-18-GHz range are rarely specified for intermodulation distortion. At lower frequencies, however, the transition time is not long enough to prevent nonlinear effects, and second- and third-order intercept points can suffer degradation. Typical values are +30 dBm for a third-order intercept, and +60 dBm for a second-order intercept.

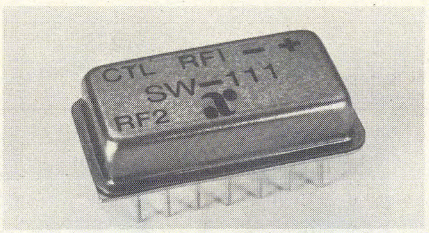
Switching speed and switching transients are two parameters that represent design trade-offs. In order to achieve high-speed switching, a certain amount of transients must be accepted. And the operating frequency bandwidth must always be considered. When unnecessary low-end frequency performance is specified, it can limit achievable speeds as well as boost transient amplitude levels. Another trade-off pair is insertion loss and isolation. Rarely does one change without affecting the other. Changes of 0.6 dB in insertion loss can mean as much as a 10-dB difference in isolation. Power operating levels can have severe consequences for all other parameters, especially isolation. The first step towards achieving a successful PIN diode switch design lies in understanding these trade-offs and specifying only those performance characteristics that are essential. ●●

References

1. Applications of PIN Diodes, Application Note 922, Hewlett-Packard Co., Palo Alto, CA.
2. PIN Diode Basics, Application Note 80200. Alpha Industries, Inc., Woburn, MA (1980).
3. PIN Diode Switching Times, Application Note 80900, Alpha Industries, Inc., Woburn, MA. (1980).
4. PIN Diode Designers Guide, Microwave Associates, 1980.
5. PIN Diode Designers Handbook and Catalog, Publication No. PD-500 Unitrode Corp., Watertown, MA (1979).
6. J.F. White, *Semiconductors Control*, Artech House Inc., Dedham, MA (1977).
7. Broadbanding the Shunt PIN Diode SPDT Switch, Application Note 957-1, Hewlett-Packard Co. (1974).

product feature

Model SW-111 is one member of a new line of PIN diode switches that covers three different frequency ranges in the 5-to-2000-MHz band. This switch operates over the full bandwidth with isolation of at least 50 dB, and up to 80 dB below 100 MHz. Its other key parameters, insertion loss and VSWR, are 2 dB and 1.5:1, respectively, across all frequencies. The SPST switch is designed to tolerate temperatures from −55 to +85°C and exhibits a typical on time of 2 μs and a typical off time of 1 μs. Its 1-dB compression point is typically +13 dBm. P&A: $175 (100 qty.); 10 wks. **Adams Russell, Anzac Div., 80 Cambridge St., Burlington, MA 01803. (617) 273-3333.**



CIRCLE NO. 393

Calibration system (continued from p. 149)

positive and negative peak detectors. Peak levels are measured by a 12-bit A-to-D converter, while modulation frequency is gauged by a 28-bit frequency counter. The AM measurement range covers from 0 to 90 percent at modulation frequencies from 30 Hz to 10 kHz and power levels from −60 to +10 dBm. Frequency modu-lation can be measured in a frequency deviation range from 0 to 300 kHz for modulation frequencies from 30 Hz to 10 kHz in the same power level range as for AM.

The many functions of the VM-24 are keyed to an internal reference source at 30 MHz. It has three output levels: 0, −20, and −30 dBm. It can be amplitude modulated by 30 percent and frequency modulated by a 1-kHz signal to a peak deviation of 50 kHz. Since these signals are microprocessor controlled, a self-test sequence can be set up to verify the accuracy of the test functions.

For flexibility, the signal generator calibrator has been designed for five possible modes of operation. The manual mode relies solely on the operator's responses to the 40-character front-panel display. A variation on this adds a tolerance factor for the characteristic being measured. The calibrator will simply display "pass" or "fail" according to the tolerance entered. A third mode, called local programmed operation, allows the operator to store up to 200 parameters via the front panel. The VM-24 can also be operated in a remote mode via the GPIB bus. In this mode, the controller commands the instrument by mnemonic codes corresponding to the front-panel push-buttons. The final mode controls the calibrator through the GPIB by direct computer interaction.

The VM-24 is relatively portable; each of its two instrument cabinets weighs about 50 lbs. Each cabinet contains its own power supply assembly and is suitable for rack mounting. P&A: $70,200; contact factory for availability. **Weinschel Engineering, One Weinschel Lane, Gaithersburg, MD 20760. (301) 948-3434, TWX: (710) 828-9705, Telex: 898352.**

CIRCLE NO. 394

The calibrator at a glance

Measurement	Specification
Power	
Frequency range	10 MHz to 18 GHz
Input range	+20 to −90 dBm
Resolution	0.01 dB
Accuracy	±0.5 dB
Attenuation	
Dynamic range	>100 dB
Resolution	0.001 dB
Accuracy	0.03 dB/10 dB
AM	
Modulation frequencies	30 Hz to 10 kHz
Percent modulation	0 to 90 percent
Power range	+10 to −60 dBm
FM	
Modulation frequencies	30 Hz to 10 kHz
Deviation range	DC to 30 kHz

Broadband DF SYSTEMS

0.5 to 18 GHz or 18 to 40 GHz with a single feed.
Includes sector scan, manual, and continuous rotation modes.
Other coverage available from 0.1 to 40 GHz.
Digital interface for computer control.
New technology lowers cost.



EM Systems, Inc. 290 SANTA ANA CT., SUNNYVALE, CA. 94086 (408) 733-0611 TWX: 910-339-9305

READER SERVICE NUMBER 63

SENIOR IC DESIGN ENGINEER

Motorola's Government Electronics Group in Arizona has an exceptional opportunity for a motivated individual to work in our custom design Integrated Circuit Facility.

It's a chance to do challenging and involving work for an experienced engineer whose interests and background are in high technology microstrip design and analysis and the processing technology required for implementation. Experience in Ka-band is required and we prefer BSEE/MSEE or BS Physics with at least 5 years MIC design background. Strong rewards are offered, plus the position offers advancement opportunities into Project/Product Management. For consideration, please send resume or call collect: Dotti Morris, 602-949-3759.

MOTOROLA INC.

Government Electronics Group

8201 E. McDowell Rd.
Scottsdale, AZ 85252
Dotti Morris, Dept. 1162

"Motorola, A World Leader in Electronics — Quality and Productivity Through Employee Participation in Management"

An Equal Opportunity/Affirmative Action Employer

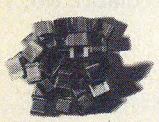
NEW

Here at last!
The chip capacitor & filter for mobile radio use.

CHIP MICA CAPACITORS

Extremely high Q and high rated voltage make these ideal for electric amplifier units.

- Extremely high Q — your No. 1 capacitor choice for high-frequency applications.
- Minimum capacitance tolerance of ±0.25% or ±0.25pF, whichever is greater.
- Excellent crack-free performance after being subjected to thermal shock. Plus — no need for pre-heating or solder containing silver.
- Highly reliable because they utilize the inherent characteristics of mica.

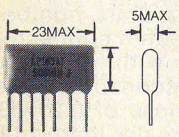


Type	Max. Capacitance (PF)		Dimensions (mm)		
	100WV	500WV	W	H	T
UC12	43		2	1.25	1.4
UC23	240	91	3.2	2.5	1.5
UC34	820	470	4.5	3.2	2.0
UC55	2000	1200	5.6	5.0	2.0

PRINTED FILTER

Save time... reduces the work process because the units are miniature and require no manual adjustment.

- Minimal dispersion and good temperature characteristics because of their monolithic mica-based structure.
- Good space factor because of their thinness.
- High reliability because few connections are required.



Type	Pass Band (MHz)	Type	Pass Band (MHz)
LP163A1	0 — 163	LP512A1	0 — 512
LP174A1	0 — 174	BP465A1	465±5
LP400A1	0 — 400	BP876A1	876±10
LP470A1	0 — 470	BP910A1	910±10

- LP's insertion loss is 0.7dB max., and input & output impedance is 50ohms.
- Can be manufactured to custom requirements if simulation data is available.

SOSHIN **SOSHIN ELECTRIC CO., LTD.**
1-18-18 Nakamagome, Ohta-ku, Tokyo, Japan. TELEX: 246-6377

READER SERVICE NUMBER 87

COMPUTER-AIDED SAWS *(continued from p. 147)*

independent and more easily transported from one computer to another. The listing in the table shows the manner in which the use of keywords (CHIRP, for example) simplifies the entry of data and the generation of graphics. The table (p. 145) gives the SPEED command file required to simulate its operation. The simulation produces a graphic output of the receiver's performance for the specified input signal (Fig. 7).

A designer may wish to examine the performance of the subsystem further by including the bandpass responses of lumped-element matching networks associated with the SAW devices, or the characteristics of interstage amplifiers. Amplitude and phase variations caused by these and other effects can translate directly into spurious side lobes in the response. These side lobes must be checked to insure that their level isn't greater than that determined by the specified spectral weighting function.

Figure 8 depicts the effect of 0.5-dB ripple Chebyshev bandpass matching networks at the input and output transducers of each SAW device. Noise can also be incorporated at key points in the procedure, and the overall simulation made as simple or as complex as desired.

The information determined from the simulation guides the design of suitable SAW devices and the specification of other key components in the signal-processing chain. As previously explained, the SAW device design in this case is almost entirely automated.

After the SAW devices have been fabricated and linked to their input and output matching networks, their responses can be measured and recorded on the automatic network analyzer system. The analyzer simulation is simply repeated with the measured SAW responses replacing their theoretical counterparts. Instead of only simulating the subsystem's potential performance, this process emulates the actual subsystem performance. This method has obvious benefits when devices must be selected from a newly fabricated batch to fulfill the required specifications of high-performance systems. In this way, it obviates the need for an individual device specification which may be difficult to set as well as leading to lower production yields by setting a higher standard than is necessary.

Complete SAW compressive receivers designed according to this process have performed very closely to predictions based on the emulation. The emulated results are easier to produce in many ways, and such synthetic test and selection procedures can be expected to become more commonplace in the future.

System applications possible

The simulation package can also be applied to design and testing on a system level. Pulse-compression radar (Fig. 9) illustrates this use of the package. This SAW compression loop has been designed and simulated according to the procedure previously described.

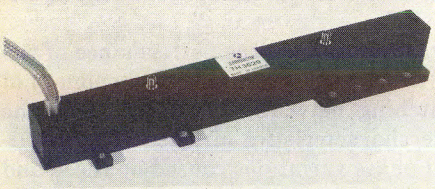
In long-pulse radars used for long-range coverage, a time-varying gain applied to compensate for the R^{-4} dependency of the received signal strength is unavoidably transferred to the pulse shape of a target return at any fixed range. This effect results in a distortion of the form:

$$d(t) = A_o(t/t_{max})^4 \qquad (2)$$

In Eq. 2, t = the return time at the range in question, and t_{max} = the return time at the maximum range. For example, if a radar has a maximum range equivalent to 330 μs (50 km) and transmits a 33-μs pulse, a target at 5 km will

TUBES

TWT generates 20 W at 7 GHz



Model TH 3628 is a traveling-wave tube designed for satellite transponders. It is capable of more than 20 W output power from 7.250 to 7.375 GHz. The tube has a typical efficiency of 43 percent, and employs an impregnated-tungsten cathode for long operating life. **Thomson CSF, Electronic Tubes Div., 38 rue Vauthier, 92100 Boulogne-Billancourt, France. (1) 604 81.75.**

CIRCLE NO. 406

TOOLS

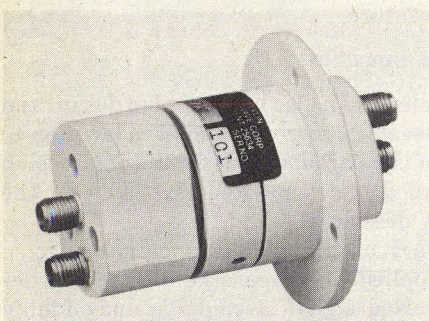
Contact springs aid in diode installation

Gold-plated contact springs offer a ready solution when installing diodes which may need to be tuned or replaced. Springs are available in diameters from 0.037 to 0.125 in. and in lengths from 0.043 to 0.142 in. The contacts feature self-inductances as low as 0.3 nH and insertion losses of 0.001 dB at 10 GHz. P&A: $750 to $999; stock. **Servometer Corp., 501 Little Falls Rd., Cedar Grove, NJ 07009. (201) 785-4630.**

CIRCLE NO. 407

PASSIVE COMPONENTS

Two-channel rotary joint bridges DC to 18 GHz



Model 2267X is a compact, dual-channel rotary joint which can handle frequencies from DC to 18 GHz with 60-dB isolation between channels. P&A: $2700; 90 days. **Kevlin Microwave Corp., 26 Conn St., Woburn, MA 01801. (617) 935-4800, TWX: (710) 393-1239.**

CIRCLE NO. 408

PASSIVE COMPONENTS

Coaxial relays offer low isolation loss

Coaxial relays in the R565000 series are designed for applications in automatic test systems, airborne scramblers, and radar. The units operate over the frequency range from DC to 18 GHz with an isolation loss of no more than 0.5 dB. The isolation is at least 70 dB from DC to 6 GHz, and at least 60 dB over the rest of the range. The VSWR is no higher than 1.5:1. Relays are available with SMA connectors in SPDT and DPDT models. **Radiall, Microndе Dept., 101 rue Philibert Hoffman, Zone Industrielle Ouest 93116, Rosny sous Bois, France. 854-80-40, Telex: RADIA A 220673F.**

CIRCLE NO. 409

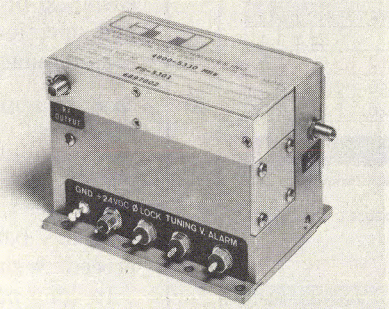
WSMA adapter spans DC to 26.5 GHz

Model 34SFSF50 is a WSMA adapter (SMA compatible) which features center conductors that can be replaced in the field. It uses a 3.5-mm connector with an air dielectric. While its specified operating range is from DC to 26.5 GHz, the adapter is usable up to 34 GHz. P&A: $150 and up; 30 days. **Wiltron Co., 805 E. Middlefield Rd., P.O. Box 7290, Mountain View, CA 94042.**

CIRCLE NO. 410

SOURCES

Phase-locked sources are remotely programmable



Phase-locked sources in the FS series can be remotely tuned via a DC tuning voltage. The units, which cover the frequency range from 1 to 19 GHz in different bandwidths, feature frequency switching times of less than 1 ms. P&A: 30 to 90 days. **Communications Techniques, Inc., 36 Rt. 10, East Hanover, NJ 07936. (201) 884-2580.**

CIRCLE NO. 411

ATTENUATORS

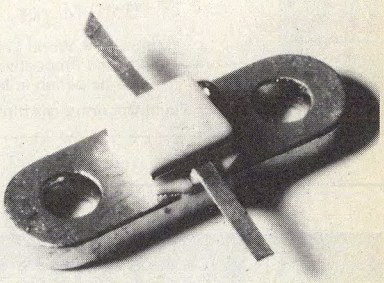
Low-cost attenuators cover DC to 1.5 GHz

The AT-75 series of 75-ohm attenuators are usable over the range from DC to 1.5 GHz. They are available in 2, 3, 6, 7, 10, 14, and 20 dB steps. These units have a typical VSWR of 1.2:1 and can handle up to 500 W on peaks. P&A: $14 to $20; stock to 30 days. **Elcom Systems, Inc., 4032 Clint Moore Rd., Boca Raton, FL 33431. (305) 994-1774.**

CIRCLE NO. 412

TRANSISTORS

Power GaAs FETs reach 10.7 GHz



Two GaAs FET power transistors have been designed for frequency use up to 10.7 GHz with 7-dB gain. Model CFX30 is rated at 100 mW output and model CFX31 will provide 250 mW output power. P&A: $125.50 (CFX30) and $145 (CFX31); (1 to 9 qty.).; stock to 8 wks. **Amperex Electronic Corp., 230 Duffy Ave., Hicksville, NY 11802. (516) 931-6200.**

CIRCLE NO. 413

CABLES AND CONNECTORS

Cable connector operates mode-free to 18 GHz

A type-N coaxial plug connector features mode-free performance from DC to 18 GHz. Part number 3001-7941-00 is a 50-ohm connector designed for use with 0.141-in. diameter cable. The connector has a maximum insertion loss of 0.21 dB and a VSWR of no greater than (1.06 + 0.006f):1 over the full frequency range. P&A: $8.13 (100 qty.); stock to 6 wks. **M/A COM, Omni Spectra Inc., 21 Continental Blvd., Merrimack, NH 03054. (603) 424-4111, TWX: (710) 366-0674.**

CIRCLE NO. 414

return a pulse that will be distorted by a nonlinear ramp with a total excursion of 11 dB within the receiver. Among other distortions, the analysis must consider amplitude limiting and phase distortions in the transmit amplifier, Doppler shift from a moving source or target, and small SAW velocity deviations caused by processing defects, aging, and temperature shift.

The same general principles for simulations at the device and subsystem level apply to system performance as well. The process usually starts with the specification of the SAW device or other components, and flows progressively through the device, subsystem, and system simulations. When the effect of each element on system performance is determined, a set of device designs which best satisfy the overall requirement can be determined by working backwards from the final system design.

Figure 10 shows the effect on the compressed pulse for a hypothetical radar system. Distortion is greatest at short ranges and almost negligible at long ranges. Unfortunately, a greater density of targets can usually be expected at closer ranges (such as seen in air traffic control). A means must be found to compensate the SAW matched filter in the receiver at some intermediate range to achieve a useful compromise.

In Fig. 11, this compensation has been accomplished for the 5-km range. Almost negligible compressed pulse distortion occurs at close ranges, and the distortion incurred near the maximum range is considered more acceptable than it would be at close range. The SPEED program allowed this solution to be found expeditiously since system parameters could be readily varied and system performance quickly determined.●●

Acknowledgment

The author wishes to give credit to the colleagues who have made many fundamental contributions to this work. In particular, M.C. Davie who developed the SPEED simulation package, and N.D.J. Miller and A.P. Malarky who developed present SAW CAD and measurement software.

REVISED

U.S. POSTAL SERVICE

STATEMENT OF OWNERSHIP, MANAGEMENT AND CIRCULATION

(Required by 39 U.S.C. 3685)

1. TITLE OF PUBLICATION	A. PUBLICATION NO	2. DATE OF FILING
MICROWAVES	7 9 7 6 8 0 0 0	2/5/82
3. FREQUENCY OF ISSUE	**A. NO. OF ISSUES PUBLISHED ANNUALLY**	**B. ANNUAL SUBSCRIPTION PRICE**
Monthly except for 2 issues in September	13	$30.00

4. COMPLETE MAILING ADDRESS OF KNOWN OFFICE OF PUBLICATION (Street, City, County, State and ZIP Code) (Not printers)

50 Essex St., Rochelle Park, Bergen County, NJ 07662

5. COMPLETE MAILING ADDRESS OF THE HEADQUARTERS OR GENERAL BUSINESS OFFICES OF THE PUBLISHERS (Not printers)

50 Essex St., Rochelle Park, NJ 07662

6. FULL NAMES AND COMPLETE MAILING ADDRESS OF PUBLISHER, EDITOR, AND MANAGING EDITOR (This item MUST NOT be blank)

PUBLISHER (Name and Complete Mailing Address)

Stacy V. Bearse, 50 Essex Street, Rochelle Park, NJ 07662

EDITOR (Name and Complete Mailing Address)

Stacy V. Bearse, 50 Essex Street, Rochelle Park, NJ 07662

MANAGING EDITOR (Name and Complete Mailing Address)

Walt J. Boisza, 50 Essex Street, Rochelle Park, NJ 07662

7. OWNER (If owned by a corporation, its name and address must be stated and also immediately thereunder the names and addresses of stockholders owning or holding 1 percent or more of total amount of stock. If not owned by a corporation, the names and addresses of the individual owners must be given. If owned by a partnership or other unincorporated firm, its name and address, as well as that of each individual must be given. If the publication is published by a nonprofit organization, its name and address must be stated.) (Item must be completed)

FULL NAME	COMPLETE MAILING ADDRESS
Hayden Publishing Co., Inc.	50 Essex St., Rochelle Park, NJ 07662
James S. Mulholland, Jr.	50 Essex St., Rochelle Park, NJ 07662

8. KNOWN BONDHOLDERS, MORTGAGEES, AND OTHER SECURITY HOLDERS OWNING OR HOLDING 1 PERCENT OR MORE OF TOTAL AMOUNT OF BONDS, MORTGAGES OR OTHER SECURITIES (If there are none, so state)

FULL NAME	COMPLETE MAILING ADDRESS
None	

9. FOR COMPLETION BY NONPROFIT ORGANIZATIONS AUTHORIZED TO MAIL AT SPECIAL RATES (Section 411.3, DMM only)

The purpose, function, and nonprofit status of this organization and the exempt status for Federal income tax purposes (Check one)

☐ (1) HAS NOT CHANGED DURING PRECEDING 12 MONTHS ☐ (2) HAS CHANGED DURING PRECEDING 12 MONTHS (If changed, publisher must submit explanation of change with this statement.)

10. EXTENT AND NATURE OF CIRCULATION	AVERAGE NO. COPIES EACH ISSUE DURING PRECEDING 12 MONTHS	ACTUAL NO. COPIES OF SINGLE ISSUE PUBLISHED NEAREST TO FILING DATE
A. TOTAL NO. COPIES (Net Press Run)	43,294	43,248
B. PAID CIRCULATION 1. SALES THROUGH DEALERS AND CARRIERS, STREET VENDORS AND COUNTER SALES	---	---
2. MAIL SUBSCRIPTION	947	1,130
C. TOTAL PAID CIRCULATION (Sum of 10B1 and 10B2)	947	1,130
D. FREE DISTRIBUTION BY MAIL, CARRIER OR OTHER MEANS SAMPLES, COMPLIMENTARY, AND OTHER FREE COPIES	41,384	41,254
E. TOTAL DISTRIBUTION (Sum of C and D)	42,331	42,384
F. COPIES NOT DISTRIBUTED 1. OFFICE USE, LEFT OVER, UNACCOUNTED, SPOILED AFTER PRINTING	963	864
2. RETURN FROM NEWS AGENTS	---	---
G. TOTAL (Sum of E, F1 and 2 - should equal net press run shown in A)	43,294	43,248

11. I certify that the statements made by me above are correct and complete

SIGNATURE AND TITLE OF EDITOR, PUBLISHER, BUSINESS MANAGER, OR OWNER: Stacy V. Bearse, Publisher/Editor

PS Form 3526 July 1981 (See Instruction on Reverse) (Page 1)

MICROWAVE TECHNOLOGY

AIRTRON

Continues to lead the way
—IN ADVANCED DESIGN
—IN MANUFACTURING
—IN MARKETING

VISIT US AT THE MTT SHOW IN DALLAS, JUNE 15, 1982 BOOTH 425.

To continue our growth we are adding proven marketing and engineering professionals. Openings are currently available for:

SENIOR DESIGN ENGINEER Magneto-Static Wave (MSW) devices. Need PHD in EE or physics with thorough knowledge and understanding of electromagnetic wave propagation.

REGIONAL SALES MANAGER BSEE or equivalent microwave background with a minimum 3-5 years solid sales experience.

EXPORT SALES MANAGER BSEE or equivalent microwave background with a minimum 3-5 years relevant export experience.

MICROWAVE/RF DESIGN ENGINEERS MSEE or at least 5 years experience in Microwave or RF circuit design of waveguide, stripline or MIC components.

Along with a challenging and professional atmosphere we offer an outstanding remuneration and benefits package. Our location in North Central New Jersey is one of the most livable (and affordable) areas in the U.S.

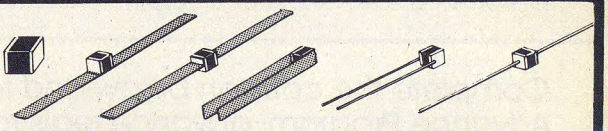
Relocation assistance? Of course!

For a personal interview please forward your resume including salary history to:
Mr. Paul Csigi, Director of Personnel
AIRTRON Division of Litton
Litton 200 East Hanover Ave., Morris Plains, New Jersey 07950
An Equal Opportunity Employer M/F

Ultra Q MICROWAVE CAPACITORS

QPL

MIL-C-55681B



CDR11 thru CDR14
CDR21 thru CDR25

write for NEW CATALOG

REPUBLIC
ELECTRONICS CORPORATION
176 E. 7th St., PATERSON, N.J. 07524
201-279-0300 TWX 710-988-5908

READER SERVICE NUMBER 88

June 1982
Vol. 21, No. 6

MICROWAVES
laser technology
A Hayden Publication



about the cover

Designers of amplifiers in the 26.5-to-40-GHz band now have an alternative to bulky and expensive Gunn-diode circuits and TWTs. In this issue, industry researchers announce that a GaAs FET has broken the 26.5-GHz barrier, and is offering substantial gains up to the 40-GHz line. (Cover photograph courtesy of Avantek, Inc., Santa Clara, CA; Randall C. Hirai, Senior Art Director.)

p. 67

departments

13 Feedback
49 R&D Roundup
58 For Your Personal Interest
62 Editorial
124 Bookshelf
126 InfoCenter
128 Looking Back
128 Looking Ahead

news

15 **Confusion mounts over DBS as FCC readies its decision.** A look at the questions posed by the emerging DBS market, including a talk with Dr. Bernard Jacobs, president of Orrox Corp.'s Satcom Division, and sketches of leading companies in the field.

22 FCC approves 930-MHz paging . . . **27** Setting radiation standards: A highly charged issue . . . **30** South Pacific islands enter satellite age . . . **35** GAO hopes Congress sees the light on laser weapons . . . **35** RCA seeks three K-band satcoms . . . **36** A new twist in antenna designs . . . **36** AEA backs education bill . . . **38** New image for Mars . . .

41 International • **43** Washington • **55** Meetings • **56** Industry

design features

67 **GaAs FET Amplifiers Reach Millimeter Waves.** In this month's cover feature, John C. Rosenberg and coworkers at Avantek show how optical lithography is helping to make K-band GaAs FETs ready for production.

71 **Multiplier Circuits Keep Phase Clean.** Lori Hoberg, of Hewlett-Packard, shows how low phase-noise microwave signals can be generated and measured.

83 **MIC Sources Hold Key To Future EW Systems.** Walter A. Crofut and Allan Reynolds, at Narda, explain how MICs can reconcile source problems of growing size and increased performance.

89 **GaAs FET Circuits Begin With Biasing Choices.** Jerry Arden, of California Eastern Labs, begins a five-part series on FET design tools by providing a review of biasing methods and considerations.

93 **GaAs FET IMD Demands Better Standard.** C. Hsieh, of Harris Corp.'s Farinon Div., offers alternatives to third-order intercept as an indicator of linearity.

97 **Shielding Barriers Block Electromagnetic Waves.** Peter S. Grant, of Technit, starts a five-part series on EMI shielding by examining how signals are attenuated through absorption, reflection, and rereflection.

product technology

99 **Product Features**—Small-signal devices keep DBS market vigil . . . **106** Three transistors take on cellular communication challenges . . . **107** Two bipolar transistors boast small price tags . . . **108** Dielectric resonator oscillator offers stable LO performance . . . **110** Versatile opamp delivers high speed and broad bandwidth

111 New Products • **119** New Literature • * **121** Application Notes

*International Editions Only.

Multiplier Circuits Keep Phase Clean

When the close-in phase noise of the signal is critical, a low-noise RF source can be multiplied to the desired microwave band. Automatic measurements of these signals can be made with a two-source method.

SIGNAL requirements at microwave frequencies have become more stringent as radar and communication systems have grown in complexity and improved in performance. Since these improvements have increased the need for generating and measuring low-noise signals, this article presents a review of phase-noise concepts and an analysis of generation and measurement techniques.

The quality of a signal can be evaluated according to either its long-term or short-term stability. Long-term stability, or drift, refers to changes in the frequency over minutes, hours, days, and longer periods. Drift results from fairly well-known phenomena, such as the aging of the crystal oscillator used as a reference source. Because these long-term variations of the signal can be predicted, designers can compensate for their effects with relative ease.

Short-term instabilities, which include fluctuations in a signal's phase or frequency that last less than a few seconds, cannot be dealt with as easily. These instabilities usually result from random phenomena.

Phase and frequency related

Since frequency and phase are related by the expression:

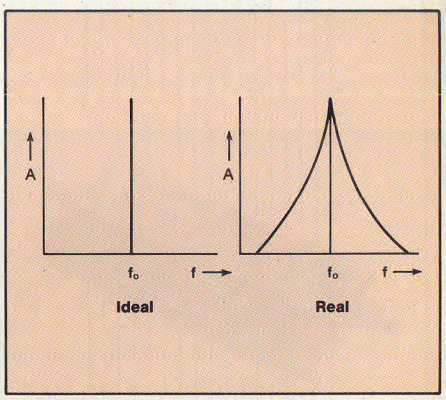
$$f(t) = \frac{1}{2\pi}\left(\frac{d\phi(t)}{dr}\right) \qquad (1)$$

either phase fluctuations or frequency fluctuations can describe the same signal. The most widely used method describes short-term instabilities as phase noise. The random nature of these instabilities is reflected in the practice of representing phase deviation as a spectral density distribution in the frequency domain.

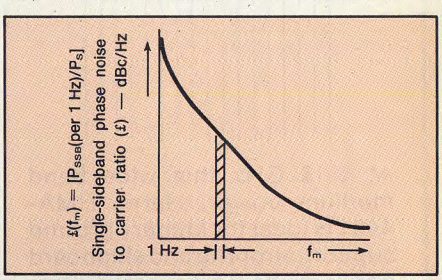
The easiest way to understand phase noise is by envisioning a spectrum analyzer display of a signal (Fig. 1) with the noise modulation sidebands frequency modulated and any residual AM modulation assumed to be negligible. A CW signal viewed on the display will not appear as a discrete spectral line (the "ideal"), but will spread modulation sidebands over frequencies both above and below the nominal frequency (the "real" waveform shown in Fig. 1).

Since the display is symmetrical, the signal can be characterized by looking at only one of its sides. Hence, the *single sideband (SSB) phase noise* is defined as the ratio of the power in one sideband (P_{SSB}), within a 1-Hz bandwidth at a specified carrier offset frequency (f_m), to the total signal power (P_S). This ratio is designated as £(f). Therefore, as Fig. 2 shows, £(f) is

(continued on next page)

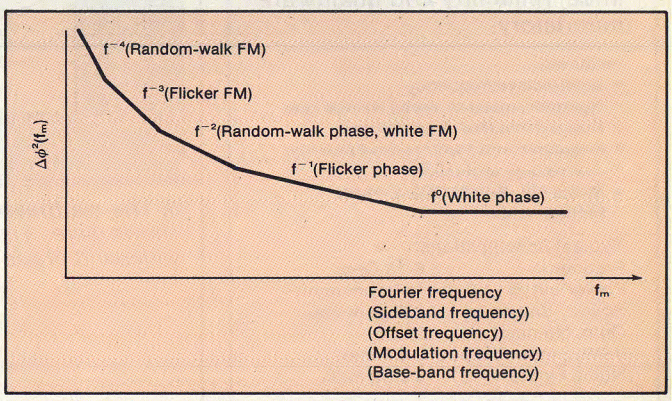


***1. Short-term instabilities** spread the carrier across modulation sidebands.*

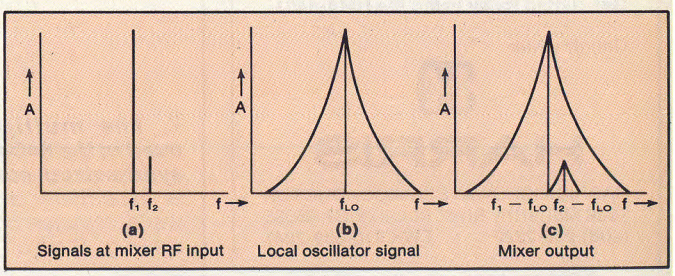


***2. A normalized SSB phase-noise ratio** describes short-term stability.*

***3. Several types of noise** produce the phase-noise spectral density distribution. Each describes a particular slope of the phase-noise curve and depends on the noise figures of the devices in the oscillator, and on the oscillator's Q factor.*

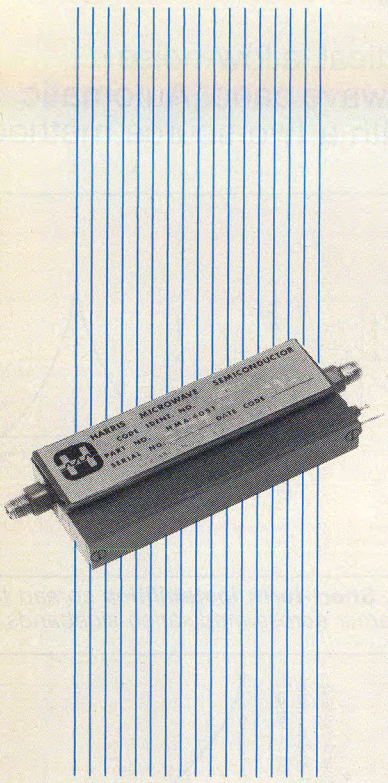


***4. LO noise can degrade a receiver's sensitivity.** When two signals (a) are downconverted, the noise of the LO (b) is transfered to the mixer products (c).*



Lori Hoberg, Product Marketing Engineer, Hewlett-Packard Co., 1620 Signal Dr., Spokane WA 99220.

ECM GaAs FET Amplifiers



At 6-18 GHz this wide band medium power, Harris HMA-4401 is ideal for Military ground support, airborne and shipboard applications. This is particularly true where superior performance, reliability and quality are mandatory.

Features:
- **Multi-octave frequency**
- **Hermetic, metal-to-metal welded case**
- **Rugged thin film construction**
- **Regulated input with reverse polarity/ overvoltage protection**
- **Meets MIL-E-5400/MIL-E-16400 requirements**

Typical Specifications

Frequency	6-18 GHz
Power out @ -1.0 db	+17 dbm min.
Power, Saturated	+23 dbm max.
Gain, Nominal	30 db
VSWR, input/output	2.0:1 max.
Noise Figure	8.0 db max.

Get started today using the HMA-4401

Call or write:

HARRIS

HARRIS MICROWAVE SEMICONDUCTOR
1530 McCarthy Blvd., Milpitas, CA 95035
(408) 262-2222 TWX 910-338-2247

READER SERVICE NUMBER 90

 (continued from p. 71)

a normalized frequency domain measure of phase fluctuation sidebands in dBc/Hz.

For phase changes much less than unity ($\Delta\phi_{RMS} \ll 1$), $\pounds(f_m)$ can be expressed as:

$$\pounds(f_m) = .5\Delta\phi_{RMS}^2 = .5\left(\frac{\Delta f_{RMS}}{f_m}\right)^2 = \frac{P_{SSB}}{P_s} \quad (2)$$

In addition, the following equations relate $\pounds(f_m)$ to the spectral densities of the phase (Eq. 3) and the frequency (Eq. 4) fluctuations of the signal:

$$S_{\Delta\phi}(f_m) = \Delta\phi_{RMS}^2 = 2\pounds(f_m) \quad (3)$$

$$S_{\Delta f}(f_m) = \Delta f_m^2(f_m) = f_m^2 S_{\Delta\phi}(f_m) = 2f_m^2\,\pounds(f_m) \quad (4)$$

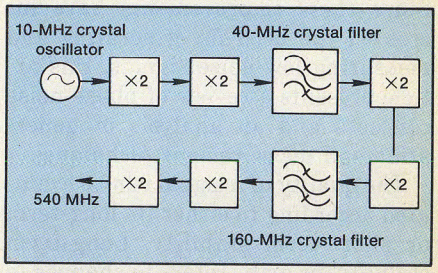
In the above expressions, $\Delta\phi_{RMS}$ = the RMS phase fluctuation, Δf_{RMS} = the RMS frequency fluctuation, $S_{\Delta\phi}$ = the spectral density of the phase fluctuations, and $S_{\Delta f}$ = the spectral density of the frequency fluctuations.

Causes of phase noise

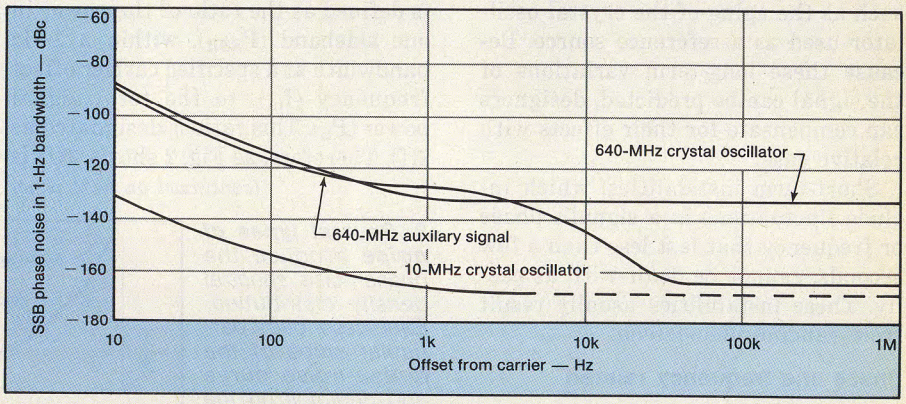
The close-in noise of a source depends on several factors. For example, the phase-noise spectral density distribution results from different types of noise: random walk, flicker, and white noise. Each describes a particular slope of the phase noise curve (Fig. 3) and depends on both the active-device characteristics in the oscillator and on the resonator's Q.[1,2]

Phase noise can be a major limiting factor in frequency conversion applications dealing with signals that span a wide dynamic range. For example, when two signals are present at the input of a high-performance heterodyne receiver (Fig. 4), they will mix with the local oscillator (LO) and be converted to lower intermediate frequencies (IF). Highly selective IF filters can separate the desired signal for amplification, detection, and baseband processing.

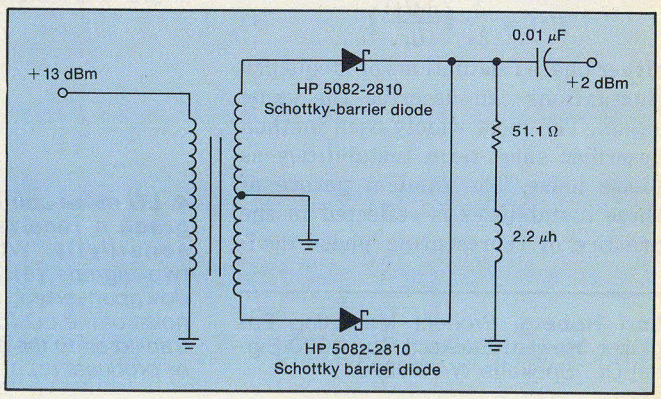
If the desired signal is the larger of



5. Synthesized sources outperform fundamental oscillators. *This scheme produces a 640-MHz reference.*



6. The synthesized source *shown in Fig. 5 produces the phase noise characteristic shown here. The monolithic crystal filters at 40 MHz and 160 MHz reduce the wideband phase noise.*



7. The multiplier used in the 640-MHz synthesized source *is essentially a full-wave rectifier circuit using Schottky diodes.*

the two, a properly designed receiver should recover it without difficulty. However, if the desired signal is the smaller of the pair, the LO phase noise becomes a critical factor.

Figures 4b and 4c show the effect of the LO's phase noise; any noise in the LO signal translates directly to the mixer products, $f_1 - f_{LO}$ and $f_2 - f_{LO}$. Notice that the translated noise of the LO in the mixer output will completely mask the smaller signal and prevent its recovery even if the receiver's IF filtering can remove the mixing product of the larger signal.

A noisy local oscillator signal can degrade both the selectivity and usable dynamic range of the receiver. Therefore, the LO design must be carefully selected.

For an application such as the receiver LO discussed above, there are several critical signal performance requirements. First, the SSB phase noise must be well known at various offsets from the carrier to insure that it is well below the selectivity specified for the receiver. The required performance can be calculated from the following:

$$\pounds(f_m) = S + C + M \qquad (5)$$

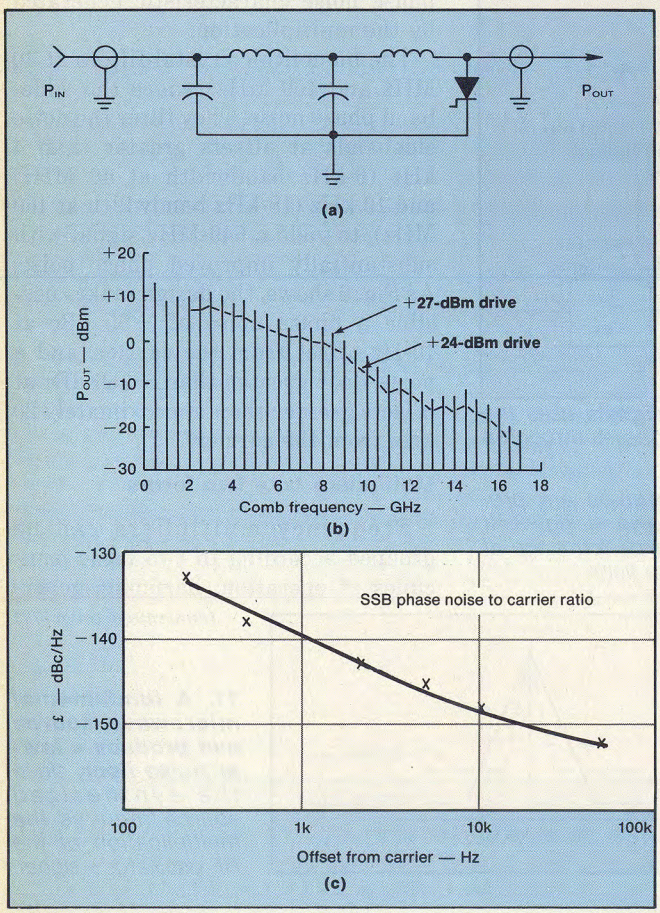
In Eq. 5, $\pounds(f_m)$ = the LO noise at the offset frequency ($f_2 - f_1$), S = the specified receiver selectivity, C = the conversion from the receiver noise bandwidth to a 1-Hz bandwidth, and M = the measurement margin. In a typical system, a measurement margin of at least 10 dB is desirable, and the bandwidth conversion, C, is given by:

$$C = 10 \log_{10} \left(\frac{\text{Receiver IF BW}}{1 \text{ Hz}} \right) \qquad (6)$$

In addition to good short-term stability, the ideal low-noise source must meet other requirements. As the IF bandwidth of receivers gets more narrow (thus increasing the selectivity) the long-term stability and resolution become more important. For this reason, synthesized signals (which are derived through mixing, multiplying, or dividing a stable reference) are becoming more popular than signals generated by fundamental oscillators.

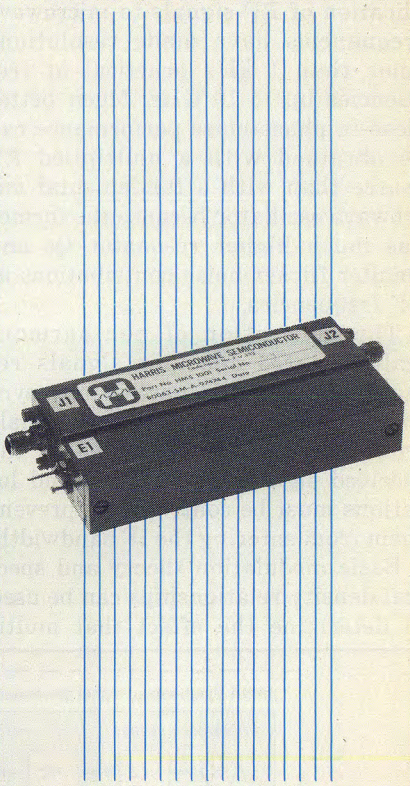
The stability and resolution of a fundamental oscillator (a tuned circuit or a resonant cavity) are limited by its components. In a synthesizer, the stability of a reference (such as a temperature-controlled crystal) is transferred directly to the output. The aging rates, which can now be achieved on the order of 10^{-10}PPM/day,

(continued on next page)



8. A simpler step-recovery-diode multiplier *will not significantly add to the phase noise after the 640-MHz reference signal has been generated. The phase noise of a typical step-recovery diode is sensitive to drive level. As the drive level is increased beyond the 24-dBm optimum, more phase noise is generated. (This level, however, must be exceeded in the final application, since the step-recovery-diode multipliers were designed for operation at 500-MHz frequency.)*

Communications
GaAs FET Amplifiers



Operating in X band, Harris GaAs FET Driver Amplifiers are ideal for many communication applications. All of this backed by our dedication to state of the art design, processing and assembly techniques.

Features:
- **Hermetic, metal-to-metal welded case**
- **Rugged thin film construction**
- **Regulated input with reverse polarity/ overvoltage protection**
- **Meets MIL-E-5400/MIL-E-16400 requirements**

Typical Specifications

Frequency	7.9 to 8.4 GHz
Power out	@ −1.0 db 200 mW to 1 W
Gain, Nominal	30 db
VSWR, input/output	1.5:1 max.
Noise Figure	7.0 db max.

Call or write today and get all the facts.
(408) 262-2222 or TWX 910-338-2247

HARRIS

HARRIS MICROWAVE SEMICONDUCTOR
1530 McCarthy Blvd., Milpitas, CA 95035
(408) 262-2222 TWX 910-338-2247

READER SERVICE NUMBER 46

eclipse drifts of several PPM/hr in fundamental generators.

The frequency resolution of a synthesizer depends, not on a resonant cavity, but on the electronics of the arithmetic operations that generate the output. Techniques such as fractional-N synthesis and the multiplication of RF signals to microwave frequencies have made resolutions finer than 1 kHz practical at frequencies up to 18 GHz. Much better close-in phase-noise performance can be obtained with a multiplied RF source than with a fundamental microwave oscillator because the former has much higher resonator Qs and smaller flicker-noise contributions at RF frequencies.

The generation of non-harmonically related spurious signals remains an intrinsic part of any synthesis process. To keep these signals from being falsely identified as the received signals, their levels and locations must be controlled to prevent them from entering the IF bandwidth.

Basic modulation theory and spectral density relationships can be used to determine the effect that multiplication has on the noise of a signal.[3] To relate $\mathcal{L}(f)$ to random or sinusoidal phase modulation, the analysis must begin with a signal having sinusoidal frequency modulation, then converted to phase modulation:

$$f = f_0 + \Delta f_{PEAK} \cos 2\pi f_m t \quad (7)$$

$$\phi = \int 2\pi f(t)dt \quad (8)$$

$$v(t) = V_S \cos\left[2\pi f_0 t + \phi(t)\right] \quad (9)$$

$$v(t) = V_S \cos\left(2\pi f_0 t + \frac{\Delta f_{PEAK}}{f_m t} \sin 2\pi f_m t\right) \quad (10)$$

In the above expressions, f_0 = the carrier frequency, Δf_{PEAK} = the maximum frequency deviation, f_m = the offset frequency, $v(t)$ = the time varying amplitude of the signal, V_S = the maximum amplitude of the signal, and ϕ = the signal's phase.

Using a small modulation index approximation, for $f_{PEAK}/f_m \ll 1$, Bessel algebra yields the single sideband phase-noise-to-carrier ratio:

$$\left(\frac{V_{SSB}}{V_S}\right) J_1\left(\frac{\Delta f_{PEAK}}{f_m}\right) = .5\,\frac{\Delta f_{PEAK}}{f_m} \approx .5\,\Delta\phi_{PEAK} \quad (11)$$

$$\mathcal{L}(f) = \left|\frac{V_{SSB}^2}{V_S}\right| \quad (12)$$

In the above expressions, V_{SSB} is the maximum amplitude of the single sideband noise. Equation 12 can be expressed in logarithmic form as:

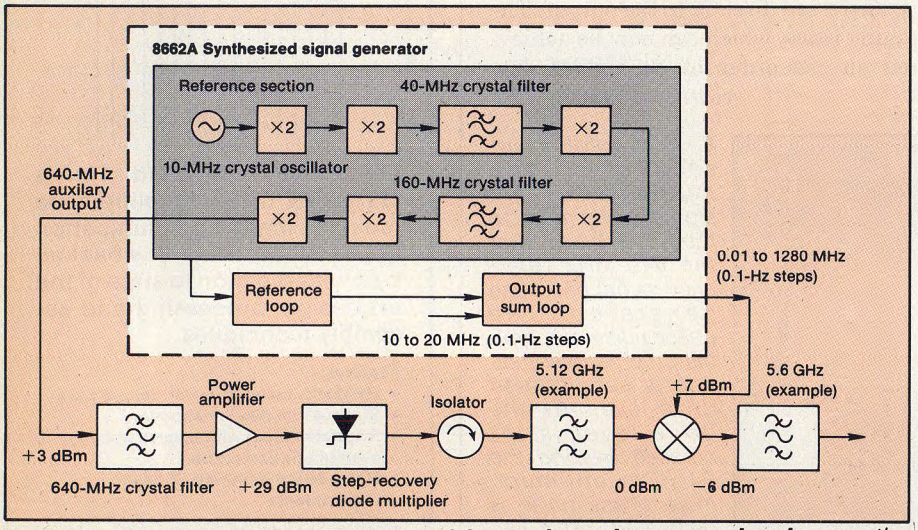
$$\mathcal{L}(f) = -6\text{dB} + 20 \log \frac{f_{PEAK}}{f_m} \quad (13)$$

The convenient form of Eq. 13 allows the increase in phase noise to be calculated when the frequency of a signal is multiplied. When a signal, $f \pm \Delta f$, is multiplied by a factor N, the frequency deviation is factored by the same amount, but the rate of modulation remains the same. Substituting for $\mathcal{L}(f)$ in Eq. 13 yields:

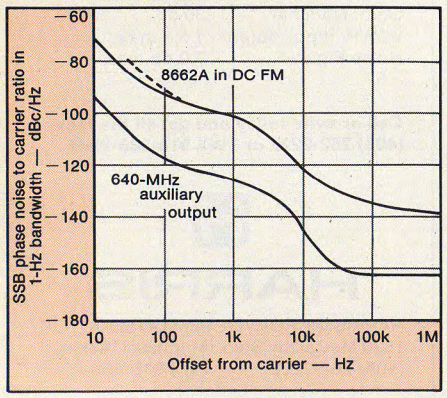
$$\frac{\mathcal{L}(Nf)}{\mathcal{L}(f)} = 20 \log\left(\frac{Nf}{f}\right) \quad (14)$$

The noise quality of the microwave signal depends on the quality of the RF source. The scheme shown in Fig. 5 can generate a clean signal at 640 MHz and is used to produce one of the reference signals of the HP8662A low noise synthesized signal generator. The 10-MHz reference is directly multiplied to a frequency of 640 MHz by using six frequency doublers. This frequency multiplication increases the phase-noise of the reference by 20 log (640/10) or 36 dB. Figure 6 shows the phase noise characteristic generated by the multiplication.

The monolithic crystal filters at 40 MHz and 160 MHz reduce the wideband phase noise. They filter the noise sidebands at offsets greater than 4 kHz (6-kHz bandwidth at 40 MHz) and 10 kHz (18-kHz bandwidth at 160 MHz), to yield a 640-MHz signal with substantially improved phase noise. As Fig. 6 shows, the design makes possible a phase noise of −95 dBc at 10-Hz offset from the carrier, and a noise floor greater than −160 dBc at offsets greater than approximately 20 kHz from the carrier.



9. This system for the generation of low-noise microwave signals *uses the 640-MHz standard described earlier. The 3-dBm reference signal passes through a 640-MHz bandpass filter before it is amplified to 29 dBm.*

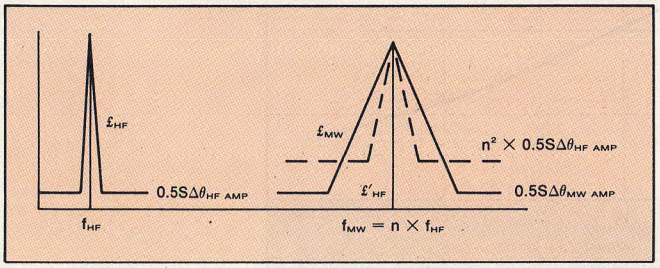


10. Clean microwave signals *are produced by the system shown in Fig. 9. It yields good close-in noise performance at some sacrifice to the noise floor.*

Multipliers take two forms

Frequency multipliers can be grouped according to two basic principles of operation: harmonic gener-

(continued on p. 77)



11. A fundamental microwave source can produce a lower noise floor, *since the synthesized source requires the multiplication of the RF oscillator's signal.*

ation by a nonlinear reactance (capacitance), and harmonic generation by nonlinear conductance.

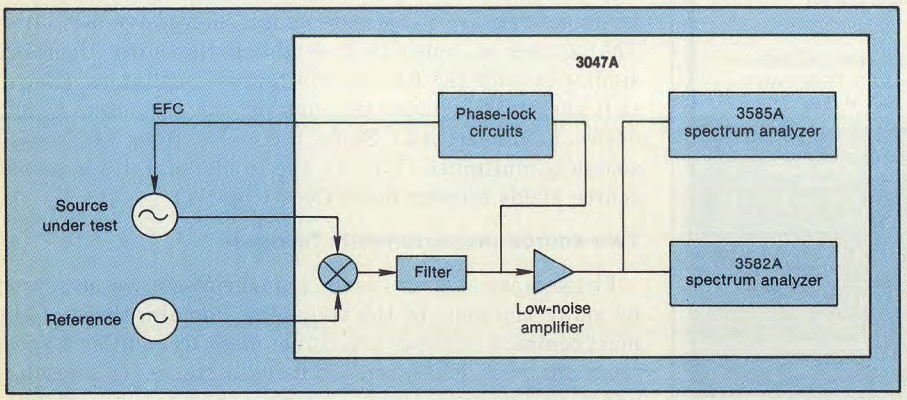
Multipliers with nonlinear capacitance typically yield more efficient, simpler circuits, but they also generate significantly more phase noise than multipliers based on nonlinear conductance. Higher AM to PM conversion efficiency, as well as charge fluctuations produced by changes in minority carrier lifetimes, are suspected of causing this difference. The multiplier that is used to generate the 640-MHz signal in Fig. 5 is, in essence, a full-wave rectifier circuit using Schottky diodes (Fig. 7). Since these diodes have low flicker noise and essentially no minority carrier storage, they serve as ideal components for low phase noise frequency multiplication.

Once a clean RF signal is generated, it can be multiplied up through the X-band region. At this point in the system, the noise of the reference signal will have reached a level at which the simpler step-recovery-diode multipliers can be used without adding any further significant noise.

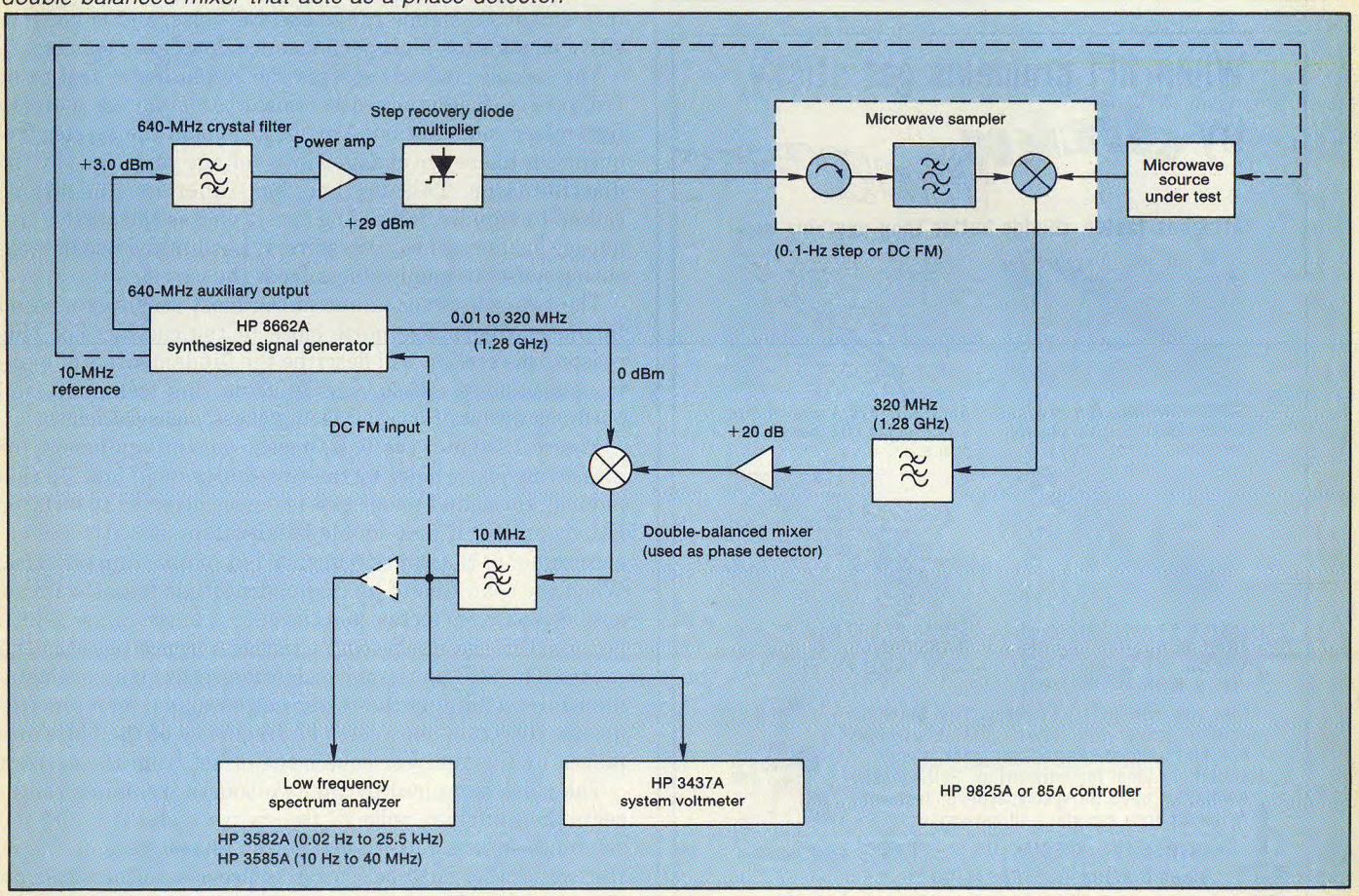
The phase noise of a typical step recovery diode is sensitive to drive level. As the drive level is increased beyond the optimum operating point (in this case, +24 dBm) more phase noise is generated. This effect becomes particularly pronounced as the pulse peak starts to drive the diode into breakdown. Figure 8 shows the circuit and its response. Note that the generator produces useful comb lines out to 18 GHz. An entire system for low-noise microwave signal generation using a 640-MHz reference signal, and a step-recover-diode multiplier, is shown in Fig. 9. This scheme starts with the 640-MHz reference signal (approximately +3 dBm) optionally available from the rear panel of the signal generator.

First, the reference signal is filtered through a 640-MHz bandpass filter to reject any 10-MHz reference or 20-MHz reference harmonic spurious sidebands that may be produced by the synthesis process in the reference section. The signal is then amplified to a level of about +29 dBm, a

(continued on next page)

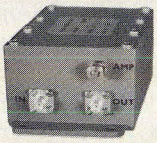


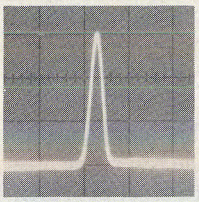
12. The two-source or phase detector technique *is the most sensitive method for measuring close-in phase noise. The signal under test is down converted to DC by a double-balanced mixer that acts as a phase detector.*



13. Automatic phase-noise measurements *can be made using the multiplication technique applied to generate low-noise microwave signals. In this case, one of the comb lines from the 640-MHz multiplier is mixed with the signal under test.*

NANOSECOND PULSE GENERATORS AVH & AVG SERIES





- 15 MODELS, 10 TO 500 VOLTS OUT
- PW 0.13 TO 5 nsec, PRF TO 1.0 MHz
- ALL SOLID STATE, LOW JITTER
- OTHER AVTECH PULSERS GIVE UP TO 350 V, PW TO 10 USEC AND PRF TO 300 MHz FOR GHz LOGIC, OPTICAL COMMUNICATONS, ATE, NUCLEAR AND OTHER APPLICATOINS.
- 70 OTHER PULSE GENERATORS, PULSE AMPLIFIERS, TRANSFORMERS, POWER SPLITTERS, BIAS TEES, AND SCOPE PROBES LISTED IN OUR NEW CATALOG

AVTECH
ELECTROSYSTEMS LIMITED

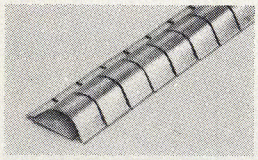
P.O. Box 3000 Ogdensburg New York 13669
P.O. Box 5611 Stn "F" Ottawa, Canada K2C 3M1
(613) 226-5772
Telex: 053-4591
TWX 610-562-8539

Germany: MICROSCAN GmbH Hamburg 040/6305067
UK: LYONS INSTRUMENTS hoddeson (09924) 67161
France: EQUIPEMENTS SCIENTIFIQUES Sa Garches 741.90.90
Japan: MEISHO ELECTRONICS Tokyo (03) 816-6581/2
Benelux: AIR—PARTS B.V. Netherlands (31) 1720-29300

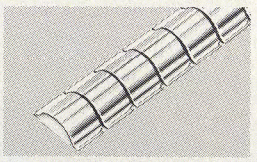
READER SERVICE NUMBER 50

When RFI problems get sticky, try sticky fingers®

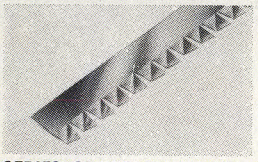
Attaches faster, shields better than anything else!



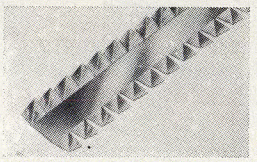
SERIES 97-500 The original Sticky Fingers with superior shielding effectiveness.



SERIES 97-520 A smaller size strip; highly effective in less space.



SERIES 97-555 New Single-Twist Series for use when space is at a premium. Measures a scant 3/8" wide.



SERIES 97-560 New ½" wide Double-Twist Series, ideal for panel divider bar cabinets.

Now you can specify the exact type beryllium copper gasket that solves just about every RFI/EMI problem. Perfect for quick, simple installation; ideal for retro-fitting. Self-adhesive eliminates need for special tools or fasteners. Write for free samples and catalog.



INSTRUMENT SPECIALTIES COMPANY, Dept. MW-1
Delaware Water Gap, PA. 18327
Telephone: (717) 424-8510

READER SERVICE NUMBER 51

KEEPING PHASE CLEAN *(continued from p. 77)*

drive level made necessary since the step-recovery-diode multiplier is optimized for 500 MHz and not 640 MHz.

To reduce spurious responses and to obtain the best conversion efficiency, a suitable bandpass filter selects the desired line element closest to the output frequency. The circulator (or isolator) absorbs unwanted reflections from the bandpass filter. The result is a clean multiple of the 640-MHz signal. This signal is mixed with the output signal from the front panel of the instrument to provide continuous frequency coverage. A final bandpass filter can be used to remove any mixing products. This system yields a clean microwave signal at a level of about −6 dBm with the typical phase-noise characteristic shown in Fig. 10.

The system described above has been optimized for close-in noise, but it does sacrifice some noise-floor performance relative to a fundamental microwave oscillator. The sources of noise that establish the noise floor are similar in both the RF and microwave oscillators. (Recall that the close-in noise depends on the resonator Q and device nonlinearities.) Since the noise floor of the RF source is multiplied (Eq. 13), the fundamental microwave source yields a lower noise floor (Fig. 11).

Two-source measurements favored

Phase noise at microwave frequencies can be measured by many methods. In the frequency domain, three of the most common methods are: direct measurement on a spectrum analyzer, measurement using a frequency discriminator, and measurements using a phase-detector or two-source technique. The first and simplest method, direct measurement on a spectrum analyzer, is limited by the instrument's dynamic range and LO noise, and is not sensitive enough for high performance, low-noise sources.

The second method requires the signal under test to be fed into a frequency discriminator such as a delay line/mixer combination. Any variations in the carrier frequency or phase are changed into voltage variations by the discriminator. This method has inherent limitations caused by rapidly decreasing sensitivity as the carrier frequency is approached, therefore, it has limited use in measuring noise at small offsets from the carrier.

The two-source technique is the most sensitive method for measuring phase noise close to the carrier. For this reason, this section will describe the fundamentals of making phase-noise measurements using this technique, and outline a system for automating these measurements.

Figure 12 shows the basic measurement equipment for measuring phase noise by the two-source technique. In this method, the signal under test is downconverted to 0 Hz, or DC, by mixing it in a double balanced mixer with a reference signal at the same frequency but in phase quadrature. When the condition of phase quadrature is met, the mixer acts as a phase detector, and the output of the mixer is proportional to the fluctuating phase difference between the inputs. The SSB phase-noise characteristics may be determined by examining the mixer output signal on a low frequency spectrum analyzer. The frequency of the noise displayed by the analyzer equals the offset from the carrier.

The noise measured by the two-source technique represents the combined noise of the source under test and the reference source. Consequently, the phase noise of one of the two sources must be known to provide definite data on the other. Usually, the noise performance of the reference source is well characterized for this purpose. The error

(concluded on p. 81)

introduced by the finite noise contribution of the reference source is given by:

$$\text{Error (dB)} = 10 \log \left(10 + \frac{P_{REF}}{P_{DUT}}\right) \quad (15)$$

In Eq. 15, P_{REF} = the actual noise power of the reference source, and P_{DUT} = the actual noise power of the source under test. The error is defined as $\pounds(f)_{MEASURED}$ minus $\pounds(f)_{ACTUAL}$ (both in dB). The noise of the reference source must be as low as possible. For example, if the noise of the reference is known to be about one-tenth that of the source under test, the noise measured using the two-source technique will be within 0.5 dB of the actual noise of the source.

In addition to the low-noise performance required of the reference source, several other characteristics should be considered. Broad frequency range, for example, will give the reference flexibility, and a frequency resolution of 0.1 or 0.2 Hz along with phase continuous switching will facilitate the setting of quadrature. The long-term stability and the electronic frequency control (EFC) of the reference must be adequate to keep the two sources at the same frequency and in quadrature. And accurate calibration requires good output level accuracy (± 1.0 dB desired). Finally, a programmable reference will allow automation of the measurement system.

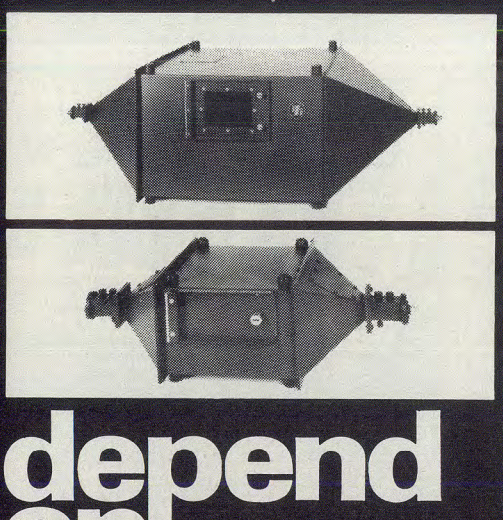
But noise performance remains the most critical specification of the reference source. Unfortunately, it is sometimes difficult to find sources that are much lower in noise than the one under test. Often, the most convenient reference source is simply another source similar to the one being tested. Both sources can be estimated to contribute equally to the measured phase noise. Thus, the actual phase-noise level of the source under test can be assumed to be one-half (or 3 dB lower than) the measured level.

If three unknown sources must be evaluated, they can be compared two at a time in three separate measurements. The absolute noise level of each source can be determined by solving three simultaneous linear equations at each measurement frequency. Since calculations like these are extremely tedious, automation is important.

The same multiplication technique described here for generating a low-noise microwave signal can be used to downconvert microwave sources for two source phase-noise measurments. A system for automatic measurements using this technique is shown in Fig. 13. In this case, one of the comb lines from the 640-MHz multiplier is mixed with the source under test. The output of the mixer is an IF frequency which is within 320 MHz of the frequency of the source under test. This IF signal is mixed with the same frequency from the front panel output of the signal generator. The result is a two-source measurement that essentially duplicates the one of Fig. 12. ●●

References

1. Scherer, D., "Today's Lesson—Learn About Low Noise Design, Part 1," *Microwaves* Vol. 18, No. 4, pp. 116-122 (April 1979).
2. Scherer, D., "Today's Lesson—Learn About Low Noise Design, Part 2," *Microwaves* Vol. 18, No. 5, pp 72-77 (May 1979).
3. Scherer, D., "Design Principles and Test Methods for Low Phase Noise RF and Microwave Sources," Hewlett Packard RF and Microwave Symposium (October 1978).



depend on ifi: Precision design TEM test chambers for accurate and broadband EMC testing

IFI's precision design and construction allows accurate E-Field generation within ± 1 db.

Each cell is equipped with a hinged access door that provides clearance for insertion of test objects, and transition panels for easy cable entry.

Larger cells can be supplied with integral E-Field Sensors, for direct readout in volts per meter.

Model CC-108—This test cell, with an operating range of DC to 800 MHz, offers an efficient means of obtaining broadband E-Field measurements in a compact, bench top application.

Model BC-100—This portable cell, specifically designed for medical and biological testing, provides a means of generating extremely high E-Fields up to 1GHz.

Model CC-103—The TEM Cell that has set industry standards, permits fully controlled testing at high E-Field levels with a moderate amount of input power.

Applications
- EMC/Susceptibility Testing
- Calibration of Field Intensity Meters
- Research & Development Applications
- Testing & Calibration of Power Density Probes

Benefits
- Cost Effective Alternative to a Full Size Screen Room
- Portable Shielded Enclosure for Lab Testing
- Protection from Hazardous Radiation During High E-Field Tests
- Useful for both Susceptibility and Emissions Measurements

"Also Depend of IFI for Broadband Amplifiers, E-Field Sensors and EMC Test Equipment"

INSTRUMENTS FOR INDUSTRY, INC.
151 Toledo Street
Farmingdale, N.Y. 11735
(516) 694-1414

READER SERVICE NUMBER 60

MIC Sources Hold Key To Future EW Systems

Performance demands are forcing microwave sources to grow in size, while also requiring more of the units to occupy the same space. MIC techniques can solve the paradox.

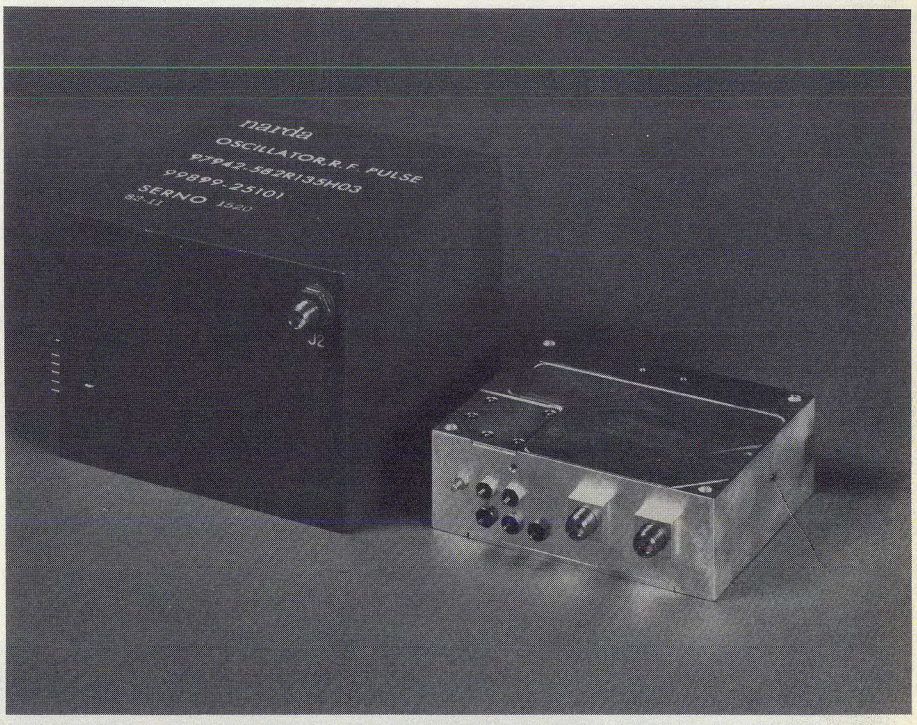
THE next generation of radar and electronic warfare systems will demand extremely high performance within the confines of aircraft and "smart" munitions. These systems are making increasing use of microwave integrated circuit (MIC) sources in programmable local oscillators, diagnostic subsystems, and radar exciters.

Microwave integrated circuit sources give higher performance than their connectorized predecessors in a fraction of the space. By using MIC Gunn diode, FET, or bipolar oscillators with coaxial or dielectric resonators, extremely low phase noise, high isolation, low spurious response, rapid switching speed, and fast settling time can be obtained in much less volume than present systems. Because the components are closer together, the effects of parasitic impedances and mismatches are minimized.

The considerable savings in size are shown in Fig. 1, where a typical MIC switched source is compared to a "connectorized" type. The unit is further detailed in Fig. 2. A schematic of the MIC version is presented in Fig. 3 and the unit's performance is shown in Table 1. The MIC switched source was developed for several current EW systems. It measures 2.5×3×1 in. and integrates three low-noise oscillators, four attenuators, a high-isolation SP3T switch, three-stage GaAs FET amplifier, low-pass filter, directional coupler, hybrid voltage regulator, oscillator control circuitry, and TTL-compatible switch driver. Any three

(continued on next page)

Walter A. Crofut, Marketing Manager, Sources and MICs, and **Allan Reynolds,** Engineering Manager, Sources, Narda Microwave Corp., Hauppauge, NY 11788.



1. The MIC switched source *takes up much less space than a similar source using connectors. Such reductions in size are required by increased performance demands. This example shows that a microwave integrated switched source for a radar warning receiver can be packaged in one-sixth of the volume required by its connectorized predecessor. This inherent size reduction also leads to superior performance, since the close component spacing minimizes parasitic impedances and mismatches.*

Table 1: MIC source specifications

Frequency	Any three between 6 and 18 GHz
Power output	+13 dBm
Phase noise	−80 dBc/Hz at 10 kHz offset
Switching speed	1μs to 1 MHz of final value
Non-selected feedthrough	70 dBc (minimum)
Environment	MIL-E-5400 (−54 to +96°C)
Frequency stability	±25 MHz (maximum)
Warm up	3 min. (maximum)
Current drain	750 mA (maximum)
Size	2.5 × 3 × 1 in.
Frequency command	TTL

oscillators in the 6-to-8-GHz range can be used without changing any of the associated components.

Unique switching required

The switches used in the MIC switched source exhibit some unique properties, which were necessitated by the need for fast settling time, and high frequency stability and high spectral purity. It was necessary for all three oscillators to operate continuously. The switch must simultaneously provide a termination to the oscillators in the off state, and a good match to the operating oscillator during and after switching. A schematic of the switch is presented in Fig. 4. If PIN-diode spacing is optimized for each frequency, more than 60-dB isolation can be achieved. Similar multipole switches are available for integration in switched sources covering the full 2-to-18-GHz band with at least 60-dB isolation.

The oscillators in the switched source can be designed to produce enough power to eliminate the need for amplification. However, an amplifier offers several advantages. High reverse isolation is provided (20 dB per stage), eliminating the need for isolators and assuring good pulling characteristics. Operating the oscillator at low power levels improves stability and phase-noise performance. Finally, FET amplifiers are reasonably efficient, and overall source power consumption is not compromised appreciably.

A choice of devices

The switched source employs Gunn-diode oscillators with coaxial resonators because the application required an unusual combination of frequency stability, high-temperature operation, mechanical tunability, and phase-noise performance. However, these MIC sources usually employ FET and bipolar oscillators with dielectric resonators on MIC substrates.

In the 6-to-18-GHz frequency range, FET dielectric resonator oscillators (DROs) are far more efficient than Gunn coaxial types and exhibit superior frequency stability with comparable phase-noise performance. For frequencies below 6 GHz, the bipolar oscillator is a better choice. For high-temperature, high-power performance above 6 GHz, a Gunn active element is often preferred in the DRO. The range of performance for DROs using bipolar, FET, and Gunn active elements is shown in Table 2.

A DRO operating at S-band frequencies can usually be built on a MIC substrate less than 1 in.^{2} in area, with size reducing in proportional to wavelength. Figures 5 and 6 show an X-band FET DRO in a drop-in package, and the frequency stability improvement realized with a dielectric resonator at 10 GHz.

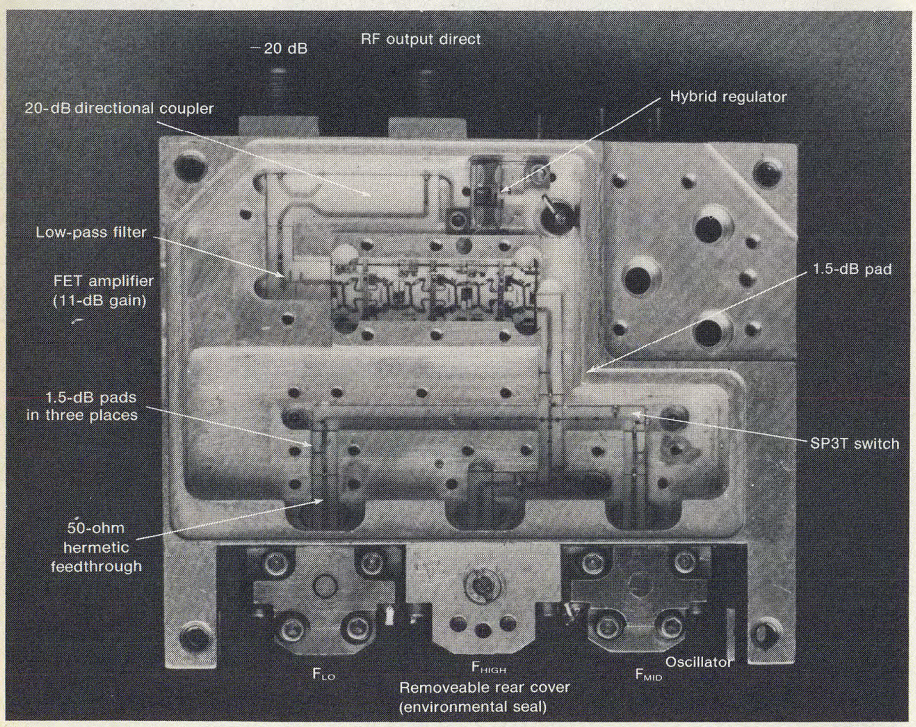
A hybrid voltage regulator assures minimum voltage pushing, can be programmed to provide temperature compensation for frequency stability, and can be incorporated easily in the MIC assembly. An isolator or amplifier can be integrated along with the oscillator to minimize frequency-

(continued on p. 86)

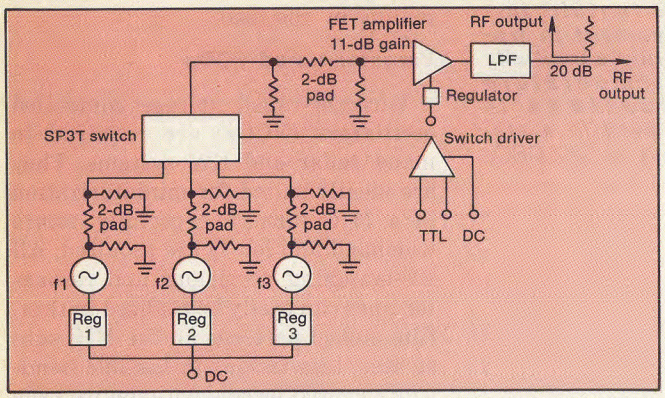
Table 2: Typical DRO characteristics

Active Element	Bipolar	FET	Gunn
Frequency range	2 to 5 GHz	2 to 18 GHz	6 to 18 GHz
Power output	+24 dBm	+18 dBm	+23 dBm
Temperature range	−54 to +85°C	−54 to +85°C	−54 to +110°C
Phase Noise[1] dBc/Hz at 10 kHz	100 dBc/Hz	90 dBc/Hz	100 dBc/Hz
Efficiency	10 to 20%	10 to 20%	1 to 3%
Stability[1]		< 2 PPM/°C	
Pushing[2]		< 4 PPM/V	
Pulling[3]		< ±5 PPM	

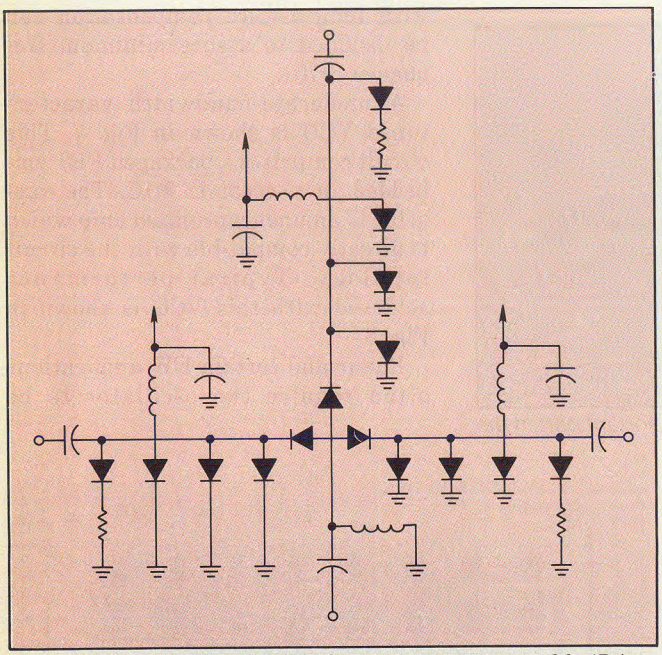
[1]Degrades with mechanical or varactor tuning
[2]With hybrid voltage regulator
[3]With isolator or buffer amplifier and 1.5 to 1 load VSWR.



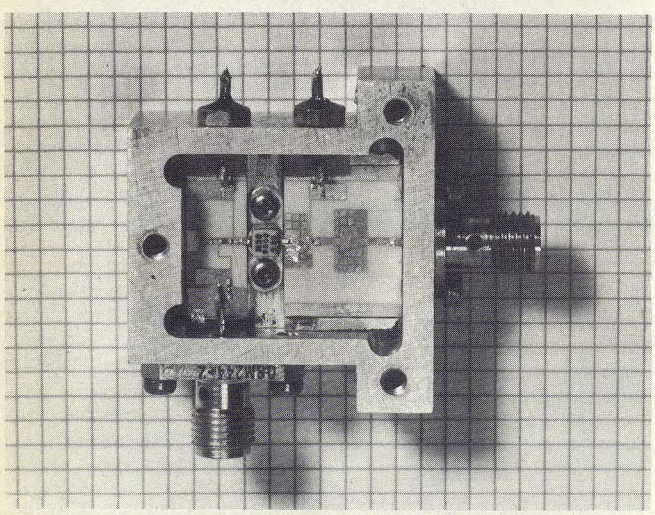
2. An interior view of the MIC source *shows the location of the 1P3T switched three-stage FET amplifier, attenuators, filters, directional coupler, and other components.*



3. The interconnection *between the oscillators, switching, control, and conditioning circuitry is apparent in this schematic.*



4. A 1P3T terminated switch *can provide up to 80-dB isolation between each of the three oscillators.*



5. An X-band FET dielectric resonator oscillator *constructed on a MIC substrate occupies less than 1 in.*[3]

We Make It Easy

to get in and out of tight spots

EASY FORM..

Semi-Rigid Coaxial Cable

MIL-C-17E Qualified

This new, semi-rigid coaxial cable called "Easy-Form" provides unique bending flexibility for applications involving mounting of preformed assemblies.

Straight cable assemblies can also be supplied for your prototype use in determining final cable configurations, without the need for special forming tools.

This cable meets all requirements of MIL-C-17E and is available in sizes .141" and .086".

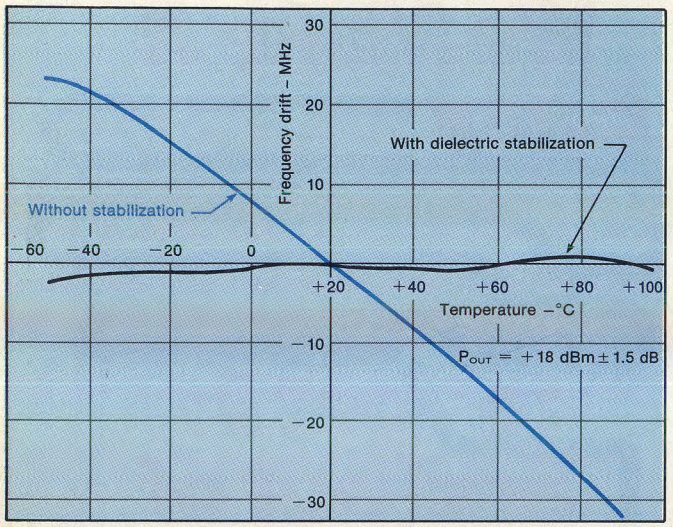
Cablewave Miniature Products

M/A-COM OMNI SPECTRA, INC.

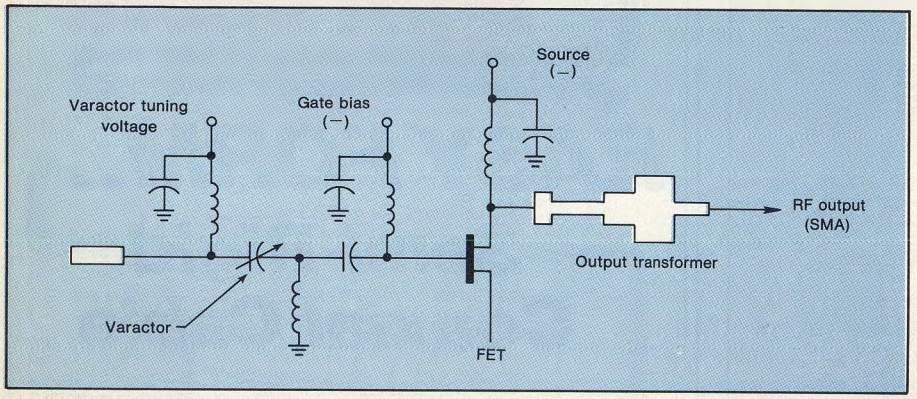
NOTE OUR NEW ADDRESS:

718 NORTH COLONY ROAD, WALLINGFORD, CT 06492
(203) 265-6560 TWX 710 476-0730

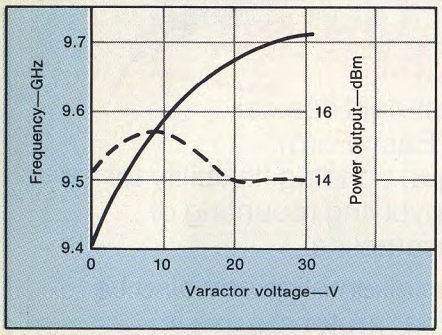
READER SERVICE NUMBER 55



***6. A tenfold improvement in frequency sensitivity to temperature variations** is achieved in a stabilized 10-GHz DRO.*

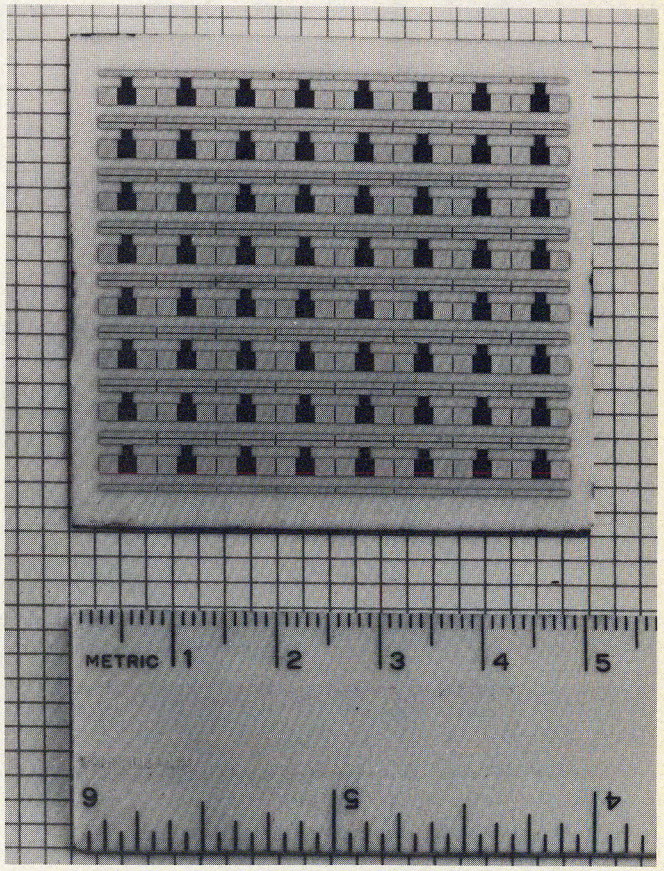


***7. Varactor-tuned voltage-controlled oscillators** can play an important part in the design of radar and electronic warfare systems.*



***8. A varactor-tuned VCO FET oscillator** provides an output of 30 mW ± 0.75 dB from 9.4 to 9.7 GHz.*

***9. Attenuators are an integral part of the switched source.** This 2 × 2 in. substrate has 64 chip attenuators.*



pulling by the load.

Varactor-tuned VCOs

Varactor-tuned voltage controlled oscillators (VCOs) are required in many radar and EW systems. They are ideally suited for miniaturization in a MIC format, especially where wideband and low Q are required. All RF-matching provisions and resonator lines can easily be realized in thin-film etched patterns on the MIC substrates. Limitations in tunable bandwidth caused by conventional package parasitics are greatly reduced by integration of unencapsulated active chips and passive components. Programmable hybrid voltage regulators with temperature compensation can be included to assure minimum frequency drift.

A moderate-bandwidth varactor-tuned VCO is shown in Fig. 7. This circuit comprises a packaged FET embedded in a ceramic MIC. The varactor is an unencapsulated chip which is directly compatible with the circuit topology. Typical performance achieved with this VCO is shown in Fig. 8.

Radar and certain EW applications often require the oscillator to be

Advertisers . . .
Products . . .
Literature.

Find them fast
in our
InfoCenter
(see p. 126)

phase-locked to a stable VHF reference. Microstrip dividers and hybrid VHF phase-locked-loop circuitry can meet this requirement. A varactor-tuned DRO can be used as a VCO in fixed-frequency, phase-locked applications to enhance the phase-noise performance.

MIC benefits and packaging

MIC construction allows many components, including couplers and filters, to be incorporated in the design with negligible cost, as they are printed with the other microstrip patterns. Resistive elements for power dividers and attenuators in chip form are easily integrated. The type of attenuator used in the switched source is shown in Figure 9. Moderate bandwidth isolators can be integrated by deposition of the proper microstrip pattern on a ferrite substrate and by adding a magnet beneath the surface.

There are several approaches to packaging MIC sources. The fully integrated approach used for the switched source offers the best size reduction. However, many source components are becoming available in "drop-in" packages, and can be integrated on a mother board using either symmetrical stripline, softboard microstrip, or alumina microstrip as a transmission line medium. The X-band DRO shown in Fig. 5 is incorporated in a standard drop-in package similar to that used for amplifiers, switches, and couplers.

Choosing a packaging technique requires assessment of several trade-offs for a given application, including size, production quantity, commonality of circuit functions, and production cost objectives. In some instances, hybrid combination of fully integrated and drop-in mother board approaches may be optimum. Commonly used functions can be incorporated as drop-in packages, and special functions integrated into the mother board transmission line medium.

The MIC assembly is typically divided into upper and lower levels. The upper level contains the microwave portion of the circuit and the lower level the support circuits such as voltage regulators, linearizers, and switch drivers. These circuits have dimensions compatible with the miniaturized microwave circuits.●●

wire, while coupling and bypass capacitors are MOS chip types. Tuning is accomplished largely by changing the distance between the bond wire inductors and the ground plane, the transmission line sections, or the adjacent bond wires. When necessary, additional tuning can be provided by bonding-in or disconnecting capacitive pads on the transmission line.

Much of the design work at 26 to 40 GHz relies on modeling techniques based on the S-parameters measured up to 26 GHz. This data makes it possible to derive an equivalent circuit model, whose accuracy can be partially verified by higher frequency measurements. In practice, it's possible to model a useful first approximation of the input and output matching circuits. The characterization of actual single-ended circuits by scalar or vector analysis then provides data that may be compared to the computer analysis of the circuit, allowing for a final modification of the gate/drain model. This, in turn, yields a more precise model of the matching structures themselves. Computer-aided design and a single iteration with measured data yields the current matching structures.

Making measurements

The S-parameter characterizations of the GaAs FETs through 26.5 GHz were made using a company-developed 18-to-26.5-GHz automatic network analyzer (ANA) system. It is a modified HP8409B system with downconverters for both the reference and test channels. These parameters were used as part of the initial gate/drain modeling, and later supplemented with complete S-parameter characterizations through 40 GHz, using a 26.5-to-40-GHz ANA (the HP8409B with an upconversion/downconversion adaptation).[3]

Most of the measurements needed for amplifier evaluation at 18 GHz and beyond can be made with reasonable accuracy over less-than-octave bandwidths through 110 GHz by using presently available instrumentation. Sweep generators (using backward-wave oscillator tubes) already exist that cover the full 26.5-to-40-GHz band with approximately + 7 dBm output power and ± 1.5 dB output flatness. Other signal sources up to 110 GHz are also available, but only for narrow-band operation. There is also a Schottky-barrier diode detector with approximately ± 2.0 dB accuracy in the 26.5-to-40-GHz range (compared to the ±0.5 dB accuracy of similar detectors at lower frequencies). Thermistor power heads and precision attenuators with ±2.0-percent accuracy are also ready for use in this band. There is even a 26-to-40-GHz diode noise source which, by using an external mixer and the sweep generator for a local oscillator, permits automatic noise figure test sets to operate in this band.

Packaging considerations and their effects on microstrip performance must be carefully evaluated at higher microwave frequencies. At a few gigaHertz, the package serves more for protection than anything else. At frequencies in X-band and above, however, it must be very carefully designed. To aid in this design, the test fixture incorporates a rather narrow channel surrounding the microstrip circuitry. This is absolutely necessary to insure that the cavity does not act as a waveguide at the high end of the operating frequency range. It also helps to minimize losses due to unwanted signal propagation and to prevent performance problems from waveguide moding. At times, it's simply impossible to design a cavity with enough room to both accommodate the circuit and not act as a waveguide or resonator. To do so requires the use of pieces of RF absorber or metal bars strategically placed to break up any potential moding (see photo, p. 67). The ultimate package for the amplifier is still under development. ●●

Acknowledgments

Avantek's semiconductor division and MIC group for 26-to-40-GHz GaAs FET development is supported in part by a Naval Electronics System Command contract and monitored technically by the Naval Research Laboratory under contract N00014-81-C-2082.

References

1. F.J. Moncrief, "Designers Push FET Amplifiers Past Ku-Band to compete with TWTAs From 18 to 26.5 GHz," *MicroWaves*, Vol. 18, No. 5, pp. 12-13 (May 1979).
2. J. Rosenberg, P. Chye, C. Huang, G. Policky, "A 25.0-40.0 GHz GaAs FET Amplifier," *1982 MTT-S International Microwave Symposium Digest*.
3. W. Kennan, "K-Band Analyzers Materialize on the FET Measurement Scene," *MicroWaves*, Vol. 20, No. 9, pp. 61, 63-68 (September 1981).
4. C. Huang, A. Herbig, R. Anderson, "Sub-Half-Micron GaAs FETs for Applications Through K Band," *1981 MTT-S International Microwave Symposium Digest*, pp. 25-27.
5. K. Kamei, S. Hori, H. Kawasaki, and T. Chigara, "Quarter Micron Gate Low Noise GaAs FET's Operable up to 30 GHz," *IEDM, Digital Technology Papers*, pp. 102-105 (1980).
6. H. Yamisaki and G.W. Kiethley, "High Performance Low Noise FET's Operating for X-Band Through Ka-Band," *IEDM Digital Technology Papers*, pp. 106-109 (1980).
7. P.H. Wolfert, J.D. Crowley, and F.B. Fank, "A Low-Noise Solid State Amplifier For Replacement of a Ka-Band TWTA," *1981 MTT-S International Microwave Symposium Digest*, p. 441.
8. Berin Fank, "InP Emerges as Near-Ideal Material for Prototype MM-Wave Devices," *MSN*, Vol. 12, No. 2, pp. 59-68 (February 1982).

Part 1: Designers: Prepare For The GaAs FET Age

GaAs FET Circuits Begin With Biasing Choices

The potential of GaAs FETs in microwave circuits is making headlines. A five-part series starting this month reviews FET design tools, beginning with biasing methods and considerations.

THREE-TERMINAL solid-state devices, in the form of GaAs FETS, are conquering areas of microwave communications and other fields that were once the domain of diodes and electron tubes. As it flourishes, the GaAs FET is changing the face of an industry and the nature of microwave design.

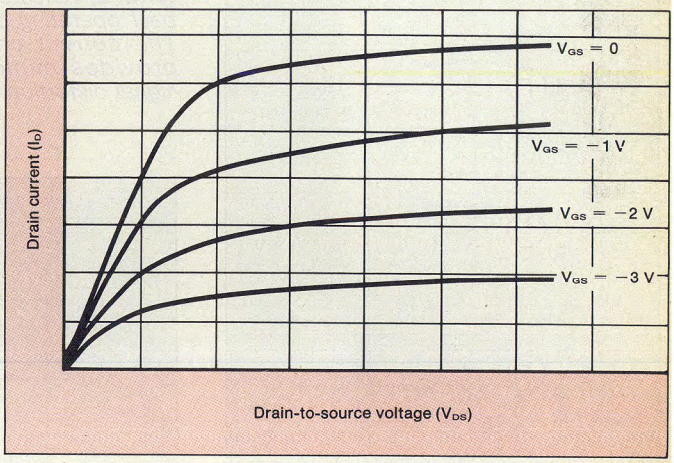
With the GaAs FET on the verge of widespread acceptance in terrestrial and space systems, the time has come to inventory design techniques that are making these applications possible. This article, and the others that follow it in the series, propose to take stock in such a manner. Biasing considerations provide the jumping-off point.

The GaAs FET is what is generally referred to as a "normally ON" device. Basically, it differs from the MOSFET in its use of a Schottky barrier at the gate instead of an oxide layer. This is an extremely important point. In other words, almost no GaAs FET gates are insulated from the channels in terms of direct current. Since a GaAs FET does not use a dielectric like a MOSFET, positive voltage applied at the gate would cause direct current to flow through it; because the gate is a very small piece of metal (0.5 × 1.0 × 2.0 μm), the gate electrodes would fuse completely in almost all cases.

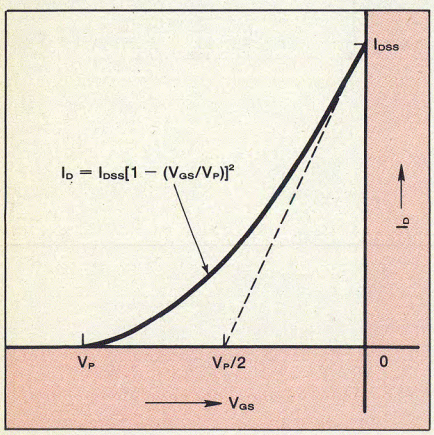
Figure 1 illustrates GaAS MESFET DC characteristics. Usually, a linear amplifier circuit supplies a bias voltage to the MESFET that ranges from I_{DSS} (saturated drain to source current, $V_{GS} = 0$) to $I_{DS} = 0$ (at pinch-off, i.e., $V_{GS} = V_P$). In this range, the voltage between the drain and the source, V_{DS}, has little effect on the current flowing through the channel, I_{DS}. The drain-to-source (channel) current is controlled by changing the gate voltage, V_{GS}. Figure 2 shows the transfer characteristics of an N-channel GaAs FET. The FET transfer characteristic is an important basic

(continued on next page)

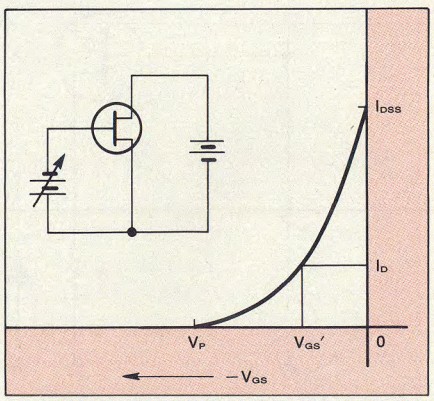
Jerry Arden (Contact), Vice President, Marketing, California Eastern Laboratories (for NEC, Inc., Japan), 3005 Democracy Way, Santa Clara, CA 95050.



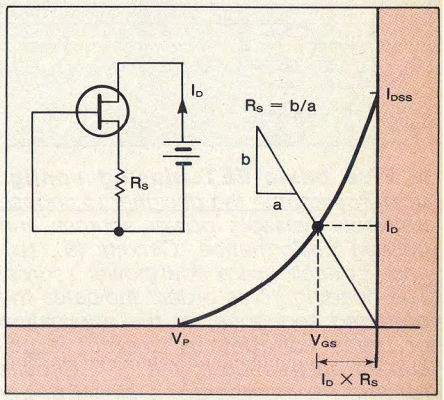
1. The GaAs MESFET DC characteristic resembles a vacuum-tube voltage/current relationship. *The drain current is mostly a function of the gate voltage, V_{GS}.*



2. The transfer characteristic of an N-channel GaAs FET *illustrates the square-law relationship between gate current and gate voltage.*



3. Dual-power-source biasing *allows the source to be directly grounded, improving high frequency response by reducing source inductance.*



4. An alternate biasing method uses a resistance, R_S, *in the source lead. This provides a form of self-bias that limits the source current.*

parameter in circuit design since it helps determine the bias conditions and operating point. The operating point in Fig. 2 is directly related to the mutual conductance, g_m.

Mutual conductance is defined as the ratio of the change in drain current to the change in gate-to-source voltage. Its square-law relationship is shown in Eq. 1:

$$I_D = I_{DSS}\left(1 - \frac{V_{GS}}{V_P}\right)^2 \qquad (1)$$

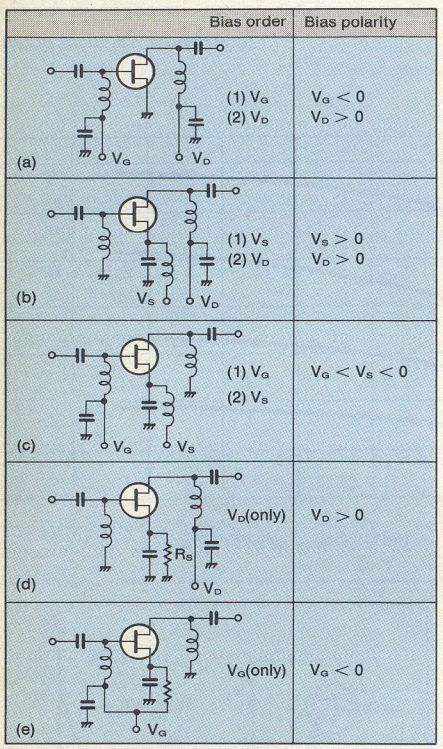
g_m is obtained when I_D in Eq. 1 is differentiated with respect to V_{GS}:

$$g_m = \frac{dI_D}{dV_{GS}} = -2\,\frac{I_{DSS}}{V_P}\left(1 - \frac{V_{GS}}{V_P}\right) \qquad (2)$$

Best bias method

GaAs FETs are biased by several methods. The dual-power-source method, shown in Fig. 3, satisfies the requirement that V_{GS} lies between pinchoff and zero volts. V_{GS} always follows the relationship:

$$V_{GS} = V_P\left(1 - \sqrt{\frac{I_D}{I_{DSS}}}\right) \qquad (3)$$



5. Five basic FET biasing configurations *enable the designer to choose between available power sources and desired performance. Circuits (a), (b), and (c) each use a dual-power source. The heading "bias order" indicates the preferred sequence for the application of these voltages to prevent large-current destruction of the FET. Circuits (d) and (e) incorporate a single power supply with a self-biasing resistance, R_S. Configuration (e) should be selected only if a negative power source is available.*

When only one power source is available, insertion of a resistance in the source lead, R_S, provides a form of self-bias that limits the source current (see Fig. 4). The voltage between the gate and source is:

$$V_{GS} = -I_D\,R_S \qquad (4)$$

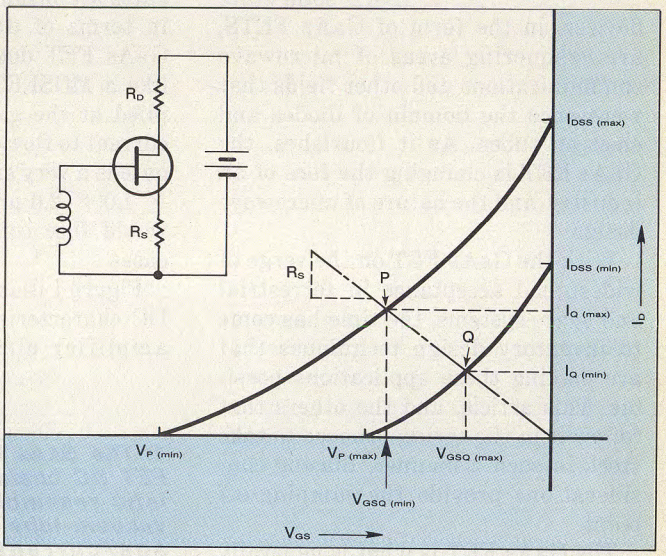
R_S is obtained by combining Eqs. 3 and 4:

$$R_S = -\frac{V_{GS}}{I_D} = -\frac{V_P}{I_D}\left(1 - \sqrt{\frac{I_D}{I_{DSS}}}\right) \qquad (5)$$

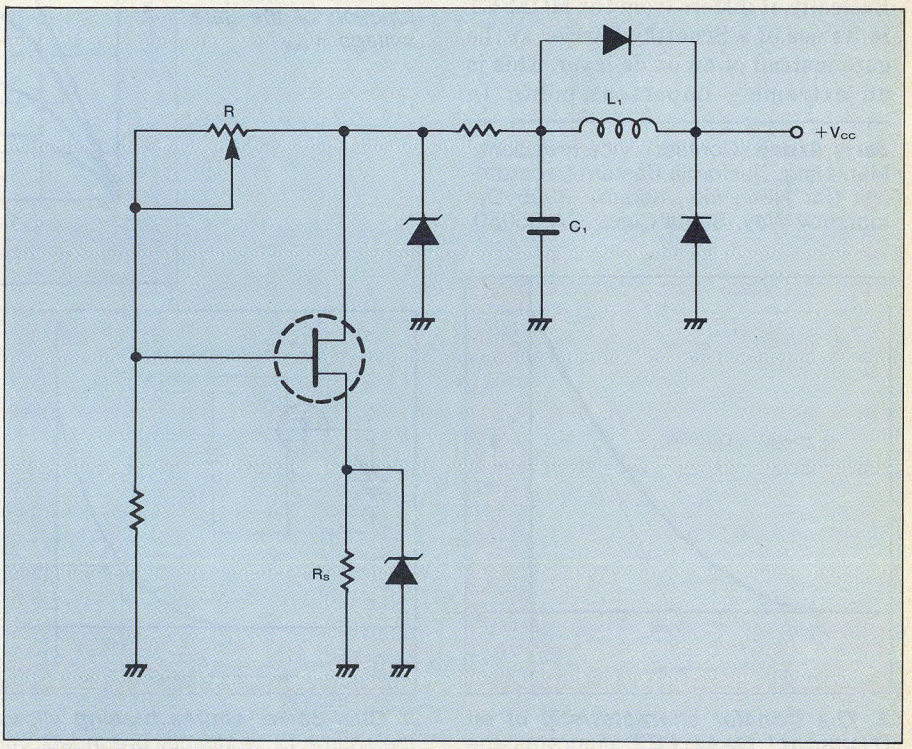
Five specific configurations effecting the two bias methods are illustrated in Fig. 5. The first, Fig. 5a, the dual-power-source bias method, improves high frequency response by directly connecting the source to ground, thereby reducing source inductance, increasing gain, and lowering noise figure.

All other bias methods require a source bypass capacitor. Even high quality capacitors introduce a loss term (tan δ) resulting from the material's dielectric properties, while chip capacitors have some inductance. Generally, if a single source (self-biasing type) is selected, Fig. 5d is

Next month this series will investigate the FET's cross modulation characteristic. Discussion will then focus on the small-signal and large-signal (or power) FET.



6. The FET locus, superimposed on the transfer characteristic, *indicates the best operating point. The correct choice provides minimum signal distortion.*



7. An actual bias circuit *requires more than the power supply and the feedback resistance. Variations among devices require additional circuit compensation, R.*

used; if the only available source is a negative one, then Fig. 5e applies.

Figure 5 also shows the *order* for adding the bias supplies when dual-power-sources are used. This prevents the occurrence of large destructive currents. With its high mutual conductance, the GaAs FET provides excellent frequency characteristics. However, if the gate voltage is near zero, g_m is maximum and oscillation may occur. Consequently, a negative bias should be applied first, followed by positive bias for the drain. While slight differences exist in bias circuits used for small-signal GaAs FETs in comparison to power GaAs FETs, the same basic techniques are utilized.

Designing an actual circuit

The bias circuit insures stable operation, as well as providing the necessary operating voltage and current. The bias locus, shown in Fig. 6, is defined by the relationship:

$$V_{GSQ} = I_Q R_S \qquad (6)$$

where I_Q, the operating point current, varies between P (maximum value) and Q (no signal). This change, ΔI_Q, causes the drain voltage to change by $R_D \Delta I_Q$. Minimum signal distortion is achieved when the operating point is fixed at the center of the bias line. This location also determines best amplifier operation with negligible D_C gate current.

I_Q is a function of both the temperature, T, and V_{GSQ}. If, with a variation in temperature of δT, I_Q changes by only δT_Q, then:

$$\delta I_Q = \frac{\partial I_Q}{\partial T}\,\delta T + \frac{\partial I_Q}{\partial V_{GSQ}}\,\delta V_{GSQ} \qquad (7a)$$

$$= \frac{\partial I_Q}{\partial T}\,\delta T - g_m\,\delta I_Q R_S \qquad (7b)$$

From this:

$$\delta I_Q\,(1+g_m R_s) = \frac{\partial I_Q}{\partial T}\,\delta T \qquad (8)$$

If $R_S = 0$ (that is, if there is no series resistance) then the drift is represented by:

$$\frac{\partial I_Q}{\partial T}\,\delta T = \delta I_Q\,(0) \qquad (9)$$

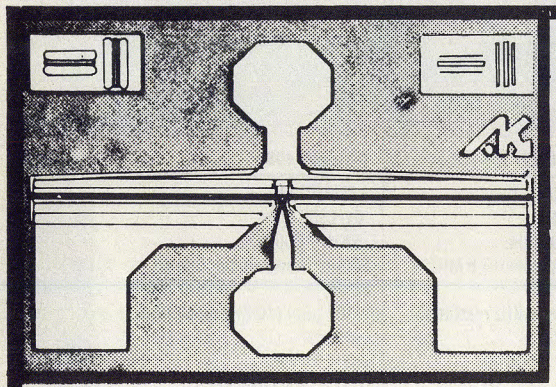
where a bias stability coefficient, S, is defined as:

$$S = \frac{I_Q \text{ fluctuations with } R_S}{I_Q \text{ fluctuations independent of } R_S}$$

$$S = \frac{\delta I_Q}{\delta I_Q(0)} = \frac{1}{1+g_m R_s} \qquad (10)$$

This means that fluctuation in the entire circuit is reduced by means of negative feedback due to R_S. This effect is particularly important when using small-signal FETs.

A complete bias circuit is illustrated in Fig. 7. Since values of I_{DSS} and V_P vary between devices, the bias circuit must be designed to accommodate these changes in order to establish an optimum and stable operating point over the expected ambient temperature range. The circuit in Fig. 7 is basically a fixed-bias circuit and not a self-bias circuit. R_S, in this case, provides a feedback mechanism. Since the voltage between the gate and the source is $V_{GS} = I_D R_s$ in a self-bias circuit, if I_D is known, R_S can be determined. With a fixed-bias circuit of the dual-source type, the gate voltage is selected independently of the quantities R_S and I_D. Consequently, R_S can be higher than the value obtained when using a self-bias circuit with a concomittant improvement in the stability coefficient, S. ●●



Avantek . . .
Years Ahead Today.

We're vertically integrated from substrates to systems, and we set industry milestones in technology, growth and opportunity.

Our on-site Stanford University Honors Program, stock participation, and profit sharing can ignite your career at Avantek.

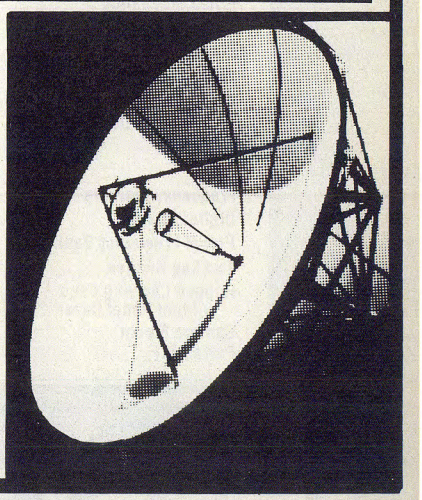
Meet us face to face in Dallas at the MTT Show in June at the Hyatt Regency, Booth 424-426.

- **MIC DESIGN**
  Thin film and hybrid, amplifiers, oscillators, subsystems
- **DIGITAL DESIGN**
  Circuit, microprocessor, hardware/software integration
- **MANUFACTURING**
  Develop and implement ATE
- **SALES/MARKETING**
  EW, International, communications

If you are unable to visit us at MTT in Dallas, we invite you to contact **Mike Birmingham at Avantek, 3175 Bowers Avenue, Santa Clara, California 95051. (408) 727-0700, extension 2436.**

Avantek

We are an equal opportunity employer.



GaAs FET IMD Demands Better Standard

The third-order intercept may not be a meaningful indicator of linearity for GaAs FET power amplifiers. Other measurement methods can give more reliable readings.

THE third-order intercept point is an imaginary power level used to indicate the linearity performance of a "well-behaved" power amplifier such as a bipolar transistor.[1, 2] Using a 2:1 ratio between the fundamental and third-order IMD components, system designers can calculate the third-order IMD level at any specific output power. Figure 1 shows a well-behaved bipolar power amplifier at 2 GHz exhibiting this 2:1 relationship. In this case, the "third-order intercept point" is approximately 10 dB higher than the 1-dB gain compression point.[3, 4, 5]

Unfortunately, GaAs FET power amplifiers are by no means well-behaved devices.[6-11] Their third-order IMD curve does not follow the 2:1 relationship with respect to the fundamental signal, nor does their IMD curve follow the 3:1 slope (Figs. 2, 3, and 4). Consequently, their IMD level cannot be calculated in the conventional manner. In fact, for most GaAs FET power amplifiers, the third-order intercept point is a meaningless term, although many power amplifier manufacturers persist in adding 10 dB to the 1-dB compression point and calling the result the third-order intercept.

Better tests exist

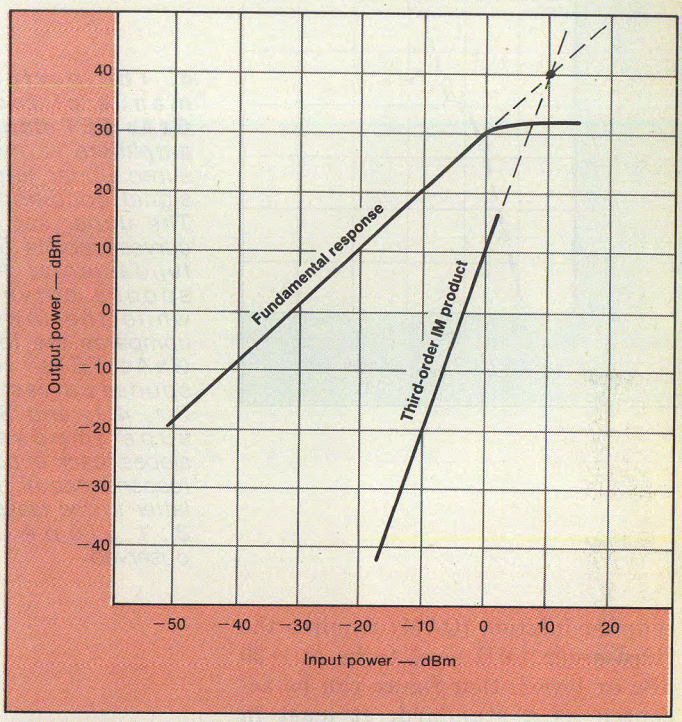
More consistent ways of gauging linearity are available. A simple two-tone test, for example, could be developed into a standardized reference that could be applied uniformly throughout the industry.

Digital radio presents an example of the manner in which this system could work. Since quadrature ampli-

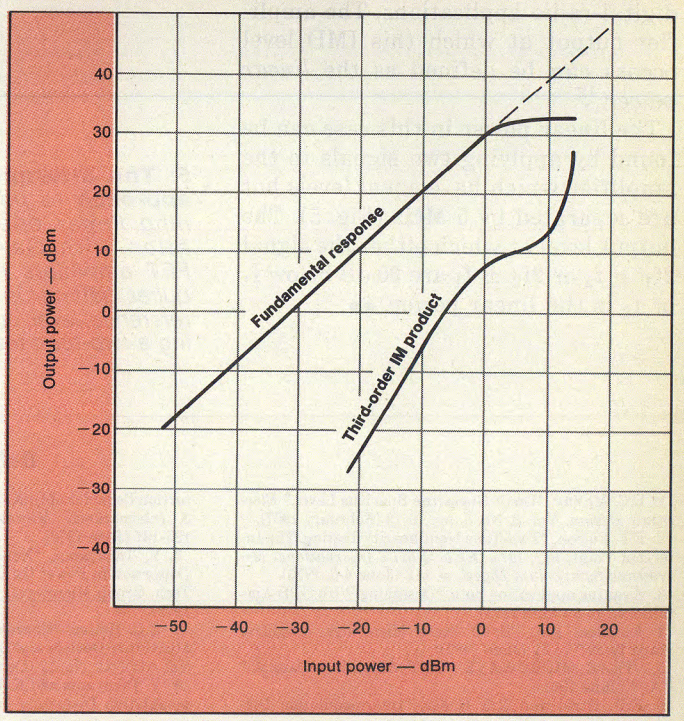
(concluded on next page)

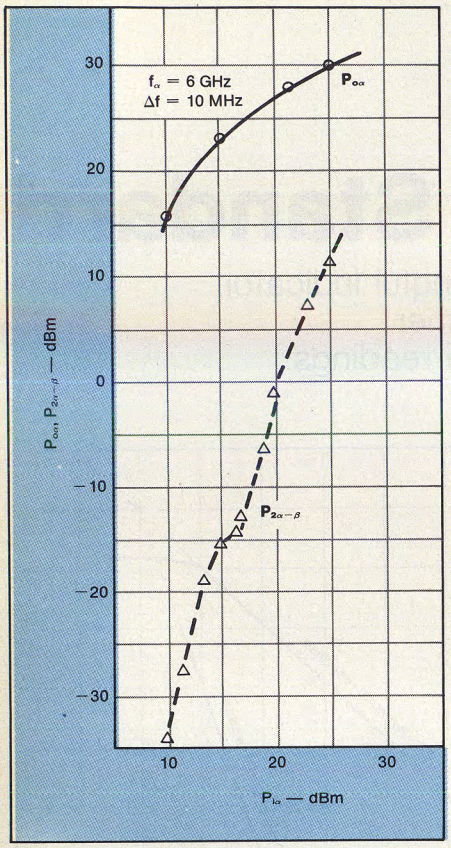
Chi Hsieh, Director of Hybrid Circuit Development, Harris Corp., Farinon Div., 1691 Bayport Ave., San Carlos, CA 94070.

***1. "Well-behaved" bipolar linear amplifiers** satisfy the classic definition of the third-order intercept point. A spread of roughly 10 dB exists between the intercept point and the 1-dB gain compression point.*

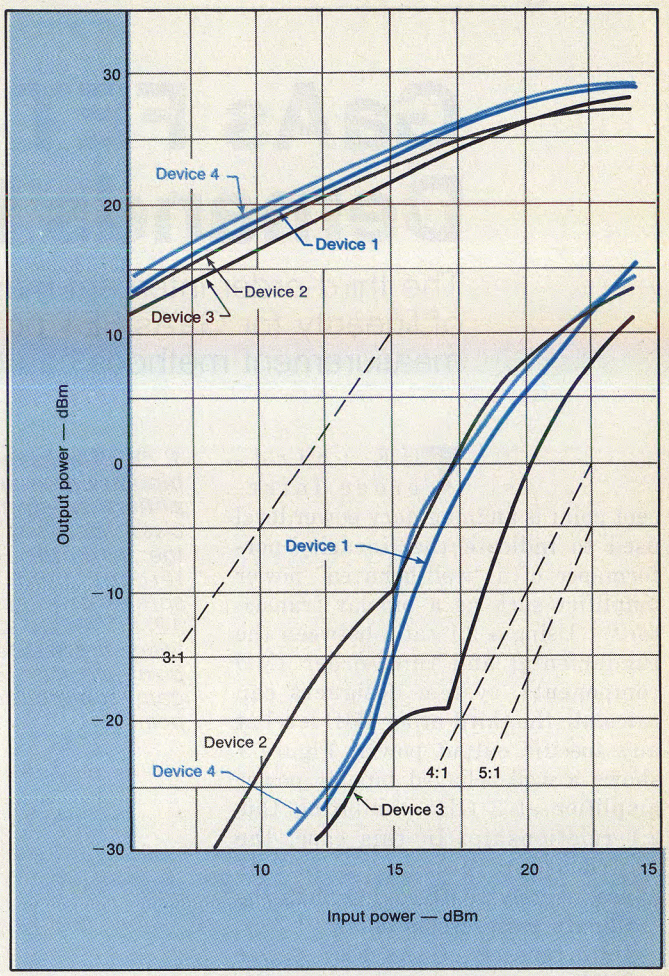


***2. GaAs FET amplifiers fundamental and third-order IMD response** curves do not satisfy classic 2:1 relationships. Other techniques must be used to determine the third-order IMD level.*





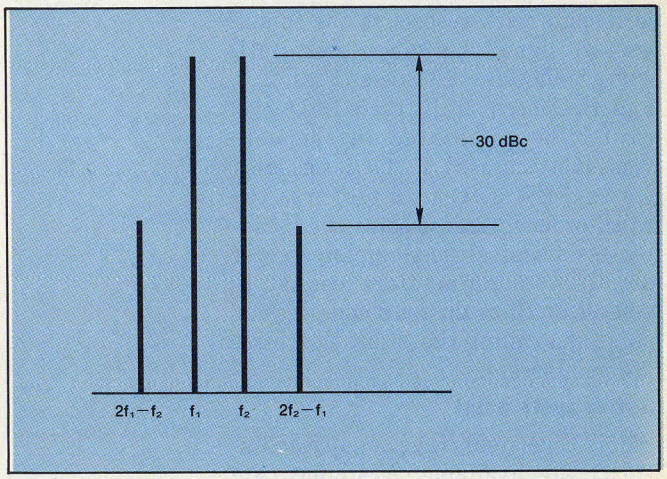
3. The fundamental and third-order IMD response *curves confirm the relationship differs from the 2:1 case.*



4. The performance of four GaAs FET linear amplifiers *is measured under large signal conditions. The upper set of curves depicts the fundamental response curves, while the lower compares the four GaAs FETs' response curves to 3:1, 4:1, and 5:1 superimposed slopes. Lack of correspondence of the latter to the classic 3:1 slope is observed.*

tude modulation (QAM) requires the third-order IMD level to be at −30 dBc or lower, that figure can be accepted as a standard, at least in digital-radio applications. The amplifier output at which this IMD level occurs can be defined as the *linear power.*[12]

The linear power in this case can be found by applying two signals to the amplifier which have equal levels but are separated by 5 MHz (Fig. 5). The output level at which either the signal $2f_1 \pm f_2$ or $2f_2 \pm f_1$ are 30 dB below f_1 or f_2 is the linear power. ●●



5. The alternate approach *to defining linear operation with GaAs FET amplifiers requires setting up a reference level during a two-tone test.*

References

1. F.C. McVay, "Don't Guess the Spurious Level," *Electronic Design,* Vol. 3, No. 3, pp. 70-73 (February 1967).
2. F.F. Fulton, "Two-Tone Nonlinearity Testing, The Intercept Point, Pi," *1973 IEEE Q-MTT International Microwave Symposium Digest,* p. 112 (June 4-6, 1973).
3. Avantek application note, "Designing With GPD Amplifiers," p. 6 (June 1972).
4. Amplica, Inc., "Solid State Microwave Amplifier Hand Book," p. 21 (June 1982).
5. TRAK MICROWAVE, "FET Amplifiers Catalog," FA. 7 (June 1981).
6. E.W. Strid and T.C. Duder, "Intermodulation Distortion Behavior of GaAs Power FETS," *1978 IEEE MTT-S International Microwave Symposium Digest,* pp. 135-137 (June 1978).
7. Y. Takayama, "Nonlinearity and Intermodulation Distortion in Power GaAs FET Amplifiers," Monograph Tech. Group Microwave, IECE of Japan. MW78-46 (July 1978).
8. G.L. Heiter, "Characterization of Nonlinearities in Microwave Devices and Systems," *IEEE Trans. on MTT,* Vol. MTT-21, No. 12 (December 1973).
9. Y. Takayama and K. Honjo, "Nonlinearity and Intermodulation Distortion in Microwave Power GaAs FET Amplifiers," NEC Technical Note, TN79901 (October 1979).
10. C. Hsieh, "Linear Amplification Techniques in 2 GHz Microwave Radios," Conference Record NTC'77, Vol. 1, pp. 16:3-1 (December 6, 1977).
11. J.A. Higgins, "Intermodulation Distortion in GaAs FETs," Rockwell Internation/Science Center, Thousand Oaks (1979).
12. TRW Data Sheet, "Microwave Linear Transistors TRW 52604," Data sheet No. 557 (May 1975).

Part 1: EMI Shielding

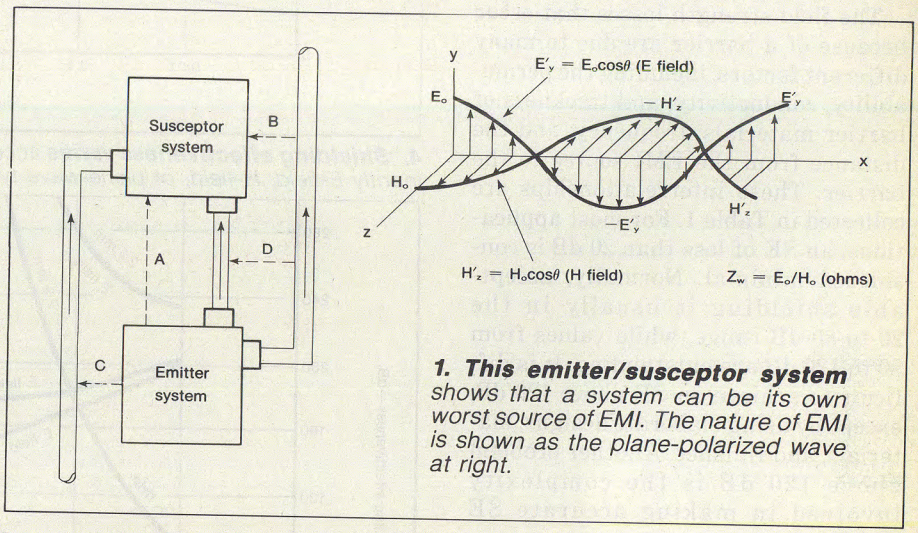
Shielding Barriers Block Electromagnetic Waves

Electromagnetic interference can hinder a system's performance by causing unwanted noise. This first in a five-part series examines how signals are attenuated through absorption, reflection, and rereflection.

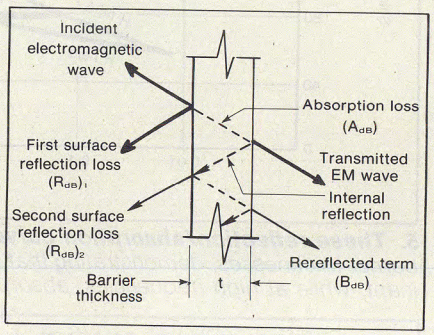
ELECTROMAGNETIC interference (EMI) is the hidden agent in every microwave design. This radiated interference is capable of impairing the performance of an electronic system or subsystem by increasing the noise level and acting as a false information signal. EMI problems are solved by establishing electromagnetic compatibility (EMC)—a near-perfect state in which an electronic system operates reliably in its intended electromagnetic environment without responding to electrical noise or generating excess electrical noise itself. This state of compatibility is usually approached by means of line filters and conductive equipment shields capable of reducing the EMI below a disruptive level.

Figure 1 presents an example of an EMI emitter/susceptor system. The emitter generates noise while the susceptor is affected by the noise. Quite often, a single device will act as both emitter and susceptor. The four lines in Fig. 1 show the different emitter-susceptor relationships. Line A represents interference that is coupled directly from the emitter to the susceptor, through radiation paths. In line B, the interconnection cables are the sources of the radiated noise. These cables can also be susceptible to EMI, as line C demonstrates. Finally, when noise in one cable is capacitively and inductively coupled to another cable, as line D indicates, excessive crosstalk results.

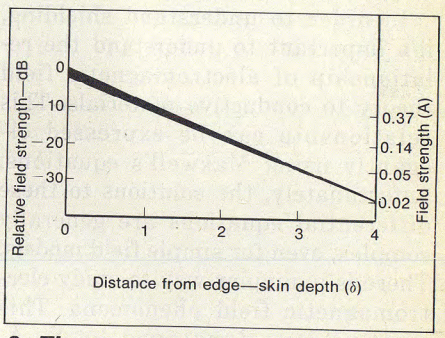
The bottom of Fig. 1 also shows, in a very simple and basic manner, the nature of electromagnetic waves. These waves consist of two oscillating fields—one electric (E), the other magnetic (H)—at right angles to each other. The electromagnetic impedance (Z_W) of the whole wave is defined as the ratio of the intensity of the E-field (in V/m) to the intensity of the H-field (in A/m). The two fields themselves have much different impedance origins. Electric fields are generated by, and most easily interact with, high-impedance voltage-driven circuits, such as straight wires or dipoles. Magnetic fields, on the other hand, are generated by and most readily interact with, low-impedance current-driven circuits, such as wire loops.



1. This emitter/susceptor system *shows that a system can be its own worst source of EMI. The nature of EMI is shown as the plane-polarized wave at right.*



2. A single electromagnetic wave *in contact with a solid conductive barrier will produce both surface reflections and internal reflections.*



3. The greater the penetration into a conductive barrier *by an electromagnetic wave, the greater the attenuation of that wave.*

Any barrier placed between an emitter and a susceptor that diminishes the strength of the interference can be thought of as an EMI shield. How well a barrier reduces the interference is commonly referred to as its shielding effectiveness (SE). The standard unit of measurement for SE is the decibel. Shielding effectiveness can be expressed as the ratio of two values of electromagnetic field strength, before and after the shield is put into place. Applicable equations are:

$$SE_{E\text{-field}} = 20 \log_{10} \frac{E_1}{E_2} \quad (1)$$

(continued on next page)

Peter Grant, EMI Product Manager, Technit, 129 Dermody St., Cranford, NJ 07016.

Table 1: Shielding effectiveness relationships

SE (dB)	Attenuation ratio	Percent attenuation
20	10^1:1	90.0
40	10^2:1	99.0
60	10^3:1	99.9
80	10^4:1	99.99
100	10^5:1	99.999
120	10^6:1	99.9999

$$SE_{H\text{-field}} = 20 \log_{10} \frac{H_1}{H_2} \qquad (2)$$

The field strength losses that occur because of a barrier are due to many different factors, including the permeability, conductivity, and thickness of barrier materials; frequency; and the distance from the EMI source to the barrier. These interrelationships are collected in Table 1. For most applications, an SE of less than 20 dB is considered minimal. Normally, acceptable shielding is usually in the 20-to-80-dB range, while values from 80 to 120 dB are outstanding. It is difficult to achieve an SE above 120 dB, except by using elaborate designs, materials, and finishes. Another problem above 120 dB is the complexity involved in making accurate SE measurements.

In order to understand shielding, it's important to understand the relationship of electromagnetic field theory to conductive materials. This relationship can be expressed elegantly using Maxwell's equations; unfortunately, the solutions to these differential equations are generally complex, even for simple field models. There is a simpler way to study electromagnetic field phenomena. This method was developed by S. A. Schelkunoff in the 1930s. Using his technique, the total shielding effectiveness (SE) of a solid conductive barrier can be expressed as the sum of the reflection (R), absorption (A), and rereflection (B) losses in dB (see Fig. 2):

$$SE = R + A + B \qquad (3)$$

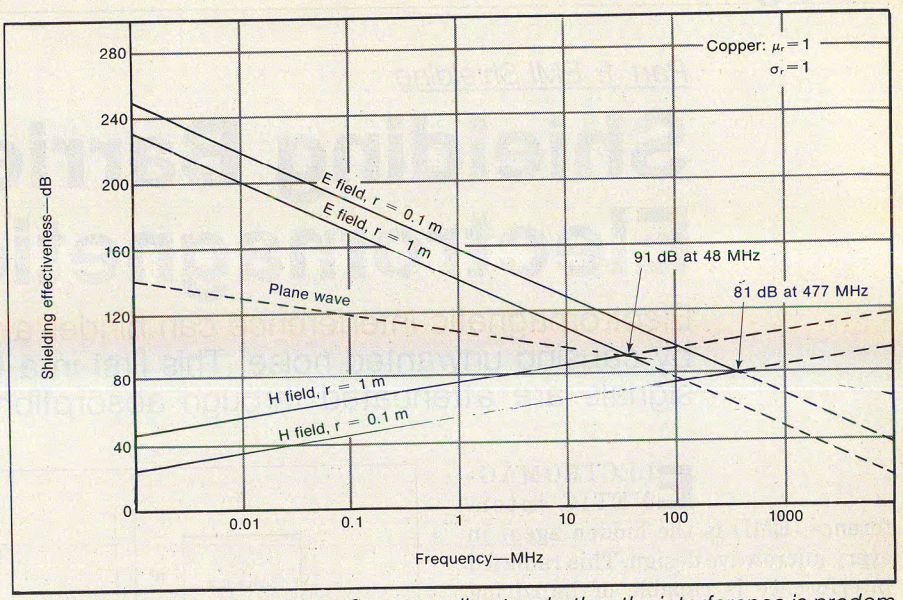
The reflection loss in this equation can be represented by:

$$R = 20 \log_{10} \frac{Z_W}{4Z_B} \qquad (4)$$

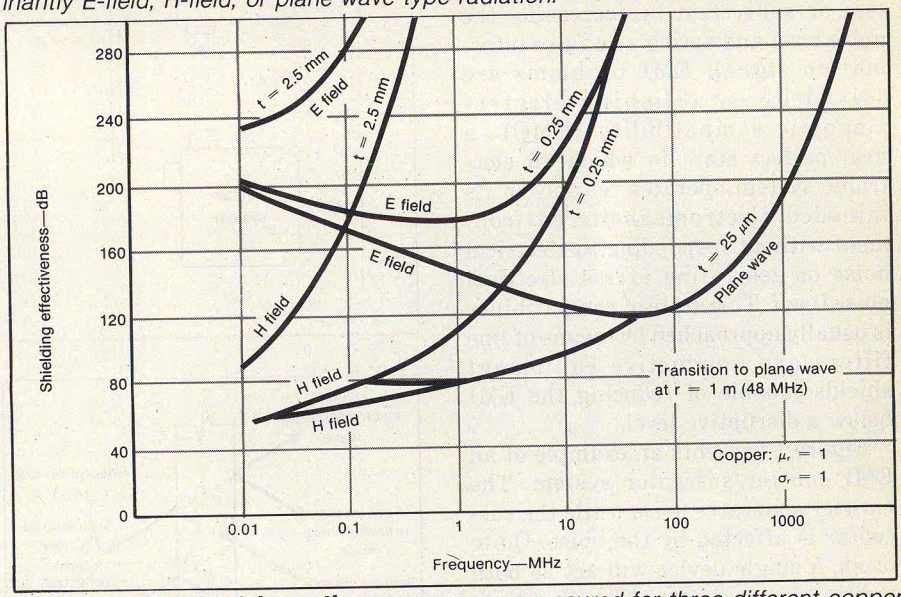
Also, the absorption loss can be written as:

$$A = 8.686\,(\alpha t) \qquad (5)$$

(concluded on p. 102)



4. Shielding effectiveness varies *according to whether the interference is predominantly E-field, H-field, or plane-wave type radiation.*



5. These reflection/absorption curves *were measured for three different copper barrier thicknesses, demonstrating that at low frequencies, reflection values are dominant, while at high frequencies, absorption values prevail.*

Table 2: Shielding terms and definitions

Terms	Description	Equivalent
A	absorption loss (dB)	$8.686\,\alpha t = 1.314(t)\,(f\mu_r\sigma_r)^{\frac{1}{2}}$
B	rereflection loss (dB)	$20 \log_{10} (1 - e^{-2\sqrt{2}(t/\delta)})$
K	impedance ratio	Z_W / Z_B
R	reflection loss (dB)	$20 \log_{10} (K + 1)^2 / 4K$
	for E-field (in m) (dB)	$321.7 - 10 \log_{10} (\mu_r/\sigma_r) f^3 r^2$
	for H-field (in m) (dB)	$14.6 - 10 \log_{10} (\mu_r/\sigma_r) f r^2$
	for plane wave (dB)	$168.1 - 10 \log_{10} (\mu_r/\sigma_r) f$
r	shield-to-source distance (m)	
Z_0	plane-wave impedance (Ω)	$(\mu_0/\epsilon_0)^{\frac{1}{2}} = 120\pi = 377$
Z_B	barrier impedance (Ω)	$3.69\lambda\ 10^{-7}\,[(\mu_r/\sigma_r)f]^{\frac{1}{2}}$
Z_W	wave impedance (Ω)	E/H
α	absorption coefficient (per cm)	$(\pi f \mu \sigma)^{\frac{1}{2}}$
δ	skin depth (cm)	$(\pi f \mu \sigma)^{-\frac{1}{2}}$
μ_r	relative permeability	1 (for air)
σ_r	relative conductivity	1 (for copper)